HYDROGEOLOGIC STUDIES AND GROUNDWATER MONITORING IN SNAKE VALLEY AND ADJACENT HYDROGRAPHIC AREAS, WEST-CENTRAL UTAH AND EAST-CENTRAL NEVADA

Edited by Hugh Hurlow

BULLETIN 135
UTAH GEOLOGICAL SURVEY
a division of
UTAH DEPARTMENT OF NATURAL RESOURCES
2014

HYDROGEOLOGIC STUDIES AND GROUNDWATER MONITORING IN SNAKE VALLEY AND ADJACENT HYDROGRAPHIC AREAS, WEST-CENTRAL UTAH AND EAST-CENTRAL NEVADA

edited by

Hugh Hurlow

Cover photo: *View northwest of Wheeler Peak and Great Basin National Park in the southern Snake Range, and the northern part of the Garrison agricultural area of Snake Valley in the foreground.*

ISBN 978-1-55791-902-1

BULLETIN 135
UTAH GEOLOGICAL SURVEY
a division of
UTAH DEPARTMENT OF NATURAL RESOURCES
2014

STATE OF UTAH
Gary R. Herbert, Governor

DEPARTMENT OF NATURAL RESOURCES
Michael Styler, Executive Director

UTAH GEOLOGICAL SURVEY
Richard G. Allis, Director

PUBLICATIONS
contact
Natural Resources Map & Bookstore
1594 W. North Temple
Salt Lake City, UT 84114
telephone: 801-537-3320
toll-free: 1-888-UTAH MAP
website: mapstore.utah.gov
email: geostore@utah.gov

UTAH GEOLOGICAL SURVEY
contact
1594 W. North Temple, Suite 3110
Salt Lake City, UT 84114
telephone: 801-537-3300
website: geology.utah.gov

CONTENTS

PLATES

DATA FOLDERS

HYDROGEOLOGIC STUDIES AND GROUNDWATER MONITORING IN SNAKE VALLEY AND ADJACENT HYDROGRAPHIC AREAS, WEST-CENTRAL UTAH AND EAST-CENTRAL NEVADA

ABSTRACT

This report presents results and analyses of hydrogeologic, geophysical, groundwater-monitoring, and hydrochemical studies and aquifer tests by the Utah Geological Survey (UGS) in Snake Valley, Tule Valley, and Fish Springs Flat, Millard and Juab Counties, west-central Utah. The primary objectives of this work were to (1) establish a new groundwater-monitoring network to improve data on baseline groundwater-level, spring-flow, and hydrochemical conditions, (2) measure the impacts of current and proposed future groundwater pumping on these baseline conditions, (3) improve understanding of geologic controls on groundwater flow in the study area, and (4) integrate the results to test previously proposed conceptual models of groundwater flow.

The study area is in the Basin and Range Province, characterized by predominantly north-south trending valleys and ranges. Faulted and folded Paleozoic carbonate rocks, Neoproterozoic and early Paleozoic siliciclastic rocks, and Mesozoic and Cenozoic intrusive rocks form the ranges and underlie the basin-fill deposits in all but the southern third of the study area, where Eocene to Miocene volcanic and shallow intrusive rocks predominate. The characteristic Basin-and-Range topography formed as late Cenozoic, steeply dipping normal faults uplifted the mountain ranges and created fault-bounded sedimentary basins in their hanging walls. Basin fill underlies the valleys and consists of predominantly coarse-grained alluvial-fan and fluvial deposits near the mountain fronts and predominantly fine-grained lacustrine and fluvial deposits in the valley centers.

New gravity data collected by the UGS in Snake Valley were combined with previous data to analyze the subsurface structure of the Quaternary-Tertiary fault-bounded sedimentary basins. Basin-fill deposits in the Snake Valley and northern and central Hamlin Valley sedimentary basins are as much as 10,000 feet (3050 m) thick, and are separated into five sub-basins by subsurface bedrock ridges that strike transverse to the valley axes. Volcanic deposits in the Indian Peak caldera complex beneath southern Hamlin Valley are locally more than 15,000 feet (4570 m) thick. The other Quaternary-Tertiary fault-bounded sedimentary basins in the study area also have complex internal structure, and their basin-fill deposits are locally more than 5000 feet (1520 m) thick.

Geologic units in the study area are grouped into 12 hydrogeologic units and classified as aquifers or confining units, based on their hydraulic properties determined by aquifer tests from previous studies of similar units in the Basin and Range Province. The most important aquifers are Quaternary to Miocene coarse-grained basin-fill deposits, upper and lower Paleozoic carbonate rocks, and fractured volcanic rocks. Confining units include Neoproterozoic to lower Paleozoic and middle Paleozoic siliciclastic rocks, Tertiary intracaldera volcanic deposits, Mesozoic and Cenozoic intrusive rocks, and fine-grained Quaternary lacustrine deposits. Partly consolidated Tertiary sedimentary and volcanic rocks in the deeper parts of the Quaternary-Tertiary fault-bounded sedimentary basins likely have hydraulic properties intermediate between those of most aquifers and confining units. Major fault zones may permit, slow, or inhibit groundwater flow across their planes depending on their geometry and the properties of the hydrogeologic units they juxtapose.

The UGS groundwater-monitoring network consists of piezometers (small-diameter wells open to discrete intervals of the aquifers) to measure groundwater levels and chemistry, and surface-flow gages to measure spring discharge. The piezometers are screened in the basin-fill, carbonate-rock, and volcanic-rock aquifers. Groundwater-monitoring sites are in mountain-front recharge, valley-floor discharge, agricultural, and interbasin-boundary zone hydrogeologic settings. The sites are adjacent to the Snake Valley part of Southern Nevada Water Authority's proposed groundwater-development project, in areas of current agricultural groundwater pumping in Utah, near environmentally sensitive and economically important springs, and along possible interbasin-flow paths.

Groundwater levels fluctuate seasonally by as much as 15 feet (5 m) in and near agricultural areas where groundwater is pumped for irrigation. Piezometers in the lower Paleozoic carbonate-rock aquifer hydrogeologic unit near

some agricultural areas fluctuate synchronously with piezometers in the basin-fill aquifer in which the pumping wells are screened, suggesting that the carbonate-rock and basin-fill aquifers are hydraulically connected at these locations. Groundwater levels near spring heads fluctuate seasonally by as much as 3 feet (0.9 m) per year in response to seasonal changes in evapotranspiration rates, and are not presently declining from year to year. The exception is Needle Point Spring in southern Snake Valley, which is near an agricultural area. Groundwater levels in the basin-fill and carbonate-rock aquifers at sites more than about 5 miles (8 km) from agricultural pumping show little regular seasonal fluctuation. Groundwater levels in Snake Valley agricultural areas declined from the late 1980s to late 2012 by average rates of 0.3 to 2.3 feet per year (0.1–0.7 m/yr) depending on location and specific time interval. Data from remote sites not affected by groundwater pumping suggest that as much as about 0.2 feet per year (0.1 m/yr) of this decline represents climatic effects, resulting from relatively lower average annual precipitation and, presumably, recharge rates following several consecutive wet years in the early 1980s.

Most hydrochemical parameters follow systematic spatial and compositional trends from the Snake Range and Deep Creek Range, to the Snake Valley, Tule Valley, and Fish Springs Flat valley floors. Total-dissolved-solids concentrations are <250 mg/L near the Snake Range, 250–1000 mg/L below the valley floors, and >1000 mg/L in some springs and wells in the northeastern part of the study area. Tritium concentration and percent modern carbon decrease progressively from the Snake Range to Fish Springs. These variations are interpreted to reflect slow regional flow from recharge to discharge areas, with relatively little input from recharge sources along the flow paths except in isolated samples. Inverse geochemical modeling of major-ion chemistry using statistically defined geochemical groups supports the conceptual model of regional flow in the Fish Springs flow system and flow paths from the Snake Range, Snake Valley, and Deep Creek Range to Tule Valley and Fish Springs.

Environmental-tracer data collectively indicate that more than half of the groundwater sampled in the Snake Valley area recharged over 1000 years ago, implying that low recharge rates and/or long flow paths characterize most of the Snake Valley groundwater system. Recently recharged groundwater occurs in parts of Snake Valley adjacent to the mountain fronts, and is likely supplied by mountain-block areas having relatively high rates of precipitation and recharge. Away from localized major sources of recharge in mountain blocks and mountain fronts, groundwater is recharged very slowly, if at all.

The UGS conducted aquifer tests at two of our groundwater-monitoring sites. At site 11, we pumped the upper Paleozoic carbonate-rock aquifer hydrogeologic unit, and monitored drawdown in three piezometers screened in the upper Paleozoic carbonate-rock aquifer and in one piezometer screened in the coarse-grained basin-fill aquifer. Hydraulic parameters estimated using standard analytical curve-matching and MLU (Multi-Layer Unsteady state) modeling methods for the carbonate-rock aquifer were 11,700 to 37,000 feet squared per day (1100–3500 m^2/d) for transmissivity, 6 to 21 feet per day (1.8–6.4 m/d) for hydraulic conductivity, and 4×10^{-4} to 1×10^{-3} for specific storage. For the basin-fill aquifer, we estimated transmissivity of 54,200 to 89,000 feet squared per day (5040–8270 m^2/d), hydraulic conductivity of 210 to 340 feet per day (64–104 m/d), and storativity of 3×10^{-4} to 4×10^{-3}. At site 3, we pumped the lower Paleozoic carbonate-rock aquifer hydrogeologic unit, and monitored drawdown in three piezometers screened in the same unit. Hydraulic parameters estimated using standard analytical curve-matching methods were 2100 to 4600 feet squared per day (200–430 m^2/d) for transmissivity, 3 to 7 feet per day (0.9–2.1 m/d) for hydraulic conductivity, and 6×10^{-5} to 2×10^{-4} for storativity. These estimates are consistent with results from aquifer tests on similar hydrogeologic units in the eastern Great Basin from other studies, and provide important reference values for future groundwater-flow models or other hydrogeologic calculations, such as those of interbasin flow presented in this report.

Spatial variations in the potentiometric surface, hydrogeologic setting, and hydrochemistry (major-ion composition, radiogenic and stable isotope concentrations) are consistent with previously proposed regional (interbasin) flow in the Fish Springs flow system from recharge in the Snake Range, through the upper and lower carbonate-rock aquifers of Snake Valley and the central and southern Confusion Range interbasin-boundary zone, to discharge in Tule Valley and Fish Springs. Evaluation of hydrogeologic and hydrochemical data supports several interbasin flow paths within the Fish Springs flow system, though some previously proposed flow paths are unlikely to accommodate significant flow. Model recharge temperatures from dissolved noble gas compositions are mostly inconsistent with other geochemical tracer data. Groundwater recharged in the Snake Valley hydrographic area may flow to Tule Valley through the central and southern Confusion Range, where it may discharge to central Tule Valley or continue to the northeast to discharge at Fish Springs. Other sources of groundwater discharging in Tule Valley and Fish Springs include flow paths from Pine and Wah Wah Valleys and the western Sevier Desert. Our work does not provide estimates of the relative proportions of these sources that

contribute to discharge in Tule Valley and Fish Springs.

Local-scale flow systems include recharge areas in the Snake Range and Deep Creek Range mountain blocks and mountain fronts, the basin-fill and shallow carbonate-rock aquifers, and discharge areas (springs and distributed areas of evapotanspiration) on the lower mountain fronts and valley floor. Groundwater in the discharge areas is younger and less chemically evolved than in the discharge areas of intermediate and regional flow systems. Recharge to intermediate-scale flow systems occurs in the same areas as the local flow systems, and discharge is from spring complexes and distributed areas of evapotranspiration on the central and eastern parts of the valley floor. Groundwater in intermediate flow systems is moderately chemically evolved, and qualitative ages are premodern to old.

Pressure to develop groundwater in west-central Utah is likely to continue in the future. Declining groundwater levels in areas of current use as determined from our groundwater monitoring, old groundwater ages, and slow recharge rates in most of the study area suggest that current groundwater use in Snake Valley is removing groundwater from storage in the basin-fill aquifer. Thus, declining groundwater levels and reduced spring flow would continue at present pumping rates. Increased future groundwater pumping would substantially increase the rate and area of groundwater-level decline and capture of discharge. Significant additional pumping of groundwater for local agricultural use or export from the hydrographic area would capture groundwater discharge that currently sustains springs, and shallow groundwater that supports sensitive-species habitat and vegetation used for irrigation and grazing.

CHAPTER 1 | INTRODUCTION

by Hugh Hurlow

View south of UGS site PW07, east-central Snake Valley, and northern Buckskin Hills in background.

Bibliographic citation for this chapter:
Hurlow, H., 2014, Introduction, Chapter 1 *in* Hurlow, H., editor, Hydrogeologic studies and groundwater monitoring in Snake Valley and adjacent hydrographic areas, west-central Utah and east-central Nevada: Utah Geological Survey Bulletin 135, p. 1–17.

CHAPTER 1 CONTENTS

FIGURES

TABLES

CHAPTER 1: INTRODUCTION

by Hugh Hurlow

1.1 PURPOSE AND SCOPE

This report presents results and analyses of hydrogeologic, geophysical, groundwater-monitoring, and hydrochemical studies by the Utah Geological Survey (UGS) in Snake Valley, Tule Valley, and Fish Springs Flat, in Millard and Juab Counties, west-central Utah (figure 1.1). The project arose in response to proposed large-scale groundwater development in east-central Nevada and west-central Utah. The general objectives of this work were to (1) establish a new groundwater-monitoring network to improve data on baseline groundwater-level, spring-flow, and geochemical conditions, (2) measure the impacts of current and proposed future groundwater pumping on these baseline conditions, (3) improve understanding of geologic controls on groundwater flow in the study area, and (4) integrate the results to test previously proposed conceptual models of groundwater flow.

The UGS study area includes Snake Valley and Hamlin Valley in Utah and Nevada, Tule Valley, Fish Springs Flat, and the western part of the Sevier Desert in western Millard, Juab, and Beaver Counties, Utah, and central and southern Spring Valley, southeastern Steptoe Valley, and Lake Valley in White Pine and Lincoln Counties, Nevada (figure 1.1; table 1.1). These hydrographic areas are in the Great Basin hydrologic region, and the carbonate-rock aquifer province of the Basin and Range physiographic province (figure 1.1 inset) (Harrill and Prudic, 1998). The focus study area, where the UGS installed new groundwater-monitoring facilities, includes Snake Valley, northern Hamlin Valley, Tule Valley, and Fish Springs Flat (figure 1.1). Hydrographic areas in the study area are thought to be connected by deep groundwater flow through the carbonate-rock aquifer, and comprise the Fish Springs multibasin flow system (Carlton, 1985) within the Great Salt Lake Desert regional flow system (Harrill and others, 1988; Harrill and Prudic, 1998) (figure 1.2).

The primary tasks of the UGS work were as follows:

1. Conduct hydrogeologic studies (chapters 2 and 4), collect new geophysical (gravity) data (chapter 3), and summarize available hydrogeologic data (chapter 4) to improve understanding of the hydrogeologic framework of the study area.
2. Establish a groundwater-monitoring network in Snake Valley and adjacent hydrographic areas in west-central Utah (chapter 5) to measure current baseline values of groundwater levels and hydrochemistry, and evaluate changes in these parameters due to possible future groundwater development and climatic variations.
3. Collect and analyze hydrochemical data from the new wells and from previously existing wells and springs, to characterize spatial variations in solute and isotope chemistry, model age, and model recharge temperature (chapter 6).
4. Conduct aquifer tests of the carbonate-rock and basin-fill aquifers to estimate their hydraulic properties (chapter 7).
5. Synthesize our new data with previously existing data to (a) evaluate previously published conceptual models of groundwater flow in the region, and (b) delineate and characterize possible local- to regional-scale groundwater-flow systems and flow paths (chapter 8).
6. Qualitatively evaluate potential impacts of proposed groundwater development, by synthesizing recent hydrogeologic and biologic studies (chapter 9).

Our results provide important new data for understanding groundwater conditions in west-central Utah and east-central Nevada, particularly (1) records of groundwater level fluctuations that will establish current trends and sensitivity to climatic fluctuations, to provide a baseline to evaluate impacts of future changes in groundwater use and climate, (2) discharge records of springs that provide habitat for environmentally sensitive species and agricultural water, and (3) subsurface lithology, water levels, chemistry, and transmissivity of the carbonate-rock aquifer, which is thought to host regional-scale groundwater flow and provide discharge to large springs, and of the basin-fill aquifer, which is currently used for agriculture in Snake Valley, and (4) the structure of the basin-fill aquifer in greater detail than was previously available.

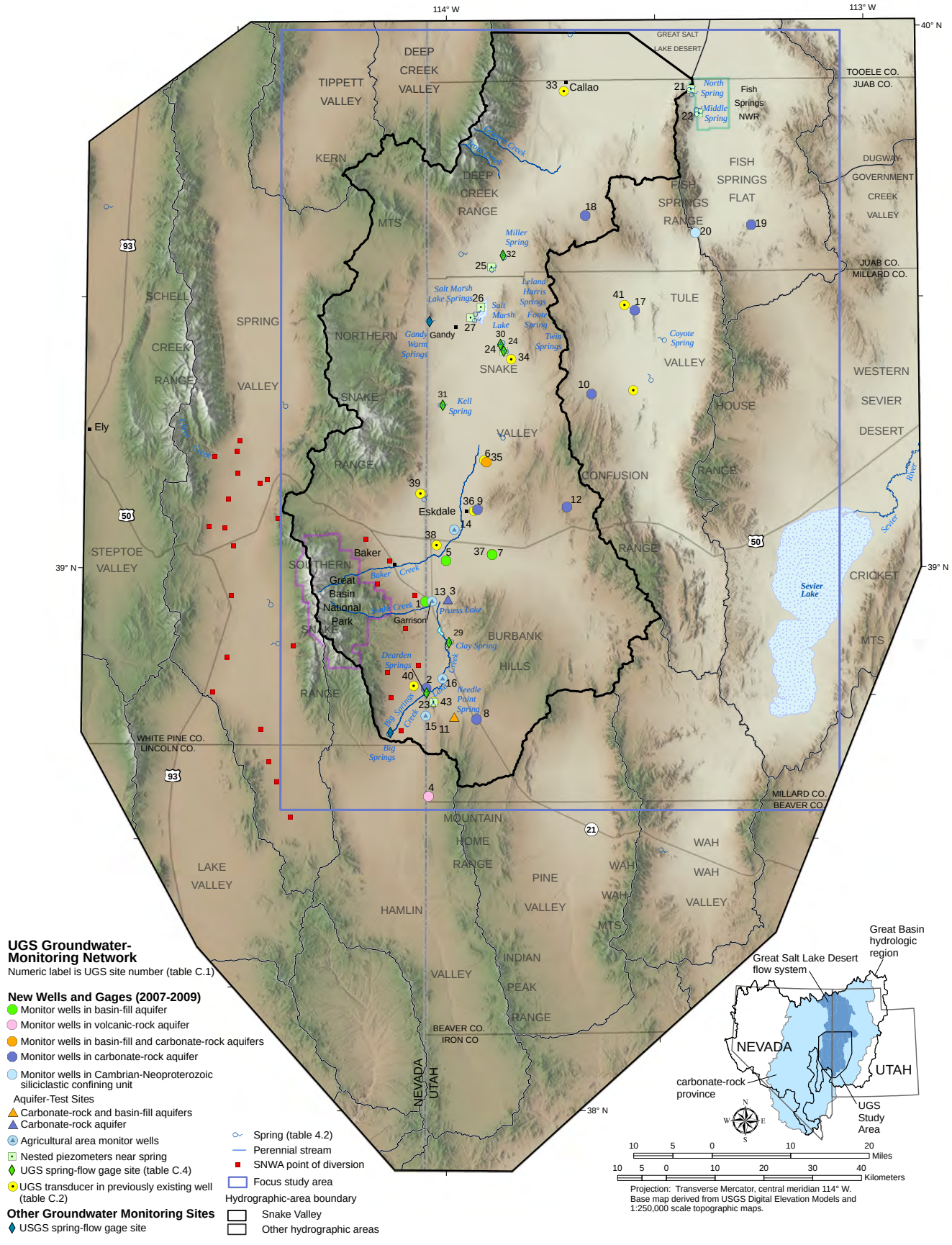

Figure 1.1. *Geographic setting of the UGS study area in west-central Utah and east-central Nevada, and locations of UGS groundwater-monitoring sites.*

Table 1.1. *Hydrographic areas and flow systems in the UGS study area.*

Hydrographic Area Name	Hydrographic Area Number[2]	Regional Flow System[3]	Area (mi²)
Deep Creek Valley[1]	253	Great Salt Lake Desert	453
Dugway-Government Creek Valley[1]	259	Great Salt Lake Desert	1171
Fish Springs Flat	258	Great Salt Lake Desert	632
Great Salt Lake Desert (West Part)[1]	261A	Great Salt Lake Desert	4648
Pine Valley	255	Great Salt Lake Desert	733
Snake Valley[4]	254	Great Salt Lake Desert	3685
Spring Valley[1]	184	Great Salt Lake Desert	1700
Tippett Valley[1]	185	Great Salt Lake Desert	347
Tule Valley	257	Great Salt Lake Desert	943
Wah Wah Valley	256	Great Salt Lake Desert	605
Steptoe Valley[1]	179	Goshute Valley	1958
Sevier Desert[1,5]	287	Sevier Lake	3981
Lake Valley	183	Colorado	550

[1] The boundaries of these hydrographic areas extend beyond the area shown on our illustrations. The surface areas cited here are for the entire hydrographic area or subarea.

[2] U.S. Geological Survey nomenclature and boundaries (Harrill and others, 1988, sheet 1), but see note 4 regarding Snake Valley.

[3] Flow systems are from Harrill and others (1988, sheet 1). Welch and others (2007, figure 41) placed southern Steptoe Valley and all of Lake Valley in the Great Salt Lake Desert regional flow system, and central Steptoe Valley in the Colorado regional flow system.

[4] The U.S. Geological Survey and the Nevada Division of Water Resources use different delineations of the Snake Valley hydrographic area. In this report UGS follows the U.S. Geological Survey delineation for hydrographic areas, and refers to Hamlin Valley as a geographic feature. When we cite reports that use the Nevada Division of Water Resources groundwater basins, we use Hamlin Valley (NV 196).

The Nevada Division of Water Resources delineates Hamlin Valley and Pleasant Valley within the U.S. Geological Survey's Snake Valley hydrographic area:

NV Groundwater Basin	NV Number	Flow System[2]	Area (mi²)
Snake Valley	195	Great Salt Lake Desert	2760
Hamlin Valley	196	Great Salt Lake Desert	813
Pleasant Valley	194	Great Salt Lake Desert	108

The Nevada Division of Water Resources uses the term "administrative groundwater basin" to refer to their water-management units <http://water.nv.gov/mapping/maps/designated_basinmap.pdf>. Their groundwater basins typically coincide with the U.S. Geological Survey's hydrographic areas except as noted for Snake Valley.

SNWA (2008, 2009a) referred to the U.S. Geological Survey's Snake Valley hydrographic area as "Big Snake Valley" to distinguish it from the Nevada Division of Water Resources' Snake Valley groundwater basin.

SNWA (2008, 2009a) and Durbin and Loy (2010) calculated groundwater budgets using the Nevada Division of Water Resources groundwater basins as acounting units, whereas Harrill and others (1988), Prudic and Harrill (1998), Welch and others (2007), Halford and Plume (2011), and Heilweil and Brooks (2011) used the U.S. Geological Survey delineation.

[5] Surface area and western boundary are those used by Durbin and Loy (2010) in their groundwater-flow model.

Data from this project will improve understanding and analysis of the hydrogeology of Snake Valley beyond the scope of this report. Continuous groundwater-level and surface-flow records will help evaluate the sensitivity of the regional groundwater supply to climatic fluctuations and pumping, and will provide a standard to assess the effects of possible future groundwater development. The monitoring wells provide convenient sampling ports for future hydrochemical analyses, particularly in the previously sparsely sampled carbonate-rock aquifers. Groundwater levels from the UGS groundwater-monitoring network have been incorporated into conceptual and numerical groundwater-flow models of the region (SNWA, 2009a, 2009b; Durbin and Loy, 2010; Halford and Plume, 2011). In the future, long-term trends, hydrochemical data, and aquifer-test results will aid the calibration of new or revised models, making them more robust predictive tools. The groundwater-level and flow data will likely be incorporated into monitoring plans associated with future water-use agreements in the region.

1.2 BACKGROUND

The UGS began its work in Snake Valley in 2004 due to concern by local and state officials and residents over proposed groundwater development in Spring and Snake Valleys, Nevada, by the Southern Nevada Water Authority (SNWA, 2012). The initial objective was to characterize the

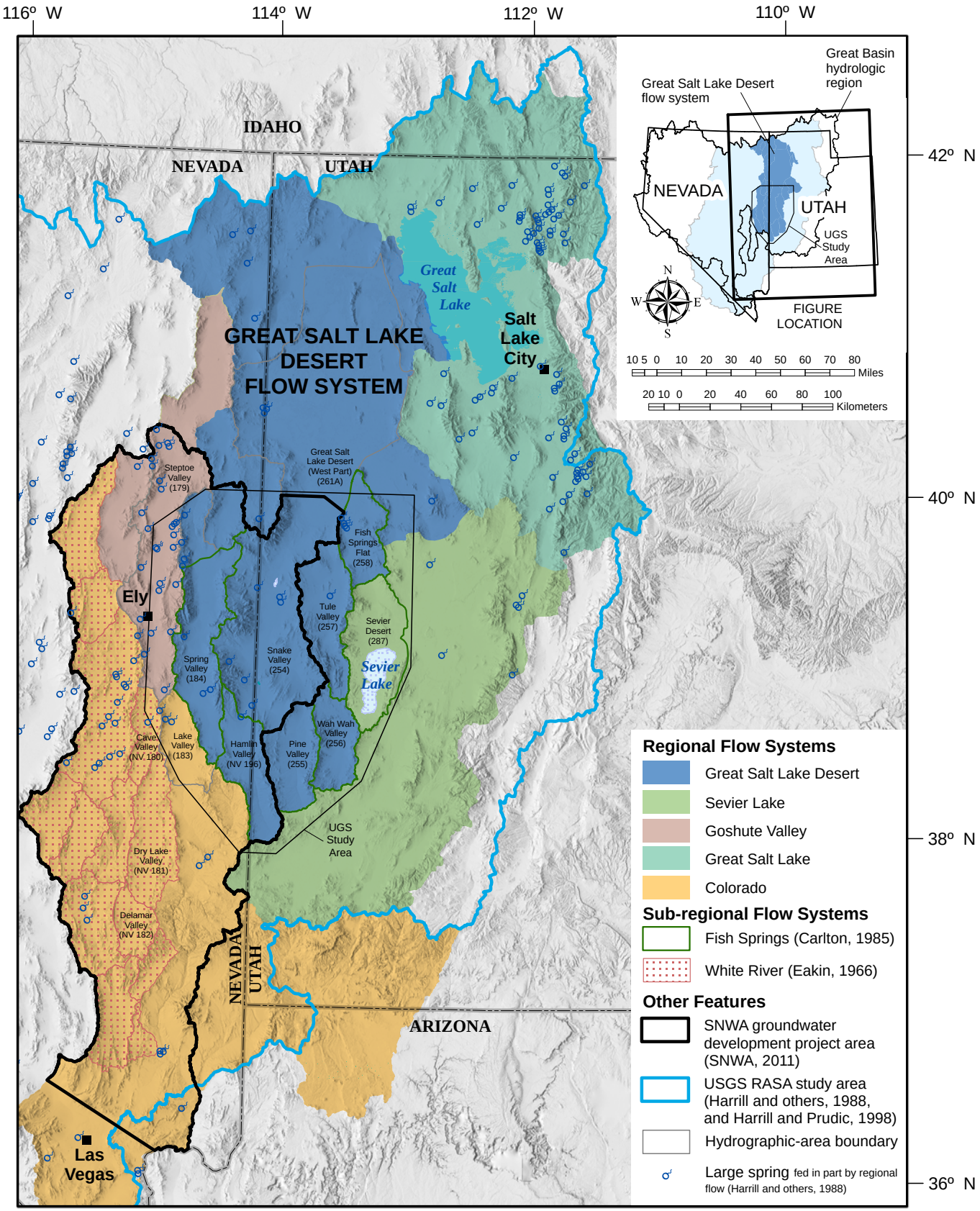

Figure 1.2. *Regional and sub-regional flow systems of the eastern Great Basin (Harrill and others, 1988). Hydrographic-area boundaries are from the U.S. Geological Survey. Harrill and others (1988), SNWA (2009a), and Heilweil and Brooks (2011) place southern Steptoe Valley and Lake Valley in the Great Salt Lake Desert regional flow system, whereas Welch and others (2007) place them in the Colorado regional flow system.*

Table 1.2. *Proposed groundwater-development projects in Snake Valley and other hydrographic areas in east-central Nevada (see figure 1.3 for locations of Snake Valley and Spring Valley applications).*

Nevada Groundwater Basin[1]	Application Numbers and Quantities[2]	Ruling Numbers and Approved Quantities[3]
Cave Valley (180)	53987, 53988: 16 cfs = 11,584 afy	6165[4]; 7.23 cfs = 5235 afy
Delamar Valley (182)	53991, 53992: 16 cfs = 11,584 afy	6166[4]; 16 cfs = 11,584 afy
Dry Lake Valley (181)	53989, 53990: 16 cfs = 11,584 afy	6167[4]; 8.34 cfs = 6042 afy
Spring Valley (184)	54003-54021: 126 cfs = 91,244 afy	6164[4,5]; 84.4 cfs = 61,127 afy
Subtotal	**174 cfs = 126,004 afy**	**116 cfs = 83,988 afy**
Snake Valley (195)	54022-54030: 70 cfs = 50,680 afy	Hearing postponed by Interim Order #3[6]
Total	**244 cfs = 176,676 afy**	**83,988 afy[7]**

cfs = cubic feet per second, afy = acre-feet per year.

[1] Nevada administrative groundwater basin name and number. See notes for table 1.1 for further explanation.

[2] Application to Nevada State Engineer (http://water.nv.gov/).

[3] Information from Nevada State Engineer (2012 a-d).

[4] Protest by the Department of the Interior on behalf of the Bureau of Indian Affairs, the Bureau of Land Management, the National Park Service, and the Fish and Wildlife Service was withdrawn subject to a Stipulated Agreement between SNWA and the Protestant (http://water.nv.gov/hearings/waterhearing/drycavedelamar/index.html).

[5] Ruling required initial development of between 32,300 and 38,000 afy for eight years with monitoring; the Nevada State Engineer may allow an additional 12,000 afy (50,000 afy total) for eight years thereafter and an additional 11,127 (61,127 afy) thereafter, depending on monitoring results.

[6] See http://water.nv.gov/Hearings/waterhearing/snakevalley/documents.html.

[7] The Nevada State Engineer approved transfer of 11,300 afy in agricultural rights in Lake Valley and 8,000 afy in agricultural rights in Spring Valley to SNWA and conversion of these rights to domestic use for inclusion in the proposed pipeline. These values are not included in the total approved quantity listed in this table.

hydrogeologic setting of Snake Valley and adjacent basins by evaluating the likely influences of stratigraphy and structure on groundwater flow (Kirby and Hurlow, 2005), compiling a geologic map, and collecting and analyzing new gravity data. In 2007 the Utah Legislature requested the UGS to establish a groundwater-monitoring network to determine baseline groundwater conditions and measure changes if future groundwater development were to occur. The network was completed in December 2009.

SNWA's proposed groundwater development in Spring and Snake Valleys is part of a larger scale plan to pump groundwater from hydrologic basins in southeastern and east-central Nevada, and convey the water to the Las Vegas area by a pipeline system (SNWA, 2012; U.S. Bureau of Land Management, 2012a, b). The northern part of this plan is the Clark, Lincoln, and White Pine Counties Groundwater Development Plan (table 1.2; figure 1.2) (SNWA, 2012). Government officials and residents of Utah are concerned about the Snake and Spring Valley segments of this plan because they would likely impact the groundwater water supply and spring-fed wetlands ecosystems in adjacent parts of Utah. The proposed wells in Snake Valley are within 6 miles (9.6 km) of the state line (figure 1.3), and some of the groundwater in the Utah part of northern Hamlin Valley and southern Snake Valley is thought to originate in Spring Valley and enter Snake Valley via subsurface interbasin flow in the carbonate-rock aquifer (Gates and Kruer, 1981; Welch and others, 2007).

The Nevada State Engineer granted water rights to SNWA in Spring, Delamar, Dry Lake, and Cave Valleys on March 22, 2012 (Nevada State Engineer, 2012a-d, rulings 6164 through 6167). The rulings granted SNWA about 67% of their combined applications in the four basins (table 1.2). Groundwater development in Spring Valley will occur in two eight-year stages subject to the results of intensive monitoring (Nevada State Engineer, 2012a, p. 115). The Nevada State Engineer's ruling allows for initial development of between 32,300 and 38,000 acre-feet per year (between 39.8 and 46.9 hm^3/yr) for eight years, during which time SNWA will monitor groundwater levels and chemistry, including four sites from the UGS groundwater-monitoring network (Nevada State Engineer, 2012a, p. 115), conduct predictive numerical modeling of the effects of the development, and submit annual reports. After that period the Nevada State Engineer may allow SNWA to pump between 42,500 and 50,000 acre-feet per year (between 52.4 and 61.7 hm^3/yr) for eight years while continuing to monitor and model the effects. The full allocation of 61,127 acre-feet per year (75.4 hm^3/yr) could be approved after the second development stage.

In Utah, several applications were filed between 2005 and 2010 for large-scale groundwater development in, and in some cases interbasin transport from, some of the hydrographic basins in the UGS primary study area (table 1.3; figure 1.3). These projects, if approved, would withdraw water from the basin-fill and/or carbonate-rock aquifers.

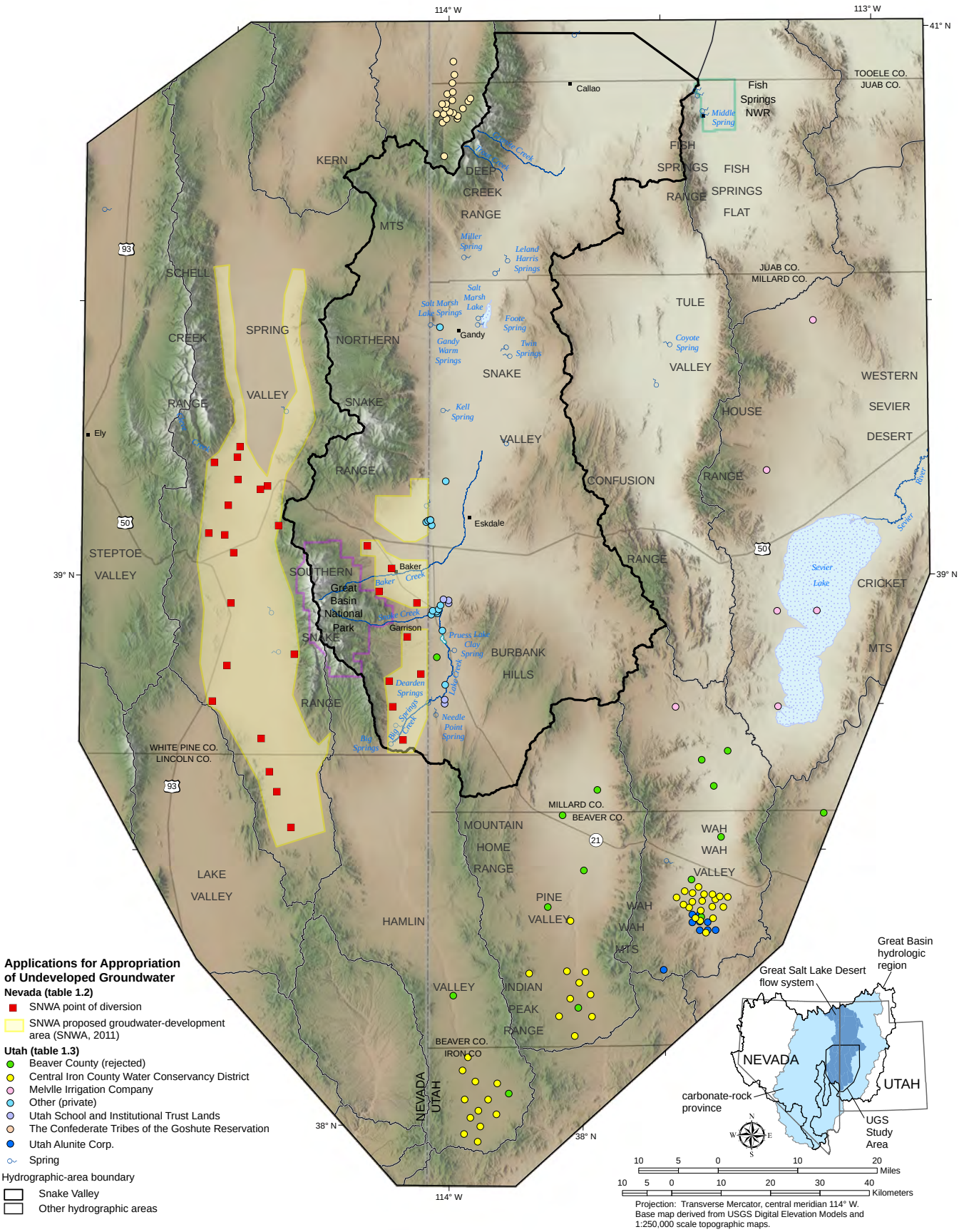

Figure 1.3. *Points of diversion for proposed groundwater-development projects in west-central Utah and east-central Nevada. See tables 1.2 and 1.3 for data and sources.*

Table 1.3. *Proposed groundwater-development projects in Snake Valley and adjacent hydrographic areas in west-central Utah (see figure 1.3 for application locations).*

Applicant[1]	Water Right Application Numbers and Quantities[2]	Status and Approved Quantities[2]
SITLA[3]	a75897; a759-33, 34, 42, 43; a79535-41: 8960 afy total (Snake Valley)	Unapproved
CICWCD[4]	a76675: 10,000 afy (Hamlin Valley) a76676: 15,000 afy (Pine Valley) a76677: 12,000 afy (Wah Wah Valley) 37,000 afy total	Unapproved
Melville Irrigation Co.	a76809: 123,000 afy (Wah Wah Valley and western Sevier Desert)	Unapproved
Goshute Tribes[5]	a77473: 35,000 afy underground, 15,000 afy surface (Deep Creek Valley)	Unapproved
Snake Valley land owners	a32297, a32318, a78574-a78577, a36268: 6590 afy total	Unapproved
Beaver County	a56999: 5069 afy (Wah Wah Valley) a57001: 3621 afy (Pine Valley) a57002: 1448 afy (Hamlin Valley) 10,138 afy total	Rejected
	a78813: 6400 afy (Hamlin Valley) a78814: 6650 afy (Wah Wah Valley) a78815: 13,900 afy (Pine Valley) 26,950 afy total	Unapproved
Utah Alunite Corp.	a79462: 6500 afy (Wah Wah Valley)	Unapproved
Total	**254,138 afy (underground)**	**244,000 pending, 10,138 rejected**

afy = acre-feet per year

[1] Application to Utah State Engineer, Department of Natural Resources/Division of Water Rights.

[2] Records available at http://www.waterrights.utah.gov/wrinfo/query.asp

[3] State of Utah School and Institutional Trust Lands Administration

[4] Central Iron County Water Conservancy District, for export to Cedar City, Utah, area.

[5] The Confederate Tribes of the Goshute Reservation; for local use.

Unapproved applications for groundwater development in Utah are for about 244,000 acre-feet per year (247 hm^3/yr), about 187,000 acre-feet per year (197 hm^3/yr) of which would be exported for use in other hydrographic basins.

The proposed groundwater-development projects in east-central Nevada and west-central Utah collectively constitute substantial pressure to develop a major portion of the groundwater resource in the region, and most of the pumped ground water would be exported for use elsewhere. The scale of the proposed development is such that, over long periods of time (tens of years) and without monitoring and mitigation programs to limit the impacts of the development, substantial drawdown of the water table would likely occur and adversely impact current use and environmental conditions in Snake Valley and adjacent hydrographic areas.

1.3 POTENTIAL EFFECTS OF PROPOSED GROUNDWATER DEVELOPMENT

Substantial (i.e., roughly 10 feet or greater) lowering of groundwater levels and capture of recharge in Snake Valley and adjacent hydrographic areas would adversely impact agricultural and domestic use, habitat for environmentally sensitive species and, potentially, air quality (U.S. Bureau of Land Management, 2012a). Lower groundwater levels cause higher agricultural production costs by requiring greater pumping lifts, deepening wells, lowering pumps, or purchasing new pumps. Eventually the ability of some users to access their legal water rights may be impaired. Lower groundwater levels and capture of groundwater discharge would lead to decreased spring discharge by lowering the hydraulic head in their source areas and reducing the groundwater-flow rate to them. The proposed

pumping may not only affect groundwater conditions near the pumping areas, but also in hydrographic basins adjacent to Snake Valley by virtue of interbasin hydraulic connectivity through deep carbonate-rock aquifers.

Springs in the study area are used for agriculture, and their pools and the spring-fed wetlands ecosystems supported by their outflow provide habitat for several environmentally sensitive species (i.e., species that are potentially threatened or endangered and/or are managed by conservation agreements) (Utah Division of Wildlife Resources, 2011). Decreased habitat quality and extent could result in listing of some species as threatened or endangered by the U.S. Fish and Wildlife Service (U.S. Fish and Wildlife Service, 2010; Utah Division of Wildlife Resources, 2011). Lowering of the water table in the valley centers to depths below the root zones of phreatophyte plants would lead to death of these plants and succession by non-phreatophytic shrub communities (Patten and others, 2007; McLendon, 2011; U.S. Bureau of Land Management, 2012a, section 3.5), and possibly soil instability and increased dust mobilization during high winds (U.S. Bureau of Land Management, 2012a, section 3.1).

Long-term lowering of the water table could also cause earth fissures due to differential shrinkage of dewatered sediment and related land-surface subsidence where geologic and hydrologic conditions favor such effects (e.g., Galloway and others, 2004; Lund and others, 2005).

Prediction of the potential effects of large-scale groundwater development in Snake Valley and adjacent basins requires knowledge of the current baseline groundwater levels, chemistry, storage and flow patterns, and understanding of the geologic controls on groundwater storage and flow in the study area. The results of this project substantially increase this data set.

1.4 PREVIOUS HYDROGEOLOGIC WORK

1.4.1 Introduction

This section summarizes the general scope and conclusions of major hydrogeologic studies that overlap spatially with the UGS study area (figure 1.4), to provide context for subsequent citations of data and interpretation of new UGS data in subsequent chapters. Figures 1.1 and 1.2 show locations of hydrographic areas and springs referenced in the following text, and figure 1.4 shows the study area locations. These studies include evaluation of geologic framework, inventories of hydrologic features, estimation of groundwater budgets, conceptual and, in some cases, numerical models of groundwater flow, and evaluations of the possible effects of future groundwater development.

1.4.2 Early Investigations

Meinzer (1911) presented the basic observational hydrology of west-central Utah, including the UGS study area. He catalogued several major spring systems, including Fish Springs, Gandy Warm Springs and the Bishop Springs complex (Foote and Twin Springs and other unnamed springs and seeps) (figure 1.1), and interpreted the magnitude, constant discharge rate, and temperature of spring flow to reflect source areas that are significantly larger than the surface-drainage basins in which the springs occur. These observations form the basis for modern interpretations of large-scale flow systems discussed in this report. The volume, mechanisms, and location of interbasin flow is an important but controversial and unresolved topic in understanding groundwater flow in the study area.

1.4.3 U.S. Geological Survey Reconnaissance Studies

The U.S. Geological Survey conducted early reconnaissance studies, in cooperation with the Nevada Department of Conservation and Natural Resources and the Utah Department of Natural Resources, to provide basic hydrogeologic, water-level, and chemical data and estimates of water budgets (recharge and discharge), groundwater storage, and developable groundwater volumes for individual hydrographic areas (figure 1.4) in east-central Nevada (Snake Valley – Hood and Rush, 1965; Spring Valley – Rush and Kazmi, 1965; Steptoe Valley – Eakin and others, 1967) and west-central Utah (Tule Valley – Stephens, 1977; Pine Valley – Stephens, 1976; Wah Wah Valley – Stephens, 1974; Fish Springs Flat – Bolke and Sumison, 1978; and southern Great Salt Lake Desert – Gates and Kruer, 1981).

Eakin (1966) described the White River flow system, which encompasses 13 hydrographic areas in east-central Nevada (figure 1.2). By combining hydrologic and hydrogeologic data, Eakin (1966) postulated that the hydrographic areas, which follow the Pleistocene White River drainage system, are hydraulically connected and constitute a sub-regional scale flow system within the Colorado regional flow system (figure 1.2) (Prudic and others, 1995, p. D70–D73) that consists of recharge areas in the northern mountains and discharge areas on the central and southern valley floors. Assuming these hydrographic areas are in hydrologic equilibrium (no long-term change in storage), Eakin (1966) proposed that the imbalance between recharge and discharge in individual basins is balanced by subsurface groundwater flow below surface-drainage divides, where

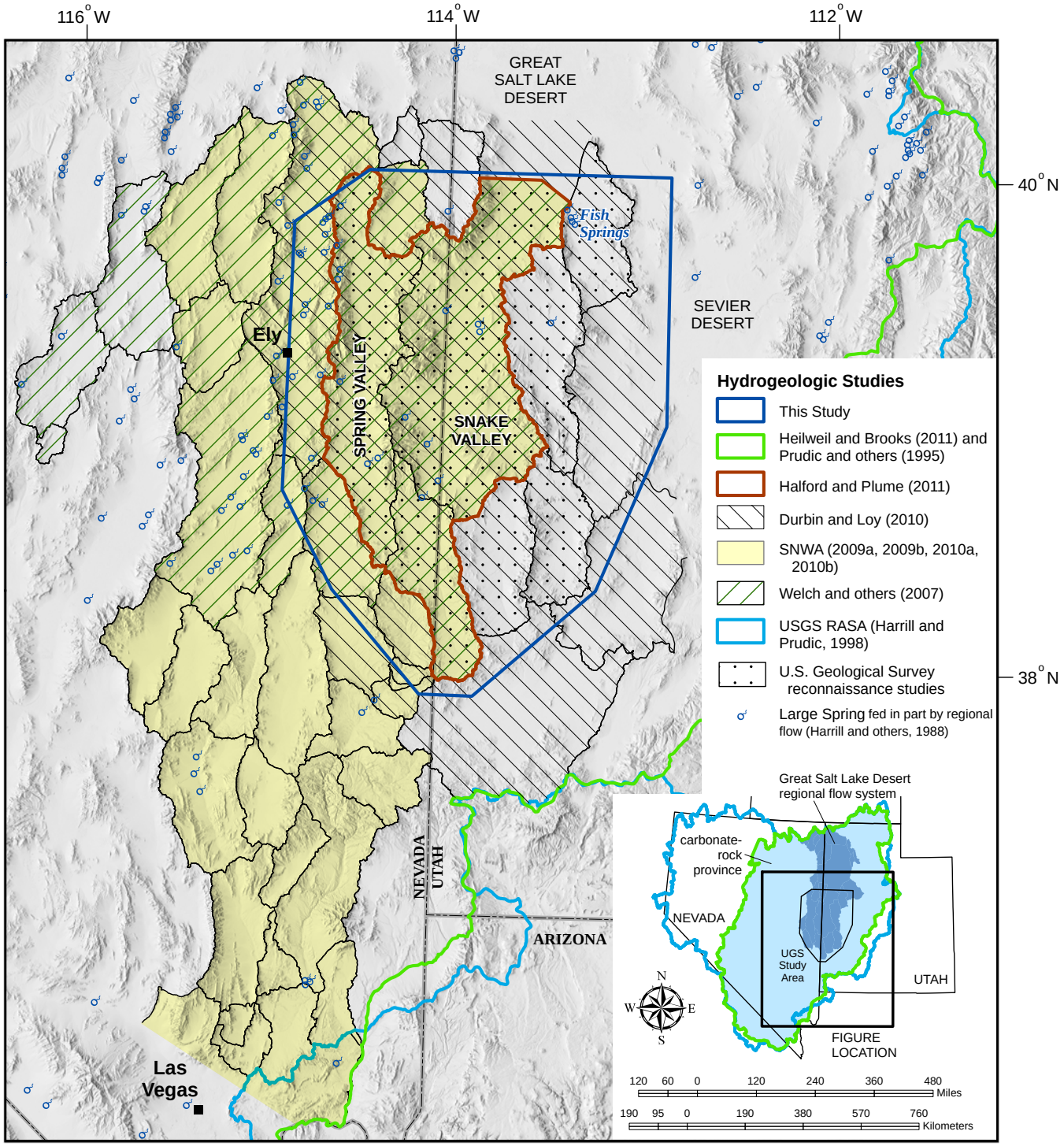

Figure 1.4. *Locations of previous hydrogeologic studies in west-central Utah and east-central Nevada discussed in the text.*

hydrogeologic conditions allow such flow.

Reconnaissance studies of hydrographic basins in western Utah included the first quantitative estimates of interbasin flow rates (summarized in Gates and Kruer, 1981, p. 31–37). In these studies, recharge estimates for Snake, Pine, and Wah Wah Valleys were greater than their discharge estimates, and Gates and Kruer (1981) regarded these basins as sources of subsurface flow. Discharge estimates for Tule Valley, Fish Springs Flat, and the southern Great Salt Lake Desert (GSLD) were substantially greater than their recharge estimates. High discharge rates in these basins are due primarily to evapotranspiration (ET) by phreatophytes and from playa on the valley floors, and large-flow springs in Tule Valley (Coyote and South and North Tule Springs), Fish Springs Flat (Fish Springs complex), and

the GSLD (Wilson Health Springs) (figure 1.1). Gates and Kruer (1981) concluded that subsurface flow from Snake, Pine, and Wah Wah Valleys is an important source of this discharge.

1.4.4 U.S. Geological Survey RASA Study

As part of its Regional Aquifer System Analysis (RASA) project, the U.S. Geological Survey conducted a regional-scale study of groundwater conditions in the basin-fill and carbonate-rock aquifers of the Great Basin, summarized by Harrill and Prudic (1998). The project included analyses of the hydrogeologic framework (Plume, 1996), groundwater chemistry (Thomas and others, 1997), and regional-scale conceptual (Harrill and others, 1988) and numerical (Prudic and others, 1995) groundwater-flow models.

Harrill and others (1988) delineated regional- to local-scale groundwater-flow systems in the Great Basin province, by identifying source areas, discharge areas, and generalized flow directions from contours of regional head. Harrill and others (1988) distinguished between shallow to intermediate-scale groundwater-flow systems in the basin-fill and carbonate-rock aquifers, and deep, regional flow systems in the carbonate-rock aquifer system, although they did not specify depth ranges. Harrill and others (1988) estimated recharge and discharge for each system, and subsurface-flow rates between hydraulically connected hydrographic areas. Harrill and others (1988) and Harrill and Prudic (1998) delineated the GSLD regional flow system, which encompasses the hydrographic areas in the UGS study area. Recharge to the GSLD flow system is mainly by infiltration of precipitation and snowmelt in the mountains bounding Snake and Spring Valleys, and the main discharge area is the western Great Salt Lake Desert.

Carlton (1985) defined the Fish Springs multibasin (referred to herein as sub-regional) flow system, which includes Snake, Hamlin, Tule, Pine, and Wah Wah Valleys, Fish Springs Flat, and western Sevier Desert (figure 1.2).

The RASA numerical flow model consists of two model layers to simulate relatively shallower flow in the basin-fill and carbonate-rock aquifers, and deeper regional flow in the carbonate-rock aquifer (Prudic and others, 1995). Simulated flow directions are mostly north to north-northeast but include local areas of east- or west-directed flow, and some flow was simulated from the Colorado and Sevier flow systems into the GSLD from the southwest and southeast, respectively. The deep-flow regions contain intermediate discharge zones such as Twin Springs in east-central Snake Valley, Coyote Spring in Tule Valley, and Fish Springs in northern Fish Springs Flat.

Schaefer and Harrill (1995) used Prudic and others' (1995) groundwater-flow model to evaluate possible drawdown from SNWA's proposed groundwater-development project. Results from this model are generalized and approximate, and are superseded by results from the models described in the following section. In the upper model layer, after 100 years of pumping at the amounts and locations in the original applications (Schaefer and Harrill, 1995, figure 8), their model shows about 100 to 350 feet (30–110 m) of drawdown at the pumping wells and up to 10 feet (3 m) of drawdown as far as 15 miles (24 km) to the east in Millard County, Utah. In the lower model layer, their model shows more than 100 feet (30 m) of drawdown around the well fields and up to 10 feet (3 m) of drawdown as far as 25 miles (40 km) to the east in Millard County.

1.4.5 Recent Studies

1.4.5.1 Introduction

Proposed groundwater development by SNWA in Nevada and by the Central Iron County Water Conservancy District and Beaver County in Utah motivated several comprehensive studies of groundwater conditions in the basin-fill and carbonate-rock aquifers in parts of east-central Nevada and west-central Utah: the U.S. Geological Survey's Basin and Range Carbonate Aquifer System (BARCAS) study (Welch and others, 2007; U.S. Geological Survey, 2011), and conceptual and numerical groundwater-flow models by SNWA (2009a, 2009b, 2010a, 2010b), Durbin and Loy (Durbin and Loy, 2010; Loy and Durbin, 2010), and the U.S. Geological Survey (Halford and Plume, 2011). Heilweil and Brooks (2011) revised estimates of groundwater availability in the Great Basin using new data and techniques.

1.4.5.2 U.S. Geological Survey BARCAS Study

The BARCAS study (Welch and others, 2007) evaluated the hydrogeology, water budget, flow systems, and available groundwater resources of the hydrographic areas in SNWA's proposed Clark, Lincoln, and White Pine Counties Groundwater Development Plan (figure 1.4). The BARCAS geologic framework analysis included development of a hydrostratigraphic and structural framework for the region, and classified the boundaries between hydrographic areas by the probability that they accommodate interbasin flow, based on hydrostratigraphy and structural geology.

The BARCAS study estimated recharge and discharge for the constituent hydrographic areas in east-central Nevada and west-central Utah. Estimates of ET, by far the greatest contributor to groundwater discharge in the Great Basin, were based on improved imagery and analysis, and on

new basin-floor climatic data. Recharge estimates used the Basin Characterization Model (BCM) (Flint and others, 2004; Flint and Flint, 2007), which calculates in-situ recharge and runoff rates based on geography, climate, and lithology (near-surface permeability) (section 4.4.4).
Lundmark and others (2007) analyzed subsurface interbasin flow rates in the BARCAS study area. Groundwater budgets in basins having greater recharge than discharge estimates were balanced by assuming subsurface outflow, whereas the groundwater budgets in basins having greater discharge than recharge estimates were balanced by assuming subsurface inflow. Lundmark and others (2007) determined that northern and southern Spring Valley, southern Steptoe Valley, and Lake Valley are sources of interbasin flow to adjacent hydrographic areas. The large discrepancy between recharge and discharge in southern Steptoe Valley lead to estimated subsurface flow rates in southern Steptoe, Lake, Spring, and Snake Valleys that were much higher than previous estimates.

1.4.5.3 SNWA Conceptual and Numerical Groundwater Flow Models

As part of the Environmental Impact Statement process, SNWA conducted comprehensive reviews and data compilation of the hydrology and hydrogeology of the hydrographic areas in and adjacent to their proposed Clark, Lincoln, and White Pine Counties Groundwater Development Plan (Dixon and others, 2007; SNWA, 2008). Their work included evaluation of the regional geology and its influence on groundwater flow and inventories of wells, springs, streams, water use, and water rights in the project area (Dixon and others, 2007; SNWA, 2008). This material formed the database for conceptual (SNWA, 2009a, 2010a) and numerical (SNWA, 2009b, 2010a, 2010b) models of groundwater flow.

The conceptual model included extensive geologic framework analyses, estimated water-budget components for the hydrographic areas including recharge rates and recharge-efficiency coefficients, discharge by ET, and subsurface inflow and outflow. The transient numerical groundwater-flow model simulated drawdown due to the combined effects of SNWA's proposed groundwater development plan and current pumping rates (SNWA, 2010b, plate 2). The model estimated drawdown under a variety of pumping scenarios.

1.4.5.4 Durbin and Loy Conceptual and Numerical Groundwater Flow Models

The U.S. Department of the Interior funded the development of conceptual (Durbin and Loy, 2010) and numerical (Loy and Durbin, 2010) groundwater-flow models for use in water-rights hearings in Utah regarding the Beaver County and Central Iron County Water Conservancy District applications (table 1.3). At the time of writing, the models are at a provisional stage of development so are not discussed thoroughly in this report. The study area included the northeastern part of the SNWA groundwater-development project area in Nevada, and Tule, Pine, and Wah Wah Valleys, Fish Springs Flat, and the western part of the Sevier Desert hydrographic areas in Utah (figure 1.4). The models included delineation of a hydrogeologic framework; estimation of recharge, discharge, and interbasin flow; calibration to steady-state groundwater levels and ET; and predictive simulation of drawdown due to a variety of future pumping scenarios.

1.4.5.5 Halford and Plume (2011)

Halford and Plume (2011) modified the RASA groundwater flow model to simulate the effects of SNWA's proposed groundwater pumping in Snake Valley on groundwater levels, spring flow, and stream flow in Great Basin National Park, adjacent parts of Snake Valley, and adjacent hydrographic areas in Utah including much of the UGS study area. Halford and Plume (2011) refined the RASA model and recalibrated it to steady state conditions in the vicinity of the Park, and simulated water-level declines and ET capture under several different pumping scenarios.

1.4.5.6 U.S. Geological Survey Great Basin Carbonate and Alluvial Aquifer Study

The U.S. Geological Survey's Great Basin Carbonate and Alluvial Aquifer System (GBCAAS) Study (Heilweil and Brooks, 2011; Brooks and others, in preparation) assesses groundwater resources in the eastern two-thirds of the Great Basin, the area underlain by the regional carbonate-rock aquifer and approximately the same area covered by the RASA carbonate-rock province numerical groundwater-flow model (Prudic and others, 1995) (figures 1.2 and 1.4). The GBCAAS study consists of regional-scale conceptual (Heilweil and Brooks, 2011) and numerical (Brooks and others, in preparation) models that include groundwater budgets for each of the 165 hydrographic areas within their study area and for the 17 major flow systems defined by Harrill and others (1988).

1.4.5.7 U.S. Bureau of Land Management Environmental Impact Statement

The Final Environmental Impact Statement (FEIS) for SNWA's Groundwater Development Project evaluated the potential environmental impacts of (1) constructing the pipeline and related facilities, and (2) the proposed groundwater development on regional groundwater, biological

(vegetation and animal), and other resources (U.S. Bureau of Land Management, 2012a). The FEIS included SNWA's comprehensive hydrogeologic studies described in section 1.4.5.3, and presented additional hydrogeologic information. The FEIS evaluated six alternative groundwater-development scenarios and recommended their Alternative F, which does not allow pipeline construction in Snake Valley and assumes that groundwater development in Delamar, Dry Lake, and Spring Valleys will comprise the amounts permitted by the Nevada State Engineer (Nevada State Engineer, 2012a-d), water rights already held by SNWA and others, and additional pumping by unspecified projects. The U.S. Bureau of Land Management (2012b) approved Alternative F in its Record of Decision, which requires SNWA to conduct an extensive monitoring, management, and mitigation program in conjunction with their groundwater development, to quantify and limit the negative environmental consequences of the pumping. Groundwater wells constructed as part of the project will require additional National Environmental Policy Act (NEPA) analyses.

1.5 ACKNOWLEDGMENTS

Funding for the installation of the Utah Geological Survey's West Desert Groundwater Monitoring network was provided by the Utah Legislature and the UGS, and both entities fund the continued maintenance of the network and data dissemination. The Utah Division of Water Rights also supports the continued maintenance of the surface-flow network and data dissemination.

The authors are grateful to the following individuals for thorough critical reviews of the manuscript: David Prudic of the University of Nevada; Lynnette Brooks, Phil Gardner, and Vic Heilweil of the U.S. Geological Survey's Utah Water Science Center; Keith Halford of the U.S. Geological Survey's Nevada Water Science Center; Andrew Burns of the Southern Nevada Water Authority; Pete Rowley and Gary Dixon, private consultants; and Roy Smith of the U.S. Bureau of Land Management.

Matt Affolter was the main well site geologist for the UGS during installation of the groundwater monitoring wells. Successful installation and operation of the real-time surface flow monitoring network would not have been possible without the assistance and expertise of Aaron Hunt, Utah Division of Water Rights.

Many local residents assisted the project. Dean Baker dug a trench for the preliminary aquifer test at site 11, and granted the UGS permission to install monitoring wells and a surface-flow gage on his property. Glen Dearden granted the UGS permission to install gages at the Dearden Springs surface-flow monitoring site, and Craig and Tom Baker helped to install the flumes there. Grant Young permitted the UGS to install flow monitoring equipment on the pipe that feeds his irrigation pivot near the Foote Spring surface-flow monitoring site and provided earth fill and heavy equipment during installation of flumes. Edward Alder and David Eldredge allowed us access to their properties to install surface-flow gages. Buck Douglas operated specialized equipment during installation of the Clay Spring surface-flow gage. We thank the owners and staff of the Border Inn and the Silver Jack Inn for their hospitality and support.

The Utah School and Institutional Trust Lands Administration (SITLA) facilitated our well drilling and surface-flow gage installation activities on property it manages for the State of Utah. Clara Stevens of the U.S. Bureau of Land Management and Jay Banta of the U.S. Fish and Wildlife Service assisted the UGS in preparing special use applications to install groundwater-monitoring wells on Federal property. The Utah Department of Transportation allowed us to store equipment and supplies at their Garrison facility. Jay Banta and Brian Allen granted the UGS permission to use U.S. Fish and Wildlife facilities during well installation and heavy equipment and personnel during surface-flow gage installation. Karl Fleming, U.S. Fish and Wildlife Service, and Krissy Wilson, Utah Division of Wildlife Resources, provided material support and funding for the surface gage installation at Miller Spring. Kevin Wheeler, Chris Crockett, and their colleagues at the Utah Division of Wildlife Resources provided biologist oversight and manual labor during surface-gage installation in sensitive species habitat.

We thank Steve Crawford, director of the U.S. Geological Survey's Western Region Research Drilling Program; Art Clark, director of the U.S. Geological Survey's Central Region Research Drilling Program; Bob Roche, Roche Well Drilling; Mike Anzalone, Anzalone Well Service, and the well drillers and assistants of these programs, for their expertise, advise, efficiency, and good humor and company during the project.

1.6 CHAPTER 1 REFERENCES

Bolke, E.L., and Sumison, C.T., 1978, Hydrologic reconnaissance of the Fish Springs Flat area, Tooele, Juab, and Millard Counties, Utah: Utah Department of Natural Resources Technical Publication No. 64, 21 p.

Brooks, L.E., and others, in preparation, Numerical groundwater-flow model of the Great Basin carbonate

and alluvial aquifer system: U.S. Geological Survey Scientific Investigations Report.

Carlton, S.M., 1985, Fish Springs multibasin flow system, Nevada and Utah: University of Nevada-Reno, M.S. thesis, 103 p.

Dixon, G.L., Rowley, P.D., Burns, A.G., Watrus, J.M., and Ekren, E.B., 2007, Geology of White Pine and Lincoln Counties and adjacent areas, Nevada and Utah—the geologic framework of regional groundwater flow systems: Las Vegas, Southern Nevada Water Authority, HAM-ED-001, variously paginated. Available *in* Southern Nevada Water Authority, 2008, Baseline characterization report for Clark, Lincoln, and White Pine Counties Groundwater Development Project, *in* U.S. Bureau of Land Management, 2012, Clark, Lincoln, and White Pine Counties Groundwater Development Project Final Environmental Impact Statement FES 12-33, Document BLM/NV/NV/ES/11-17+1793.

Durbin, T., and Loy, K., 2010, Development of a groundwater model, Snake Valley region, eastern Nevada and western Utah: U.S. Department of the Interior: Online, http://www.blm.gov/ut/st/en/prog/more/doi_groundwater_modeling.html, accessed July 2, 2010.

Eakin, T.E., 1966, A regional interbasin ground-water system in the White River area, southeastern Nevada: Water Resources Research, v. 2, p. 251–271.

Eakin, T.E., Hughes, J.L., and Moore, D.O., 1967, Water-resources appraisal of Steptoe Valley, White Pine and Elko Counties, Nevada: Nevada Department of Conservation and Natural Resources, Water Resource Reconnaissance Series Report 42, 62 p.

Flint, A.L., Flint, L.E., Hevesi, J.A., and Blainey, J.M., 2004, Fundamental concepts of recharge in the desert southwest—a regional modeling perspective, *in* Hogan, J.F., Phillips, F.M., and Scanlon, B.R., eds., Groundwater recharge in a desert environment—the southwestern United States: American Geophysical Union, Water Science and Application Series, 9, p. 159–184.

Flint, A.L., and Flint, L.E., 2007, Application of the basin characterization model to estimate in-place recharge and runoff potential in the Basin and Range carbonate-rock aquifer system, White Pine County, Nevada, and adjacent areas in Nevada and Utah: U.S. Geological Survey Scientific Investigations Report 2007-5099, 20 p.

Galloway, D., Jones, D.R., and Ingebritsen, S.E., 2004, Land subsidence in the United States: U.S. Geological Survey Circular 1182, 178 p.

Gates, J.S., and Kruer, S.A., 1981, Hydrologic reconnaissance of the southern Great Salt Lake Desert and summary of the hydrology of west-central Utah: Utah Department of Natural Resources Technical Publication 71, 55 p.

Halford, K.J., and Plume, R.W., 2011, Potential effects of groundwater pumping on water levels, phreatophytes, and spring discharges in Spring and Snake Valleys, White Pine County, Nevada, and adjacent areas in Nevada and Utah: U.S. Geological Survey Scientific Investigations Report 2011-5032, 52 p.

Harrill, J.R., Gates, J.S., and Thomas, J.M., 1988, Major ground-water flow systems in the Great Basin region of Nevada, Utah, and adjacent states: U.S. Geological Survey Hydrologic Investigations Atlas HA-694-C, scale 1:1,000,000, 2 sheets.

Harrill, J.R., and Prudic, D.E., 1998, Aquifer systems in the Great Basin region of Nevada, Utah, and adjacent states; summary report: U.S. Geological Survey Professional Paper 1409-A, p. 66.

Heilweil, V.M., and Brooks, L.E., editors, 2011, Conceptual model of the Great Basin carbonate and alluvial aquifer system: U.S. Geological Survey Scientific Investigations Report 2010-5193.

Hood, J.W., and Rush, F.E., 1965, Water-resources appraisal of the Snake Valley area, Utah and Nevada: Utah State Engineer Technical Publication No. 14, p. 43.

Kirby, S., and Hurlow, H.A., 2005, Hydrogeologic setting of the Snake Valley hydrologic basin, Millard County, Utah, and White Pine and Lincoln Counties, Nevada—implications for possible effects of proposed water wells: Utah Geological Survey Report of Investigations 254, 39 p.

Loy, K., and Durbin, T., 2010, Simulation results report eastern Nevada–western Utah regional groundwater flow model: U.S. Department of the Interior: Online, http://www.blm.gov/ut/st/en/prog/more/doi_groundwater_modeling.html, accessed July 2, 2010.

Lund, W.R., DuRoss, C.B., Kirby, S.M., McDonald, G.N., Hunt, G., and Vice, G.S., 2005, The origin and extent of earth fissures in Escalante Valley, southern Escalante Desert, Iron County, Utah: Utah Geological Survey Special Study 115, 28 p.

Lundmark, K.W., Pohll, G.M., and Carroll, R.W.H., 2007, A steady-state water budget accounting model for the carbonate aquifer system in White Pine County, Nevada, and adjacent areas in Nevada and Utah: University of Nevada, Desert Research Institute Publication 41235, 56 p.

McLendon, T., 2011, Potential effects of change in depth to water on vegetation in Spring Valley, Nevada: Southern Nevada Water Authority, variously paginated: Online, http://water.nv.gov/hearings/past/springetal/browseabledocs/Exhibits%5CSNWA%20Exhibits/SNWA_Exh_037_McLendon%20Report.pdf, accessed July 26, 2011.

Meinzer, O.E., 1911, Ground water in Juab, Millard, and Iron Counties Utah: U.S. Geological Survey Water Supply Paper 277, 162 p.

Nevada State Engineer, 2012a, Spring Valley ruling 6164: Online, http://water.nv.gov/hearings/past/springetal/browseabledocs/Final%20Rulings/Spring%20Valley%20Ruling%206164.pdf, accessed 3/26/2012.

Nevada State Engineer, 2012b, Cave Valley ruling 6165: Online, http://water.nv.gov/hearings/past/springetal/browseabledocs/Final%20Rulings/Cave%20Valley%20Ruling%206165.pdf, accessed 3/26/2012.

Nevada State Engineer, 2012c, Dry Lake Valley ruling 6166: Online, http://water.nv.gov/hearings/past/springetal/browseabledocs/Final%20Rulings/Dry%20Lake%20Valley%20Ruling%206166.pdf, accessed March 26, 2012.

Nevada State Engineer, 2012d, Delamar Valley ruling 6167: Online, http://water.nv.gov/hearings/past/springetal/browseabledocs/Final%20Rulings/Delamar%20Valley%20Ruling%206167.pdf, accessed March 26, 2012.

Patten, D.T., Rouse, L., and Stromberg, J.C., 2007, Isolated spring wetlands in the Great Basin and Mojave Deserts, USA—potential response of vegetation to groundwater withdrawal: Environmental Management (doi: 10.1007/s00267-007-9035-9).

Plume, R.W., 1996, Hydrogeologic framework of aquifer systems in the Great Basin region of Nevada, Utah, and adjacent states: U.S. Geological Survey Professional Paper 1409-B, 64 p.

Prudic, D.E., Harrill, J.R., and Burbey, T.J., 1995, Conceptual evaluation of regional ground-water flow in the carbonate-rock province of the Great Basin, Nevada, Utah, and adjacent states: U.S. Geological Survey Professional Paper 1409-D, 102 p.

Rush, F.E., and Kazmi, S.A.T., 1965, Water-resources appraisal of Spring Valley, White Pine and Lincoln Counties, Nevada: Nevada Department of Conservation and Natural Resources Water Resources Reconnaissance Report 33, 39 p.

Schaefer, D.H., and Harrill, J.R., 1995, Simulated effects of proposed ground-water pumping in 17 basins of east-central and southern Nevada: U.S. Geological Survey Water-Resources Investigations Report 95-4173, 71 p.

Southern Nevada Water Authority, 2008, Baseline characterization report for Clark, Lincoln, and White Pine Counties Groundwater Development Project, *in* U.S. Bureau of Land Management, 2012, Clark, Lincoln, and White Pine Counties Groundwater Development Project Final Environmental Impact Statement: FES 12-33, Document BLM/NV/NV/ES/11-17+1793.

Southern Nevada Water Authority, 2009a, Conceptual model of groundwater flow for the central carbonate-rock province—Clark, Lincoln, and White Pine Counties Groundwater Development Project, *in* U.S. Bureau of Land Management, 2012, Clark, Lincoln, and White Pine Counties Groundwater Development Project Final Environmental Impact Statement: FES 12-33, Document BLM/NV/NV/ES/11-17+1793.

Southern Nevada Water Authority, 2009b, Transient numerical model of groundwater flow for the central carbonate-rock province—Clark, Lincoln, and White Pine Counties Groundwater Development Project, *in* U.S. Bureau of Land Management, 2012, Clark, Lincoln, and White Pine Counties Groundwater Development Project Final Environmental Impact Statement: FES 12-33, Document BLM/NV/NV/ES/11-17+1793.

Southern Nevada Water Authority, 2010a, Addendum to the groundwater flow model for the central carbonate-rock province—Clark, Lincoln, and White Pine Counties Groundwater Development Project, *in* U.S. Bureau of Land Management, 2012, Clark, Lincoln, and White Pine Counties Groundwater Development Project Final Environmental Impact Statement: FES 12-33, Document BLM/NV/NV/ES/11-17+1793.

Southern Nevada Water Authority, 2010b, Simulation of groundwater development scenarios using the transient numerical model of groundwater flow for the central carbonate-rock province—Clark, Lincoln, and White Pine Counties Groundwater Development Project, *in* U.S. Bureau of Land Management, 2012, Clark, Lincoln, and White Pine Counties Groundwater Development Project Final Environmental Impact Statement: FES 12-33, Document BLM/NV/NV/ES/11-17+1793.

Southern Nevada Water Authority, 2012, Southern Nevada Water Authority Clark, Lincoln, and White Pine Counties Groundwater Development Project Conceptual Plan of Development November 2012: Online, http://www.snwa.com/assets/pdf/ws_gdp_copd.pdf, accessed March 19, 2014.

Stephens, J.C., 1974, Hydrologic reconnaissance of

the Wah Wah Valley drainage basin, Millard and Beaver Counties, Utah: Utah Department of Natural Resources Technical Publication No. 47, 45 p.

Stephens, J.C., 1976, Hydrologic reconnaissance of the Pine Valley drainage basin, Millard, Beaver, and Iron Counties, Utah: Utah Department of Natural Resources Technical Publication No. 51, 31 p.

Stephens, J.C., 1977, Hydrologic reconnaissance of the Tule Valley drainage basin, Juab and Millard Counties, Utah: Utah Department of Natural Resources Technical Publication No. 56, 29 p.

Thomas, J.M., Welch, A.H., and Dettinger, M.D., 1997, Geochemistry and isotope hydrology of representative aquifers in the Great Basin region of Nevada, Utah, and adjacent states: U.S. Geological Survey Professional Paper 1409-C, 100 p.

U.S. Bureau of Land Management, 2012a, Clark, Lincoln, and White Pine Counties Groundwater Development Project Final Environmental Impact Statement: FES 12-33, Document BLM/NV/NV/ES/11-17+1793.

U.S. Bureau of Land Management, 2012b, Clark, Lincoln, and White Pine Counties Groundwater Development Project Record of Decision: Document BLM/NV/NV/ES/11-17+1793.

U.S. Fish and Wildlife Service, 2010, Endangered and threatened wildlife and plants-12-month finding on a petition to list the least chub as threatened or endangered: Federal Register, v. 75, no. 119, p. 35, 398–35, 424.

U.S. Geological Survey, 2011, Basin and Range carbonate aquifer Website: Online, http://nevada.usgs.gov/barcass/index.htm, accessed numerous times during 2004 through 2011.

Utah Division of Wildlife Resources, 2011, Utah sensitive species list: Online, http://dwrcdc.nr.utah.gov/ucdc/ViewReports/SSLAppendices20110329.pdf, 150 p., accessed January 4, 2012.

Welch, A.H., Bright, D.J., and Knochenmus, L.A., 2007, Water resources of the Basin and Range carbonate-rock aquifer system, White Pine County, Nevada, and adjacent areas in Nevada and Utah: U.S. Geological Survey Scientific Investigations Report 2007-5261, 96 p.

CHAPTER 2 | GEOLOGIC FRAMEWORK

by Hugh Hurlow

View north of monitor-well drilling at UGS site PW17, north-central Tule Valley. Outcrop in foreground is Silurian Laketown Dolomite of the lower Paleozoic carbonate-rock aquifer hydrogeologic unit.

Bibliographic citation for this chapter:
Hurlow, H., 2014, Geologic framework, Chapter 2 *in* Hurlow, H., editor, Hydrogeologic studies and groundwater monitoring in Snake Valley and adjacent hydrographic areas, west-central Utah and east-central Nevada: Utah Geological Survey Bulletin 135, p. 19–28.

CHAPTER 2 CONTENTS

FIGURES

CHAPTER 2: GEOLOGIC FRAMEWORK

by Hugh Hurlow

2.1 PHYSIOGRAPHIC AND GEOLOGIC SETTING

The UGS study area is in the eastern Basin and Range Province of the western intermontane United States (figure 2.1). The Basin and Range Province is characterized by generally north-south trending mountain ranges that are 10 to 50 miles (16–80 km) long and 2 to 10 miles (3–33 km) wide, separated by valleys of similar dimensions. Most mountain fronts (transition between ranges and valleys; Wilson and Guan, 2004) are relatively abrupt and are mantled by alluvial fans that emanate from canyons in the ranges. In the UGS study area, valley-floor elevations range from about 4250 to 6550 feet (1300–2000 m), and the highest parts of the ranges are about 8,000 to 13,000 feet (2440–3960 m) above sea level.

Figures 2.2 and 2.3 and plate 1 show the geologic units and major structures in the study area. The predominant topographic grain results from displacement on north-south striking, Quaternary to Miocene normal-fault zones, where the ranges are in the uplifted footwalls, the valleys are the sedimentary basins on the down-dropped hanging walls, and the major normal-fault zones are along the mountain fronts (Stewart, 1998). Roughly east-west trending ranges or range-spurs and bedrock highs buried below the valley floors reflect either transverse faults (Faulds and Varga, 1998) or volcanic edifices that predated the Basin and Range normal faulting (Best and Christiansen, 1991).

Mountain ranges in the northern two-thirds of the study area are predominantly composed of Paleozoic carbonate rocks that are complexly to slightly faulted and folded (figures 2.2 and 2.3; plate 1). Parts of the Schell Creek and Snake Ranges and the southern Deep Creek Range are composed of Neoproterozoic to Early Cambrian quartzite and schist. In the Snake Range and Deep Creek Range, these rocks are intruded by Tertiary and Mesozoic granitic rocks, and rocks near the intrusions are metamorphosed to greenschist to (locally) amphibolite grade. Ranges in the southwestern part of the study area are composed of Oligocene volcanic and volcaniclastic rocks of the Indian Peak Caldera Complex.

2.2 STRATIGRAPHIC AND STRUCTURAL EVOLUTION

The following summary of the geologic history of the UGS study area provides a basic outline of how the rocks and sediments that form the aquifers and confining units attained their present composition and geometry. Chapter 4 presents more details about the composition, texture, hydraulic properties, and hydrogeologic significance of the geologic units in the study area.

During Neoproterozoic to Early Cambrian time, up to 10,000 feet (3000 m) of siliciclastic deposits (sand, silt, and mud) accumulated in shallow-marine and nonmarine depositional environments on a subsiding continental margin during and after continental rifting (Armstrong, 1968b; Stewart, 1972; Hintze and Kowallis, 2009). From Late Cambrian to Late Devonian time, marine-carbonate reef and platform depositional environments dominated and up to 20,000 feet (6100 m) of predominantly carbonate deposits accumulated as the western North American continental margin continued to subside. These conditions changed in Late Devonian through Late Mississippian time, when up to 3000 feet (900 m) of marine silt and clay, and minor interbedded sand and carbonate deposits, accumulated in a marine sedimentary basin east of the Antler orogenic belt, which formed by thrust faulting and folding about 125 to 200 miles (200–320 km) west of the UGS study area (Dickinson, 2006, and references therein). Slowly subsiding marine-shelf conditions returned to the study area from Late Mississippian to Late Triassic time, when about 9000 feet (2700 m) of sand and carbonate deposits accumulated. Only scant Mesozoic sedimentary rocks are preserved in the study area due to later tectonic events, but rocks in adjacent regions record deposition of siliciclastic deposits in shallow marine, fluvial, and eolian environments.

The tectonic and depositional setting of the study area changed dramatically in Late Jurassic to Early Cretaceous time, when the Sevier fold and thrust belt began to form (Armstrong, 1968a; Allmendinger, 1992; DeCelles, 2004; DeCelles and Coogan, 2006). In east-central Nevada and west-central Utah, thrust faults and related folds transported most of the Neoproterozoic and Paleozoic stratigraphic section over 125 miles (200 km) to the east. The major Sevier structures are exposed about 150 miles (240 km) east of the study area. Rocks that now comprise the

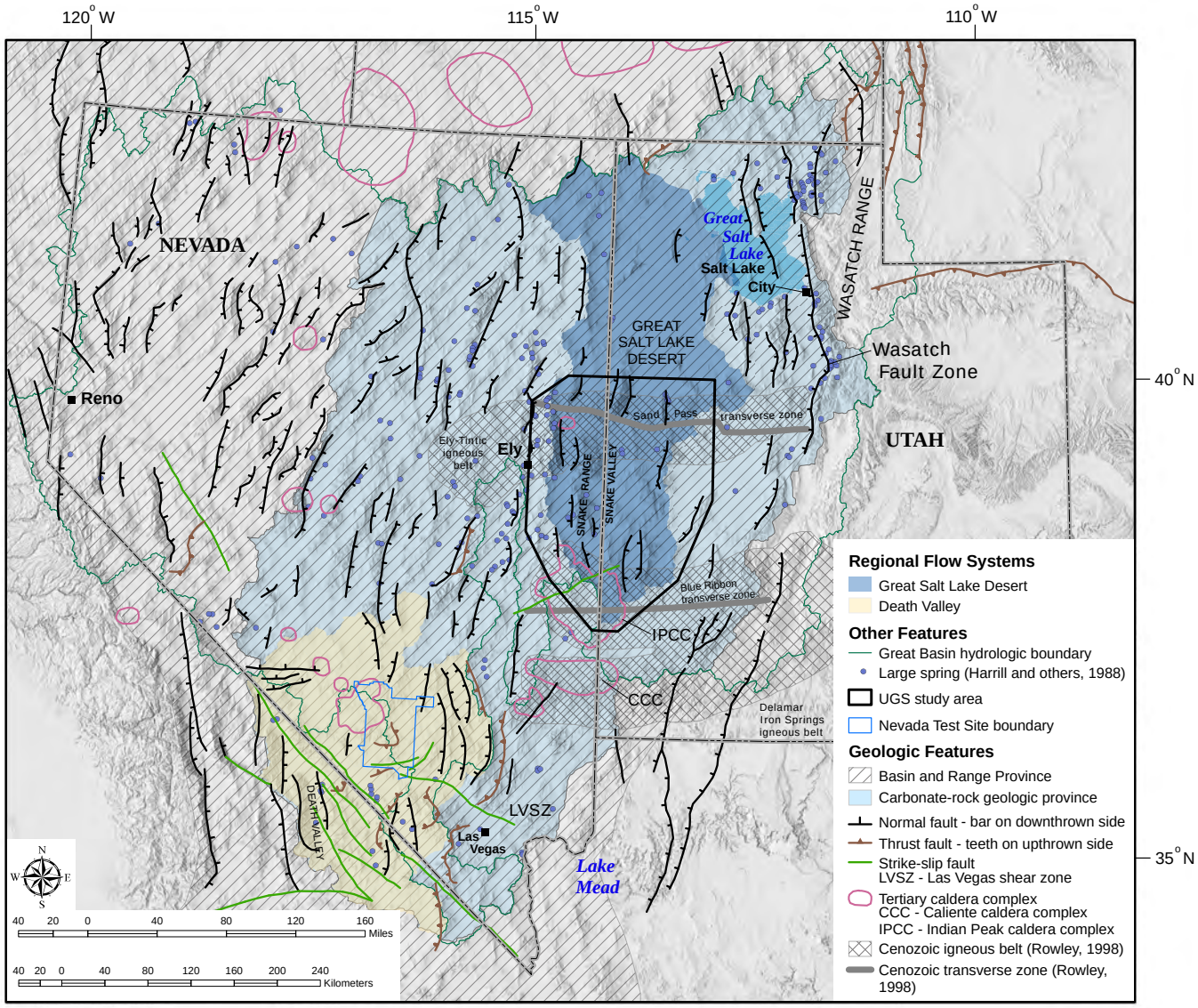

Figure 2.1. *Regional tectonic setting of Utah, Nevada, and parts of adjacent states.*

mountain ranges in the UGS study area moved eastward above Sevier thrust faults and were uplifted, causing erosion of most Triassic and Jurassic rocks (Long, 2012). Sevier thrust belt structures exposed in the UGS study area include the Mountain Home thrust fault and related folds and thrust faults in the northern Mountain Home Range (Hintze and Best, 1987), the Confusion Range syncline and thrust faults (Hose, 1977; Hintze and Davis, 2002a), the Wah Wah and Blue Mountain thrust faults in the southern Wah Wah Mountains (Morris, 1983; Steven and others, 1990), and the Frisco thrust in the San Francisco Mountains (Morris, 1983; Steven and others, 1990; Hintze and Kowallis, 2009) (figure 2.3). Displacement in the Sand Pass-Kern Mountains transverse zone (figures 2.1 and 2.3) may also have occurred during this time (Rowley, 1998). Minor thrust faults, steeply dipping reverse and transcurrent faults, and folds are exposed in most of the ranges. Many of these faults lack firm age control because they cut only Paleozoic rocks, and may have experienced displacement during the Sevier thrust belt formation and/or Tertiary extensional faulting. Plutons intruded the Snake Range and House Range near the beginning (Middle to Late Jurassic), and the Kern Mountains and the Snake Range near the end (Late Cretaceous), of Sevier deformation.

Beginning in late Eocene or early Oligocene time, the dominant tectonic regime in the UGS study area changed to volcanism and crustal extension. Eocene and Oligocene volcanic deposits formed in the Thomas Range and Drum Mountains in the northeastern part of the study area (Hintze and Kowallis, 2009), and are preserved east of Sacramento Pass in west-central Snake Valley (Miller and Grier, 1995), below northern Spring Valley, and in mountain ranges in the northeastern part of the study area (plate 1). All of these deposits are part of the regional-scale Ely-Tintic igneous belt, localized along the east-west trending Sand

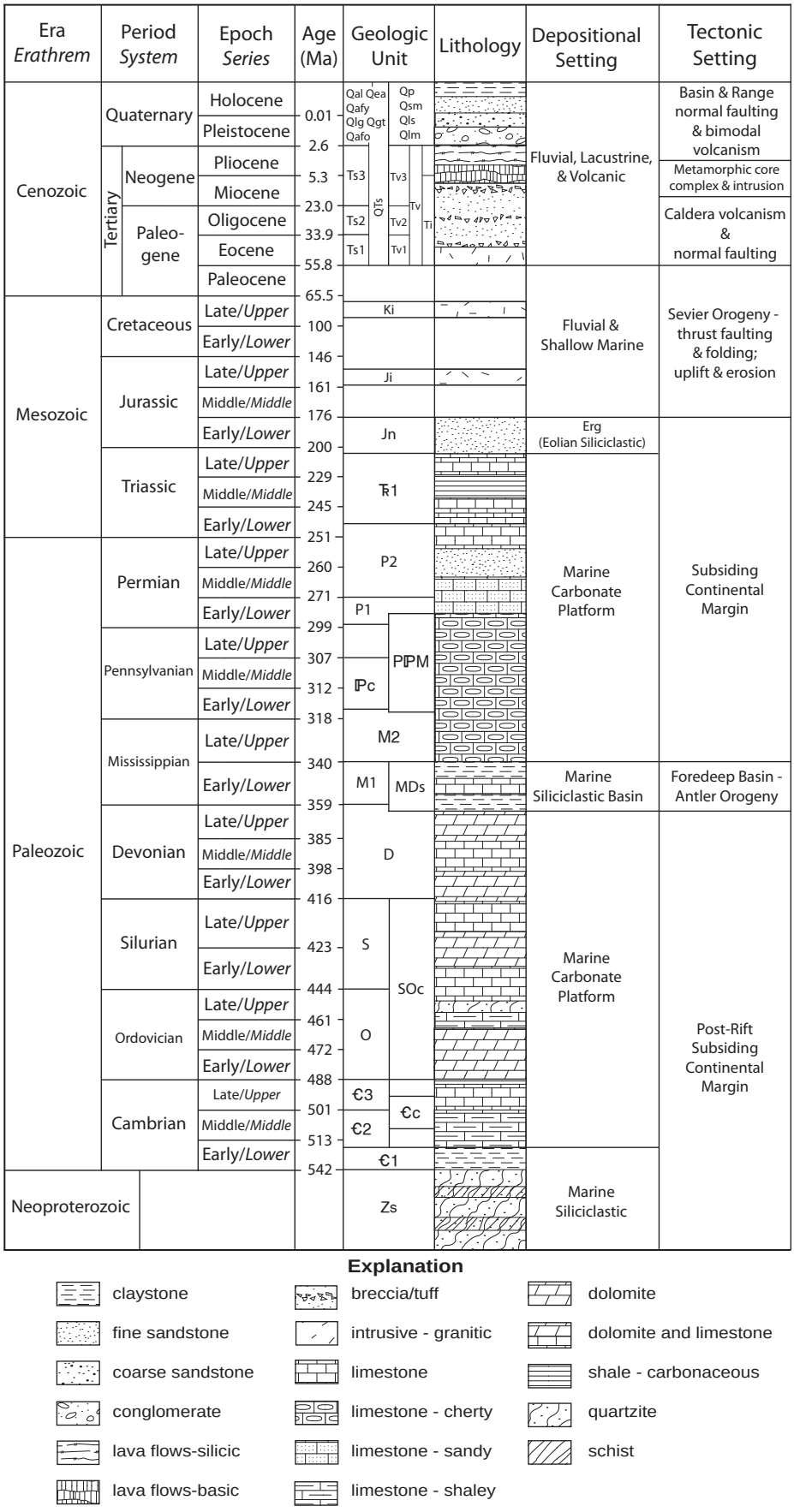

Figure 2.2. *Generalized stratigraphy, depositional settings, and tectonic history of geologic units in the UGS study area.*

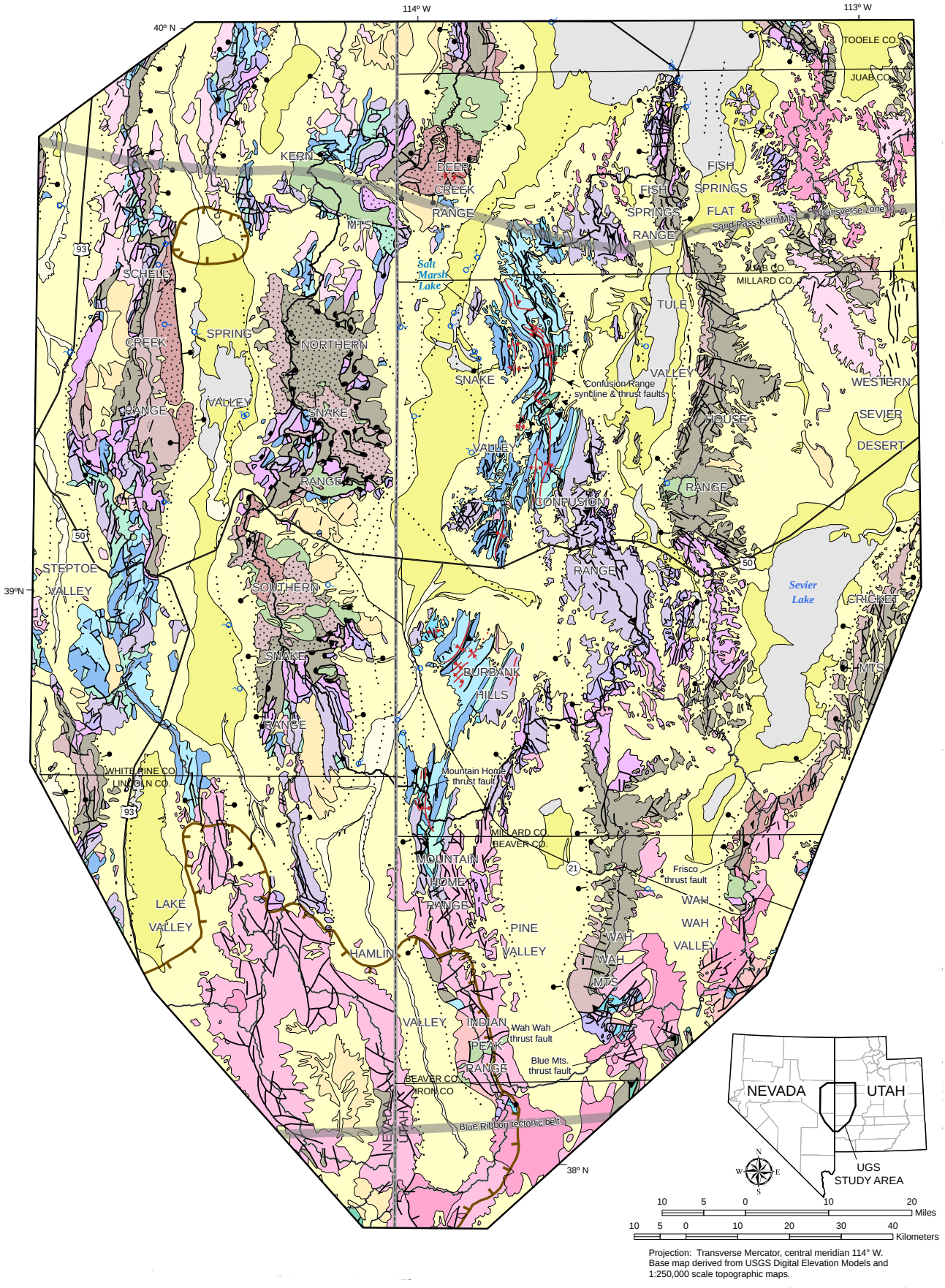

Figure 2.3. *Simplified geologic map of the study area.*

Figure 2.3. *continued*

Pass transverse zone (a steeply dipping fault zone having a complex displacement history) (figure 2.1) (Rowley, 1998). Localized crustal extension along steeply dipping normal faults occurred in parts of the study area (Best and Christiansen, 1991).

In the southern part of the study area, the Indian Peak caldera complex formed during Oligocene to early Miocene time (Best and others, 1989). The resultant volcanic rocks include welded tuff, flows, breccia, and volcaniclastic deposits, are over 12,000 feet (3700 m) thick in places, and compose most exposures in the Indian Peak Range and White Rock Mountains. These volcanic and related volcaniclastic deposits form most of the basin fill in southern Hamlin and Pine Valleys. Their compositions include dacite, andesite, and rhyolite, similar to volcanic rocks that form near convergent tectonic-plate margins. The Indian Peak caldera complex is part of the regional-scale Delamar-Iron Springs igneous belt, localized along the east-west trending Blue Ribbon transverse zone (figure 2.1) (Rowley, 1998).

Basin-and-Range faulting in the UGS study area began in early Miocene time (about 20 Ma; Rowley and others, 2009, p. 256), when steeply dipping (>45°) normal-fault zones formed a regional pattern of north-south trending mountain ranges and adjacent depositional basins, defining the modern basin-range topography (Stewart, 1998). Transverse accommodation zones having complex displacement and faulting patterns truncate many of the major range-bounding normal-fault zones (Faulds and Varga, 1998). The Sand Pass transverse zone (Rowley, 1998) formed an accommodation zone between the range-bounding normal-fault zones along the eastern margins of the northern Snake Range and Deep Creek Range, and between the normal-fault zones bounding the northern House Range and southern Fish Springs Range.

Miocene to Quaternary basin fill in the hanging walls of the Basin-and-Range normal-fault zones includes interbedded alluvial, lacustrine, volcaniclastic, and volcanic deposits that overlie Eocene to Oligocene volcanic and volcaniclastic deposits in the deeper structural basins (Plume, 1996; Dixon and others, 2007; Welch and others, 2007, p. 28; Rowley and others, 2009; Halford and Plume, 2011). Basins have approximately symmetric geometry where they are bounded on either side by planar range-bounding fault zones, or are asymmetric where they thicken toward listric range-bounding fault zones (see further discussion in section 3.3.3). Mid- to late-Miocene-age, "bimodal" (basalt and rhyolite) composition volcanism continued in and around the Indian Peak caldera complex, depositing up to 4000 feet (1200 m) of tuff and flow rock. Lower volume bimodal volcanism occurred in the northern Confusion Range, and a substantial eruptive center formed in the Thomas Range in the northeastern part of the study area.

The Snake Range decollement is a gently east-dipping fault zone along the eastern slopes of the Snake Range, is predominantly Miocene, and had a complex structural evolution (Bartley and Wernicke, 1984; Gans and others, 1985; Miller and others, 1999; Rowley and others, 2009). Detailed discussion of the various hypotheses for the structural evolution of the Snake Range decollement is beyond the scope of this report, but unresolved issues that have hydrogeologic implications include the poorly-known eastward projection of the decollement into the Snake Valley, and amount of displacement on the steeply dipping Basin and Range normal-fault zones along the eastern mountain front of the Snake Range. These faults likely influence groundwater flow below the Snake Range mountain front and western Snake Valley (Rowley and others, 2009) (section 4.3.2).

Discontinuous fault scarps along parts of the northern Snake Range, House Range, and Fish Springs Range fronts cut Quaternary alluvial-fan deposits, indicating that extensional faulting is active locally in the study area. During Pleistocene to early Holocene time, Lake Bonneville occupied most of the valley floors in the study area except southern Snake Valley, Hamlin Valley, and Pine Valley. Lacustrine deposits include shoreline to shallow-water sand and gravel bars on the range slopes and lake-bottom clay and silt in the valley centers (plate 1). Predominantly fine-grained lacustrine deposits are at least 100 feet (30 m) thick at three UGS monitoring-well sites on the Snake Valley floor.

2.3 CHAPTER 2 REFERENCES

Allmendinger, R.W., 1992, Fold and thrust tectonics of the western United States exclusive of the accreted terranes, *in* Burchfiel, B.C., Lipman, P.W., and Zoback, M.L., editors, The Cordilleran orogen—Coterminous U.S.: Boulder, Colorado, Geological Society of America, The Geology of North America, v. G-3, p. 583–607.

Armstrong, R.L., 1968a, Sevier orogenic belt in Nevada and Utah: Geological Society of America Bulletin, v. 79, p. 429–458.

Armstrong, R.L., 1968b, The Cordilleran miogeosyncline in Nevada and Utah: Utah Geological and Mineralogical Survey Bulletin 78, 58 p.

Bartley, J.M., and Wernicke, B.P., 1984, The Snake Range decollement interpreted as a major extensional shear

zone: Tectonics, v. 8, p. 647–657.

Best, M.G., and Christiansen, E.H., 1991, Limited extension during peak Tertiary volcanism, Great Basin of Nevada and Utah: Journal of Geophysical Research, v. 96, p. 13509–13528.

Best, M.G., Christiansen, E.H., and Blank, R.H., Jr., 1989, Oligocene caldera complex and calc-alkaline tuffs and lavas of the Indian Peak volcanic field, Nevada and Utah: Geological Society of America Bulletin, v. 101, p. 1076–1090.

Burchfiel, B.C., Cowan, D.S., and Davis, G.A., 1992, Tectonic overview of the Cordilleran orogen in the western United States, *in* Burchfiel, B.C., Lipman, P.W., and Zoback, M.L., editors, The Cordilleran orogen—Coterminous U.S.: Boulder, Colorado, Geological Society of America, The Geology of North America, v. G-3, p. 407–479.

DeCelles, P.G., 2004, Late Jurassic to Eocene evolution of the Cordilleran thrust belt and foreland basin system, western U.S.A.: American Journal of Science, v. 304, p. 105–168.

DeCelles, P.G., and Coogan, J.C., 2006, Regional structure and kinematic history of the Sevier fold-and-thrust belt, central Utah: Geological Society of America Bulletin, v. 118, p. 841–864.

Dickinson, W.R., 2006, Geotectonic evolution of the Great Basin: Geosphere, v. 2, p. 353–368.

Dixon, G.L., Rowley, P.D., Burns, A.G., Watrus, J.M., and Ekren, E.B., 2007, Geology of White Pine and Lincoln Counties and adjacent areas, Nevada and Utah—the geologic framework of regional groundwater flow systems: Las Vegas, Southern Nevada Water Authority, HAM-ED-001, variously paginated. Available *in* Southern Nevada Water Authority, 2008, Baseline characterization report for Clark, Lincoln, and White Pine Counties Groundwater Development Project, *in* U.S. Bureau of Land Management, 2012, Clark, Lincoln, and White Pine Counties Groundwater Development Project Final Environmental Impact Statement FES 12-33, Document BLM/NV/NV/ES/11-17+1793.

Faulds, J.E., and Varga, R.J., 1998, The role of accommodation and transfer zones in the regional segmentation of extended terranes, *in* Faulds, J.E., and Stewart, J.H., editors, Accommodation zones and transfer zones—the regional segmentation of the Basin and Range Province: Boulder, Colorado, Geological Society of America Special Paper 323, p. 1–45.

Gans, P.B., Miller, E.L., McCarthy, J., and Ouldcott, M.L., 1985, Tertiary extensional faulting and evolving ductile-brittle transition zones in the northern Snake Range and vicinity—new insights from seismic data: Geology, v. 13, p. 189–193.

Greene, D.C., and Herring, D.M., 2013, Structural architecture of the Confusion Range, west-central Utah—a Sevier fold thrust belt and frontier petroleum province: Utah Geological Survey Open-File Report 613, 22 p., 6 plates.

Halford, K.J., and Plume, R.W., 2011, Potential effects of groundwater pumping on water levels, phreatophytes, and spring discharges in Spring and Snake Valleys, White Pine County, Nevada, and adjacent areas in Nevada and Utah: U.S. Geological Survey Scientific Investigations Report 2011-5032, 52 p.

Heilweil, V.M., and Brooks, L.E., editors, 2011, Conceptual model of the Great Basin carbonate and alluvial aquifer system: U.S. Geological Survey Scientific Investigations Report 2010-5193, 192 p., 2 plates.

Hintze, L.F., and Best, M.G., 1987, Geologic map of the Mountain Home Pass and Miller Wash quadrangles, Miller and Beaver Counties, Utah, and Lincoln County, Nevada: U.S. Geological Survey Miscellaneous Field Studies Map MF-1950, scale 1:24,000.

Hintze, L.F., and Davis, F.D., 2002a, Geologic map of the Tule Valley 30′ x 60′ quadrangle and parts of the Ely, Fish Springs, and Kern Mountains 30′ x 60′ quadrangles, northwest Millard County, Utah: Utah Geologic Survey Map 186, scale 1:100,000.

Hintze, L.F., and Davis, F.D., 2002b, Geologic map of the Wah Wah Mountains North 30′ x 60′ quadrangle and part of the Garrison 30′ x 60′ quadrangle, southwest Millard County and part of Beaver County, Utah: Utah Geological Survey Map 182, scale 1:100,000.

Hintze, L.H., and Kowallis, B.J., 2009, Geologic history of Utah: Provo, Utah, Brigham Young University Geology Studies, Special Publication 9, 225 p.

Hintze, L.F., Willis, G.C., Laes, D.Y.M., Sprinkel, D.A., and Brown, K.D., 2000, Digital geologic map of Utah: Utah Geological Survey Map 179DM (CD), 1:500,000).

Hose, R.K., 1977, Structural geology of the Confusion Range, west-central Utah: U.S. Geological Survey Professional Paper 971, 9 p., 1 plate, scale 1:125,000.

Long, S.P., 2012, Magnitudes and spatial patterns of erosional exhumation in the Sevier hinterland, eastern Nevada and western Utah, U.S.A.—insights from a Paleogene paleogeographic map: Geosphere, v. 8, p. 881–901 (doi: 10.1130/GES00783.1).

Ludington, S., Moring, B.C., Miller, R.J., Flynn, K.,

Hopkins, M.J., Stone, P., Bedford, D.R., and Haxel, G.A., 2005, Preliminary integrated geologic map databases for the United States—western states: California, Nevada, Arizona, and Washington: U.S. Geological Survey Open-File Report 2005-1305.

Miller, E.L., Dumitru, T.A., Brown, R.W., and Gans, P.B., 1999, Rapid Miocene slip on the Snake Range–Deep Creek Range fault system, east-central Nevada: Geological Society of America Bulletin, v. 111, p. 886–905.

Miller, E.L., and Grier, S.P., 1995, Geologic map of Lehman Caves 7.5′ quadrangle, White Pine County, Nevada: U.S. Geological Survey Map GQ-1758, scale 1:24,000.

Morris, H.T., 1983, Interrelations of thrust and transcurrent faults in the central Sevier orogenic belt near Leamington, Utah, *in* Miller, D.M., Todd, V.R., and Howard, K.A., editors, Tectonic and stratigraphic studies in the eastern Great Basin: Geological Society of America Memoir 157, p. 75–81.

Plume, R.W., 1996, Hydrogeologic framework of aquifer systems in the Great Basin region of Nevada, Utah, and adjacent states: U.S. Geological Survey Professional Paper 1409-B, 64 p.

Rowley, P.D., 1998, Cenozoic transverse zones and igneous belts in the Great Basin, western United States—their tectonic and economic implications, *in* Faulds, J.E., and Stewart, J.H., editors, Accommodation zones and transfer zones—the regional segmentation of the Basin and Range Province: Boulder, Colorado, Geological Society of America Special Paper 323, p. 195–228.

Rowley, P.D., Dixon, G.L., Burns, A.G., and Collins, C.A., 2009, Geology and hydrogeology of the Snake Valley area, western Utah and eastern Nevada, *in* Tripp, B.T., Krahulec, K., and Jordan, J.L., editors, Geology and geologic resources and issues of western Utah: Utah Geological Association Publication 38, p. 251–269.

Steven, T.A., Morris, H.T., and Rowley, P.D., 1990, Geologic map of the Richfield 1° x 2° quadrangle, west-central Utah: U.S. Geological Survey Miscellaneous Investigation Series Map I-1901, scale 1:250,000.

Stewart, J.H., 1972, Initial deposits in the Cordilleran geosyncline—evidence of a Late Precambrian (<850 m.y.) continental separation: Geological Society of America Bulletin, v. 83, p. 1345–1360.

Stewart, J.H., 1980, Geology of Nevada: Nevada Bureau of Mines and Geology Special Publication 4, 136 p.

Stewart, J.H., 1998, Regional characteristics, tilt domains, and extensional history of the late Cenozoic Basin and Range Province, western North America, *in* Faulds, J.E., and Stewart, J.H., editors, Accommodation zones and transfer zones—the regional segmentation of the Basin and Range Province: Boulder, Colorado, Geological Society of America Special Paper 323, p. 47–74.

U.S. Geological Survey, 2008, Quaternary fault and fold database for the United States: Online, http://earthquake.usgs.gov/hazards/qfaults/, accessed September 9, 2011.

Welch, A.H., Bright, D.J., and Knochenmus, L.A., 2007, Water resources of the Basin and Range carbonate-rock aquifer system, White Pine County, Nevada, and adjacent areas in Nevada and Utah: U.S. Geological Survey Scientific Investigations Report 2007-5261, 96 p.

Wilson, J.L., and Guan, H., 2004, Mountain-block hydrology and mountain-front recharge, *in* Phillips, F.M., Hogan, J., and Scanlon, B., editors, Groundwater recharge in a desert environment—the Southwestern United States: Washington, D.C., American Geophysical Union, p. 113–137.

CHAPTER 3 | GRAVITY STUDY

by Hugh Hurlow

View east of Salt Marsh Lake playa and Salt Marsh Range, central Snake Valley.

Bibliographic citation for this chapter:
Hurlow, H., 2014, Gravity study, Chapter 3 *in* Hurlow, H., editor, Hydrogeologic studies and groundwater monitoring in Snake Valley and adjacent hydrographic areas, west-central Utah and east-central Nevada: Utah Geological Survey Bulletin 135, p. 29–55.

CHAPTER 3 CONTENTS

FIGURES

TABLES

CHAPTER 3: GRAVITY STUDY

by Hugh Hurlow

3.1 INTRODUCTION

Valleys in the Basin and Range Province overlie Tertiary to Quaternary normal-fault-bounded, syntectonic sedimentary basins. Geophysical and drilling data show that most of these basins (1) are up to 10,000 feet (3000 m) deep, and a few are locally over 16,000 feet (5000 m) deep (Saltus and Jachens, 1995), and (2) are structurally complex below their relatively smooth topographic surfaces (Anderson and others, 1983; Saltus and Jachens, 1995; Schlishce and Anders, 1996; Faulds and Varga, 1998; Mankinen and others, 2006; Watt and Ponce, 2007). The structurally complex basins consist of two or more sub-basins separated by buried or topographically subdued intrabasin ridges that strike at a high angle to the basin margins. The intrabasin ridges are typically composed of highly fractured bedrock. This structural complexity results in variable basin-fill thickness patterns and buried or exposed intrabasin bedrock highs and ridges, as illustrated by isopach (depth to bedrock or geophysical basement) maps (Saltus and Jachens, 1995; Mankinen and others, 2006; Watt and Ponce, 2007; Mankinen and McKee, 2009).

Analysis of gravity data can delineate the structure of sedimentary basins where exploration-grade seismic-reflection data are sparse or unavailable. Thickness variations in unconsolidated to weakly consolidated basin-fill sediment (including both clastic and volcanic deposits), by virtue of their density contrast with consolidated bedrock, produce spatial variations in the vertical component of the gravitational field measured on the land surface. The measured gravity field can be numerically modeled to estimate the thickness and geometry of the basin fill. Use of independent constraints on basin-fill thickness such as well logs substantially improves the ability of geophysical models to produce geologically reasonable estimates of structure and basin-fill thickness.

Mankinen and others (2006), Watt and Ponce (2007), and Mankinen and McKee (2009) presented interpretations of gravity and magnetic data in the BARCAS study area, including Snake Valley. Isopach maps in these publications show that the sedimentary basin below Snake Valley and northern Hamlin Valley is composed of four roughly north-south trending sub-basins, with depositional centers in northern Hamlin Valley adjacent to the Limestone Hills; south-central Snake Valley near Baker, Nevada; central Snake Valley south of Gandy, Utah; and northern Snake Valley south of Callao, Utah. Where the valley is widest, the maximum thickness of the sub-basins ranges from approximately 9000 to 15,000 feet (2700–4600 m). Where the valley narrows, the sub-basins are separated by roughly east-west trending intrabasin structural highs concealed by younger Quaternary sediment. The eastern part of the Indian Peak caldera complex, a roughly circular, 45-mile (72 km) diameter structure filled with 1500 to 12,000 feet (500–3700 m) of volcanic and shallow intrusive rocks, underlies southern Hamlin Valley (Watt and Ponce, 2007). Based on aeromagnetic data, Watt and Ponce (2007, figure 6) interpreted that plutons underlie the basin fill in south-central Snake Valley from Sacramento Pass to Ferguson Desert and adjacent parts of the Snake and Confusion Ranges, and in northern Snake Valley from the Kern Mountains to Callao.

3.2 METHODS

Previously existing gravity data were obtained from the Pan American Center for Earth and Environmental Sciences (PACES) (2007) and the U.S. Geological Survey (figure 3.1; table DF1 in Gravity Data folder accompanying this report). To provide greater resolution for the Snake Valley depositional basin, I collected and processed 445 new data points during 2006 (figure 3.1; appendix A) using a Lacoste-Romberg G-series meter borrowed from the University of Utah Department of Geology and Geophysics. Repeat measurements indicated that readings were accurate to within 0.02 milligal (mGal). Instrument drift was assumed linear and was quantified by occupying a drift base four to five times per day, including the first and last measurements of each day. Absolute gravity base 2360-1 in Baker, Nevada (appendix A) was occupied at the beginning and end of every day of data collection to provide a reference value for data reduction. The coordinates and elevation of each gravity station were measured using a Trimble 5800 series GPS system in real-time kinetic mode (stationary base and mobile "rover" antennae). Typical uncertainties were <3 cm (1.18 in) for horizontal coordinates and 3 to 6 cm (1.18–2.36 in) for elevation.

New data collection emphasized closely spaced (0.5 mile [0.8 km]) stations along linear traverses that crossed the entire valley width, including stations on bedrock where accessible (figure 3.1). In addition, most of the proposed

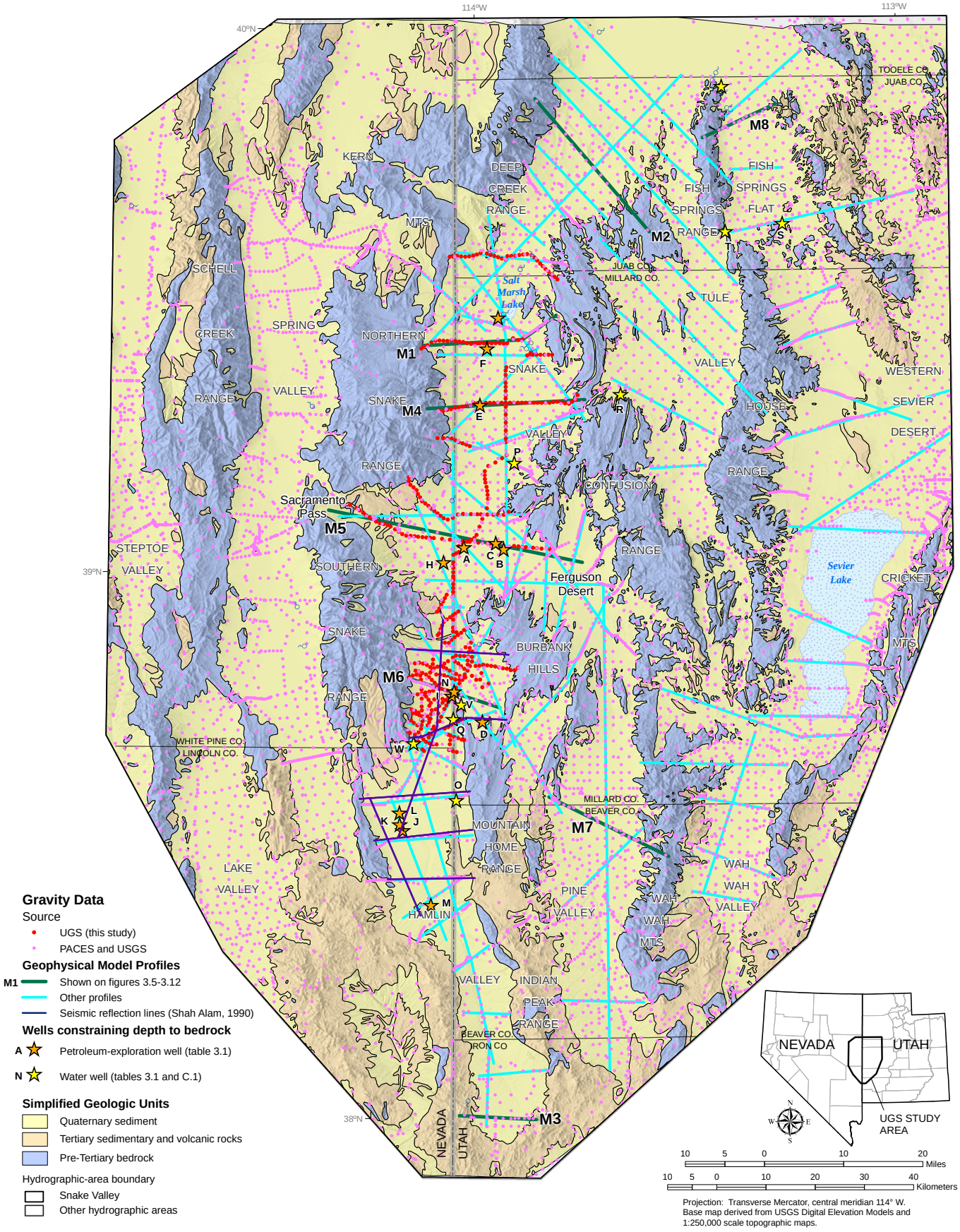

Figure 3.1. *Gravity data stations used in this study, including new UGS stations and previously existing stations. M1 through M8—geophysical model profiles.*

SNWA groundwater development area along the eastern flank of the southern Snake Range was covered with 0.5-mile (0.8 km) station spacing. The close station spacing limited the scope of new data collection to central and southern Snake Valley, but enabled construction of two-dimensional numerical models to estimate the basin-fill geometry.

Raw data were corrected for the effects of earth tide, instrument drift, latitude, elevation (free-air and Bouguer corrections), and local and regional topographic variations (terrain correction) using standard equations and constants (appendix A; Blakely, 1995; Geosoft, Inc., 2010). The resulting value for each station is the Corrected Bouguer Anomaly (CBA), which varies with the density and thickness of subsurface sediment and rock. The primary goal of the gravity-data analysis was to combine the UGS, PACES, and USGS data to allow detailed modeling along selected traverses to delineate the structure of the sedimentary basins that underlie the valleys in the study area. To improve consistency between the UGS and PACES data sets, terrain corrections for the PACES stations were recalculated using the software used to process the UGS data. The consistency of the two data sets can be evaluated by comparing results from 21 coincident stations. The CBA values of UGS stations are 0.46 ± 0.20 mGal greater than coincident stations in the PACES data set. The difference is primarily due to different elevation estimates of the stations: the average elevation difference is 0.67 ± 1.06 m (2.2 ± 3.48 ft), and the average difference in free-air anomaly is 0.43 ± 0.28 mGal. The UGS and U.S. Geological Survey data are consistent at coincident stations.

The CBA values for the combined UGS, PACES, and U.S. Geological Survey data were further reduced to isostatic residual anomaly (IRA) values (figure 3.2) (Jachens and Roberts, 1981) to remove the gravity field due to variations in the density and thickness of Earth's crust below about 20,000 feet (6000 m) depth. The IRA values of coincident UGS and PACES data are consistent to within 0.02 ± 0.10 mGal, justifying combining all data for subsequent analyses. Spatial variations in the IRA principally reflect variations in basin-fill thickness, but may also include variations in bedrock density from the standard assumed value of 2.67 g/cm^3. In the study area, such variations would result from the presence of plutonic rocks (less dense than 2.67 g/cm^3), or mafic intrusive or Precambrian rocks (denser than 2.67 g/cm^3) in the upper crust (Watt and Ponce, 2007). The east-west and north-south horizontal gradients of the IRA grid were calculated to aid in locating major basin-bounding normal faults and other structures (figure 3.3; section 3.3.3).

Aeromagnetic data for the UGS study area were compiled from PACES and gridded at 50 m (164 ft) node spacing using a minimum curvature algorithm (figure 3.4). The grid was sampled at the locations of the gravity stations, and used in conjunction with the gravity data in selected numerical models of basin-fill structure.

Basin-fill geometry was numerically modeled from the IRA values along 87 linear traverses in the study area (locations shown on figure 3.1), using the code GM-SYS (Geosoft, Inc., 2010). Models in central and southern Snake Valley are based predominantly on UGS data, whereas models in the rest of the study area include PACES and U.S. Geological Survey data only. Most models trend perpendicular to the valley floors, span the entire valley width, and include stations on bedrock at either end. Models parallel to the valley-floor axes were constructed to ensure consistency among the valley-perpendicular models, and the modeled depth to bedrock was constrained to be equal at model intersection points. Wells that penetrate the basin fill-bedrock contact are sparse in the study area (figure 3.1), but were used to constrain model traverses where possible. Aeromagnetic data were also roughly modeled in selected traverses as explained in section 3.3.

The models use the depth-density function derived by Saltus and Jachens (1995) for Quaternary-Tertiary sedimentary and volcanic basin-fill deposits in the Basin and Range Province (appendix A) and an average bedrock density of 2.67 g/cm^3. The depth-density function accounts for increased density with increasing depth due to compaction and cementation. Basin-fill thickness and geometry have substantially greater uncertainty for depths greater than about 3900 feet (1200 m) (Saltus and Jachens, 1985). The thickness of the basin-fill geophysical model layers are determined from well logs where such data are available, or are set to standard depths below land surface where well data are absent.

3.3 RESULTS

3.3.1 Isostatic Residual Anomaly Map

Low IRA values beneath the valley floors reflect thick accumulations of unconsolidated to semiconsolidated basin-fill deposits in the normal-fault-bounded sedimentary basins that formed during Tertiary to Quaternary time (Watt and Ponce, 2007). The lowest IRA values occur in Steptoe, Spring, Lake, Snake, and Pine Valleys. Low IRA values also occur in Wah Wah and Tule Valleys, western Sevier Desert, and Fish Springs Flat. Where low IRA values coincide with high aeromagnetic anomaly values, the basin

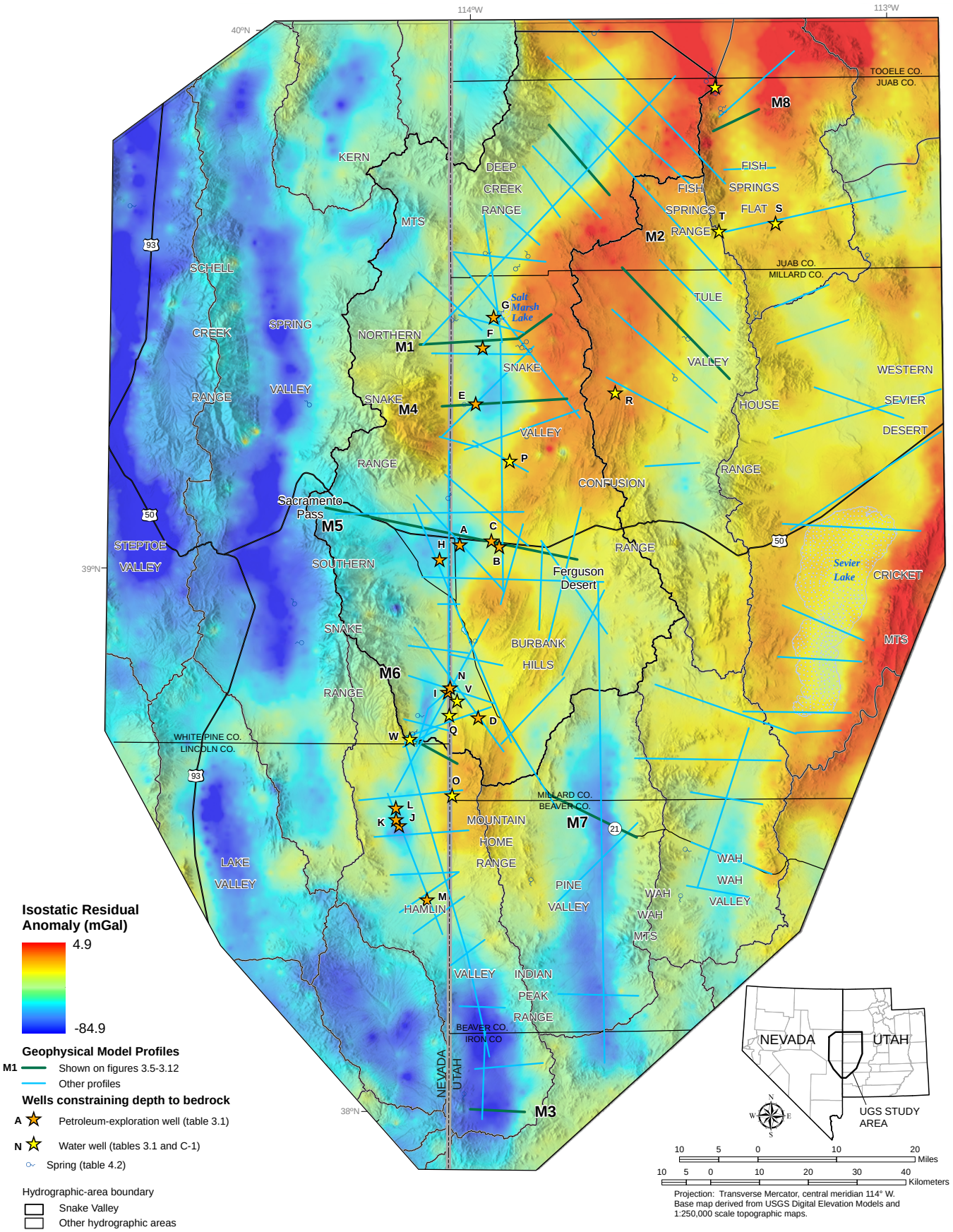

Figure 3.2. *Isostatic residual gravity anomaly field for the UGS study area.*

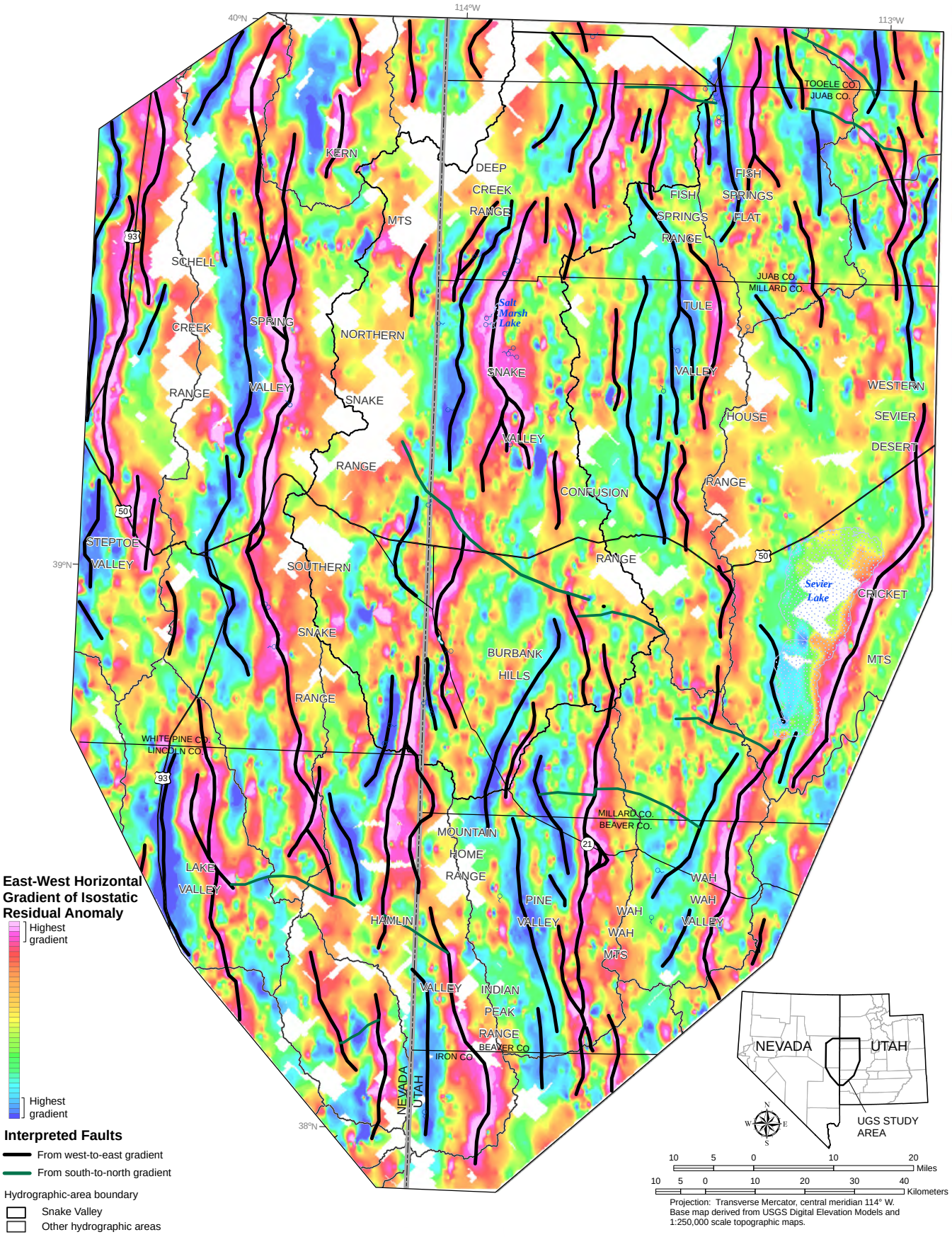

Figure 3.3a. *Horizontal gradients of the isostatic residual gravity anomaly field and interpreted faults. West-to-east gradient.*

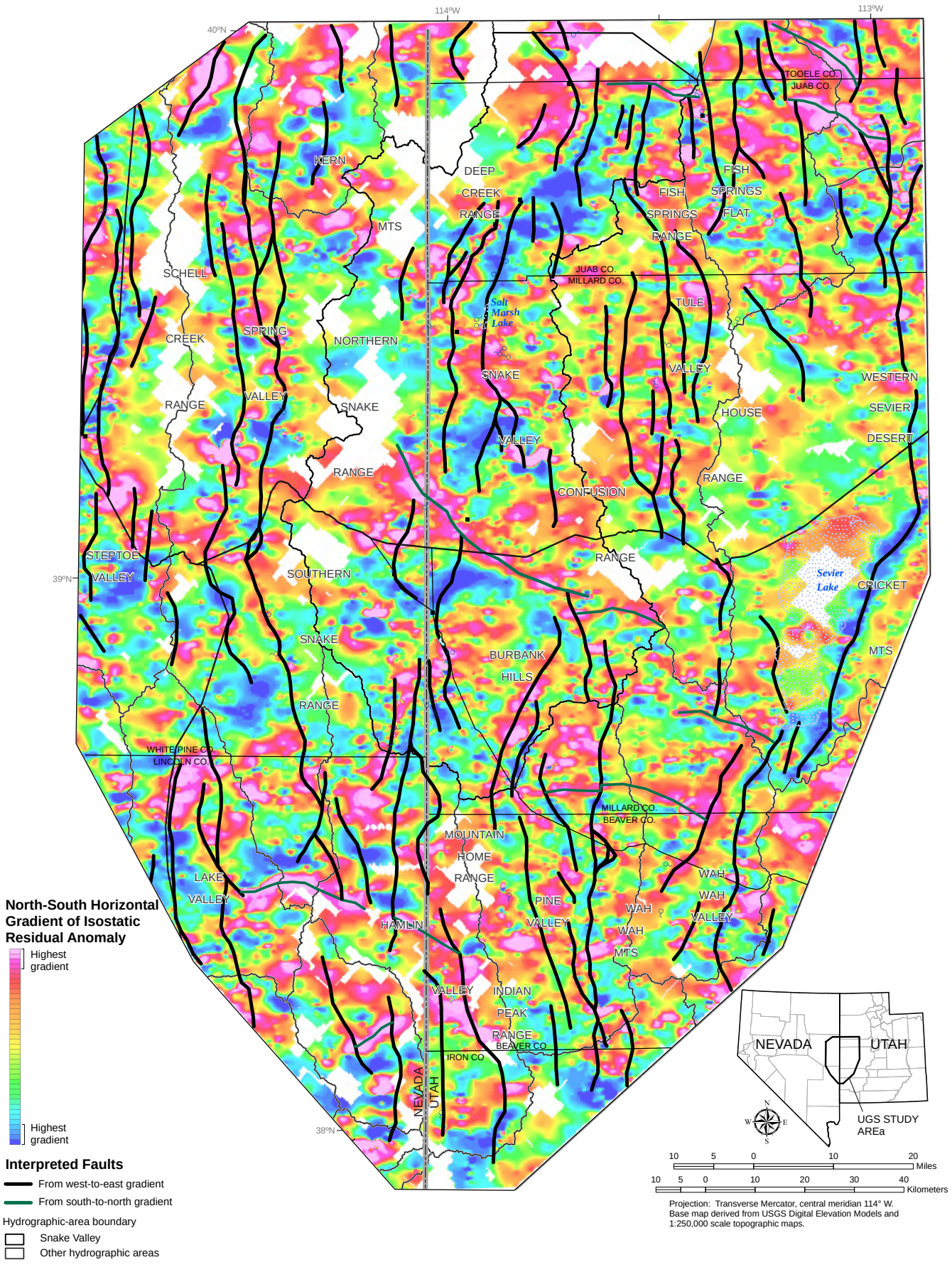

Figure 3.3b. *Horizontal gradients of the isostatic residual gravity anomaly field and interpreted faults. South-to-north gradient.*

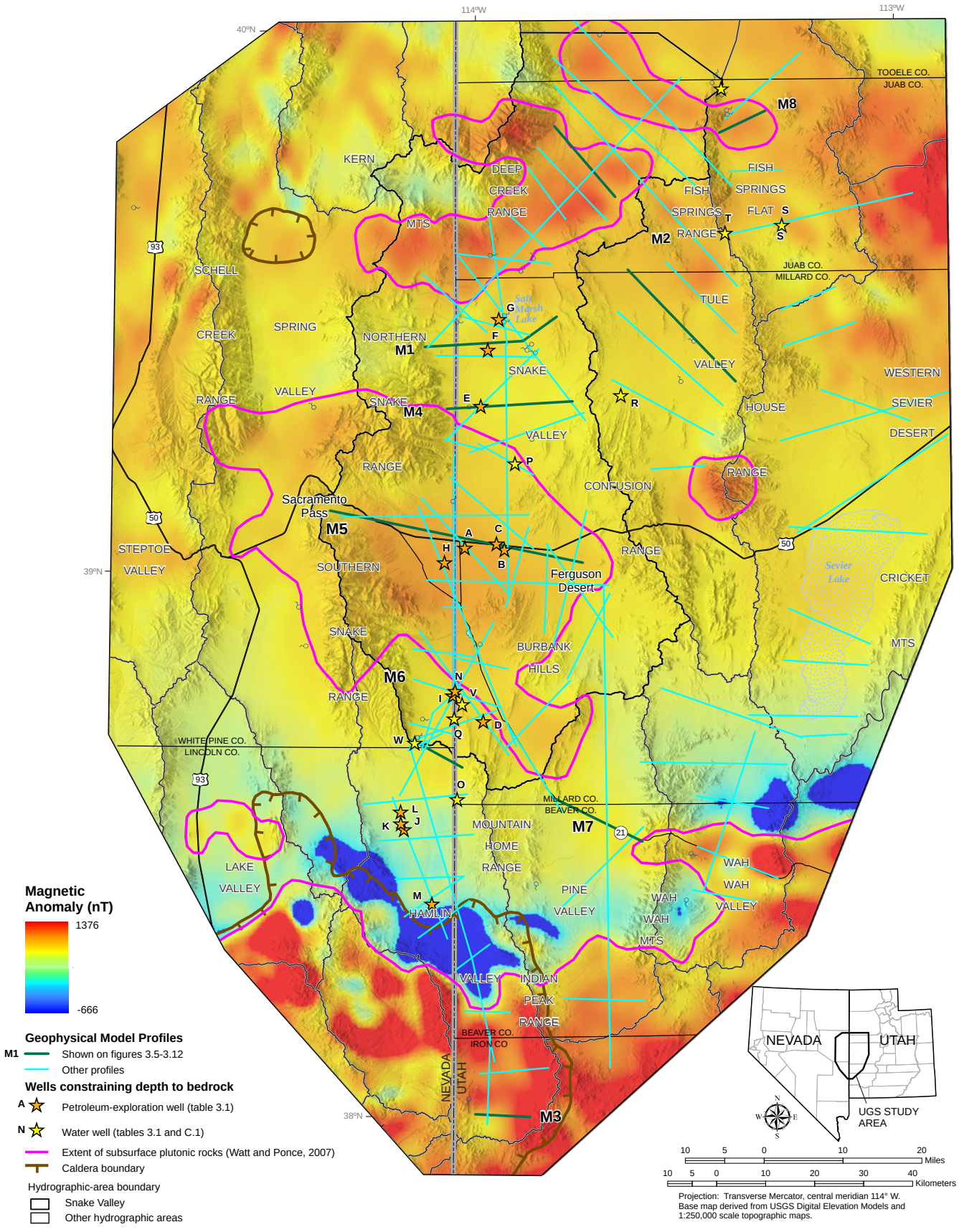

Figure 3.4. *Aeromagnetic anomaly field for the study area. Data are from PACES <http://research.utep.edu/Default.aspx?alias=research.utep.edu/paces>. Locations of subsurface plutonic rocks are after Watt and Ponce (2007, figure 4).*

fill likely contains significant amounts of volcanic detritus and/or the sedimentary basin is underlain by plutonic rocks having high magnetic susceptibility (Watt and Ponce, 2007). These conditions are evident below northern Snake Valley, central Snake Valley, southern Hamlin Valley, and parts of Tule Valley, western Sevier Desert, Spring Valley, and Steptoe Valley (Watt and Ponce, 2007). The roughly circular pattern of low IRA values and high aeromagnetic anomaly values in southern Hamlin Valley and ranges and valleys to the west is caused by thick accumulations of volcanic and shallow intrusive rocks of the Indian Peak caldera complex (Watt and Ponce, 2007).

The highest IRA values occur along a north-northeast trending band from the northern Mountain Home Range to the northern Fish Springs Range in the central part of the study area, below the southern House Range and Cricket Mountains in the southeastern part of the study area, and below the Thomas Range in the northeastern corner of the study area (figure 3.2). The high IRA values likely result from a variety of geologic conditions, depending on location (section 3.4).

The aeromagnetic data were modeled in only a general way on selected geophysical profiles, due to the absence of susceptibility data. To match the aeromagnetic profiles in the better-constrained models, the upper basin-fill model geophysical layer was assigned a susceptibility value of 0 (dimensionless), the middle layer was assigned variable susceptibility of 0 to 0.0015, and the deepest layer was assigned a uniform susceptibility of 0.0015. These deeper basin-fill deposits are likely Tertiary in age and contain a larger proportion of volcanic detritus, and so may have higher magnetic susceptibility, than the younger sediments. Parts of the adjacent bedrock (geophysical basement) were also assigned a susceptibility value of 0.0015 as needed to fit the aeromagnetic data.

Major basin-bounding normal-fault zones can be identified from the IRA gradient field (figure 3.3), because they produce sharply defined, linear bands of high horizontal IRA gradient along the range-valley margins that result from the juxtaposition of basin fill and bedrock along the fault plane (Mankinen and McKee, 2009). Figure 3.3a shows the horizontal IRA gradient calculated from west to east, in which steep gradients from high to low IRA values, shown in blue shades, represent the steeply dipping (i.e., fault-bounded) western boundaries of depositional basins, and steep gradients from low to high IRA values, shown in pink shades, represent the steeply dipping (i.e., fault-bounded) eastern boundaries of depositional basins. Most major range-bounding faults in the study area strike north-south, so produce the greatest density contrast in the east-west direction. The south-to-north horizontal gradient field reveals several east-west and northeast-striking density contrasts interpreted as faults (figure 3.3b). Northwest- to west-striking faults are interpreted to bound the northern part of the central Snake Valley, northern Pine Valley, and northern Wah Wah Valley depositional basins, and form the northern boundary of the Indian Peak caldera complex.

3.3.2 Two-Dimensional Geophysical Model Profiles

The primary goal of the geophysical modeling was to delineate basin-fill geometry. Figures 3.5 through 3.12 show example model profiles selected from the 87 models that were generated to produce the isopach map. Magnetic susceptibility data are not available for rocks in the study area, so the aeromagnetic data were only roughly modeled in selected traverses, using typical cited magnetic susceptibility values (Geosoft, Inc., 2010) to aid in structural interpretations. The following paragraphs describe some general features and problems with the models, and section 3.3.3 presents structural interpretations.

Models that include wells for which depth to bedrock is known and that have stations on bedrock at both ends are considered to be the most reliable. During the cross-correlation process, these models were used to constrain the intersecting models. The more reliable models, however, were not without problems. Several models in northern Snake Valley cannot simultaneously match the gravity anomaly at both ends and accommodate the well data. For example, geophysical model profile M1 (figure 3.5) matches the constraints of having bedrock stations (zero-thickness basin fill) at is western end and the depth to bedrock from a petroleum-exploration well in western Snake Valley (F, table 3.1), but does not fit the gravity data in its eastern part. As noted in section 3.2, IRA values in the northern Confusion Range are unusually high, suggesting that this area is underlain by rocks denser than 2.67 g/cm^3, but no subsurface information exists about the nature of these rocks. Rather than modeling this area with arbitrary, non-unique bedrock geometry and density, the model is left unmatched to the gravity data and the cross section on figure 3.5 depicts a generalized area having density greater than 2.67 g/cm^3. The geometry of the basin fill in the eastern part of this and the other models that extend from the northern Snake Range to the northern Confusion Range has greater uncertainty than in their western and central parts.

In some models, the aeromagnetic data are useful in resolving problems with the gravity data. For example, several models in northern Snake Valley that extend from the Deep Creek Range to the northern Confusion Range show a decrease or relatively small increase in IRA value

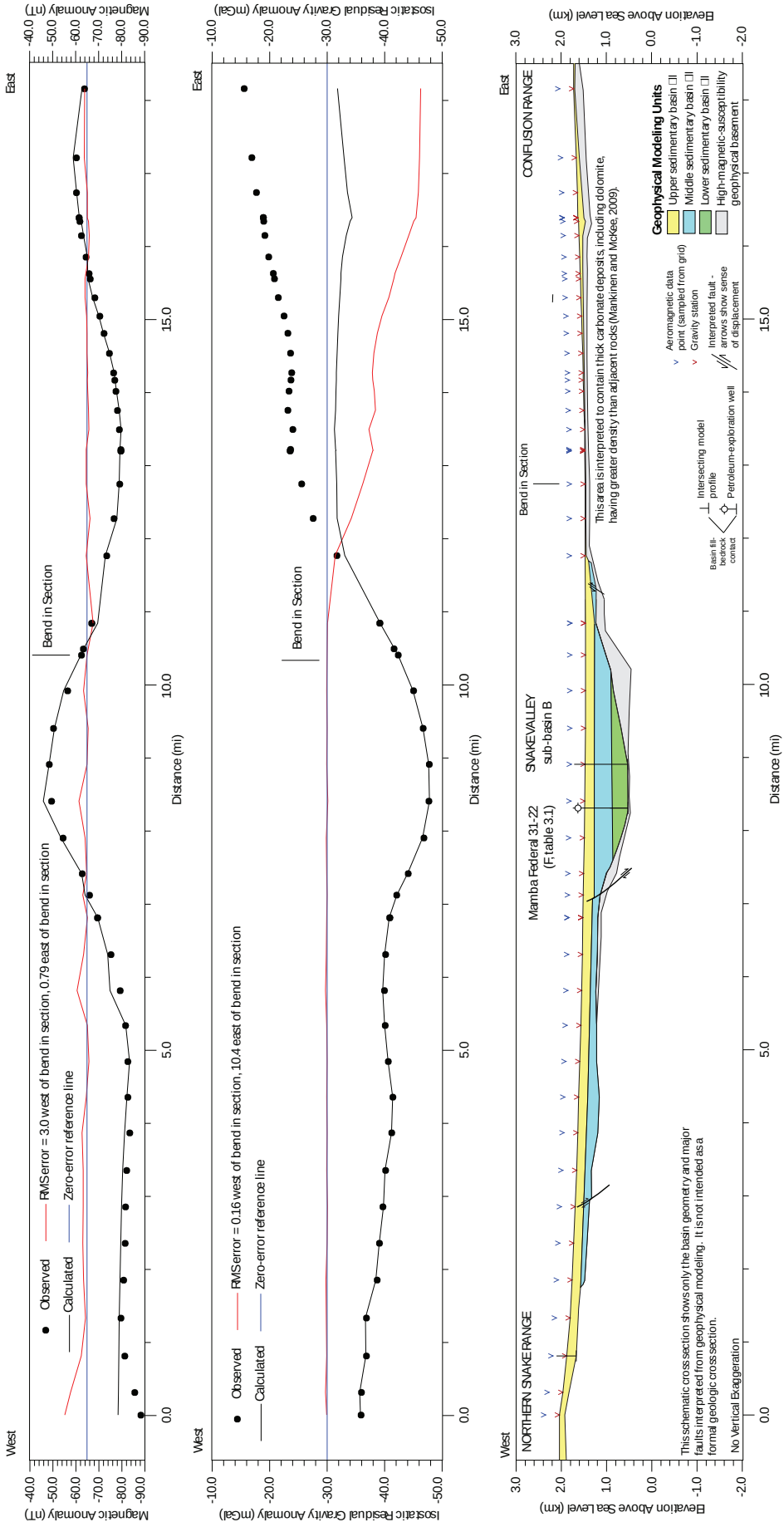

Figure 3.5. *Geophysical model profile M1 from Marble Canyon, northern Snake Range, to the northern Confusion Range. See figure 3.1 for profile location.*

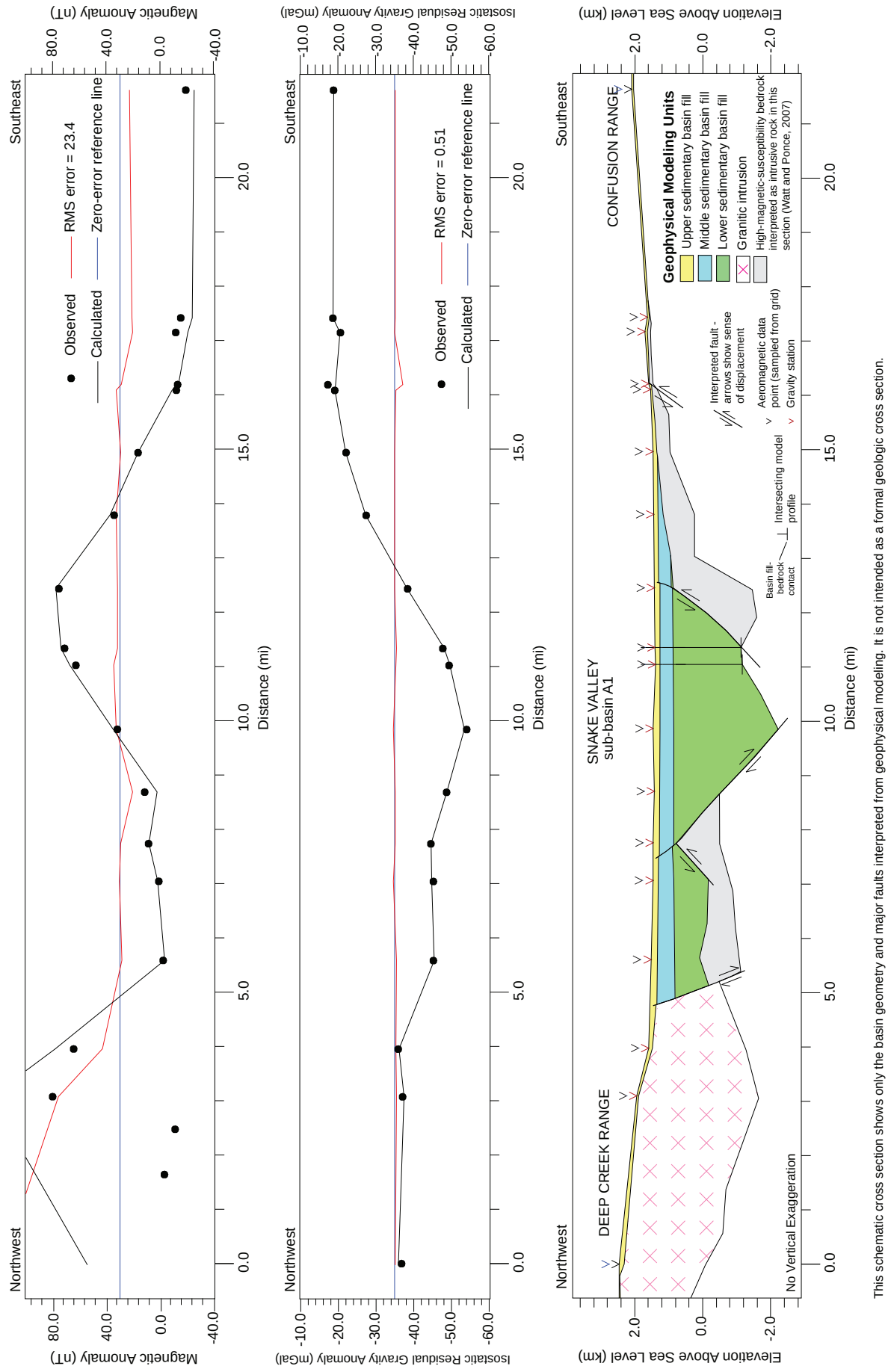

This schematic cross section shows only the basin geometry and major faults interpreted from geophysical modeling. It is not intended as a formal geologic cross section.

Figure 3.6. *Geophysical model profile M2 from the Deep Creek Range to the northern Confusion Range. See figure 3.1 for profile location.*

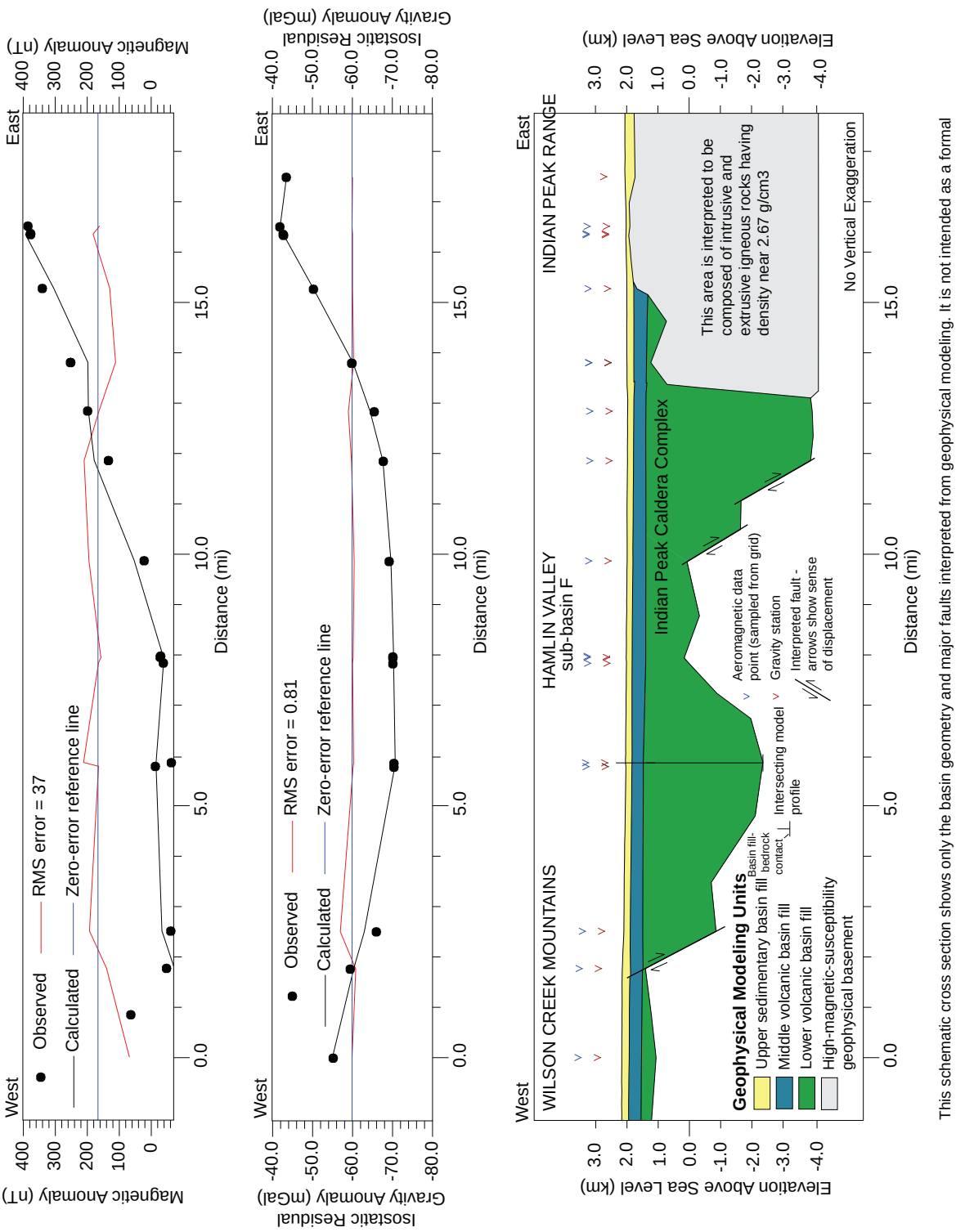

This schematic cross section shows only the basin geometry and major faults interpreted from geophysical modeling. It is not intended as a formal geologic cross section.

Figure 3.7. *Geophysical model profile M3 through southern Hamlin Valley. See figure 3.1 for profile location.*

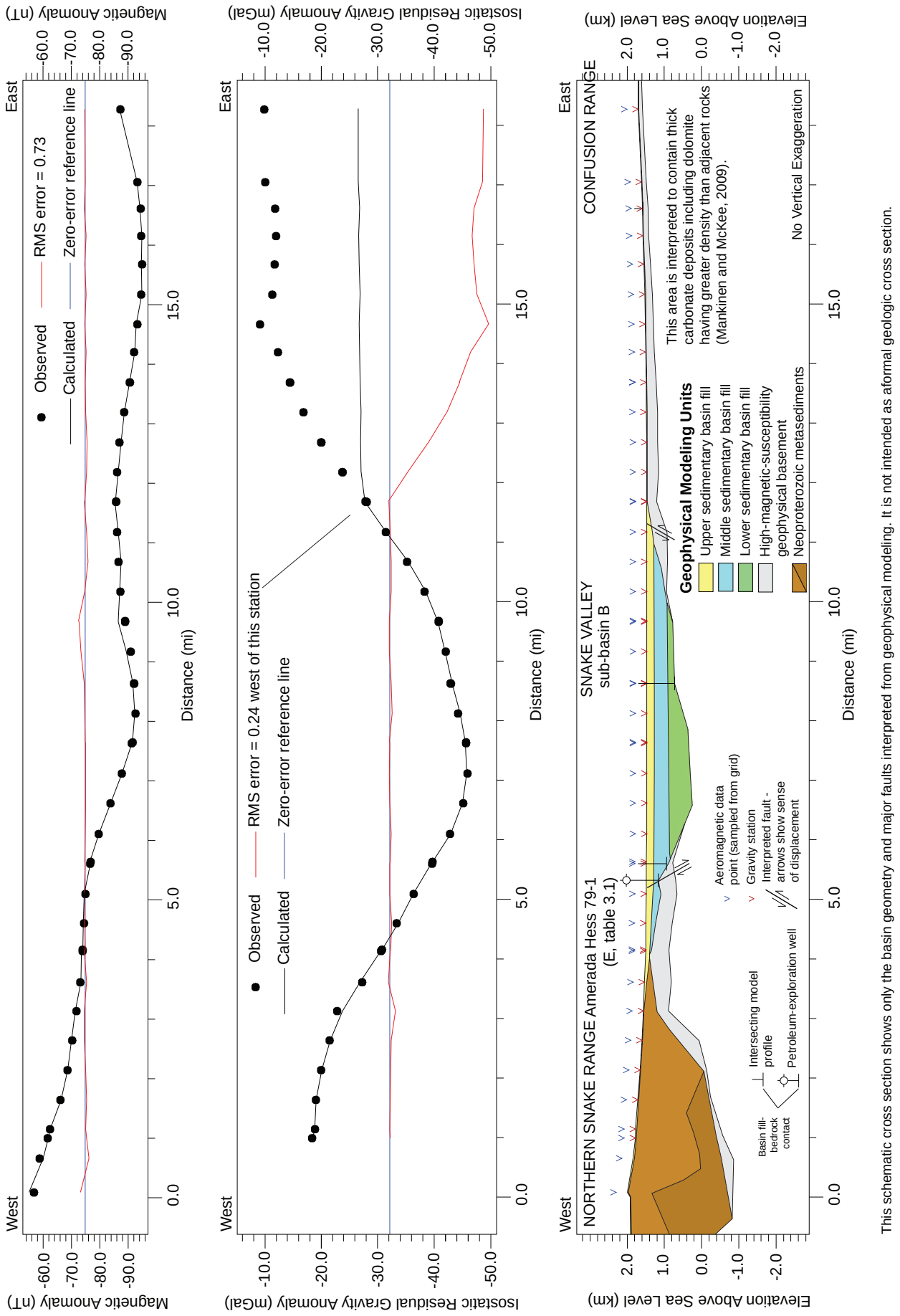

This schematic cross section shows only the basin geometry and major faults interpreted from geophysical modeling. It is not intended as aformal geologic cross section.

Figure 3.8. *Geophysical model profile M4 from the northern Snake Range to the Confusion Range. See figure 3.1 for profile location.*

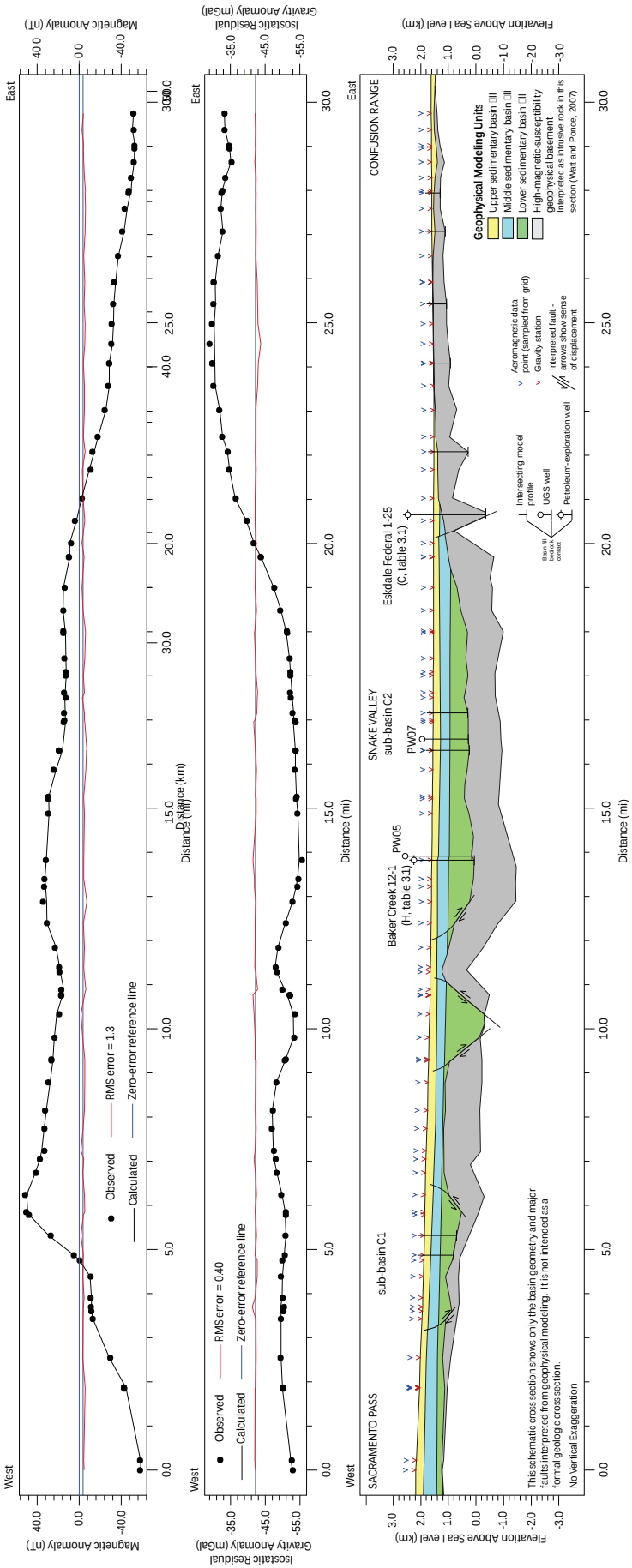

Figure 3.9. *Geophysical model profile M5 from Sacramento Pass to the central Confusion Range. See figure 3.1 for profile location.*

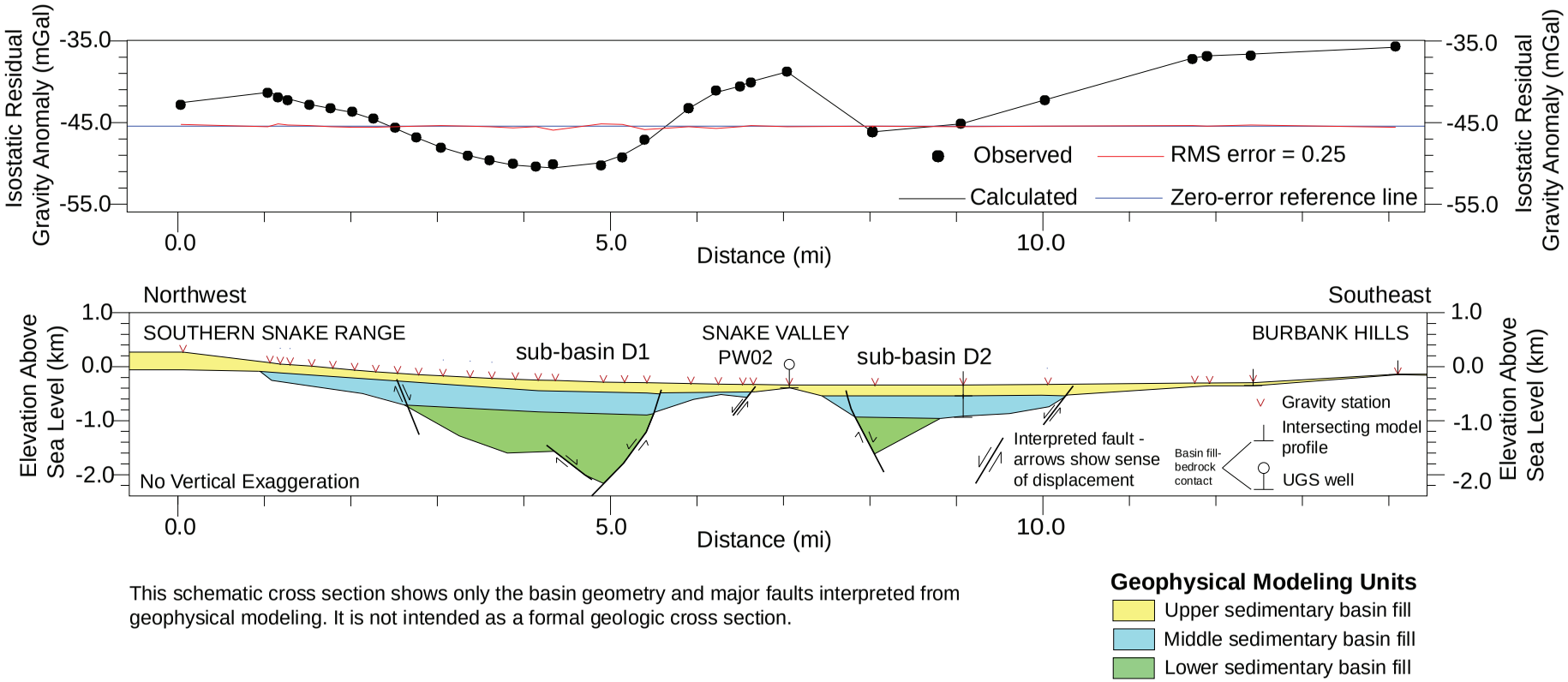

Figure 3.10. *Gravity model profile M6 from the southern Snake Range to the Burbank Hills. See figure 3.1 for profile location.*

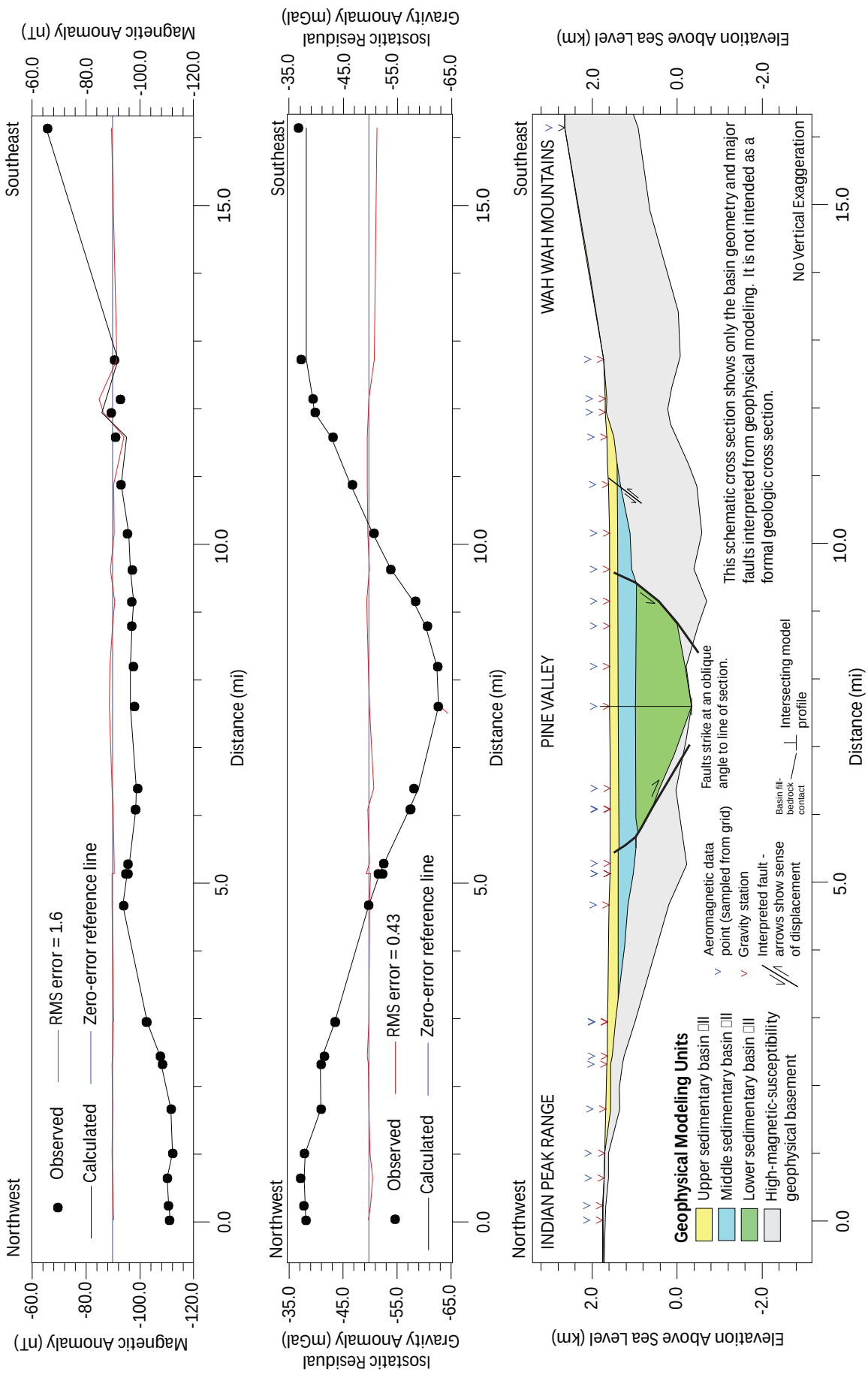

Figure 3.11. *Gravity model profile M7 through central Pine Valley. See figure 3.1 for profile location.*

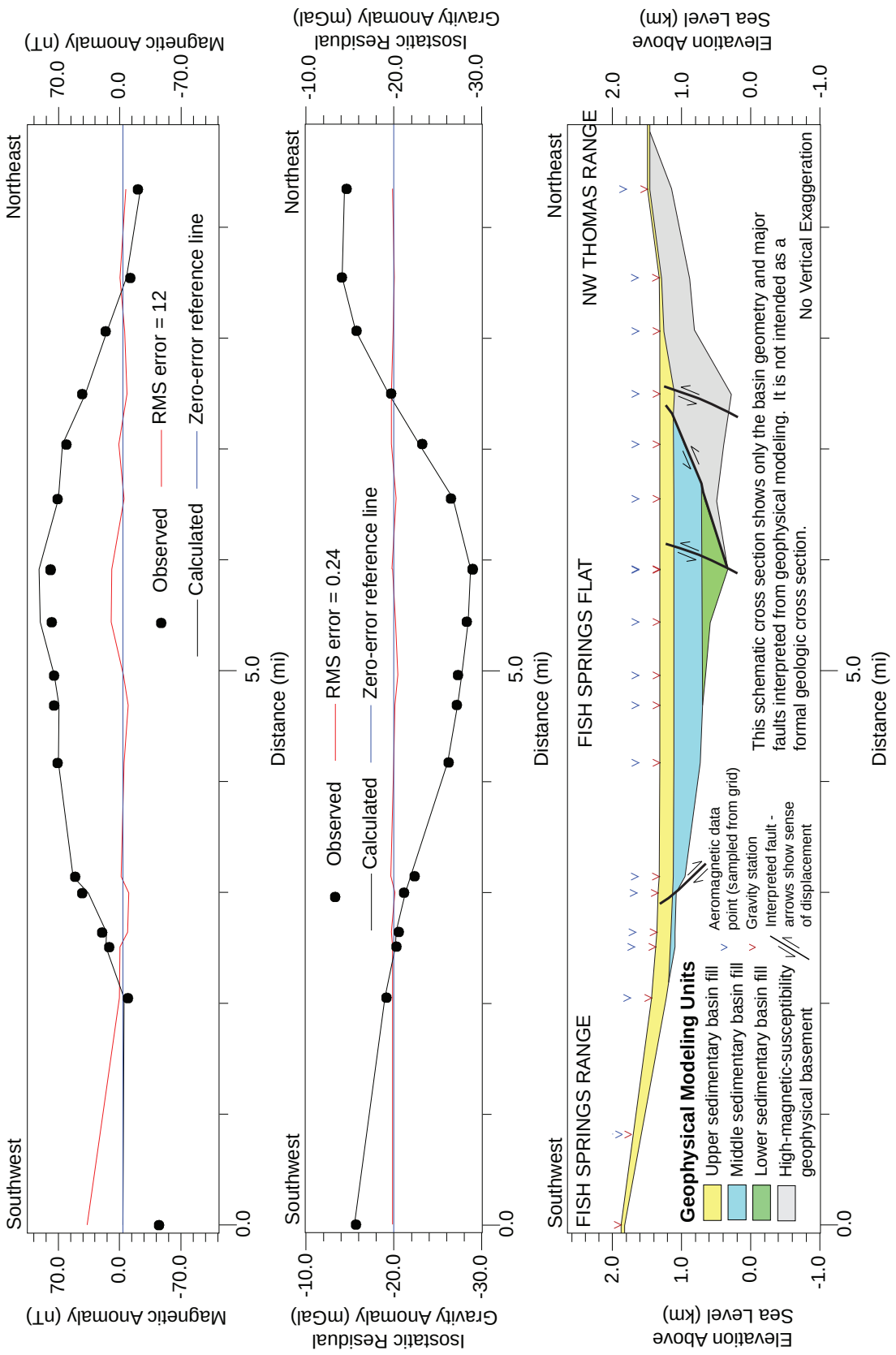

Figure 3.12. *Gravity model profile M8 from the Fish Springs Range to the northwestern Thomas Range. See figure 3.1 for profile location.*

Table 3.1. *Records of wells having logs that constrain depth to bedrock.*

Well Label	Operator	Well Name	Location[1]									Depth to Bedrock (ft)[2]	Bedrock Formation[3]	Well Number[4]
			X	Y	Latitude	Longitude	Township	Range	Section	County	Elevation			
A	SHELL OIL COMPANY	1 BAKER CREEK UNIT	238280	4326108	39.046	-114.025	20S	19W	19	Millard	5088	4610	€1 (€Zs)	4302711037
B	NEWMAN, LARRY A	1-25 ESKDALE-FEDERAL	246328	4325461	39.043	-113.931	20S	19W	25	Millard	5025	>4047	TD in Tertiary rocks	4302730006
C	NEWMAN, LARRY A	1-23 ESKDALE-FEDERAL	244756	4326722	39.054	-113.950	20S	19W	23	Millard	5026	>7373	TD in Tertiary rocks	4302730007
D	COMMODORE RESOURCES CORP	1-B NEEDLE ANTICLINE	240874	4290547	38.727	-113.981	24S	19W	16	Millard	5666	475	PIPM (LPzc)	4302730011
E	AMERADA HESS	79-1	242475	4354904	39.305	-113.987	17S	19W	28	Millard	4865	1034	O (LPzc)	4302730013
F	EQUITABLE RESOURCES ENERGY CO	MAMBA FEDERAL 31-22	244285	4366340	39.409	-113.970	16S	19W	22	Millard	4870	2820	M2 (MPzs)	4302730038
G	EQUITABLE RESOURCES ENERGY CO	COBRA STATE 12-36	246735	4372524	39.465	-113.944	15S	19W	36	Millard	4825	2672	S (LPzc)	4302730034
H	J.R. BACON	BAKER CREEK 12-1	234039	4323203	39.017	-114.072	13N	70E	12	White Pine	5125	4610	O (LPzc)	2703305288
I	COMMODORE RESOURCES CORP	OUTLAW FEDERAL 1	234815	4295987	38.773	-114.052	10N	70E	1	White Pine	5444	1254	PIPM (LPzc)	2703305245
J	FLETCHER, C.H.	FLETCHER 1	223943	4268994	38.527	-114.167	8N	70E	30	White Pine	5740	>7481	TD in Tertiary rocks	2701705206
K	FALCON ENERGY	HAMLIN WASH 19-1	223330	4270216	38.537	-114.174	8N	70E	19	White Pine	5721	4183	D (LPzc)	2701705223
L	FALCON ENERGY	HAMLIN WASH 18-1	223394	4272597	38.559	-114.174	8N	70E	18	White Pine	5711	3060	Tv2 (Tv2) at 2600 ft; D (LPZC) at 3060 ft	2701705225
M	FRONTIER EXPLORATION	COBB CREEK FEDERAL 11-1	229170	4253611	38.390	-114.101	6N	70E	11	White Pine	5959	352	D (LPzc)	2701705217
N	UTAH GEOLOGICAL SURVEY	PW02	235287	4296878	38.781	-114.047	23S	20W	25	Millard	5459	30	P1 (UPzc)	384651114025101
O	UTAH GEOLOGICAL SURVEY	PW04	234988	4274763	38.581	-114.043	26S	20W	2	Millard	6180	110	Tv2 (Tv2)	383452114023401
P	UTAH GEOLOGICAL SURVEY	PW06	249081	4342927	39.199	-113.905	18S	18W	32	Millard	5001	343	P1 (UPzc)	391156113541902
Q	UTAH GEOLOGICAL SURVEY	PW15	234940	4291254	38.730	-114.049	24S	20W	14	Millard	5528	175	P1 (UPzc)	384347114025601
R	UTAH GEOLOGICAL SURVEY	PW10	271127	4356179	39.324	-113.655	17S	16W	16	Millard	5266	308	PIPM (LPzc)	391926113391801
S	UTAH GEOLOGICAL SURVEY	PW19	305150	4389822	39.634	-113.271	14S	13W	2	Juab	4635	190	S (LPzc)	393803113161601
T	UTAH GEOLOGICAL SURVEY	PW20	293508	4388586	39.621	-113.406	14S	14W	10	Juab	4721	60	€1 (€Zs)	393714113242001
U	UTAH GEOLOGICAL SURVEY	SG21	293663	4418108	39.887	-113.413	11S	14W	3	Juab	4310	28	S (LPzc)	395312113244803
V	UTAH GEOLOGICAL SURVEY	SG23	236641	4294137	38.756	-114.030	24S	20W	1	Juab	5450	30	P1 (UPzc)	384521114014701
W	U.S. GEOLOGICAL SURVEY	SW of Big Springs	226707	4286601	38.687	-114.153	9N	70E	32	White Pine	6020	480	PIPM (LPzc)	384112114091101

[1] X and Y in NAD83 12N, latitude and longitude in WGS84, Elevation in NAVD88. Public Land Survey coordinates are relative to Sale Lake Baseline and Meridian for wells in Millard and Juab Counties, and Mount Diablo Baseline and Meridian for wells in White Pine County.

[2] Depth to bedrock in petroleum-exploration well logs (wells A through M) from Utah Division of Oil, Gas, and Minng data (http://oilgas.ogm.utah.gov/Data_Center/DataCenter.cfm), in UGS groundwater-monitoring well boreholes (wells N through V) from UGS records (chapter 5 and table C.1), and in USGS well (well W) from R. Plume (written communication, 08/19/2011).

[3] Geologic unit (plate 2); hydrogeologic unit (figure 4.1) in parentheses.

[4] Well numbers are American Petroleum Institute Number for wells A through M, and U.S. Geological Survey well numbers for wells N through W.

and an increase in magnetic anomaly at their western ends. This relation suggests the presence of intrusive rock in the mountain block, confirmed by model M2 which overlies the Ibapah pluton at its western end (figure 3.6). Intrusive rocks also likely underlie the Snake Valley basin fill east of the Deep Creek Range (Watt and Ponce, 2007; Mankinen and McKee, 2009). Some of the deeper basin fill shown on geophysical profile M2 (figure 3.6) may instead be intrusive rock, so the modeled basin fill thickness is a maximum value.

Models within the Indian Peak caldera complex (geophysical model profile M3, figure 3.7) and up to 10 miles (16 km) north of the northern caldera boundary use a depth-dependent density model for volcanic rocks (appendix A; Saltus and Jachens, 1995). The thickness of volcanic rocks in the basin fill is known only in petroleum-exploration wells J, K, and L, about 8 to 10 miles (13–16 km) north of the northern caldera boundary in central Hamlin Valley (figure 3.1; table 3.1). Details of the transition from dominantly volcanic and volcaniclastic material to detritus derived primarily from Paleozoic rocks in the lower basin fill of northern Hamlin Valley are not known, but the volcanic rocks thin rapidly northward in exposures north of the caldera boundary, so the transition likely occurs over about 10 miles (16 km).

3.3.3 Schematic Isopach Map and Structural Interpretations

3.3.3.1 Introduction

This section describes the thickness distribution and structure of basin-fill deposits in the study area from the model profiles (figures 3.5–3.12), isopach map (figure 3.13), analysis of the horizontal gradient of the IRA (figure 3.3), and geologic map (plate 1). To construct the schematic isopach map of basin-fill deposits, model points on the basin fill-geophysical basement contact surfaces in all 87 two-dimensional models were exported to real-world coordinates, and basin-fill thickness was calculated as the difference between the land-surface elevation and the elevation of the contact. These points were combined with points along the basin fill-bedrock contact designated as zero-thickness into a single database. Basin-fill thickness values were then checked against the geologic map, gridded, and contoured (figure 3.13). Figure 3.14 shows the interpreted subsurface structures. Criteria for identifying subsurface faults include (1) geologic map relations, including fault scarps, the projection of mapped faults below the basin fill, and abrupt linear topographic breaks between valleys and ranges, (2) linear bands of high horizontal gradient in the IRA, and (3) in geophysical model profiles, abrupt changes in the slope of the contact between basin fill and geophysical basement. In the following discussion, "valley axis" refers to an imaginary line connecting points of lowest valley-floor elevation along its geometric long axis; "mountain front" refers to the transition between valley floor and mountain range (Wilson and Guan, 2004); "sedimentary basin" refers to the accumulation of sedimentary and, in some basins, volcanic deposits below the valley; "depositional center" refers to the area of thickest basin-fill accumulation within a sedimentary basin or sub-basin; and "basin fill-geophysical basement contact" refers to the surface separating model units used to represent basin fill and consolidated rock in geophysical model profiles.

3.3.3.2 Snake Valley and Hamlin Valley

The Snake Valley and northern Hamlin Valley sedimentary basins together consist of six sub-basins (A through F, figures 3.13 and 3.14) separated by transverse basement highs concealed below the upper part of the basin fill. Welch and others (2007) delineated similar sub-basin boundaries in Snake and Hamlin Valleys.

Sub-basin A beneath northern Snake Valley east of the Deep Creek Range includes a larger, deeper northeastern depositional center and a smaller southwestern depositional center (A1 and A2, respectively, figures 3.13 and 3.14). The northeastern depositional center (A1) attains a maximum thickness of over 10,000 feet (3000 m) about 6 miles (10 km) southeast of the Deep Creek Range, and includes a subsurface bedrock horst (geophysical model profile M2, figure 3.6). Northwest of this horst, the basin fill thickens toward the major normal-fault zone that defines the southeastern margin of the Deep Creek Range. Sub-basin A is coincident with high aeromagnetic anomaly values, suggesting that plutonic rocks underlie the basin and/or that the basin fill contains large amounts of volcanic rock or sediment derived from igneous rocks (Watt and Ponce, 2007; Mankinen and McKee, 2009).

Sub-basin B beneath north-central Snake Valley extends from its southern boundary about 5 miles (8 km) north of Eskdale to the Millard-Juab County line. The main part of sub-basin B trends north, lies below the valley axis, contains three depositional centers, and attains a maximum thickness of 9000 feet (2700 m). The southern part of sub-basin B is interpreted as an asymmetric graben that thickens toward its relatively gently dipping (~30°) western boundary fault (geophysical model profile M4, figure 3.8). The main basin-bounding faults are 2 to 4 miles (3–6 km) toward the valley axis from the nearest mountain front. The northern part of sub-basin B is wider and consists of several roughly symmetrical, north-south-trending grabens that are up to 4000 feet (1200 m) thick. The western end of model profile M4 has relatively high IRA values, suggesting the

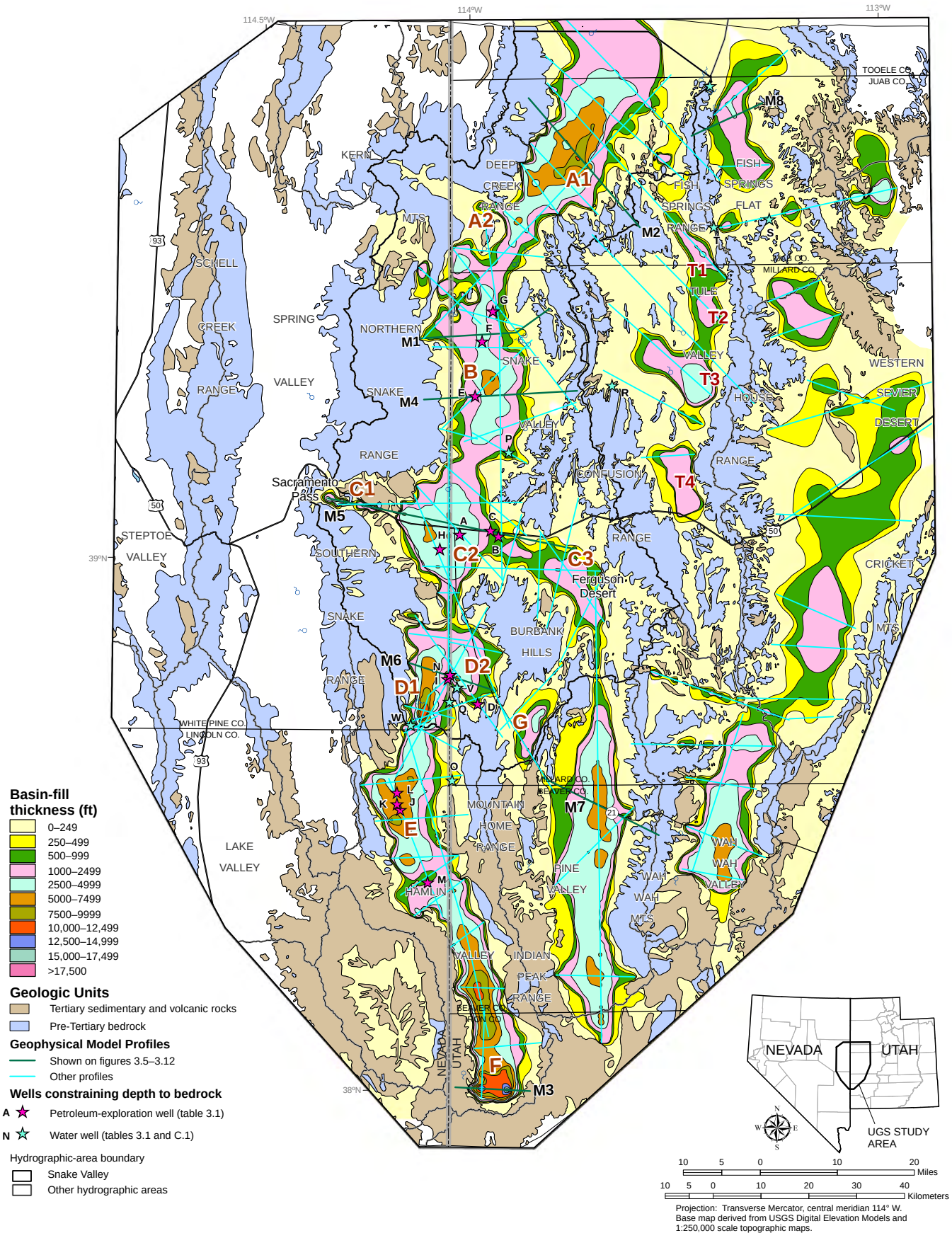

Figure 3.13. *Schematic isopach map of basin-fill deposits in the study area. A through F—Snake and Hamlin valley sub-basins (section 3.3.3.2); G—Antelope Valley sub-basin (section 3.3.3.2); T1 through T4—Tule Valley sub-basins (section 3.3.3.3).*

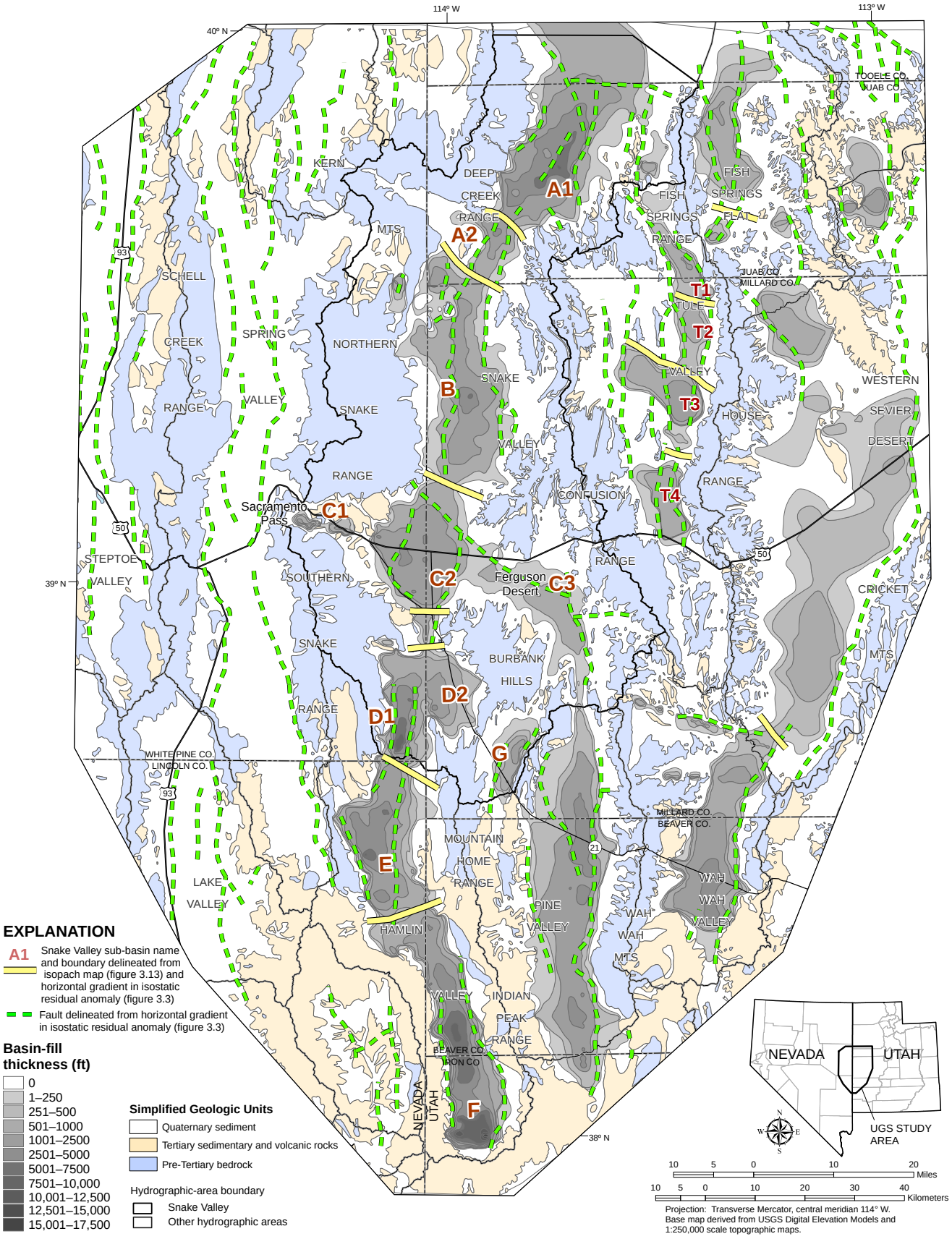

Figure 3.14. *Subsurface structures interpreted from two-dimensional geophysical model profiles and the horizontal gradient of the isostatic residual gravity anomaly. A through F—Snake and Hamlin valley sub-basins (section 3.3.3.2); G—Antelope Valley sub-basin (section 3.3.3.2); T1 through T4—Tule Valley sub-basins (section 3.3.3.3).*

presence of rocks denser than 2.67 g/cm^3. This inference is consistent with the geology of this part of the northern Snake Range, where Precambrian quartzite is exposed, the structurally deepest exposure in the Snake Range. These rocks may be denser than 2.67 g/cm^3, causing the higher IRA values there. The positions of the depositional centers and main basin-forming normal-fault zones suggest that the older, deeper part of sub-basin B initially formed as a relatively narrow graben. In this interpretation, displacement on the original basin-forming faults waned as new, steeply dipping normal faults formed to the west and east, expanding the area of the depositional basin. The latter faults define the present basin-range topography but did not produce the deepest part of the depositional basin.

Snake Valley sub-basin C is a structurally and stratigraphically complex, composite basin (figures 3.9, 3.13, and 3.14) that includes (1) a narrow, sharply defined, east-southeast-trending depositional center (C1) from Sacramento Pass to west-central Snake Valley, (2) a broad, roughly circular depositional center (C2) centered below U.S. Highway 6/50, and (3) a relatively narrow, southeast-trending depositional center (C3) below Ferguson Desert. Depositional center C1 is interpreted as an internally faulted graben composed of the Tertiary conglomerate and volcaniclastic, volcanic, and lacustrine deposits mapped in the adjacent hills (Miller and Grier, 1995), and is up to 4000 feet (1200 m) thick. Depositional center C2 is over 6000 feet (1800 m) thick in its deepest part, and is likely composed of sedimentary, volcanic, and volcaniclastic deposits similar to the Tertiary rocks that compose depositional center C1. Depositional center C2 is bounded on its west and east sides by northwest-southeast striking normal faults, and on its north side by a northwest-striking fault interpreted from the south-to-north horizontal IRA gradient (figures 3.3b and 3.14). Geophysical model profile M5 (figure 3.9) shows that depositional center C2 contains two concealed bedrock horsts and gradually tapers eastward. Watt and Ponce (2007), based on aeromagnetic data, suggested that depositional center C2 is underlain by plutonic rocks. The logs of petroleum-exploration wells in sub-basin C do not denote plutonic rocks, although they possibly were encountered but misinterpreted as volcanic rocks in the basin fill. Geophysical model profile M5 does not depict plutonic rocks below the basin fill. The modeled basin-fill depth would be shallower if they are present. Depositional basin C3 is up to 2500 feet (800 m) thick, and is interpreted here as a graben bounded by northwest-striking normal faults.

Sub-basin D beneath southern Snake Valley comprises two straight, north-south trending grabens (depositional centers D1 and D2, figures 3.13 and 3.14; geophysical model profile M6, figure 3.10). The larger, western graben (D1) is below the valley floor east of the southern Snake Range and west of a mostly concealed, northwest-trending horst defined by a gravity high and sparse bedrock exposures. This horst is the continuation of the ridge denoted as Needle Point Mountain in the northwestern Mountain Home Range. Dearden Springs (sections 4.5.3 and 5.3) issue from bedrock exposures of this horst along Lake Creek. The western graben (D1) is about 14,000 feet (4300 m) thick in its deepest part, and the eastern graben (D2) is locally over 7500 feet (2800 m) thick. The boundary between sub-basins D and E is interpreted as a buried transverse intrabasin ridge below the surface-drainage divide between southern Snake Valley and northern Hamlin Valley.

Sub-basin E beneath northern Hamlin Valley fills a north-trending, asymmetric graben that is over 11,000 feet (3400 m) thick immediately east of the basin-forming normal-fault zone that bounds the eastern margin of the Limestone Hills. Logs of petroleum-exploration wells (J, K, and L, table 3.1) show that sub-basin E contains 400 to 1000 feet (122–305 m) of volcanic rocks in the middle of the Tertiary basin fill, and anhydrite deposits up to 250 feet (76 m) thick.

Low IRA values beneath southern Hamlin Valley and adjacent areas in east-central Nevada result from thick accumulations of relatively less dense (compared to Paleozoic rocks) volcanic and shallow intrusive rocks of the Indian Peak caldera complex (sub-basin F, figures 3.13 and 3.14) (Watt and Ponce, 2007). The approximate caldera boundary is based on geologic mapping (Dixon and others, 2007). The south-to-north horizontal IRA gradient shows a linear high-gradient band below the mapped northern caldera boundary. Geophysical model profile M3 (figure 3.7) illustrates the subsurface structure of the Indian Peak caldera complex in its thickest part (locally over 18,000 feet [5000 m]) near the southern boundary of Hamlin Valley. The northern caldera boundary defines the boundary between sub-basins E and F.

Sub-basin G underlies Antelope Valley, in the Snake Valley hydrographic area east of southern Snake Valley, and is an asymmetric half-graben that is over 2500 feet (800 m) thick in its deepest part adjacent to the normal-fault zone that bounds the western margin of the southern Tunnel Spring Mountains.

3.3.3.3 Tule Valley

The Tule Valley sedimentary basin contains four sub-basins (T1 through T4, figures 3.13 and 3.14) west of the House Range, between the range-bounding normal-fault zone and several north-south striking horsts in the valley center. The northern sub-basin T1 trends north-northwest, is locally over 5000 feet (1500 m) thick, and is bounded by

the northern House Range and the southern Fish Springs Range on the northeast, and by the eastern Middle Range on the northwest. Sub-basin T1 is interpreted here as a structurally complex, composite basin that formed due to displacement on the normal-fault zones along the western margins of the Fish Springs and House Ranges, and on the Sand Pass transverse zone (Rowley, 1998) which trends west-southwest through the pass between these ranges and through the northern part of sub-basin T1.

Tule Valley sub-basin T2 is up to 2000 feet (610 m) thick in the hanging wall of the normal-fault zone along the western margin of the House Range. The largest sub-basin, T3, trends northwest, is over 5000 feet (1500 m) thick in its deepest part, and is a graben bounded by the western House Range normal-fault zone and by two northwest-striking transverse faults (figure 3.14). West of sub-basin T3, these transverse faults bound several horsts and grabens that form the Coyote Hills and include Coyote Spring, an important groundwater discharge point in Tule Valley (figure 3.14). Sub-basin T4 trends northwest, and is bounded by the western House Range normal-fault zone adjacent to the highest part of the range.

3.3.3.4 Pine Valley

The Pine Valley sedimentary basin trends north-south below the valley axis and is up to 6000 feet (1800 m) thick in two distinct depositional centers. In northwest-to-southeast profile, the contact between basin fill and geophysical basement resembles the bottom of a sailboat, having gently inward-sloping outer margins that thicken abruptly to form an asymmetric "keel" at the basin center in which the eastern keel margin is steeper (geophysical model profile M7, figure 3.11). The Pine Valley sedimentary basin is interpreted as a composite graben, in which normal faults bound the keel and the outer basin margins, and the eastern keel-bounding fault has the greatest displacement. The keel-bounding faults are 4 to 5 miles (6–8 km) west of the eastern mountain front and 5 to 6 miles (8–10 km) east of the western mountain front, and do not cut the upper part of the basin fill, whereas the normal-fault zones that form the present basin-range boundaries cut the upper part of the basin fill and are, therefore, interpreted as younger and having less displacement. The basin is interpreted to have initially formed during Tertiary time as a narrow, straight-sided graben below the present valley axis, that widened when active faulting stepped outward from the basin center.

3.3.3.5 Wah Wah Valley and Western Sevier Desert

The Wah Wah Valley sedimentary basin trends north-northeast below the valley axis, and includes a larger, southern depositional center that is locally over 7000 feet (2100 m) thick and a smaller, northern depositional center that is over 4000 feet (1200 m) thick. Both depositional centers are asymmetric, having steeper eastern boundaries. The Wah Wah Valley sedimentary basin is interpreted as an asymmetric graben in which displacement is greater on the eastern basin-bounding normal-fault zone and displacement and basin thickness increase from north to south. The interpreted basin-bounding faults are 2 miles (3 km) or less from the mountain fronts, and the shape of the basin fill-geophysical basement contact suggests that the eastern basin-bounding normal-fault zone has substantially great displacement than the western normal-fault zone.

In the western Sevier Desert, the depositional basin beneath Sevier Lake trends northeast and is bounded on its eastern margin by a normal-fault zone along the northwestern front of the Cricket Mountains. This basin has depositional centers below southern Sevier Lake (over 2500 feet [800 m] thick in its deepest part) and 25 miles (40 km) to the northeast (over 1000 feet [300 m] thick), and is symmetric in geophysical model profiles. Its geometry is similar to sedimentary basins in Nevada that Anderson and others (1983) interpreted as having formed above distributed crustal stretching and subsidence. In this interpretation, the basin-bounding faults were among many distributed faults that controlled basin development, in contrast to the interpretation that most other basins in the study area formed primarily due to displacement along range-bounding fault zones.

3.3.3.6 Fish Springs Flat

The Fish Springs Flat sedimentary basin includes three depositional centers. The northern depositional center is over 3000 feet (900 m) thick and is asymmetric, thickening toward the normal-fault zone along the eastern Fish Springs Range mountain front (geophysical model profile M8, figure 3.12). The middle depositional center is locally over 2000 feet (600 m) thick and has a more symmetric profile, thickening slightly toward a gently east-dipping basin-bounding normal-fault zone. The southern depositional center is over 1000 feet (300 m) thick and is bounded by, and thickens toward, a normal fault along its western boundary. This depositional center is also along strike of the Sand Pass transverse zone and, like Tule Valley sub-basin T1, may have formed as a pull-apart basin in a structurally complex fault-intersection zone.

3.4 DISCUSSION

In the platform used for data reduction (Geosoft, Inc., 2010), the terrain correction is calculated from a digital elevation model (DEM) grid having 30-meter (98 ft) node

spacing and does not include the traditional inner terrain correction estimate derived from observations of topography near each station (Hammer, 1939). Although care was taken not to occupy stations having steep slopes within 100 feet (31 m) of the gravity meter, the DEM probably does not completely account for topography within 100 feet (31 m) of some of the stations in mountain canyons. For these stations, the terrain correction and CBA values calculated here are probably lower than they should be. This problem should not substantially affect the isopach map derived from the two-dimensional model profiles, because the profiles use only the first one to three bedrock stations to constrain minimum basin-fill thickness.

The variations in the isostatic residual gravity anomaly (figure 3.2) are similar to those shown by Mankinen and others (2006, figure 4), Watt and Ponce (2007, figure 3 and plate 1), and Mankinen and McKee (2009, figure 2), although my IRA values are about 8 to 10 mGal lower. Because I used the same data except for the new UGS stations, which are consistent with the previously existing data as noted in section 3.2, the difference may result from differences in scale, DEM, or algorithm used to calculate the regional field that is subtracted from the CBA to generate the IRA.

Mankinen and McKee (2009) attributed the high IRA values below the northern Confusion Range to the presence in the subsurface of thick sections of Paleozoic carbonate rocks, which contain a relatively high proportion of dolomite. Dolomite is denser than most other sedimentary rocks in the region, so thick sections of dolomitic carbonate may produce excess mass relative to adjacent areas. The same explanation may apply to IRA highs below the Burbank Hills and northern Mountain Home Range. Mankinen and McKee (2009) suggested that the high IRA values below the northern Snake Range and Cricket Mountains are due to the presence of metamorphosed Neoproterozoic quartzite closer to the land surface than in other parts of the study area.

The high IRA values beneath the Thomas Range and southern Great Salt Lake Desert cannot be explained by the presence of dolomite-rich carbonate rocks or metamorphosed Neoproterozoic rocks near the surface. The surface geology, high IRA values, high aeromagnetic anomaly, and two-dimensional geophysical modeling collectively suggest that rocks denser and having higher magnetic susceptibility than the Paleozoic carbonate rocks underlie the Thomas Range.

Differences among the isopach map presented in this study and those of Mankinen and others (2006), Watt and Ponce (2007), and Mankinen and McKee (2009), are likely due to different assumptions in calculating the IRA values, and different methods for converting the IRA values to basin-fill thickness. The present study used the same petroleum-exploration wells as the previous studies, and additional constraints on depth to bedrock provided by nine of the new UGS groundwater-monitoring wells (table 3.1). Mankinen and others (2006, figure 10) and Mankinen and McKee (2009, figure 6) applied inversion modeling of their entire data set to derive depth to pre-Cenozoic geophysical basement. This approach estimates a value for each grid cell and minimizes the uncertainty of the grid as a whole. The UGS study used inversion modeling along selected traverses having a high concentration of data points, and profiles that contain wells constraining depth to bedrock are assigned greater weight when cross-correlating the model traverses and constructing the isopach map. The isopach map presented here (figure 3.13) was derived by gridding a data set that consists of depth-to-bedrock values along the model traverses and points along the mapped bedrock-basin fill contact that were assigned a depth-to-bedrock value of zero.

The faults interpreted from the IRA horizontal-gradient field were drawn along the centers of the linear bands marking the highest gradients. These bands coincide with the position of the greatest density contrast along the fault planes, probably near the midpoint of the section of the fault plane that juxtaposes basin fill and bedrock. The map traces of these interpreted faults are the vertical projection from the fault plane at depth to the surface, whereas fault traces on geologic maps (e.g., plate 1) show the intersection of the fault with the land surface. The map traces of range-bounding normal-fault zones defined from the horizontal IRA gradient, therefore, are closer to the valley axis than their surface traces. The horizontal separation on the map between these two traces is inversely proportional to the fault dip.

Shah Alam (1990) interpreted the structural geology and stratigraphy of the Tertiary-Quaternary sedimentary basin below southern Snake Valley and northern Hamlin Valley from migrated stacked sections and depth sections of five east-west and two north-south trending seismic-reflection lines. Geophysical model traverses calculated in this study closely follow the east-west seismic-reflection lines (figure 3.1). The shape and maximum depth of basin-fill deposits in the model geophysical profiles from this study closely match Shah Alam's (1990) interpretive depth sections for three of the five east-west seismic-reflection profiles. The primary basin-bounding normal-fault zones are typically steeper in the geophysical model profiles than in the seismic-reflection profiles. In the northern of the three seismic-reflection profiles in Hamlin Valley, the basin fill is about 7500 feet (2300 m) thicker at its maximum depth

in the geophysical model profile than in the depth section derived from the seismic-reflection line. These differences are likely due to different interpretations of density and seismic velocity of subsurface units along this profile, or to the greater uncertainty of the geophysical modeling for deeper sedimentary basins. Along the northeast-trending seismic-reflection profile from Big Springs to the Burbank Hills in southern Snake Valley, the maximum basin-fill thickness from this study and in Mankinen and McKee (2009) is about 9000 feet (2700 m) greater than in the seismic-reflection depth section. Shah Alam (1990, figure 12c) presented a gravity model based on the depth section, that does not match the observed gravity data in the area of maximum basin depth. The depth-density distribution and/or seismic velocity distribution are evidently anomalous in this area compared to the rest of the study area.

3.5 CHAPTER 3 REFERENCES

Anderson, R.E., Zoback, M.L., and Thompson, G.A., 1983, Implications of selected subsurface data on the structural form and evolution of some basins in the northern Basin and Range Province, Nevada and Utah: Geological Society of America Bulletin, v. 94, p. 1055–1072.

Blakely, R.J., 1995, Potential theory in gravity and magnetic applications: Cambridge, England, Cambridge University Press, 441 p.

Dixon, G.L., Rowley, P.D., Burns, A.G., Watrus, J.M, and Ekren, E.B., 2007, Geology of White Pine and Lincoln Counties and adjacent areas, Nevada and Utah—the geologic framework of regional groundwater flow systems: Las Vegas, Southern Nevada Water Authority, HAM-ED-001, variously paginated. Available *in* Southern Nevada Water Authority, 2008, Baseline characterization report for Clark, Lincoln, and White Pine Counties Groundwater Development Project, *in* U.S. Bureau of Land Management, 2012, Clark, Lincoln, and White Pine Counties Groundwater Development Project Final Environmental Impact Statement FES 12-33, Document BLM/NV/NV/ES/11-17+1793.

Faulds, J.E., and Varga, R.J., 1998, The role of accommodation and transfer zones in the regional segmentation of extended terranes, *in* Faulds, J.E., and Stewart, J.H., editors, Accommodation zones and transfer zones—the regional segmentation of the Basin and Range Province: Geological Society of America Special Paper 323, p. 1–45.

Geosoft Inc., 2010, Montaj gravity and terrain correction v. 7.1: Toronto, Ontario, Canada, Geosoft Incorporated, 50 p.

Hammer, S., 1939, Terrain corrections for gravimeter stations: Geophysics, v. 4, p. 184–194.

Jachens, R.C., and Roberts, C.W., 1981, Documentation of program, ISOCOMP, for computing isostatic residual gravity: U.S. Geological Survey Open-File Report 81-574, 26 p.

Mankinen, E.A., and McKee, E.H., 2009, Geophysical setting of western Utah and eastern Nevada between latitudes 37°45′ and 40°N, *in* Tripp, B.T., Krahulec, K., and Jordan, J.L., editors, Geology and geologic resources and issues of western Utah: Utah Geological Association Publication 38, p. 271–286.

Mankinen, E.A., Roberts, C.W., McKee, E.H., Chuchel, B.A., and Moring, B.C., 2006, Geophysical data from the Spring and Snake Valleys area, Nevada and Utah: U.S. Geological Survey Open-File Report 2006-1160, 36 p.

Miller, E.L., and Grier, S.P., 1995, Geologic map of the Lehman Caves quadrangle, White Pine County, Nevada: U.S. Geological Survey Map GQ-1758, scale 1:24,000.

Pan American Center for Earth and Environmental Sciences (PACES), 2007, Gravity and aeromagnetic data: Online, http://research.utep.edu/Default.aspx?alias=research.utep.edu/paces, accessed January 9, 2007.

Rowley, P.D., 1998, Cenozoic transverse zones and igneous belts in the Great Basin, western United States—their tectonic and economic implications, *in* Faulds, J.E., and Stewart, J.H., editors, Accommodation zones and transfer zones—the regional segmentation of the Basin and Range Province: Geological Society of America Special Paper 323, p.195–228.

Saltus, R.W., and Jachens, R.C., 1995, Gravity and basin depth maps of the Basin and Range Province, western United States: U.S. Geological Survey Map GP-1012, scale 1:2,500,000.

Schlische, R.W., and Anders, M.H., 1996, Stratigraphic effects and tectonic implications of the growth of normal faults and extensional basins, *in* Beratan, K.K., editor, Reconstructing the history of Basin and Range extension using sedimentology and stratigraphy: Geological Society of America Special Paper 303, p. 183–203.

Shah Alam, A.H.M., 1990, Crustal extension in the southern Snake Range and vicinity, Nevada-Utah—an integrated geological and geophysical study: Baton Rouge, Louisiana State University, Ph.D.

dissertation, 126 p.

Watt, J.T., and Ponce, D.A., 2007, Geophysical framework investigations influencing ground-water resources in east-central Nevada and west-central Utah: U.S. Geological Survey Open-File Report 2007-1163, 43 p.

Welch, A.H., Bright, D.J., and Knochenmus, L.A., 2007, Water resources of the Basin and Range carbonate-rock aquifer system, White Pine County, Nevada, and adjacent areas in Nevada and Utah: U.S. Geological Survey Scientific Investigations Report 2007-5261, 96 p.

Wilson, J.L., and Guan, H., 2004, Mountain-block hydrology and mountain-front recharge, *in* Phillips, F.M., Hogan, J., and Scanlon, B., editors, Groundwater recharge in a desert environment—the southwestern United States: Washington, D.C., American Geophysical Union, p. 113–137.

CHAPTER 4 | HYDROGEOLOGICAL SETTING

by Hugh Hurlow

Flowing wells in northern Snake Valley, Deep Creek Range in the background.

Bibliographic citation for this chapter:
Hurlow, H., 2014, Hydrogeological setting, Chapter 4 *in* Hurlow, H., editor, Hydrogeologic studies and groundwater monitoring in Snake Valley and adjacent hydrographic areas, west-central Utah and east-central Nevada: Utah Geological Survey Bulletin 135, p. 57–90.

CHAPTER 4 CONTENTS

FIGURES

TABLES

CHAPTER 4: HYDROGEOLOGIC SETTING

by Hugh Hurlow

4.1 INTRODUCTION

This chapter summarizes previous work on the hydrogeologic setting of the UGS study area. Most recent hydrogeologic data are from geologic framework, data compilation, and groundwater-flow modeling studies from the U.S. Geological Survey's RASA (Harrill and others, 1988; Harrill and Prudic, 1998) and BARCAS (Welch and others, 2007) projects, and SNWA's proposed groundwater-development project (Dixon and others, 2007; SNWA, 2009a; U.S. Bureau of Land Management, 2012). Additional data and interpretations on hydrostratigraphy and hydraulic properties are from extensive site characterization for the proposed nuclear waste repository at the Nevada Test Site and associated groundwater-flow modeling of the Death Valley Regional Flow System, 180 miles (290 km) southwest of the UGS study area (figure 2.1) (Belcher and others, 2001; Belcher, 2004; Fenelon and others, 2010).

4.2 HYDROSTRATIGRAPHY

4.2.1 Introduction

The lithostratigraphic units on plates 1 and 2 consist of one or more geologic formations delineated by lithology and age. In this report these simplified map units are further categorized into hydrogeologic units, defined as groups of geologic formations having similar known or inferred hydraulic properties and which are typically classified as either aquifers or confining units (figures 4.1 and 4.2; appendix B). Some hydrogeologic units have intermediate hydraulic properties, or their hydraulic properties vary due to regional compositional changes or varying geologic structure (Winograd and Thordarson, 1975; Laczniak and others 1996; Belcher and others, 2001; Welch and others, 2007). The hydrogeologic units defined in this report (section 4.2.2; appendix B) are similar to those of Plume (1996), Dixon and others (2007), and Sweetkind and others (2007), although the unit nomenclature is somewhat different.

4.2.2 Hydrogeologic Units

Cenozoic geologic formations in the study area consist of Miocene to Quaternary unconsolidated to semi-consolidated, predominantly clastic deposits denoted as "younger basin fill"; Eocene to Oligocene consolidated to semi-consolidated, sedimentary, volcaniclastic, and volcanic rocks denoted as "older basin fill"; and Eocene to Oligocene volcanic rocks (figures 4.1 and 4.2; appendix B).

Younger basin-fill deposits are grouped into three hydrogeologic units: (1) the coarse-grained basin-fill aquifer (QTcs, Miocene to Holocene) composed mainly of alluvial-fan and stream deposits, (2) the fine-grained basin-fill confining unit (QTfs, Miocene to Holocene) composed mainly of fine-grained lacustrine deposits, and (3) volcanic-flow rocks (Tvf, Miocene and Pliocene). Hydrogeologic unit QTcs is the most heavily used aquifer in the study area, and is pumped for irrigation. The thickness of units QTcs and QTfs combined is difficult to determine, but they are 1000 to 1500 feet (300–450 m) thick in boreholes at several UGS groundwater-monitoring sites (appendix B). The coarse- and fine-grained deposits are interlayered, reflecting varying predominance of alluvial and lacustrine depositional environments, and the average grain size of the coarse-grained deposits likely decreases toward the valley axes, creating confined conditions there. These deposits accumulated in sedimentary basins below the present-day valleys due to normal faulting and associated valley-floor subsidence that define the present-day Basin-and-Range topography (chapters 2 and 3).

Older basin-fill deposits form a sedimentary-rock aquifer (Ts) (figures 4.1 and 4.2; appendix B). Unit Ts is exposed in the Sacramento Pass area of the Snake Range, where it is about 1100 to 3700 feet (330–1130 m) thick and is composed of alluvial, lacustrine, and volcanic rocks (Miller and Grier, 1995). Unit Ts also occurs along the eastern flank of the southern Snake Range where it consists of coarse-grained volcaniclastic rocks (Whitebread, 1969). The composition, distribution, and thickness of this unit in the sedimentary basins that underlie the valleys in the study area are not known except in several petroleum-test wells in Hamlin Valley, in which the unit includes over 2,000 feet (>600 m) of evaporite deposits, clay, lacustrine limestone, and volcanic tuff (appendix B). These deposits likely formed during the early stages of Basin-and-Range extension (Rowley and others, 2009) or earlier, localized normal faulting of lower magnitude (Best and Christiansen, 1991). Eocene to Oligocene sedimentary rocks in the northwestern Schell Creek Range in the northwestern part of the study area formed in a large sedimentary basin in

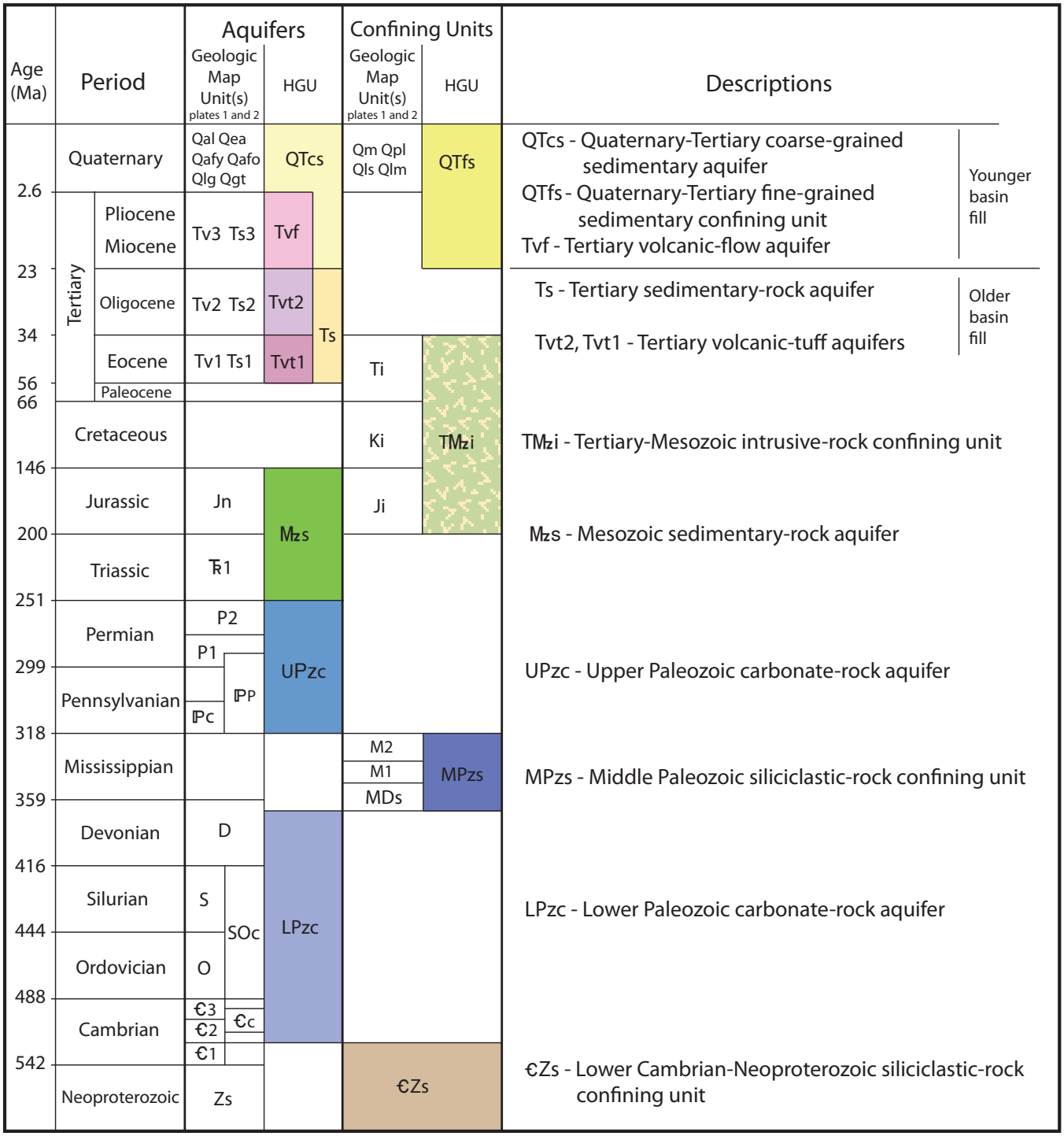

Figure 4.1. *Hydrogeologic units (HGU) in the study area.*

eastern Nevada that predated Basin-and-Range tectonism (Dixon and others, 2007, p. 4–15).

The volcanic rocks erupted from caldera complexes including the large Indian Peak caldera complex in the southern part of the broader UGS study area and adjacent parts of Nevada and Utah (Best and others, 1989), and accumulated within and adjacent to the calderas. Variations in thickness and depositional facies do not follow the same patterns as the younger deposits because the present-day Basin-and-Range topography had not yet formed (e.g., compare figures 8 and 14 of Sweetkind and others, 2007). Welded-tuff deposits may form fractured-rock aquifers, whereas poorly sorted volcanic-breccia deposits likely form low-hydraulic-conductivity aquifers or confining units. These ash-flow tuff units vary from over 2000 feet

(>600 m) thick near the caldera margins to less than 500 feet (<150 m) thick below Garrison, Utah (Sweetkind and others, 2007, figure 14). Volcanic deposits in the Indian Peak caldera complex are locally over 15,000 feet (>4600 m) thick (figures 3.7 and 3.14), and shallow intracaldera intrusive rocks and related hydrothermal alteration likely reduce hydraulic conductivity.

Plutonic rocks range from Jurassic to Miocene in age; are predominantly granitic composition; crop out in the Snake Range, Deep Creek Range, House Range, and San Francisco Mountains (plate 1; figure 4.2); and are grouped into hydrogeologic unit TMzi (figure 4.1). Granitic intrusive rocks may occur below parts of central and northern Snake Valley (figure 3.4), based on interpretation of aeromagnetic data by Watt and Ponce (2007) and Mankinen and McKee (2009). Based on comparison with the geologic setting of adjacent ranges (plate 1), these concealed intrusions likely form plutons and stocks in Paleozoic rocks. These plutonic rocks have extremely low primary porosity and may transmit some groundwater through connected fractures, but form low-hydraulic-conductivity masses where present in the saturated zone (Plume, 1996). The exception may be adjacent to normal-fault zones, where the plutonic rocks may transmit groundwater through dense fracture networks (section 4.2.3).

Mesozoic sedimentary rocks (Mzs) include early Mesozoic limestone, fine-grained sandstone and shale, and middle Mesozoic eolian sandstone. These rocks were eroded from most of the study area during Mesozoic Sevier fold-and-thrust tectonics (Long, 2012), and are present in the southeastern part of the study area as structural blocks of limited continuity cut by thrust faults, and in the axis of the Confusion Range syncline where they are above the saturated zone. Their presence and extent in the saturated zone below the valley floors is poorly known and likely restricted, so they are not considered an important aquifer in our study area.

Upper Paleozoic (Upper Mississippian to Permian) carbonate rocks are grouped into hydrogeologic unit UPzc, which is nearly 7000 feet thick (2100 m) and forms a major regional aquifer in the study area (Plume, 1996; Dixon and others, 2007; Sweetkind and others, 2007). The most important formations in this hydrogeologic unit are interbedded limestone and fine-grained, calcareous sandstone of the Permian Arcturus Formation (about 2700 feet [800 m] thick), and cherty bioclastic limestone of the Late Mississippian-Early Permian Ely Limestone (about 1900 feet [600 m] thick) (figures 4.1 and 4.2; appendix B). Groundwater flows through joints and faults, and solution widening likely increases the hydraulic conductivity of the carbonate rocks (section 4.2.3; appendix B). Hydrogeologic unit UPzc crops out in mountains in the central part of the study area where it is extensively folded and faulted (figure 4.2), and is present in the subsurface below the valleys nearby where it accommodates local- to regional-scale groundwater flow.

Middle Paleozoic rocks are predominantly carbonaceous or calcareous shale that form a 2700-foot-thick (800 m) confining hydrogeologic unit (MPzs) between the two Paleozoic carbonate-rock aquifer hydrogeologic units (figure 4.1; appendix B). The Mississippian Chainman Formation and the Mississippian-Devonian Pilot Shale are the main formations, and crop out in the central part of the study area where they are complexly folded and faulted (figure 4.2), defining structural groundwater compartments (section 4.3.2; appendix E).

Middle to lower Paleozoic carbonate rocks form the thickest (up to 18,000 feet [5500 m] thick) and most extensively exposed hydrogeologic unit (LPzc) in the study area (figures 4.1 and 4.2; appendix B). These geologic units are composed of Middle Cambrian through Devonian, interbedded limestone and dolomite. Devonian through Ordovician limestone and dolomite occur extensively in mountain ranges and in the subsurface in the central part of the study area, and contain very little shale. This part of the hydrogeologic unit likely accommodates significant local- to regional-scale groundwater flow. The Ordovician Eureka Quartzite (550–620 feet [170–190] thick) occurs at the base of the upper third of the stratigraphic sequence, is densely fractured where observed throughout the study area, and therefore does not likely form a confining layer. Shale-rich layers are more common in the Upper and Middle Cambrian rocks, and this part of the hydrogeologic unit may have overall lower hydraulic conductivity. The LPzc hydrogeologic unit crops out in ranges and is present in the saturated zone in the northwestern quarter and eastern third of the study area, and is extensively faulted except in the House Range where it forms a largely intact, east-dipping homocline. Solution features, including caves, are common in outcrop and presumably exist where the unit is present below the water table where geochemical and flow conditions are favorable, greatly increasing the local hydraulic conductivity of these rocks.

Lower Cambrian to Neoproterozoic quartzite and schist are at least 15,000 feet (4600 m) thick and form a confining hydrogeologic unit (CZs) that crops out in the Schell Creek Range and southern Deep Creek Range in the northeastern part of the study area, and in the northern San Francisco Mountains and southern Cricket Range in the southeastern part. The quartzite has little or no primary porosity and is typically cut by joints, so hydraulic conductivity is low compared to the carbonate rocks. Schist layers in the

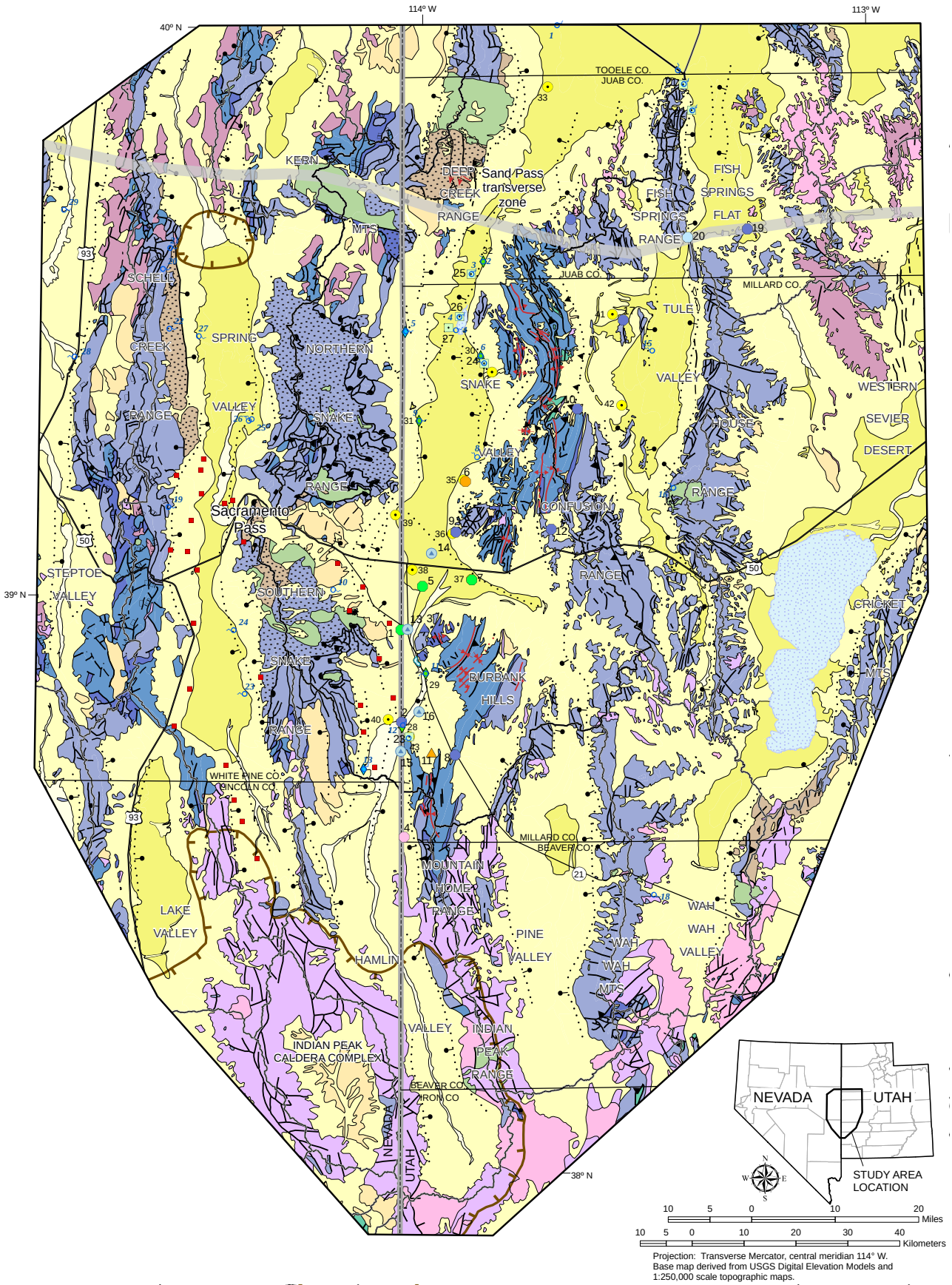

Figure 4.2. *Hydrogeologic map of the UGS study area. The map was derived by grouping the map units shown on plate 1 into the hydrogeologic units shown on figure 4.1.*

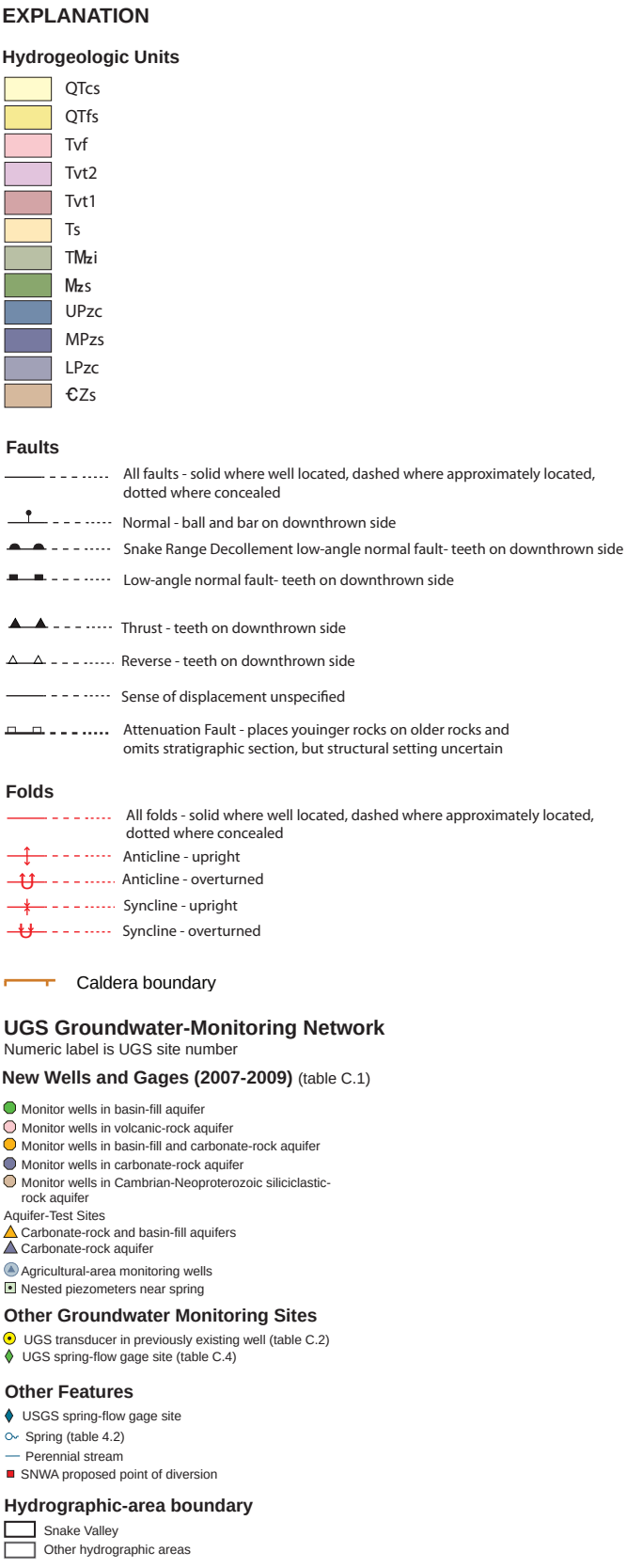

***Figure 4.2**. continued*

Neoproterozoic rocks likely form barriers to cross-bedding groundwater flow and limits the extent of fractures, further limiting the hydraulic conductivity of this unit. This hydrogeologic unit likely conducts groundwater locally where joint density in the quartzite is high, but is a regional confining unit (Plume, 1996).

4.2.3 Hydraulic Properties of Hydrogeologic Units

The hydraulic properties of geologic materials are quantified by their hydraulic conductivity and porosity, which describe their capacity to transmit and store groundwater, respectively. The hydraulic properties of unconsolidated sedimentary deposits are determined by their texture (grain size, sorting, layering, and cementation), which establish the amount of interconnected pore space that can store and transmit groundwater (Fetter, 1994, p. 87–93). Pre-Tertiary rocks in the Basin and Range Province typically have low primary porosity and hydraulic conductivity, whereas secondary porosity and hydraulic conductivity, derived from interconnected fractures, may be higher (Winograd and Thordarson, 1975; Dettinger and others, 1995; Belcher and others, 2001). Solution widening of fractures likely contributes significantly to the secondary hydraulic conductivity of the upper and lower Paleozoic carbonate-rock aquifers (Winograd and Thordarson, 1975). Tertiary sedimentary and volcanic rocks have a wide range of primary textures and degree of consolidation, so may be dominated by either primary or secondary hydraulic conductivity and porosity (Winograd and Thordarson, 1975; Plume, 1996; Belcher and others, 2001).

Table 4.1 and figure 4.3 summarize hydraulic-conductivity and storage-coefficient estimates for the hydrogeologic units used in this study. Hydraulic properties are typically estimated from aquifer tests, preferably those that include a pumping well and at least one monitoring well (Belcher and others, 2001). Figure 4.3 shows that whereas the ranges in estimated hydraulic conductivity overlap substantially, the hydrogeologic units can be classified into aquifers and confining units by their geometric means. An exception is hydrogeologic unit QTfs, which is a confining unit based on its predominant grain size and texture dominated by layered silt and clay, but has hydraulic-conductivity estimates similar to those for the coarse-grained younger basin-fill hydrogeologic unit QTcs. Belcher and others (2001) suggested that aquifer-test results from unit QTfs are mainly from wells screened in coarse-grained beds within the finer-grained sediment.

Aquifer-test data for hydrogeologic units in the UGS study area are relatively sparse. Chapter 7 summarizes results from the UGS aquifer tests in Snake Valley. The U.S. Geological Survey (2010) and Halford and Plume (2011,

Table 4.1. *Hydraulic-property estimates for hydrogeologic units in the study area.*

Source	HGU[2]	Hydraulic Conductivity (ft/day)[1]			Specific Yield[1]		Storativity[1]	
		Geometric Mean[3]	Median	Range	Mean[3]	Range	Mean[3]	Range
Dettinger and others (1995)	UPzc and LPzc[5]	–	4.5	0.01–940	–	–	–	–
	MPzs and €Zs	–	0.015	–	–	–	–	–
Belcher and others (2001)[4]	QTcs and Ts	7	–	0.003–427	0.03	0.0004–0.2	–	–
	QTfs	10	–	0.01–112		0.01	0.01	$9x10^{-5}$–0.04
	Tvt1, Tvt2, Tvf	0.3	–	$3x10^{-6}$–591	0.03	0.00 –0.2	0.001	$4x10^{-5}$–0.004
	TMzi	0.03	–	0.002–3	–	–	–	–
	UPzc	0.3	–	$3x10^{-5}$–2690	–	–	0.003	$8x10^{-4}$–0.006
	MPzs	0.03	–	0.01–1.3	–	–	–	–
	LPzc	0.3	–	$3x10^{-5}$–2690	–	–	0.003	$8x10^{-4}$–0.006
	€Zs	$2x10^{-5}$	–	$1x10^{-7}$–16	–	–	–	–
Sweetkind and others (2007)	QTcs	5	10	0.0002–431	–	–	–	–
	QTfs	8	19	0.01–111	–	–	–	–
	Tvf	1	2	0.04–14	–	–	–	–
	Ts	0.2	0.4	0.0001–21	–	–	–	–
	Tvt1, Tvt2	8	37	0.09–179	–	–	–	–
	TMzi	0.03	0.01		–	–	–	–
	UPzc	1	3	0.0003–1045	–	–	–	–
	MPzs	0.06	0.1	0.0001–3	–	–	–	–
	LPzc	4	4	0.009–2704	–	–	–	–
	€Zs	$2x10^{-6}$	$2x10^{-7}$	$9x10^{-8}$–15	–	–	–	–
SNWA (2009a)	QTcs and QTfs	–	–	4–38	–	0.01–0.2	–	$2x10^{-4}$–0.035
	UPzc and LPzc[5]	–	–	5–64	–	–	–	–
Dong and Halford (2010)[6]	QTcs [6]	3.9	–	3.0–4.8	0.15	0.12–0.18	–	–
	QTfs [6]	0.18	–	0.13–0.22	–	–	–	–
Dong and others (2010)[6]	QTs undiff.[6]	0.6	–	–	0.13	0.12–0.13	–	–
	UPzc[6]	11	–	7–15	0.003	0.001–0.006	–	–
Halford and Plume (2011)	QTcs and QTfs[7]	–	–	–	0.05	–	–	–
	Tvt1, Tvt2	0.06	–	–	–	–	–	–
	UPzc and LPzc[6]	–	–	7–32[8]	–	0.001–0.006	–	–
	UPzc and LPzc[7]	–	–	1–110[8]	–	0.02–0.04	–	–
UGS (this study)[9]	QTcs (site 11)	275	–	210–340	0.28	–	–	–
	UPzc (site 11)	15	–	6–21	$5.5x10^{-5}$	$1.6–8.9x10^{-5}$	.01	0.006–0.017
	LPzc (site 3)	4	3	3–7	0.014	$4.8x10^{-5}$–0.03	$1.3x10^{-4}$	$6.2x10^{-5}$–$2.4x10^{-4}$

– value not reported

[1] Most reported values are from aquifer tests associated with research at the Nevada Test Site and adjacent areas.

[2] The hydrogeologic units (HGUs) listed in this table are those defined in this study. The reported values are for HGUs defined in the references. The HGUs in the cited reports have different nomenclature but encompass lithologically similar geologic units.

[3] The geometric mean is reported for hydraulic conductivity because these data are typically log-normally distributed, whereas the arithmetic mean is reported for storage parameters because they are typically normally distributed (Belcher and others, 2001).

[4] Values from Belcher and others (2001) are from their table 2, converted from the metric system. Values reported for carbonate-rock aquifers are for hydrogeologic units UPzc and LPzc combined, and include fractured and unfractured carbonate rocks.

[5] Reported values are for fractured Paleozoic carbonate rocks, undifferentiated.

[6] Values from irrigation aquifer tests.

[7] Values from conventional aquifer tests, chiefly of SNWA test wells in Spring Valley.

[8] Estimated from transmissivity estimates of Halford and Plume (2011, table 1) assuming aquifer thickness of 500 to 1000 feet.

[9] See chapter 7 and tables 7.4 and 7.5.

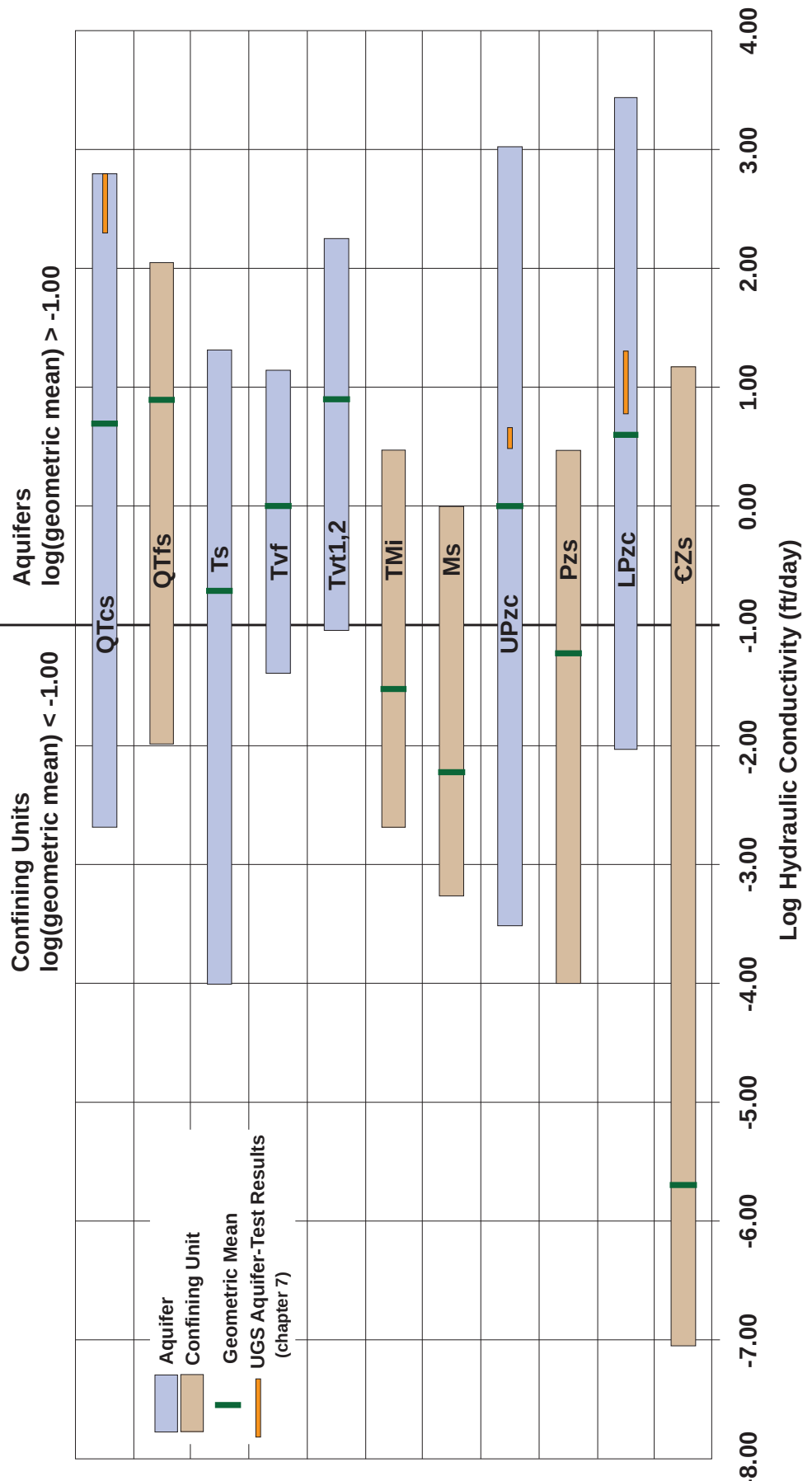

Figure 4.3. *Ranges and geometric means of hydraulic-conductivity estimates from aquifer tests for the hydrogeologic units defined in the study area, derived from the data in table 4.1. For this data set, aquifers and confining units can be delineated as having geometric means greater than or less than 0.1 ft/day (0.03 m/day) (log values of -1.00), respectively, with the exception of hydrogeologic unit QTfs. This unit is appropriately classified as a confining unit based on sediment grain size and texture, and Belcher and others (2001) suggested that the anomalously high hydraulic-conductivity estimates come from aquifer tests on wells screened in coarser-grained, more transmissive beds within predominantly fine-grained units.*

p. 13) summarized results of conventional aquifer tests on three wells in the basin-fill aquifer (transmissivity estimates ranged from 400 to 10,000 ft^2/day [37–930 m^2/day]) and two wells in the carbonate-rock aquifer (transmissivity estimates ranged from 300 to 11,000 ft^2/day [28–1020 m^2/day]) in Snake and Spring valleys on the flanks of the southern Snake Range. Dong and Halford (2010) and Dong and others (2011) used seasonal water-level declines associated with agricultural pumping to estimate transmissivity, hydraulic conductivity, and specific yield for the basin-fill aquifer in Snake Valley near Baker, Nevada, and in Lake Valley, and for the basin-fill and carbonate-rock aquifers in southern Snake Valley (table 4.1). Their estimates are derived from one to two orders of magnitude greater pumping and aquifer volumes than standard aquifer tests, and yield hydraulic-property estimates within the same range.

More data are available from extensive aquifer testing in southern Nevada (Dettinger and others, 1995) and the Nevada Test Site and adjacent areas in east-central Nevada (Belcher and others, 2001; Belcher, 2004). The geologic formations, hydrogeologic units, structural geology, and hydrogeologic setting of the Nevada Test Site region are generally similar to those of east-central Nevada and west-central Utah (Harrill and Prudic, 1998; Belcher, 2004), so hydraulic properties estimated from those studies provide ranges of values that serve as reasonable approximations for the hydrogeologic units in our study area. Differences in depositional environment, composition, and structural setting between comparable geologic units in the two regions may result in somewhat different ranges and mean values. SNWA (2009a) summarized aquifer-test data and interpretations for wells in their project area.

Hydraulic-conductivity estimates determined from aquifer tests generally decrease with observation-well depth for all common aquifer types in the eastern Basin and Range, but a range of up to five orders of magnitude can be measured at any given depth (Belcher and others, 2001, figure 4). For example, the mean hydraulic conductivity of the upper and lower Paleozoic carbonate-rock aquifer of about 2 feet per day (0.6 m/day) has been measured at up to 4000 feet (1200 m) depth. This value provides a reasonable (if perhaps arbitrary) estimate of the maximum depth of significant groundwater flow in our study area, though deeper flow may occur (Van Denburgh and Rush, 1974, p. 31, and Thomas and others, 1990, p. 56).

Uncertainty exists over how transmissivity and hydraulic-conductivity estimates derived from conventional aquifer tests should be extrapolated to regional-scale values (Schulze-Makuch and others, 1999). Calibrated steady-state groundwater-flow models (Prudic and others, 1995; SNWA, 2009a; Halford and Plume, 2011) provide an alternate method to estimate the large-scale magnitude and distribution of hydraulic conductivity, and typically result in lower hydraulic-property estimates than those derived from aquifer tests, most of which involve wells preferentially screened in parts of the aquifers having the highest hydraulic conductivity (D. Prudic, written communication, 2013).

4.3 GEOLOGIC STRUCTURES

4.3.1 Introduction

Geologic structures influence groundwater flow by altering the geometry and physical continuity of hydrogeologic units, by creating large-scale preferred pathways or barriers to flow related to hydrogeologic unit geometry and fault-zone hydraulic-conductivity structure, and by changing secondary porosity and hydraulic conductivity. Faults may tilt, bend, or sever aquifers, and juxtapose hydrogeologic units having contrasting hydraulic properties (e.g., Winograd and Thordarson, 1975; Faunt, 1997; Sweetkind and others, 2004; Dixon and others, 2007; Sweetkind and others, 2007). Faults and joints may increase hydraulic conductivity by providing connected flow pathways, whereas thick, fine-grained fault-zone materials, veins, and cement in fault cores form barriers to flow across their surfaces. Folds tilt stratigraphic units, changing the orientation of bedding planes and, therefore, the direction of hydraulic-conductivity anisotropy due to sedimentary layering and texture, and may induce tensional fractures or pressure-solution features in their hinge zones (Twiss and Moores, 1992, p. 314–321), all of which may direct flow parallel to the fold axis.

4.3.2 Faults

4.3.2.1 Juxtaposition of Hydrogeologic Units

Faults that juxtapose hydrogeologic units having contrasting hydraulic properties can significantly influence groundwater flow (e.g., Allan, 1989; Haneberg, 1995; Caine and Forster, 1999). Where the higher-hydraulic-conductivity unit is upgradient, groundwater flows vertically and/or laterally along the fault, depending on the distribution of hydraulic gradient and hydraulic conductivity in adjacent areas, toward zones having higher hydraulic conductivity. Groundwater that flows upward along the fault may emerge at the surface to form a spring if the head in the aquifer is at or above the local land-surface elevation, or across the fault where another aquifer is present on the opposite side. Where the fault zone forms a low-hydraulic-

conductivity barrier (section 4.3.2.2), similar patterns of groundwater flow and hydraulic gradient result. Where the higher-hydraulic-conductivity unit is downgradient, cross-fault flow is generally less restricted, subject to variations in the hydraulic conductivity of the fault zone itself, and the hydraulic gradient in the downgradient unit is lower. In both cases, the hydraulic gradient is steepest in and adjacent to the fault zone, where the contrast in hydraulic conductivity is abrupt.

The hydrogeologic units juxtaposed across major fault zones likely vary laterally and vertically. Pre-faulting structure and fault displacement vary along typical major fault planes, resulting in juxtaposition of different pairs of hydrogeologic units at different locations, producing spatially variable cross-fault hydraulic-conductivity contrasts (Allan, 1989; Haneberg, 1995; Caine and Forster, 1999). These variations in hydraulic-conductivity distribution likely result in complex patterns of hydraulic gradient and flow along and across fault zones. Large fault zones likely accommodate groundwater flow across their planes where relatively high-hydraulic-conductivity hydrogeologic units are on either side of the fault zone and where fault-zone fabrics and geometry do not form barriers to flow.

In the UGS study area, examples of major faults that may influence groundwater flow include range-bounding normal-fault zones, intrabasin normal faults, the Mountain Home thrust fault, the Sand Pass transverse fault zone, and the Snake Range decollement. These faults have sufficient displacement to juxtapose aquifer hydrogeologic units against confining hydrogeologic units, and likely have heterogeneous fault-zone structure and fabrics that affect groundwater flow (section 4.3.2.2).

Most range-bounding normal-fault zones in the study area juxtapose bedrock hydrogeologic units in their footwalls against coarse-grained basin-fill aquifers in their hanging walls. Hydraulic head is typically higher in the footwalls due to closer proximity to the high-elevation recharge zones, and lower in the hanging walls, so that the general hydraulic gradient is toward the valleys approximately normal to the topographic slope and to the strike of the normal-fault zones. The hydraulic-conductivity structure of the fault zones and distribution of hydrogeologic units may modify local flow directions. Examples include the normal-fault zones along both sides of the Snake Range, Limestone Hills, Schell Creek Range, and Fish Springs Range; along the eastern Deep Creek Range mountain front; and along the western Confusion Range (in northern Snake Valley), Mountain Home Range, House Range, Wah Wah Mountains, San Francisco Mountains, and Cricket Mountains mountain fronts (figure 4.2; plate 1). Most subsurface flow likely crosses the range-bounding normal-fault zones downgradient from areas of greatest precipitation (section 4.4) where the footwall is composed of carbonate-rock aquifer hydrogeologic units. Manning and Solomon (2005) provide geochemical evidence for flow from the mountain block to the basin-fill aquifer across the Wasatch fault zone, a major range-bounding normal-fault zone that forms the boundary between the Wasatch Range and the Salt Lake Valley basin, northern Utah.

The western boundary of the Confusion Range in northern Snake Valley strikes approximately normal to the regional hydraulic gradient (section 4.5). Cross section B–B′ (plate 2) shows that the middle Paleozoic siliciclastic-rock confining hydrogeologic unit dips west below Snake Valley, and crops out in a structurally complex fault-cored anticline-syncline pair in the western Confusion Range. This geometry likely restricts eastward groundwater flow from Snake Valley into the Confusion Range, and the range-bounding normal-fault zone may localize Twin Springs and Foote Reservoir Spring in east-central Snake Valley.

Cross sections by Rowley and others (2009, plate 2) provide examples of intrabasin normal faults below east-central Snake Valley, southern Snake Valley, Tule Valley, and northern Pine Valley that may influence groundwater flow. Where the intrabasin faults strike at a high angle to the regional hydraulic gradient (east-central Snake Valley and Tule Valley), groundwater flow may deviate from the direction of greatest hydraulic gradient toward the surface or laterally toward areas of higher hydraulic conductivity or lower hydraulic gradient. Where the intrabasin faults strike nearly parallel to the hydraulic gradient (southern Snake Valley, Pine Valley, and Wah Wah Valley), the faults may not substantially alter flow direction and may provide high-hydraulic conductivity flow paths (section 4.3.2.3).

The Mountain Home thrust fault in the northern Mountain Home Range places the lower Paleozoic carbonate-rock aquifer hydrogeologic unit and the tightly folded middle Paleozoic siliciclastic-rock confining hydrogeologic unit in its hanging wall over the upper Paleozoic carbonate-rock aquifer hydrogeologic unit in its footwall (plate 1; cross section B–B′, figure 7.4; Hintze and Best, 1987). North of the Mountain Home Range, the thrust fault and associated folds plunge north in the subsurface below southern Snake Valley, and the hydraulic gradient is to the north. The thrust faults and steeply dipping bedding likely provide highly transmissive pathways for south-to-north groundwater flow and the fault planes, bedding, and north-striking siliciclastic-rock confining hydrogeologic unit likely inhibit east-west groundwater flow.

The Sand Pass transverse fault zone in the southern Deep Creek Range juxtaposes the upper Paleozoic carbonate-rock hydrogeologic unit against quartzite and schist of the Cambrian-Proterozoic hydrogeologic unit (figure 4.2), a stratigraphic throw of about 28,000 feet (8500 m). Pre-fault structure here was likely complex, and the fault zone may also have accommodated transcurrent displacement of uncertain sense at some time in its history (Rowley, 1998). Between the southern Fish Springs Range and the northern House Range, the Sand Pass transverse fault zone is an accommodation zone between range-bounding normal-fault systems having opposite displacement directions, and has likely experienced normal, reverse, and strike-slip displacements during a protracted history. The Sand Pass transverse fault zone likely forms a high-hydraulic-conductivity pathway for generally east-west directed groundwater flow where the hydraulic gradient is close to parallel to the fault-zone strike.

Plume (1996) and Sweetkind and others (2007) interpreted the Snake Range decollement as a barrier to groundwater flow where it dips gently east in the subsurface east of the Snake Range. Where exposed, brittle and plastic fault-zone fabrics suggest that the decollement has low cross-fault transmissivity and may restrict recharge along the mountain front or upward flow of groundwater below the valley center. The subsurface geometry of the Snake Range decollement is not well known (Gans and others, 1985; McGrew, 1993; Gans and others, 1999), and Dixon and others (2007) and Rowley and others (2009) suggested that it does not project eastward below Snake Valley and is cut by range-bounding normal-fault zones that likely influence groundwater flow to a much greater degree.

4.3.2.2 Fault-Zone Geometry

Structural, paleoseismic, and seismic-reflection data show that range-bounding normal-fault zones in the Basin and Range and other continental rift zones throughout the world are not simple planar features, but consist of geometric segments up to tens of miles long separated by structurally complex boundary zones (figure 4.4) (de Polo and others, 1991; Faulds and Varga, 1998). For example, Machette and others (1991) divided the 240-mile-long (390 km) Wasatch fault zone (figure 2.1; figure 4.4a) into 10 geometric segments having trace lengths of 7 to 43 miles (11–69 km), and Bruhn and others (1987) divided the Salt Lake City segment of the Wasatch fault zone into 11 sections, 2 to 8 miles (3–13 km) long (figure 4.4b). The strike, dip, displacement vector, and rupture history typically vary among the segments and sections within a fault zone (Bruhn and others, 1987; Janecke, 1993).

Fault segments or sections intersect at segment- or section-boundary zones, characterized by dense, distributed faulting and folding oriented obliquely to the main fault zone (e.g., Bruhn and others, 1987, p. 338; Janecke, 1993, figure 2; Faulds and Varga, 1998). Normal-fault segment boundaries also typically intersect, or are cut by, faults that strike at a high angle to their planes (see examples in Bruhn and others, 1987, and Janecke, 1993). The central, straight to gently curved parts of some fault zones between segment-boundary zones are composed of multiple overlapping segments of limited lateral and vertical extent and irregular shape, separated by lenses of less-deformed rock (Kattenhorn and Pollard, 2001, figure 6). The major range-bounding normal-fault zones in the UGS study area likely have structure similar to the well-studied fault zones cited here and shown in figure 4.4.

The segmented, heterogeneous nature of fault zones along strike and within the fault plane suggests that their hydraulic-conductivity structure is highly variable for both cross-fault and fault-parallel groundwater flow, as confirmed by numerous studies (e.g., Bruhn and others, 1987; Faulds and Varga, 1998; do Nascimento and others, 2005; Zhang and others, 2011). For these reasons, segment-boundary zones and parts of some fault planes are areas of significant potential fault-parallel and cross-fault groundwater flow (Bruhn and others, 1987; Curewitz and Karson, 1997; Faulds and Varga, 1998; Kattenhorn and Pollard, 2001; Stewart, 2001; Hess and others, 2009; Bonson and others, 2012). In segment-boundary zones, dense fracture arrays oblique to the main fault planes and cross-cutting faults are potential pathways for cross-fault groundwater flow. Along the main fault planes, cross-fault groundwater flow may occur through lenses of less-deformed rock or where aquifers are juxtaposed.

4.3.2.3 Fault-Zone Fabrics

Fault zones are composed of a central core, which accommodates the majority of displacement between rock blocks, and adjacent damage zones on both sides of the core that are highly fractured but accommodate relatively little displacement (figure 4.4c) (Sibson, 1994; Caine and others, 1996; Bastesen and others, 2009; Faulkner and others, 2010). Core zones include fault gouge and breccia surrounding relatively undeformed blocks, small-displacement slip surfaces, and filled veins, depending on displacement history, rock type, and temperature, pressure, and presence of fluids during displacement (Sibson, 1994; Bastesen and others, 2009; Faulkner and others, 2010). Damage zones are composed chiefly of dense networks of joints and small-displacement faults (Caine and others, 1996). The geometry, relative volumetric proportions, and degree of development of damage and core zones are heterogeneous at all scales within a fault zone (Caine and others, 1996;

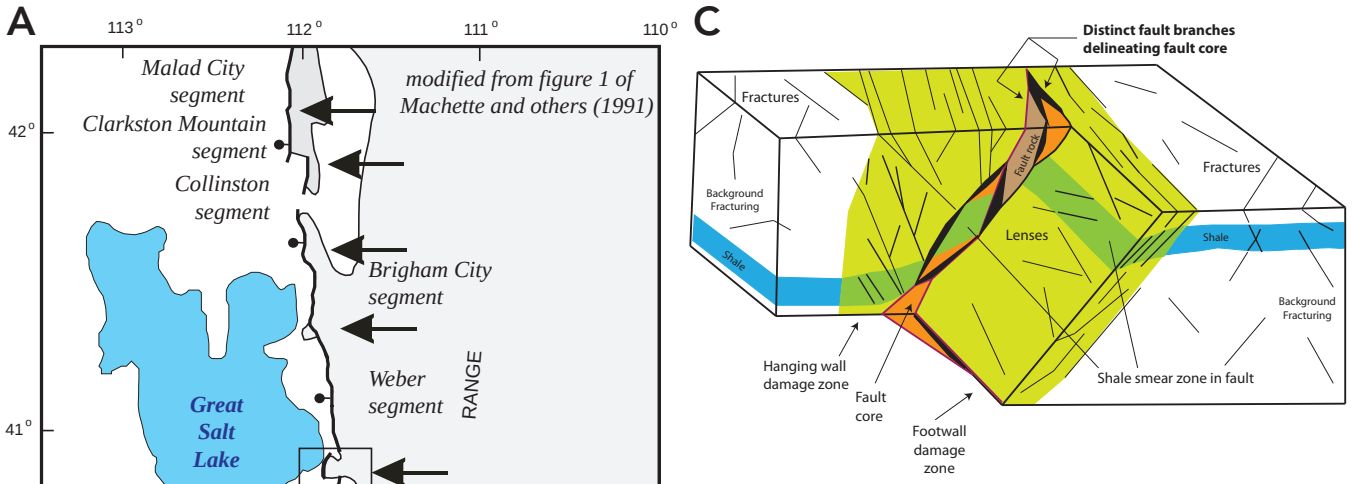

Figure 4.4. *Structural styles of range-bounding normal-fault zones in the Basin and Range Province, and general model of fault-zone structure. These examples illustrate the characteristic structural style of major normal fault zones, to provide models of the structural style and heterogeneity that likely characterize the range-bounding normal-fault zones in the UGS study area.* ***A.*** *Characteristic fault-zone structure at a scale of several hundred kilometers, as illustrated by the segments of the Wasatch fault zone, Utah (Machette and others, 1991, figure 1). The Wasatch fault zone is 240 miles (384 km) long and contains 10 segments that range from 7 to 43 miles (11–69 km) long. The segments overlap at their ends in structurally complex segment-boundary zones. See figure 2.1 for location.* ***B.*** *Characteristic fault-zone structure at a scale of several tens of miles. Fault sections of the Salt Lake City segment of the Wasatch fault zone, Utah, after Bruhn and others (1987, figure 2). The Salt Lake City segment includes 11 sections that overlap in structurally complex section-boundary zones, which form potential pathways for cross-fault groundwater flow.* ***C.*** *Characteristic fault-zone structure, as illustrated by a generic model of fault-zone structure, including fault core composed of very fine grained gouge and less-deformed lenses, and adjacent hanging-wall and footwall damage zones characterized by abundant slip surfaces and joints (Lindanger and others, 2007, figure 1). The fault cores are dominated by thick and physically continuous gouge, and impede cross-fault groundwater flow, whereas less-deformed lenses provide potential pathways for cross-fault flow. High fracture density in the damage zones permits fault-parallel groundwater flow.*

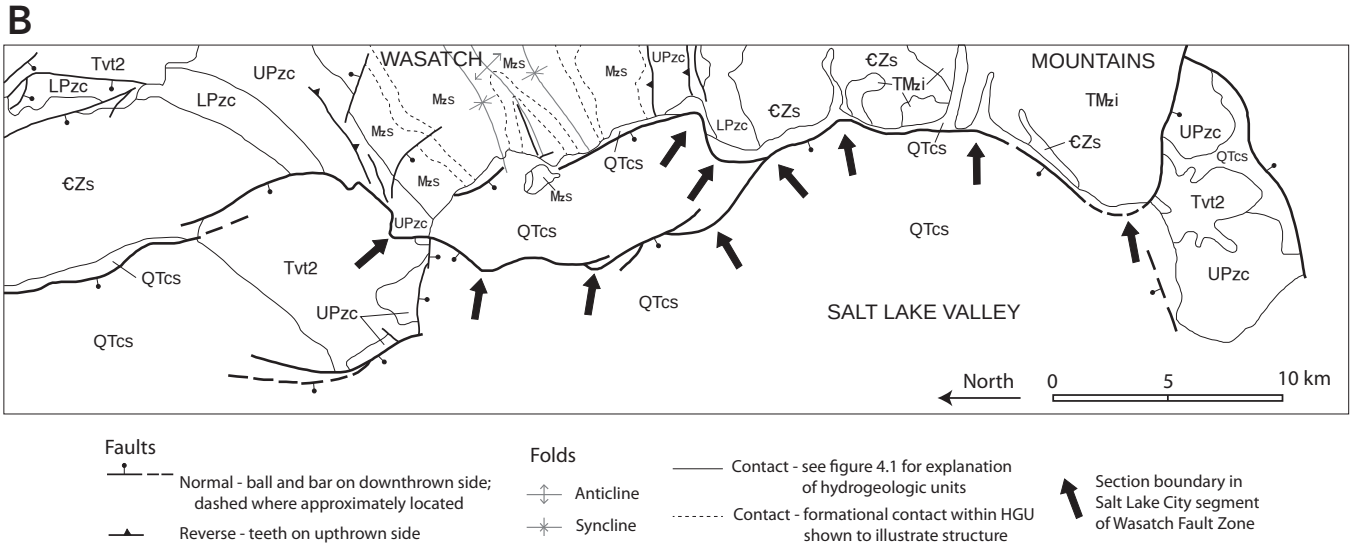

Bastesen and others, 2009; Faulkner and others, 2010). Most large-displacement fault zones likely impede cross-fault flow and enhance fault-parallel flow over much of their surfaces, but the natural heterogeneity of fault geometry and permeability structure described in the preceding paragraphs indicates that groundwater can cross fault zones in places. Due primarily to the extremely fine grain size and common presence of clay minerals in gouge, the hydraulic conductivity of fault cores may be as small as 1 x 10^{-6} times that of damage zones and undeformed rocks (Caine and others, 1996; Caine and Forster, 1999). Vein formation and/or cementation of the fault core by precipitation of minerals from fluids circulating along the fault plane would reduce or eliminate cross-fault permeability (Caine and Forster, 1999; Bastesen and others, 2009). Damage zones typically have substantially greater hydraulic conductivity than undeformed rock due to higher fracture density and absence of gouge (Caine and others, 1996; Caine and Forster, 1999).

The hydrogeologic implications of the nature and variation of fault-zone fabrics can be summarized as follows: (1) sections of faults having well-developed core zones form barriers to cross-fault flow, (2) sections of faults having poorly developed core zones may permit cross-fault flow, (3) well-developed damage zones form conduits for fault-parallel flow, and (4) each of these architectural variations may occur at different places within a large fault zone. Contrasts in hydraulic conductivity among fault core, damage zone, and relatively undeformed wall rock, and their geometry relative to the hydraulic gradient, largely control fluid-flow patterns along and across faults (Haneberg, 1995; Caine and Forster, 1999). For example, fault-parallel flow is favored where adjacent architectural elements have greatly contrasting hydraulic conductivities, whereas a fault having similar hydraulic properties to adjacent rocks may have little effect on groundwater flow (Haneberg, 1995; Caine and Forster, 1999).

The hydrogeologic character of a fault zone also depends on the lithology of the rock units it displaces. Faults that cut shale-rich formations may develop abundant clay-rich gouge and incorporate lenses of plastically deformed shale (figure 4.4c). This "shale smear" fault-zone structure forms reservoir seals in petroleum fields (e.g., Gibson, 1994), and would likely form a barrier to cross-fault groundwater flow. In the UGS study area, displacement of the middle Paleozoic siliciclastic-rock confining hydrogeologic unit likely forms shale smears in range-bounding normal-fault zones. Possible examples from Rowley and others (2009) include a west-side-down normal fault near the eastern margin of Snake Valley on their cross section X–X′, an east-side-down normal fault below Ferguson Desert on their cross section V–V′, and the normal fault that bounds the west side of the Mountain Home Range on their cross section U–U′.

4.3.2.4 State of Stress

The state of stress in a fault zone can influence groundwater flow by selectively widening the apertures of fractures oriented close to normal to the minimum horizontal principal stress direction (Sibson, 1994; Faulds and others, 2006; Faunt, 1997). In the Death Valley region, for example, extension and the minimum horizontal principal stress are oriented northwest-southeast, and steeply dipping, dominantly northeast-striking faults tend to transmit more groundwater than northwest-striking faults (Sweetkind and others, 2004; Faunt, 1997). The minimum horizontal principal stress is likely also northwest-southeast in our study area, parallel to measured values in the southern Wasatch Front, Nevada Test site, and central Nevada (Zoback, 1989; Smith and Arabasz, 1991). Steeply dipping, northeast-striking faults in the broader UGS study area may have greater permeability than faults in other orientations, though we are unaware of data that directly support this assumption.

4.3.3 Folds

The axial planes of folds are the loci of joints, faults, pressure-solution features, and veins due to high bending and shearing strains (Twiss and Moores, 1992, p. 314–321). Based on extensive well-field and structural data, Huntoon (1993) concluded that anticlinal hinge zones promote groundwater flow parallel to their axial planes due primarily to solution widening of joints and faults formed by bending tension. Another factor promoting flow parallel to the axial planes of folds may be that bedding generally strikes parallel to the axial planes, and hydraulic conductivity is typically greater parallel to bedding than normal to it in layered rocks, creating an overall anisotropic hydraulic-conductivity structure that favors flow parallel to axial planes.

UGS groundwater-monitoring site 11 is in the hinge zone of an anticline in the hanging wall of the Mountain Home thrust fault (chapter 7). Analyses of the aquifer-test results are inconclusive with respect to horizontal anisotropy of hydraulic conductivity in the upper Paleozoic carbonate-rock aquifer hydrogeologic unit. I assume that the axial planes of folds throughout the study area form relatively high-conductivity groundwater-flow pathways, due to the combination of transmissive joints parallel to the axial planes and greater hydraulic conductivity parallel to tilted bedding planes than perpendicular to them.

4.3.4 Other Geologic Features

4.3.4.1 Unconformities

Boreholes at UGS groundwater-monitoring sites 2, 4, 6, 10, 11, 15, 19, 21, and 23 penetrate the unconformity between alluvial-fan basin-fill deposits and underlying bedrock. The unconformity at all of these sites except 4 is near or below the water table. Bedrock formations are the Permian Arcturus Formation of the upper Paleozoic carbonate-rock aquifer hydrogeologic unit (UPzc) at sites 2, 6, 15, and 23, welded tuff of the middle volcanic-tuff hydrogeologic unit (Tvt2) at site 4, the Permian-Mississippian Ely Limestone of the upper Paleozoic carbonate-rock hydrogeologic unit at sites 10 and 11, the Silurian Laketown Dolomite(?) at site 21, and the Ordovician-Cambrian Notch Peak Formation at site 19, both of the lower Paleozoic carbonate-rock aquifer hydrogeologic unit. Drilling encountered substantial lost circulation problems at the unconformity in all of these boreholes, especially those that penetrate the Arcturus Formation, suggesting that significant transmissivity exists along the unconformity between alluvial fans and underlying aquifer hydrogeologic units in much of the study area. The high transmissivity probably results from a combination of the relatively coarse-grained texture of the alluvial-fan deposits and open fractures in the bedrock units due to weathering while they were exposed. Recharge and hydraulic connection between basin-fill and bedrock hydrogeologic units are likely high where alluvial-fan deposits overlie bedrock units. Results from the aquifer test at UGS groundwater-monitoring site 11 also suggest good hydraulic connection across the basin fill-bedrock unconformity (chapter 7). Where lakebed deposits overlie bedrock, silt and clay may fill the weathered fractures and the unconformity is not likely a significant hydrogeologic feature. Where volcanic rocks overlie bedrock, ash or flow rock may partially fill the weathered fractures, reducing their transmissivity.

4.3.4.2 Calderas

Along caldera margins, volcanic breccia and tuff deposits are typically poorly sorted, and shallow intrusive rocks, steeply dipping faults, and hydrothermal alteration may occur (Sweetkind and others, 2004; Dixon and others, 2007). All of these features reduce the hydraulic conductivity of rocks normal to their margins, and calderas are typically interpreted as barriers to groundwater flow (Plume, 1996; Sweetkind and others, 2004; Welch and others, 2007; SNWA, 2009a). The northern margin of the Indian Peak Caldera complex (figure 4.2 and plate 1) likely inhibits north-south groundwater flow, except where it is cut by north-striking faults.

4.4 Climate and Surface Water

The climate in west-central Utah and east-central Nevada is temperate and arid to semi-arid, with hot and dry summers punctuated by thunderstorms, and cold, moist winters (Houghton and others, 1975). In the valleys and foothills, summer temperatures range from 50 to 96 degrees Fahrenheit (10–30°C) and winter temperatures range from 12 to 44 degrees Fahrenheit (-7–7°C) (low and high average daily temperatures, respectively; Western Regional Climate Center, 2011). Because mean annual precipitation is relatively low and highly variable, and falls predominantly on the mountains, perennial streams and springs form relatively small and isolated, but important, surface-water resources (figure 4.5).

Precipitation in the study area comes mainly from Pacific storms in the winter and spring, and from Pacific or Gulf of Mexico storms in the summer (Western Regional Climate Center, 2011). Mean annual precipitation is about 6 to 7 inches per year (15–18 cm/yr) at valley-floor climate stations (figure 4.6) (Western Regional Climate Center, 2011) and about 13 to 30 inches per year (33–76 cm/yr) at mountain climate stations (figure 4.7) (U.S. Geological Survey, 2011). The PRISM model of precipitation distribution in the United States (Daly and others, 1994) projects mean annual precipitation of up to 38 inches per year (96 cm/yr) in the highest-elevation parts of the Schell Creek and southern Snake Ranges (figure 4.8). Annual precipitation varies substantially from year to year, as illustrated by statistics from Western Regional Climate Center (2011) data that show standard deviations of 23% to 39% at stations having long-term records (figure 4.6).

From the early 1980s to the early 2010s, annual precipitation in west-central Utah was above average during the early to mid 1980s and the mid to late 1990s, and in the 2010–2011 water year (figure 4.9). Annual precipitation was below average during the late 1980s, and much below average from 1999 to the early 2000s. A record driest year occurred during the 2011–2012 water year (figure 4.9).

Surface water includes perennial streams in the mountains and some mountain fronts, Pruess Lake reservoir, and wet playa surfaces including Sevier Lake and Salt Marsh Lake (figure 4.5). In Snake Valley, perennial streams are in the Deep Creek and Snake Ranges, where mean annual discharge varies from about 0.2 to 9.5 cfs, (6–269 L/sec) and seven streams have average discharge of more than 4 cfs (113 L/sec) (SNWA, 2008a). Pruess Lake is an impounded reservoir at the end of Lake Creek, 4 miles (6 km) south of Garrison, Utah. Surface water occurs intermittently on playa surfaces in southern and northern Spring Valley, northern Snake Valley, southern Great Salt Lake Desert,

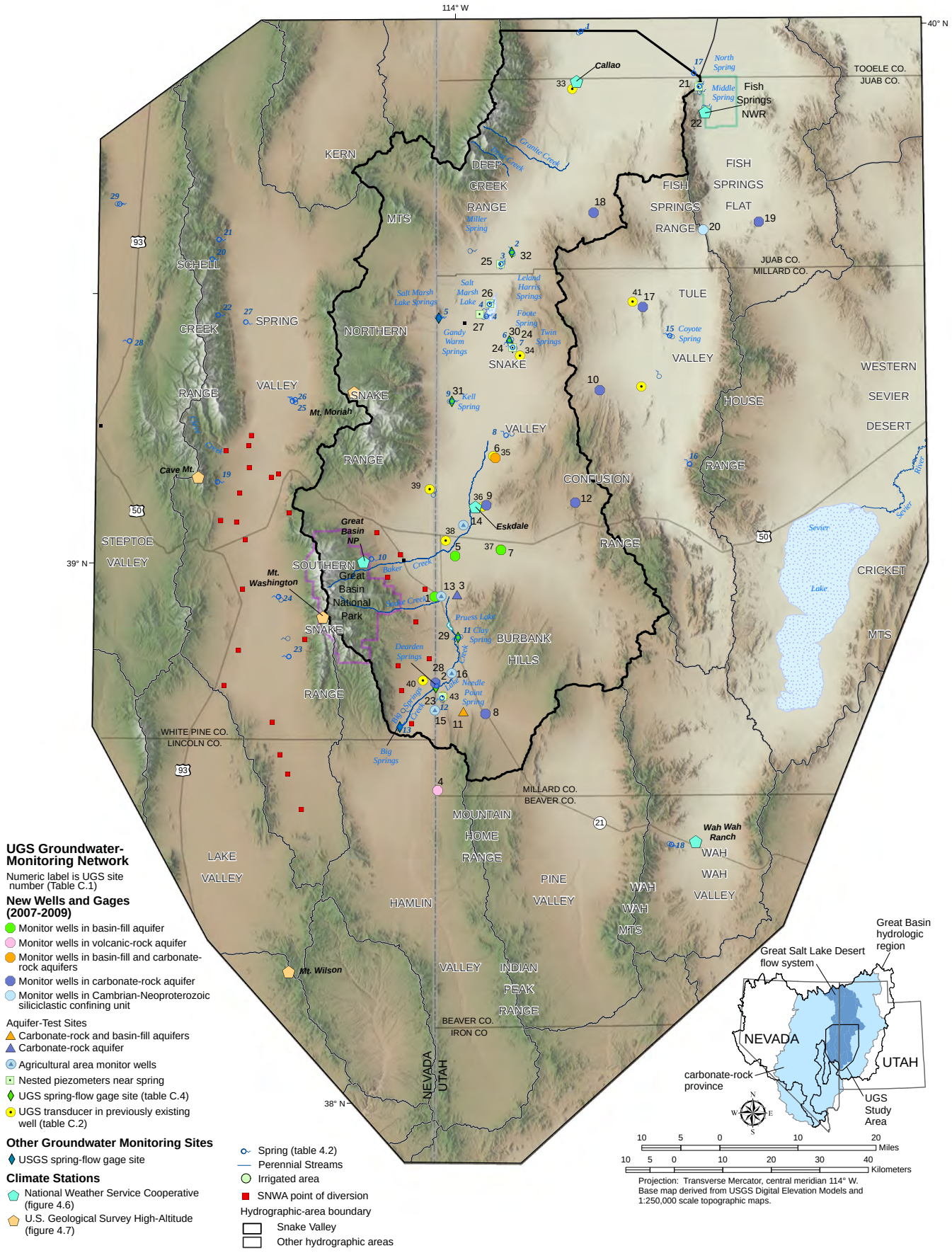

Figure 4.5. *Hydrologic setting of the UGS study area.*

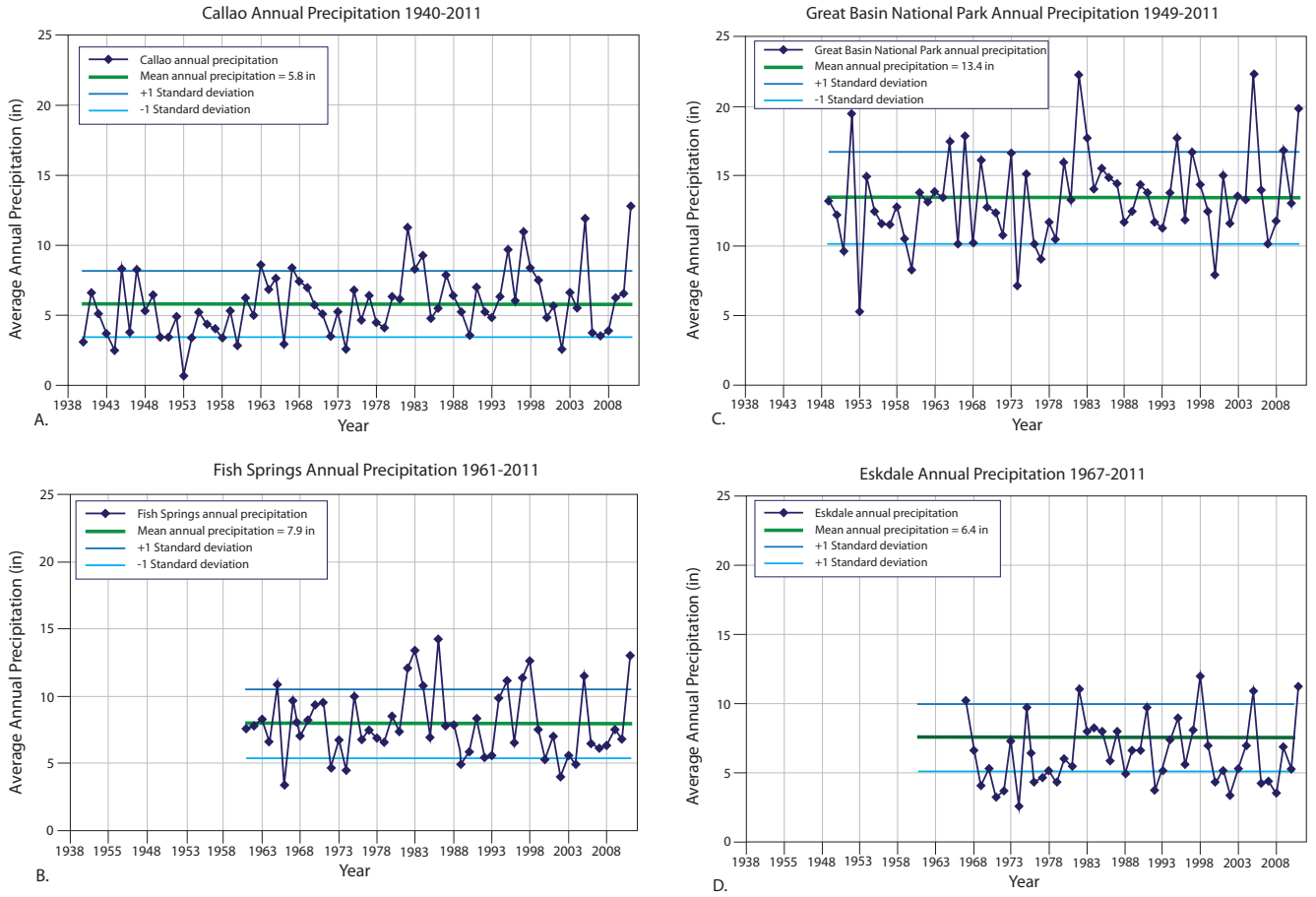

Figure 4.6. *Mean annual precipitation records from National Weather Service Cooperative Network climate stations in the UGS study area, accessed through the Western Regional Climate Center (http://www.wrcc.dri.edu/summary/Climsmut.html). A. Precipitation record for Callao station. B. Precipitation record for Fish Springs National Wildlife Refuge station. C. Precipitation record for Great Basin National Park station. D. Precipitation record for Eskdale station.*

central Tule Valley, northern Fish Springs Flat, and Sevier Lake (Welch and others, 2007; SNWA, 2008; Durbin and Loy, 2010).

4.5 GROUNDWATER

4.5.1 Occurrence and Movement

The vast majority of current groundwater use in the study area is from the basin-fill aquifer (Laczniak and others, 2007; U.S. Bureau of Land Management, 2012), but significant pressure exists for future groundwater development from the carbonate-rock aquifers (section 1.2). The carbonate-rock aquifer hydrogeologic units also transmit major quantities of groundwater in the mountain blocks, below low intermontane passes, and below the basin fill (Harrill and Prudic, 1998; Sweetkind and others, 2007; SNWA, 2009a). Volcanic-rock aquifers occur below the younger or older basin-fill deposits of Hamlin, Pine, and Wah Wah Valleys, and in mountain blocks in and adjacent to the Indian Peak caldera complex in the southern part of the study area (figure 4.2).

Figure 4.10 shows potentiometric-surface contours of groundwater, compiled from Wilson (2007), SNWA (2008), Gardner and others (2011), and Heilweil and Brooks (2011). Gardner and others (2011) presented water-level data from southern Spring, Snake, Pine, Wah Wah, and Tule Valleys and Fish Springs Flat from an extensive well-measurement campaign in March 2010, and contoured water levels from the basin-fill and carbonate-rock aquifers together. For areas not covered by Gardner and others (2011), figure 4.10 shows contours from Wilson (2007) in northern Spring, Steptoe, and Lake Valleys, and from Heilweil and Brooks (2011) in the mountain blocks. Heilweil and Brooks' (2011) mountain-block potentiometric-surface contours are based on the elevations of perennial streams and springs having discharge greater than 300 gallons per minute, which they assume are connected to the groundwater-flow system. Where the studies overlap, figure 4.10 shows the contours

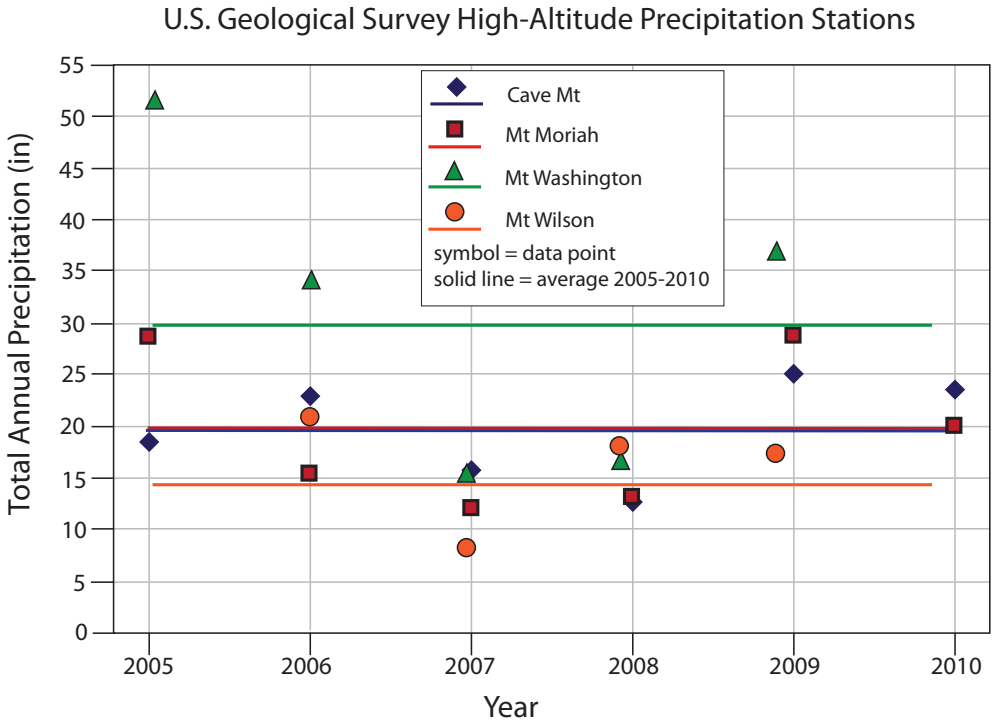

Figure 4.7. *Precipitation records from U.S. Geological Survey high-altitude climate stations in the UGS study area (http://wdr.water.usgs.gov/adrgmap/index.html).*

of Gardner and others (2011) instead of those from the other sources. Where contours from different studies intersect, (i.e., at the edges of the area contoured by Gardner and others [2011]), contours are slightly modified to produce smooth variations.

The potentiometric-surface contours from the four sources are generally consistent, especially near wells, but some important differences exist. Gardner and others (2011) and Heilweil and Brooks (2011) contoured water-level data from the three main aquifer types together, whereas Wilson (2007) and SNWA (2008) provided separate maps for water levels in the basin-fill and carbonate-rock aquifers. Gardner and others (2011) argued that combining potentiometric levels from the basin-fill, carbonate-rock, and volcanic-rock aquifers is valid based on available water-level data that suggest the aquifers are hydraulically connected over most of their study area. Groundwater levels, drilling data, and aquifer tests from our work (section 4.2) suggest that the basin-fill aquifer and the underlying carbonate- and volcanic-rock aquifer hydrogeologic units are hydraulically connected below the mountain fronts. The degree of hydraulic connection between the older basin-fill and carbonate-rock hydrogeologic units is presumably lower below the valley centers, where the older basin-fill aquifer is likely thick and has low hydraulic conductivity, than below the mountain fronts. The potentiometric surfaces in the basin-fill and carbonate-rock aquifers may diverge below the valley centers, but the difference cannot be predicted without water-level data. Data on the potentiometric-surface elevation in aquifers below 1000 feet (300 m) depth are sparse. Of the 271 wells used for data compilation from Gardner and others (2011) (which includes the UGS data) and Welch and others (2007) combined, only 12 are greater than 1000 feet (300 m) deep.

SNWA's (2008, appendices C and E) potentiometric-surface contours are generally similar to those in figure 4.10, except in the following areas. In central and northern Snake Valley, SNWA's (2008) 4400- to 4900-foot (1341–1493 m) contours are U-shaped, with the vertex convex-south to southwest and the eastern limb striking parallel to the eastern Snake Valley margin. In contrast, Gardner and others (2011) project their contours southeast into the Confusion Range. Part of this difference results from SNWA's (2008) approach of contouring water levels in the basin-fill aquifer separately from those in the carbonate aquifer, and part is due to their interpretation that groundwater does not readily move from the basin-fill aquifer in Snake Valley into the carbonate-rock aquifer in the Confusion Range.

SNWA (2008) does not show contours in the carbonate-rock aquifers east of Snake Valley, and closes the 5600-foot (1707 m) contour in northern Spring Valley, in contrast to Wilson (2007) who leaves the contour open on the north end facing Tippett Valley. This difference is consistent with the contrasting interpretations of the two studies on inter-

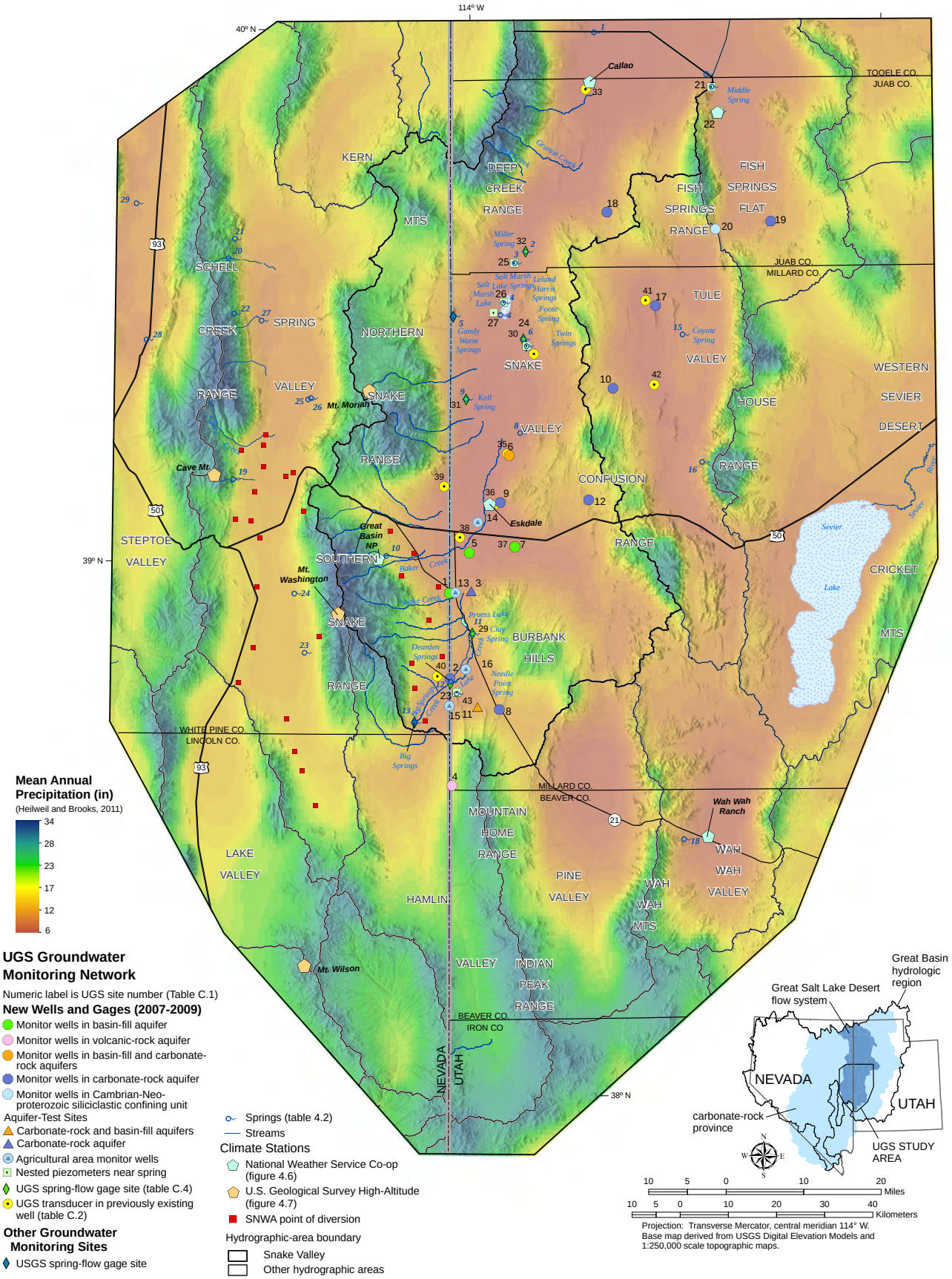

Figure 4.8. *Mean annual precipitation in the UGS study area, based on PRISM data (Daly and others, 1994, coverage from Heilweil and Brooks, 2011).*

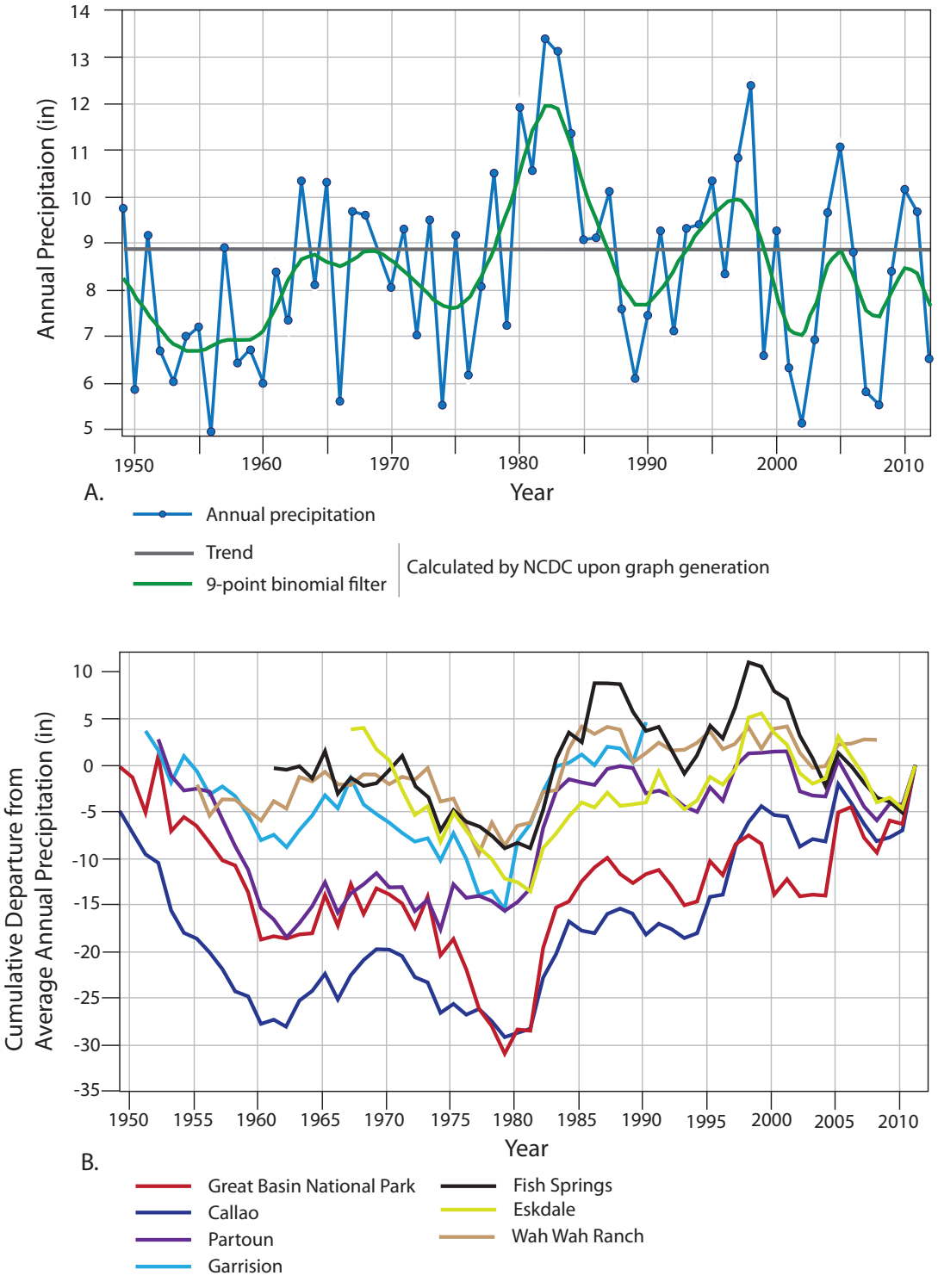

Figure 4.9. *A. Time-series precipitation plot for western Utah, 1949 to 2011, obtained online from the National Climatic Data Center (NCDC), accessed October 16, 2012. The plot can be reproduced using the following link: <http://www.ncdc.noaa.gov/temp-and-precip/time-series/index.php?parameter=pcp&month=12&year=2011&filter=ytd&state=42&div=1>. B. Cumulative departure from average annual precipitation, 1949 to 2011, for National Climatic Data Center Co-op climate stations in the study area, calculated from data obtained online at <http://www.wrcc.dri.edu/summary/Climsmut.html>. See figure 4.5 for station locations.*

basin flow from Spring to Tippett Valleys, which SNWA (2008, 2009a) discounts whereas Wilson (2007) favors.

SNWA's (2008) water-level contours in southern Steptoe Valley are U-shaped and convex-south, whereas Wilson (2007) projects the contours southeast into the southern Schell Creek Range. Potentiometric-surface contours in the carbonate-rock aquifer in the two studies contrast in a similar manner. SNWA (2008) discounts significant interbasin flow from southern Steptoe Valley to the south and southeast, whereas Welch and others (2007) interpret that major groundwater flow occurs out of southern Steptoe Valley to northern Lake Valley and southern Spring Valley.

Steep hydraulic gradients, expressed by closely spaced groundwater-level contours, occur along the eastern and western margins of central and southern Spring Valley, along the western margin of Snake Valley, in northwestern Tule Valley, and in central Pine Valley (figure 4.10). Steep hydraulic gradients below the Spring Valley, Snake Valley, and Steptoe Valley mountain fronts may result from the large difference in potentiometric-surface elevations between groundwater in the mountain blocks and that in the basin centers, or may reflect the presence of low-hydraulic-conductivity range-bounding normal-fault zones. In northwestern Tule Valley, the steep gradients may exist because basin-fill deposits are thin, so the groundwater is in rocks of the upper and lower Paleozoic carbonate-rock aquifer and middle Paleozoic siliciclastic confining unit hydrogeologic units. The hydraulic gradient and the dip direction are both east, so groundwater must flow across bedding planes and through the middle Paleozoic siliciclastic confining hydrogeologic unit, resulting in lower effective transmissivity compared to bedding-parallel flow through carbonate-rock aquifers or the basin fill. In central Pine Valley, water levels are several hundred feet deep and groundwater is likely in the older basin-fill and volcanic-rock hydrogeologic units, so the relatively steep gradients there likely reflect the lower hydraulic conductivity of these hydrogeologic units compared to that of the basin-fill and carbonate-rock aquifers. Low hydraulic gradients exist below central Snake Valley and central Tule Valley, where groundwater resides in relatively high-hydraulic conductivity basin-fill and carbonate-rock aquifer hydrogeologic units, respectively (Prudic and others, 1995; Halford and Plume, 2011).

4.5.2 Effects of Structures

The horizontal component of groundwater flow is parallel to the maximum hydraulic gradient (i.e., normal to the contour lines) in isotropic aquifers (Fetter, 1994, p. 153–155). Although this principle provides a reasonable guide to interpreting regional flow directions in the study area, exceptions may occur. Metamorphic rocks and/or intrusive bodies form low-permeability barriers to intermediate- to deep-level groundwater flow below the Snake Range, Deep Creek Range, and in the southern part of the study area (Plume, 1996, plate 1). These low-hydraulic-conductivity masses may divert groundwater flow around their margins, causing the flow direction to deviate from the maximum gradient direction (Harrill and Prudic, 1998, figure 8). Range-bounding normal-fault zones and the Sand Pass transverse fault likely form high-hydraulic-conductivity flow paths parallel to their strikes, and may divert groundwater flow away from the maximum gradient direction where the gradient direction and fault strike are not close to parallel, for example along the Spring and Snake Valley margins and in central Tule Valley.

Flow direction may deviate from the principal hydraulic-gradient direction where the bulk hydraulic-conductivity tensor is anisotropic (Fetter, 1994, p. 155), for example where a well-defined structural grain (i.e., predominant strike of faults, folds, and bedding) or significant lateral permeability contrast in aquifer materials exist (Ritzi and Andolsek, 1992; Zhang and Sanderson, 1995), a likely condition in much of the study area (Dixon and others, 2007; SNWA, 2009a; Durbin and Loy, 2010).

4.5.3 Water-Level Trends

The following paragraphs briefly summarize groundwater-level trends in the UGS groundwater-monitoring network and selected wells monitored by the U.S. Geological Survey through September 2013. Plate 3 presents hydrographs, and table C.1 presents completion and water-level data for these wells. The U.S. Geological Survey has measured groundwater levels in some wells in the UGS study area annually since 1980 or before. Plate 4 presents hydrographs and table C.3 presents completion and water-level data for these wells. Chapter 5 describes water-level trends and presents preliminary interpretations in terms of precipitation and groundwater pumping trends, for both sets of wells.

Monitoring wells within about 3 miles (4.8 km) of the approximate geographic centers of current agricultural pumping areas (figure 4.5) measure groundwater-level changes associated with groundwater pumping for irrigation, and include wells screened in the basin-fill and carbonate-rock aquifers. Depending on location, groundwater levels decline by less than one foot to 15 feet (4.6 m) during the pumping season and recover during the winter months (sites AG13–16, SG23, Snake Valley north MX, and Callao, plate 3). Annual groundwater levels in most piezometers in the agricultural-area sites declined steadily from the beginning of the period of record to winter 2010, and increased substantially during spring and summer

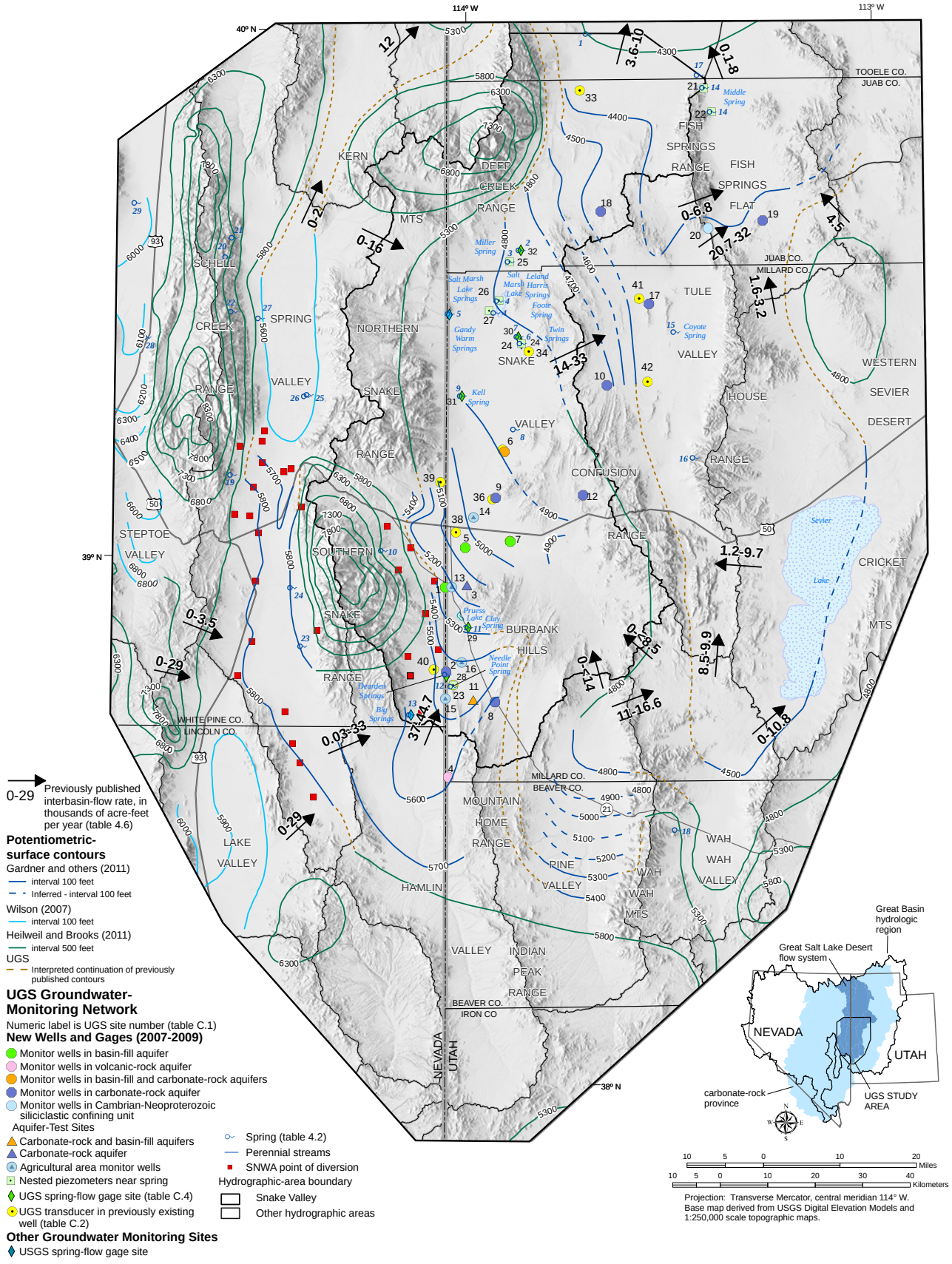

Figure 4.10. *Groundwater levels in the basin-fill and carbonate-rock aquifers in the study area, from Wilson (2007), SNWA (2009a), Gardner and others (2011), and Heilweil and Brooks (2011), and previously published interbasin flow-rate estimates in west-central Utah and east-central Utah (black arrows and associated labels). See table 4.6 for interbasin flow-estimate values and sources.*

2011. Higher runoff probably provided more recharge than in previous years, and the relatively wet, cool spring likely allowed pumps to be turned on later and used less than in previous years. Groundwater levels declined during summer and fall 2012, following the driest spring and summer on record in western Utah.

Spring-gradient sites consist of two or three nested piezometers, near ecologically and economically important springs, to measure the upward hydraulic gradient that feeds spring discharge. Evapotranspiration in nearby spring-fed wetlands causes groundwater levels in the spring-gradient site piezometers to fluctuate by 0.5 to 3 feet (0.15–0.9 m) seasonally, and no year-to-year change in water levels occurred between 2008 and 2011 (sites SG21–27, plate 3).

UGS groundwater-monitoring network sites in remote parts of the study area were designed to measure baseline groundwater conditions far from the effects of groundwater pumping and high evapotranspiration, and to better understand regional-scale flow within and between hydrographic areas. Wells are screened in the basin-fill, carbonate-rock, and volcanic-rock aquifers, and one is screened in the Lower Cambrian-Neoproterozoic siliciclastic-rock confining unit. Groundwater levels at most of these sites did not vary significantly from 2007 or 2008 to June 2012. Groundwater levels at sites on mountain fronts rose slightly in response to the high-precipitation winter of 2011–2012, whereas sites in the valley floors showed little or no change.

The U.S. Geological Survey has measured groundwater levels in some wells in the broader UGS study area annually since 1980 or before (plate 4; table C.3). Groundwater levels in nearly all of these wells rose during the middle to late 1980s in response to recharge from unusually high precipitation in 1982 through 1985, and declined gradually from the late 1980s or early 1990s through 2012. Groundwater levels in some wells rose in late 2010 and early 2011. Groundwater levels in wells in and near agricultural areas increased by up to 15 feet (4.6 m) during the middle 1980s, and declined to below 1980 levels by late 2010. In remote parts of Snake Valley, Tule Valley, Fish Springs Flat, and Wah Wah Valley, groundwater levels increased by three feet or less during the middle to late 1980s, and declined to near 1980 levels by the late 2000s.

4.5.4 Springs

Springs in the study area occur in mountain, mountain-front, and valley-floor settings, and their discharge ranges from seasonal seeps to 15 cfs (425 L/sec) (SNWA, 2008a; Durbin and Loy, 2010; U.S. Bureau of Land Management, 2012, appendix F3.3.1). Most springs are "cold" (temperature less than 21.1°C [70°F]), but several are "warm" (21.1 to 32.2°C [70–116°F) and two are "hot" springs (>32.2°C [116°F]; McGill Spring in Steptoe Valley and Wilson Health Springs in northern Fish Springs Flat) (SNWA, 2008). Table 4.2 lists springs in the study area having mean annual discharge greater than 0.11 cubic feet per second (50 gallons per minute [3 L/min]). The UGS monitors surface flow from five springs or spring complexes in the study area (chapter 5), including, from north to south, Miller Spring, Foote Spring, Twin Springs (north and south pools), Kell Spring, Clay Spring, and Dearden Springs. The elevations of non-perched springs help to constrain the potentiometric surface of their source aquifers, and spring-water chemistry provides important constraints on groundwater-flow paths (chapter 6).

Mountain springs are part of local-scale groundwater-flow systems, and are characterized by relatively low discharge, cold temperature, and low total-dissolved-solids (table 4.2; table D.1), compared to most mountain-front and valley-floor springs. Mountain springs typically occur where canyon walls intersect the local water table, where low-permeability strata impede downward flow (contact springs), or where faults juxtapose higher-permeability rocks or sediment upgradient against lower-permeability rocks or sediment downgradient (fault springs).

Mountain-front springs typically occur in the distal parts of alluvial fans, and are likely part of local-scale groundwater flow systems. Their catchment areas consist primarily of the mountain drainages that feed the alluvial fans in which the springs occur. Important exceptions include the Fish Springs complex, Gandy Warm Springs, and Big Springs, which are localized along range margins by major range-bounding normal-fault zones and whose sources include local and regional flow systems (chapter 6). Mountain-front springs in the UGS study area may be (1) localized by faults that juxtapose bedrock and unconsolidated deposits or unconsolidated deposits of contrasting hydraulic conductivity, (2) contact springs caused by progressive fining and thinning and consequent decreased transmissivity of the alluvial-fan deposits toward the valley floor; or (3) contact springs where the alluvial fan toe is cut by a pluvial shoreline.

Valley-floor springs in the UGS study area occur between the alluvial-fan toe and the valley axis, and the distance from the closest recharge areas suggests that they are fed by intermediate- to regional-scale flow systems. Some, such as the Leland Harris and Salt Marsh Lake complexes in Snake Valley, are contact springs where lakebed deposits are cut by erosional features related to lower lake levels or post-lake streams, and some, such as Twin and Foote Reservoir

Table 4.2. *Mean annual discharge estimates for selected springs in the UGS study area.*

Map #	Hydrographic Area	Spring	Discharge[1] afy	cfs	gpm	Source[5]	Temperature[8]	Geographic Setting	Structural Type[9]
1	Snake Valley	Redden Spring	516	0.71	**320**	e	Cold	Valley Floor	Contact
2	Snake Valley	Miller Spring	254	0.35	157	c	Cold	Valley Floor	Fault
3	Snake Valley	Leland Harris spring comlex	**17**	0.02	11	b	Cold	Valley Floor	Contact
4	Snake Valley	Salt Marsh Lake spring complex	**6,700**	9.25	4,154	b	Cold	Valley Floor	Fault
5	Snake Valley	Gandy Warm Springs	10,870	**15.00**	6,726	d	Warm	Mountain Front	Fault
6	Snake Valley	Foote Spring[2]	2,014	**2.78**	1,247	c	Cold	Valley Floor	Fault
7	Snake Valley	Twin Springs[2]	1,949	**2.69**	1,206	c	Cold	Valley Floor	Fault
8	Snake Valley	Knoll Springs	5 32	0.01 0.04	**3** 20	a b	Cold	Valley Floor	Fault
9	Snake Valley	Kell Spring	87	**0.12**	54	c	Cold	Mountain Front	Fault
10	Snake Valley	Rowland Spring	1,645	**2.27**	1,018	d	Cold	Mountain	Fault
11	Snake Valley	Clay Spring	239	**0.33**	148	c	Cold	Mountain Front	Fault
12	Snake Valley	Dearden Springs complex[3] (a.k.a. Stateline Springs)	4,464	**6.16**	2,762	c	Cold	Valley Floor	Fault
13	Snake Valley	Big Springs[4]	7,334 **6,700** 4,420	10.14 9.25 **6.10**	**4,547** 4,154 2,735	a b d	Cold	Mountain Front	Fault
14	Fish Springs Flat	Fish Springs complex	29,668 **22,334** 20,768	41.02 30.82 **28.66**	**18,393** 13,847 12,852	a[6] b[6] d[7]	Warm	Mountain Front	Fault
15	Tule Valley	Coyote Spring	**515**	0.71	319	b	Warm	Valley Floor	Fault
16	Tule Valley	Painter Spring	6	0.01	**4**	f	Cold	Mountain	Contact
17	Great Salt Lake Desert	Wilson Health Springs complex	163 **176**	0.23 0.24	**101** 109	a b	Hot	Valley Floor	Fault
18	Wah Wah Valley	Wah Wah Springs	**1,161**	1.60	720	b	Cold	Mountain Front	Fault
19	Spring Valley	Bastian Spring	**1,850**	2.55	1,147	b	Cold	Mountain Front	Contact
20	Spring Valley	Kalamazoo Creek Spring	**1,790**	2.47	1,110	b	Cold	Mountain	Contact
21	Spring Valley	Muncy Creek Spring	**1,617**	2.23	1,003	b	Cold	Mountain	Fault
22	Spring Valley	North Creek Spring	**1,609**	2.22	998	b	Cold	Mountain	Contact
23	Spring Valley	Minerva Spring	439	0.61	**272**	a	Cold	Valley Floor	Fault
24	Spring Valley	The Cedars	120	0.17	**75**	a	Warm	Mountain Front	Fault
25	Spring Valley	North Millick Spring	456	0.63	**283**	a	Cold	Valley Floor	Fault
26	Spring Valley	South Millick Spring	763	1.05	**473**	a	Cold	Valley Floor	Fault
27	Spring Valley	Keegan Spring	376	0.52	**233**	a	Cold	Valley Floor	Fault
28	Steptoe Valley	McGill Spring	7,636	10.56	**4,734**	a	Warm	Valley Floor	Fault
29	Steptoe Valley	Monte Neva Spring	1,047	1.45	**649**	a	Hot	Valley Floor	Fault

[1] Afy = acre-feet per year, cfs = cubic feet per second, gpm = gallons per minute. Value in boldface is reported by the source publication; values in regular font are converted from reported value
[2] Estimated Twin Springs discharge is the sum of average values from UGS gages downstream from the north and south pools. Estimated Foote Spring discharge is average of measurements made when no flow to irrigation pivot occurs.
[3] Estimated Dearden Springs complex discharge is the difference between values from gages upstream and downstream from the spring complex (chapter 5).
[4] U.S. Geological Survey gage is below confluence of streams from two spring heads.
[5] Data Sources
a) SNWA (2008a) b) Durbin and Loy (2010) c) UGS gage (<http://geology.utah.gov/databases/groundwater/map.php?proj_id=1>)
d) USGS gages (<http://wdr.water.usgs.gov/adrgmap/index.html>) e) Gates and Kruer (1981) f) Stephens (1977)
[6] Sum of values from gages at ten springs in complex.
[7] Sum of values from gages at seven springs in complex from U.S. Fish and Wildlife Service (2004, p. 16).
[8] Temperature: Cold - <21.1°C Warm - 21.1 to 32.2°C Hot - >32.2°C
[9] Based on SNWA (2008a), Kistinger and others (2009), and the senior author's interpretation from published geologic maps and field inspection.

springs in Snake Valley and Coyote Spring in Tule Valley, are localized by faults. Coyote and Dearden (also known as Stateline) Springs are unusual valley-floor springs because they are fault-localized springs that emanate from bedrock where it is juxtaposed against basin fill, a structural setting that is more typical of valley-margin springs.

Spring flow forms pools, streams, and wetlands, and most of this water is consumed by evapotranspiration; therefore spring flow is typically included in discharge estimates for groundwater-budget analysis of hydrographic basins (Prudic and others, 1995; Welch and others, 2007; SNWA, 2009a). The surface flow may be used for crop irrigation (for example, Foote Spring in Snake Valley) or stock watering (most springs in the study area), and/or the associated vegetation is used for grazing. All substantial springs in the study area have associated water rights (Snake Valley water rights are compiled in Appendix F3.3.2 of U.S. Bureau of Land Management, 2012).

Spring pools, outflow streams, and associated wetlands and riparian vegetation form habitat for a wide variety of wildlife species, including several listed as sensitive species by the Utah Division of Wildlife Resources (2011). Utah sensitive species include (1) those listed by the U.S. Fish and Wildlife Service as candidate, threatened, or endangered, (2) conservation agreement species, for which agreements are in place to preserve habitat and maintain populations in order to avoid Federal listing, and (3) species of concern, deemed as potential conservation species or potential candidates for Federal listing (Utah Division of Wildlife Resources, 2011). Spring-fed pools and streams form the only suitable habitat for the aquatic sensitive species in the study area—the least chub, Columbia spotted frog, northern leopard frog, and several species of spring snail. These species use the shallow vegetated margins of the wetland complexes for reproduction. Least chub use shallow vegetated areas to spawn, and Columbia spotted frogs attach egg masses to emergent vegetation in these areas. Even a slight reduction in surface-water elevation would cause significant negative impacts to these shallow habitats, and could short-circuit the life cycles of these two species (Utah Division of Wildlife Resources, 2011).

4.5.5 Groundwater Budgets

4.5.5.1 Introduction

Groundwater budgets are an accounting of the inflow (recharge) and outflow (discharge) of groundwater in a defined geographic area and aquifer system. The hydrogeologic studies summarized in section 1.4 quantify the groundwater budgets of hydrographic areas and, in some cases, regional flow systems, in parts of west-central Utah and east-central Nevada (tables 4.3 through 4.6). The typical goals of estimating groundwater budgets are to quantify the amount of developable groundwater in a hydrographic area (Gates and Kruer, 1981; Welch and others, 2007), and to provide input parameters for groundwater-flow models that characterize groundwater-flow systems and predict the potential impacts of pumping (Harrill and Prudic, 1998; Schaefer and Harrill, 1995; SNWA, 2009a; Loy and Durbin, 2010; Halford and Plume, 2011). Groundwater budgets include estimates of recharge from precipitation that falls within the hydrographic area and resultant runoff and base flow, and subsurface interbasin flow from adjacent hydrographic area(s). Discharge estimates include evapotranspiration and subsurface interbasin flow to adjacent hydrographic areas. The UGS study area contains few perennial streams, none of which cross hydrographic-area boundaries.

4.5.5.2 Recharge

Recharge to the aquifers in the study area is chiefly from in-place infiltration of precipitation and snowmelt in areas that receive more than 8 inches per year (20.3 cm/yr) long-term average annual precipitation (Maxey and Eakin, 1949; Prudic and others, 1995; Laczniak and others, 2007; SNWA, 2009a). Other important recharge sources include infiltration of runoff and base flow from stream channels where they cross alluvial fans, and irrigation return flow.

SNWA (2009a) and Durbin and Loy (2010) estimated recharge using "modified Maxey-Eakin" approaches, in which mean annual recharge is calculated as a function of mean annual precipitation. The percentage of annual precipitation that becomes recharge is expressed as a recharge coefficient, which increases with increasing precipitation. Recharge-efficiency coefficients are not well known, and are typically calibrated so that total recharge balances discharge within a hydrologically closed hydrographic area or flow system. SNWA (2009a, table 9–4) cited uncertainties of about 14% to 38% for the recharge estimates they calculated for the hydrographic areas in our study area.

The Basin Characterization Model (BCM) (Flint and Flint, 2007; Flint and others, 2011) estimates in-place recharge and runoff as functions of precipitation rate, snowmelt, sublimation, evapotranspiration, and temperature, all of which vary spatially and temporally, and of soil-storage capacity and bedrock hydraulic conductivity, which vary spatially. The minimum uncertainty of BCM recharge estimates is about 50% (Flint and others, 2011). The BCM method also includes estimates of runoff from the mountain block, about 10% to 15% of which recharges to the basin-fill aquifer (Laczniak and others, 2007; Heilweil

Table 4.3. *Recharge estimates in acre-feet per year for hydrographic areas in the UGS study area. Values are rounded to the nearest 100 acre-feet per year.*

Hydrographic Area	USGS Recon. [1]	USGS RASA[2]	BARCAS[3]	SNWA[4]	DOI[5]	USGS GBCAAS[6]
Snake Valley[a]	100,000	102,000	111,300	151,000	124,500	160,000
Tule Valley	7600	8000	n/a	n/a	8400	13,000
Fish Springs Flat	4000	4000	n/a	n/a	4,200	1600
Pine Valley	21,000	21,000	n/a	n/a	22,000	27,000
Wah Wah Valley	7000	7000	n/a	n/a	5400	6000
Spring Valley	75,000	75,000	93,100	81,300	75,400	110,000
Steptoe Valley	85,000	85,000	154,000	91,700	83,000	86,000

n/a value not estimated

Conceptual model studies: 1) Eakin and others (1967) and Gates and Kruer (1981) and references therein, 2) Harrill and others (1988), 3) Laczniak and others (2007) and references therein, 4) SNWA (2009a), 5) Durbin and Loy (2010), 6) Heilweil and Brooks (2011).

[a] Includes Snake Valley, Hamlin Valley, and Pleasant Valley hydrographic areas.

Table 4.4. *Groundwater discharge estimates in acre-feet per year for hydrographic areas in the UGS study area. Values are rounded to the nearest 100 acre-feet per year.*

Hydrographic Area	USGS Recon.[1]	USGS RASA[2,a]	BARCAS[3]	SNWA[4]	DOI[5,b]	USGS GBCAAS[6]
Snake Valley[c]	87,000	72,000	132,200	132,500	112,0000	130,000
Tule Valley	40,000	32,000	n/a	n/a	24,500	38,000
Fish Springs Flat	35,000	35,000	n/a	n/a	20,100	34,000
Pine Valley	7100	5000	n/a	n/a	5400	0
Wah Wah Valley	1500	n/a	n/a	n/a	1,300	1500
Spring Valley	70,000	n/a	75,600	75,400	82,000	82,000
Steptoe Valley	70,000	n/a	101,500	101,500	73,100	110,000

n/a value not estimated

Conceptual model studies: 1) Eakin and others (1967) and Gates and Kruer (1981) and references therein, 2) Prudic and others (1995), 3) Laczniak and others (2007) and references therein, 4) SNWA (2009a), 5) Durbin and Loy (2010), 6) Heilweil and Brooks (2011).

[a] Values reported here are from the RASA numerical model and cannot be directly compared to the recharge estimates from Harrill and others (1988) listed in table 4.3.
[b] Values reported here are the sum of groundwater ET and surface outflow (base flow) derived from groundwater (Durbin and Loy, 2010, table 3.1-1).
[c] Includes Snake Valley, Hamlin Valley, and Pleasant Valley hydrographic areas.

Table 4.5. *Difference between recharge and discharge estimates in acre-feet per year for hydrographic areas in the UGS study area. Values are rounded to the nearest 100 acre-feet per year.*

Hydrographic Area	USGS Recon.[1]	USGS RASA[a]	BARCAS[3]	SNWA[4]	DOI[5]	USGS GBCAAS[6]
Snake Valley[b]	13,000	-	(20,900)	18,500	12,500	30,000
Tule Valley	(32,400)	-	n/a	n/a	(16,100)	(23,000)
Fish Springs Flat	(31,000)	-	n/a	n/a	(15,900)	(32,400)
Pine Valley	13,900	-	n/a	n/a	16,600	27,000
Wah Wah Valley	5500	-	n/a	n/a	4100	4500
Spring Valley	5000	-	17,500	5900	(6600)	28,000
Steptoe Valley	15,000	-	52,500	(9800)	9900	(24,000)

n/a value not estimated – outside of study area

Conceptual model studies: 1) Eakin and others (1967) and Gates and Kruer (1981) and references therein, 3) Laczniak and others (2007) and references therein, 4) SNWA (2009a), 5) Durbin and Loy (2010), 6) Heilweil and Brooks (2011).

[a] Harrill and others (1988) estimated recharge but not discharge for individual hydrographic basins in the eastern Great Basin, whereas Prudic and others (1995) estimated discharge from their numerical groundwater flow model. The two quantities cannot be directly compared.
[b] Includes Snake Valley, Hamlin Valley, and Pleasant Valley hydrographic areas.

and Brooks, 2011). Recharge estimates using the BCM method are generally consistent with those from other methods except where carbonate rocks receive high annual precipitation (Welch and others, 2007, figure 23).

Recharge estimates for the hydrographic areas in the UGS study area by the four recent conceptual models of groundwater conditions (Flint and Flint, 2007; SNWA, 2009a; Durbin and Loy, 2010; Flint and others, 2011) are consistent within the uncertainty of the methods, except for Snake and Steptoe Valleys. The recharge estimates for Snake Valley of 151,000 acre-feet per year (186 hm^3/yr) by SNWA (2009a) and 160,000 acre-feet per year (197 hm^3/yr) by Heilweil and Brooks (2011) are 50 to 60% greater than the lowest of the previously published estimates (table 4.3). The recharge estimate for Steptoe Valley of 154,000 acre-feet per year (190 hm^3/yr) by Flint and Flint (2007) and Laczniak and others (2007) is 40% to 45% greater than other published estimates. Use of a relatively high hydraulic-conductivity value to calculate infiltration rate in the BCM (Flint and Flint, 2007; Flint and others, 2011) lead to greater estimates of in-place recharge compared to the recharge-efficiency coefficient in the modified Maxey-Eakin method, which does not account for variations in lithology.

4.5.5.3 Discharge

Discharge of groundwater from aquifers in the UGS study area occurs primarily through evapotranspiration (ET) by phreatophytic desert shrubs (Laczniak and others, 2007, figure 24; Moreo and others, 2007; SNWA, 2009a). Significant evapotranspiration from grassland, meadowland, and marshland environments also occurs. The vast majority of pumped groundwater is used for irrigation of cropland and is, therefore, consumed by evapotranspiration (Laczniak and others, 2007; SNWA, 2009a). Laczniak and others (2007, appendix A) estimated average annual groundwater pumping of about 35,000 acre-feet (43 hm^3) in Snake Valley, 17,500 acre-feet (22 hm^3) in Spring Valley, and 25,000 acre-feet (31 hm^3) in Steptoe Valley. SNWA (2009b, table C-5) estimated average annual groundwater pumping of about 21,881 acre-feet (27 hm^3) in Snake Valley, 5,390 acre-feet (6.7 hm^3) in Spring Valley, and 11,373 acre-feet (14 hm^3) in Steptoe Valley. Reported uncertainties for discharge estimates for the hydrographic areas in our study area range from 10% to 38% (Zhu and others, 2007; SNWA, 2009a). Discharge estimates from the four recent conceptual models of groundwater conditions (Laczniak and others, 2007; SNWA, 2009a; Durbin and Loy, 2010; Heilweil and Brooks, 2011) are consistent within the reported uncertainty of the methods.

4.5.5.4 Groundwater Budgets and Interbasin Flow

Water-budget analysis can be used to identify hydrographic areas that are likely sources or sinks for interbasin flow. Heilweil and Brooks (2011) noted that the uncertainty of water-budget estimates for individual hydrographic areas makes quantifying interbasin flow tenuous, and concluded that interbasin flow can be interpreted only for hydrographic areas for which the difference between recharge and discharge estimates is greater than 30%. In the UGS study area, the difference between recharge and discharge estimates is substantially greater than 30 % for Pine Valley, Wah Wah Valley, Tule Valley, and Fish Springs Flat in all five published studies listed in tables 4.3 through 4.5. Pine and Wah Wah Valleys have excess recharge and are likely sources for interbasin flow, whereas Tule Valley and Fish Springs Flat have excess discharge and likely receive interbasin flow from other hydrographic areas. The excess discharge in Tule Valley and Fish Springs Flat combined exceeds the excess recharge in Pine and Wah Wah Valleys combined by about 11,000 to 44,000 acre-feet per year (13.6–54.3 hm^3/yr). This excess discharge must be supplied by interbasin flow from Snake Valley and/or from other upgradient hydrographic areas east of the study area.

Published estimates of recharge and discharge are highly variable for Snake, Spring, and Steptoe valleys (tables 4.3 through 4.5). In most studies, the difference between recharge and discharge in these three hydrographic areas is less than 30%, with the exceptions of Laczniak and others (2007) for Steptoe Valley and Heilweil and Brooks (2011) for Spring Valley. The residuals estimated by Heilweil and Brooks (2011) for Snake Valley, Laczniak and others (2007) for Spring Valley, and Eakin and others (1967) and Heilweil and Brooks (2011) for Steptoe Valley are between 20% and 30%, suggesting that they are potential candidates for interbasin flow pending more accurate water-budget analyses. The difference between recharge and discharge estimates in the five studies varies substantially for each of these hydrographic areas (table 4.5), suggesting that the water budgets for these hydrographic areas are difficult to estimate but could be improved by additional work.

Table 4.6 and figure 4.10 show estimates of interbasin-flow rates among the hydrographic areas in west-central Utah and east-central Nevada from recent conceptual and numerical groundwater-flow models. The range of estimated flow rates reflects the relatively high level of uncertainty in quantifying interbasin flow, due to the uncertainty in estimates of recharge and discharge for hydrographic areas, and the lack of water-level data from the bedrock aquifers near the hydrographic-area boundaries. Recently published numerical groundwater-flow models provide estimates of interbasin-flow rates across some of the hydrographic-area

Table 4.6. *Estimated interbasin groundwater-flow rates in acre-feet per year, through selected hydrographic-area boundaries in the UGS study area.*

Hydrographic Areas	USGS Reconnaissance[1]	USGS RASA[2] Conceptual Model	USGS RASA[2] Numerical Model	BARCAS[3]	SNWA[4]	DOI[5]
Southern Spring Valley to southern Snake Valley	4000	4000	?	33,000	5700	300
Northern Spring Valley to northern Snake Valley	0	0	0	16,000	0	0
Northern Hamlin Valley to southern Snake Valley	0	?	?	37,000	44,700	37,600
Central Snake Valley to Tule Valley	24,000	22,000 or 33,000	14,000	29,000 - w	15,000[x]	17,200
Northern Snake Valley to Great Salt Lake Desert	10,000	10,000 - v	?	w	11,500[x]	3600
Tule Valley to Fish Springs Flat	32,000[q]	27,000	21,300	n/a	n/a	20,700
Northern Snake Valley to Fish Springs Flat	0	?	6800	n/a	n/a	0
Pine Valley to Wah Wah Valley	14,000 - r	11,000 - t	?	n/a	n/a	16,600
Pine Valley to Snake Valley	r	t	?	n/a	n/a	0
Wah Wah Valley to Tule Valley	8500 – s1 – s2	8500 – u1 – u2	9000	n/a	n/a	9900
Wah Wah Valley to Snake Valley	s1	u1	0	n/a	n/a	0
Wah Wah Valley to western Sevier Desert	s2	u2	0	n/a	n/a	10,800
Western Sevier Desert to Tule Valley	n/a	9000	1200	n/a	n/a	9700
Western Sevier Desert to Fish Springs Flats	n/a	?	1600	n/a	n/a	3200
Fish Springs Flat to Great Salt Lake Desert	<0.1	v	?	n/a	n/a	8000
Dugway/Government Creek to Fish Springs Flat	n/a	?	4500	n/a	n/a	n/a
Southern Steptoe Valley to southern Spring Valley	0	0	0	n/a	n/a	5000
Southern Steptoe Valley to Lake Valley	0	0	0	18,900	0	0
Lake Valley to southern Spring Valley	0	0	0	29,000	0	0

n/a interbasin flow value not estimated – outside of study area
? interbasin flow assumed to occur but not quantified

Conceptual model studies: 1) Eakin and others (1967) and Gates and Kruer (1981) and references therein, 2) Harrill and others (1988) (conceptual) and Prudic and others (1995) (numerical) 3) Laczniak and others (2007) and references therein, 4) SNWA (2009a, table I-2), 5) Durbin and Loy (2010, table 3.1-1).

The reports cited in this table treat the hydrographic-area boundary between Snake and Hamlin Valleys differently. The USGS reconnaissance and RASA reports did not distinguish Snake and Hamlin Valleys as separate hydrographic basins and, therefore, did not provide separate water-budget estimates for Hamlin Valley. Laczniak and others (2007) sub-divided Snake Valley into sub-basins, but their sub-basin boundaries do not coincide with the hydrographic-area boundary delineated by the Nevada State Engineer. The value of interbasin flow from northern Hamlin to southern Snake Valley cited here is the sum of their estimate of interbasin flow from southern Spring Valley to northern Hamlin Valley and the excess recharge in their sub-basin 5 of Snake Valley, which occupies the southern half of Hamlin Valley. SNWA (2009a) and Loy and Durbin (2010) provided interbasin flow-rate estimates for northern Hamlin Valley to southern Snake Valley across the hydrographic-area boundary.

[q] Estimated total outflow from Tule Valley was 32,000 afy; relative proportion to Fish Springs Flats and northern Snake Valley not specified.
[r] Estimated total outflow from Pine Valley was 14,000 afy; relative proportion to Wah Wah Valley (14,000-r) and east-central Snake Valley (r) not specified.
[s] Estimated total outflow from Wah Wah Valley was 8500 afy; relative proportions to Tule Valley (8500-s1-s2), east-central Snake Valley (s1), and Sevier Desert (s2) not specified.
[t] Estimated total outflow from Pine Valley was 11,000 afy; relative proportion to Wah Wah Valley (11,000-t) and east-central Snake Valley (t) not specified.
[u] Estimated total outflow from Wah Wah Valley was 8500 afy; relative proportions to Tule Valley (8500-u1-u2), east-central Snake Valley (u1), and Sevier Desert (u2) not specified.
[v] Estimated total inflow to southern Great Salt Lake Desert was 10,000 afy; relative proportions from Snake Valley (10,000-v) and Fish Springs Flat (v) not specified.
[w] Estimated total outflow from central and northern Snake Valley was 29,000 afy; relative proportions to Tule Valley (29,000-w) and Great Salt Lake Desert (w) not specified.
[x] Values are from table 8-1 of SNWA (2009a). In SNWA (2009a, table I-7), the estimated total outflow from Snake Valley was 24,000 afy; relative proportions to Tule Valley and southern Great Salt Lake Desert not specified.

boundaries of interest in this study (table 4.6; figure 4.10) (SNWA, 2009a; Durbin and Loy, 2010). These rates are based largely on water-budget analyses, so depend on the accuracy of recharge and discharge estimates. The water-budget analyses in these models cover many hydraulically connected hydrographic areas, and interbasin-flow rates are balanced with respect to the water budgets of each hydrographic area and the entire model area. Lundmark and others (2007) derived their interbasin-flow rates using a spreadsheet solver that included water-budget estimates for all of the hydrographic areas in their study area, and minimized the total uncertainty.

All of the studies cited here agree that discharge by spring flow and evapotranspiration in Tule Valley and Fish Springs Flat is supported by interbasin flow from adjacent hydrographic areas, though flow-rate estimates vary. General agreement exists that some interbasin flow occurs (1) from southern Spring Valley to northern Hamlin Valley, (2) from Snake Valley to Tule Valley and to the southern Great Salt Lake Desert, (3) from Tule Valley, western Sevier Desert, and Dugway/Government Creek Valley into Fish Springs Flat, (4) from northern Pine Valley to northern Wah Wah Valley, and (5) from northern Wah Wah Valley to Tule Valley and/or western Sevier Desert. Consensus does not exist regarding interbasin flow paths on figure 4.10 and table 4.6 having a zero lower estimate.

The most controversial proposed interbasin flow paths are from southern Steptoe Valley to southern Spring Valley and Lake Valley, and from Lake Valley to southern Spring Valley (Laczniak and others, 2007; Lundmark and others, 2007; SNWA, 2009a). About two thirds of the flow from Lake Valley to southern Spring Valley proposed by Laczniak and others (2007) and Lundmrk and others (2007) represents "pass-through" flow from southern Steptoe Valley. As noted in section 4.5.4, the high interbasin flow-rate estimates from southern Steptoe Valley from the BARCAS study (Flint and Flint (2007; Laczniak and others, 2007; Lundmark and others, 2007) result from a high recharge-rate estimate for the southern Egan and Schell Creek Ranges, which bound Spring Valley and are composed of the carbonate-rock aquifer hydrogeologic units. Re-evaluation of the BCM model for this area (Heilweil and Brooks, 2011) and estimates using modified Maxey-Eakin methods by SNWA (2009a) and Durbin and Loy (2010) (tables 4.3 through 4.5) suggest that recharge and discharge rates in southern Steptoe Valley are more closely in balance and, therefore, that substantially less interbasin flow occurs from southern Steptoe Valley to Lake Valley and southern Spring Valley than Flint and Flint (2007), and Lundmark and others (2007) proposed.

4.6 CHAPTER 4 REFERENCES

Allan, U.S., 1989, Model for hydrocarbon migration and entrapment within faulted structures: American Association of Petroleum Geologists Bulletin, v. 73, p. 803–811.

Bastesen, E., Braathen, A., Nottveit, H., Gabrielsen, R.H., and Skar, T., 2009, Extensional fault cores in micritic carbonate—case studies from the Gulf of Corinth, Greece: Journal of Structural Geology, v. 31, p. 403–420.

Belcher, W.R., editor, 2004, Death Valley regional groundwater flow system, Nevada and California—hydrogeologic framework and transient ground-water flow model: U.S. Geological Survey Scientific Investigations Report 2004-5205.

Belcher, W.R., Elliot, P.E., and Geldon, A.L., 2001, Hydraulic-property estimates for use with a transient ground-water flow model of the Death Valley regional ground-water flow system, Nevada and California: U.S. Geological Survey Water-Resources Investigations Report 01-4120, 28 p.

Best, M.G., Christiansen, E.H., and Blank, R.H., Jr., 1989, Oligocene caldera complex and calc-alkaline tuffs and lavas of the Indian Peak volcanic field, Nevada and Utah: Geological Society of America Bulletin, v. 101, p. 1076–1090.

Best, M.G., and Christiansen, E.H., 1991, Limited extension during peak Tertiary volcanism, Great Basin of Nevada and Utah: Journal of Geophysical Research, v. 96, p. 13509–13528.

Bonson, C.G., Walsh, J.J., and Carboni, V., 2012, The role of faults in localizing mineral deposits in the Irish Zn-Pb orefield: Structural Geology and Resources, Australian Institute of Geologists, v. 56, p. 8–11.

Bruhn, R.L., Gibler, P.R., and Parry, W.T., 1987, Rupture characteristics of normal faults—an example from the Wasatch fault zone, Utah, *in* Coward, M.P., Dewey, J.F., and Hancock, P.L., editors, Continental extensional tectonics: Geological Society Special Publication 28, p. 337–353.

Caine, J.S., Evans, J.P., and Forster, C.B., 1996, Fault zone architecture and permeability structure: Geology, v. 24, p. 1025–1028.

Caine, J.S., and Forster, C.B., 1999, Fault zone architecture and fluid flow—insights from field data and numerical modeling, *in* Haneberg, W.C., Mozley, P.S., Moore, J.C., and Goodwin, L.B., editors, Faults and subsurface fluid flow in the shallow crust: American

Geophysical Union Geophysical Monograph 113, p. 101–127.

Carlton, S.M., 1985, Fish Springs multibasin flow system, Nevada and Utah: University of Nevada-Reno, M.S. thesis, 103 p.

Curewitz, D., and Karson, J.A., 1997, Structural settings of hydrothermal outflow—fracture permeability maintained by fault propagation and interaction: Journal of Volcanology and Geothermal Research, v. 79, p. 149–168.

Daly, C., Neilson, R.P., and Phillips, D.L., 1994, A statistical-topographic model for mapping climatological precipitation over mountainous terrain: Journal of Applied Meteorology, v. 33, p. 140–158.

dePolo, C.M., Clark, D.G., Slemmons, D.B., and Ramelli, A.R., 1991, Historical surface faulting in the Basin and Range province, western North America—implications for fault segmentation: Journal of Structural Geology, v. 13, p. 123–136.

Dettinger, M.D., Harrill, J.R., Schmidt, D.L., and Hess, J.W., 1995, Distribution of carbonate-rock aquifers and the potential for their development, southern Nevada and parts of Arizona, California, and Utah: U.S. Geological Survey Water-Resources Investigations Report 91-4146, 100 p.

Dixon, G.L., Rowley, P.D., Burns, A.G., Watrus, J.M, and Ekren, E.B., 2007, Geology of White Pine and Lincoln Counties and adjacent areas, Nevada and Utah—the geologic framework of regional groundwater flow systems: Las Vegas, Southern Nevada Water Authority, HAM-ED-001, variously paginated. Available *in* Southern Nevada Water Authority, 2008, Baseline characterization report for Clark, Lincoln, and White Pine Counties Groundwater Development Project, *in* U.S. Bureau of Land Management, 2012, Clark, Lincoln, and White Pine Counties Groundwater Development Project Final Environmental Impact Statement: FES 12-33, Document BLM/NV/NV/ES/11-17+1793.

do Nascimento, A.F., Lunn, R.J., and Cowie, P.A., 2005, Modeling the heterogeneous hydraulic properties of faults using constraints from reservoir-induced seismicity: Journal of Geophysical Research, v. 110, B09201, doi:10.1029/2004JB003398.

Dong, W., and Halford, K.J., 2010, Analysis of water level fluctuations from pumpage for irrigation during multiple drought years in Snake Valley, HA195, near Baker, NV: Online, http://nevada.usgs.gov/water/aquifertests/snake_valley_n.cfm?studyname=snake_valley_n, 18 p., June 4, 2013.

Dong, W., Naranjo, R.C., and Halford, K.J., 2011, Analysis of water level fluctuations from pumpage for irrigation during multiple drought years in Snake Valley, HA195, near Needle Point and south of Garrison, Utah: Online, http://nevada.usgs.gov/water/aquifertests/Snake_needle_point.cfm?studyname=Snake_needle_point, 16 p., accessed June 4, 2013.

Durbin, T., and Loy, K., 2010, Development of a groundwater model, Snake Valley region, eastern Nevada and western Utah: U.S. Department of the Interior: Online, http://www.blm.gov/ut/st/en/prog/more/doi_groundwater_modeling.html, accessed July 2, 2010.

Eakin, T.E., 1966, A regional interbasin ground-water system in the White River area, southeastern Nevada: Water Resources Research, v. 2, p. 251–271.

Eakin, T.E., Hughes, J.L., and Moore, D.O., 1967, Water-resources appraisal of Steptoe Valley, White Pine and Elko Counties, Nevada: Nevada Department of Conservation and Natural Resources, Water Resource Reconnaissance Series Report 42, 62 p.

Faulds, J.E., Coolbaugh, M.F., Vice, G.S., and Edwards, M.L., 2006, Characterizing structural controls of geothermal fields in the northwestern Great Basin—a progress report: Geothermal Resources Council Transactions, v. 30, p. 69–76.

Faulds, J.E., and Varga, R.J., 1998, The role of accommodation and transfer zones in the regional segmentation of extended terranes, *in* Faulds, J.E., and Stewart, J.H., editors, Accommodation zones and transfer zones—the regional segmentation of the Basin and Range Province: Boulder, Colorado, Geological Society of America Special Paper 323, p. 1–45.

Faulkner, D.R., Jackson, C.A.L., Lunn, R.J., Schlische, R.W., Shipton, Z.K., Wibberly, C.A.J., and Withjack, M.O., 2010, A review of recent developments concerning the structure, mechanics, and fluid flow properties of fault zones: Journal of Structural Geology, v. 32, p. 1557–1575.

Faunt, C.C., 1997, Effect of faulting on ground-water movement in the Death Valley region, Nevada and California: U.S. Geological Survey Water-Resources Investigations Report 95-4132, 42 p.

Fenelon, J.M., Sweetkind, D.S., and Laczniak, R.J., 2010, Groundwater flow systems at the Nevada Test Site, Nevada—a synthesis of potentiometric contours, hydrostratigraphy, and geologic structures: U.S. Geological Survey Professional Paper 1771, 54 p.

Fetter, C.W., 1994, Applied hydrogeology: New York, Macmillan College Publishing Company, 691 p.

Flint, A.L., and Flint, L.E., 2007, Application of the Basin Characterization Model to estimate in-place recharge and runoff potential in the Basin and Range carbonate-rock aquifer system, White Pine County, Nevada, and adjacent areas in Nevada and Utah: U.S. Geological Survey Scientific Investigations Report 2007-5099, 20 p.

Flint, A.L., Flint, L.E., and Masbruch, M.D., 2011, Appendix 3: Input, calibration, uncertainty, and limitations of the Basin Characterization Model, *in* Heilweil, V.M., and Brooks, L.E., editors, 2011, Conceptual model of the Great Basin carbonate and alluvial aquifer system: U.S. Geological Survey Scientific Investigations Report 2010-5193, p. 149-163.

Gans, P.B., Miller, E.L., McCarthy, J., and Ouldcott, M.L., 1985, Tertiary extensional faulting and evolving ductile-brittle transition zones in the northern Snake Range and vicinity—New insights from seismic data: Geology, v. 13, p. 189-193.

Gans, P.B., Miller, E.L., and Lee, J., 1999, Geologic map of the Spring Mountain Quadrangle, Nevada: Nevada Bureau of Mines and Geology Field Studies Map 18, scale 1:24,000.

Gardner, P.M., Masbruch, M.D., Plume, R.W., and Buto, S.G., 2011, Regional potentiometric surface map of the Great Basin carbonate and alluvial aquifer system in Snake Valley and surrounding areas, Juab, Millard, and Beaver Counties, Utah, and White Pine and Lincoln Counties, Nevada: U.S. Geological Survey Scientific Investigations Map 3193.

Gates J.S., and Kruer, S.A., 1981, Hydrologic reconnaissance of the southern Great Salt Lake Desert and summary of the hydrology of west-central Utah: Utah Department of Natural Resources Technical Publication 71, 55 p.

Gibson, R.G., 1994, Fault-zone seals in siliciclastic strata of the Columbus Basin, offshore Trinidad: American Association of Petroleum Geologists Bulletin, v. 78, p. 1372–1385.

Halford, K.J., and Plume, R.W., 2011, Potential effects of groundwater pumping on water levels, phreatophytes, and spring discharges in Spring and Snake Valleys, White Pine County, Nevada, and adjacent areas in Nevada and Utah: U.S. Geological Survey Scientific Investigations Report 2011-5032, 52 p.

Haneberg, W.C., 1995, Steady state groundwater flow across idealized faults: Water Resources Research, v. 31, p. 1815–1820.

Harrill, J.R., Gates, J.S., and Thomas, J.M., 1988, Major ground-water flow systems in the Great Basin region of Nevada, Utah, and adjacent states: U.S. Geological Survey Hydrologic Investigations Atlas HA-694-C, scale 1:1,000,000, 2 sheets.

Harrill, J.R., and Prudic, D.E., 1998, Aquifer systems in the Great Basin region of Nevada, Utah and adjacent states—summary report: U.S. Geological Survey Professional Paper 1409-A, p. 66.

Heilweil, V.M., and Brooks, L.E., editors, 2011, Conceptual model of the Great Basin carbonate and alluvial aquifer system: U.S. Geological Survey Scientific Investigations Report 2010-5193.

Hess, S., Fairley, J.P., Bradford, J., Lyle, M., and Clement, W., 2009, Evidence for composite hydraulic architecture in an active fault system based on 3D seismic reflection, time-domain electromagnetics, and temperature data: Near Surface Geophysics, v. 7, p. 341–352.

Hintze, L.F., and Best, M.G., 1987, Geologic map of the Mountain Home Pass and Miller Wash quadrangles, Millard and Beaver Counties, Utah, and Lincoln County, Nevada: U.S. Geological Survey Miscellaneous Field Studies Map MF-1950, scale 1:24,000.

Hood, J.W., and Rush, F.E., 1965, Water-resources appraisal of the Snake Valley area, Utah and Nevada: Utah State Engineer Technical Publication No. 14, p. 43.

Houghton, J.G., Sakamoto, C.M., and Gifford, R.O., 1975, Nevada's weather and climate: Nevada Bureau of Mines and Geology Special Publication 2, 78 p.

Huntoon, P.W., 1993, The influence of Laramide foreland structures on modern ground-water circulation in Wyoming artesian basins, *in* Snoke, A.W., Steidtmann, J.R., and Roberts, S.M., editors, Geology of Wyoming: Geological Survey of Wyoming Memoir No. 5, p. 756–789.

Janecke, S.U., 1993, Structures in segment boundary zones of the Lost River and Lemhi faults, east central Idaho: Journal of Geophysics, v. 98, p. 16,223–16,238.

Kattenhorn, S.A., and Pollard, D.D., 2001, Integrating 3-D seismic data, field analogs, and mechanical models in the analysis of segmented normal faults in the Wytch Farm oil field, southern England, United Kingdom: American Association of Petroleum Geologists Bulletin, v. 85, p. 1183–1210.

Kistinger, G.M., Prieur, J.P., Rowley, P.D., and Dixon, G.L., 2009, Characterization of streams and springs in the Snake Valley area, Utah and Nevada, *in* Tripp, B.T., Krahulec, K., and Jordan, J.L., editors, Geology and geologic resources and issues of western Utah: Utah Geological Association Publication 38, p. 300–323.

Laczniak, R.J., Cole, J.C., Sawyer, D.A., and Trudeau, D.A., 1996, Summary of hydrogeologic controls on ground-water flow at the Nevada test site, Nye County, Nevada: U.S. Geological Survey Water-Resources Investigations Report 96-4109, 59 p.

Laczniak, R.J., Flint, A.L., Moreao, M.T., Knochenmus, L.A., Lundmark, K.W., Pohll, G., Carroll, R.W.H., Smith, J.L., Welborn, T.L., Heilweil, V.M., Pavelko, M.T., Hershey, R.L., Thomas, J.M., and Lyles, B.F., 2007, Ground-water budgets, in Welch, A.H., Bright, D.J., and Knochenmus, L.A., 2007, Water resources of the Basin and Range carbonate-rock aquifer system, White Pine County, Nevada, and adjacent areas in Nevada and Utah: U.S. Geological Survey Scientific Investigations Report 2007-5261, p. 43–82.

Lindanger, M., Gabrielsen, R.H., and Braathen, A., 2007, Analysis of rock lenses in extensional faults: Norwegian Journal of Geology, v. 87, p. 361–372.

Long, S.P., 2012, Magnitudes and spatial patterns of erosional exhumation in the Sevier hinterland, eastern Nevada and western Utah, U.S.A.—insights from a Paleogene paleogeographic map: Geosphere, v. 8, p. 881–901 (doi: 10.1130/GES00783.1).

Loy, K., and Durbin, T., 2010, Simulation results report eastern Nevada—western Utah regional groundwater flow model: U.S. Department of the Interior: Online, http://www.blm.gov/ut/st/en/prog/more/doi_groundwater_modeling.html, accessed July 2, 2010.

Machette, M.N., Personius, S.F., Nelson, A.R., Schwartz, D.P., and Lund, W.R., 1991, The Wasatch fault zone, Utah—segmentation and history of Holocene earthquakes: Journal of Structural Geology, v. 13, p. 137–149.

Mankinen, E.A., and McKee, E.H., 2009, Geophysical setting of western Utah and eastern Nevada between latitudes 37°45′ and 40°N, *in* Tripp, B.T., Krahulec, K., and Jordan, J.L., editors, Geology and geologic resources and issues of western Utah: Utah Geological Association Publication 38, p. 271–286.

Manning, A.H., Solomon, D.K., 2005, An integrated environmental tracer approach to characterizing groundwater circulation in a mountain block: Water Resources Research, v. 41, W12412 (doi: 10.1029/2005WR004178).

Mason, J.L., Atwood, J.W., and Buettner, P.S., 1985, Selected test-well data from the MX-missile siting study, Tooele, Juab, Millard, Beaver, and Iron Counties, Utah: U.S. Geological Survey Open-File Report 85-347, 13 p.

Maxey, G.B., and Eakin, T.E., 1949, Groundwater in White River Valley, White Pine, Nye, and Lincoln Counties, Nevada: Nevada Water Resources Bulletin 8, 61 p.

McGrew, A.J., 1993, The origin and evolution of the southern Snake Range decollement, east central Nevada: Tectonics, v. 12, p. 21–34.

Miller, E.L., and Grier, S.P., 1995, Geologic map of Lehman Caves 7.5′ quadrangle, White Pine County, Nevada: U.S. Geological Survey Map GQ-1758, scale 1:24,000.

Moreo, M.T., Laczniak, R.J., and Stannard, D.I., 2007, Evapotranspiration rate measurements of vegetation typical of ground-water discharge areas in the Basin and Range carbonate-rock aquifer system, White Pine County, Nevada, and adjacent areas in Nevada and Utah, September 2005–August 2006: U.S. Geological Survey Scientific Investigations Report 2007-5078, 36 p.

National Climatic Data Center, 2012, National precipitation and temperature maps: Online, http://www.ncdc.noaa.gov/temp-and-precip/maps.php?ts=12&year=2011&month=9&imgs[]=Divisionalprank&submitted=Submit, accessed October 18, 2012.

Plume, R.W., 1996, Hydrogeologic framework of aquifer systems in the Great Basin region of Nevada, Utah, and adjacent states: U.S. Geological Survey Professional Paper 1409-B, 64 p.

Prudic, D.E., Harrill, J.R., and Burbey, T.J., 1995, Conceptual evaluation of regional ground-water flow in the carbonate-rock province of the Great Basin, Nevada, Utah, and adjacent states: U.S. Geological Survey Professional Paper 1409-D, 102 p.

Ritzi, R.W., Jr., and Andolsek, R.H., 1992, Relation between anisotropic transmissivity and azimuthal resistivity surveys in shallow, fractured carbonate flow systems: Ground Water, v. 30, p. 774–780.

Rowley, P.D., 1998, Cenozoic transverse zones and igneous belts in the Great Basin, western United States—their tectonic and economic implications, *in* Faulds, J.E., and Stewart, J.H., editors, Accommodation zones and transfer zones—the regional segmentation of the Basin and Range Province: Boulder, Colorado, Geological Society of America Special Paper 323, p. 195–228.

Rowley, P.D., Dixon, G.L., Burns, A.G., and Collins, C.A., 2009, Geology and hydrogeology of the Snake Valley area, western Utah and eastern Nevada, *in* Tripp, B.T., Krahulec, K., and Jordan, J.L., editors, Geology and geologic resources and issues of western Utah: Utah

Geological Association Publication 38, p. 251–269.

Schaefer, D.H., and Harrill, J.R., 1995, Simulated effects of proposed ground-water pumping in 17 basins of east-central and southern Nevada: U.S. Geological Survey Water-Resources Investigations Report 95-4173, 71 p.

Schulze-Makuch, D., Carlson, D.A., Cherkauer, D.S., and Malik, P., 1999, Scale dependency of hydraulic conductivity in heterogeneous media: Ground Water, v. 37, p. 904–919.

Sibson, R.H., 1994, Crustal stress, faulting, and fluid flow, *in* Parnell, J., editor, Geofluids—origin, migration, and evolution of fluids in sedimentary basins: Geological Society of London Special Publication 78, p. 69–84.

Smith, R.B., and Arabasz, W.J., 1991, Seismicity of the intermountain seismic belt, *in* Slemmons, D.B., Engdahl, E.R., Zoback, M.D., and Blackwell, D.D., editors, Neotectonics of North America: Boulder, Colorado, Geological Society of America, Decade Map Volume 1, p. 185–227.

Southern Nevada Water Authority, 2008, Baseline characterization report for Clark, Lincoln, and White Pine Counties Groundwater Development Project, *in* U.S. Bureau of Land Management, 2012, Clark, Lincoln, and White Pine Counties Groundwater Development Project Final Environmental Impact Statement: FES 12-33, Document BLM/NV/NV/ES/11-17+1793.

Southern Nevada Water Authority, 2009a, Conceptual model of groundwater flow for the central carbonate-rock province—Clark, Lincoln, and White Pine Counties Groundwater Development project, *in* U.S. Bureau of Land Management, 2012, Clark, Lincoln, and White Pine Counties Groundwater Development Project Final Environmental Impact Statement: FES 12-33, Document BLM/NV/NV/ES/11-17+1793.

Southern Nevada Water Authority, 2009b, Transient numerical model of groundwater flow for the central carbonate-rock province—Clark, Lincoln, and White Pine Counties Groundwater Development Project, *in* U.S. Bureau of Land Management, 2012, Clark, Lincoln, and White Pine Counties Groundwater Development Project Final Environmental Impact Statement: FES 12-33, Document BLM/NV/NV/ES/11-17+1793.

Southern Nevada Water Authority, 2010, Addendum to the groundwater flow model for the central carbonate-rock province—Clark, Lincoln, and White Pine Counties Groundwater Development Project, *in* U.S. Bureau of Land Management, 2012, Clark, Lincoln, and White Pine Counties Groundwater Development Project Final Environmental Impact Statement: FES 12-33, Document BLM/NV/NV/ES/11-17+1793.

Stephens, J.C., 1977, Hydrologic reconnaissance of the Tule Valley drainage basin, Juab and Millard Counties, Utah: Utah Department of Natural Resources Technical Publication No. 56, 29 p.

Stewart, S.A., 2001, Displacement distributions on extensional faults: Implications for fault stretch, linkage, and seal: American Association of Petroleum Geologists Bulletin, v. 85, p. 587–599.

Sweetkind, D.S., Belcher, W.R., Faunt, C.C., and Potter, C.J., 2004, Chapter B geology and hydrogeology, *in* Belcher, W.R., editor, Death Valley regional groundwater flow system, Nevada and California—hydrogeologic framework and transient ground-water flow model: U.S. Geological Survey Scientific Investigations Report 2004-5205, p. 27–98.

Sweetkind, D.S., Knochenmus, L.A., Ponce, D.A., Wallace, A.R., Scheirer, D.S., Watt, J.T., and Plume, R.W., 2007, Hydrogeologic framework, *in* Welch, A.H., Bright, D.J., and Knochenmus, L.A., 2007, Water resources of the Basin and Range carbonate-rock aquifer system, White Pine County, Nevada, and adjacent areas in Nevada and Utah: U.S. Geological Survey Scientific Investigations Report 2007-5261, p. 11–42.

Thomas, J.M., Schaefer, D.H., and Dettinger, M.D., 1990, Use of geochemical data to trace ground-water flow which could affect oil migration in carbonate-rock aquifers of eastern Great Basin, Nevada and Utah [abs.], *in* Flanigan, D.H., Garside, L.J., and Hansen, M., editors, Oil fields and geology of Pine Valley, Eureka County area, Nevada: Reno, Nevada, Nevada Petroleum Society, 1990 Fieldtrip Guidebook, 74 p.

Twiss, R.J., and Moores, E.M., 1992, Structural Geology: New York, W.H. Freeman and Company, 532 p.

U.S. Bureau of Land Management, 2012, Clark, Lincoln, and White Pine Counties Groundwater Development Project Final Environmental Impact Statement: FEIS 12-33, Document BLM/NV/NV/ES/11-17+1793.

U.S. Fish and Wildlife Service, 2004, Comprehensive conservation plan—Fish Springs National Wildlife Refuge: Online, http://www.fws.gov/mountain-prairie/planning/ccp/ut/fhs/fhs.html, accessed December, 2012.

U.S. Geological Survey, 2010, Aquifer tests: Carson City, Nevada, U.S. Geological Survey Nevada Water Science Center: Online, http://nevada.usgs.gov/water/aquifertests/index.htm, accessed June 4, 2013.

U.S. Geological Survey, 2011, Basin and Range carbonate aquifer website: Online, http://nevada.usgs.gov/barcass/index.htm, accessed numerous times during 2004 through 2011.

Utah Division of Wildlife Resources, 2011, Utah sensitive species list: Online, http://dwrcdc.nr.utah.gov/ucdc/ViewReports/SSLAppendices20110329.pdf, 150 p., accessed January 4, 2012.

Van Denburgh, A.S., and Rush, F.E., 1974, Water resources appraisal of Railroad and Penoyer Valleys, east-central Nevada: Nevada Division of Water Resources, Reconnaissance Report 60, 61 p.

Watt, J.T., and Ponce, D.A., 2007, Geophysical framework investigations influencing ground-water resources in east-central Nevada and west-central Utah: U.S. Geological Survey Open-File Report 2007-1163, 43 p.

Welch, A.H., Bright, D.J., and Knochenmus, L.A., 2007, Water resources of the Basin and Range carbonate-rock aquifer system, White Pine County, Nevada, and adjacent areas in Nevada and Utah: U.S. Geological Survey Scientific Investigations Report 2007-5261, 96 p.

Western Regional Climate Center, 2011, Cooperative climatological data summaries—Utah: Online, http://www.wrcc.dri.edu/summary/Climsmut.html, accessed numerous times during 2012.

Whitebread, D.H., 1969, Geologic map of the Wheeler Peak and Garrison quadrangles, Nevada and Utah: U.S. Geological Survey Miscellaneous Geologic Investigations Series Map I-578, scale 1:48,000

Wilson, J.L., and Guan, H., 2004, Mountain-block hydrology and mountain-front recharge, *in* Phillips, F.M., Hogan, J., and Scanlon, B., editors, Groundwater recharge in a desert environment—the southwestern United States: Washington, D.C., American Geophysical Union, p. 113–137.

Wilson, J.W., 2007, Water-level surface maps of the carbonate-rock and basin-fill aquifers in the Basin and Range carbonate-rock aquifer system, White Pine County, Nevada, and adjacent areas in Nevada and Utah: U.S. Geological Survey Scientific Investigations Report 2007-5089, 9 p., 2 plates.

Winograd, I.J., and Thordarson, W., 1975, Hydrogeologic and hydrochemical framework, south-central Great Basin, Nevada-California, with special reference to the Nevada Test Site: U.S. Geological Survey Water-Supply Paper 712-C, 126 p.

Zhang, X., and Sanderson, D.J., 1995, Anisotropic features of geometry and permeability in fractured rock masses: Engineering Geology, v. 40, p. 65–75.

Zhang, L., Luo, X., Vasseur, G., Yu, C., Yong, W., Lei, Y., Song, C., Yu, L., and Yan, J., 2011, Evaluation of geological factors in characterizing fault connectivity during hydrocarbon migration—application to the Bohai Bay basin: Marine and Petroleum Geology, v. 28, p. 1634–1647.

Zhu, J., Young, M.H., and Cablk, M.E., 2007, Uncertainty analysis of estimates of ground-water discharge by evapotranspiration for the BARCAS study area: University of Nevada, Desert Research Institute Publication 41234, 36 p.

Zoback, M.L., 1989, State of stress and modern deformation of the northern Basin and Range Province: Journal of Geophysical Research, v. 94, p. 7105–7128.

CHAPTER 5 | UGS GROUNDWATER-MONITORING NETWORK

by Hugh Hurlow, J. Lucy Jordan, and Kevin Thomas

View northwest of drilling operations at UGS groundwater-monitoring site 3. Irrigated fields in the northern end of the Garrison agricultural area are in the middle distance, and the Snake Range is in the background.

Bibliographic citation for this chapter:
Hurlow, H., Jordan, J.L., and Thomas, K., 2014, UGS groundwater-monitoring network, Chapter 5 *in* Hurlow, H., editor, Hydrogeologic studies and groundwater monitoring in Snake Valley and adjacent hydrographic areas, west-central Utah and east-central Nevada: Utah Geological Survey Bulletin 135, p. 91–124.

CHAPTER 5 CONTENTS

FIGURES

TABLES

CHAPTER 5: UGS GROUNDWATER-MONITORING NETWORK

by Hugh Hurlow, J. Lucy Jordan, and Kevin Thomas

5.1 INTRODUCTION

In March 2007 the Utah State Legislature requested the UGS to establish a long-term (50+ years) groundwater-monitoring network in Snake Valley and adjacent areas, in response to concerns over potential drawdown from proposed large-scale groundwater development projects in east-central Nevada and west-central Utah (section 1.2). The UGS groundwater-monitoring network was completed in spring 2009 and includes wells and spring gages in Snake Valley, and wells in Tule Valley and Fish Springs Flat (figure 5.1; table C.1).

The objectives of the UGS groundwater-monitoring network are (1) determine baseline spatial and temporal water-level and chemical trends to evaluate possible future changes in local and regional groundwater-flow systems, (2) establish groundwater-monitoring wells near the planned pumping wells and areas of current groundwater use to assess their potential impacts on groundwater levels and chemistry in Utah, (3) monitor discharge from selected springs, (4) conduct aquifer tests to measure the hydraulic properties of, and hydraulic connectivity between, the basin-fill and carbonate-rock aquifers, and (5) evaluate groundwater-flow systems within Snake Valley and from Snake Valley to Fish Springs National Wildlife Refuge.

The UGS web-based groundwater-data server (section 5.2.3) provides access to water-level data, lithologic and geophysical logs, well-construction information for the new wells, water-level data from the pre-existing wells, and surface-flow data. The lithologic and geophysical logs are also available in data folders on this CD.

New well sites are in a variety of hydrologic settings, including (1) the basin-fill and carbonate-rock aquifers in agricultural areas in which groundwater is pumped for crop irrigation, (2) the basin-fill and carbonate-rock aquifers in remote areas, (3) the carbonate-rock aquifer along the proposed groundwater-flow path from Snake Valley to Fish Springs (Harrill and others, 1988; Prudic and others, 1995), and (4) spring systems that host sensitive aquatic species and consist of multiple upwelling points and therefore cannot be gauged. Nested piezometers are screened at different depths to evaluate vertical hydraulic gradients. Where possible, piezometers are installed in the basin-fill and carbonate-rock aquifers at the same groundwater-monitoring site to evaluate the hydraulic connectivity between the two aquifers.

5.2 WELL CONSTRUCTION AND MONITORING

5.2.1 Well Drilling and Completion

Drilling methods varied depending on the aquifer material, target depth, and environmental conditions at each site. Drillers used the mud-rotary technique with a tricone bit for boreholes in the basin-fill aquifer, except for the shallow boreholes at the agricultural-area sites which were drilled with a cable-tool rig. For boreholes in bedrock aquifers, drillers used the air-rotary hammer method with a button bit, with injected water or foam when appropriate (figure 5.2a). At sites where piezometers were installed in both the basin-fill and bedrock aquifers, the drillers used the mud-rotary technique in the basin fill, and sealed the borehole with high-density grout at least 20 feet (6.1 m) above and below the contact. At sites where the groundwater level was below the contact, the drillers installed steel casing in the borehole to just below the contact, then drilled the bedrock using the rotary air-hammer method. Lost circulation problems were common at the basin fill-bedrock contact. At spring-gradient sites, the drillers used an auger bit (figure 5.2b) or a Geoprobe hydraulic press (figures 5.2c and 5.2d), which do not require introduction of drilling fluids, to prevent potential contamination of spring pools inhabited by sensitive species. The exception is the deepest borehole at site SG21 (North Spring, Fish Springs National Wildlife Refuge), which penetrated the carbonate-rock aquifer using mud-rotary drilling, but site topography, shallow borehole depth, and setback from the spring allowed the drillers to preclude contamination of the spring pool. Use of hydraulic press and auger drilling limited the depth of the spring-gradient piezometers to just over 100 feet, depending on aquifer materials encountered. A UGS geologist monitored and logged all drilling (data folder DF-2).

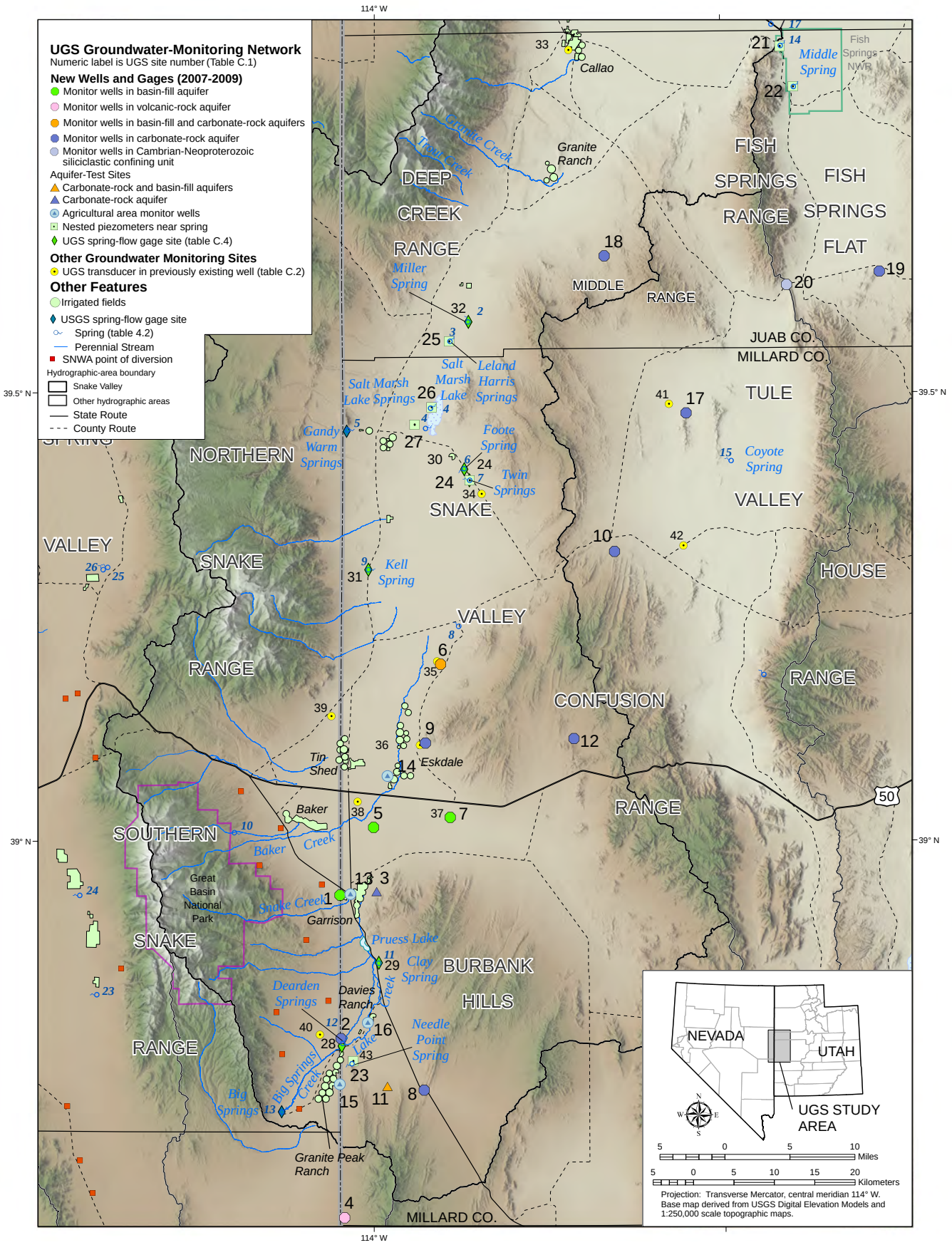

Figure 5.1. *Geographic and hydrologic setting of the UGS west desert groundwater-monitoring network. New monitor wells are at sites 1–27, and new spring-discharge monitoring equipment are at sites 24 and 28–32.*

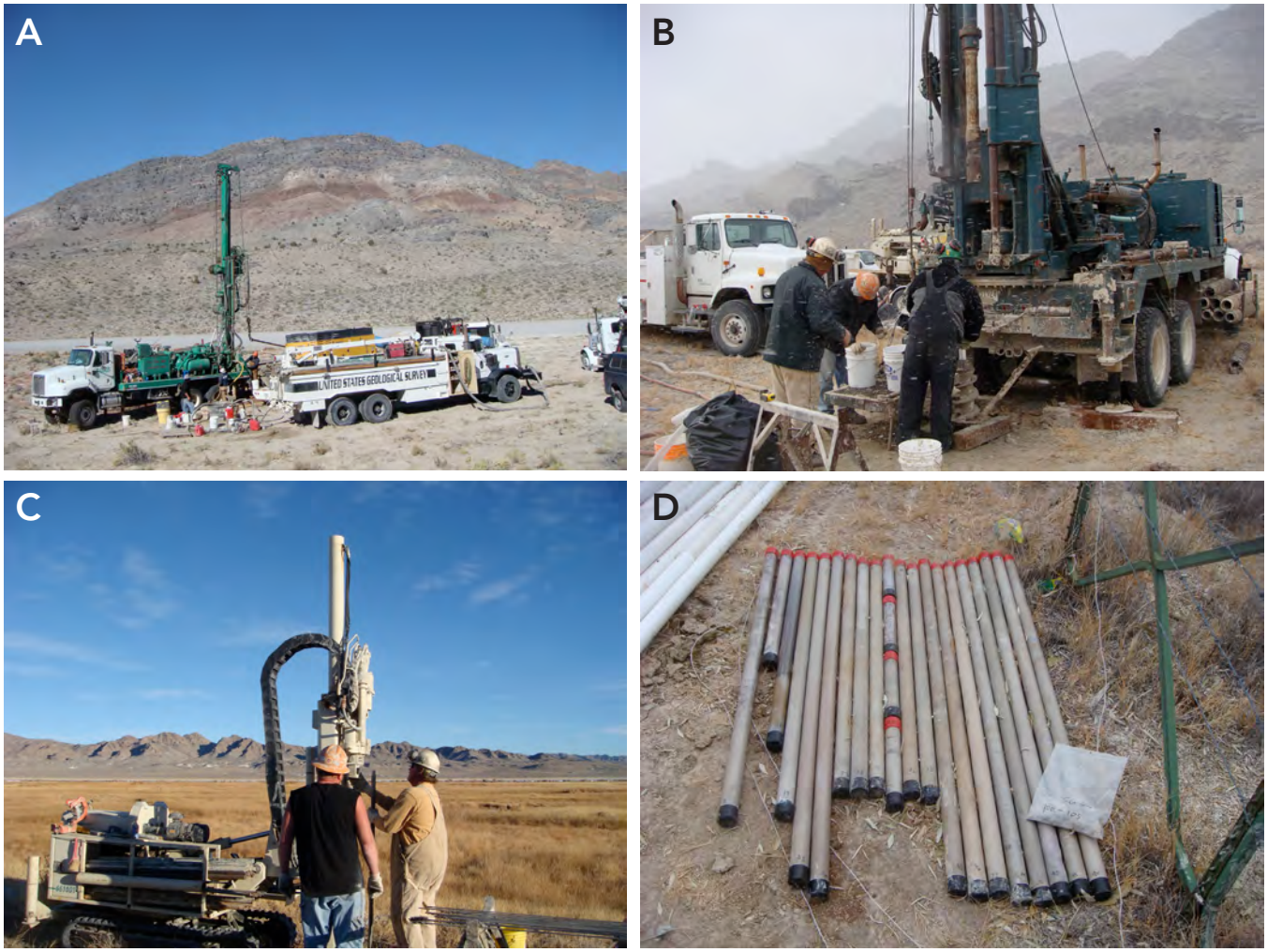

Figure 5.2. *Well drilling for the UGS west desert groundwater-monitoring network.* ***A.*** *View north of site 20 (Sand Pass) drilling using the air-hammer method. Brown rocks in background are densely fractured Prospect Mountain Quartzite of the Lower Cambrian-Neoproterozoic siliciclastic-rock hydrogeologic unit. Gray rocks in middle distance are densely fractured and veined Cambrian limestone and dolomite displaced by southeast-side-down normal faults. Gray rocks above Prospect Mountain Quartzite are Cambrian limestone and dolomite of the lower Paleozoic carbonate-rock aquifer hydrogeologic unit.* ***B.*** *View west of drilling borehole for piezometer SG21C at North Spring, using a hollow-stem auger bit.* ***C.*** *Coring the younger basin-fill aquifer hydrogeologic unit at UGS groundwater-monitoring site 25 (Leland Harris spring complex), using a Geoprobe hydraulic press.* ***D.*** *Core of the younger basin-fill aquifer hydrogeologic unit at UGS groundwater-monitoring site 24 (Twin Springs), obtained using a Geoprobe hydraulic press.*

Well completion followed Utah code (http://waterrights.utah.gov/wellinfo/handbook.pdf) and varied depending on borehole diameter and geologic conditions (table C.1). Completed boreholes contain one to three PVC piezometers (2.0-inch-diameter [5.1 cm] or, rarely, 1.0- or 2.5-inch-diameter [2.5–6.4 cm]) except piezometer PW18A, which is steel due to high groundwater temperature in this well (chapter 6; Blackett, 2011). Most piezometers have one 20-foot-long (6.1 m) screened interval at their base. Screen length is 40 feet (12.2 m) in low-yield boreholes, and 5 or 10 feet (1.5–3.1 m) at the spring-gradient sites. The annular space surrounding the screens is filled with well-sorted sand. The annular space surrounding unscreened parts of the boreholes is filled with bentonite grout to seal the borehole from hydraulic connection with the aquifer and to prevent hydraulic connection between screened intervals in multiple-completion (more than one piezometer) boreholes (figure 5.3).

Wells in the UGS network are named according to the following conventions.

1. The first two letters are the type of geographic/hydrologic setting: AG stands for agricultural area, PW stands for paired well, for sites where the goal was to install piezometers in both the basin-fill and carbonate-rock aquifers or more than one piezometer in the carbonate-rock aquifer, and SG stands for spring-gradient. Early in the project, our

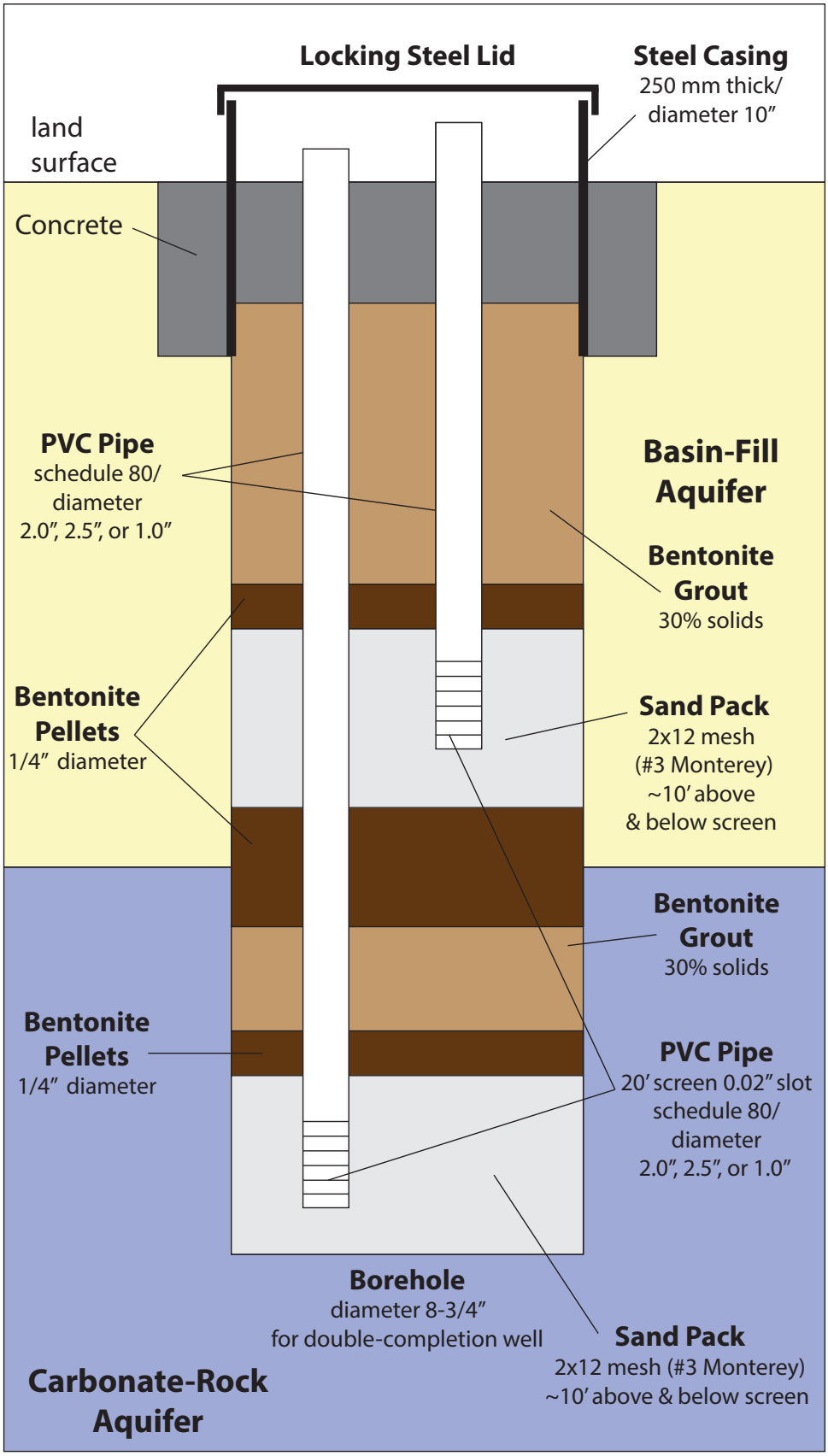

Figure 5.3. *Schematic well-completion diagram for example UGS groundwater-monitoring well in basin-fill and bedrock aquifers.*

strategy for the PW wells did not work for sites 1 and 7, where the borehole did not reach bedrock, and site 4, where the groundwater level was below the basin fill. We changed our site-placement strategy to ensure that the wells would intercept the bedrock, so several PW wells are not in basin-fill deposits.

2. The number following the site type is the UGS site number.
3. The letter following the site number denotes the piezometer, in order of increasing depth. For example, AG13C is the deepest of three piezometers (AG13A, AG13B, and AG13C) at UGS site 13, in an agricultural area (Garrison in this example).

5.2.2 Geophysical Well Logging

Using UGS-owned geophysical well logging equipment, we logged most of the boreholes for natural gamma radiation, resistivity (16- and 64-inch [41- and 163-cm] normal and lateral), and temperature (data folder DF-3). We measured borehole diameters using a caliper tool, and conducted sonic logs on boreholes that penetrate bedrock. Blackett (2011) measured detailed temperature logs of many of the deepest piezometers in the network.

Gamma logs measure natural gamma radiation emitted by the surrounding rock or sediment, and are useful for identifying clay and shale zones, as well as igneous units. Resistivity logs measure the resistance of the surrounding rock or sediment to an electrical current and are useful for identifying high-porosity zones. Sonic logs measure the time in which a sound wave travels one foot through the material surrounding the well. The travel time depends on the density of the material and can be used to estimate porosity. Caliper logs record the diameter of the borehole and can be useful for identifying fracture zones, as well as aiding in the interpretation of the other logs.

We determined the screened intervals within general target depths based on rock type, porosity, fracturing, and likely hydrologic isolation from other borehole intervals. We used the geophysical and lithologic logs, and increases in water production during drilling, to select screened intervals within those target-depth ranges that appeared most likely to yield groundwater.

5.2.3 Transducers and Water-Level Data Processing

All piezometers in the UGS groundwater-monitoring network are equipped with pressure transducers that record hourly. Transducer models include Global Water WL400, Solinst Levelogger Gold, and Solinst Levelogger Junior. Data are downloaded on-site quarterly, corrected for barometric fluctuations and barometric well efficiency where necessary, and posted to the UGS groundwater-monitoring data portal (http://geology.utah.gov/databases/groundwater/projects.php). The transducer data are calibrated to water-level measurements taken with electrical sounders at the time the data are downloaded.

Solinst Barologgers, installed at sites 3, 10, and 19, measure barometric pressure hourly. Barometric corrections for Solinst Leveloggers and all barometric efficiency corrections are performed using the Barologger data. The Global Water transducers are vented and do not require barometric correction.

5.3 GROUNDWATER-LEVEL TRENDS

5.3.1 Introduction

This section summarizes groundwater-level trends in the UGS groundwater-monitoring network (2007 or 2008 to September 2013), and longer-term records from selected wells monitored by the U.S. Geological Survey (1981 to 2013). Plate 3 and table C.1 present water-level data and completion information for the UGS wells, respectively. The UGS groundwater-monitoring network includes 67 transducers in wells constructed for this project, and 11 transducers installed in previously existing wells. Most of the pre-existing wells, hereafter referred to as MX wells, were installed during 1979 and 1980 as part of a regional assessment of groundwater resources associated with the MX Missile-Siting Investigation (Bunch and Harrill, 1984; Mason and others, 1985). Transducer records for most of these wells began in mid-2006, whereas transducer records for most new UGS wells began in 2007 or 2008. At the time of writing, therefore, five to seven years of data are available from the UGS groundwater monitoring network, sufficient to make preliminary observations, but not detailed analyses, of trends related to climate variations and groundwater pumping. Some wells in the study area have been measured annually or semi-annually by the U.S. Geological Survey since 1980 or earlier, providing a long-term but less detailed record of water-level variations (table C.3; plate 4; Gardner and others, 2011), and are also discussed in this section. Unless otherwise noted, the standard reference for comparing annual groundwater levels is early March, the most common time for repeated measurements because most groundwater levels are near their highest annual level, having recovered from the previous irrigation season, and groundwater pumping for

the current year has not yet begun.

The following sections cite approximate rates of groundwater-level declines observed in some of the piezometers monitored by the UGS and U.S. Geological Survey (table 5.1). Time periods of the rates of change vary depending on the period of record, and are approximate. For piezometers in the UGS groundwater-monitoring network, rates of change are estimated from the difference in groundwater levels measured in early March (unless otherwise noted) from year to year. For piezometers measured annually by the U.S. Geological Survey, simple linear regression lines were calculated for time periods showing consistent trends, and the goodness-of-fit statistic (R^2) is cited.

5.3.2 Agricultural-Area Monitoring Sites

Figure 5.1 shows informally named and delineated agricultural areas in the UGS study area, determined by the senior author based on identification of irrigated fields by inspection of aerial photography, field inspection, and compilation of water-well logs. In monitor wells within about 5 miles (8 km) of the approximate geographic centers of current agricultural pumping areas, groundwater levels decline during the summer irrigation season in response to pumping and recover during the fall and winter months. At several sites, groundwater levels declined overall from 2008 to early 2011, rose in early to mid-2011 in response to greatly above-normal winter 2010 and spring 2011 precipitation (figure 4.9) then, after the record driest 2012 water year (figure 4.9; National Climatic Data Center, 2012), returned to previous levels (plate 3).

5.3.2.1 Northern Snake Valley

In the Callao agricultural area in northern Snake Valley, the groundwater level at site 33 fluctuated seasonally by 1.5 to 2.5 feet (0.46–0.76 m) from November 2007 to November 2010, based on bi-annual measurements by a local rancher using an electronic tape (figure 5.1; table C.2; plate 3). The groundwater level in this open, unused well rose about 9 feet (2.7 m) (plate 3) from early April to mid-June, 2011, after the high precipitation winter and early spring, then declined nearly 10 feet during the summer irrigation season. At the beginning of the 2012 irrigation season (mid-April), the water level was more than 2 feet (0.6 m) higher than the same time in previous years. Pumping during the 2012 irrigation season caused the groundwater level to decline about 8 feet (2.4 m) to the lowest recorded value during the period of record.

5.3.2.2 South-Central Snake Valley

UGS groundwater-monitoring sites 9, 36 (Eskdale MX), 14, 5, 38 (Baker Creek well), and 39 (Snake Valley North MX) record groundwater-level changes related to pumping in the Eskdale and Tin Shed agricultural areas (figure 5.1; tables C.1 and C.2). Groundwater levels in piezometers PW09A (screen midpoint at 255 feet [78 m] depth) and PW09B (screen midpoint at 710 feet [216 m] depth), both in Silurian dolomite of the lower Paleozoic carbonate-rock aquifer hydrogeologic unit, show a downward vertical gradient of about 0.004 (based on groundwater-level data in table C.1) and fluctuate seasonally by about 1 foot (0.3 m). From 2008 to 2013, groundwater levels in both piezometers fluctuated seasonally by about 0.1 to 0.2 feet (0.03–0.06 m) in response to groundwater pumping in the Eskdale area (plate 3). From March 2008 to March 2012, the groundwater level in piezometer PW09A decreased by about 1.8 feet (0.6 m), an average rate of decline of about 0.4 feet per year (0.12 m/yr), and in piezometer PW09B decreased about 2.4 feet (0.7 m), an average rate of decline of about 0.5 feet per year (0.2 m/yr) (table 5.1; plate 3). Drilling records and geophysical logs suggest moderate to high subsurface fracture density and, during drilling, groundwater entered the borehole at about 200 gallons per minute (760 L/min). From 2006 to 2013, the groundwater level in the Eskdale MX well fluctuated seasonally by about 1 foot (0.3 m), in response to groundwater pumping in the Eskdale area (plate 3). The groundwater level in this well decreased about 1.9 feet (0.6 m), an average rate of decline of about 0.4 feet per year (0.12 m/yr) (table 5.1; plate 3).

Site 14 contains three piezometers having screen midpoints at 55, 130, and 270 feet (17, 40, and 82 m), all completed in the younger basin-fill aquifer hydrogeologic unit (figure 5.1; table C.1). The piezometers show upward vertical hydraulic gradients of about 0.03 between piezometers AG1C and AG14A, and about 0.04 between piezometers AG14C and AG14B. From 2009 to 2012, groundwater levels fluctuated seasonally by about 0.5 to 2 feet (0.15–0.61 m) in piezometers AG14A, AG14B, and AG14C (plate 3). The peak annual groundwater level in all three piezometers occurred in early May, and declined by about 0.2 to 0.4 feet (0.06–0.12 m), an average rate of decline of about 0.1 feet per year (0.03 m) (table 5.1; plate 3).

At site 5, the shallower two piezometers, PW05A and PW05B, are screened in the younger basin-fill aquifer hydrogeologic unit, whereas the deepest piezometer, PW05C, is screened in the older basin-fill aquifer hydrogeologic unit (Ts) (table C.1). Groundwater levels in all three piezometers changed abruptly during 2009 as a result of final development by pumping to purge the wells before chemical sampling (plate 3). Groundwater levels at site 5 define an upward hydraulic gradient of about 0.02 to 0.03, and increased slightly in spring 2012, interpreted as a delayed response to recharge from high precipitation

during the 2010-2011 winter and spring. From 2009 to 2013, groundwater levels in piezometer PW05A decreased by about 2.4 feet (0.7 m), an average rate of decline of about 0.9 feet per year (0.3 m/yr); groundwater levels in piezometer PW05B and PW05C decreased by about 1.1 feet (0.3 m), an average rate of decline of about 0.3 feet per year (0.1 m/yr) (table 5.1; plate 3). At least some of this protracted decline is likely due to groundwater pumping for irrigation in the Eskdale-Baker area.

The Shell-Baker Creek well (site 38; figure 5.1; tables 5.1 and C.2) is screened in the younger basin-fill aquifer hydrogeologic unit, and is about 2.3 miles (3.7 km) northwest of site 5. From late October 2011 to late April 2012, the groundwater level in this well increased by about 0.3 feet (0.1 m) (table 5.1; plate 3), interpreted as a delayed response to recharge from high-precipitation during the 2010–2011 winter and spring. From 2008 to 2013, groundwater levels in the Shell-Baker Creek well decreased by about 2.4 feet (0.7 m), an average rate of decline of about 0.5 feet per year (0.2 m/yr) (table 5.1; plate 3), similar to the trends observed in piezometer PW05A.

The Snake Valley North MX well (site 39) is about 2.5 miles (4 km) northwest of the nearest agricultural pumping, and is screened in the younger basin-fill aquifer hydrogeologic unit (QTcs) from 74 to 94 feet (23–29 m) (table C.2). From 2009 to 2013, groundwater levels in this well fluctuated seasonally by about 0.3 to 1 foot (0.1–0.3 m) (table 5.1; plate 3) in response to groundwater pumping to the southeast. The groundwater level in this well decreased about 2.5 feet (0.8 m), an average rate of decline of about 0.6 feet per year (0.2 m/yr) (table 5.1; plate 3).

5.3.2.3 Garrison Area

UGS groundwater-monitoring sites 13, 1, and 3 record groundwater-level changes related to pumping in the Garrison agricultural area. Site 13 includes three piezometers having screen midpoints at 75, 148, and 295 feet (23, 45, and 90 m), all in the younger basin-fill aquifer hydrogeologic unit (QTcs) (table C.1). In 2009 and 2010, groundwater levels fluctuated seasonally by about 4.6 to 6.9 feet (1.4–2.1 m) in piezometer AG13A, and by about 12.6 to 16.6 feet (3.8–5.1 m) in piezometers AG13B and AG13C (plate 3), respectively, in response to groundwater pumping in the Garrison agricultural area. From late October 2010 to early June 2011, groundwater levels rose nearly 14 feet (4.3 m) in piezometer AG13A, and nearly 24 feet (7.3 m) in piezometers AG13B and AG13C. During the 2012 irrigation season, groundwater levels declined by nearly 14 feet (4.3 m) in piezometer AG13A, and nearly 25 feet (7.6 m) in piezometers AG13B and AG13C (table 5.1; plate 3), by far the greatest irrigation-season declines during the period of record.

Site 1 includes three piezometers having screen midpoints at 250, 955, and 1607 feet (76, 291, and 490 m). Piezometer PW01A is completed in sediment of the younger basin-fill aquifer hydrogeologic unit (QTcs), and piezometers PW01B and PW01C are completed in the older basin-fill aquifer hydrogeologic unit (Ts) (table C.1). From 2008 to 2010, groundwater levels in piezometers PW01A and PW01B fluctuated seasonally by about 2 to 5 feet (0.6–1.5 m) in response to pumping (plate 3). The peak annual groundwater level in both piezometers occurred in mid-April to early May, and in piezometer PW01A decreased by about 5.7 feet (1.7 m), an average rate of decline of 1.8 feet per year (0.6 m/yr), and in piezometer PW01B declined by about 4.5 feet (1.4 m), and average rate of decline of 1.4 feet per year (0.4 m/yr) (table 5.1; plate 3). During the 2012 irrigation season, groundwater levels in piezometers PW01A and PW01B declined by over 6 feet (1.8 m), to levels similar to those prior to the high-precipitation 2010–2011 winter. Piezometer PW01C still contained drilling mud at the time of writing, and showed very slow recovery after attempts to develop the well by low-flow pumping, so we are unsure to what extent its water level represents the piezometric level in this very low-hydraulic-conductivity unit, and exclude it from our data presentation.

Site 3 includes three monitor wells and one pumping well, all completed in the lower Paleozoic carbonate-rock aquifer hydrogeologic unit. In chapter 7 we present more details about the structural setting of this site, and describe and interpret the aquifer test we conducted here. The screen midpoints for piezometers PW03A and PW03B are at 300 and 840 feet (91 and 256 m), respectively (table C.1), and a fault zone lies between the two screens (see data folder DF-2 Lithologic Logs). From 2007 to April 2010, groundwater levels in piezometers PW03A and PW03B declined by about 9.4 and 9.2 feet (2.9 and 2.8 m), respectively, an average rate of decline about 3.1 feet per year (-0.9 m/yr) (table 5.1; plate 3). Groundwater levels in piezometers PW03A and PW03B rose 11 and 12 feet (3.3 and 3.7 m), respectively, between late April and late October 2011 (plate 3), a delayed response to recharge during the high-precipitation 2010–2011 winter and spring. Seasonal changes in groundwater levels of about 1 to 2 feet (0.3–0.6 m) are superposed on this overall decline in groundwater levels. Groundwater levels rose during the summer and declined during the winter and early spring, out of phase with the timing of recharge and pumping for irrigation. We interpret the seasonal variations to reflect time-delayed pressure signals from spring recharge, summer groundwater pumping, and fall/winter recovery. The signal is delayed and damped due to the distance from the recharge areas in the southern Snake Range mountain block and mountain

Table 5.1. *Estimated rates of change of groundwater levels from UGS data.*

UGS Site Number[1]	Piezometer	Average Rate of Change[2] (ft/yr)	Time Period	Hydrogeologic Unit	Screened Interval
AGRICULTURAL AREAS					
Northern Snake Valley					
33	Callao	-11.3	06/2011–09/2012	QTcs	126
South-Central Snake Valley					
Eskdale-Tin Shed area					
9	PW09A	-0.4	2008–2013	LPzc	245–265
	PW09B	-0.5	2008–2013	LPzc	700–720
36	Eskdale MX	-0.4	2008–2013	QTcs	77–97
14	PW14A	-0.1	2009–2012	QTcs	45–65
	PW14B	-0.1	2009–2012	QTcs	120–140
	PW14C	-0.1	2009–2012	QTcs	260–280
5	PW05A	-0.6	2009–2013	QTcs	138–158
	PW05B	-0.4	2009–2013	QTcs	610–650
	PW05C	-0.3	2009–2013	Ts	925–965
38	Baker Creek	-0.5	2008–2013	QTcs	69–76
39	SVN MX	-0.6	2009–2013	QTcs	74–94
Garrison area					
13	AG13A	0.05	2009–2010	QTcs	65–85
	AG13B	0.05	2009–2010	QTcs	138–158
	AG13C	0.05	2009–2010	QTcs	285–305
1	PW01A	-1.8	2008–2010	QTcs	240–260
	PW01B	-1.4	2008–2010	QTcs	945–965
3	PW03A	-3.1	2007–2010	LPzc	280–320
	PW03B	-3.1	2007–2010	LPzc	820–860
Southern Snake Valley					
16	AG16A	-0.4	2009–2013	QTcs	50–60
	AG16B	-0.4	2009–2013	QTcs	80–100
	AG16C	-0.4	2009–2013	QTfs	305–315
2	PW02A	-0.3	2009–2013	UPzc	405–425
	PW02B	-0.03	2009–2013	UPzc	615–635
40	SVS MX	-0.05	2009–2013	QTcs	77–97
15	AG15A	-0.4	2009–2012	QTcs	159–179
23	SG23A	-0.4	2008–2013	QTcs	16–46
	SG23B	-0.4	2009–2013	QTcs	55–60

Table 5.1. *continued*

UGS Site Number[1]	Piezometer	Average Rate of Change[2] (ft/yr)	Time Period	Hydrogeologic Unit	Screened Interval
REMOTE SITES					
South-Central Snake Valley					
Eskdale-Tin Shed area					
6	PW06A & B	-0.2	2008–2013	QTcs	see table C.1
	PW06C & D	-0.2	2008–2013	UPzc	see table C.1
35	PW06 MX	-0.2	2009–2013	QTcs	77–97
7	PW07A	-0.2	2008–2013	QTcs	530–570
	PW07B	-0.2	2008–2013	Ts	1245–1285
37	PW07 MX	-0.3	2009–2013	QTcs	77–97
Southern Snake Valley-Northern Hamlin Valley					
8	PW08A	-0.7	2009–2011	UPzc	140–160
	PW08A	0.9	2011–2013	UPzc	140–160
	PW08B	-0.7	2009–2011	UPzc	380–400
	PW08B	1	2011–2013	UPzc	380–400
11	PW11B	0.05	2009–2012	QTcs	435–455
	PW11C-E	0.05	2009-2012	UPzc	see table C.1
4	PW04A	0.09	2009–2013	Tvt2	730–750
	PW04B	0.09	2009–2013	Tvt2	895–915
Central Confusion Range North-Central Snake Valley, and Middle Range					
12	PW12A	0.1	2009–2012	LPzc	1593–1633
34	TS MX	-0.06	2008–2013	QTcs	78–98
18	PW18A	-0.1	2010–2013	LPzc	970–990
Tule Valley and Fish Springs Flat					
10	PW10A	-0.7	2009–2011	UPzc	649-669
	PW10A	0.4	2011–2013	UPzc	649-669
	PW10B	-0.9	2009–2011	UPzc	718–738
	PW10B	0.6	2011–2013	UPzc	718–738
42	CTV MX	0.05	2009–2013	QTcs	100–380
41	CK MX	0.1	2010–2013	QTcs	161–181
17	PW17A-C	0.05	2009–2013	LPzc	see table C.1
20	PW20A	0.4	04/11–09/11	CZs	545–565
19	PW19A-C	0.4	04/11–09/11	LPzc	see table C.1

[1] See tables C.1 and C.2 for more detailed well information.

[2] Approximate rate of change calculated by difference between groundwater levels measured in early March.

front, an effect of the hydraulic diffusivity of the basin-fill and carbonate-rock aquifers (Bredehoeft, 2011). The long-term decline likely results from removal of groundwater from storage by the irrigation pumping. These hydrographs show that the basin-fill and carbonate-rock aquifers are hydraulically connected in this area.

5.3.2.4 Southern Snake Valley

In southern Snake Valley, groundwater pumping for agriculture occurs at the Granite Peak Ranch in Nevada and the Davies Ranch in Utah (figure 5.1). Groundwater levels in piezometers at UGS groundwater-monitoring sites 16, 2, Snake Valley South MX, 23, and 15 fluctuate seasonally in response to this pumping. At site 16 near Davies Ranch, piezometers AG16A and AG16B are screened in the younger basin-fill aquifer hydrogeologic unit (QTcs) (screen midpoints at 55 and 90 feet [17 and 27 m] depth, respectively) (table C.1). From 2009 to 2012, groundwater levels in piezometers AG16A and AG16B fluctuated seasonally by about 8 and 18 feet (2.4 and 5.5 m), respectively, (plate 3) in response to groundwater pumping at Davies Ranch. The peak annual groundwater level in both piezometers occurred in late April to early May, and in piezometer AG16A decreased by about 1.2 feet (0.4 m), an average rate of decline of about 0.4 feet per year (0.12 m/yr), and in piezometer AG16B decreased by about 1.1 feet (0.3 m), an average rate of decline of about 0.4 feet per year (0.12 m/yr) (table 5.1; plate 3). In piezometer AG16C, screened in dense clay of the younger basin-fill confining hydrogeologic unit (QTfs) (screen midpoint at 310 feet [94 m] depth), the groundwater level showed a slight response to pumping and decreased by about 1.2 feet (0.4 m) from 2009 to March 2013, an average rate of decline of about 0.4 feet per year (0.12 m/yr) (table 5.1).

Piezometers PW02A and PW02B (screen midpoints at 415 and 625 feet [126 and 190 m], respectively) are in fractured calcareous sandstone of the Permian Arcturus Formation of the upper Paleozoic carbonate-rock aquifer hydrogeologic unit (table C.1). Site 2 is near the likely northward continuations of normal faults that mark the western margin of the Mountain Home Range (figure 3.13). From 2009 to 2013, groundwater levels fluctuated seasonally by about 0.6 to 1.2 feet (0.2–0.4 m) in both piezometers (plate 3), in response to groundwater pumping at Granite Peak Ranch. The peak annual groundwater level in both piezometers occurred in late April to early May, and in piezometer PW02A decreased by about 0.9 feet (0.3 m), an average rate of decline of about 0.3 feet per year (0.1 m/yr), and in piezometer PW02B decreased by about 0.8 feet (0.2 m), an average rate of decline of about 0.3 feet per year (0.1 m/yr) (table 5.1; plate 3). Because these piezometers respond to groundwater pumping from the basin-fill aquifer at Granite Peak Ranch, we infer that the carbonate-rock and basin-fill aquifers are hydraulically connected at this site.

The Snake Valley South MX well (site 40) is screened from 77 to 97 feet (23–30 m) in alluvial-fan deposits of the younger basin-fill aquifer hydrogeologic unit (QTcs) (table C.2). From 2009 to 2013, the groundwater level in this well fluctuated seasonally by about 0.3 to 0.4 foot (0.09–0.1 m) (plate 3), likely in response to groundwater pumping at Granite Peak Ranch about 2.5 miles (4 km) to the southeast. The peak annual groundwater level occurred in late April to early May, and did not decline significantly.

Piezometer AG15A is screened from 159 to 179 feet (48–55 m) below land surface in alluvial-fan deposits of the younger basin-fill aquifer hydrogeologic unit (QTcs) (table C.1). Drilling encountered significant lost circulation problems and reduced penetration rate at 178 feet (54 m) depth, suggesting that the borehole reached the contact between the basin-fill and carbonate-rock aquifers. Based on limited cuttings returns, the carbonate-rock aquifer here is the Permian Arcturus Formation. From 2009 to 2013, the groundwater level in piezometer AG15A fluctuated seasonally by about 2.2 to 3.5 feet (0.7–1.1 m) (plate 3), in response to groundwater pumping at Granite Peak Ranch. The peak annual groundwater level occurred in late April to early May, and decreased by about 1.2 feet (0.4 m), an average rate of decline of about 0.4 feet per year (0.12 m/yr) (table 5.1; plate 3).

The piezometers at site 23 (Needle Point Spring) are screened in alluvial-fan deposits of the younger basin-fill aquifer hydrogeologic unit (QTcs). The U.S. Bureau of Land Management installed piezometer SG23A in 2001. Drilling of piezometer SG23B for this project encountered significant lost circulation problems and reduced penetration rate at 65 feet (20 m) depth, suggesting that the borehole reached the basin fill-bedrock contact. The Permian Arcturus Formation is exposed on the low ridge west of the borehole, and we infer that it underlies the basin-fill deposits below the groundwater-monitoring site. From 2009 to 2012, groundwater levels fluctuated seasonally by about 1.6 to 2.5 feet (0.5–0.8 m) in piezometer SG23A (BLM groundwater-monitoring well), and by about 1.7 to 3.0 feet (0.5–0.9 m) in piezometer SG23B (plate 3), in response to groundwater pumping at Granite Peak Ranch. The peak annual groundwater level in both piezometers occurred in late April to early May, and in piezometer SG23A decreased by about 1.5 feet (0.5 m), an average rate of decline of about 0.4 feet per year (0.12 m/yr), and in piezometer SG23B decreased by about 0.9 feet (0.3 m), an average rate of decline of about 0.4 feet per year (0.1 m/yr) (table 5.1; plate 3).

5.3.3 Remote Sites

5.3.3.1 South-Central Snake Valley

Groundwater levels at UGS groundwater-monitoring sites more than about 5 miles (8 km) from the approximate geographic centers of current agricultural pumping areas or spring-fed wetland systems showed faint or no seasonal variation in response to pumping and local evapotranspiration. Groundwater levels at most of these sites showed a relatively minor increase during early 2012 that is interpreted as a delayed response to recharge from high precipitation during the 2011–2012 winter and spring.

In the Baker-Eskdale area of south-central Snake Valley, UGS groundwater-monitoring sites 6 and 7 are between about 5 to 17 miles (8–27 km) from the geographic centers of groundwater pumping for irrigation (figure 5.1). At site 6, UGS piezometers PW06A and PW06B and a nearby MX well (site 35) are completed in the younger basin-fill aquifer hydrogeologic unit, and piezometers PW06C and PW06D are completed in the Permian Arcturus Formation of the upper Paleozoic carbonate-rock aquifer hydrogeologic unit (tables C.1 and C.2). These rocks are in the gently east-dipping limb of the Confusion Range syncline, and are highly fractured as determined from drilling records and geophysical logs. From 2008 to 2013, groundwater levels in these five piezometers were nearly identical, and declined by about 1 foot (0.3 m) (plate 3), an average rate of decline of about 0.2 feet per year (0.05 m/yr). The close similarity between groundwater levels in piezometers in the basin-fill and bedrock aquifers, and severe lost-circulation problems at the basin fill-bedrock contact during drilling, indicate that the two aquifers are hydraulically connected.

At site 7, piezometer PW07A and an MX well (site 37) are screened in the younger basin-fill aquifer hydrogeologic unit, and the deeper piezometer, PW07B, is screened in the older basin-fill aquifer hydrogeologic unit (Ts) (tables C.1 and C.2). Groundwater levels at site 7 define a slight downward hydraulic gradient of about 0.003 to 0.01. From 2008 to 2013, groundwater levels in the MX well decreased by about 1.1 feet (0.3 m), an average rate of decline of about 0.3 feet per year (0.08 m/yr); groundwater levels in piezometers PW07A and PW07B decreased by about 0.7 feet (0.2 m), an average rate of decline of about 0.2 feet per year (0.05 m/yr) (table 5.1; plate 3).

5.3.3.2 Southern Snake Valley and Northern Hamlin Valley

Piezometers at UGS groundwater-monitoring site 8 (PW08A, 140–160 feet [43–49 m], and PW08B, 380–400 feet [116–122 m]) are screened in the Ely Limestone of the upper Paleozoic carbonate-rock aquifer hydrogeologic unit (table C.1). From 2008 to 2011, groundwater levels in both piezometers decreased by about 1.7 feet (0.5 m), an average rate of decline of about 0.7 feet per year (0.2 m/yr) (table 5.1; plate 3). From July 2011 to October 2012, the groundwater levels in both piezometers rose about 1.2 feet (0.40 m) in response to relatively high precipitation during the 2011–2012 winter and spring (table 5.1; plate 3). The slight downward vertical hydraulic gradient suggests that site 8 is in a recharge zone.

Site 11 includes one piezometer (PW11B) in the basin-fill aquifer hydrogeologic unit, and three piezometers (PW11C, PW11D, and PW11E) in the Ely Limestone of the upper Paleozoic carbonate-rock aquifer hydrogeologic unit (table C.1). In chapter 7 we present more details about the structural setting of this site, and describe and interpret the aquifer test we conducted there. Groundwater levels in the four piezometers are nearly identical, and were approximately constant over the period of record. The aquifer-test results confirm that the basin-fill and carbonate-rock aquifers are hydraulically connected at site 11.

Piezometers PW04A (730–750 feet [222–229 m]) and PW04B (895–915 feet [273–279 m]) are screened in fractured, welded ash-flow tuff of the volcanic-rock aquifer hydrogeologic unit (table C.1). Groundwater levels in the two piezometers are nearly identical, show no significant seasonal fluctuation, and increased by about 0.3 feet (0.1 m) from 2009 to 2013. These are the only piezometers in the network in the volcanic-rock aquifer. Site 4 is in the hanging wall of the west-side-down normal-fault zone that bounds the western margin of the northern Mountain Home Range.

5.3.3.3 Central Confusion Range, North-Central Snake Valley, and Middle Range

Other remote UGS groundwater-monitoring sites in the Snake Valley hydrographic area include site 12 in the central Confusion Range, the Twin Springs MX well in eastern-north-central Snake Valley, and site 18 in the northern Middle Range.

Piezometer PW12A is screened from 1593 to 1633 feet (486–498 m) in the Devonian Guilmette Formation of the lower Paleozoic carbonate-rock aquifer hydrogeologic unit (table C.1). Rocks exposed at the surface dip gently east and have low fracture density. The groundwater level is 1427 feet (435 m) below land surface, and the groundwater-level elevation is more similar to that in Tule Valley than Snake Valley. Site 12 is in the hypothetical zone of interbasin flow from Snake Valley to Tule Valley and is east of Little Valley, an intermontane valley in the Confusion

Range, which is bounded on its east side by a west-side-down normal fault (plate 1). Exposures of this fault in a wash about 2.3 miles (3.7 km) northwest of site 12 reveal dense deformation bands in sandy facies of the Guilmette Formation (appendix E). These deformation bands likely impede cross-fault groundwater flow (e.g., Antonellini and Aydin, 1994), suggesting that groundwater at site 12 may not be connected to groundwater moving northeast from Snake Valley through the Confusion Range. Groundwater levels showed a slight increase from 2008 to 2013, but the variable reproducibility of measuring such deep groundwater levels due to possible stretching of the measuring tape and possible long-term stretching and occasional replacement of the cable from which the transducer hangs, suggest that the significance of this trend is uncertain.

The Twin Springs MX well (site 34) is about 1.2 miles (1.9 km) southeast of Twin Springs, and is screened in the younger basin-fill aquifer hydrogeologic unit (table C.2; plate 3). From 2008 to 2013, groundwater levels in this well fluctuated seasonally by about 0.2 to 0.3 feet (0.06–0.09 m), likely in response to evapotranspiration because the site is far from any site of groundwater pumping for irrigation, and decreased by about 0.3 feet (0.09 m).

At site 18, a single piezometer is screened from 970 to 990 feet (296–302 m) in limestone and dolomite of the Devonian Guilmette Formation of the lower Paleozoic carbonate-rock aquifer hydrogeologic unit (table C.1). On the surface the rocks dip gently south and are not extensively fractured, and drilling records and geophysical logs do not suggest that the borehole encounters faults or highly fractured zones. Equipment problems in this well prevented continuous monitoring of groundwater levels, but existing data suggest no significant seasonal variations and a nearly 1-foot (0.3 m) decline during 2011.

5.3.3.4 Tule Valley and Fish Springs Flat

The UGS groundwater-monitoring network in Tule Valley includes two sites in the basin-fill aquifer, two sites in the carbonate-rock aquifer, and one site in the lower Cambrian-Neoproterozoic siliciclastic-rock confining hydrogeologic unit. The UGS continuously monitors groundwater levels in the Coyote Knolls MX well (site 41) in northern Tule Valley, and in the Central Tule Valley MX well (site 42), both screened in the upper basin-fill aquifer hydrogeologic unit (table C.2; plate 3). During the period of record, groundwater levels in these wells did not fluctuate seasonally and increased slightly.

Site 17 includes three piezometers screened in dolomite of the lower Paleozoic carbonate-rock aquifer hydrogeologic unit. Groundwater levels in these piezometers are nearly identical, showed slight seasonal variation, and increased by about 0.2 feet from 2009 to 2013. Site 17 is in the footwall of an east-side-down normal fault that bounds a north-south-striking horst in north-central Tule Valley. Drilling records and geophysical logs do not indicate that the rock is extremely fractured. The borehole is likely not in the damage zone of the normal fault, but could be hydraulically connected to it by fractures.

Site 10 is on the eastern Confusion Range mountain front, in a possible zone of interbasin flow from Snake Valley to Tule Valley. Both piezometers are in the Ely Limestone of the upper Paleozoic carbonate-rock aquifer hydrogeologic unit. Basin-fill deposits are 300 feet (90 m) deep at this site, but the groundwater level is significantly deeper. The groundwater level in piezometer PW10A declined at a rate of about 0.7 feet per year (0.2 m/yr) from early June 2009 to early June 2011, then from early June 2011 to early March 2013 increased by 0.7 foot (0.2 m), an average rate of about 0.4 feet per year (0.12 m/yr) (table 5.1). From August 2008 to early June 2011, the groundwater level in piezometer PW10B decreased by about 2.4 feet (0.7 m), an average rate of decline of about 0.9 feet per year (0.3 m/yr), then increased by 1.1 feet (0.3 m) from early June 2011 to early March 2013, an average rate of increase of about 0.6 feet per year (0.2 m/yr) (table 5.1; plate 3). This site is far from any area of groundwater pumping, so these groundwater-level trends are most likely related to variations in recharge. The screen midpoints in the two piezometers are 69 feet (21 m) apart, and groundwater levels define an upward hydraulic gradient of about 0.3. The middle Paleozoic siliciclastic-rock confining hydrogeologic unit, projected from outcrops to the south along its north-south strike and nearly vertical dip, is likely present below the basin-fill aquifer about 0.5 to 1.5 miles (0.8–2.4 km) east of site 10. The upward hydraulic gradient may result from impedance of eastward groundwater flow by this unit (Gardner and others, 2011).

Piezometer PW20A is in the topographic pass between the northern House Range and the southern Fish Springs Range, in the northeast corner of the Tule Valley hydrographic area, and is the only well in the UGS network screened (545–565 feet [166–172 m]) in the Lower Cambrian-Proterozoic siliciclastic-rock confining hydrogeologic unit (table C.1). The groundwater level in this piezometer was constant from late 2008 to early 2011, then from late April to late September 2011 rose by about 0.4 feet (0.12 m) (plate 3) likely in response to recharge in the northern House Range and southern Fish Springs Range from unusually large precipitation during winter 2010 to spring 2011. Site 20 is in the zone of interbasin flow from Tule Valley to Fish Springs Flat. Groundwater at site 20 is entirely within the Lower Cambrian Prospect

Mountain quartzite, which is highly fractured in its upper 300 feet (90 m) (data folder DF-2 Lithologic Logs) and, therefore, may transmit groundwater from Tule Valley to Fish Springs Flat. Based on field observations by the senior author, rocks within 1 mile (1.6 m) of site 20 are densely fractured, suggesting that this could be a broad zone of interbasin flow. Such flow would, however, need to cross range-bounding faults on either side of Sand Pass. The range-bounding faults on the western margin of the House Range and on the eastern margin of the Fish Springs Range have opposite displacement directions, so the Sand Pass area is a displacement-transfer zone and is likely densely fractured below the land surface. The tip zones (ends of faults along strike) of major range-bounding fault zones likely contain dense fracturing of variable orientation, and are more favorable for trans-fault groundwater flow than the central part of the faults (chapter 4).

Site 19 is in the southern part of the Fish Springs Flat hydrographic area, about 15 miles (24 km) south of Fish Springs. The site is in the hanging wall of the east-side-down normal fault that defines the Table Knoll horst, and the three piezometers are completed in limestone of the Cambrian Orr Formation of the lower Paleozoic carbonate-rock aquifer hydrogeologic unit. Drilling records and geophysical logs do not indicate that the borehole crosses the fault or is in its damage zone. Groundwater levels in the three piezometers are nearly identical, remained constant from early March 2008 to late April 2011, then increased by about 0.4 feet (0.12 m) from late April to late September 2011 (plate 3) in response to recharge from unusually high precipitation during the previous winter, and remained constant through early March 2013. Groundwater here is warm (about 30°C [86°F]) (Blackett, 2011), possibly due to upwelling of deep groundwater along the normal fault.

5.3.4 Spring-Gradient Sites

The UGS groundwater-monitoring sites near springs consist of two or three nested piezometers equipped with five-foot-long screens at their bases. Screen midpoints in the shallowest, intermediate, and deepest piezometers range from 9.5 to 22.5 feet (2.9–6.9 m), 35.5 to 62.5 feet (11–19 m), and 58.5 to 112.5 feet (18–34 m) below land surface, respectively (table C.1). The objective of these sites is to measure the vertical hydraulic gradient that drives spring flow where discharge cannot be gaged. The exception is Twin Springs (site 24) where nested piezometers are near the north pool, which has a UGS surface-flow gage in its outflow channel (section 5.4), to examine the relationship between discharge and the vertical hydraulic gradient within 100 feet (31 m) of the land surface. Seasonal fluctuations reflect evapotranspiration during the summer followed by recovery of groundwater levels during the winter and spring, and no significant long-term trends are observed.

Spring-gradient sites in Snake Valley are at Twin Springs (site 24), Salt Marsh Lake spring complex (site 26), Leland Harris spring complex (site 25), and Needle Point Spring (site 23; section 5.3.2.4). Groundwater levels in these piezometers fluctuated by about 0.5 to 3 feet (0.15–0.9 m) seasonally, with lowest levels during the summer months and highest levels during the late winter/early spring months (plate 3), in response to evapotranspiration in the spring-fed wetlands ecosystems that are supported by the spring flow. The upward vertical hydraulic gradient was about 0.03 at Twin Springs and the Leland Harris spring complex, and about 0.06 at Salt Marsh Lake spring complex.

Spring-gradient sites in Fish Springs National Wildlife Refuge are at North Spring (site 21) and Middle Spring (site 22). At North Spring, groundwater levels fluctuated by 0.3 feet (0.09 m) seasonally. The average upward vertical hydraulic gradient between the deepest and shallowest piezometers was 0.08. Piezometer SG21C is screened from 56 to 66 feet (17–20 m) in bedrock of the lower Paleozoic carbonate-rock aquifer hydrogeologic unit (table C.1), so the groundwater elevation in this piezometer more closely represents the hydraulic head that drives discharge from the Fish Springs complex than in the other piezometers. At Middle Spring, groundwater levels fluctuated by 0.3 feet (0.09 m) seasonally (plate 3), and the average upward hydraulic gradient was 0.3. The groundwater level in piezometer SG22A showed no apparent long-term trend (plate 3). The groundwater level in piezometer SG22B was nearly 8 feet (2.4 m) above land surface, and declined by about 1.5 feet (0.46 m) from mid-2009 to mid-2011, then increased by about 1.5 feet (0.46 m) in late 2011. The decrease occurred gradually, whereas the increase occurred during a time when the packer in the well was not functioning properly. We are, therefore, unsure how accurately the water levels measured in piezometer SG22B reflect the piezometric level of groundwater near Middle Spring.

5.3.5 Long-Term Trends—U.S. Geological Survey Data

The U.S. Geological Survey has recorded groundwater levels in some wells in the greater UGS study area annually to quarterly since 1981 or before (table C.3; plate 4). These wells are either MX wells screened at 87 to 97 feet (27–30 m) or 187 to 197 feet (57–60 m) below land surface in the basin-fill aquifer, or wells in agricultural areas (table C.3; plate 4). Groundwater levels in nearly all of these wells increased during the early to mid- or late-1980s in response to recharge from unusually high precipitation in

1981 through 1985, then declined gradually through 2012 (plate 4). Groundwater levels in some wells rose in 2011 in response to recharge from unusually high precipitation in late 2010 and early 2011.

In northern Snake Valley, the early March (pre-pumping season) groundwater level in an irrigation well in the southwest part of the Callao agricultural area (site 45, table C.3; plate 4) increased by 2.1 feet (0.6 m) from 1980 to 1984, then from 1986 to 2013 decreased by about 5.1 feet (1.6 m), a rate of decline of about 0.16 feet per year (0.05 m/yr) (R^2 = 0.79) (table 5.2; plate 4). The groundwater level in an unused well in Partoun, (site 46, table C.3; plate 4) about 20 miles (32 km) south of Callao at the base of the southern Deep Creek Range mountain front, increased by about 2 feet (0.6 m) from 1981 to 1988, was approximately constant until 1998, decreased by about two feet through 2005, and increased by about 1 foot (0.3 m) through 2013 (plate 4).

In west-central Snake Valley near the Mt Moriah quarry yard, where groundwater is used for quarry operations and by local residents but not for irrigation, the groundwater level in the well monitored by the U.S. Geological Survey (site 47, table C.3; plate 4) increased by about 4.6 feet (1.4 m) from 1980 to 1984, then decreased by 6.1 feet (1.9 m) to 2005, and was erratic but increased slightly overall through 2013.

In south-central Snake Valley near the Eskdale and Tin Shed agricultural areas, groundwater levels generally rose from the early 1980s to the late 1980s, then declined steadily to 2013 (plate 4). From 1992 to 2013 (available period of record), the groundwater level in the Snake Valley North MX well (site 39, table C.3; plate 4) decreased about 4.4 feet (1.3 m), an average rate of decline of about 0.36 feet per year (0.1 m/yr) (R^2 = 0.95) (table 5.2; plate 4). From 1988 to 2013, the groundwater level in the Shell-Baker Creek well (site 38, table C.3; plate 4) decreased by about 6.3 feet (1.9 m), an average rate of decline of about 0.24 feet per year (0.07 m/yr) (R^2 = 0.85) (table 5.2). This time period included two intervals of greater rates of groundwater-level declines (from 1988 to 1998, 0.35 feet per year [0.11 m/yr, R^2 = 0.98], and from 2001 to 2013, 0.4 feet per year [0.12 m/yr, R^2 = 0.96]) (table 5.2).

From 1989 to 2013, the groundwater level in the site 6 MX well (site 35, table C.3; plate 4) decreased by about 3.9 feet (1.2 m), an average rate of decline of about 0.18 feet per year (0.05 m/yr) (R^2 = 0.98) (table 5.2). From 1998 to 2013, the groundwater level in the site 7 MX well (site 37, table C.3; plate 4) decreased by about 2.3 feet (0.7 m), an average rate of decline of about 0.18 feet per year (0.05 m/yr) (R^2 = 0.97) (table 5.2). From 1987 to 2013, the groundwater level in the Eskdale MX well (site 36, table C.3; plate 4) decreased by about 8.8 feet (2.7 m), an average rate of decline of about 0.35 feet per year (0.11 m/yr) (R^2 = 0.98), and this time period included an interval of substantially greater rate of groundwater-level decline (from 2001 to 2005, 0.71 feet per year [0.22 m/yr], R^2 = 0.93) (table 5.2).

In south-central Snake Valley in the Garrison agricultural area, the groundwater level in the well monitored by the U.S. Geological Survey (site 48, table C.3; plate 4) varied strongly compared to long-term records from most other wells in the study area, and closely followed precipitation variations recorded at Great Basin National Park climate station (figure 4.6c). From 1980 to 1986, the groundwater level in this well increased by about 12.9 feet (3.9 m), then decreased by 17.4 feet (5.3 m) to 1993, increased by 12.3 feet (3.8 m) to 1999, decreased by 8.5 feet (2.6 m) to 2005, increased by 8.5 feet (2.6 m) to 2006, decreased by 9.8 feet feet (2.6 m) to 2010, and increased by 6.3 feet (1.9 m) to 2012 (plate 4).

In southern and east-central Snake Valley (sites 40 and 34, respectively), Tule Valley (sites 52, 51 and 41), Fish Springs Flat (sites 49 and 50), Pine Valley (site 53), and Wah Wah Valley (sites 54 and 55) (table C.3; plate 4), groundwater levels increased by about 0.5 to 2 feet (0.2–0.6 m) during the mid- to late-1980s, then gradually declined to near-1980 levels by the late 2000s.

5.3.6 Groundwater-Level Trends Compiled in the U.S. Bureau of Land Management's FEIS

Groundwater levels in pumping wells in the Eskdale agricultural area declined by about 3 to 10 feet (0.9–3.1 m) from about 1990 to 2010, a rate of about 0.15 to 0.5 feet per year (0.095–0.2 m/yr), as measured by the well operators and reported in the FEIS (U.S. Bureau of Land Management, 2012, p. 3.3–46). Inspection of logs of wells in this area indicates that all are screened in the basin-fill aquifer. At Needle Point Spring, surface flow ceased in 2001 and groundwater levels declined by about 6 feet (1.8 m) from 2001 to 2010 (U.S. Bureau of Land Management, 2012, p. 3.3–25).

5.3.7 Discussion of Groundwater-Level Trends

This section provides some preliminary interpretations of groundwater-level trends and their causes in Snake Valley and adjacent hydrographic areas, based on data from the UGS groundwater-monitoring network, which have high measurement frequency but a relatively short period of record, and the U.S. Geological Survey data, which are much less detailed but include at least 30 years of record for most wells. More robust analyses and interpretations can

be made from the UGS data after at least 10 years of record have accumulated (Taylor and Alley, 2001, p. 15–16). In this section groundwater-level trends are compared primarily to annual precipitation data from the Great Basin National Park climate station (figure 5.4a) because these are the only long-term climate data from a main recharge area in the UGS study area. The U.S. Geological Survey's high-altitude precipitation data (figure 4.7) are also from the main recharge area, but span only six years (2005 through 2010).

Groundwater-level hydrographs at monitoring sites in the UGS study area vary according to distance from areas of groundwater pumping. Groundwater levels at sites within about 5 miles (8 km) of agricultural areas responded to groundwater pumping by decreasing during the summer irrigation season and recovering to pre-pumping levels during the winter and early spring. Groundwater levels at remote sites (disregarding the spring-gradient sites) show slight or no seasonal variation. Groundwater levels at sites on valley floors far from recharge areas show little or no correlation with precipitation records, whereas those along mountain fronts, especially near perennial streams that run out onto the mountain front, show greater year-to-year variation that generally correlates with variations in annual precipitation.

Groundwater levels near recharge areas show greater variation than those in valley centers, for wells in both agricultural areas and remote areas. Groundwater levels in wells in the UGS groundwater-monitoring network in Garrison (sites 1, 3, and 13, plate 3) showed the greatest response to high precipitation during the 2010–2011 winter and early spring. Some recharge in this area likely occurs from infiltration of runoff in Snake Creek, which likely had greater-than-usual flow rate during this time. Long-term groundwater-level records from wells at Callao (sites 44 and 45), Partoun (site 46), Mt Moriah Quarry (site 47), and Garrison (site 48) (plate 4) varied markedly in concert with variations in precipitation (table 5.2; plate 4), likely due to their proximity to the area of concentrated groundwater recharge and surface runoff in the northern Snake Range and southern Deep Creek Range, respectively.

Groundwater levels at remote monitoring sites in valley centers or near ranges having low recharge rates changed negligibly during the period of record of UGS monitoring and long-term monitoring by the U.S. Geological Survey (plates 3 and 4), whereas groundwater levels at remote monitoring sites near mountain fronts showed greater variation. Groundwater levels at sites 4, 12, 17, 18, 19, and 20 (plate 3) varied little during the period of record, except for step increases of 0.2 to 0.4 feet during 2011, but with little change before or after. Site 8 in southern Snake Valley and site 10 in west-central Tule Valley showed similar patterns of decreasing groundwater levels from 2009 to 2011 and increasing groundwater levels from 2011 to 2013, at higher rates than recorded at other remote sites (table 5.1; plate 3). The changes at site 8 may be due to hydrostatic pressure effects from local recharge in the southern Snake Range, Buckskin Hills, and northern Mountain Home Range, and the changes at site 10 may be due to hydrostatic pressure effects from local recharge in the Confusion Range.

Plots of groundwater hydrographs and cumulative departure from average annual precipitation can help identify baseline groundwater-level variations due to temporal variations in precipitation and, by inference, recharge, and identify wells that are influenced by groundwater pumping. Burden and others (2012, p. vii) defined and described interpretation of cumulative departure from average annual precipitation as follows:

> [the cumulative departure plot is] a graph of the departure or difference between the average annual precipitation and the value of precipitation for each year, plotted cumulatively. A cumulative plot is generated by adding the departure from average precipitation for the current year to the sum of departure values for all previous years in the period of record. A positive departure, or greater-than-average precipitation, for a year results in a graph segment trending upward; a negative departure results in a graph segment trending downward. A generally downward-trending graph for a period of years represents a period of generally less-than-average precipitation, which commonly causes and corresponds with declining water levels in wells. Likewise, a generally upward-trending graph for a period of years represents a period of greater-than-average precipitation, which commonly causes and corresponds with rising water levels in wells. However, increases or decreases in withdrawals of groundwater from wells also affect water levels and can change or eliminate the correlation between water levels in wells and the graph of cumulative departure from average precipitation.

Figure 5.4a shows annual precipitation and cumulative departure for the Great Basin National Park (GBNP) climate station operated by the National Climatic Data Center from 1981 to 2012, and figure 5.4b shows cumulative departure plots for five stations in the UGS study area. This time period was chosen because it is the most common period of record for annual measurements by the U.S. Geological Survey of MX wells, which were installed

Table 5.2. *Estimated rates of change of groundwater levels from U.S. Geological Survey data.*

UGS Site Number[1]	Piezometer	Average Rate of Change[2] (ft/yr)	Time Period	Hydrogeologic Unit	Screened Interval
AGRICULTURAL AREAS					
Northern Snake Valley					
45	Callao shallow	-0.16 (R^2 = 0.79)	1986–2013	QTcs	126
		-0.28 (R^2 = 0.96)	1986–1997		
		-0.36 (R^2 = 0.97)	1998–2005		
		-0.75 (R^2 = 0.99)	2006–2009		
South-Central Snake Valley					
Eskdale–Tin Shed area					
36	Eskdale MX	1.1 (R^2 = 0.96)	1981–1987	QTcs	77–97
		-0.35 (R^2 = 0.98)	1987–2013		
		-0.71 (R^2 = 0.93)	2001–2005		
38	Shell-Baker Creek	0.94 (R^2 = 0.97)	1982–1986	QTcs	69–76
		-0.24 (R^2 = 0.85)	1988–2013		
		-0.35 (R^2 = 0.98)	1988–1999		
		-0.40 (R^2 = 0.96)	2001–2013		
39	Snake Valley North MX	-0.36 (R^2 = 0.95)	1991–2013	QTcs	74–94
Garrison area					
48	Garrison	1.9 (R^2 = 0.97)	1978–1986	QTcs	80–300
		-2.3 (R^2 = 0.92)	1986–1993		
		1.8 (R^2 = 0.84)	1993–1999		
		-1.4 (R^2 = 0.89)	1999–2005		
		-2.5 (R^2 = 0.94)	2006–2011		
		-0.42 (R^2 = 0.27)	1999–2013		
Southern Snake Valley					
40	Snake Valley South MX	-0.04 (R^2 = 0.89)	2009–2013	QTcs	77–97
REMOTE SITES					
South-Central Snake Valley					
Eskdale–Tin Shed area					
35	PW06 MX	0.26 (R^2 = 0.95)	1984–1989	QTcs	77–97
		-0.18 (R^2 = 0.98)	1989–2013		
37	PW07 MX	0.27 (R^2 = 0.98)	1988–1996	QTcs	77–97
		-0.18 (R^2 = 0.97)	1998–2013		
Northern Snake Valley					
46	Partoun	0.25 (R^2 = 0.74)	1981–1988	QTcs	–
		-0.09 (R^2 = 0.70)	1988–2007		
		0.11 (R^2 = 0.74)	2007–2013		
		-0.1 (R^2 = 0.71)	1988–2013		

Table 5.2. *continued*

UGS Site Number[1]	Piezometer	Average Rate of Change[2] (ft/yr)	Time Period	Hydrogeologic Unit	Screened Interval
Central Snake Valley					
34	TS MX	0.03 (R^2 = 0.52)	1981–2001	QTcs	78–98
		-0.07 (R^2 = 0.88)	2001–2013		
47	Mt Moriah Quarry	1.3 (R^2 = 0.72)	1981–1984	QTcs	–
		-0.23 (R^2 = 0.78)	1985–2005		
		negligible	2006–2013		
Tule Valley and Fish Springs Flat					
42	Central Tule Valley MX	0.26	1981–1987	QTcs	100–380
		negligible	1988–2013		
41	Coyote Knolls MX	0.18	1981–1989	QTcs	161–181
		negligible	1990–2013		
50	SW Fish Springs Flat	0.01 (R2 = 0.81)	1981–1994	QTcs	177–197
		-0.03 (R2 = 0.84)	1994–2013		

[1] See table C.3 for more detailed well information.

[2] Approximate rate of change calculated by simple linear regression for values where an R^2 is cited, or by difference between groundwater levels measured in early March.

in 1979 and 1980 and, therefore, provide a long-term record of groundwater-level variations.

The plots in figure 5.4b are divided into periods of predominantly above-average and below-average precipitation. On figure 5.4b, vertical lines through inflection points on the cumulative departure plot of the GBNP data define predominantly greater-than-average precipitation periods from 1981 to 1987, 1994 to 1998, 2005 to 2006, and 2008 to 2011, separated by periods of less-than-average precipitation. Because GBNP is in part of the principal recharge area for the basin-fill and carbonate-rock aquifers in Snake Valley (section 4.5.4), these records can be used as a qualitative proxy for groundwater recharge assuming that they represent precipitation on the entire recharge area of the Snake Range and Deep Creek Range. The cumulative departure plot for the GBNP climate station can be compared to changes in groundwater levels in wells to delineate the degree of connection of the aquifers in which the wells are screened to the recharge area. Wells that display groundwater-level trends that do not correlate with precipitation changes are likely influenced by other hydrologic factors, primarily groundwater pumping.

In Snake Valley, groundwater-level variations near recharge areas qualitatively correlate with variations in precipitation at GBNP, including wells in agricultural areas (Callao, site 45 figure 5.5a; Garrison, site 48, figure 5.5b) and remote areas (Partoun, site 46, figure 5.5c; Mt. Moriah Quarry yard, site 47, figure 5.5d). Groundwater levels in wells in south-central Snake Valley, near the Eskdale and Tin Shed agricultural areas (Eskdale MX, site 36, figure 5.5e; PW06 MX, site 36, figure 5.5f; PW07 MX, site 37, figure 5.5g; Shell-Baker Creek, site 38, figure 5.5h; Snake Valley North MX, site 54, figure 5.5i) increased by about 0.3 to 1 foot per year (0.1–0.3 m/yr) in response to greater-than-average precipitation during the early to mid-1980s, then declined from the late 1980s or early 1990, depending on location, to 2013.

During the time of overall declining groundwater levels, two periods of greater-than average precipitation occurred, from 1994 to 1998 and from 2004 to 2006, but had little effect on groundwater levels, at least in comparison to the early 1980s. The exception is the Shell-Baker Creek well, which may have received some local recharge from flow in Baker Creek. Although records of changes in groundwater pumping are not available, groundwater pumping is the most likely cause of the decoupling of groundwater level trends from precipitation variations in this area. Dong and Halford (2010) estimated average effective groundwater withdrawals in south-central Snake Valley of about 7800 to 16,000 acre-feet per year for the 2000 through 2004 irrigation seasons, based on total groundwater pumped (from crop area and estimated application rates), minus return flow (estimated at 20% of pumped value). Dong and others (2011) estimated average effective groundwater withdrawals in southern Snake Valley of about 4500 to 6600 acre-feet per year for the 2000 through 2004 irrigation seasons, using the same approach as Dong and Halford (2010).

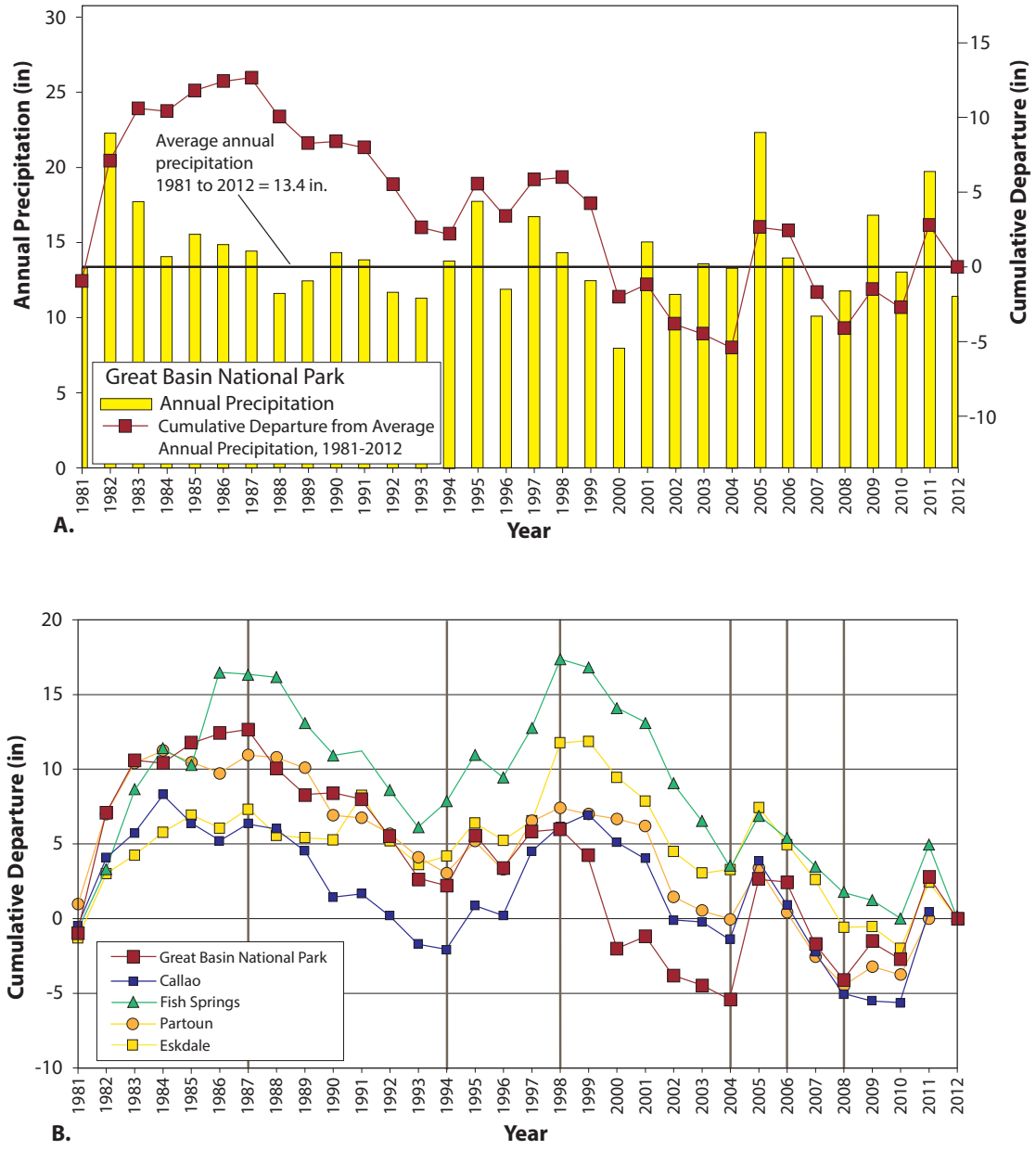

Figure 5.4. *Cumulative departure from average annual precipitation for selected National Climate Data Center Co-op stations in the UGS study area, 1981 to 2012. The data were accessed from the Western Regional Climate Center (http://www.wrcc.dri.edu/summary/Climsmut.html). Figure 4.10 shows station locations. See section 5.3.7 for description of cumulative departure plots. The plots are used here to identify temporal trends in precipitation, and to aid interpretation of groundwater-level hydrographs (figure 5.5).* ***A.*** *Plots of annual precipitation and cumulative departure for the Great Basin National Park Co-op station. Periods of generally above-average precipitation occurred from 1981 to 1987, 1994 to 1998, 2005 to 2006, and 2008 to 2011. Periods of generally below-average precipitation occurred from 1987 to 1994, 1998 to 2005, and 2007 to 2008. These periods are interpreted to represent times of relatively high and low recharge rates, respectively, to aquifers in Snake Valley.* ***B.*** *Plots of cumulative departure for five Co-op stations in the study area, showing that trends in annual precipitation were generally similar throughout the UGS study area, so that groundwater-level hydrographs from throughout the study area can be directly compared.*

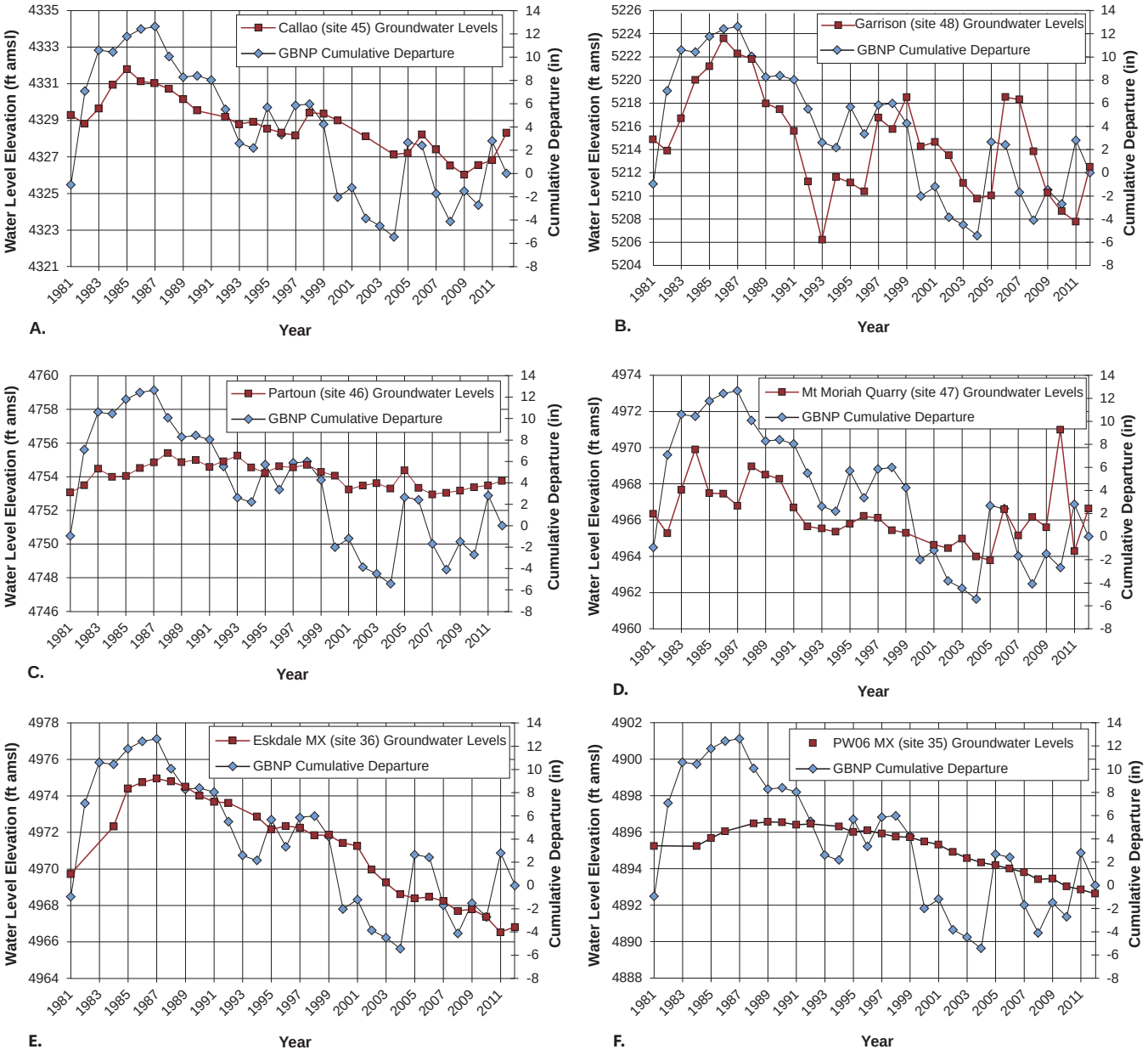

Figure 5.5. *Groundwater levels in wells monitored annually by the U.S. Geological Survey and cumulative departure from average annual precipitation from the National Climate Data Center Co-op station at Great Basin National Park, 1981 to 2012. Water-level data are from the U.S. Geological Survey's National Water Information System (http://waterdata.usgs.gov/nwis/gw), and cumulative departure values were calculated from precipitation data obtained from the Western Regional Climate Center (http://www.wrcc.dri.edu/summary/Climsmut.html). See table C.3 for well information.* ***A.*** *Groundwater levels in a well in Callao (site 45) in the southwestern part of the Callao agricultural area (figure 5.1; table C.3) that is pumped for irrigation. Groundwater levels measured in early March, before the irrigation season, generally correlated with annual precipitation trends with a one- to two-year time lag.* ***B.*** *Groundwater levels in a well in Garrison (site 48) in the Garrison agricultural area (figure 5.1; table C.3). Groundwater levels generally correlated with annual precipitation trends, with a one-year time lag.* ***C.*** *Groundwater levels in an unused well in Partoun (site 46) (figure 5.1; table C.3). Groundwater levels generally correlated with annual precipitation trends.* ***D.*** *Groundwater levels in the Mt Moriah Quarry Yard well (site 47) (figure 5.1; table C.3). Groundwater levels generally correlated with annual precipitation trends.* ***E.*** *Groundwater levels in the Eskdale MX well (site 36) east of the Eskdale agricultural area (figure 5.1; table C.3). Groundwater levels rose during the high-precipitation years 1981 to 1987, and declined thereafter (table 5.2) despite several periods of increased precipitation. The rate of decline increased during a period of lower-than-average annual precipitation from 2000 to 2004, and decreased during periods of greater-than-average precipitation from 1996 to 1998 and 2004 to 2006.* ***F.*** *Groundwater levels in the PW06 MX well (site 35) north-northeast of the Eskdale agricultural area (figure 5.1; table C.3). Groundwater levels rose during and after the greater-than-average precipitation years 1981 to 1987, and declined thereafter (table 5.2) despite several periods of greater-than-average precipitation.*

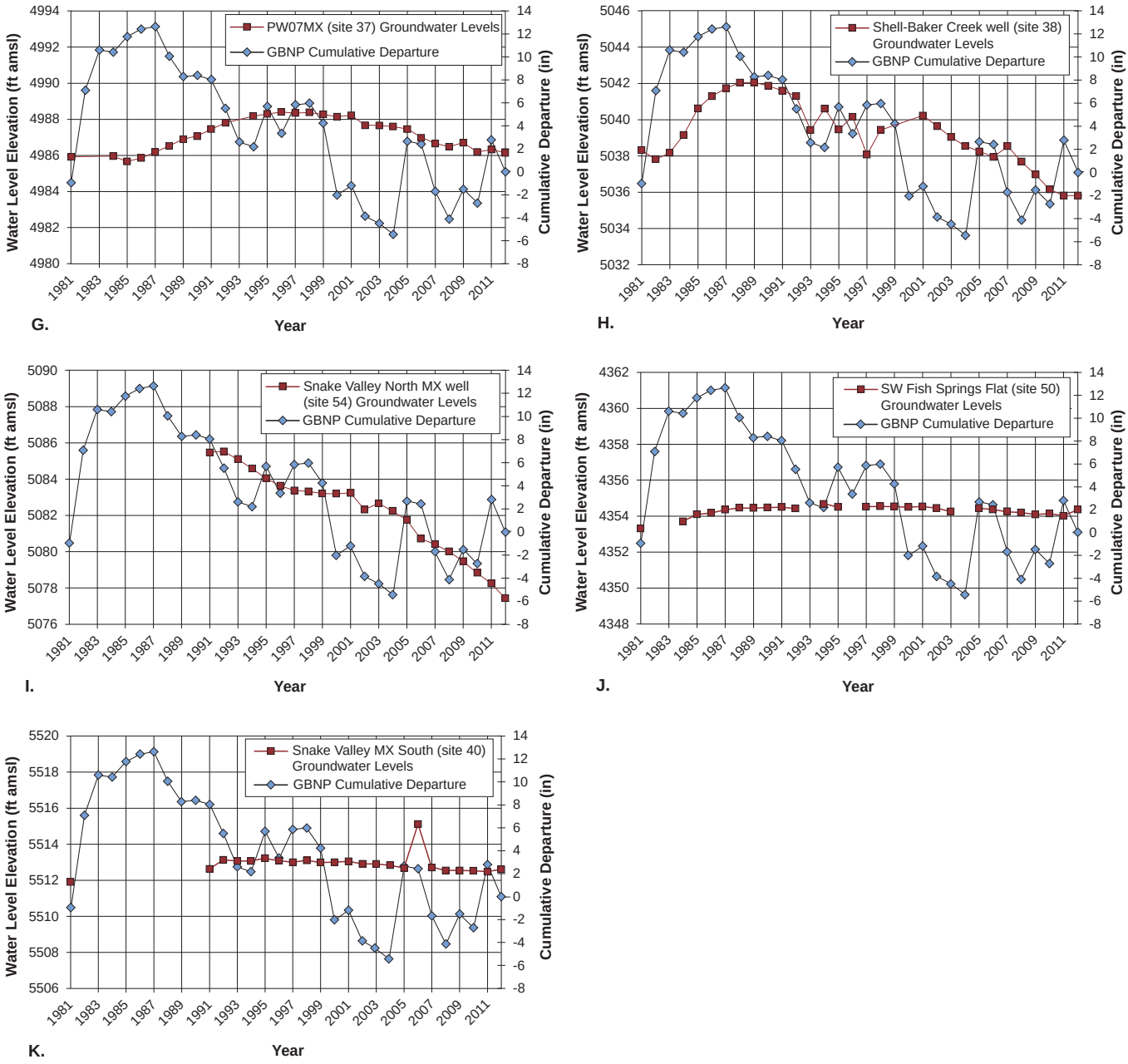

Figure 5.5. *continued* ***G.*** *Groundwater levels in the PW07 MX well (site 37) southeast of the Eskdale agricultural area (figure 5.1; table C.3). Groundwater levels rose during and after the greater-than-average precipitation years 1981 to 1987, and declined thereafter (table 5.2) despite several periods of greater-than-average precipitation.* ***H.*** *Groundwater levels in the Shell-Baker Creek well (site 38) southwest of the Eskdale agricultural area and southeast of the Tin Shed agricultural area (figure 5.1; table C.3). Groundwater levels generally correlated with variations in annual precipitation.* ***I.*** *Groundwater levels in the Snake Valley north MX well (site 39) northwest of the Tin Shed agricultural area (figure 5.1; table C.3). Groundwater levels rose during the high-precipitation years 1981 to 1987, and declined thereafter (table 5.2) despite several periods of greater-than-average precipitation. The rate of decline increased after 2003.* ***J.*** *Groundwater levels in the SW Fish Springs Flat MX well (site 50) (figure 5.1; table C.3). Groundwater levels remained constant and did not correlate with annual precipitation trends.* ***K.*** *Groundwater levels in the Snake Valley South MX well (site 40) northwest of the Granite Peak Ranch agricultural area (figure 5.1; table C.3). Groundwater levels remained constant and did not correlate with annual precipitation trends, except for a sharp increase in 2006 in response to high precipitation in 2006.*

In south-central Snake Valley, comparison of groundwater-level changes and cumulative departure curves for wells far from and within areas of groundwater pumping yields approximate maximum rates of change due to variations in precipitation from 1981 to 2013. Groundwater levels in the MX wells at sites 35 (PW06 MX) and 37 (PW07 MX) fluctuate seasonally by about 0.06 feet and 0.25 to 0.4 feet, respectively (plate 3). Site 37 is on a dry playa with abundant greasewood, so seasonal groundwater fluctuations there may be related to evapotranspiration rather than groundwater pumping. Dong and Halford (2010) did not include sites 35 and 37 in their regional aquifer-test analysis of irrigation pumping in south-central Snake Valley, but visual inspection of their figure 8 suggests that these sites are at the outer limit of drawdown related to groundwater pumping. Long-term groundwater levels in these wells may only slightly, if at all, reflect decreasing groundwater levels due to pumping in the Eskdale agricultural area (section 5.3.6).

Groundwater levels increased at average rates of 0.26 feet per year from 1984 to 1989 at site 35, and at 0.27 feet per year from 1988 to 1996 at site 37 (table 5.2; plate 4), in response to greater-than-average annual precipitation from 1981 to 1987 (figure 5.4). The delayed response of groundwater levels to the increased recharge from precipitation reflects slow transmission of the hydrostatic pressure wave and groundwater flow through the basin-fill aquifer.

Groundwater levels declined at average rates of 0.21 feet per year from 1989 to 2012 at site 35, and at 0.18 feet per year from 2009 to 2013 at site 37 (table 5.2; plate 4), in response to lower-than-average annual precipitation from 1988 to 2004 and 2006 to 2008 (figure 5.4). The rate of decline of groundwater levels at both wells after the late 1980s of about 0.2 feet per year (0.06 m/yr), provides a reasonable estimate of maximum changes in groundwater levels due to variations in precipitation. This is a maximum estimated rate of change because the declines may include some drawdown from groundwater pumping. In summary, of the rates of decline of groundwater levels observed in south-central Snake Valley from the late 1980s to present, up to about 0.2 feet per year (0.06 m/yr), could be attributed to generally decreasing rates of recharge due to overall lower-than-average annual precipitation.

The rates and magnitudes of groundwater-level change in response to variations in precipitation and recharge likely varied throughout Snake Valley and adjacent hydrographic areas. For example, MX wells in east-central Snake Valley (Twin Springs MX well, site 34), Tule Valley (Coyote Knolls MX well, site 41), and Fish Springs Flat (SW Fish Springs Flat MX well, site 50, figure 5.5j) that are much farther from areas of recharge and groundwater pumping showed substantially less increase during the early to mid 1980s and less decline beginning in the late 1980s compared to sites 35 and 37 (plate 4).

In southern Snake Valley, the Snake Valley South MX well on the southern Snake Range mountain front (site 40, figure 5.5k) showed only one instance of response to increased precipitation, and is not strongly affected by nearby irrigation (Dong and others, 2011). This well may be screened in a perched or otherwise hydraulically isolated part of the basin-fill aquifer. Long-term records from wells not affected by the groundwater pumping are not available to estimate how much of this decline may result from lower recharge rates after the late 1980s.

5.4 SPRING-FLOW MONITORING

5.4.1 Introduction

The UGS and the Utah Division of Water Rights installed equipment to measure discharge at springs that could be impacted by future groundwater development. These springs have water rights on record and/or their outflow supports spring-fed wetlands ecosystems that provide habitat for sensitive aquatic species (section 4.5.3). In all, ten gages are in place at six sites and the real-time data are streamed to the Utah Department of Natural Resources via radio telemetry. We can make only preliminary interpretations about average values and variations in discharge because the period of record is between three and four years for the flow gages and some sites encountered equipment problems.

5.4.2 Instrumentation

Each of the ten flow-measurement gages is equipped with some type of primary flow measuring equipment (table C.4), a radio modem, an antenna, and, since May 2013, a back-up data logger. Power is supplied by a marine-grade 12-volt battery recharged by 10- to 50-watt solar panels or by the electrical grid where available. We determined the best flow measuring device for each site based on the range of probable discharge, the level of accuracy and reliability of the device, and the geography and physical characteristics of the stream channel or spring head. Flumes (figures 5.6a, 5.6b, and 5.6c) are located at sites where debris clogging may be an issue or where flow comes from a culvert. A 90-degree v-notch weir was retrofitted into one existing concrete spring collection box (figure 5.6d), and ultrasonic flow meters were attached to existing discharge pipes at two sites (figure 5.6e).

Figure 5.6. *Instrumentation at surface-flow measurement sites.* ***A.*** *20 cfs ramp flume at West Middle Ditch (site 28) and large stilling well, solar panel, and antenna to left of flume.* ***B.*** *3-foot Parshall flume at East Middle Ditch (site 28).* ***C.*** *8-inch Palmer Bowlus flume to left of stilling well and instrument box on pole downgradient of the earthen dam at Miller Spring (site 32).* ***D.*** *90-degree v-notch weir plate (lower left) and float on pulley (upper right) attached to a shaft encoder (concealed in metal box) at Clay Spring (site 29).* ***E.*** *Ultrasonic flow meter transducers attached to discharge pipe at Kell Spring (site 31).* ***F.*** *Shaft encoder and pulley system inside a stilling well.*

Figure 5.6. *continued* ***G.*** *Weatherproof box housing radios, solar panel power controller, and data card inside protective metal box.*

In the case of flumes and weirs, a shaft encoder and pulley/float/weight system housed inside a stilling well (figure 5.6f) translates the depth of water in the flume or weir (stage) to a signal. The ultrasonic flow meters calculate the velocity of the water in the pipe using sonic reflectance and calculate the flow in the pipe using this velocity. The stage or flow signal is read every 10 to 15 minutes and telemetered via radio modems (figure 5.6g) to our connection to the Utah Department of Natural Resources (DNR) network at the Utah Department of Transportation station in Garrison, Utah. Stage is converted to flow using either standard rating tables for the particular flume or weir or rating tables we have made using in-stream flow metering. Discharge data are available in real time from the Division of Water Rights (part of DNR) on their website (http://www.waterrights.utah.gov/distinfo/realtime_info.asp). The UGS reviews these data quarterly and places the quality-controlled data and information relevant to a site's discharge on the UGS groundwater-monitoring data portal (http://geology.utah.gov/databases/groundwater/projects.php).

5.4.3 Geologic Setting and Discharge Records

5.4.3.1 Miller Spring

Miller Spring is in northern Snake Valley, 0.2 miles (0.32 km) east of the valley-floor axis and about 0.15 miles (0.24 km) west of the western margin of alluvial-fan deposits that emanate from the northern Confusion Range to the east (figure 5.7). The spring discharges from fine-grained lacustrine deposits of the younger basin-fill confining hydrogeologic unit into an impounded pool. The spring does not coincide with a mapped fault, but is about 2000 feet (610 m) east of the axis of a north-south striking fault interpreted from the horizontal gradient in the isostatic residual gravity field (figures 3.14 and 5.7). As discussed in section 3.4, map traces of faults interpreted from gravity gradients show the position of the faults at depth and, therefore, do not coincide to their surface traces. If this fault dips west, its surface trace likely lies near Miller Spring and it may localize the spring.

From mid 2010 to September 2013, discharge from Miller Spring ranged from about 0.2 to 0.45 cubic feet per second (6–13 L/sec) and averaged 0.3 ± 0.05 cubic feet per second (8 ± 1 L/sec) (figure 5.8). Discharge measurements were higher for a brief period during very cold weather in early 2011, and we suspect ice was interfering with the normal operation of the flow-monitoring equipment. The earthen dam that impounds the spring discharge leaked by varying amounts in 2012 and 2013, which produced less-than-actual discharge values.

5.4.3.2 Twin Springs and Foote Reservoir Spring

The UGS monitors flow from Twin Springs and Foote Reservoir Spring in the Bishop Springs area (figure 5.9). Twin Springs and Foote Reservoir Spring issue from the distal part of a composite alluvial-fan deposit west of the central Confusion Range (figure 5.9). Hintze and Davis (2002a) show no faults below or near these springs, and they are about 2.5 miles (4.0 km) east of the nearest fault interpreted from the horizontal gradient in the isostatic residual gravity field (figure 3.14). Kistinger and others (2009) and Rowley and others (2009) show a northwest-striking normal fault below Twin Springs and Foote Reservoir Spring, and a parallel normal fault to the southwest. We have not investigated the area in detail, but we also interpret Twin Springs and Foote Reservoir Spring to lie along a northwest-striking, southwest-side-down normal fault, based on reconnaissance mapping and inspection of aerial photographs. The Bishop Springs area also includes several seeps southwest of Foote Reservoir Spring and a spring about 0.75 miles (1.2 km) southwest of Foote Reservoir Spring known as Central Pool, which may occur along

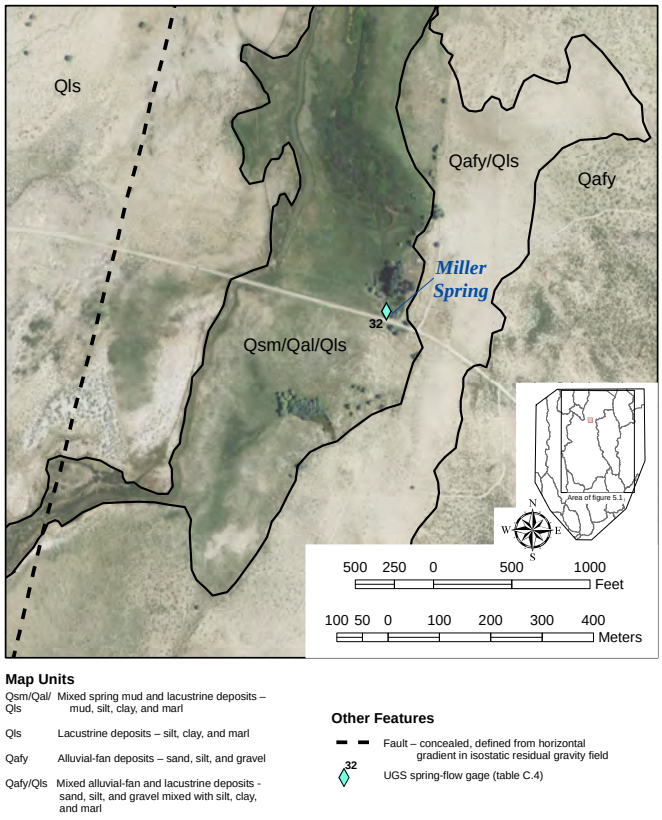

Figure 5.7. *Geographic and geologic setting of the Miller Spring area (site 32, table C.4), northern Snake Valley, based on reconnaissance mapping by the senior author. Contact locations are approximate.*

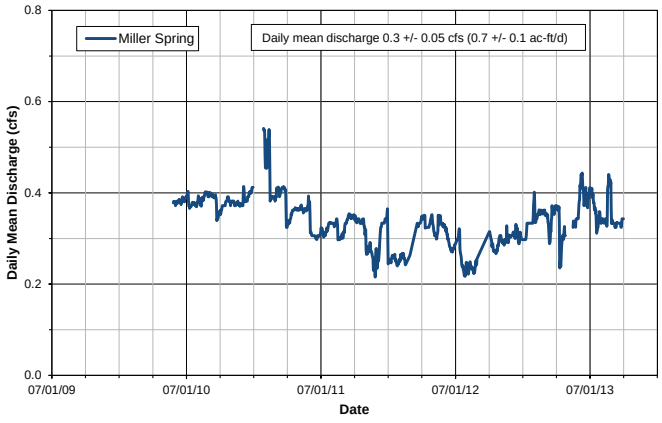

Figure 5.8. *Hydrograph of daily mean discharge from Miller Spring (site 32, table C.4). Ice possibly affected measurements in January–February 2011. Leak in dam affected measurements in 2012 and 2013.*

a separate northwest-striking fault, or along a northeast-striking fault in the hanging wall of the fault that localizes Twin Springs and Foote Reservoir Spring.

Twin Springs has a north orifice and a south orifice located approximately 150 feet apart; each orifice is surrounded by a pool of clear water and drained by a distinct outflow stream channel. UGS flumes are installed in each channel

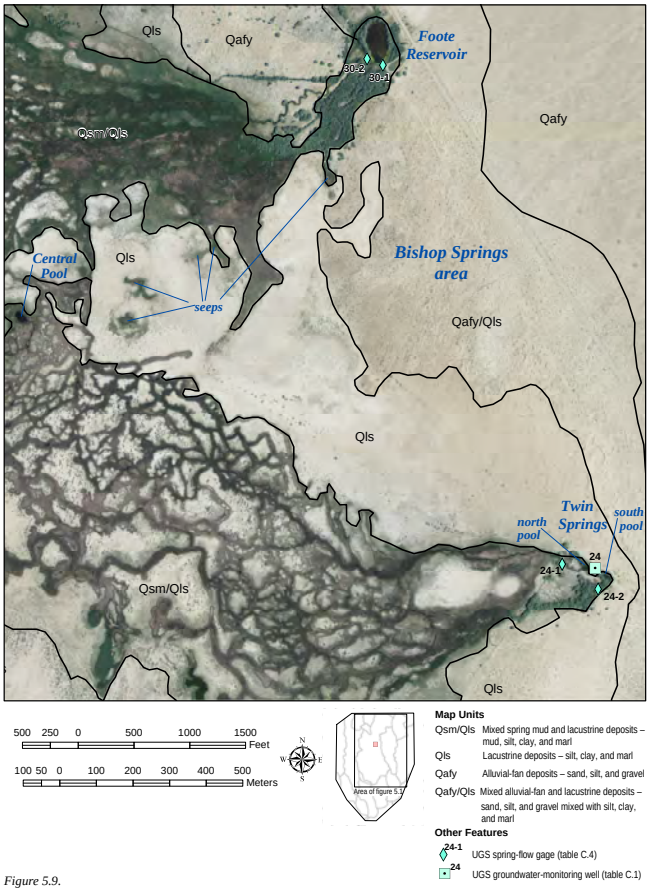

Figure 5.9.

Figure 5.9. *Geographic and geologic setting of the Bishop Springs area, east-central Snake Valley (sites 24 and 30, table C.4). Surficial geology is based on reconnaissance mapping by the senior author. Contact locations are approximate.*

roughly 100 to 200 feet downstream from the pools. Discharge from Twin Springs north orifice varies from about 1.3 to 1.6 cubic feet per second (37–45 L/sec), and averages 1.4 ± 0.05 cubic feet per second (40 ± 1 L/sec) (figure 5.10). Discharge from Twin Springs south orifice varies from about 1.1 to 1.5 cubic feet per second (31–43 L/sec), and averages 1.3 ± 0.07 cubic feet per second (37 ± 2 L/sec) (figure 5.10). During the 3 years of record, discharge from the south orifice increased by about 0.2 cubic feet per second in the late fall and early winter, whereas no seasonal variation in discharge was observed from the north orifice.

Discharge from Foote Reservoir Spring is impounded in Foote Reservoir, which has two outlets, one to an outflow stream and the other into a pipe that supplies an irrigation pivot about 1.5 miles (2.4 km) to the northwest, complicating record interpretation. When the irrigation pivot is operating, the discharge measured at the pivot with an ultrasonic flow meter must be added to the discharge through a flume in the reservoir outlet channel. The average measured discharge from Foote Reservoir Spring is 3.0 ± 0.3 cubic feet per second (85 ± 9 L/sec) (figure 5.11). Most variation in the combined discharge apparent in figure 5.11

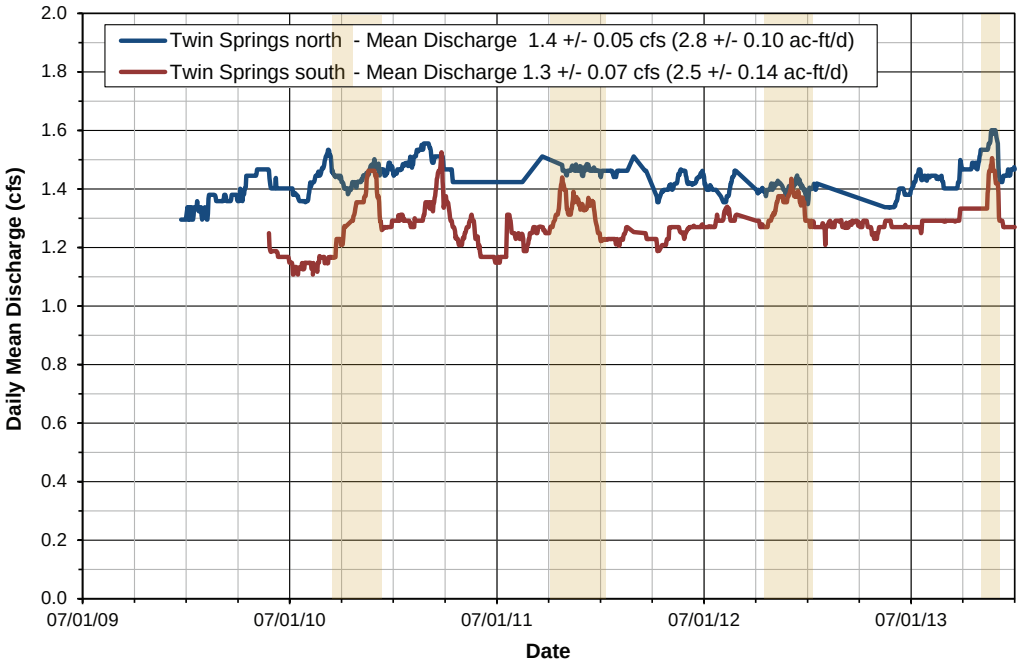

Figure 5.10. *Hydrographs of daily mean discharge from Twin Springs north and south orifices (site 24, table C.4). Apparent increase in discharge from the south orifice each fall is shaded.*

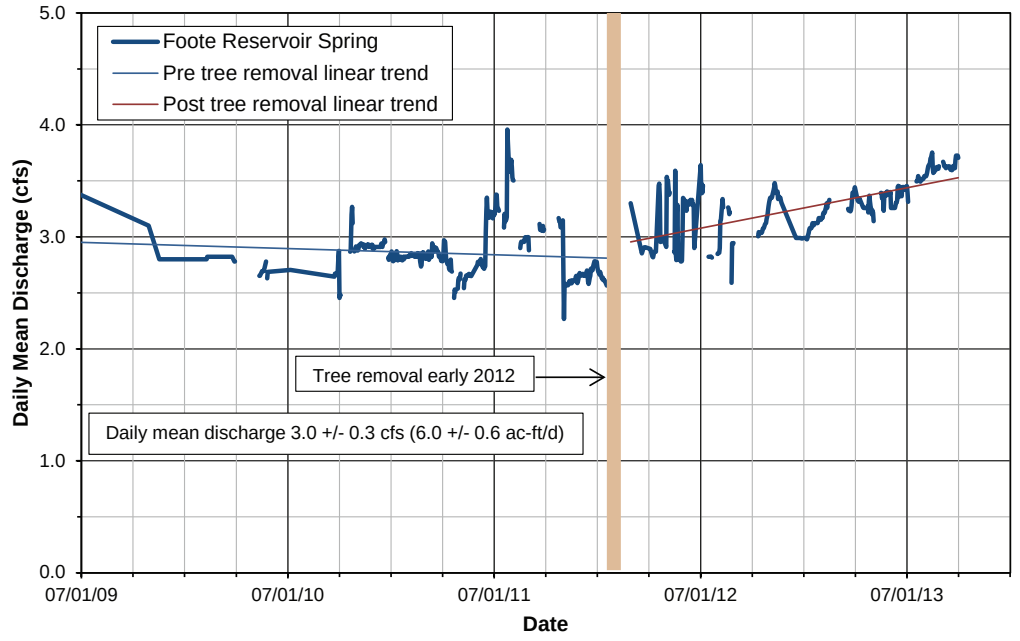

Figure 5.11. *Hydrograph of combined daily mean discharge from Foote Reservoir outflow and irrigation pivot (site 30, table C.4). Periods of rapid increase and decrease in calculated discharge are often due to non-equilibrium flow after the irrigation pivot is cycled on and off. Discharge increased following removal of 13 acres of large trees surrounding the spring area; however, the long-term effect of tree removal on discharge is unknown.*

coincides with changes in water routing between the reservoir and the pivot.

Utah Division of Wildlife Resources personnel removed a small forest of Russian olive (*Eleagnus angustifolia*) trees covering approximately 13 acres around Foote Reservoir and the outlet stream in late January/early February 2012. A linear regression on pre-tree-removal discharge (figure 5.11) shows a slight downward trend, whereas the discharge after the trees were removed trends up. Non-native Russian olive and saltcedar trees have been implicated in increased water loss from riparian systems through evapotranspiration in the West since the 1980s (Nagler and others, 2010). Recent research on removal of Russian olive and saltcedar trees on riparian ecosystems in the West (Nagler and others, 2010) suggests that removal of these two non-native trees may not conserve water in the stream as compared to water consumption by native cottonwood and willow species; however, the Foote Reservoir area did not support large trees before the spread of Russian olive over the past two decades. Reported rates of evapotranspiration for mixed stands of saltcedar and Russian olive average approximately 1 meter per year (Nagler and others, 2010), somewhat higher than salt grass and other grasses (Shafroth and others, 2005). Our data suggest more water is flowing in the stream channel since the removal of the trees. Discharge trends will be closely monitored as the area vegetates.

5.4.3.3 Kell Spring

Kell Spring is in west-central Snake Valley, in fine-grained lakebed deposits of the younger basin-fill confining hydrogeologic unit, about 900 feet (274 m) east of the eastern margin of Quaternary alluvial-fan deposits that emanate from the northern Snake Range (figure 5.12). Hintze and Davis (2002a) show an approximately north-striking, east-side-down normal fault that cuts surficial deposits and passes directly through Kell Spring. This fault may control the location of the spring by juxtaposing basin-fill deposits of contrasting hydraulic properties. Discharge from Kell Spring has increased slightly over the period of record and averaged 0.13 ± 0.02 cubic feet per second (3.7 ± 0.6 L/sec) (figure 5.13). Most discharge variations shown on figure 5.13 are due to temporary vegetation blockages in the pipe through the small earthen dam surrounding the spring head.

5.4.3.4 Clay Spring

Clay Spring is in southern Snake Valley, on the western flank of the northern Burbank Hills and about 0.3 miles (0.5 km) east of Lake Creek (figure 5.14). The spring issues from coarse-grained, poorly sorted, semi-consolidated alluvial-fan deposits of the younger basin-fill aquifer hydrogeologic unit. Hintze and Davis (2002b) do not show a fault near Clay Spring, and reconnaissance field inspection by the senior author was inconclusive regarding the presence of a fault. Clay Spring is in an inactive ephemeral stream bed, and the basin-fill deposits dip gently east, so the spring may be a contact spring where the gully intersects the water table above a low-permeability bed. Discharge from Clay Spring has averaged 0.3 ± 0.02 cubic feet per second (9 ± 0.6 L/sec) (figure 5.15), and shows a slight downward trend.

5.4.3.5 Dearden Springs

Dearden Springs (aka Stateline Springs) are on the Dearden Ranch in southern Snake Valley, about 1200 feet (370 m) east of the Utah-Nevada border (figure 5.16). The Dearden Springs complex consists of at least seven spring heads along a 0.4-mile-long (0.6 km) stretch of Lake Creek, and the springs issue from fine-grained, densely jointed calcareous sandstone of the Permian Arcturus Formation of the upper Paleozoic carbonate-rock hydrogeologic unit (figure 5.17).

Downstream of the Dearden Springs complex, Lake Creek splits into two channels. The UGS estimates discharge from the spring complex as the difference between the combined flow through a flume in each channel, and a flume upstream of the springs (figures 5.16). This configuration provides an estimate of the discharge from the spring complex, but does not account for other possible gains to and losses from the stream, such as seepage from intermittently used irrigation canals on either side of Lake Creek, or loss from the stream bed to the basin-fill or bedrock aquifers. We estimate the total uncertainty on individual estimates of daily mean discharge from the spring complex is 0.5 cfs (14 L/sec). This precision can be improved by gaging flow in the canals and estimating seepage to the stream.

Daily mean discharge from the Dearden Springs complex ranges from about 4 to 8 cubic feet per second (113–227 L/sec) and averages 5.9 ± 0.9 cubic feet per second (167 ± 26 L/sec) (figure 5.18). The overall trend since UGS began measuring spring discharge at this site is downward. Spring flow shows periodic changes, despite gaps in the record. Peak flow occurred between mid December and mid March, and minimum flow occurred between early August and mid September. Peak flow and the transition from declining flow to increasing flow coincided with periods of greatest mean monthly precipitation measured in Great Basin National Park (figure 4.9d). The transition from increasing to decreasing flow was abrupt and occurred before the beginning of the irrigation season for the Granite Peak Ranch agricultural operation, the northern well of

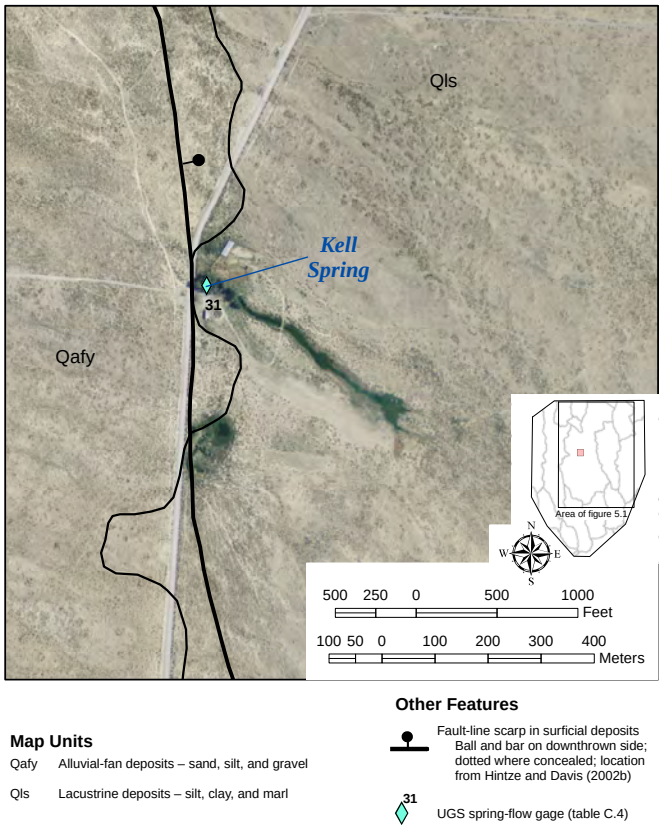

Figure 5.12. *Geographic and geologic setting of the Kell Spring area, west-central Snake Valley (site 31, table C.4), based on reconnaissance mapping by the senior author. Contact locations are approximate.*

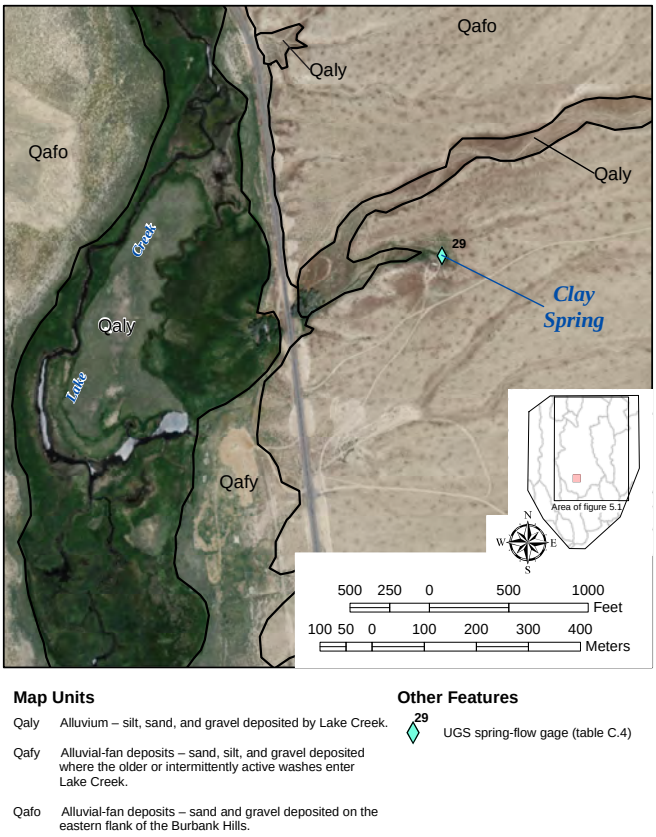

Figure 5.14. *Geographic and geologic setting of the Clay Spring area, southern Snake Valley (site 29, table C.4), based on reconnaissance mapping by the senior author. Contact locations are approximate.*

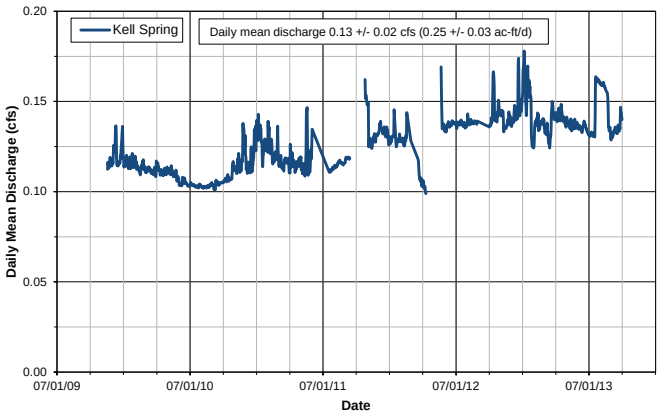

Figure 5.13. *Hydrograph of daily mean discharge from Kell Spring (site 31, table C.4). Higher than average flows are occasionally observed after vegetation is cleaned from the pond outlet. Not all high-flow periods are caused by removing blockages. Flow decrease in late March 2012 likely was caused by vegetation build up in the outlet pipe from pond.*

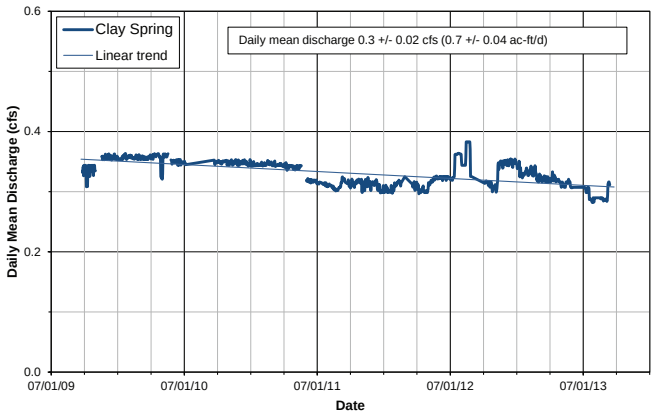

Figure 5.15. *Hydrograph of daily mean discharge from Clay Spring (site 29, table C.4). Discharge is trending downward slightly.*

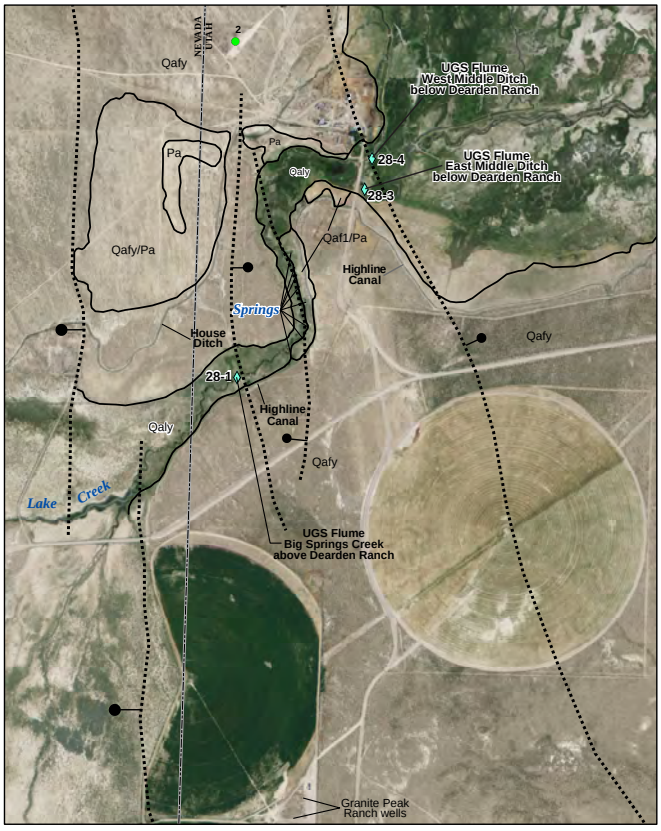

Figure 5.16. *Geographic and geologic setting of the Dearden Springs area, southern Snake Valley (site 28, table C.4), based on reconnaissance mapping by the senior author. Contact locations are approximate.*

Figure 5.17. *Groundwater issuing from fractured, fine-grained calcareous sandstone of the Permian Arcturus Formation of the upper Paleozoic carbonate-rock aquifer hydrogeologic unit at Dearden Springs (site 28, table C.4).*

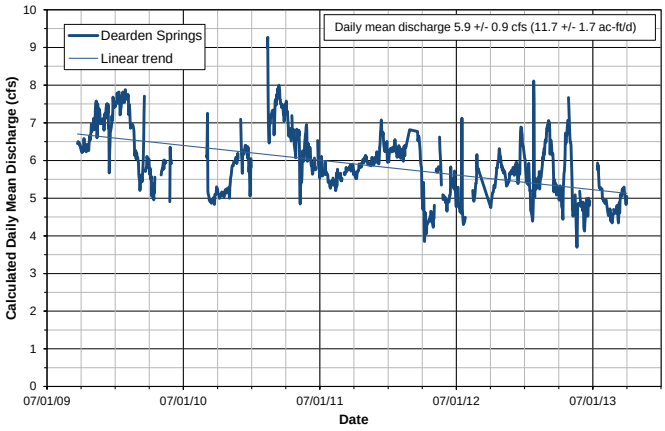

Figure 5.18. *Hydrograph of daily mean discharge from Dearden Springs (site 28, table C.4), calculated as the difference between the sum of discharge at the gages downstream from the springs (East Middle Ditch and West Middle Ditch) and the gage upstream from the springs (Big Springs Creek above Dearden Ranch). The trend in Dearden Springs discharge over 3 years of measurement is downward. Normally, the discharge measurements for a few hours after the irrigation operators route water between ditches is removed from the record. During unknown periods, some surface flow or bank infiltration from other irrigation ditches may enter the stream between the upper and lower gages, thereby inflating the calculated discharge. Although this flow is intermittent and estimated to be less than 0.5 acre-feet per day, the accuracy of the calculated discharge is affected. Ice may affect gages in the winter months.*

which is about 0.8 miles (1.3 km) south of the southern end of the Dearden Springs complex. The roughly annual trend of increasing and decreasing flow periods observed through March 2012 changed to a higher frequency cycle of increasing and decreasing flow beginning in April 2012. Better information about the duration and volume of groundwater pumping at Granite Peak Ranch and a longer period of record for spring discharge are needed to evaluate whether or how much groundwater pumping at Granite Peak Ranch affects spring discharge.

5.5 WETLANDS MONITORING

UGS assisted with installation of 60 shallow piezometers in five spring-fed wetlands ecosystems in Snake Valley as part of a project to establish baseline physical habitat conditions of wetlands, funded by the U.S. Environmental Protection Agency (Three Parameters Plus, 2010; Hooker and others, 2011). This project is done in coordination with the Utah Division of Wildlife Resources, which monitors the populations of sensitive aquatic species in the spring pools and wetlands. Data are available on the UGS groundwater-monitoring data portal (http://geology.utah.gov/databases/groundwater/map.php?proj_id=1), and results will be presented and interpreted in a separate report.

5.6 CHAPTER 5 REFERENCES

Antonellini, M., and Aydin, A., 1994, Effect of faulting on fluid flow in porous sandstones, petrophysical properties: American Association of Petroleum Geologists Bulletin, v. 78, p. 355–377.

Blackett, R.E., 2011, Temperature profiles of water monitoring wells in Snake Valley, Tule Valley, and Fish Springs Flat, Millard and Juab Counties, Utah: Utah Geological Survey Open-File Report 578, 13 p.

Bredehoeft, J.D., 2011, Monitoring regional groundwater extraction—the problem: Ground Water, v. 49, no. 6, p. 808-814 (doi: 10.1111/j.1745-6584.2011.00799.x).

Bunch, R.L., and Harrill, J.R., 1984, Compilation of selected hydrologic data from the MX missile-siting investigation, east-central Nevada and western Utah: U.S. Geological Survey Open-File Report 84-702, 123 p.

Burden, C.B., Allen, D.V., Christiansen, H.K., Downhour, P., Eacret, E.J., Fisher, M.J., Gibson, T.L., Holt, C.M., Howells, J.H., Slaugh, B.A., Smith, L., and Whittier, N.R., 2012, Groundwater conditions in Utah, spring of 2012: Utah Department of Natural Resources Cooperative Investigations Report No. 53, 118 p.

Dong, W., and Halford, K.J., 2010, Analysis of water level fluctuations from pumpage for irrigation during multiple drought years in Snake Valley, HA195, near Baker, NV: Online, http://nevada.usgs.gov/water/aquifertests/snake_valley_n.cfm?studyname=snake_valley_n, 18 p., accessed June 4, 2013.

Dong, W., Naranjo, R.C., and Halford, K.J., 2011, Analysis of water level fluctuations from pumpage for irrigation during multiple drought years in Snake Valley, HA195, near Needle Point and south of Garrison, Utah: Online, http://nevada.usgs.gov/water/aquiferests/Snake_needle_point.cfm?studyname=Snake_needle_point, 16 p., accessed June 4, 2013.

Gardner, P.M., Masbruch, M.D., Plume, R.W., and Buto, S.G., 2011, Regional potentiometric surface map of the Great Basin carbonate and alluvial aquifer system in Snake Valley and surrounding areas, Juab, Millard, and Beaver Counties, Utah, and White Pine and Lincoln Counties, Nevada: U.S. Geological Survey Scientific Investigations Map 3193.

Harrill, J.R., Gates, J.S., and Thomas, J.M., 1988, Major ground-water flow systems in the Great Basin region of Nevada, Utah, and adjacent states: U.S. Geological Survey Hydrologic Investigations Atlas HA-694-C, scale 1:1,000,000, 2 sheets.

Hintze, L.F., and Davis F.D., 2002a, Geologic map of the Tule Valley 30′ x 60′ quadrangle and parts of the Ely, Fish Springs, and Kern Mountains 30′ x 60′ quadrangles, northwest Millard County, Utah: Utah Geologic Survey Map 186, scale 1:100,000.

Hintze, L.F., and Davis F.D., 2002b, Geologic map of the Wah Wah Mountains North 30′ x 60′ quadrangle and part of the Garrison 30′ x 60′ quadrangle, southwest Millard County and part of Beaver County, Utah: Utah Geological Survey Map 182, scale 1:100,000.

Hooker, T.H., Jordan, J.L., and Emerson, R., 2011, Intensive monitoring of spring discharge and wetland hydrology to understand aquifer dynamics and the consequences for excessive ground-water withdrawal: Geological Society of America Abstracts with Programs, v. 43, no. 4, p. 60.

Kistinger, G.M., Prieur, J.P., Rowley, P.D., and Dixon, G.L., 2009, Characterization of streams and springs in the Snake Valley area, Utah and Nevada, *in* Tripp, B.T., Krahulec, K., and Jordan, J.L., editors, Geology and geologic resources and issues of western Utah: Utah Geological Association Publication 38, p. 300–323.

Mason, J.L., Atwood, J.W., and Buettner, P.S., 1985, Selected test-well data from the MX-missile siting study, Tooele, Juab, Millard, Beaver, and Iron Counties, Utah: U.S. Geological Survey Open-File Report 85-347, 13 p.

National Climatic Data Center, 2012, National precipitation and temperature maps: Online, http://www.ncdc.noaa.gov/temp-and-precip/maps.php?ts=12&year=2011&month=9&imgs[]=Divisionalprank&submitted=Submit, accessed October 18, 2012.

Prudic, D.E., Harrill, J.R., and Burbey, T.J., 1995, Conceptual evaluation of regional ground-water flow in the carbonate-rock province of the Great Basin, Nevada, Utah, and adjacent states: U.S. Geological Survey Professional Paper 1409-D, 102 p.

Nagler, P.L., Shafroth, P.B., LaBaugh, J.W., Snyder, K.A., Scott, R.L., Merritt, D.M., and Osterberg, J., 2010, The potential for water savings through the control of saltceder and Russian olive, *in* Shafroth, P.B., Brown, C.A., and Merritt, D.M., editors, 2010, Saltcedar and Russian olive control demonstration act science assessment: U.S. Geological Survey Scientific Investigations Report 2009-5247, 143 p.

Rowley, P.D., Dixon, G.L., Burns, A.G., and Collins, C.A., 2009, Geology and hydrogeology of the Snake Valley area, western Utah and eastern Nevada, *in* Tripp, B.T., Krahulec, K., and Jordan, J.L., editors, Geology and geologic resources and issues of western Utah: Utah Geological Association Publication 38, p. 251–269.

Shafroth, P.B., Cleverly, J.R., Dudley, T.L., Taylor, J.P., Van Ripper, C., Weeks, E.P., and Stuart, J.N., 2005, Control of *Tamarix* in the Western United States—implications for water salvage, wildlife use, and riparian restoration: Environmental Management, v. 35, p. 231–246.

Taylor, C.J., and Alley, W.M., 2001, Ground-water-level monitoring and the importance of long-term water-level data: U.S. Geological Survey Circular 1217, 68 p.

Three Parameters Plus, 2010, Baseline physical habitat conditions of wetlands in Snake Valley, Utah—final report: Unpublished contract report prepared for the Utah Department of Natural Resources, Endangered Species Program, 2 volumes.

U.S. Bureau of Land Management, 2012, Clark, Lincoln, and White Pine Counties Groundwater Development Project Final Environmental Impact Statement FES 12-33: Document BLM/NV/NV/ES/13-2+1793.

CHAPTER 6

HYDROCHEMISTRY, WATER QUALITY, DISSOLVED GAS, AND ISOTOPIC DATA FOR GROUNDWATER IN THE SNAKE VALLEY AREA AND IMPLICATIONS FOR GROUNDWATER FLOW PATHS

by Stefan Kirby, Janae Wallace, and Mike Lowe

Pumping piezometers PW03A and PW03B at site 3 for hydrochemical sampling.

Bibliographic citation for this chapter:
Kirby, S., Wallace, J., and Lowe, M., 2014, Hydrochemistry, water quality, dissolved gas, and isotopic data for groundwater in the Snake Valley area and implications for groundwater flow paths, Chapter 6 *in* Hurlow, H., editor, Hydrogeologic studies and groundwater monitoring in Snake Valley and adjacent hydrographic areas, west-central Utah and east-central Nevada: Utah Geological Survey Bulletin 135, p. 125–194.

CHAPTER 6 CONTENTS

FIGURES

TABLES

CHAPTER 6: HYDROCHEMISTRY, WATER QUALITY, DISSOLVED GAS, AND ISOTOPIC DATA FOR GROUNDWATER IN THE SNAKE VALLEY AREA AND IMPLICATIONS FOR GROUNDWATER FLOW PATHS

by Stefan Kirby, Janae Wallace, and Mike Lowe

6.1 INTRODUCTION

6.1.1 Background

Groundwater chemistry is a basic characteristic that influences end use of the resource and also provides information about the origin, fate, and evolution of groundwater within a hydrogeologic system. The relative quality of groundwater is defined by concentrations of major and trace dissolved chemical constituents. These dissolved constituents change due to mineral-water interaction, mixing, fluid dilution or concentration, and a host of other processes along groundwater flow paths, and therefore provide constraints on groundwater movement and evolution (Kehew, 2000).

The isotopic and dissolved-gas composition of groundwater can also be used to evaluate potential flow paths and recharge or discharge relationships in the aqueous system (Clark and Fritz, 1997; Stute and Schlosser, 2000). Common isotopes measured in groundwater include the stable isotopes ^{18}O, ^{2}H, and ^{13}C, and the radiogenic isotopes ^{3}H and ^{14}C. These isotopes are either directly incorporated in the water molecule, in the case of ^{18}O, ^{2}H, and ^{3}H, or present as dissolved inorganic carbon (DIC) primarily as the bicarbonate anion at typical values of pH, in the case of ^{13}C and ^{14}C. Relative concentrations of these isotopes can define areas of recharge and discharge, flow paths, and apparent age of groundwater (Clark and Fritz, 1997). Measured concentrations of dissolved noble gases in groundwater can be used to model the temperature and atmospheric pressure conditions at the water table at the point of recharge. The dissolved gas concentrations of isotopes of H and He may be used for additional apparent age estimates (Stute and Schlosser, 2000).

In this chapter we present the results of groundwater and dissolved-gas sampling in the Snake Valley area, and use the results to evaluate hypothesized flow paths and the nature of the regional groundwater system. The dissolved chemical, isotopic, and gas composition of groundwater, in conjunction with measured groundwater elevation, constitute the primary measurements of a groundwater system and must therefore be accounted for by any conceptual or numerical model that covers a given flow system. Taken together, dissolved solute chemistry, isotopic composition, and dissolved-gas composition of groundwater can provide fundamental, and in many cases, unique data concerning the groundwater system and provide meaningful control on the recharge-to-discharge pathways of regional groundwater flow.

6.1.2 Previous Work

Meinzer (1911) conducted the first evaluation of groundwater resources that included Snake Valley and adjacent basins in western Utah. Meinzer (1911) noted that groundwater quality from wells and springs in mountainous areas and alluvial slopes is generally good and suitable for irrigation purposes, but that groundwater in the central parts of valleys (especially shallow groundwater) and desert/playa areas may be too saline for culinary use. Meinzer (1911) documented that one flowing well in the Callao area (SE1/4 section 1, T. 11 S., R. 17 W., Salt Lake Base Line and Meridian [SLBM]) yielded water with a total-dissolved-solids (TDS) concentration of 249 mg/L.

Snyder (1963) conducted a geologic and hydrologic reconnaissance of west-central Utah, including Snake Valley and adjacent basins, to determine the availability of stock water. Snyder (1963) concluded that most of the area yielded groundwater of suitable quality for stock watering except the northern parts of Snake Valley and Fish Springs Flat, which border the Great Salt Lake Desert.

Hood and Rush (1965) conducted a more detailed evaluation of groundwater resources in Snake Valley, which included analyses of 26 water samples from wells and springs. Their estimated TDS concentrations for 17 samples from Utah ranged from 152 to 10,100 mg/L, but most samples ranged from 200 to 600 mg/L (Hood and Rush, 1965, table 8). A 112-foot-deep (34 m) Bureau of Land Management well (NW1/4SW1/4SE1/4 section 30,

T. 11 S., R. 15 W., SLBM) in northern Snake Valley just south of the Great Salt Lake Desert (Hood and Rush, 1965, plate 1, table 8) yielded groundwater with the highest TDS of 10,100 mg/L. Nitrate-as-nitrate concentrations for groundwater from 16 wells and springs in Utah ranged from 0 to 12 mg/L (Hood and Rush, 1965, table 8), but most of the wells had concentrations of less than 2 mg/L. The well that yielded groundwater with a nitrate-as-nitrate concentration of 12 mg/L (drinking water-quality [health] standard 45 mg/L) was 120 feet (37 m) deep and located in the SW1/4SW1/4NW1/4 section 6, T. 22 S., R. 19 W., SLBM, near Garrison (Hood and Rush, 1965, plate 1, table 8). Hood and Rush (1965) reported most groundwater as mixed calcium-magnesium-sodium-bicarbonate type, but groundwater from wells and springs near basin margins as predominately calcium-magnesium-bicarbonate type, and shallow groundwater near the Great Salt Lake Desert as sodium-chloride type. Hood and Rush (1965) attributed high-temperature discharge water (81°F [27°C]) from Warm Springs near Gandy to igneous sources or active fault zones.

Stephens (1974) conducted a hydrologic reconnaissance of Wah Wah Valley, which included analyses of 20 groundwater samples from 15 wells. TDS concentrations ranged from 99 to 4550 mg/L (Stephens, 1974, table 9), but most sources yielded water having less than 1000 mg/L TDS. Groundwater from two wells completed in igneous rocks exceeded 3000 mg/L TDS, and also exceeded secondary drinking water-quality standards for chloride and sulfate (250 mg/L for both) (Stephens, 1974, table 9). Stephens (1974) reported groundwater having the lowest TDS concentrations from wells completed in quartzite or carbonate rocks.

Stephens (1976) conducted a hydrologic reconnaissance of Pine Valley, which included analyses of 12 groundwater samples from eight springs, two wells, and one mine. TDS concentrations ranged from 94 to 732 mg/L (Stephens, 1976, table 9), but most sources yielded water having less than 250 mg/L TDS. The lowest TDS concentrations were from wells completed in quartzite, and groundwater having the highest TDS concentrations (greater than 500 mg/L) was from springs issuing from volcanic or carbonate rocks.

Stephens (1977) conducted a hydrologic reconnaissance of Tule Valley, which included analyses of eight groundwater samples from four springs and three wells. TDS concentrations ranged from 516 to 1580 mg/L (Stephens, 1977, table 8), but most sources yielded water less than 1000 mg/L TDS. The two groundwater samples exceeding 1000 mg/L TDS were from springs.

Bolke and Sumsion (1978) conducted a hydrologic reconnaissance of the Fish Springs Flat area, which included analyses of 11 groundwater samples from nine springs and two wells. TDS concentrations ranged from 1740 to 22,400 mg/L (Bolke and Sumsion, 1978, table 8). Bolke and Sumsion (1978) concluded that groundwater in the Fish Springs Flat area was sodium-chloride type and not suitable for drinking.

Gates and Kruer (1981) conducted a hydrologic reconnaissance of west-central Utah, which included Snake Valley and adjacent areas, and mapped water quality based on data collected as part of the studies discussed above, a brine resource assessment by Nolan (1928), two water-data reports (U.S. Geological Survey, 1977, 1978), and new groundwater samples analyzed as part of their study. Gates and Kruer's (1981) data were mostly from the southern Great Salt Lake Desert, but included two samples from Snake Valley and one sample from Wah Wah Valley. TDS concentrations in the basin-fill aquifer ranged from 94 mg/L in southern Pine Valley to greater than 200,000 mg/L in the southern Great Salt Lake Desert (Gates and Kruer, 1981, plate 3). Gates and Kruer (1981) noted that fresh (potable) groundwater could be obtained from all of the basins except Fish Springs Flat, which had large areas having greater than 1000 mg/L TDS, and that the southern Great Salt Lake Desert north of Callao yielded groundwater having greater than 35,000 mg/L due to saline Lake Bonneville deposits and because it was the regional groundwater discharge area (primarily by evapotranspiration). Gates and Kruer (1981) also estimated the apparent age of groundwater discharging from springs in the Fish Springs Flat area based on ^{14}C analyses to range from 8300 to 11,400 years at Cold Spring, and 12,500 to 15,600 years at Percy Spring.

Carlton (1985) evaluated hydrochemistry in the Fish Springs multibasin flow system, including Snake Valley and adjacent areas, to construct a groundwater-flow model to analyze regional groundwater movement. Part of this analysis was based on silica geothermometry, stable isotopes, and ^{14}C. Carlton (1985, table 2) analyzed groundwater samples from Fish, Coyote, and Warm Springs near Gandy, and Twin Springs for the stable isotopes of ^{18}O and ^{2}H, the radiogenic isotopes of ^{3}H and ^{14}C, temperature, and silica, and Knoll Spring and an unnamed spring nearby for temperature and silica. Isotopic concentrations ranged from -121 to -109‰ for deuterium, and from -15.5 to -13.6‰ for ^{18}O; deuterium versus ^{18}O for all samples plotted below the meteoric water line of Craig (1961). Apparent age estimates using ^{14}C ranged from 7200 to 23,400 years (Carlton, 1985, see table 2); Warm Springs near Gandy yielded the youngest age and Coyote and Fish Springs yielded the oldest ages. Carlton (1985) concluded, based on combined temperature and silica data, that the

minimum depth of circulation of groundwater feeding the springs was about 5000 feet (1500 m).

Schaefer and others (2005) evaluated groundwater quality in the carbonate-rock aquifer in Snake Valley and adjacent areas in Utah and Nevada, and collected samples from 10 sites in Utah, including Warm Springs near Gandy and Fish Springs (Schaefer and others, 2005, figure 5, table 1); these samples were analyzed for major anions and cations, nutrients, trace elements, dissolved organic carbon, volatile organic carbon compounds, pesticides, radon, and microbiology (as reported in Tibbetts and others, 2004, p.448–452), and ^{18}O, deuterium, and tritium (Schaefer and others, 2005, table 2). Warm Springs near Gandy yielded calcium-bicarbonate type water, and Fish Springs yielded sodium-chloride type water (Schaefer and others, 2005, figure 8). Coliform bacteria was detected in Warm Springs near Gandy (Schaefer and others, 2005, table 2). Based on data by Thomas and others (1996), Schaefer and others estimated that Warm Springs near Gandy yielded modern groundwater (16.4 pCi/L), and water from Fish Springs has an apparent age of 9000 years based on data from Gates and Kruer (1981).

Hershey and others (2007) described water quality and evaluated recharge altitude and residence time using model recharge temperatures derived from dissolved-gas compositions and tritium/helium dating, evaluated groundwater flow paths using water chemistry and environmental isotopes, and estimated groundwater ages, travel times, and velocities as part of the Basin and Range Carbonate-rock Aquifer System (BARCAS) study, which included Snake Valley. Warm Springs near Gandy, Caine Spring, and Needle Point Spring well were sampled for stable isotopes and dissolved gases, but the Warm Springs near Gandy sample was stripped of gases (Hershey and others, 2007, table 2). Although most springs and wells in Snake Valley yielded calcium-bicarbonate type groundwater, mixed calcium-magnesium-sodium-bicarbonate type and sodium-chloride type groundwater was also encountered in some areas (Hershey and others, 2007). Hershey and others concluded that most groundwater was recharged at temperatures (0–5°C) indicative of mountain-block recharge; Caine Spring was one of the exceptions, having dissolved-gas recharge temperatures (6–12°C) indicative of a relatively low-elevation minimum recharge altitude (1700 m). Based on tritium concentrations, Hershey and others (2007, table 3) concluded groundwater from Caine Spring and Needle Point Spring well was recharged prior to the early 1950s, and that groundwater from Warm Springs near Gandy had at least some component of post-1950s recharge. Based on water-rock reaction modeling, Hershey and others (2007) estimated groundwater travel times along a Spring Valley to Snake Valley flow path to be less than 1000 to 6000 years and groundwater velocities of 20 to 100 feet (6–30 m) per year.

Knochemus and others (2007) evaluated groundwater quality relative to drinking-water standards for the BARCAS study area. For chemical constituents having more than 25 sampling sites, only arsenic and fluoride exceeded primary drinking-water standards at more than one site (Knochemus and others, 2007, table 4).

Gillespie (2008) presented a conceptual model of groundwater flow in Spring Valley, Nevada, and Snake Valley, Nevada and Utah, using solute chemistry, radioactive isotopes (tritium and ^{14}C), and stable isotopes (^{18}O, deuterium, and ^{13}C) in groundwater; hydrochemical groundwater modeling using these data was incorporated into the conceptual model and used to test the plausibility of flow paths. Gillespie (2008) found that groundwater from siliciclastic and plutonic rocks generally had the lowest TDS concentrations, averaging 171 mg/L, compared to groundwater from volcanic rocks, which averaged 228 mg/L, and groundwater from carbonate rocks, which averaged 466 mg/L. In general, TDS concentrations increased to the north-northeast, possibly due to the interaction of groundwater with carbonate bedrock and/or lake sediments (Gillespie, 2008). Gillespie (2008) identified tritium in most basin-fill aquifer groundwater in Snake Valley and ^{14}C activities ranging from about 70 to less than 20 percent modern carbon (pMC) (Gillespie, 2008, figure 12); groundwater having low ^{14}C content was generally along the eastern margin of Snake Valley. These results were summarized and used to support a conceptual model where groundwater in Spring and Snake Valleys derives from local recharge and interbasin flow is not required (Gillespie and others, 2012).

Acheampong and others (2009) described the chemistry and isotopic concentrations of groundwater in the Snake Valley area based on 370 sample locations in Nevada and Utah. Based on the distribution of major water types, stable isotopes, and tritium concentrations, Acheampong and others (2009) concluded that the main source of recharge in the Snake Valley area is precipitation in the Deep Creek, Snake, and House Ranges.

Blackett (2011) collected temperature profiles for 23 of the 68 monitoring wells established by the Utah Geological Survey at 27 sites from 2007 to 2009 in Snake Valley and adjacent areas. Maximum bottom-hole temperatures ranged from 53°F (12°C) at 180 feet (55 m) in basin fill near Needle Point Spring (well AG15) in southern Snake Valley to 117°F (47°C) at 1000 feet (305 m) in the Devonian Guillmette Formation on the northwest flank of the Middle Range (well PW 18) in northeastern Snake Valley. Thermal

gradients range from near zero near Garrison (well PW01C) in southern Snake Valley to 6.7°F/100 feet (123°C/km) on the northwest flank of the Middle Range (well PW 18) in northeastern Snake Valley.

6.1.3 Groundwater Sampling, Analysis, and Data Compilation

Groundwater samples were collected between June 2006 and October 2011 from a variety of sources, including springs, existing wells, and new monitoring wells. Springs were sampled using a peristaltic pump or low-flow submersible pump with the sampling tubing or pump inlet placed as near as possible to the main orifice or point of discharge as far beneath the water surface as possible. Wells were sampled via one of three different techniques that included existing pumps and supply lines, a portable down-hole submersible pump, or airlift.

Airlift samples were collected from drilling rigs following completion and development of many of the new monitoring wells. The air-lift method uses high-pressure air injected below the water level to force water out of the well. All air-lifted samples may therefore be contaminated due to atmospheric gas exchange and consequent pH and mineral saturation changes in a given sample. Because of the potential for sample contamination, as many as possible of the air-lift samples were resampled using either a standard downhole sampling pump or a positive displacement Bennet pump.

All pumped samples were collected after being purged of at least three well casing volumes of water. Samples were collected as near the wellhead or pump outlet as possible, following standard field sampling protocol outlined by Wilde and others (1998). Field parameters, including specific conductance, temperature, pH, dissolved oxygen, and total dissolved-gas pressure, were measured using a calibrated multiparameter probe. Samples for dissolved cations and anions, and arsenic, were filtered using a standard 0.45 micrometer filter.

Dissolved ions, arsenic, and nitrate samples were analyzed at one of the following laboratories: the U.S. Geological Survey National Water Quality Laboratory in Denver, Colorado; the Utah State Bureau of Chemical and Environmental Services Water Quality Laboratory in Salt Lake City, Utah; or the Brigham Young University Hydrogeochemistry Laboratory in Provo, Utah.

Samples for stable isotopes of hydrogen and oxygen were collected from either unfiltered or filtered (0.45 micrometer) water in amber glass containers with polyseal caps or polyethylene bottles sealed with no air space in the container. Stable isotope samples were analyzed at either the Brigham Young University Hydrogeochemistry Laboratory, or the U.S. Geological Survey Stable Isotope Laboratory in Reston, Virginia.

Samples for carbon isotopes were collected from filtered water in amber glass containers with polyseal caps or polyethylene bottles. All carbon samples were collected by filling the sample bottle from the bottom and allowing water to overflow until several bottle volumes had flushed through the bottle. Bottles were then sealed with rinsed caps to minimize contact with the air and air space in the bottle. Carbon isotope samples were analyzed via AMS methods at either the University of Georgia Center for Applied Isotope Studies or the National Ocean Sciences Accelerator Mass Spectrometry Facility (NOSAMS) at the Woods Hole Oceanographic Institution in Woods Hole, Massachusetts. Samples for tritium were collected from either unfiltered or filtered (0.45 micrometer) water in amber glass containers with polyseal caps or polyethylene bottles. Tritium samples were analyzed at either the University of Utah Dissolved Gas Laboratory in Salt Lake City, Utah, or at the Brigham Young University Hydrogeochemistry Laboratory.

Samples for noble gas analysis were collected either during sample pumping using sealed copper tubes or via passive diffusion samplers. Copper tube samples were collected directly from sampling pump discharge and sealed to avoid the presence of bubbles in the samples. Diffusion samplers were allowed to equilibrate for at least 24 hours prior to being removed and promptly crimped and sealed. Total dissolved gas pressure was measured in situ using a Hydrolab sonde or a dedicated total dissolved gas pressure probe placed near the position of the diffusion sampler and allowed to properly equilibrate. Diffusion samplers were placed as near to the screened interval as possible in the case of wells or as deep and near as possible to the main orifice of groundwater discharge in the case of springs. All noble gas analyses were performed by the University of Utah Dissolved Gas Laboratory.

Nearly all samples (124 of the total 141) included in the dataset had intial cation-anion charge balance within ± 5% (table D.1). For 17 samples the reported concentration of a single solute was adjusted to achieve electroneutrality. For each of these samples the solute to adjust was chosen based on hydrochemical analysis in the AquaCHEM software package as well as comparison with geochemically similar samples that are charge balanced.

Additional groundwater samples were compiled from available recent publications and used to augment the samples collected during this study (table D.2). External samples were selected based on data completeness, sample

location, and a minimum difference in anion and cation charge balance of ± 5% for all but two samples; for these two samples, a single anion or cation concentration was back-calculated to achieve electroneutrality via methodology similar to that described above. Compiled samples are assumed to have been collected and analyzed by standard sampling and laboratory techniques analogous to those used for pumped samples collected in this study. More detailed descriptions of sample collection and analysis for compiled sites are available from their source reports listed in table D.2. All compiled samples include basic field parameters of temperature, pH, and conductivity, as well as laboratory measurements of major solute concentrations and stable isotopes. Additional analyses of TDS, nitrate, arsenic, stable isotopes, and radiogenic isotopes of tritium and carbon are included where available for compiled samples. All subsequent analyses and discussions will focus on various subsets of sample data contained in the collected and compiled datasets.

6.2 GROUNDWATER CHEMISTRY AND STATISTICAL ANALYSIS

6.2.1 General Chemistry

6.2.1.1 Introduction

Analysis of groundwater chemistry is based on a select set of 88 samples collected during this study combined with sample data compiled from recent publications for 66 additional samples (table 6.1). Subsequent use of the term "dataset" in this chapter refers to this select set of 154 new and compiled hydrochemical samples.

Samples in the dataset cover an area roughly 100 miles (60 km) north to south by 50 miles (30 km) east to west in western Utah and adjoining parts of Nevada (figure 6.1). The sample locations range from upland springs in the Snake Range to wells and springs at Fish Springs, and a variety of newly completed and previously existing wells and springs in between. Depth of sampled intervals in wells ranges from near land surface in the case of springs to over 1200 feet (370 m) at several deep monitoring wells. Half (77) of all samples in the dataset and all but two of the samples from the compiled dataset are from springs. Samples from wells are generally from screened intervals within 750 feet (230 m) of the land surface (figure 6.2).

Each sample record also contains basic information for the geologic unit from which the sample was collected. For samples collected from wells, this represents the unit at the screened interval. The geologic unit for spring samples collected during this study is the hydrogeologic unit at the spring head. For compiled spring samples, the geologic unit was interpreted from the compiled geologic map (plate 1). Geologic unit designations follow those presented in chapter 3. Most samples are from the basin-fill (QTcs) or Paleozoic carbonate-rock (UPzc and LPzc) aquifers (figure 6.2). The remaining samples were collected from bedrock units that include the lower Paleozoic and Neoproterozoic quartzites (€Zs) and Tertiary-age sedimentary or igneous rocks (Ts and Tv).

6.2.1.2 Field Parameters

Field parameters obtained during sampling provide a broad measure of the character of groundwater in the study area. Every sample in the dataset includes basic field parameters of pH, specific conductance, and temperature. Median pH for the 154 samples in the dataset is 7.24, with a maximum of 8.2 and minimum of 5.95. Specific conductance is a measure of the conductive ionic content and is controlled by the solute content of a solution (Kehew, 2000). Specific conductance at the sampling temperature ranges from a minimum of 41.5 µS/cm to a maximum of 8310 µS/cm; the median value is 1184 µS/cm. Temperature measured during sampling is a crude proxy for downhole temperatures and may be affected by heating due to pumping and/or cooling or heating due to air temperature during sampling. For the entire dataset, the median temperature irrespective of sampling depth is 14.9°C. Temperature of the groundwater samples ranged between 3.5 and 50.1°C. Blackett (2011) presented vertical temperature profiles of many of the new wells completed by the UGS.

6.2.1.3 Groundwater Temperature

Analysis of groundwater temperature data recorded during sampling of springs and wells provides generalized information for the temperature characteristics of the regional groundwater system. Groundwater temperature generally increases along flow paths from areas of recharge to areas of discharge. During recharge in areas of shallow groundwater, the groundwater temperature is nearly equal to (generally 1 to 2°C greater than) the local mean annual air temperature (Domenico and Schwartz, 1997; Anderson, 2005). Following recharge, groundwater temperature may increase, depending on crustal heat flow, depth of circulation, and residence time. Spatial trends in groundwater temperature can therefore be an important indicator of areas of relative recharge and discharge, depth of groundwater circulation, and regional trends in crustal heat flux (Domenico and Schwartz, 1997). Because of the variability of well completion depths, and subsequent lack of spatial coverage for wells completed at depths greater than 300 feet (100 m), only wells screened within 300 feet

Table 6.1. *Samples used for water quality and geochemical analysis.*

Station ID[1]	Location	Longitude[2]	Latitude	Water elev (ft)[3]	Screen Mid (ft)[4]	Geology[5]	Sample date	pH	Temp (°C)	Cond (µS/cm)	K (mg/L)	Na (mg/L)	Ca (mg/L)	Mg (mg/L)	Cl (mg/L)	SO_4 (mg/L)	HCO_3 (mg/L)	Water Type[6]	TDS (mg/L)[7]	As (µg/L)	NO_3+ NO_2(mg/L)	Calcite[8]	Dolomite	Gypsum	Halite	Group[9]
2	PW01A	-114.049	38.941	5215.40	250	QTcs	7/29/09	7.54	14.80	416	1.19	12.40	47.70	19.00	13.40	22.60	216.00	Ca-HCO3	230	1.21	0.91	0.04	-0.12	-2.35	-8.32	3
4	PW01B	-114.049	38.941	5214.50	955	Ts	7/29/09	7.57	16.70	352	1.37	18.80	32.40	17.20	12.70	23.76	185.00	Ca-HCO3	196	2.09	0.32	-0.13	-0.29	-2.47	-8.17	3
7	PW02B	-114.047	38.781	5430.30	625	UPzc	7/30/09	7.63	17.70	369	3.87	31.00	27.30	15.50	11.10	26.80	189.00	Ca-HCO3	218	41.60	0.47	-0.12	-0.23	-2.49	-8.01	3
9	PW03A	-113.996	38.945	5120.90	290	LPzc	5/19/09	7.20	13.10	800	4.20	39.00	74.00	39.00	44.00	75.00	341.00	Ca-HCO3	530	4.30	1.30	-0.01	-0.12	-1.76	-7.33	4
11	PW03B	-113.996	38.946	5125.50	840	LPzc	5/18/09	7.20	13.20	818	4.40	41.00	75.00	41.00	44.00	77.00	343.00	Ca-HCO3	490	4.60	1.30	0.00	-0.09	-1.75	-7.31	4
12	PW03P	-113.997	38.946	5128.90	571	LPzc	3/24/09	7.21	13.50	823	4.94	39.30	77.80	42.40	50.40	75.50	326.00	Ca-HCO3	450	3.65	1.25	-0.16	-0.27	-3.08	-7.56	4
16	PW05A	-114.001	39.016	5027.00	148	QTcs	7/29/09	7.38	17.70	353	1.16	12.80	38.60	15.70	10.50	22.88	185.00	Ca-HCO3	206	2.23	0.11	-0.22	-0.59	-2.41	-8.42	3
17	PW05B	-114.001	39.016	5042.20	630	QTcs	7/29/09	8.20	16.70	268	3.14	44.10	9.56	4.77	6.64	25.60	127.00	Na-HCO3	194	9.66	0.22	-0.17	-0.40	-2.89	-8.06	3
19	PW05C	-114.001	39.016	5043.40	870	QTcs	5/19/09	8.20	14.30	368	8.60	46.00	15.00	11.00	6.90	31.00	166.00	Na-HCO3	240	20.00	0.20	0.08	0.23	-2.65	-8.03	3
21	PW06A	-113.905	39.199	4893.20	160	QTcs	9/18/09	7.11	18.60	668	3.40	31.60	56.70	28.30	41.40	55.30	294.00	Ca-HCO3	360	6.09	0.39	-0.17	-0.38	-1.97	-7.45	4
23	PW06B	-113.905	39.199	4893.60	325	QTcs	5/19/09	7.50	17.70	730	5.00	89.00	46.00	22.00	49.00	74.00	289.00	Na-HCO3	490	18.00	0.30	0.09	0.12	-1.94	-6.93	4
26	PW06C	-113.905	39.199	4893.80	380	UPzc	5/19/09	7.30	18.10	757	4.20	57.00	43.00	26.00	49.00	55.00	274.00	Na-HCO3	490	13.00	0.30	-0.14	-0.24	-2.08	-7.12	4
32	PW07A	-113.892	39.029	4975.10	550	QTcs	7/28/09	8.02	16.30	435	10.40	62.00	15.10	10.20	13.10	47.10	182.00	Na-HCO3	276	14.90	0.14	-0.04	-0.01	-2.49	-7.63	3
35	PW07B	-113.892	39.029	4973.90	1265	QTcs	5/19/09	7.80	13.78	2475	41.00	300.00	160.00	70.00	70.00	1100.00	61.00	Na-SO4	1900	4.30	0.16	-0.07	-0.29	-0.59	-6.31	5
38	PW08B	-113.929	38.723	5627.20	390	UPzc	5/18/09	7.50	14.87	433	2.10	9.50	42.00	25.00	15.00	16.00	233.00	Ca-HCO3	250	2.70	1.30	-0.03	-0.07	-2.56	-8.39	3
40	PW09A	-113.926	39.110	4950.30	255	LPzc	9/18/09	7.02	17.70	602	4.85	52.30	53.50	24.90	61.90	50.10	286.00	Ca-HCO3	406	10.50	--	-0.31	-0.71	-2.03	-7.06	4
44	PW11B	-113.982	38.728	5451.20	445	Ts	5/18/09	7.60	14.90	598	2.20	50.00	41.00	28.00	17.00	100.00	226.00	Mg-HCO3	420	4.40	0.28	0.00	0.05	-1.84	-7.63	4
46	PW11C	-113.982	38.728	5451.30	529	UPzc	5/18/09	7.50	15.10	628	2.00	49.00	44.00	28.00	21.00	86.00	257.00	Mg-HCO3	410	3.40	0.30	-0.01	0.00	-1.87	-7.55	4
48	PW11E	-113.982	38.728	5451.40	1149	UPzc	5/18/09	7.40	15.60	651	1.90	27.00	51.00	29.00	21.00	55.00	249.00	Ca-HCO3	370	2.70	0.30	-0.03	-0.10	-1.99	-7.80	4
51	AG13A	-114.034	38.942	5195.50	75	QTcs	11/21/08	6.98	13.20	1007	1.55	18.60	112.00	35.80	200.00	35.10	186.00	Ca-Cl	650	1.06	1.62	-0.31	-0.93	-1.93	-7.00	4
52	AG13B	-114.034	38.948	5186.90	148	QTcs	11/21/08	7.50	12.60	380	1.18	13.70	48.00	19.10	22.50	23.76	191.00	Ca-HCO3	214	1.38	0.46	-0.09	-0.40	-2.32	-8.05	3
53	AG13C	-114.034	38.948	5186.30	295	QTcs	11/21/08	7.12	12.50	359	1.12	12.40	44.60	18.40	14.40	15.55	200.00	Ca-HCO3	192	1.37	0.47	-0.47	-1.16	-2.52	-8.28	3
54	AG14A	-113.981	39.074	4983.90	55	QTcs	2/3/09	7.36	14.00	205	1.42	13.30	19.70	6.94	12.40	7.09	102.00	Ca-HCO3	134	2.86	0.20	-0.80	-1.85	-3.11	-8.30	3
55	AG14B	-113.981	39.074	4984.00	130	QTcs	12/4/08	6.01	12.70	176	1.68	18.50	25.20	6.94	16.66	22.56	99.00	Ca-HCO3	130	4.82	0.88	-2.09	-4.57	-2.52	-8.03	3
56	AG14C	-113.981	39.074	4989.60	270	QTcs	12/4/08	7.14	13.00	280	1.99	18.40	29.50	22.58	24.62	33.33	158.00	Mg-HCO3	174	4.55	0.24	-0.72	-1.39	-2.36	-7.88	3
57	AG15A	-114.049	38.730	5447.50	169	QTcs	11/19/08	6.72	13.60	423	2.72	13.20	43.00	24.20	13.60	12.70	252.00	Ca-HCO3	248	4.34	0.41	-1.08	-2.22	-2.62	-8.28	3
59	AG16A	-114.009	38.799	5395.40	55	QTcs	7/30/09	6.88	12.70	1476	4.87	147.00	104.00	54.00	220.00	211.00	356.00	Na-Cl	984	12.60	0.29	-0.25	-0.62	-1.29	-6.08	4
61	AG16B	-114.009	38.799	5385.50	90	QTcs	7/30/09	7.59	13.50	432	4.34	26.40	33.70	21.40	23.10	28.40	187.00	Mg-HCO3	284	18.50	0.44	-0.14	-0.30	-2.39	-7.76	3
63	AG16C	-114.009	38.799	5400.80	310	QTcs	7/30/09	7.86	20.70	3050	18.50	603.00	21.30	25.90	10.40	1071.92	410.00	Na-SO4	2228	50.70	--	0.02	0.40	-1.48	-6.86	4
66	PW17A	-113.551	39.478	4424.80	170	LPzc	5/19/09	7.07	16.57	2270	13.00	120.00	240.00	90.00	140.00	810.00	200.00	Ca-SO4	1800	16.00	0.66	-0.02	-0.22	-0.54	-6.40	5
73	PW19B	-113.271	39.635	4438.70	395	LPzc	6/9/09	6.13	33.70	4420	52.20	500.00	191.00	54.50	744.33	320.00	576.00	Na-Cl	2736	25.10	0.18	-0.35	-0.81	-1.07	-5.11	6
75	PW19C	-113.271	39.634	4438.80	450	LPzc	5/19/09	6.40	33.50	4577	70.00	630.00	210.00	65.00	1000.00	300.00	592.00	Na-Cl	2600	16.00	0.16	-0.05	-0.17	-1.10	-4.90	6
77	SG21C	-113.413	39.887	4307.30	61	LPzc	6/9/09	7.03	24.70	4410	40.50	624.00	99.10	59.20	895.95	384.00	268.00	Na-Cl	2660	9.63	0.22	-0.18	-0.23	-1.23	-4.91	6
78	SG22B	-113.395	39.841	4326.00	59	QTcs	2/5/09	7.01	28.20	3110	39.10	435.00	96.50	52.70	621.00	277.00	300.00	Na-Cl	1826	12.10	0.15	-0.07	-0.02	-1.33	-5.22	6
79	SG23B	-114.030	38.756	5442.80	58	QTcs	11/19/08	7.45	13.80	464	7.00	20.40	34.00	24.30	25.00	31.30	188.00	Mg-HCO3	252	4.50	1.97	-0.31	-0.58	-2.35	-7.83	3
80	SG24B	-113.863	39.404	4817.90	46	QTcs	11/20/08	7.15	15.00	763	6.15	57.10	69.60	32.20	65.60	51.30	318.00	Ca-HCO3	430	6.16	0.21	-0.12	-0.37	-1.94	-6.99	4
81	SG24C	-113.863	39.403	4820.20	113	QTcs	11/20/08	6.92	16.50	730	5.49	67.70	50.60	34.50	53.90	83.00	282.00	Na-HCO3	412	8.21	0.33	-0.47	-0.87	-2.01	-7.01	4
82	SG25A	-113.892	39.559	4786.20	23	QTcs	11/20/08	7.15	12.80	550	5.01	42.90	55.90	26.60	33.10	171.00	138.00	Ca-HCO3	338	5.14	0.64	-0.52	-1.19	-2.15	-7.39	3
83	SG25B	-113.892	39.559	4786.60	63	QTcs	11/20/08	7.28	13.90	463	3.34	43.60	39.40	19.90	19.80	27.50	242.00	Ca-HCO3	266	4.59	0.49	-0.28	-0.67	-2.36	-7.61	3
84	SG25C	-113.892	39.559	4789.20	113	QTcs	11/20/08	7.10	13.70	435	3.34	49.30	30.10	15.30	16.90	23.40	241.00	Na-HCO3	248	3.62	0.51	-0.64	-1.38	-2.51	-7.62	3
85	SG25D	-113.896	39.559	4788.30	43	QTcs	7/10/09	7.63	20.60	648	3.85	49.90	43.30	22.20	65.90	37.90	260.00	Na-HCO3	394	4.62	0.28	0.22	0.43	-2.23	-7.05	4
86	SG26B	-113.918	39.485	4795.70	43	QTcs	2/5/09	7.22	13.10	487	5.20	35.90	41.60	20.70	18.90	46.80	242.00	Ca-HCO3	294	5.95	0.28	-0.34	-0.80	-2.11	-7.71	3
87	SG26C	-113.917	39.485	4796.90	85	QTcs	2/5/09	7.40	14.30	446	5.18	35.50	27.70	21.50	17.20	38.56	216.00	Mg-HCO3	284	7.52	0.47	-0.35	-0.62	-2.35	-7.76	3
88	SG27A	-113.943	39.465	4819.20	16	QTcs	2/4/09	6.98	12.80	768	5.35	51.80	66.20	29.10	84.10	41.00	274.00	Ca-HCO3	452	6.58	--	-0.36	-0.90	-2.03	-6.92	4
89	(C-13-14)25dac[19mx]	-113.364	39.660	4352.40	187	QTcs	7/10/09	6.82	16.80	4120	48.00	604.00	159.00	98.30	987.57	330.00	536.00	Na-Cl	2702	28.10	0.81	-0.01	0.01	-1.14	-4.88	6
90	(C-16-18)26cba[twin mx]	-113.846	39.388	4848.50	88	QTcs	7/28/09	7.79	16.30	714	6.98	49.30	53.90	32.10	50.30	62.70	282.00	Ca-HCO3	424	9.75	0.26	0.42	0.84	-1.95	-7.17	4
91	(C20-18)32abd[PW7 mx]	-113.892	39.029	4986.20	87	QTcs	7/28/09	7.39	15.60	609	3.24	42.80	47.80	24.20	36.30	52.30	258.00	Ca-HCO3	352	7.27	0.21	-0.06	-0.19	-2.04	-7.37	4

Table 6.1. *continued*

Station ID[1]	Location	Longitude[2]	Latitude	Water elev (ft)[3]	Screen Mid (ft)[4]	Geology[5]	Sample date	pH	Temp (°C)	Cond (µS/cm)	K (mg/L)	Na (mg/L)	Ca (mg/L)	Mg (mg/L)	Cl (mg/L)	SO_4 (mg/L)	HCO_3 (mg/L)	Water Type[6]	TDS (mg/L)[7]	As (µg/L)	NO_3+ NO_2(mg/L)	Calcite[8]	Dolomite	Gypsum	Halite	Group[9]
92	Indian Trail well	-113.638	39.375	4644.20	240	QTcs	6/13/06	7.23	14.71	1950	4.13	62.09	186.50	90.51	90.59	683.84	125.80	Ca-SO4	--	--	--	-0.16	-0.42	-0.66	-6.86	5
94	Tule Mx #1 well	-113.458	39.095	4421.20	520	QTcs	6/13/06	7.73	17.53	1550	11.09	238.40	25.15	21.55	224.33	124.68	259.30	Na-Cl	--	--	--	0.04	0.35	-2.04	-5.87	4
95	Big Spring	-114.132	38.698	5575.00	--	QTcs	6/14/06	7.35	17.10	413	0.66	4.33	49.28	19.85	8.60	9.50	232.40	Ca-HCO3	--	--	--	0.09	0.18	-2.74	-9.01	2
96	Davies well	-114.006	38.798	5400.40	40	QTcs	6/14/06	7.51	15.44	608	1.35	26.20	44.83	33.26	31.26	35.45	270.90	Mg-HCO3	--	--	--	0.09	0.29	-2.24	-7.65	4
97	Shell-Baker well	-114.025	39.049	5036.00	80	QTcs	6/14/06	7.39	15.19	355	0.38	8.84	45.04	8.59	23.77	10.12	155.40	Ca-HCO3	--	--	--	-0.22	-0.91	-2.68	-8.22	2
98	Twin Springs	-113.866	39.404	4812.00	--	QTcs	6/14/06	7.08	19.60	794	2.53	49.49	59.85	26.23	62.28	61.41	275.20	Ca-HCO3	--	--	--	-0.26	-0.66	-1.90	-7.07	4
99	West Buckskin well	-113.942	39.097	4985.00	--	QTcs	6/14/06	7.09	14.48	744	1.99	31.03	57.53	28.58	46.69	59.97	273.90	Ca-HCO3	--	--	--	-0.27	-0.63	-1.92	-7.40	4
100	Persey Spring	-113.392	39.832	4318.00	--	QTcs	6/15/06	7.24	24.20	3280	30.68	441.96	91.95	49.94	556.12	374.07	281.40	Na-Cl	--	--	--	-0.02	-0.03	-1.21	-5.24	6
101	Mirror Spring	-113.395	39.849	4316.00	--	QTcs	6/15/06	7.17	23.40	3260	30.98	432.61	99.16	49.04	553.83	378.81	298.40	Na-Cl	--	--	--	-0.11	-0.31	-1.16	-5.24	6
102	North Spring	-113.413	39.887	4307.00	--	QTcs	6/15/06	7.93	23.61	5160	39.12	717.64	120.00	62.32	1210.97	386.86	276.00	Na-Cl	--	--	--	0.78	1.61	-1.19	-4.73	6
104	Coyote Springs	-113.487	39.424	4420.00	--	QTcs	6/3/08	7.12	28.41	2444	35.50	371.00	71.10	42.30	439.00	314.00	262.00	Na-Cl	--	18.00	0.47	-0.14	-0.12	-1.36	-5.43	6
106	(C-15-15)30bdd-1	-113.577	39.488	4423.80	173	QTcs	6/5/08	7.12	17.00	2198	15.90	132.00	260.00	88.90	137.00	879.00	199.70	Ca-SO4	--	20.20	1.03	0.06	-0.10	-0.49	-6.38	5
108	(C-18-15)36cdd-1	-113.485	39.193	4335.50	--	QTcs	9/8/08	7.50	14.20	2340	37.50	328.00	64.80	68.80	528.00	324.00	141.74	Na-Cl	--	3.10	15.80	-0.26	-0.29	-1.37	-5.37	5
109	PW06D	-113.905	39.199	4893.64	543	UPzc	9/9/08	7.30	17.70	674	4.40	44.30	58.30	25.70	51.60	52.00	274.86	Ca-HCO3	--	8.70	0.91	-0.01	-0.13	-1.98	-7.21	4
110	PW09B	-113.925	39.110	4949.30	710	LPzc	9/9/08	7.30	16.30	678	3.70	33.90	61.80	29.60	42.40	55.20	285.95	Ca-HCO3	--	5.80	1.78	0.01	-0.08	-1.94	-7.41	4
111	(C-20-17)9cad-1 BLM LVW	-113.763	39.081	4880.00	715	QTcs	9/9/08	7.59	16.00	1317	4.50	64.70	112.00	76.50	99.30	431.00	175.02	Mg-SO4	--	0.80	0.48	0.20	0.45	-1.00	-6.79	5
113	SG23A	-114.030	38.756	5442.80	45	QTcs	9/10/08	7.80	12.21	355	3.20	18.20	30.70	15.30	23.60	27.20	140.51	Ca-HCO3	--	4.70	9.16	-0.10	-0.34	-2.41	-7.90	3
114	C20	-113.712	39.898	4323.18	506	QTcs	10/20/10	7.18	17.58	428	2.13	48.60	72.60	15.40	140.00	26.20	160.00	Ca-Cl	436	--	1.52	-0.26	-0.94	-2.17	-6.73	4
115	C32 (C-11-17)11aaa-1	-113.721	39.888	4332.00	480	QTcs	10/20/10	6.96	15.17	696	2.87	68.50	17.70	5.90	39.60	24.10	169.00	Na-HCO3	250	1.23	1.83	-1.05	-2.37	-2.69	-7.11	3
116	RSW02	-113.701	39.993	4297.14	53	QTcs	10/20/10	7.12	17.87	866	5.93	116.00	33.30	27.20	187.00	42.00	174.00	Na-Cl	494	3.18	3.78	-0.63	-1.10	-2.31	-6.24	4
117	CO2	-113.698	39.988	4295.41	40	QTcs	10/20/10	7.47	15.67	428	3.02	66.80	17.30	12.30	68.50	22.10	131.00	Na-HCO3	260	4.26	0.46	-0.66	-1.25	-2.75	-6.88	3
118	C9	-113.702	39.914	4317.00	70	QTcs	10/20/10	7.03	13.07	518	3.91	33.40	66.10	17.20	53.70	48.75	228.00	Ca-HCO3	336	--	5.26	-0.36	-1.13	-1.92	-7.30	4
119	C29	-113.725	39.898	4331.80	125	QTcs	1/20/11	7.10	16.43	811	3.19	55.20	84.10	20.40	190.00	39.30	102.00	Ca-Cl	582	<1.0	0.80	-0.50	-1.38	-1.95	-6.55	4
120	C199	-113.719	39.883	4332.60	126	QTcs	1/20/11	6.72	14.04	641	2.41	61.50	69.20	12.00	105.00	34.50	198.00	Ca-HCO3	398	<1.0	0.91	-0.70	-1.96	-2.05	-6.75	4
121	(C-11-16)36cdb	-113.598	39.817	4411.00	137	QTcs	1/20/11	7.78	37.19	8310	53.40	1410.00	473.00	131.00	2190.00	1870.00	181.00	Na-Cl	5964	16.90	<0.1	0.99	1.85	-0.25	-4.27	5
122	Kell Spring	-114.008	39.304	4935.00	--	QTcs	12/6/10	7.46	14.09	406	1.55	23.50	42.60	18.80	32.20	24.80	197.00	Ca-HCO3	258	1.21	0.81	-0.14	-0.45	-2.36	-7.66	3
123	SG24a	-113.863	39.404	4817.86	17	QTcs	1/20/11	6.66	14.32	697	5.81	56.60	72.30	31.00	65.30	82.30	300.00	Ca-HCO3	466	8.04	0.16	-0.59	-1.36	-1.72	-7.00	4
124	SG21a	-113.413	39.887	4304.24	22	QTcs	1/20/11	6.41	22.22	4250	49.60	714.00	116.00	68.40	1180.00	403.00	292.00	Na-Cl	2626	9.05	0.21	-0.74	-1.40	-1.18	-4.74	6
125	SG21b	-113.413	39.887	4304.34	36	QTcs	1/20/11	6.48	22.67	4735	47.90	843.00	113.00	67.70	1430.00	419.00	290.00	Na-Cl	2900	4.90	0.27	-0.70	-1.30	-1.20	-4.59	6
126	SG22a	-113.395	39.841	4314.09	22	QTcs	1/20/11	6.40	28.06	2914	41.80	462.00	98.90	55.10	655.00	397.00	302.00	Na-Cl	1836	11.90	0.18	-0.69	-1.27	-1.19	-5.18	6
127	PW04b	-114.043	38.581	5588.60	905	Tv	11/3/10	7.66	15.20	459	3.25	14.40	43.90	19.20	54.80	18.60	145.00	Ca-HCO3	--	4.80	3.29	-0.04	-0.22	-2.46	-7.65	3
128	PW10b	-113.655	39.324	4746.50	728	UPzc	11/4/10	7.24	15.50	1400	2.53	27.00	121.00	70.70	342.00	27.50	166.00	Ca-Cl	--	0.50	1.06	-0.06	-0.14	-2.08	-6.62	4
129	PW18	-113.669	39.654	4430.00	980	LPzc	11/5/10	7.25	45.90	5725	22.80	585.00	475.00	129.00	1150.00	1350.00	177.00	Na-Cl	--	0.70	2.55	0.65	1.19	-0.29	-4.92	5
130	Well 22	-113.209	39.629	4437.57	509	QTcs	6/15/11	6.79	22.96	3624	19.20	631.00	94.40	64.40	1050.00	230.00	336.00	Na-Cl	2184	2.99	0.84	-0.34	-0.53	-1.46	-4.83	6
131	Ibex Well	-113.377	38.928	4430.20	515	QTcs	6/15/11	7.35	20.16	873	11.90	130.00	32.60	25.00	125.00	126.00	214.00	Na-Cl	556	20.40	0.47	-0.32	-0.48	-1.88	-6.37	4
132	Wah Wah Well	-113.305	38.678	4434.40	294	QTcs	6/15/11	7.60	16.23	2121	14.40	372.00	50.80	39.10	614.00	167.00	157.00	Na-Cl	1290	22.70	2.41	-0.15	-0.19	-1.71	-5.25	4
133	Guyman Well	-113.686	38.640	4783.25	340	QTcs	6/15/11	7.55	16.71	303	3.81	30.00	23.10	14.50	26.40	48.20	122.00	Na-HCO3	212	11.60	1.86	-0.47	-0.91	-2.29	-7.64	3
134	Mountain Home Spring	-113.957	38.581	7140.00	--	UPzc	6/16/11	6.84	9.54	1169	4.23	48.00	198.00	46.40	93.40	334.00	384.00	Ca-SO4	872	<1.0	0.06	-0.05	-0.62	-0.85	-6.93	4
136	Antelope Spring	-113.349	38.377	5520.00	--	Tv	6/28/11	7.87	18.56	622	4.42	50.80	54.30	19.90	125.00	40.60	132.00	Ca-Cl	448	11.40	0.99	0.23	0.30	-2.09	-6.76	4
139	Gyp Seep	-114.003	38.678	6410.00	--	UPzc	6/29/11	6.43	18.71	4196	2.07	207.00	557.00	128.00	1280.00	367.00	264.00	Ca-Cl	4402	2.82	0.04	-0.17	-0.70	-0.67	-5.25	5
140	Pw17c	-113.551	39.478	4424.80	570	LPzc	10/6/11	7.07	16.20	2206	12.50	98.70	279.00	71.90	144.00	825.00	196.00	Ca-SO4	1732	5.64	0.22	0.03	-0.29	-0.47	-6.47	5
141	Dearden Ranch Spring	-114.045	38.776	5420.00	--	UPzc	10/7/11	7.49	15.74	329	3.18	18.10	26.30	14.50	13.80	30.00	138.00	Ca-HCO3	214	8.89	1.16	-0.43	-0.89	-2.43	-8.14	3
201	Kious Spring	-114.159	38.986	5984.23	--	Ts	6/19/92	7.56	14.20	440	1.62	27.20	52.80	7.69	34.00	13.80	198.00	Ca-HCO3	--	--	2.35	0.06	-0.52	-2.50	-7.58	2
202	Barrel Spring	-114.055	38.131	7520.00	--	Tv	5/21/04	7.72	9.80	380	0.52	16.50	55.70	6.12	18.80	10.70	193.00	Ca-HCO3	--	--	3.50	0.17	-0.49	-2.57	-8.04	2
203	Cedar Cabin Spring	-114.223	38.797	7949.45	--	LPzc	7/13/05	7.55	9.60	432	0.92	5.15	60.10	21.20	5.00	5.70	272.00	Ca-HCO3	--	2	2.30	0.16	-0.02	-2.85	-9.12	2
204	DecathonSpring	-114.279	38.807	8260.00	--	LPzc	7/14/05	6.89	7.60	525	0.44	2.79	109.00	7.84	3.40	11.40	325.00	Ca-HCO3	--	--	<0.04	-0.21	-1.50	-2.33	-9.56	2
205	Mustang Spring	-114.272	38.863	10160.73	--	LPzc	7/14/05	7.09	4.30	329	0.30	1.15	63.60	4.56	0.80	5.50	218.00	Ca-HCO3	--	<1.0	<0.04	-0.43	-1.99	-2.78	-10.55	2

Table 6.1. *continued*

Station ID[1]	Location	Longitude[2]	Latitude	Water elev (ft)[3]	Screen Mid (ft)[4]	Geology[5]	Sample date	pH	Temp (°C)	Cond (µS/cm)	K (mg/L)	Na (mg/L)	Ca (mg/L)	Mg (mg/L)	Cl (mg/L)	SO_4 (mg/L)	HCO_3 (mg/L)	Water Type[6]	TDS (mg/L)[7]	As (µg/L)	NO_3+ NO_2(mg/L)	Calcite[8]	Dolomite	Gypsum	Halite	Group[9]
206	South Spring (D7)	-114.176	38.804	7447.48	--	LPzc	7/14/05	6.87	9.70	502	0.44	2.21	62.90	29.80	2.60	3.40	343.00	Ca-HCO3	--	<1.0	2.04	-0.41	-1.03	-3.09	-9.78	2
207	SpringCreekSpring	-114.113	38.910	6130.00	--	LPzc	7/16/05	7.26	12.90	380	1.07	6.85	64.40	8.44	6.70	12.50	227.00	Ca-HCO3	--	<1.0	1.55	-0.11	-0.93	-2.46	-8.88	2
208	GandySprings	-114.037	39.460	5235.00	--	LPzc	8/2/06	7.10	27.00	483	4.80	28.30	52.30	16.80	25.60	22.10	253.00	Ca-HCO3	--	--	--	-0.13	-0.38	-2.36	-7.72	3
209	UnnamedSpring#4	-114.196	38.833	8140.00	--	LPzc	7/28/05	6.43	6.10	713	0.97	6.16	134.00	22.30	6.60	17.90	474.00	Ca-HCO3	--	<1.0	<0.04	-0.48	-1.70	-2.12	-8.94	2
210	Unnamed Spring #5 (D10)	-114.170	38.851	6980.00	--	LPzc	7/28/05	6.97	11.90	524	1.15	9.51	59.10	32.60	9.20	9.20	322.00	Ca-HCO3	--	1	4.12	-0.33	-0.77	-2.70	-8.61	2
211	CobbSpring	-113.987	38.542	7510.00	--	UPzc	7/28/05	7.31	11.70	790	6.30	21.70	73.20	59.20	14.80	24.70	502.00	Mg-HCO3	--	<1.0	0.53	0.23	0.52	-2.27	-8.06	4
212	UnnamedSpring#12	-114.216	39.307	9180.00	--	CZs	10/25/05	7.24	7.60	222	0.58	4.27	36.70	3.18	2.40	4.20	130.00	Ca-HCO3	--	<0.5	1.24	-0.65	-2.29	-3.07	-9.50	2
213	Unnamed Spring, 195 N16 E69 19 1	-114.261	39.230	8034.75	--	LPzc	10/26/05	7.39	9.20	550	0.75	8.93	71.30	30.40	6.60	35.40	322.00	Ca-HCO3	--	--	0.66	0.11	-0.04	-2.04	-8.77	2
214	UnnamedSpring#13	-114.287	39.178	7390.00	--	LPzc	10/26/05	7.48	9.90	1249	1.12	69.00	80.60	95.40	83.60	234.00	437.00	Mg-HCO3	--	0.9	0.44	0.28	0.75	-1.36	-6.82	4
215	RyanSpring	-113.929	38.331	7240.00	--	Tv	11/19/05	7.07	7.80	565	0.83	23.20	84.90	7.54	41.50	22.80	264.00	Ca-HCO3	--	3.1	1.46	-0.22	-1.42	-2.12	-7.55	2
216	MerrilsCampSpring	-113.866	38.188	8120.00	--	TMzi	11/19/05	7.21	8.40	270	0.35	7.63	39.80	5.24	6.50	5.40	156.00	Ca-HCO3	--	0.6	0.84	-0.56	-1.92	-2.95	-8.82	2
217	RipgutSpring	-114.039	38.248	6760.00	--	Tv	11/19/05	6.95	18.70	258	8.02	17.90	23.80	4.37	17.00	6.40	116.00	Ca-HCO3	--	2	2.04	-1.00	-2.48	-3.09	-8.05	3
218	Unnamed Spring #1 (WM-8)	-114.160	38.303	6850.37	--	Tv	6/19/06	7.35	10.40	377	0.98	15.90	47.20	8.85	45.50	14.00	128.00	Ca-HCO3	--	--	3.50	-0.43	-1.45	-2.51	-7.67	2
219	Butcher Spring	-114.015	38.030	7148.93	--	Tv	6/23/06	7.10	10.10	218	1.01	10.80	25.50	5.44	18.10	10.90	78.30	Ca-HCO3	--	--	8.28	-1.12	-2.79	-2.80	-8.22	3
220	Caine Spring	-114.048	39.138	5031.82	--	QTcs	8/2/06	7.65	14.50	412	2.17	16.33	43.84	17.38	31.44	22.76	180.20	Ca-HCO3	--	--	--	0.03	-0.14	-2.37	-7.83	3
221	Clay Spring	-113.993	38.865	5446.00	--	QTcs	8/2/06	7.00	13.70	608	2.29	8.13	70.31	35.35	14.03	131.27	224.00	Ca-HCO3	--	--	--	-0.40	-0.91	-1.52	-8.50	4
222	Cold Spring	-113.956	39.455	4859.56	--	QTcs	8/2/06	7.34	14.10	661	6.35	62.20	59.86	19.81	34.41	38.85	347.30	Ca-HCO3	--	--	--	0.09	-0.12	-2.09	-7.23	4
223	Knoll Spring	-113.879	39.240	4880.00	--	QTcs	8/2/06	6.74	19.90	689	6.32	48.35	64.47	26.53	49.76	54.73	302.50	Ca-HCO3	--	--	--	-0.46	-1.03	-1.94	-7.19	4
224	Needle Pt Spring Box	-114.030	38.756	5447.38	--	QTcs	8/3/06	7.97	12.40	342	3.97	15.80	30.30	15.16	25.14	28.86	145.50	Ca-HCO3	--	--	--	0.08	0.02	-2.39	-7.93	3
225	North Little Springs	-114.113	38.689	5568.60	--	QTcs	8/3/06	7.27	12.60	330	1.43	3.51	50.00	18.35	4.76	6.54	244.40	Ca-HCO3	--	--	--	-0.18	-0.64	-2.86	-9.31	2
226	MX Well 100 (N11 E70 36BDDD)	-114.067	38.781	5470.00	100	QTcs	9/1/06	7.94	12.70	330	1.86	8.29	27.08	21.91	25.89	11.17	175.20	Mg-HCO3	100	--	--	0.08	0.25	-2.86	-8.20	3
227	MX-Observation (N08 E69 35CDDD)	-114.199	38.506	5663.00	90	QTcs	9/1/06	7.76	17.80	404	6.91	26.48	35.18	16.40	19.82	28.00	215.00	Ca-HCO3	90	--	--	0.16	0.25	-2.38	-7.83	3
228	Unnamed Spring #7 (SN-29)	-114.227	39.302	9438.95	--	LPzc	9/16/06	7.59	6.30	310	0.33	2.62	61.20	4.33	2.00	5.63	193.00	Ca-HCO3	--	--	1.64	0.04	-1.02	-2.78	-9.80	2
229	Unnamed Spring #9 (SN-31)	-114.206	39.298	9514.41	--	CZs	9/16/06	6.98	5.60	59	0.60	2.72	7.03	1.50	1.57	3.57	29.50	Ca-HCO3	--	--	0.04	-2.23	-5.10	-3.72	-9.84	1
230	Unnamed Spring #10 (SN-33)	-114.238	39.423	8180.94	--	LPzc	9/17/06	7.18	10.50	503	0.73	14.40	90.50	5.77	13.60	15.50	293.00	Ca-HCO3	--	--	<0.04	0.00	-1.06	-2.27	-8.25	2
231	Marble Spring (SN-34)	-114.284	39.455	9002.60	--	LPzc	9/17/06	8.10	6.70	500	0.41	3.84	88.10	18.30	3.90	7.48	330.00	Ca-HCO3	--	--	<0.04	0.88	1.14	-2.60	-9.36	2
232	Unnamed Spring #17 (SN-35)	-114.145	39.275	10078.71	--	CZs	10/8/06	6.71	7.60	176	0.60	2.08	32.90	3.30	1.25	2.13	112.00	Ca-HCO3	--	--	<0.08	-1.28	-3.48	-3.39	-10.09	2
233	Unnamed Spring #18 (SN-36)	-114.144	39.267	9596.43	--	CZs	10/8/06	7.13	5.10	192	0.56	2.01	34.80	3.90	0.85	1.98	121.00	Ca-HCO3	--	--	<0.08	-0.85	-2.62	-3.40	-10.27	2
234	Unnamed Spring #19 (SN-37)	-114.141	39.263	9297.87	--	CZs	10/8/06	6.84	4.60	126	0.65	2.35	21.10	2.93	1.30	2.40	74.70	Ca-HCO3	--	--	0.62	-1.55	-3.94	-3.48	-10.00	1
235	Unnamed Spring #20 (SN-38)	-114.265	38.950	9527.53	--	TMzi	10/9/06	6.25	5.10	62	1.08	3.85	6.30	1.39	1.71	2.51	29.20	Ca-HCO3	--	--	<0.08	-3.02	-6.67	-3.91	-9.66	1
236	Unnamed Spring #21 (SN-39)	-114.260	38.951	9711.26	--	TMzi	10/9/06	6.96	4.30	94	1.06	4.51	11.10	2.63	1.22	2.88	50.60	Ca-HCO3	--	--	0.80	-1.86	-4.34	-3.64	-9.74	1
237	Unnamed Spring #22 (SN-40)	-114.268	38.955	9412.70	--	QTcs	10/9/06	6.28	4.60	61	0.57	3.98	7.17	1.22	1.08	1.29	33.20	Ca-HCO3	--	--	0.31	-2.89	-6.53	-4.15	-9.84	1
238	Unnamed Spring #23 (SN-41)	-114.269	38.956	9353.65	--	QTcs	10/9/06	5.95	5.00	42	0.43	2.81	4.55	0.88	0.73	1.69	22.00	Ca-HCO3	--	--	<0.08	-3.57	-7.84	-4.20	-10.16	1
239	Unnamed Spring #24 (SN-42)	-114.250	39.069	6646.96	--	TMzi	10/9/06	7.52	15.10	430	1.24	22.80	59.30	8.91	33.70	18.40	190.00	Ca-HCO3	--	--	2.61	0.06	-0.49	-2.34	-7.66	2
240	Coyote Spring	-113.958	39.584	5120.00	--	QTcs	10/11/06	8.19	15.20	936	4.60	110.00	63.00	55.00	94.00	71.00	450.00	Na-HCO3	--	6	<0.5	1.00	2.16	-1.92	-6.57	4
241	Pipe Spring	-114.281	39.197	7946.17	--	LPzc	10/14/06	7.16	11.90	430	1.87	10.84	68.84	32.77	14.06	17.87	371.00	Ca-HCO3	--	--	--	-0.03	-0.23	-2.37	-8.37	2
242	Rowland Spring	-114.208	39.009	6584.16	--	QTcs	10/14/06	7.01	10.60	128	0.73	5.86	24.82	4.27	5.55	5.49	98.00	Ca-HCO3	--	--	--	-1.11	-2.85	-3.10	-9.00	3
243	Marmot Spring	-114.242	38.988	7641.05	--	CZs	10/15/06	7.05	10.00	90	0.84	6.38	12.42	2.78	0.80	0.79	62.10	Ca-HCO3	--	--	--	-1.54	-3.62	-4.18	-9.79	1

Table 6.1. *continued*

Station ID[1]	Location	Longitude[2]	Latitude	Water elev (ft)[3]	Screen Mid (ft)[4]	Geology[5]	Sample date	pH	Temp (°C)	Cond (µS/cm)	K (mg/L)	Na (mg/L)	Ca (mg/L)	Mg (mg/L)	Cl (mg/L)	SO_4 (mg/L)	HCO_3 (mg/L)	Water Type[6]	TDS (mg/L)[7]	As (µg/L)	NO_3+ NO_2(mg/L)	Calcite[8]	Dolomite	Gypsum	Halite	Group[9]
244	SnakeCampsite#2	-114.153	38.913	6490.00	--	LPzc	10/15/06	7.46	8.30	193	1.16	8.16	43.07	5.83	8.93	8.03	161.00	Ca-HCO3	--	--	--	-0.28	-1.33	-2.76	-8.65	2
245	SnakeCreekRiver	-114.221	38.921	7600.00	--	LPzc	10/15/06	8.00	3.50	70	0.72	3.19	16.87	3.09	1.16	3.00	69.50	Ca-HCO3	--	--	--	-0.53	-1.81	-3.47	-9.91	1
246	Wilson Health Spring	-113.432	39.906	4293.00	--	QTcs	3/26/08	7.04	50.10	36300	340.00	7780.00	780.00	210.00	13000.00	1600.00	200.00	Na-Cl	20000	98	<0.5	--	--	--	--	--
247	House Spring	-113.396	39.850	4315.00	--	QTcs	3/26/08	6.56	24.60	3380	45.00	460.00	100.00	58.00	640.00	380.00	300.00	Na-Cl	--	11	0.78	0.54	1.04	-0.45	-2.87	6
248	Deadman Spring	-113.407	39.878	4310.00	--	LPzc	3/26/08	6.29	18.70	3910	53.00	620.00	110.00	71.00	900.00	410.00	340.00	Na-Cl	--	8.4	<0.5	-0.86	-1.64	-1.16	-4.90	6
250	Laird Spring	-113.052	39.574	5935.89	--	Tv	9/29/08	7.24	17.30	3040	17.00	160.00	220.00	45.00	610.00	140.00	260.00	Ca-Cl	--	2.6	5.10	0.34	0.24	-1.23	-5.63	5
251	North Canyon Spring	-113.323	39.470	6700.00	--	LPzc	9/29/08	7.88	18.60	3610	4.30	410.00	84.00	52.00	740.00	170.00	260.00	Na-Cl	--	1.4	11.00	0.56	1.18	-1.55	-5.14	4
252	Walter Spring	-113.403	39.870	4308.00	--	QTcs	9/29/08	8.07	22.20	3390	48.00	480.00	86.00	55.00	710.00	390.00	320.00	Na-Cl	--	3.4	<0.5	0.84	1.80	-1.25	-5.11	6
253	Antelope Spring (C-17-12)30ba (Unlisted #1)	-113.248	39.313	5770.06	--	QTcs	9/29/08	7.71	18.20	572	1.20	35.00	42.00	23.00	50.00	16.00	250.00	Ca-HCO3	--	1.2	3.20	0.25	0.49	-2.59	-7.32	4
254	Lime Spring	-113.917	39.664	5385.74	--	QTcs	9/30/08	7.74	18.10	1111	5.70	98.00	78.00	36.00	190.00	130.00	220.00	Na-Cl	--	0.52	<0.5	0.40	0.72	-1.55	-6.32	4
255	Trough Spring	-113.912	39.693	5793.83	--	QTcs	9/30/08	7.25	16.60	679	2.00	30.00	73.00	16.00	55.00	130.00	150.00	Ca-SO4	--	<0.4	0.51	-0.25	-0.94	-1.49	-7.35	4
256	Skunk Spring	-113.647	39.298	5480.00	--	UPzc	10/1/08	7.59	20.10	3440	5.30	180.00	240.00	150.00	772.50	300.00	260.00	Mg-Cl	--	<0.4	<0.5	0.69	1.47	-1.00	-5.50	5
257	Tule Spring	-113.515	39.351	4423.55	--	QTcs	10/1/08	7.28	29.30	1560	20.00	190.00	62.00	33.00	230.00	250.00	250.00	Na-Cl	--	17	1.00	0.01	0.12	-1.44	-5.98	4
258	Painter Spring	-113.441	39.186	5478.02	--	TMzi	10/1/08	7.91	15.80	898	2.70	95.00	66.00	14.00	120.00	36.00	310.00	Na-HCO3	--	1.1	<0.5	0.66	0.86	-2.10	-6.51	4
259	Kiln Spring	-113.507	38.394	5773.95	--	Tv	10/2/08	7.08	14.30	937	1.60	31.00	110.00	38.00	110.00	39.00	420.00	Ca-HCO3	--	2.1	11.00	0.14	0.01	-1.92	-7.04	4
260	Buckhorn Spring	-113.840	38.340	6674.20	--	QTcs	10/2/08	7.57	15.40	525	2.30	53.00	49.00	4.40	36.00	15.00	240.00	Ca-HCO3	--	4.7	3.10	0.13	-0.57	-2.51	-7.27	2
261	Mud Spring	-113.860	38.426	6660.00	--	QTcs	10/2/08	7.48	13.90	774	1.40	35.00	62.00	30.00	78.00	30.00	290.00	Ca-HCO3	--	2.1	7.90	0.16	0.20	-2.19	-7.12	4
262	Willow Spring (Wah Wah Valley)	-113.492	38.313	6154.04	--	Tv	10/2/08	7.02	17.20	1532	1.90	83.00	180.00	47.00	260.00	160.00	450.00	Ca-HCO3	--	6.5	<0.5	0.29	0.24	-1.22	-6.27	4
263	Willow Spring (Pine Valley)	-113.837	38.412	6281.00	--	QTcs	10/2/08	7.11	13.90	2420	1.50	96.00	210.00	89.00	510.00	250.00	270.00	Ca-Cl	--	3.2	<0.5	0.14	0.09	-1.03	-5.92	5
264	Water Hollow Spring	-113.643	38.284	7324.40	--	CZs	10/2/08	7.19	14.80	167	0.83	8.00	18.00	4.20	11.00	4.00	70.00	Ca-HCO3	--	7.6	<0.5	-1.14	-2.70	-3.36	-8.57	3
265	Miller Spring	-113.865	39.580	4768.39	--	QTcs	10/23/08	7.58	11.30	1145	13.00	100.00	83.00	42.00	100.00	190.00	370.00	Na-HCO3	--	6.5	<0.5	0.37	0.59	-1.38	-6.57	4
266	South Tule Spring	-113.519	39.334	4427.00	--	QTcs	10/1/08	7.60	24.80	1465	20.00	190.00	56.00	31.00	240.00	165.00	240.00	Na-Cl	--	20	<0.1	0.23	0.54	-1.62	-5.95	4

[1] Station ID corresponds with those in tables A.6.1 and A.6.2.

[2] Coordinates are in NAD GCS 1983 projection.

[3] Water elevation is the measured groundwater elevation at sample site.

[4] Screen midpoint in feet below land surface. -- indicates spring sites or unknown screen depths.

[5] Hydrogeologic units (figure 4.1). QTcs = Quaternary Tertiary coarse-grained basin fill aquifer, Ts = Tertiary sedimentary-rock aquifer, Tv = Tertiary volcanic-rock aquifer, TMzi = Tertiary Mesozoic intrusive confining unit, UPzc = upper Paleozoic carbonate-rock aquifer, LPzc = lower Paleozoic carbonate-rock aquifer, CZs = Cambrian-Neoproterozoic siliciclastic-rock confining unit.

[6] Water type calculated using Aquachem.

[7] Total dissolved solids, solids as residue at 180°C.

[8] Mineral phase saturation indices calculated using PHREEQC.

[9] Geochemical group calculated by hierarchical cluster analysis, see text for details.

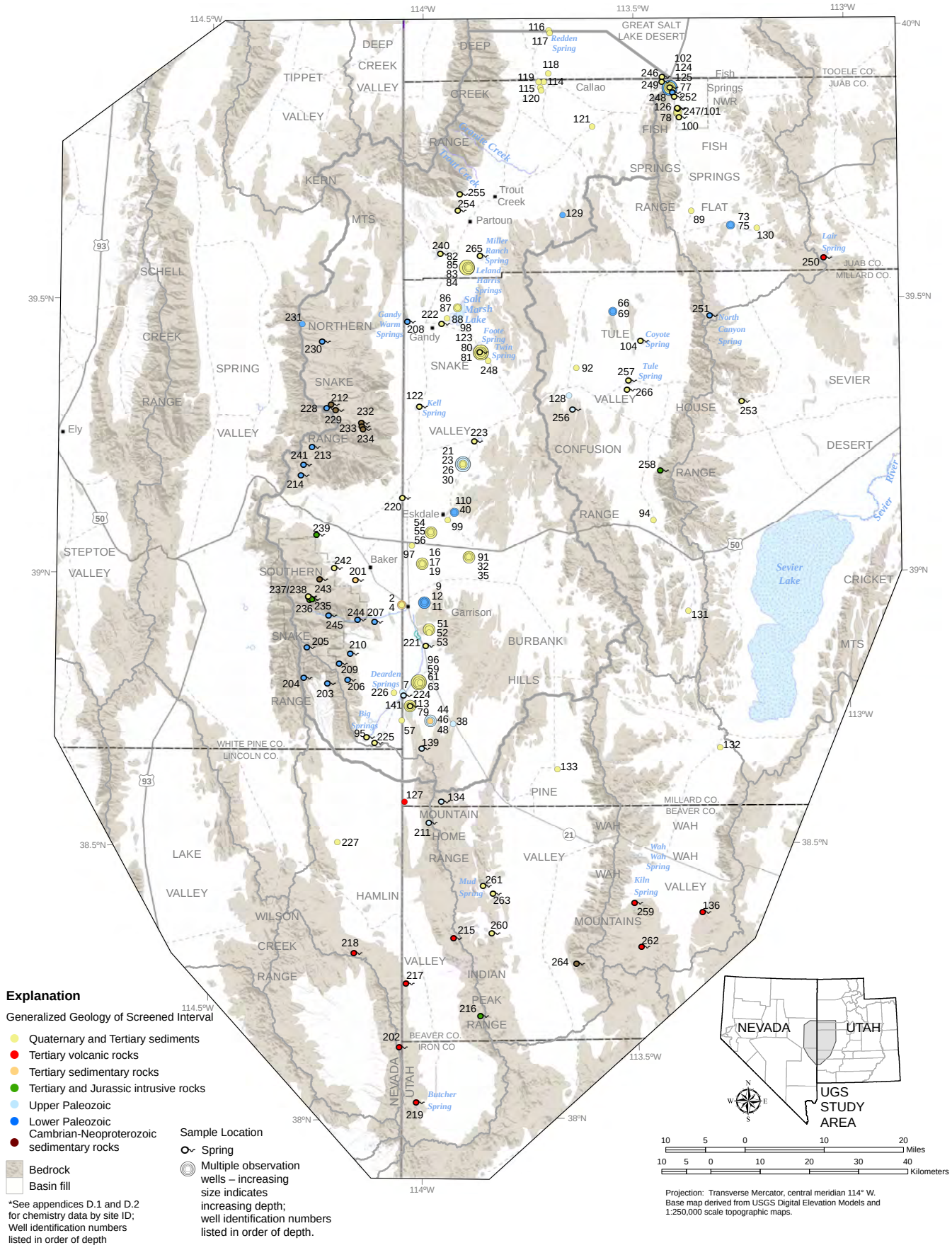

Figure 6.1. *Wells and springs in the UGS study area sampled for hydrochemistry.*

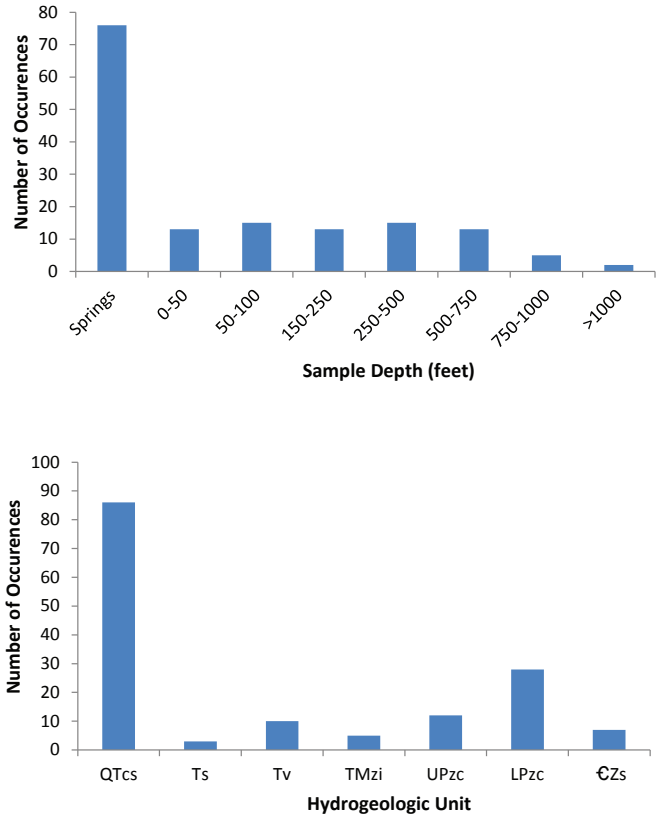

Figure 6.2. *Depths and screened geologic units of sampled wells and springs. Hydrogeologic units (figure 4.1):* QTcs, *Quaternary-Tertiary coarse-grained sedimentary aquifer;* Ts, *Tertiary sedimentary-rock aquifer;* TMzi, *Tertiary-Mesozoic intrusive-rock confining unit;* UPzc, *upper Paleozoic carbonate-rock aquifer;* LPzc, *lower Paleozoic carbonate-rock aquifer;* €Zs, *Cambrian-Neoproterozoic siliciclastic-rock confining unit.*

(100 m) of the land surface or springs are examined in the subsequent analysis. These 124 samples are assumed to represent the temperature of the uppermost part of the aquifer system.

Groundwater temperatures are lowest in and near the Snake Range and Deep Creek Range and along the western part of Snake Valley (figure 6.3). Groundwater along the floor of Snake Valley ranges between 13 and 20°C. Most sites in Tule Valley and Fish Springs Flat have shallow groundwater temperatures near or greater than 20°C. The highest measured groundwater temperatures occur at the lowest elevations near the north end of the Fish Springs Range. High groundwater temperatures in low-elevation areas including Tule Valley and Fish Springs Flat likely result from deeper and longer flow paths and/or possibly higher local heat flux in these areas. Lower temperatures generally indicate areas of active recharge and/or higher rates of groundwater movement. Across the study area groundwater temperature generally increases from higher elevations in and adjacent to the mountains to lower elevations on the valley floors (figure 6.4).

6.2.1.4 Major Solute Concentrations

Box and whisker plots of the principal dissolved ions show the distribution of solute concentrations in the study area (figure 6.5). The concentrations of the major dissolved cations (Ca, Mg, K, and Na) and anions (Cl, SO_4) vary by several orders of magnitude. The concentrations of the anion HCO_3 is an exception, varying by a single order of magnitude. The distribution of concentrations of the major solutes have means and 1-standard deviation uncertainties that are generally in the lower third of the range of concentrations. A number of the higher concentrations are above the 1-standard-deviation uncertainty for a given constituent. This type of distribution is generally skewed to the largest concentrations and median concentrations can be considered more representative of typical values. Median concentrations for the cations Ca, Mg, K, and Na are 56.7, 24.2, 3.2, and 39 mg/L, respectively. Median concentrations for the anions Cl, SO_4, and HCO_3 are 41.4, 37.9, and 240 mg/L, respectively. Mean concentrations for these constituents are substantially higher in all cases except HCO_3, which is slightly lower.

6.2.2 Water Quality

6.2.2.1 Introduction

Basic groundwater quality across the Snake Valley area is defined by water chemistry type, TDS, nitrate, and arsenic concentration (table 6.1). Major ion chemistry of each sample is simplified by using standard water type nomenclature (Freeze and Cherry, 1979; Kehew, 2000) that classifies a given sample according to dominant cation and anion (e.g., Ca-HCO_3 or Na-Cl). Water type was calculated using the Aquachem software. TDS concentrations for 50 samples that lack laboratory TDS measurements were calculated based on specific conductance data; the remaining samples use laboratory-reported TDS values. Water quality data are examined in detail for the basin-fill carbonate-rock, and Tertiary volcanic-rock aquifers.

6.2.2.2 Hydrochemical Facies

Hydrochemical facies vary from calcium-bicarbonate (Ca-HCO_3) to sodium-chloride (Na-Cl). No samples contained potassium as the dominant cation. Most samples (84 of 154, or 55%) are calcium-bicarbonate facies, and all bicarbonate facies including magnesium-bicarbonate and sodium-bicarbonate together constitute 70% of all samples. The next most common facies contain chloride as the dominant anion and calcium, magnesium, and sodium as the principal cations; together, these samples constitute 24% of all the samples. Sulfate facies constitute the remaining 6% of the dataset. A Piper diagram (figure 6.6)

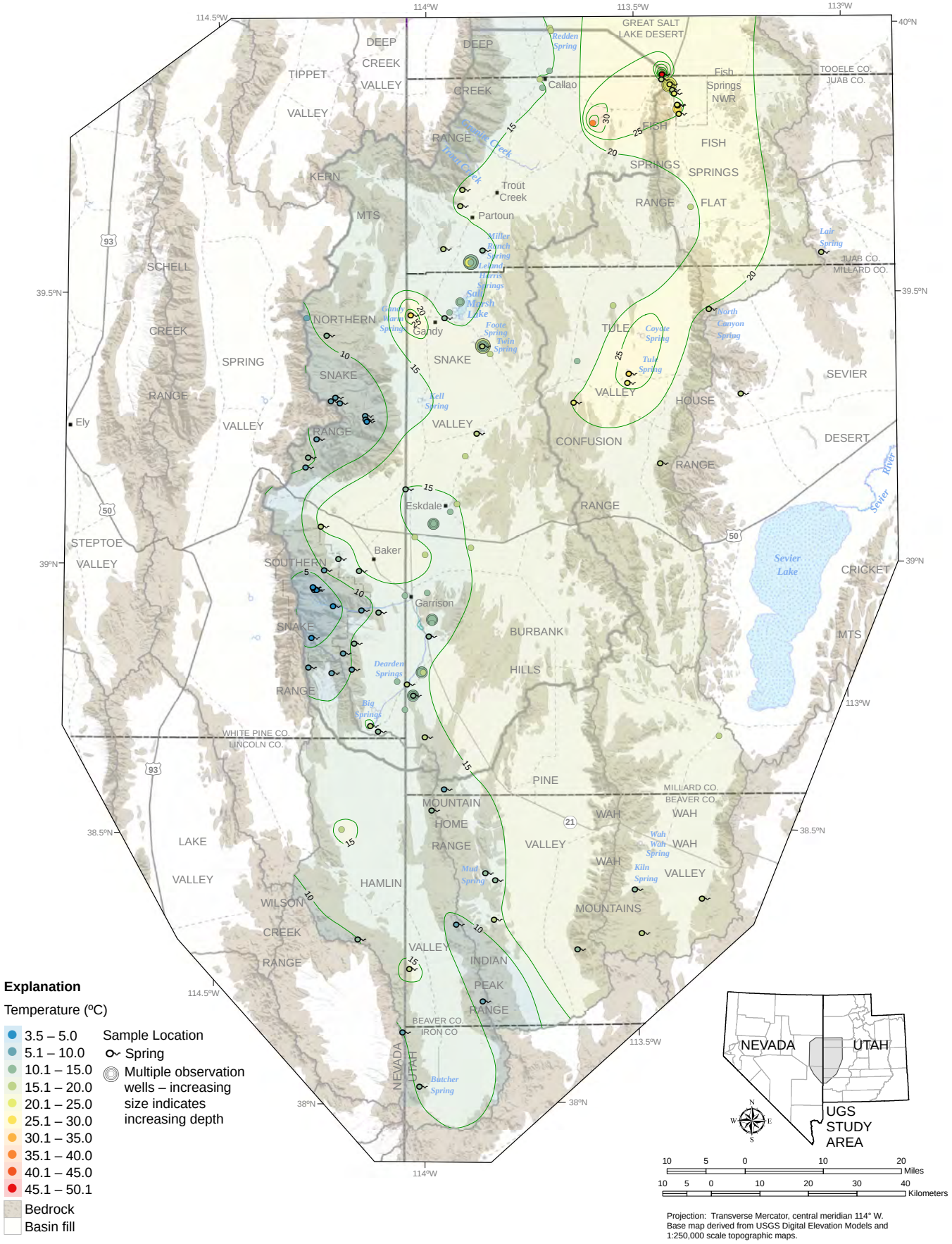

Figure 6.3. *Generalized aquifer temperatures from select wells and springs in the UGS study area (table 6.1).*

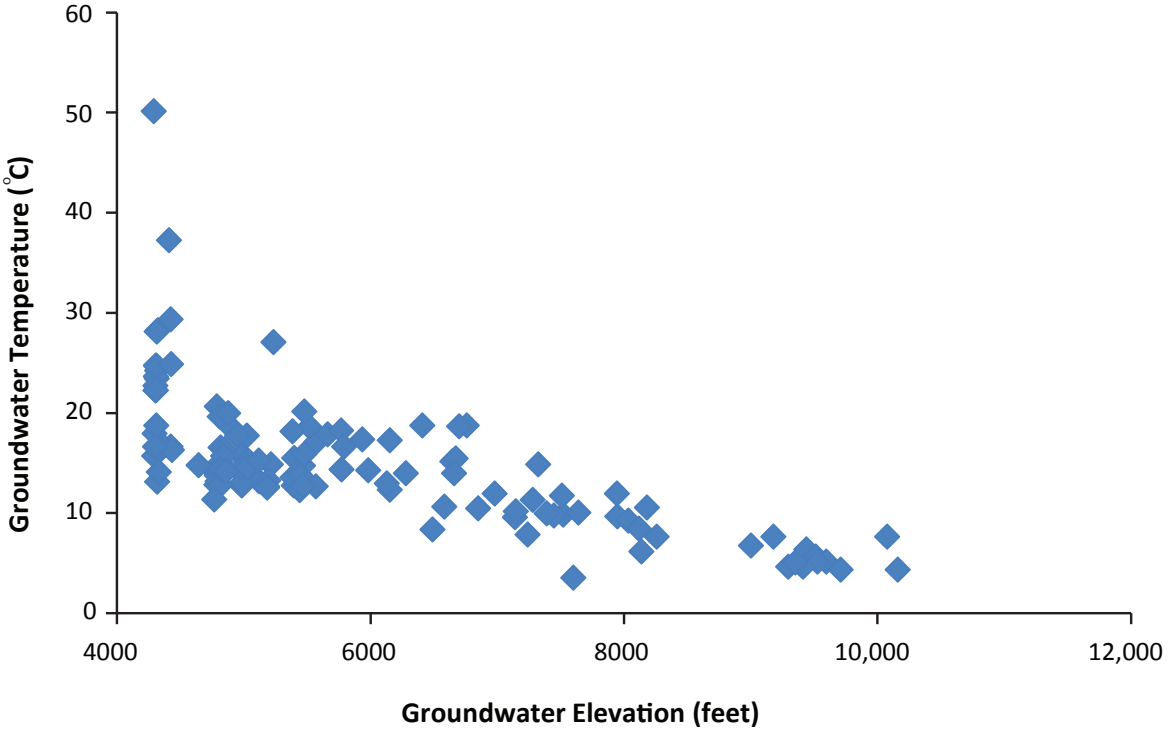

Figure 6.4. *Groundwater temperature measured during sampling versus static groundwater-level elevation for wells and springs screened within 300 feet (100 m) of the land surface. Temperature increases with decreasing elevation.*

of general chemistry indicates that groundwater chemistry is variable and spans a range from dilute bicarbonate to concentrated sodium-chloride facies. The dominant facies are calcium-magnesium-bicarbonate and calcium-sodium-magnesium-bicarbonate, followed by calcium-bicarbonate facies.

The distribution of hyodrochemical facies follows systematic patterns across the study area (figure 6.7). Groundwater near the Snake Range and across much of Snake Valley is dominated by bicarbonate and either calcium or magnesium. Sulfate and chloride groundwater types occur to the east in parts of Tule, Pine, and Wah Wah Valleys. Discharge areas near Coyote Spring in Tule Valley and to the north at and near Fish Springs have sodium-chloride water types (figure 6.7). Sulfate water types occur in Tule Valley and at several other isolated locations. Water type generally ranges between calcium-bicarbonate water types in recharge areas near the Snake Range to sodium-chloride water types in areas of major discharge including Fish Springs and Tule Valley. Sulfate water types are fewer but generally occur in a zone between chloride and bicarbonate water types.

6.2.2.3 Total-Dissolved-Solids Concentrations

TDS concentrations are from 75 springs and 80 wells (figures 6.8 and 6.9). TDS concentrations in Snake Valley area groundwater are generally below 1000 mg/L; elevated TDS concentrations exist locally in the basin-fill and bedrock aquifers. Groundwater from basin fill with low TDS concentrations exists in wells and springs near groundwater recharge areas along the eastern margin of the Snake Range in the western part of the study area (figure 6.8). Groundwater from bedrock having low TDS concentrations exists in springs in the Snake Range and in a well in the Mountain Home Range in the western and southwestern part of the study area (figure 6.9). The poorest quality groundwater for both basin-fill and bedrock aquifers, in terms of high TDS, exists in the Great Salt Lake Desert and Fish Springs Flat in the northeast part of the study area (figures 6.8 and 6.9), which are regional groundwater discharge areas. For basin-fill and bedrock aquifers, TDS increases along groundwater flow paths due to water-rock interaction and fluid concentration near areas of major evapotranspiration.

TDS concentrations in Snake Valley and adjacent areas range from 26 to 6400 mg/L with an outlier concentration of 20,000 mg/L from Wilson Health Springs at the northern end of the Fish Springs Range (figure 6.8); the average TDS concentration for the basin-fill aquifer, excluding springs of unknown geology but including alluvial-sourced springs, is 825 mg/L, and the median value is 398 mg/L.

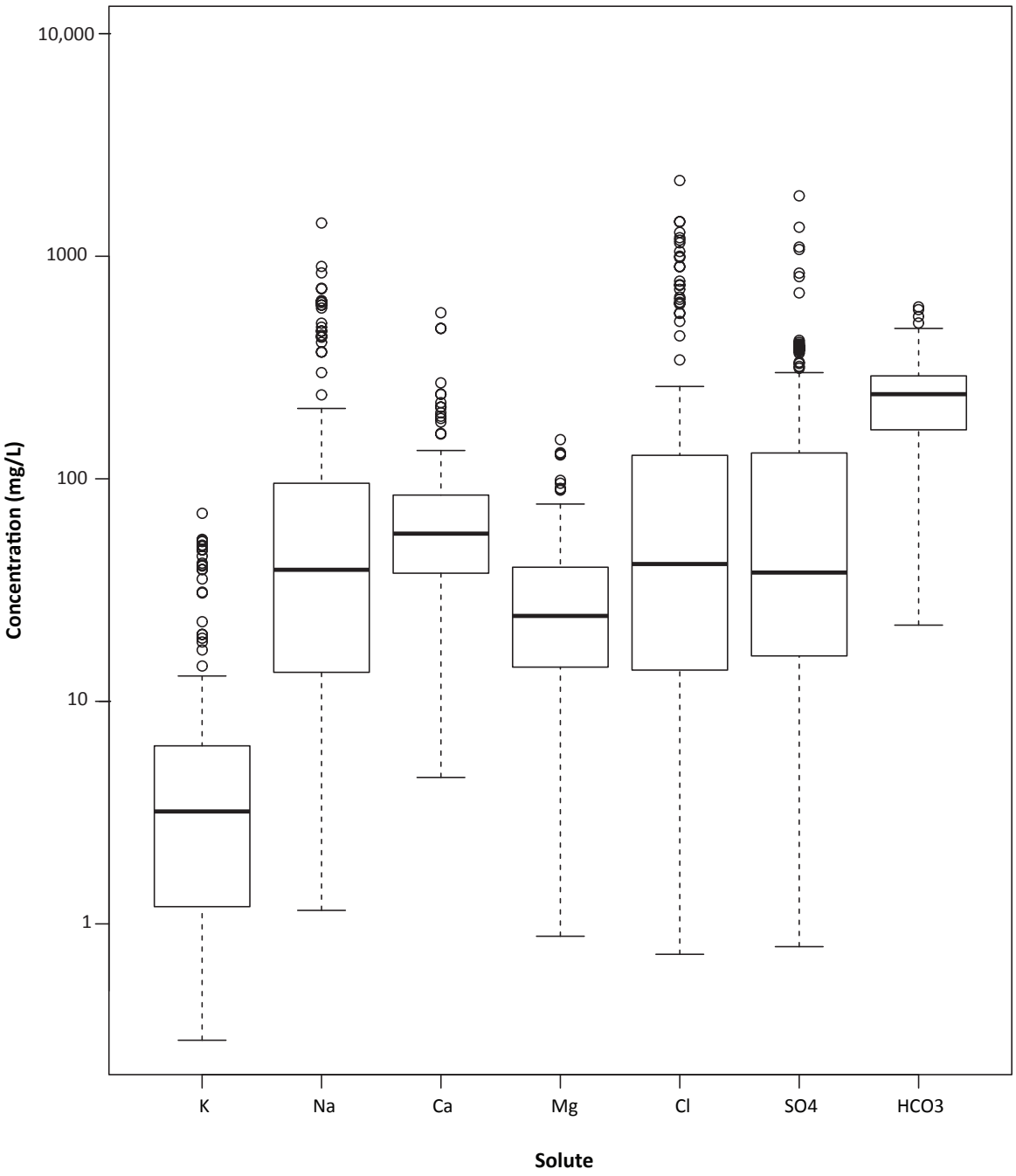

Figure 6.5. *Box and whisker plots of major solute concentrations for wells and springs (table 6.1). The thick horizontal lines are the medians and the upper and lower edge of the boxes represent the 25th and 75th percentiles, respectively. The dashed lines extend to the 10th and 90th percentiles. Circles represent solute concentrations of individual samples.*

Samples from bedrock, including seven springs with known geologic sources, have a mean concentration of 1235 mg/L and median of 490 mg/L. TDS concentrations for groundwater samples from about 21% of the samples are above 1000 mg/L. Groundwater having TDS concentrations less than 500 mg/L in Snake Valley ranges from 26 to 494 mg/L and comprises 65% of all data samples; 79% of samples have TDS concentrations less than 1000 mg/L. Water having TDS greater than 3000 mg/L exists in six of 155 samples (4%).

We examined wells in three depth categories based on screened-interval depth: shallow, medium, and deep (less than 150 feet [45 m], 150 to 300 feet [45-90 m], and greater than 300 feet [90 m], respectively). For all wells in the shallow category, the average TDS is 793 mg/L; for

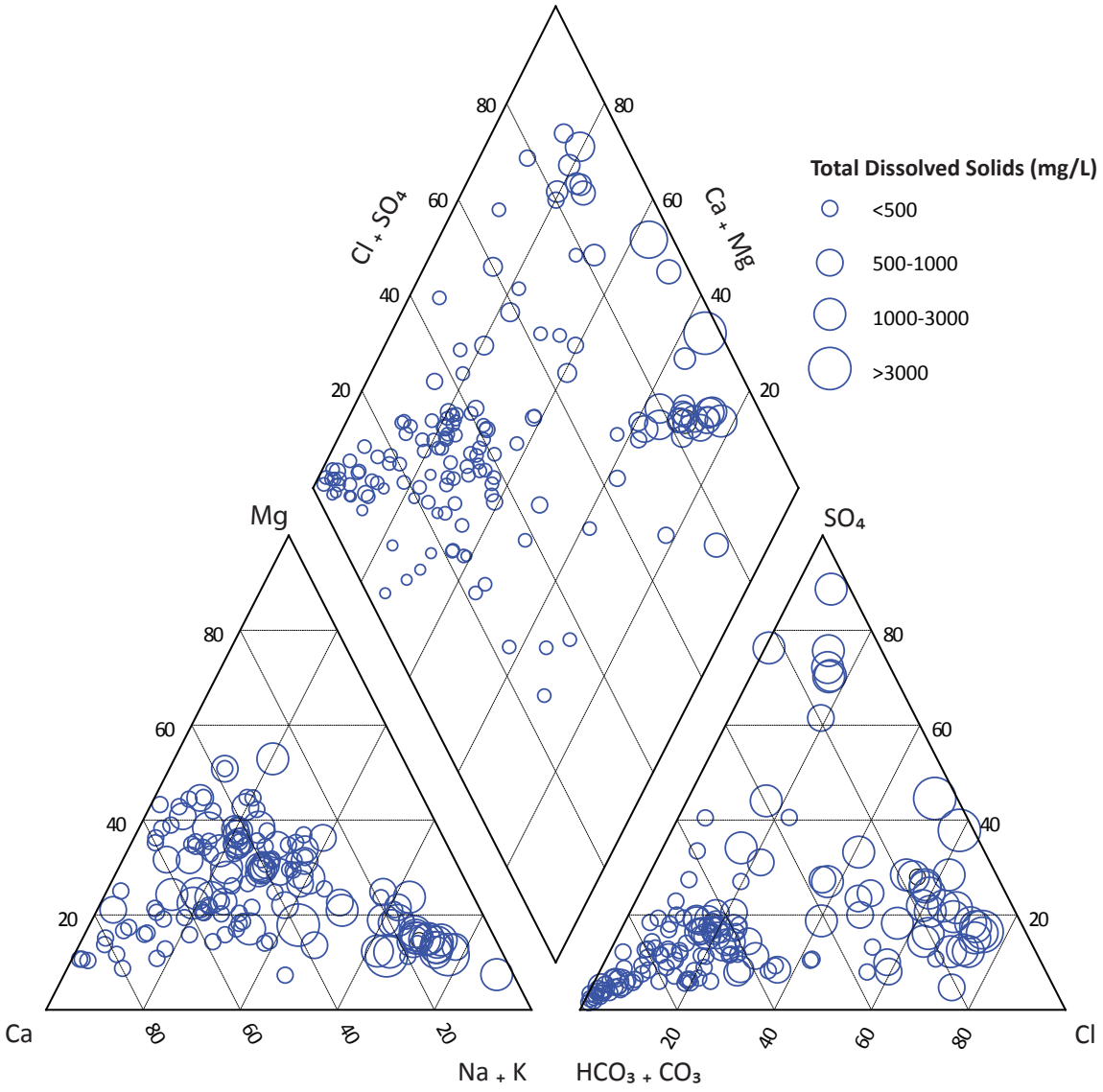

Figure 6.6. *Piper diagram for select wells and springs (table 6.1).*

medium-depth wells, the average TDS is 920 mg/L; and deep wells average 891 mg/L. For basin-fill samples in the depth categories, average TDS for shallow, medium, and deep wells is 739 mg/L, 855 mg/L, and 776 mg/L, respectively. For bedrock wells, average TDS for wells having a screened-interval depth greater than 300 feet (90 m) is 844 mg/L. The lowest TDS is found in shallow-depth-category wells screened in basin-fill deposits.

6.2.2.4 Nitrate Concentrations

Nitrate values in groundwater from 129 samples range from less than 0.04 mg/L (non-detect) to 15.8 mg/L (figure 6.10; table 6.1). Nitrate concentration was below detection at 17% of the sites. Average nitrate concentration for the remaining 83% is 1.6 mg/L, with a median of 0.47 mg/L for all samples including non-detects. Average nitrate concentration, excluding non-detects, is 1.05 mg/L for samples from the basin-fill aquifer, 0.89 mg/L for bedrock samples, and 2.8 mg/L for springs of unknown geology. Nitrate concentration is less than 1 mg/L for 70% of all of the groundwater samples. Approximately 88% of the samples have nitrate concentration less than 3 mg/L. Three samples (2%) exceeded the U.S. Environmental Protection Agency (2011) nitrate maximum contaminant level (MCL) of 10 mg/L. Overall, nitrate concentrations in the basin-fill and bedrock aquifers are low, especially compared to other rural areas in Utah (see, for example, Lowe and Wallace, 1999; Lowe and others, 2002, 2003). The highest nitrate concentrations (>10 mg/L) exist in wells and springs (especially North Canyon Spring and Kiln Spring) (figure 6.10) located in the eastern part of the study area. Nitrate concen-

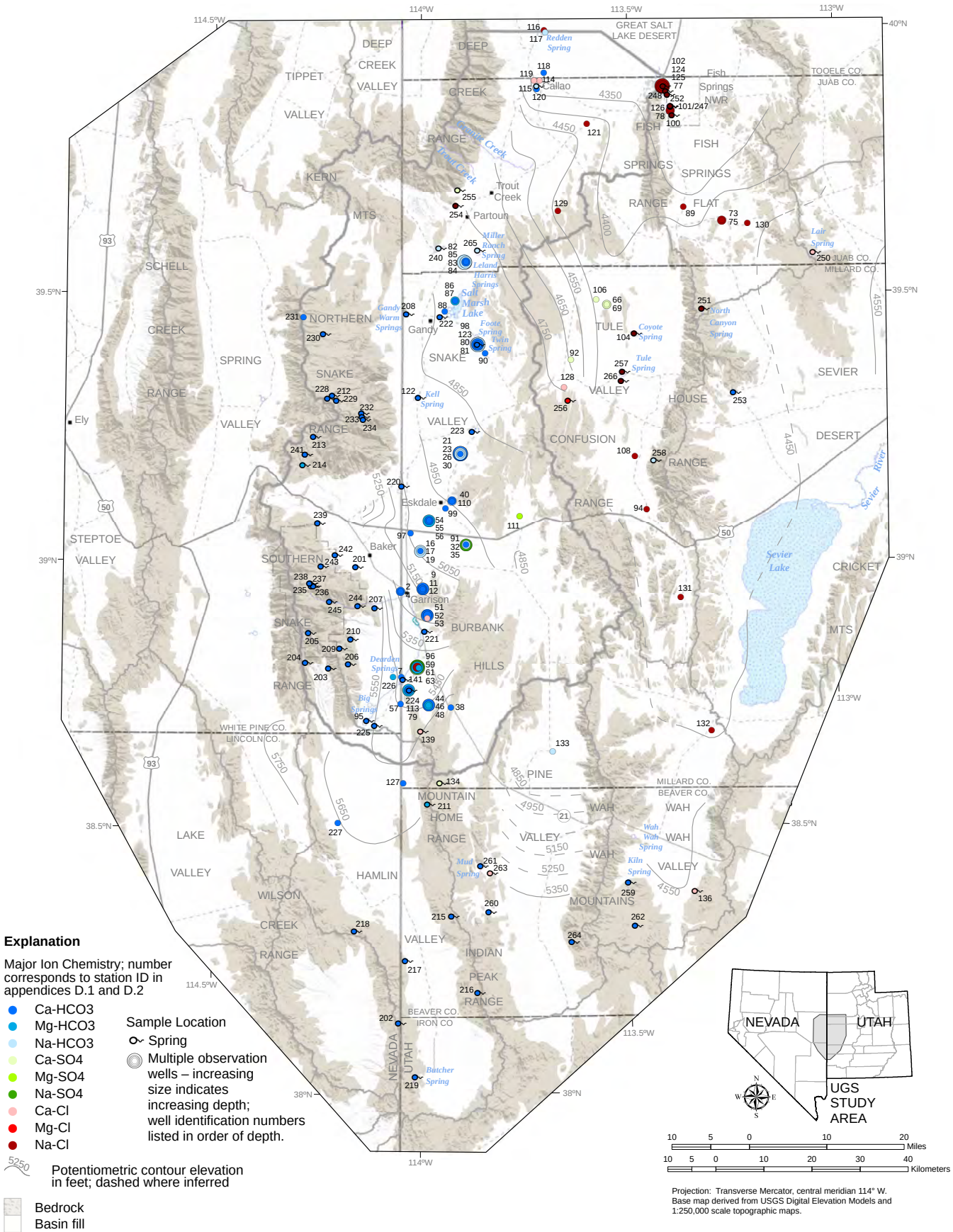

Figure 6.7. *Major-ion chemistry for select wells and springs in the UGS study area (tables 6.1 and 6.3). Potentiometric contours simplified from Gardner and others (2011).*

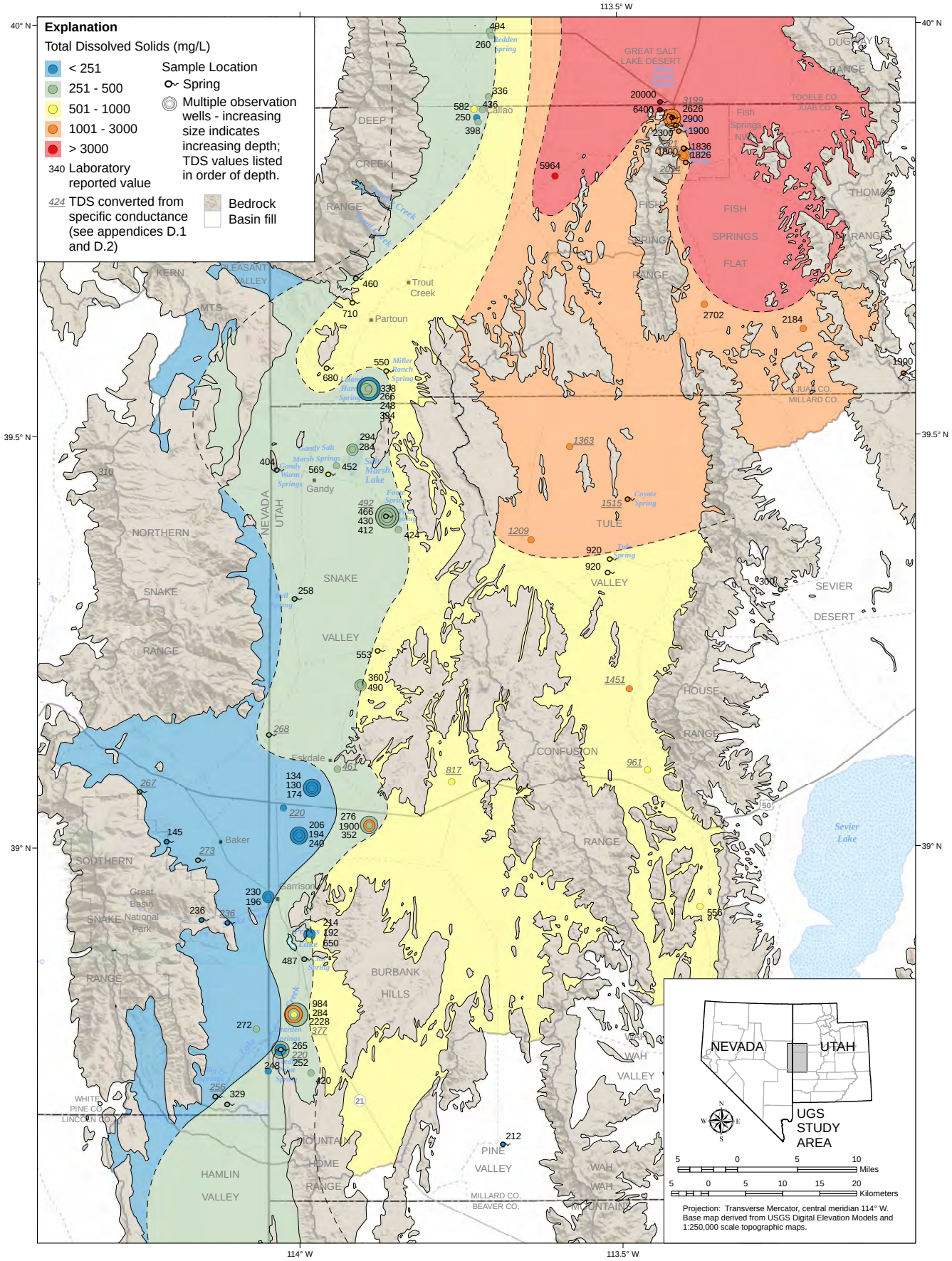

Figure 6.8. *Total-dissolved-solids concentrations for select wells and springs in the basin-fill aquifer in the UGS study area (table 6.1).*

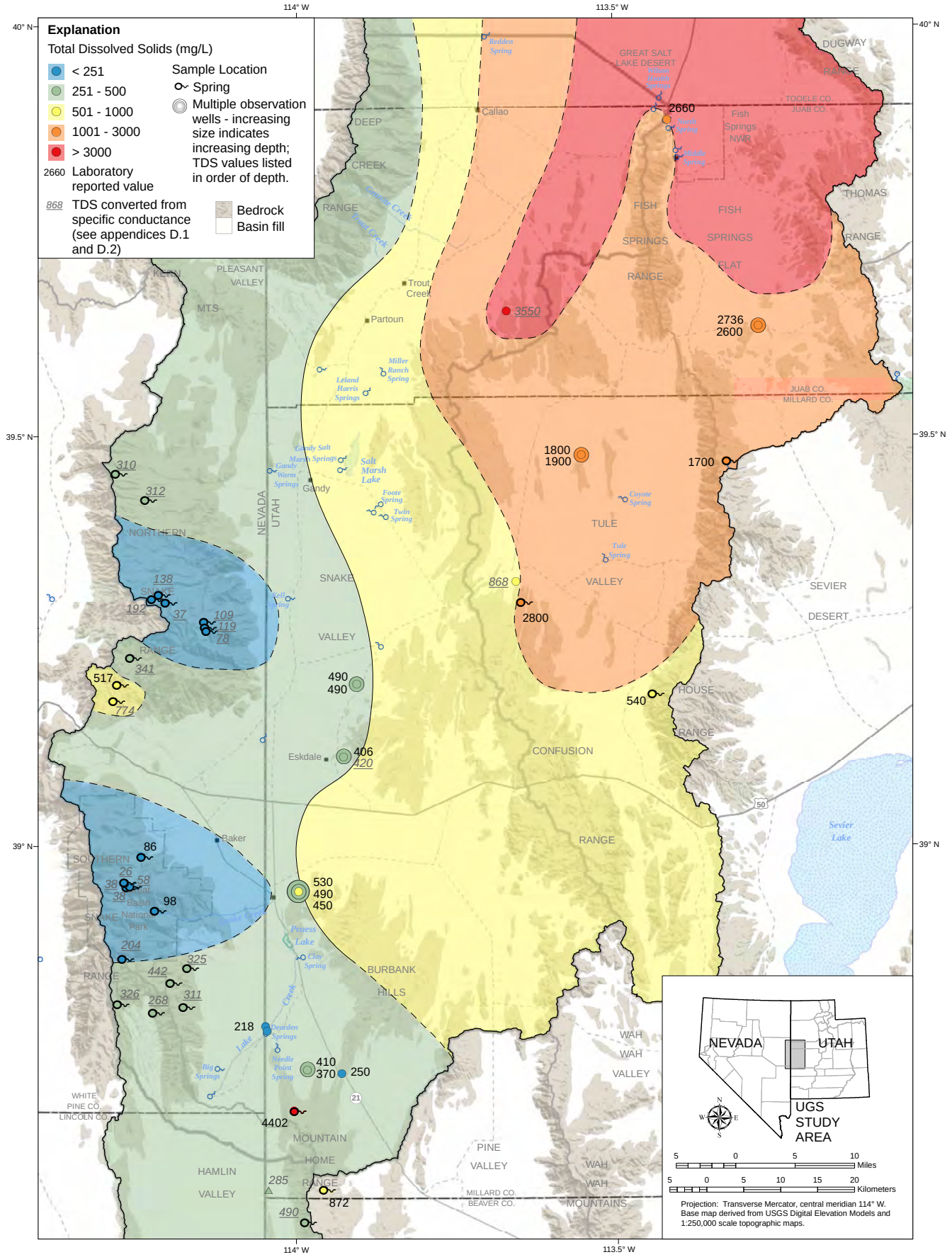

Figure 6.9. *Total-dissolved-solids concentrations for select wells and springs in the bedrock aquifers in the UGS study area (table 6.1).*

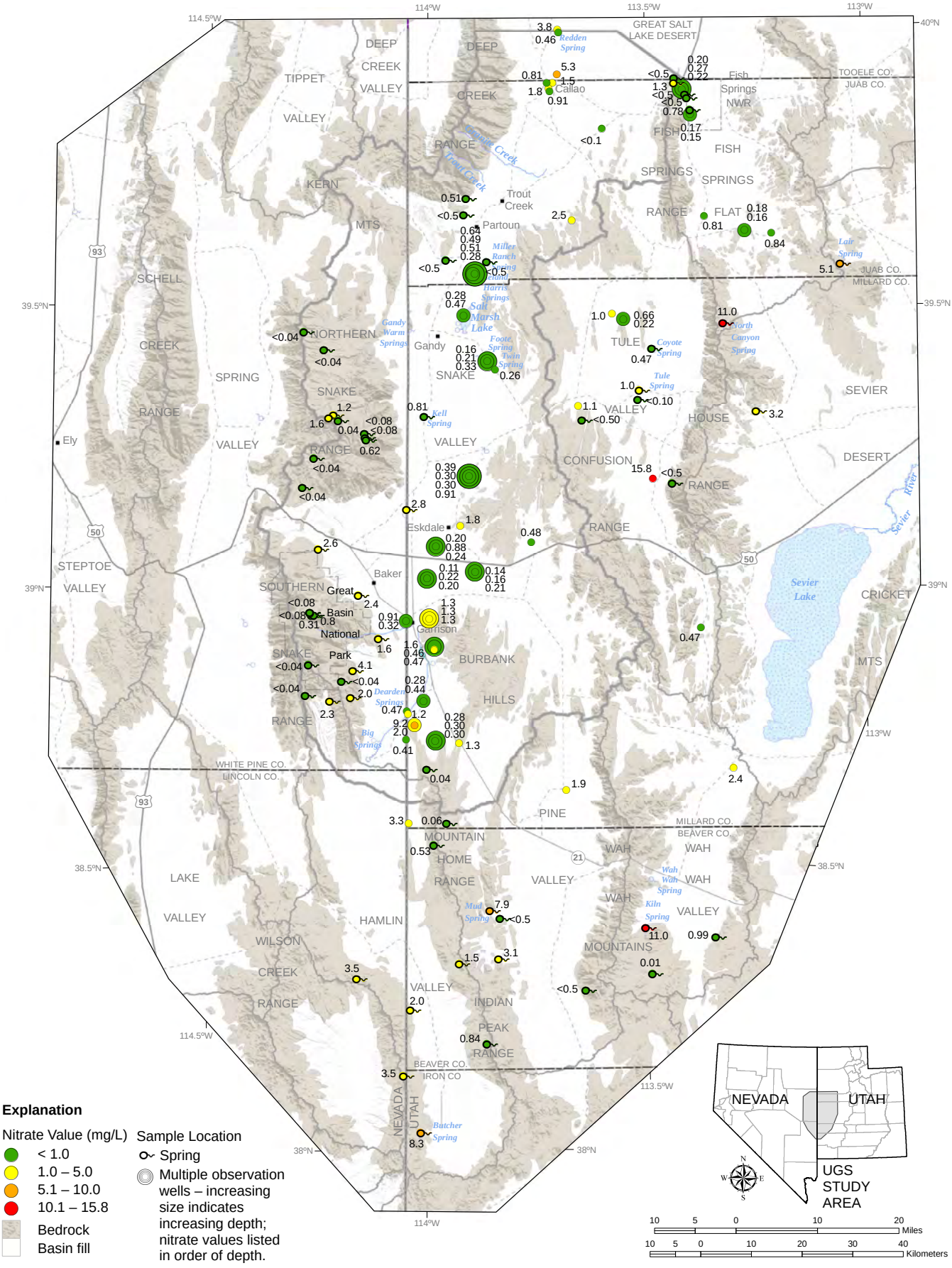

Figure 6.10. *Nitrate concentrations for select wells and springs in the UGS study area (table 6.1).*

trations are sporadic and vary throughout the study; sample sites having nitrate concentrations between 5 and 10 mg/L are typically springs and alluvial wells. The source of high nitrate concentrations is uncertain and not associated with a particular land use.

6.2.2.5 Arsenic Concentrations

Arsenic concentrations in groundwater from 112 samples range from less than 0.5 µg/L (non-detect) to 98 µg/L, and average 7.9 µg/L (table 6.1). The high concentration of 98 µg/L is from Wilson Health Springs (figure 6.11). The range of arsenic concentrations from bedrock wells is 0.5 to 41.6 µg/L with an average of 7.9 µg/L. Arsenic concentrations average 8.7 µg/L for all alluvial samples, and 6.7 µg/L for springs of unknown geology (3.7 µg/L when Wilson Health Springs is excluded). Distribution of arsenic concentrations were evaluated on the basis of sample depth (shallow, medium, and deep) using the same criteria as described above in the TDS section. For all shallow wells, the average arsenic concentration is 6.4 µg/L; for medium-depth wells, the average concentration is 10.2 µg/L; and average arsenic concentration is 14 µg/L for deep wells. Twenty-three percent of all of the arsenic samples exceed 10 µg/L, the U.S. Environmental Protection Agency (2011) drinking water quality standard, and 43% of all of the samples exceed 5 µg/L. Samples having less than 1 µg/L arsenic concentration represent about 16% of all data samples. Overall, arsenic concentrations in the basin-fill and bedrock aquifers are variable, but high in many places. The highest arsenic concentrations (>10 µg/L) exist in springs and deep alluvial wells (figures 6.11 and 6.12) located generally in the eastern part of the study area and may be related to localized dissolution of arsenic-rich minerals. Of 70 samples having arsenic concentrations and apparent age data, the majority (82%) of wells having concentrations that exceed the 10 µg/L standard are categorized as "old" water (apparent age greater than 1000 years), and 28 of 33 samples having arsenic concentrations greater than 5 µg/L are categorized as "old"; only 2 of those 33 are "modern" (apparent age less than 50 years). Overall, springs (excluding Wilson Health Springs) have the lowest arsenic concentrations with 74% of springs of unknown geology below 5 µg/L and 32% below 1 µg/L. A weak correlation exists between high arsenic concentration and temperature (and TDS), especially in the Fish Springs area in the northeastern part of the basin.

6.2.2.6 Other Chemical Constituents

Secondary drinking-water standards (U.S. Environmental Protection Agency, 2011) were exceeded in 32 samples for sulfate (12 springs and 29 wells) and 28 for chloride (14 springs and 14 wells); these constituents are not harmful to human health, but may impart an unpleasant taste, odor, or color to the water.

6.2.3 Groundwater Chemistry Statistical Analysis

6.2.3.1 Introduction

Major solute chemistry is a basic characteristic of groundwater that determines its quality and influences end use, and is controlled by in large part by water-rock interactions as the groundwater moves through a flow system (Freeze and Cherry, 1979; Kehew, 2000). This section examines the distribution of solute concentrations across the Snake Valley study area and uses these data in conjunction with simple statistical techniques and inverse hydrochemical models to determine the composition and variation across the study area. These results and discussion were first presented by Kirby (2012).

Statistical analysis of groundwater chemistry is based on a select set of 88 samples collected during this study combined with sample data compiled from recent publications for 66 additional samples (tables D.1 and D.2). Subsequent use of the term "dataset" in this section refers to the combined set of 154 new and compiled hydrochemical samples (table 6.1).

6.2.3.2 Factor Analysis

The correlation between the major solutes and their control on the total variability of dissolved chemistry can be objectively analyzed via a statistical factor analysis (Dawd and Feth, 1967). Factor analysis is a scale-independent mathematic reduction that calculates synthetic variables retaining the inherent variability in samples and across a data array. This variability is represented in a number of simplified factors calculated for each sample. These objective factors may then be interpreted in the context of the original variables and samples to constrain numeric variability and correlation across a data array (Everitt and Torsten, 2006). Factor analysis can therefore provide a robust mathematical basis for understanding the relationship between various aqueous species and their interrelation in a hydrogeologic system (Dawd and Feth, 1967; Dalton and Upchurch, 1978; Usunoff and Guzmán-Guzmán, 1989; Suk and Lee, 1999; Koonce and others, 2006).

For this study we used R-Mode factor analysis to assess the correlation and similarities between the major dissolved constituents. The factor analysis was performed on a matrix that included the concentrations of seven principal solute compounds (Ca, Mg, Na, K, Cl, SO_4, and HCO_3) using the open source R statistical software (Everitt and Torsten, 2006; R Development Core Team, 2012). The statistical

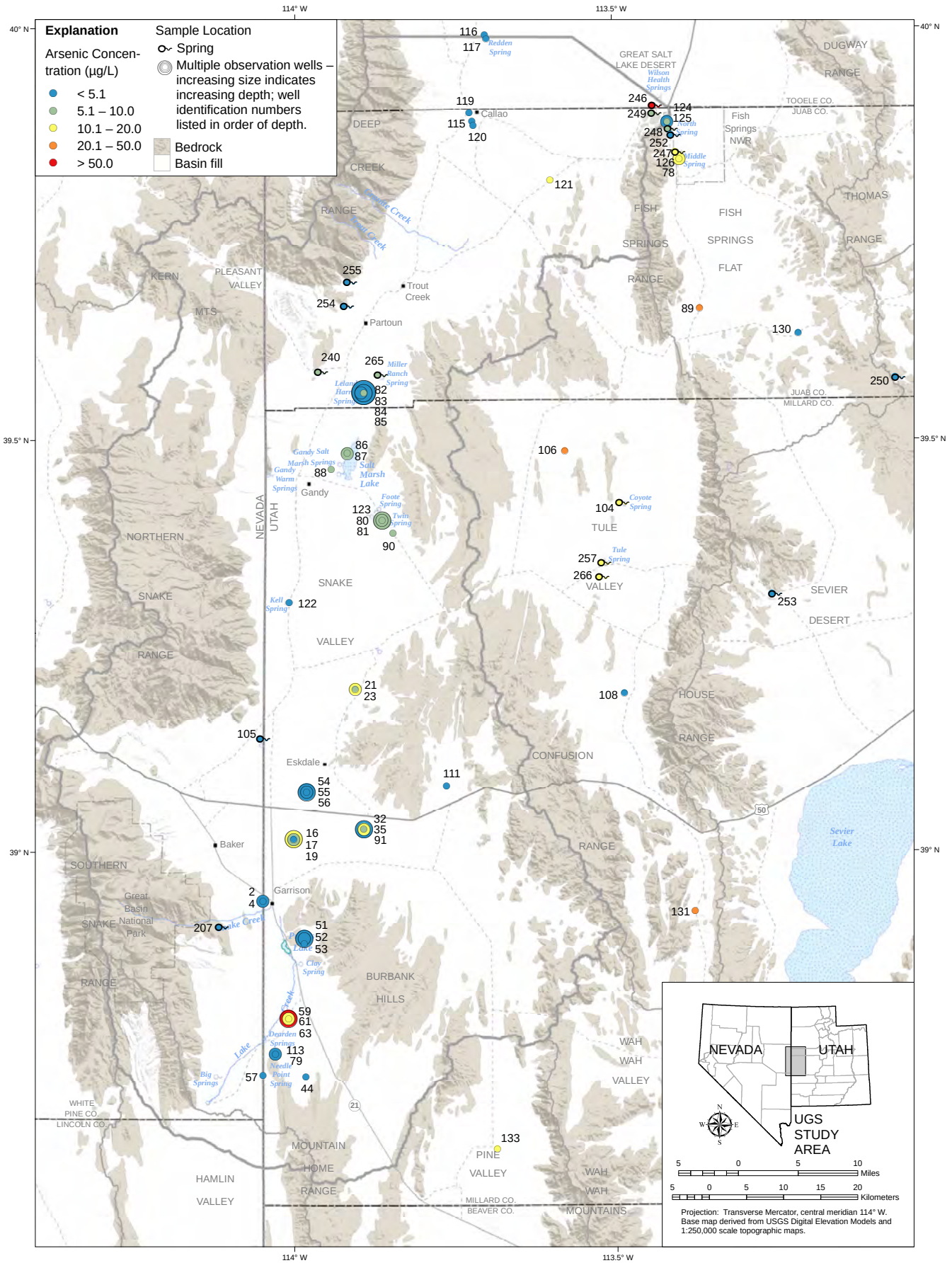

Figure 6.11. *Arsenic concentrations for select wells and springs in the basin-fill aquifer in the UGS study area (table 6.1).*

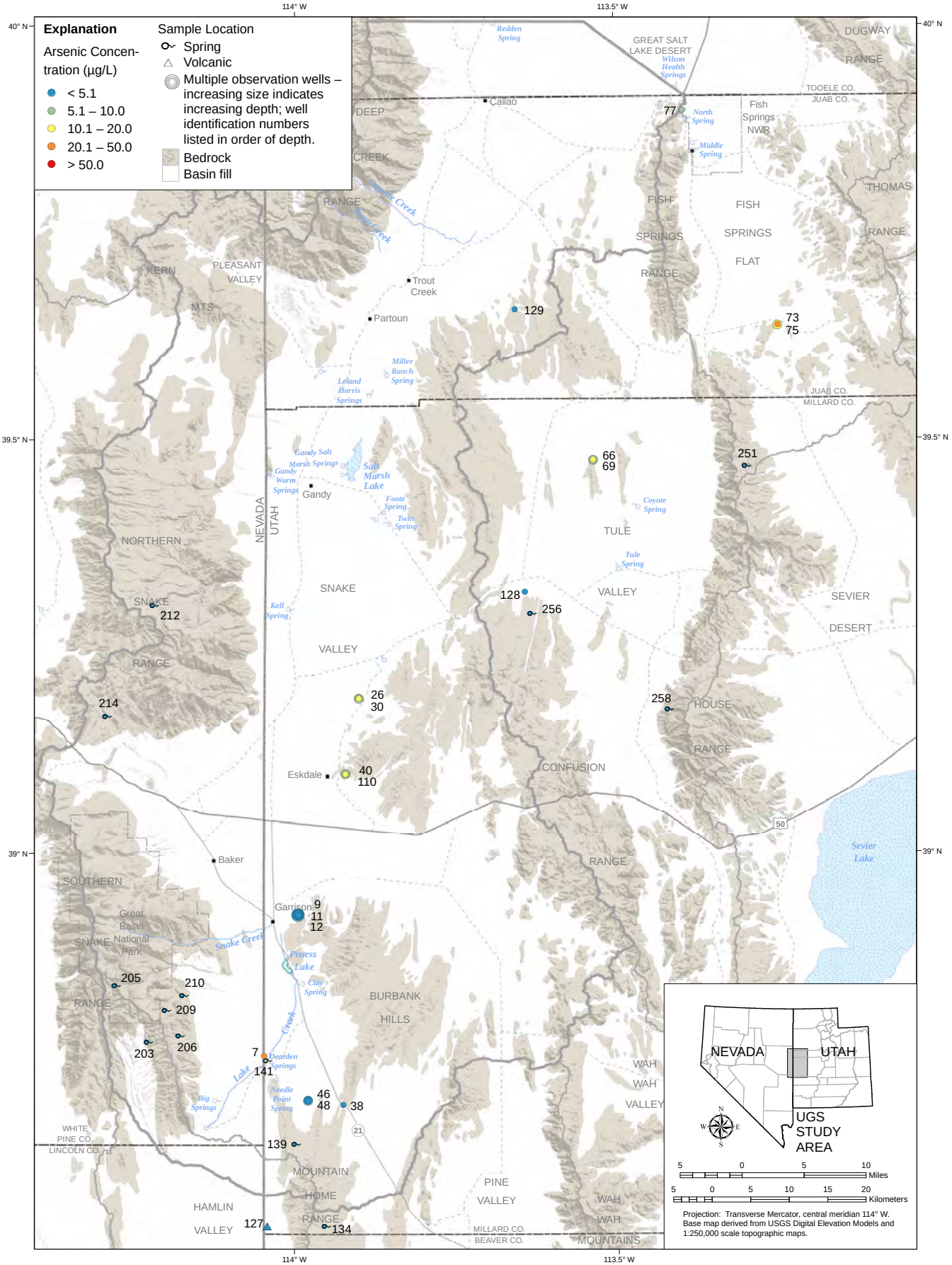

Figure 6.12. *Arsenic concentrations for select wells and springs in the bedrock aquifers in the UGS study area (table 6.1).*

routine included a standard factor analysis with varimax rotation and calculation of Bartlett scores for each factor and each sample. This method calculated three unique factors that together describe 79% of the variance across all samples (table 6.2).

Factor 1 accounts for 33% of the total variance and is driven primarily by changes in sodium, chloride, and potassium. Variability in the concentration of sodium is likely driven by a combination of halite dissolution, fluid concentration from evapotranspiration, and ion exchange. Changes in potassium concentration in carbonate-dominated settings commonly result from either clay mineral, potassium feldspar, or sylvite dissolution (Kehew, 2000). Changes in the chloride concentration in meteoric groundwater systems result primarily from dissolution of halite, or less likely may be the result of fluid concentration from evaporation or fluid mixing (Domenico and Schwartz, 1997).

Factor 2 accounts for 29% of the total variance. This factor is controlled by concentrations of magnesium, calcium, and sulfate, which are likely driven by variable amounts of dissolution or precipitation of calcite, dolomite, and gypsum. Hydrochemical linkages among these constituents in similar carbonate settings have been attributed to de-dolomitization reactions (Back and others, 1983; Plummer and others, 1990). Calcium and magnesium may also be involved in ion exchange reactions that may occur with clay minerals, and to a lesser degree with carbonate minerals (Kehew, 2000).

Factor 3 describes 17% of the variation and is primarily correlated to sulfate and sodium concentrations. Changes in the concentration of sulfate may result from dissolution of gypsum. Changes in sodium concentration may result from a combination of halite dissolution, fluid concentration from evapotranspiration, and ion exchange.

Taken together, the factor analysis results can be explained by water-rock (aquifer) interaction in the form of mineral dissolution or precipitation and ion exchange as the reactions that could account for much of the observed variability in solute concentration across the dataset. The changes in solute concentration may result either from residence-time-dependent sequential water-rock interactions, or localized geologic conditions along a given flow path.

Table 6.2. *Summary of factor analysis.*

Solute	Factor 1	Factor 2	Factor 3
Ca	0.216	0.922	0.192
Cl	0.853	0.468	0.206
HCO_3	0.311	0.101	–
K	0.754	0.128	0.449
Mg	0.37	0.742	0.281
Na	0.835	0.236	0.492
SO_4	0.237	0.566	0.787
Eigenvalue	2.331	2.023	1.221
Total Variance (%)	33	29	17
Cumulative Variance (%)	33	62	79

6.2.3.3 Cluster Analysis

Groundwater samples from the dataset are statistically grouped via a cluster analysis into hydrochemical facies based on differences and similarities in the concentrations of the seven principal solutes. Cluster analysis is a multivariate statistical technique used to delineate statistically distinct groups. During cluster analysis samples are intercorrelated based on multiple parameters and grouped with one another based on the relative variability among the parameters of a given sample (Everitt and Torsten, 2006; Templ and others, 2008). The concentrations of the seven principal dissolved constituents were input into the R software package and all data transformation and statistical analyses were calculated using standard R routines and functions (Everitt and Torsten, 2006; R Development Core Team, 2012). The dataset was first log-transformed and then standard Z scores were calculated for the entire dataset following the method of Guler and Thyne (2006) and references therein. After data transformation and standardization, we performed a hierarchical cluster analysis using the Ward method and standard Euclidean scores to group the data. Clusters were extracted from these data and labeled. Numerous techniques exist for determining the appropriate number of clusters to extract from a dataset, all of which rely to varying degrees on subjective decisions (Templ and others, 2008). For this analysis, we used the sum-of-squares method to give a range of possible numbers of clusters that were statistically valid (Suk and Lee, 1999; Everitt and Torsten, 2006; Guler and Thyne, 2006). The sum-of-squares method yields between five and nine clusters that reasonably group the data. Each of these options was run and the results examined for both spatial coherence and cluster coherence based on plots of the previously calculated factor scores and spatial distribution of the groups. A total of six clusters (referred to hereafter as hydrochemical groups) were identified based on this analysis (figures 6.13 and 6.14; table 6.3).

To assess the dispersion of the grouped data, the coefficient of variation (COV) was calculated for each group and dissolved constituent. The COV is the standard deviation divided by the mean and it represents a scale-

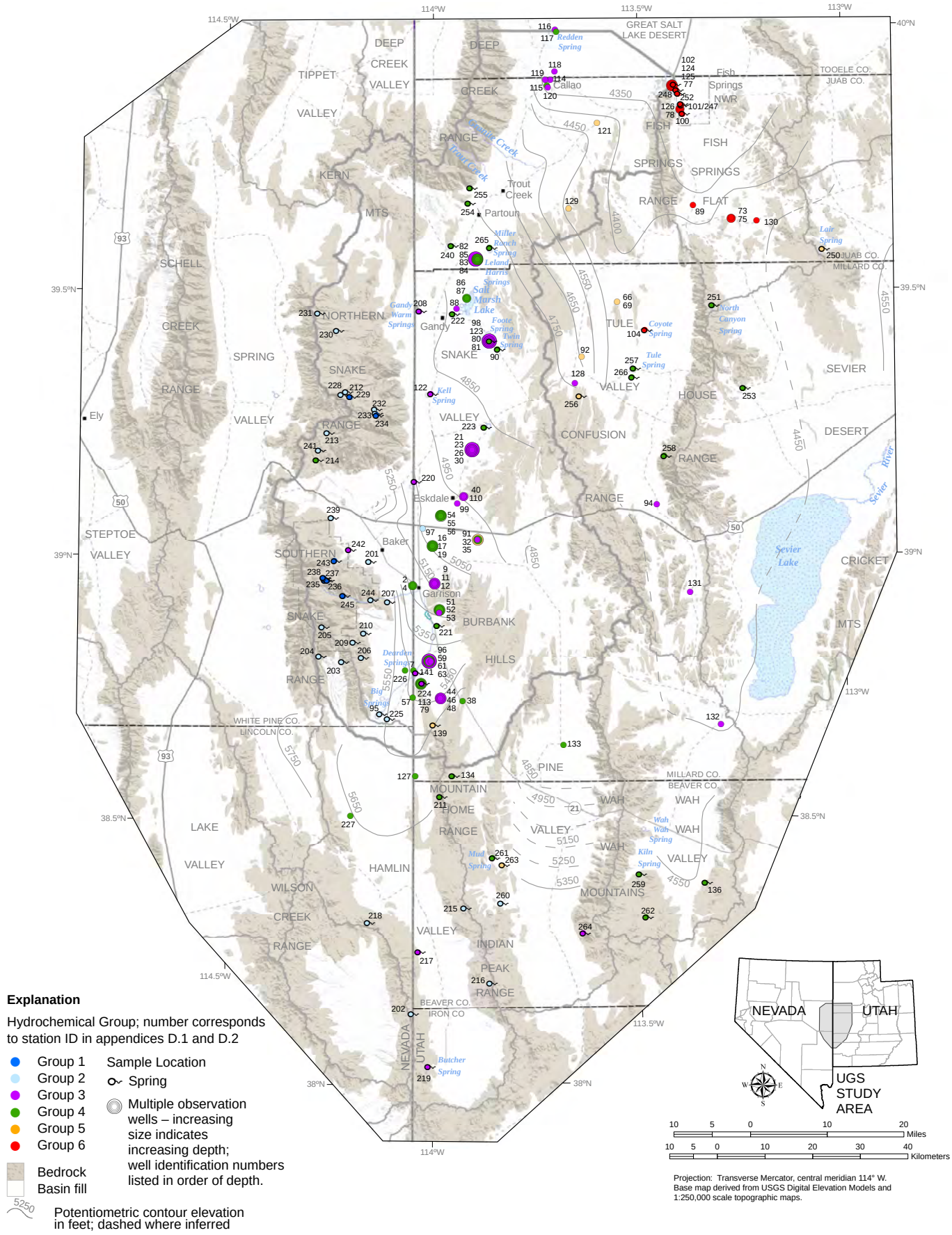

Figure 6.13. *Hydrochemical groups based on cluster analysis (table 6.3). Potentiometric contours simplified from Gardner and others (2011).*

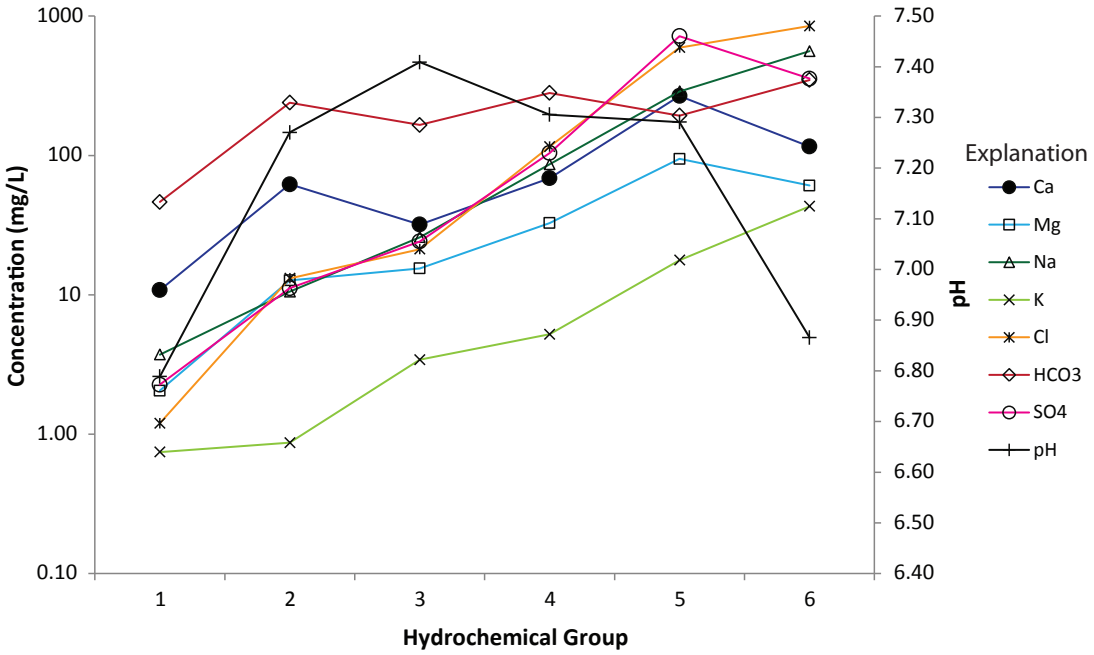

Figure 6.14. *Summary of group-mean hydrochemistry based on cluster analysis (table 6.3).*

independent metric that can compare dispersion among the various groups and dissolved constituents. COV is similar for given dissolved constituents for most groups (table 6.4, figure 6.15). Sulfate, chloride, and sodium are the dissolved constituents having the greatest range of COV across the groups; other constituents have a smaller range. These results suggest that these groupings are valid and that subsequent discussion and comparison of group mean chemistry provide relevant summaries of the hydrochemistry of the groups.

The six hydrochemical groups reflect variations in physiographic locations, water-rock interactions, and recharge or discharge relationships along flow paths. Hydrochemical groups indicate spatial control on groundwater chemistry and groupings vary systematically from west-southwest toward the east-northeast (figures 6.16 and 6.17). The spatial distribution, and consequently hydrochemical evolution, of the groups may therefore generally follow topographic flow paths from group 1 to group 6. Group-mean field parameters of temperature and conductivity, as well as solute concentrations of sodium, chloride, and potassium, generally increase along potential flow paths from group 1 to 6 (figure 6.16). The group-mean values for calcium, magnesium, and sulfate also generally increase from group 1 to 5, with the largest values for group 5 and lower values of these constituents in group 6. Bicarbonate and pH do not vary uniformly among the groups. Values for deuterium, a stable isotope of hydrogen, overlap at least in part across all six groups (figure 6.16).

The mean hydrochemistry of group 1 yields a calcium-bicarbonate water type (figure 6.17). All group 1 samples come from mountain springs in the Snake Range. Most of these springs occur in parts of this range that are underlain by siliclastic sedimentary or felsic plutonic rocks in addition to the more typical carbonate rocks. This group is typical of the highest elevation extent of the regional groundwater system and the recharge that occurs in these areas. This group can also be considered typical of recharge settings where bedrock consists at least partially of siliciclastic sedimentary or felsic plutonic rocks.

The mean hydrochemistry of group 2 yields calcium-magnesium-bicarbonate water type that is typical of groundwater in carbonate terrains (Kehew, 2000). This group has a significantly lower mean groundwater elevation and higher temperature than group 1, and includes mountain springs as well as springs and wells in the upper part of the basin fill in western Snake Valley. Groundwater in this group is typical of recent recharge in carbonate or other bedrock in the mountain ranges with relatively high precipitation rates as well as recharge to adjoining basin fill from upland runoff. Both group 1 and 2 typify hydrochemistry of the major recharge zones in the Snake Valley study area.

Groundwater of group 3 is calcium-magnesium-sodium-bicarbonate type and includes wells and springs primarily in basin fill in western Snake Valley. This group represents the upper middle part of the flow system, and the

Table 6.3. *Summary of group-mean chemistry and mineral saturation.*

Group	Number of samples	Water Elevation[1] (ft)	pH	Conductivity (µS/cm)	Temperature (°C)	Water Type[2]	Group-mean chemistry Ca (mg/L)	Mg (mg/L)	Na (mg/L)	K (mg/L)	Cl (mg/L)	HCO_3 (mg/L)	SO_4 (mg/L)	Mineral saturation[3] Calcite	Dolomite	Gypsum	Halite	Sylvite
1	8	9007	6.79	76	5.3	Ca-HCO3	10.82	2.05	3.72	0.74	1.2	46.35	2.27	-2.06	-4.81	-3.75	-9.83	-9.89
2	26	7624	7.27	406	10	Ca-Mg-HCO3	62.06	12.69	10.53	0.87	13.12	239.05	11.16	-0.14	-0.86	-2.53	-8.39	-8.88
3	37	5313	7.41	373	14.8	Ca-Mg-Na-HCO3	31.96	15.48	25.87	3.42	21.24	165.61	24.17	-0.37	-0.84	-2.46	-7.8	-8.12
4	54	5209	7.31	965	16.1	Na-Ca-Mg-HCO3-Cl-SO4	68.68	32.77	86.31	5.2	115.72	280.92	104.11	0.01	-0.08	-1.67	-6.58	-7.25
5	13	5004	7.29	3222	20.1	Na-Ca-Cl-SO4	267.48	94.51	287.96	17.74	593.95	193.17	717.68	0.27	0.37	-0.6	-5.42	-6.12
6	16	4342	6.87	3812	24.9	Na-Cl	116.01	60.81	560.39	43.16	848.36	348.11	355.86	-0.16	-0.26	-1.2	-4.98	-5.61

[1] Water elevation is the average potentiometric elevation for all samples in a given group (mean sea level datum).

[2] Water type calcuated from group-mean chemistry.

[3] Mineral saturation calculation for group-mean chemistry using PHREEQC.

Table 6.4. *Coefficient of variation for hydrochemical groups.*

Group	Coeffecient of variation[1] K (mg/L)	Na (mg/L)	Ca (mg/L)	Mg (mg/L)	Cl (mg/L)	SO_4 (mg/L)	HCO_3 (mg/L)
1	0.314	0.348	0.533	0.433	0.283	0.414	0.443
2	0.585	1.066	0.378	0.784	1.047	0.663	0.375
3	0.685	0.649	0.358	0.422	0.594	0.948	0.292
4	0.858	1.221	0.465	0.448	1.165	1.432	0.303
5	0.936	1.272	0.550	0.326	1.060	0.698	0.318
6	0.267	0.235	0.329	0.209	0.329	0.152	0.321

[1] Coefficient of variation is the standard deviation divided by the mean for a given constituent and group.

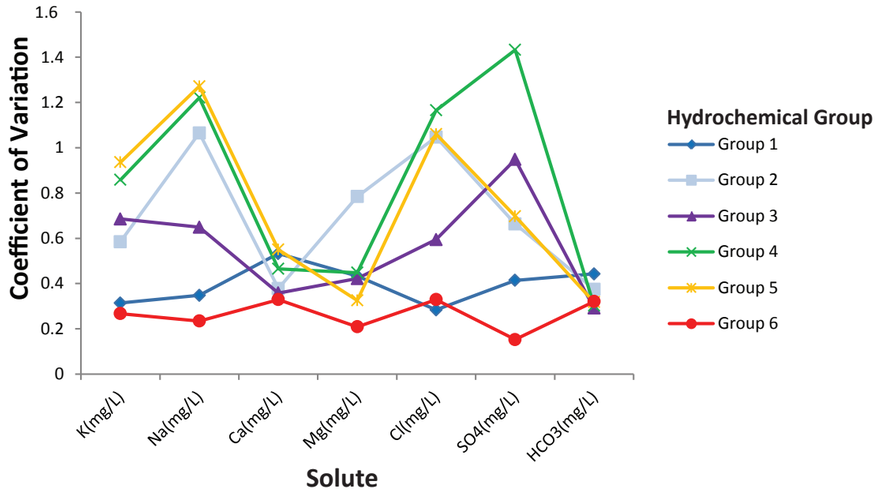

Figure 6.15. *Coefficient of variation versus solute concentration for hydrochemical groups.*

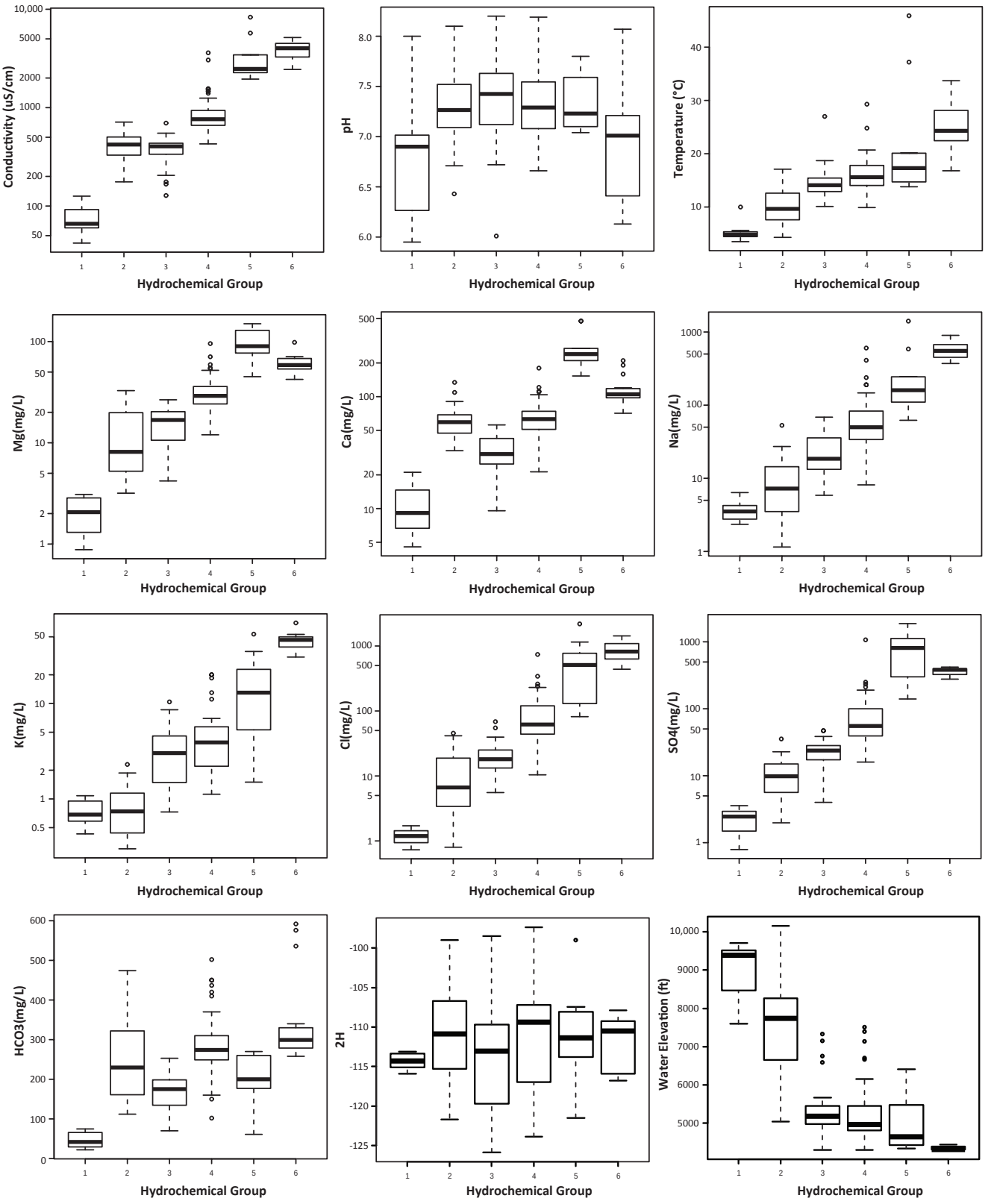

Figure 6.16. *Box and whisker plots for major solute concentrations, field parameters, and the stable isotope deuterium (^2H) for the grouped dataset. The thick horizontal lines are the medians and the upper and lower edges of the boxes represent the 25th and 75th percentiles respectively. The dashed lines extend to the 10th and 90th percentiles; circles indicate outliers. Water elevation is the potentiometric surface elevation of a given sample site.*

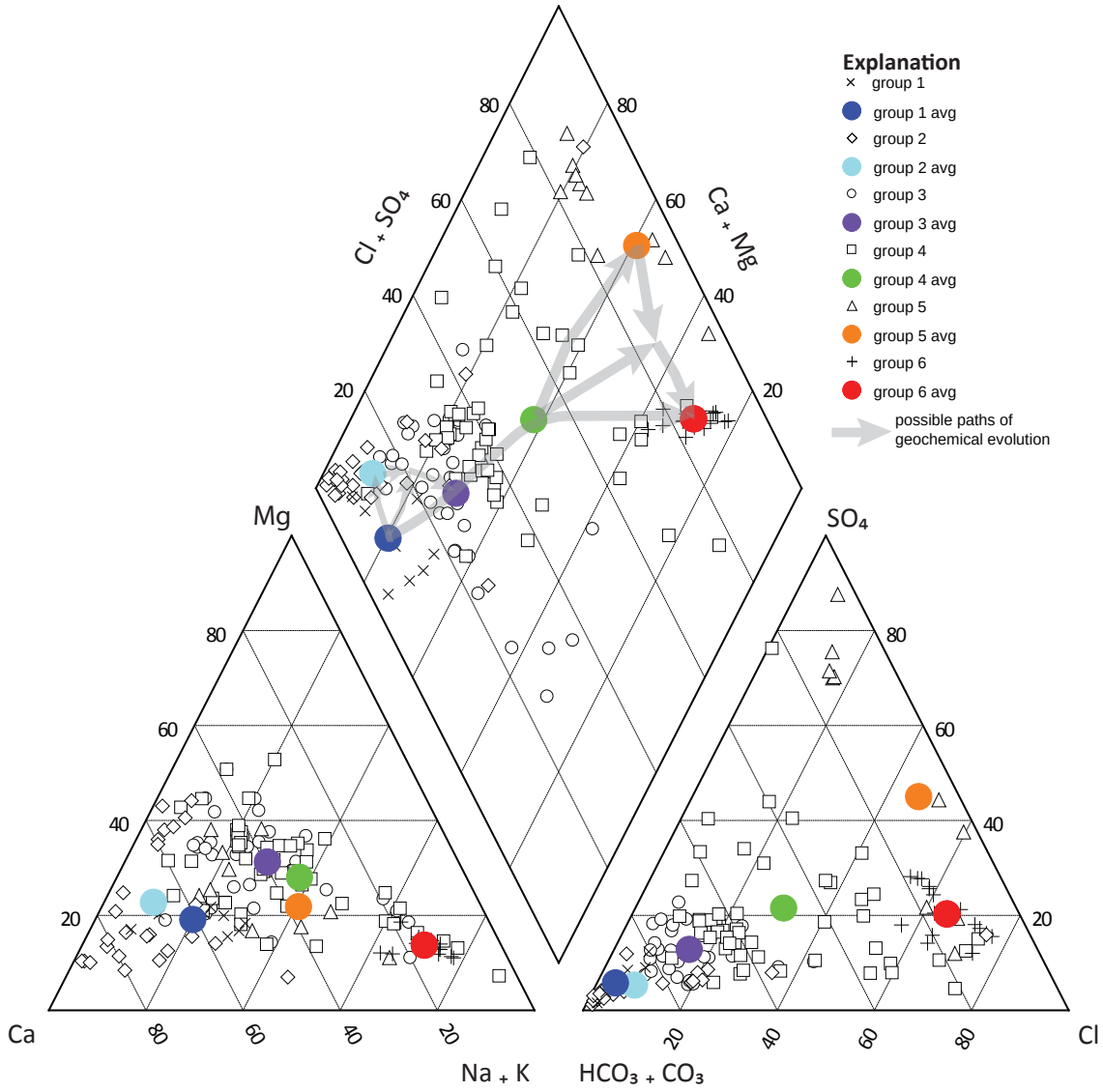

Figure 6.17. *Piper diagram of grouped geochemical samples. Data for individual samples and group-mean average values are given in tables 6.1 and 6.3, respectively. Paths of geochemical evolution are based on plausible inverse geochemical models.*

increase in dissolved constituents relative to groups 1 and 2 is likely the result of water-mineral interactions and ion exchange that occur in the basin-fill aquifer. Groundwater chemistry of group 3 may also result from mixing of local recharge with either group 1 or 2 groundwater near areas of discharge.

Group 4 comprises the largest number of samples and is sodium-calcium-magnesium-bicarbonate-chloride-sulfate water type. Samples in this group occur in a variety of settings, including the basin fill of Snake Valley and Tule Valley, and mountain springs in ranges east of Snake Valley. The increase in solute concentrations relative to group 3 likely results from increased distance and time since recharge and corresponding increases in water-mineral interaction, ion exchange, and possibly evaporative fluid concentration in the case of shallow groundwater beneath central and western Snake Valley and in areas with low recharge rates. Mineral-water interaction in this group may have occurred along longer flow paths in either basin fill or bedrock settings, and this group may include groundwater that has flowed from bedrock to basin fill or basin fill to bedrock. Several samples in this group from mountain springs in ranges east of Snake Valley have higher solute concentrations than comparable upland springs in group 2, possibly due to lower recharge rates and longer residence times in these drier eastern areas.

Group 5 includes samples with high concentrations of sulfate relative to other groups and is sodium-calcium-

chloride-sulfate water type. The high solute concentrations in this group suggest that significant water-mineral interaction and/or dissolution has occurred in these samples. Significant dissolution of sulfate, calcium, and magnesium minerals (gypsum, dolomite, and calcite) in bedrock or basin fill could account for the hydrochemistry of group 5.

Group 6 consists of sodium-chloride water type and includes samples from springs and wells, in bedrock and basin fill, having the lowest groundwater elevations in the study area. Samples in this group are confined to low-elevation parts of Fish Springs Flat and Tule Valley. High concentrations of sodium and chloride in this group may result from significant mineral dissolution and/or fluid concentration due to evaporation or evapotranspiration in and near major areas of discharge. This group represents a groundwater discharge zone and the relative end of chemical evolution of the groundwater in the study area.

6.2.3.4 Mineral Saturation Indices

To better understand hydrochemical evolution across the study area, saturation indices of major mineral and gas phases relevant to the study were calculated from group-mean and individual sample chemistry using the PHREEQC hydrochemical modeling program (Parkhurst and Appello, 1999). Calculated saturation values can range from negative (undersaturated) to positive (oversaturated). Undersaturation indicates a tendency to dissolve a given phase whereas oversaturation indicates a tendency to precipitate a given phase (Parkhurst and Appello, 1999). The phases included in the analysis are calcite, dolomite, gypsum, halite, and sylvite, and these phases are used to constrain inverse hydrochemical models in subsequent sections.

Group-mean chemistry yields oversaturation for calcite in group 4, and oversaturation for calcite and dolomite in group 5 (table 6.5, figure 6.18). All other phase and group combinations are undersaturated for the phases examined. These results indicate that, with respect to the mineral phases examined, sampled groundwaters will generally tend to dissolve minerals from the aquifer matrix except in group 4 and 5 waters, where there is an oversaturation of calcite and/or dolomite. Fracture- and pore-space-filling cement, primarily in the form of calcite, may be locally precipitated by groundwater in groups 4 and 5. Oversaturation of calcite may in part result from increases in water temperature along low-elevation flow paths. Conversely, groundwater typical of the remaining groups would tend to dissolve calcite (or dolomite) filling fractures and pore space in the aquifer matrix. The relative coherence of samples relative to a given group mean varies across the six groups. Samples in groups 1, 2, and 6 vary little from the calculated group-mean compositions, whereas groups 3, 4, and 5 have substantially greater variability. To address variability among individual samples within a given group, subsequent inverse hydrochemical modeling explores models using discrete samples along possible flow paths.

Statistical groups provide a useful and independent simplification of the hydrochemical evolution across the entire study area. Based on individual-sample and group-mean hydrochemistry, and the geographic distribution of the groups, a general path of hydrochemical evolution is inferred from the upgradient-dilute calcium-bicarbonate groundwater of group 1 to the downgradient-concentrated sodium-chloride groundwater of group 6. The systematic change in solute composition along potential flow paths suggests that groundwater in the study area undergoes hydrochemical evolution as it travels from high-elevation areas of recharge to low-elevation areas of discharge. To test this possibility, a series of inverse hydrochemical models that account for changes in chemistry via defined reactions was constructed using the PHREEQC program.

6.2.4 Inverse Hydrochemical Modeling

6.2.4.1 Introduction

Inverse modeling in the PHREEQC software package employs a chemical mass balance approach that attempts to quantify the type and amount of aqueous, mineral, and gas-phase reactions that can account for observed changes in water chemistry between samples (Parkhurst and Appello, 1999). In any hydrochemical modeling the validity of results is strongly dependent on the input data, proper conceptualization of the system, and a reasonable correlation between any formulated models and real-world conditions. Model results are not unique and do not represent absolute solutions for hydrochemical evolution. Instead, these results are intended to show the most plausible hydrochemical reactions that can account for changes in groundwater chemistry across the study area.

We developed two types of inverse hydrochemical models; those using group-mean hydrochemistry as initial and final waters (group-mean models, section 6.2.4.2), and those using individual samples along hypothetical flow paths (flow path models, section 6.2.4.3). Inverse hydrochemical models for group-mean chemistry examine general hydrochemical evolution across the study area and provide simple estimates of the processes that can account for the variation in major ion chemistry. Hydrochemical models using individual sample compositions as initial and final waters examine water evolution along hypothetical flow paths. All models use the same parameters described below and differ only in the initial and final waters considered.

Table 6.5. *Group-mean hydrochemical model results.*

Model	Initial[1]	% initial	Initial	% initial	Final	Sum residual error[2]	Mineral mass transfer (mMoles/kg)[3] Calcite	Min	Max	Dolomite	Min	Max	CO_2 (gas)	Min	Max	Gypsum	Min	Max	Halite	Min	Max	Sylvite	Min	Max	CaX	Min	Max	MgX	Min	Max	NaX	Min	Max
A	Group 1	100			Group 2	7.45	0.88	0.72	0.98	0.44	0.38	0.5	1.91	1.74	2.13	0.09	0.08	0.11	0.34	0.3	0.36	--	--	--	--	--	--	--	--	--	--	--	--	--
B.1	Group 2	100			Group 3	No model																										
B.2	Group 1	53	Group 2	47	Group 3	4.6	0.24	0.13	0.35	--	--	--	--	--	--	0.18	0.13	0.22	0.34	0.17	0.46	0.07	0.06	0.08	-0.59	-0.77	-0.41	0.35	0.19	0.46	0.48	0.25	0.74
B.3	Group 1	100			Group 3	4.37	1.06	1.04	1.33	--	--	--	0.89	0.78	1.28	0.23	0.2	0.26	0.5	0.42	0.57	0.07	0.06	0.08	-0.79	-0.96	-0.66	0.55	0.48	0.62	0.47	0.26	0.67
C	Group 3	100			Group 4	5.51	-0.52	-0.92	-0.05	0.78	0.52	0.91	1.31	0.94	1.72	0.83	0.7	0.97	2.62	2.21	3.03	0.05	0.02	0.07	--	--	--	--	--	--	--	--	--
D	Group 4	100			Group 5	4.94	--	--	--	-0.42	-0.66	-0.2	-1.09	-1.75	-0.5	5.65	5.55	6.3	14.09	11.61	15.27	0.32	0.26	0.38	--	--	--	2.83	2.22	3.6	-5.67	-7.2	-4.45
E.1	Group 5	100			Group 6	No model																										
E.2	Group 5	46	Group 4	54	Group 6	2.88	1.08	0.38	1.73	--	--	--	2.32	1.24	3.33	--	--	--	14.01	9.03	18.58	0.83	0.66	1.01	-2.24	-3.96	-0.53	--	--	--	4.49	1.07	7.92
E.3	Group 4	100			Group 6	7.3	0.46	0.07	0.75	--	--	--	1.48	0.83	2.07	2.26	2.15	2.51	20.07	17.86	22.59	0.97	0.85	1.1	-1.41	-1.54	-1.13	1.41	1.13	1.54	--	--	--

[1] Initial and final solutions, % initial is model computed fraction.

[2] Sum residual error is the model computed error term for a given model.

[3] Mineral phases, positive mass transfer values represent phase dissolution and negative values represent phase precipitation. Min and max are the upper and lower bounds based on the error for a given phase. X indicates ion exchange of a given cation.

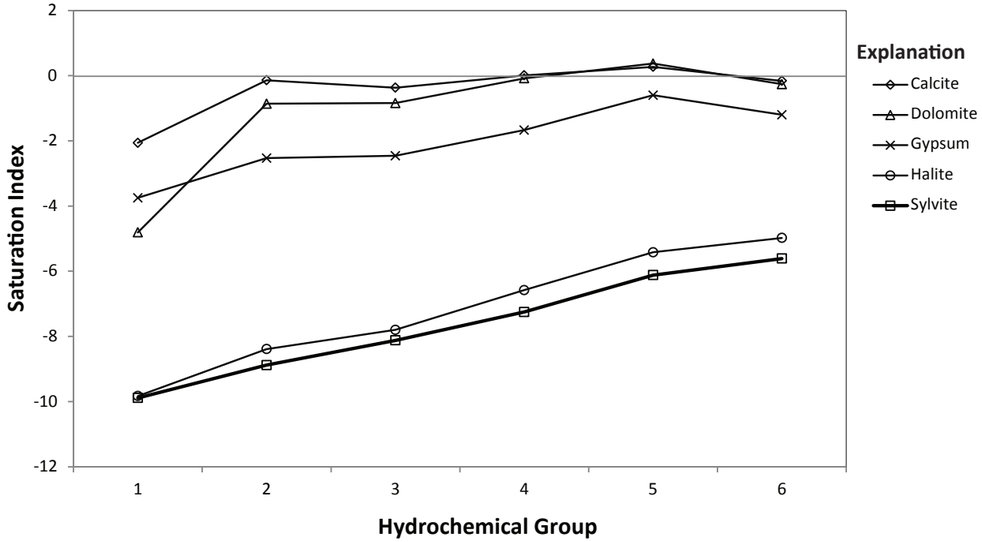

Figure 6.18. *Summary of group-mean mineral saturation indices. Positive values represent oversaturation and negative values represent undersaturation with respect to a given mineral phase.*

Five basic model scenarios for chemical evolution between hydrochemical groups (labeled models A through E in tables 6.5 and 6.6) were considered. These models cover stepwise chemical evolution from hydrochemical group 1 to hydrochemical group 6 (i.e., group 1 to 2, group 2 to 3, etc.). Initial and final samples are either the group-mean chemistry for a given group, or discrete samples along hypothetical flow paths. PHREEQC allows the consideration of error in the initial and final solutions, and an error factor of 10% is used for all models. Actual error in hydrochemical models among group-mean chemistry is the sum of analytical errors of samples within a given group and may therefore be substantially larger than 10%. This error term is not intended as an accurate accounting of error propagated through the inverse hydrochemical models, particularly models based on group-mean chemistry. It is instead a value that yields consistent constraints on model results for hydrochemical models constructed for both group-mean chemistry and hypothetical flow paths.

Mineral phases in the models are based on the likely reactive mineralogical components of bedrock and basin fill in the study area, which are in turn based on lithologic descriptions in published geologic mapping (Hintze and Davis, 2002a, 2002b, 2003). The phases considered for the modeling include CO_2 gas, calcite, dolomite, gypsum, halite, sylvite, and cation exchange. Calcite and dolomite are abundant in Paleozoic rocks that either bound the principal aquifer or served as a major source of sediment for the basin fill that comprises the principal aquifer. Gypsum may occur in parts of the basin fill or bedrock, and halite and sylvite may be present in basin fill, particularly in low-elevation parts of the study area (Oviatt, 1991; Hintze and Davis, 2003). Evapotranspiration and consequent fluid concentration may also account for increases in concentrations of dissolved constituents, but it is not considered in the models presented herein. Cation exchange is also considered for these models and occurs in many hydrochemical settings, primarily on clay minerals, but also less commonly on carbonate minerals (Plummer and others, 1990; Kehew, 2000). Exchange species include variable, model-computed portions of calcium and magnesium exchanging for sodium ions. Constraints in all models are the group-mean values of calcium, magnesium, sodium, potassium, chloride, bicarbonate, and sulfate.

Based on the inputs described above, one or more models for each of the five initial and final conditions was computed in PHREEQC. Most sets of initial and final waters produce multiple models, and in these cases a single model is chosen that minimizes the computed sum-of-residuals error term and results in the minimum mass transfer. Each model must also satisfy the previously calculated mineral saturation indices, and only mineral phases that are oversaturated in the final solution should precipitate and minerals that are undersaturated should dissolve in solution.

Model results are shown in graphs of calculated mineral dissolution or precipitation for a given set of initial and final waters (figure 6.19, appendix A.6.3). Results also include the error calculated by PHREEQC assuming a range of ± 10% for the concentration of the major solutes in initial and final solutions. Additional model-computed parameters include the relative amount of initial solutions for models that involve fluid mixing, and a sum-of-residuals term representing a measure of error associated with each model (tables 6.5 and 6.6). In the case where no model resulted for a given set of initial and final solutions, additional models were run that included mixing of upgradient groups and using other potentially upgradient groups as intitial solutions. All models use the same mineral phases, hydrochemical constraints, and error ranges previously described. Results are discussed in detail for models based on group-mean waters, and results from defined flow paths summarized with an emphasis on differences between these results and those of the group-mean models.

6.2.4.2 Group-Mean Model Results

Model A represents the hydrochemical evolution of groundwater from group 1 to group 2 and among the models includes the smallest computed mass transfers (figure 6.19, table 6.5). Mineral dissolution of calcite, dolomite, and halite, and dissolution of CO_2 gas are included in this model. All mass transfers are less than 1 mMole of mineral per kilogram of water except CO_2 gas, which was calculated at 1.91 mMole/kg. The modeled reactions are likely typical of groundwater as it moves through the shallow groundwater system in areas of recharge and includes the addition of relatively low-pH meteoric waters or recently recharged groundwater. Contribution of CO_2 gas in the model may result from the incorporation of soil gases in the groundwater either during recharge or along the base of the vadose zone. This model supports hydrochemical evolution between group 1 and group 2 waters.

Model B examines the hydrochemical evolution between groundwater of group 2 and group 3. A model of group 3 water evolving directly from group 2 water was not possible within the given constraints, so two additional models were run. Model B.2 examines mixing of water from groups 1 and 2 and mineral-phase reactions to produce group 3 waters, and model B.3 evolves group 1 water into that of group 3. These models have varying amounts of mineral dissolution and ion exchange. Ion exchange in both models includes varying amounts of sodium and magnesium exchanging for calcium ions. Ion exchange may occur on clay minerals known to exist in the

Table 6.6. *Inverse hydrochemical model results for flow paths.*

Inverse Chemical Model[1]	Model	Initial[2]	%Initial	Initial	%Initial	Final	Sum residual error[3]	Mineral mass transfer (mMoles/kg)[4]																								
								Calcite	Min	Max	Dolomite	Min	Max	CO_2 (gas)	Min	Max	Gypsum	Min	Max	Halite	Min	Max	Sylvite	Min	Max	CaX	Min	Max	MgX	Min	Max	NaX	Min	Max
Deep Creek	D	254	100			121	6.51	--	--	--	--	--	--	-0.16	-0.21	-0.12	18.24	16.14	20.33	49.89	48.67	62.06	1.23	1.08	1.38	-8.31	-11.64	-4.90	3.94	3.25	4.63	8.73	1.14	14.60
	E.1	121	100			77	No Model																											
	E.2	254	84	121	16	77	3.52	0.55	0.05	1.04	--	--	--	1.33	0.67	1.98	--	--	--	10.84	3.96	15.76	0.69	0.51	0.87	-1.63	-3.07	-0.46	--	--	--	3.27	0.91	6.15
	E.3	254	100			77	7.94	--	--	--	--	--	--	0.65	0.64	0.78	2.65	2.24	3.19	19.61	16.69	22.26	0.89	0.77	1.01	-2.32	-3.10	-1.65	0.82	0.57	1.21	3.00	1.20	5.07
Gandy Springs	B	231	100			208	No Model																											
	C	208	100			222	7.80	-0.78	-1.13	-0.48	0.82	0.66	0.99	0.81	0.50	1.17	0.17	0.11	0.24	0.21	0.01	0.41	0.04	0.01	0.07	--	--	--	-0.75	-0.85	-0.53	1.51	1.06	1.71
	D	222	100			129	5.60	-1.35	-1.72	-1.17	--	--	--	-1.78	-2.32	-1.52	12.29	12.25	13.16	31.59	27.81	34.60	0.42	0.35	0.50	--	--	--	4.51	3.90	5.13	-9.02	-10.25	-7.79
	E.1	129	100			77	No Model																											
Northern Snake Range	A	229	100			232	No Model																											
	B	232	100			122	8.17	0.80	0.72	0.82	--	--	--	--	--	--	0.23	0.21	0.26	0.85	0.82	0.95	0.02	0.02	0.03	-0.72	-0.73	-0.64	0.72	0.64	0.73	--	--	--
	C	122	100			81	9.71	1.02	0.90	1.29	--	--	--	1.64	1.41	2.13	0.28	0.20	0.36	1.11	1.11	1.12	0.11	0.10	0.11	-0.55	-0.76	-0.40	0.55	0.40	0.76	--	--	--
	D	81	100			129	5.08	-1.25	-1.62	-1.07	--	--	--	-1.99	-2.59	-1.72	12.16	12.14	12.88	31.04	27.19	33.70	0.43	0.36	0.49	--	--	--	3.99	3.40	4.60	-7.99	-9.20	-6.81
	E.1	129	100			77	No Model																											
	E.2	81	72	129	28	77	2.68	--	--	--	--	--	--	--	--	--	--	--	--	14.58	9.03	19.94	0.76	0.61	0.92	-2.17	-3.27	-0.80	0.00	0.00	0.00	4.34	1.59	6.55
	E.3	81	100			77	3.99	--	--	--	--	--	--	--	--	--	3.47	3.02	3.93	22.60	19.76	25.44	0.88	0.76	1.00	-2.73	-3.61	-1.86	1.12	0.74	1.49	3.23	0.87	5.52
Snake Creek	A	245	100			207	6.61	0.99	0.89	1.06	0.22	0.18	0.26	1.94	1.87	2.09	0.10	0.08	0.12	0.15	0.12	0.17	0.01	0.00	0.01	--	--	--	--	--	--	--	--	--
	B	207	100			2	9.41	--	--	--	--	--	--	-0.28	-0.39	-0.23	0.08	0.07	0.10	0.19	0.16	0.25	--	--	--	-0.51	-0.55	-0.47	0.51	0.47	0.55	--	--	--
	C	2	100			26	7.48	0.51	0.36	0.70	--	--	--	0.79	0.56	1.11	0.34	0.26	0.42	0.93	0.74	1.12	0.08	0.06	0.09	-0.98	-1.13	-0.80	0.35	0.14	0.47	1.26	0.96	1.51
	D	26	100			140	6.61	-4.07	-5.04	-3.29	1.79	1.49	2.17	-0.36	-0.83	-0.03	8.08	7.14	8.95	2.10	1.89	2.36	0.21	0.17	0.26	--	--	--	--	--	--	--	--	--
	E.1	140	100			77	No Model																											
	E.2	26	57	140	43	77	6.69	--	--	--	0.22	0.00	0.43	0.73	0.05	1.35	--	--	--	21.95	18.74	25.05	0.84	0.69	0.98	-1.39	-2.64	-0.53	--	--	--	2.78	1.07	5.28
	E.3	26	100			77	9.33	--	--	--	--	--	--	0.30	0.11	0.48	3.03	2.98	3.23	23.16	21.76	25.80	0.93	0.82	1.05	-1.49	-1.69	-1.37	1.49	1.37	1.69	--	--	--
Southern Snake Range	B	95	100			57	7.39	0.18	0.10	0.25	--	--	--	1.86	1.64	2.29	0.03	0.01	0.06	0.09	0.02	0.16	0.05	0.04	0.06	-0.38	-0.45	-0.30	0.23	0.13	0.27	0.30	0.21	0.45
	C	57	100			11	7.11	--	--	--	0.55	0.44	0.65	--	--	--	0.62	0.58	0.75	0.82	0.63	1.00	0.04	0.02	0.06	-0.29	-0.37	-0.16	--	--	--	0.57	0.32	0.75
	D	11	100			111	4.09	-1.52	-1.97	-1.16	--	--	--	-2.32	-2.99	-1.82	3.72	3.16	4.22	1.31	1.16	1.49	--	--	--	-1.46	-1.95	-0.98	1.46	0.98	1.95	--	--	--
	E.1	111	100			104	No Model																											
	E.2	11	76	111	24	104	4.69	--	--	--	--	--	--	--	--	--	1.70	0.91	2.40	9.99	8.38	11.63	0.80	0.69	0.90	-2.07	-3.00	-1.26	--	--	--	4.14	2.52	6.00
	E.3	11	100			104	No Model																											
Pine Valley	B	260	100			133	No Model																											
	C	133	100			131	5.151	1.04	0.65	1.26	--	--	--	1.30	0.80	1.58	0.81	0.63	0.99	2.36	2.11	3.04	0.21	0.17	0.25	-1.62	-1.91	-1.12	0.40	0.27	0.60	2.43	1.29	2.87
	D.1	131	100			108	No Model																											
	D.2	133	79	131	21	108	5.41	--	--	--	--	--	--	--	--	--	3.05	2.33	3.26	11.85	10.11	14.28	0.82	0.64	0.97	-2.10	-2.44	-1.64	2.10	1.64	2.44	--	--	--
	D.3	133	100			108	9.67	0.01	0.00	0.03	--	--	--	--	--	--	3.16	2.69	3.26	12.85	11.77	14.32	0.86	0.76	0.97	-2.18	-2.47	-1.89	2.18	1.89	2.47	--	--	--
	E.1	108	100			104	4.25	1.20	0.80	1.61	--	--	--	1.72	1.18	2.26	--	--	--	--	--	--	--	--	--	-1.05	-1.79	-0.30	-1.09	-1.55	-0.63	4.28	1.87	4.92
	E.2	131	41	108	59	104	6.09	0.91	0.47	1.35	--	--	--	1.34	0.75	1.94	1.00	0.20	1.40	--	--	--	0.22	0.04	0.40	-1.42	-2.50	-1.27	--	--	--	2.83	2.53	4.99
	E.3	131	100			104	6.18	0.39	0.01	0.69	--	--	--	0.68	0.14	1.14	1.63	1.50	2.02	8.49	8.32	9.98	0.60	0.48	0.73	-0.89	-0.99	-0.53	0.89	0.53	0.99	--	--	--
North Canyon Spring	E.3	251	100			77	3.57	--	--	--	--	--	--	0.79	0.62	0.99	2.23	1.66	2.81	5.59	0.69	8.23	0.93	0.81	1.04	-1.86	-2.89	-0.82	--	--	--	3.71	1.64	5.78
Laird Spring	E.1	250	100			77	3.39	--	--	--	--	--	--	0.27	0.08	0.48	2.55	2.00	3.09	9.22	5.28	11.90	0.60	0.46	0.75	-6.12	-6.91	-4.94	0.59	0.16	1.02	11.06	8.58	13.50

[1] Model names and IDs correspond with those in the text, figure 6.20, and figure D.1.

[2] Initial and final solutions, % initial is model computed fraction.

[3] Sum residual error is the model computed error term for a given model.

[4] Mineral phases, positive mass transfer values represent phase dissolution and negative values represent phase precipitation. Min and max are the upper and lower bounds based on the error for a given phase. X indicates ion exchange of a given cation.

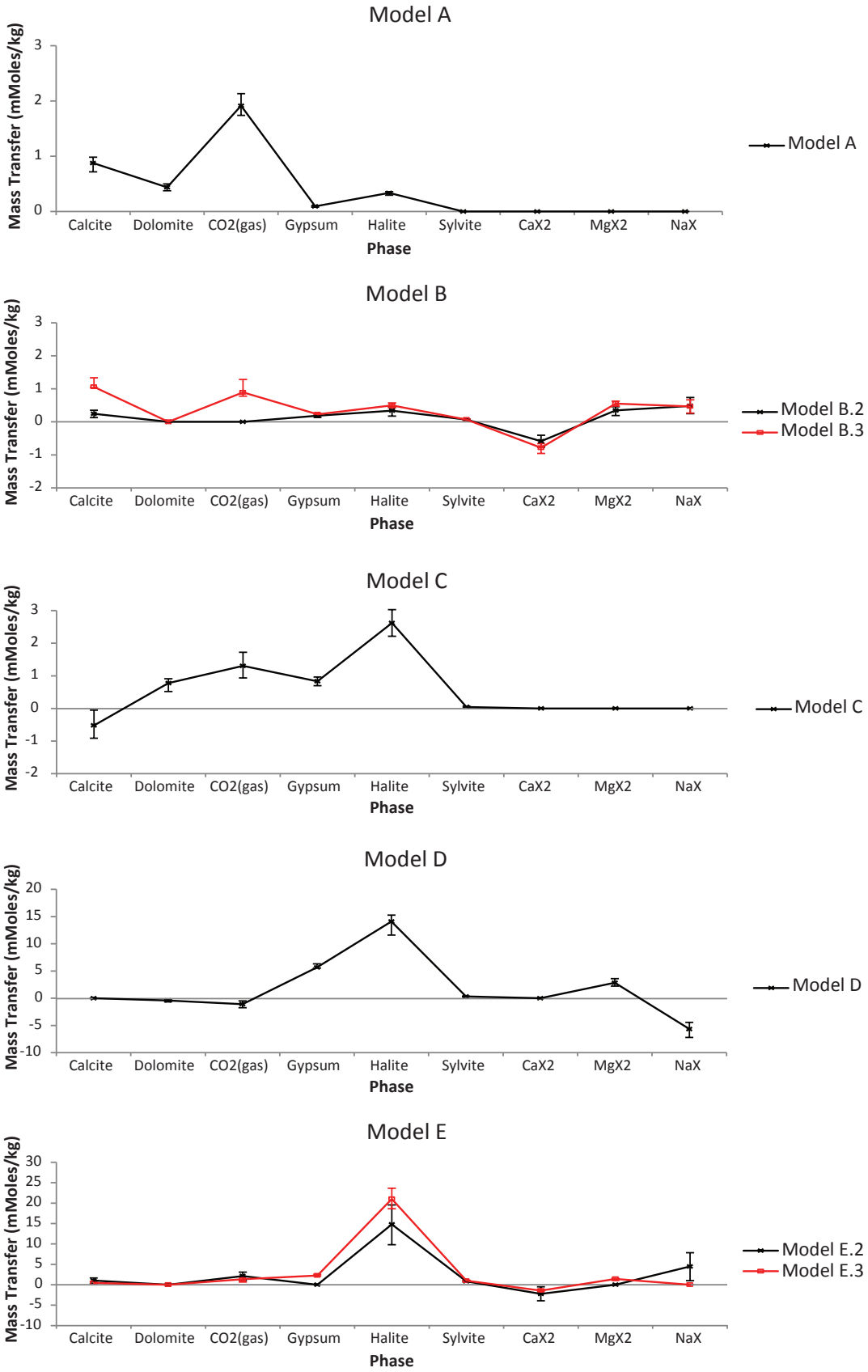

Figure 6.19. *Mass transfer graphs of inverse geochemical models. Positive values represent dissolution and negative values indicate precipitation of a given phase. Error bars calculated assuming 10% error in initial and final fluid composition. CaX2, MgX2, and NaX are cation exchange phases. See text for detailed description of modeling.*

basin fill that is typical of sample sites for most of group 3. The mixing model (B.2) includes nearly equal fractions of group 1 and group 2 water combined that hydrochemically evolves to make group 3 waters. Assuming general conservation of water mass, mixing may occur where flow lines converge, typically at points of spring flow and discharge. A number of spring samples (e.g., Dearden Springs) are represented within group 3 waters and may account for this apparent discrepancy and allow for mixing of upgradient waters to produce this group. Model B.3 evolves group 1 water to group 3 water and differs from model B.2 by requiring greater amounts of calcite and CO_2 gas dissolution. The lack of a plausible direct hydrochemical link between group 2 and 3 waters may imply that flow paths connecting these groups include mixing of other water types, such as group 1 in the case of model B.2, or perhaps the addition of direct recharge via infiltration of meteoric water or stream runoff. These models together support a conceptual model of valley spring discharge either due to a converging mixture of flow paths, or long residence times capable of more mineral dissolution, or both. Alternatively, hydrochemical evolution of water to group 3 may be driven by mineral phases not considered in these models.

Model C represents the hydrochemical evolution of water from group 3 to group 4. This model includes dissolution of mineral phases, including dolomite, gypsum, and halite, as well as dissolution of CO_2 gas. Dissolution of halite is the largest mass transfer in this model. No ion exchange was required for this model; instead, a small amount of calcite, less than 1 mMole/kg, is precipitated from the system. This precipitation is supported by mineral saturation indices that show group 4 water is saturated to slightly oversaturated with respect to calcite. This model implies a simple and direct hydrochemical link between group 3 and 4 water and may also indicate the potential for localized calcite mineral infilling of void space (i.e., potentially reduced permeability due to calcite precipitation as groundwater moves between these two groups).

Model D represents the hydrochemical evolution between group 4 and group 5. Group 5 waters contain significant concentrations of sulfate relative to the other groups, and model D requires the dissolution of nearly 6 mMoles/kg of gypsum. Significant dissolution of halite is also required for this model as well as ion exchange of magnesium for calcium and sodium. The large amount of gypsum dissolution implies water from group 4 travels through material with significant quantities of gypsum to reach group 5 waters. Gypsum is known to occur in the basin fill, particularly at the lower elevations and in Paleozoic bedrock units (e.g., the Plympton Formation in the Confusion Range [Hintze and Davis, 2002b, 2003]), potentially implying hydrochemical evolution of groundwater across the Confusion Range between groups 4 and 5 (figure 6.13). Alternatively, recharge originating in the Confusion Range could also dissolve gypsum present in these rocks.

Model E is the final step in the hydrochemical evolution of groundwater from group 5 to group 6. The initial case of group 5 to group 6 produced no possible models within the assumed constraints and phases, so two additional models to derive group 6 waters were constructed. Models E.2 and E.3 considered initial mixing of group 4 and 5 waters, and group 4 initial water, respectively, followed by hydrochemical evolution to group 6 water. Both of these alternatives yielded viable results with similar mineral dissolutions marked by significant dissolution of halite and minor dissolution of other phases, and relatively minor magnesium- and sodium-for-calcium ion exchange. Halite is known to occur in the basin fill in low elevations of Fish Springs Flat and Tule Valley (Oviatt, 1991; Hintze and Davis, 2002b). Alternatively, increases in the concentration of sodium and chloride may result from the mixing of deep basin brines with shallower groundwater or evaporative concentration in discharge zones.

6.2.4.3 Flow Path Model Results

Regional groundwater flow is constrained by Darcy's law and depends on aquifer permeability and hydraulic head. Within the study area there is relatively large uncertainty with respect to permeability and hydraulic gradient across basin boundaries. There is, however, sufficient hydraulic gradient and permeability in certain areas that interbasin flow may occur (see chapters 4 and 8). If interbasin flow occurs in certain areas, simple hydrochemical models should allow upgradient water to evolve into downgradient water along hypothesized flow paths. The models presented in this section examine plausible hydrochemical reactions that can account for hydrochemical evolution along hypothesized flow paths. These results do not require connection along flow paths, but instead add support for flow paths that are supported by Darcy's law.

Initial and final samples were chosen along select flow paths delineated in chapter 8. These models examine eight hypothesized flow paths that represent groundwater evolution across most of the study area (figure 6.20). Model results are constrained by mineral saturation indices calculated for all initial and final solutions. Complete model results are summarized in table 6.6 and graphs of mass transfer are shown in figure D.1. Models are delineated by path name (Gandy Springs path) and reaction model (E, E.1 etc.), and nomenclature is consistent such that models for different paths represent evolution between the same hydrochemical groups. Model results are summarized below, emphasizing results that differ substantially from

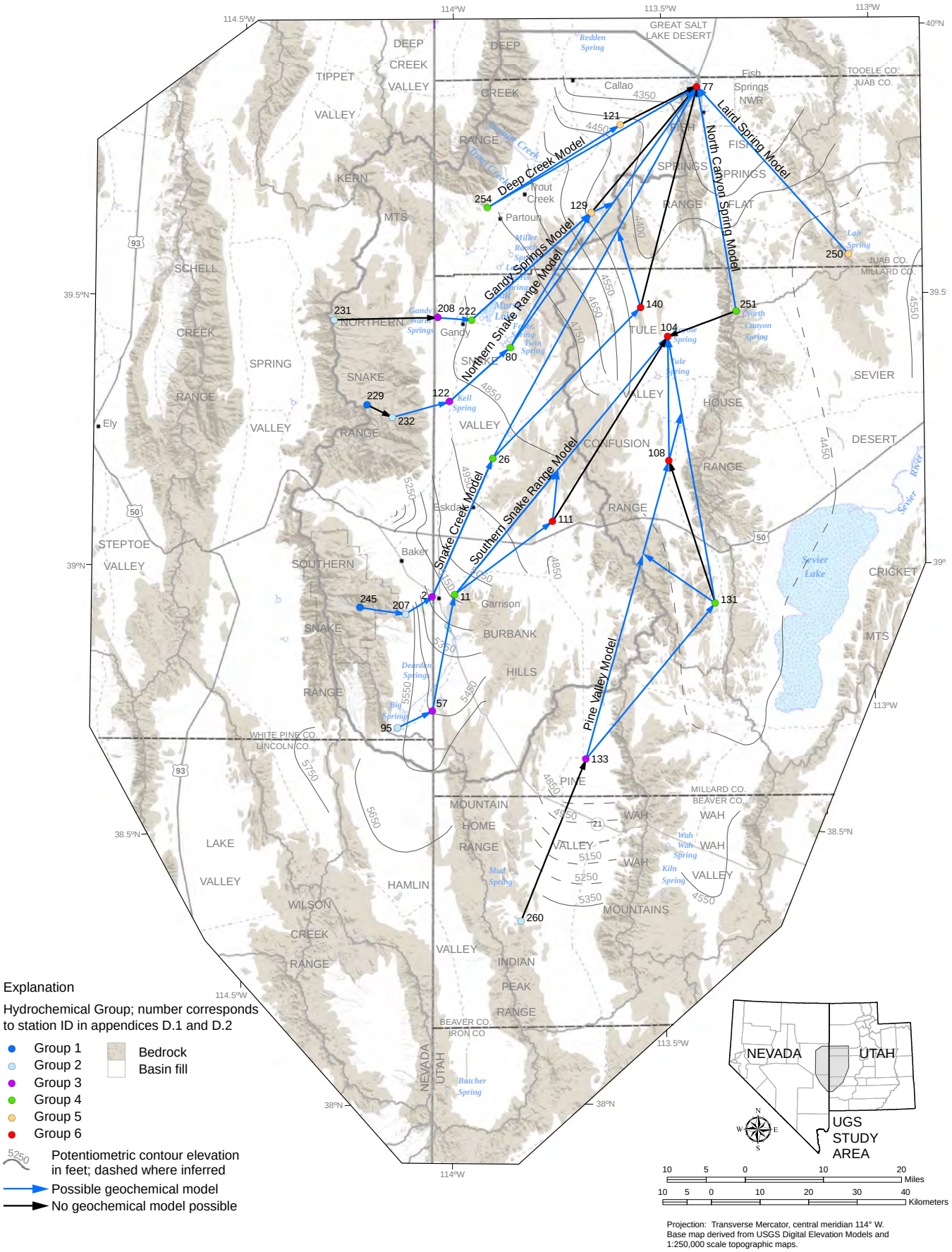

Figure 6.20. *Inverse hydrochemical models along flow paths. Complete data are presented in tables D.1 and D.2. Potentiometric contours simplified from Gardner and others (2011).*

those of the group-mean chemistry models, or where no model is possible.

The Deep Creek path extends from group 4 water, southeast of the Deep Creek Range, to group 5 water in the north end of Snake Valley, and ends with group 6 water at Fish Springs (figure 6.20). Mass transfer along Deep Creek path model D requires dissolution of halite and gypsum that is several times that of the corresponding group-mean model D. No direct model is possible from group 5 to 6 water along this path; instead, mixing of group 4 and 5 and group 4 alone can evolve into group 6 water. Mixing of flow paths is likely in areas of discharge near Fish Springs and these models are broadly similar to those for model E of the group-mean chemistry models.

The Gandy Springs path extends from an upland group 2 spring in the northern Snake Range through Gandy Springs (aka Warm Springs near Gandy), Cold Springs, and the northern Confusion Range to Fish Springs. No model was possible between group 2 and group 3 water at Gandy Springs. This result mirrors that of group-mean model B and implies that mixing of waters may be required to produce the Gandy Springs chemistry. Mixing could occur among various waters recharged in the northern Snake Range. The final model of this path is shared with the northern Snake Range path. No direct model is possible between group 5 and 6 waters along this path, and mixing is required along the final model. Alternately, group 4 water may evolve directly into group 6 water found at Fish Springs.

The northern Snake Range path includes samples from group 1 through 6 and extends from upland parts of the Snake Range across Snake Valley to the northern Confusion Range and Fish Springs. No model is possible between group 1 and 2 waters along this path. However, in contrast to the group-mean models, mixing is not required to produce group 3 water along this path. Models C and D along this path are similar to the group-mean models and support the possibility of groundwater evolution across this part of Snake Valley and into the adjoining Confusion Range.

The Snake Creek path includes group 1 to 6 waters. The path begins along the upper reaches of Snake Creek in the Snake Range and extends across Snake Valley and through the Confusion Range to Tule Valley and Fish Springs. Model results A through C support hydrochemical groundwater evolution between upland groundwater in the Snake Range and groundwater to the north and east in Snake Valley. Model D along this path is similar to the group-mean models and supports the possibility of groundwater in eastern Snake Valley evolving into groundwater in adjoining Tule Valley. The final model E again requires either mixing of group 4 and 5 samples or direct evolution of group 4 to produce group 6 water at Fish Springs.

The southern Snake Range path begins at Big Springs and extends north and east along the floor of Snake Valley. The final model of the path extends across the Confusion Range to Coyote Spring in Tule Valley. Models B through D support a continuum of hydrochemical evolution of groundwater across this part of Snake Valley and into the western edge of the Confusion Range. The final model E to Coyote Spring and across the Confusion Range was only possible via mixing of group 4 and 5 waters.

The Pine Valley path extends from southern Pine Valley northward through the Confusion Range to Wah Wah and Tule Valleys, ending at Coyote Springs. Water levels along this path are poorly constrained relative to the other flow paths. Because of this, model results that imply connection between Pine Valley and areas to the north are more conjectural than those of other paths. No model was possible between group 2 and 3 waters along this path. Models were possible between group 3 and 4 and between group 3 and 5 waters. No model was possible between group 4 and 5 waters. Models were possible from both group 4 and 5 to the group 6 water at Coyote Spring; this supports mixing and convergence of flow paths near Coyote Spring.

Two flow paths from areas south and east of Fish Springs were considered. These models begin with either group 4 (North Canyon Spring path) or group 5 (Laird Spring path) waters and extend to group 6 water at Fish Springs. The North Canyon Spring path produced a viable model that is similar to the corresponding model based on group-mean chemistry for direct evolution of group 4 into group 6 water, implying that some water discharging at Fish Springs may originate in the House Range. No model was possible between group 4 water at North Canyon Spring and Coyote Spring to the west in Tule Valley. Along the Laird Spring path group 5 water may evolve into group 6 water via gypsum and halite dissolution and calcium-for-sodium ion exchange. This result implies that, at least locally, group 5 water may evolve directly into group 6 water without mixing, and that water discharging at Fish Springs may be partially sourced from the east.

Hydrochemical models along hypothesized flow paths closely follow model results for the group-mean chemistry in most cases. These results support the general hydrochemical evolution presented for group-mean chemistry and imply the possibility of interconnection within Snake Valley and locally across the Confusion Range into Tule Valley and to Fish Springs. Many of these models imply at least some degree of mixing among groundwater types is occurring among the hydrochemical groups, particularly

in low-elevation parts of the study area. Mixing in these areas is expected from a general convergence of flow paths that is typical of discharge areas and springs. The models also suggest that group 5 and group 6 water both represent hydrochemically distinct parts of discharge in the regional groundwater system. Four paths between Snake Valley and either Tule Valley or Fish Springs yielded no model between groups 5 and 6. The relative hydrochemical difference between the two groups may result from localized aquifer geology and not necessarily one-way hydrochemical evolution. The possible direct evolution of group 4 to group 6 implies a link between these two water types. Group 4 water, typical of large parts of the basin-fill aquifer in Snake Valley and Tule Valley, could evolve into the group 6 water found at major regional discharge areas at Fish Springs and Coyote Springs in Tule Valley.

6.3 DISSOLVED GAS AND ISOTOPIC DATA

6.3.1 Dissolved Gas Data

6.3.1.1 Introduction

Dissolved gases in groundwater provide information concerning the temperature and pressure conditions at which recharge occurred and the time since recharge. Noble gases (helium, neon, argon, krypton, and xenon) are chemically inert and occur in known concentrations in the atmosphere. The relative concentrations of these gases are determined by Henry's law solubility equations that are generally driven by changes in temperature and pressure (elevation) (Stute and Schlosser, 2000). As groundwater is recharged, it dissolves noble gases present in the vadose zone in concentrations that depend primarily on the temperature, pressure, and salinity conditions at the time of recharge (Aeschbach-Hertig and others, 1999). By assuming elevation (pressure) at the time of recharge it is possible to model the temperature under which recharge occurred (Aeschbach-Hertig and others, 2000). In addition to estimates of the recharge conditions, the concentrations of dissolved helium isotopes may be used to estimate time of residence within the groundwater system. The dissolved concentrations of helium and tritium in groundwater may be used to constrain time since recharge and provide quantitative ages for the tritiogenic (young) component of groundwater (Solomon and Cook, 2000) and qualitative age of the old component of groundwater (Solomon, 2000).

Water recharging within a few hundred feet of the land surface generally equilibrates at a temperature equal to or slightly warmer than the mean annual temperature at a given location. In areas of significant topographic relief, and consequently wide temperature range (typical of the Snake Valley area) at which groundwater may recharge, estimates of recharge temperature can provide constraints on the spatial distribution of recharge and the potential connectivity of flow paths (Manning and Solomon, 2003). In the Snake Valley area mean annual temperatures range from near 15°C (59°F) at low elevations (4200 feet [1280 m]) near Fish Springs to below 0°C (32°F) at the highest elevations (greater than 11,000 feet [3350 m]) of the Snake Range and Deep Creek Range (Harrill and Prudic, 1998). Recharge temperatures in shallow water-table settings lacking significant geothermal heat flux should therefore be between 0 and 15°C (32–59°F) for groundwater in the Snake Valley area. Calculated recharge temperatures greater than 15°C (59°F) may result from deep (greater than several hundred feet) recharge where the geothermal gradient significantly affects the temperature of the base of the vadose zone (Vic Heilweil, U.S. Geological Survey, verbal communication, 2009). High calculated recharge temperatures may also result from gas loss (gas stripping) either in the aquifer (Thomas and others, 2003) or upon sample collection. Long-term climate change may also affect recharge temperatures, and groundwater recharged during the late Pleistocene may have lower calculated recharge temperatures for a given elevation.

Modeled dissolved gas recharge temperatures depend strongly on the assumptions and methods used to calculate equilibrium concentrations of noble gases during recharge; chief among these is the compensation for excess air incorporated in the recharge zone. Excess air can result in the inclusion of dissolved gas concentrations that are greater than atmospheric at the location of recharge (Aeschbach-Hertig and others, 2000). The modeled dissolved gas recharge temperature is based on assumptions for the composition and amount of excess air (Solomon, 2000).

Gardner and Heilweil (2014) analyzed helium isotopic concentrations in the Snake Valley area. For this study, helium isotope data for select sites are presented in the subsequent tritium section to calculate apparent ages of the young tritium-bearing fraction of groundwater samples that have both tritium greater than 0.5 TU and complete dissolved gas measurements.

6.3.1.2 Dissolved Gas Results

The modeled recharge temperatures are the work of P. Gardner with the U.S. Geological Survey Utah Water Science Center. Complete discussion of dissolved gas data and recharge temperature modeling methods were presented by Gardner and Heilweil (2014). The dissolved gas recharge temperature was calculated using measured concentrations of ^{20}Ne, ^{40}Ar, ^{84}Kr, and ^{129}Xe via the closed equilibrium

(CE) dissolved gas model (Aeschbach-Hertig and others, 2000). Multiple iterations of the CE model were run via an Excel spreadsheet and macro provided by the University of Utah Dissolved Gas Laboratory. This technique employs additional model parameters of fractionation and excess air that are solved for in addition to the recharge temperature for the measured dissolved gas concentrations via multiple iterations that minimize the misfit between measured and modeled parameters following techniques presented by Aeshcbach-Hertig and others (1999). In the study area the elevation at which recharge occurred is not known and the CE model is used to calculate maximum and minimum possible recharge temperatures based on maximum and minimum possible elevation of recharge for a given site. Maximum elevation is the highest possible water-table altitude upgradient from a sample site (yielding the lowest possible recharge temperature) and minimum elevation is generally the altitude of the water table where the sample was collected (yielding the highest possible temperature of recharge). Subsequent discussion of recharge temperature will examine the average recharge temperature that lies between the maximum and minimum possible recharge temperatures. Gardner and Heilweil (2014) presented detailed determination of recharge temperatures that account for regional and time-dependent temperature lapse rates.

The sample set includes 59 dissolved gas samples from the collected or compiled databases (table 6.7). The dissolved gas data include analyses from Snake Valley and adjoining Tule Valley and Fish Springs Flat. Sample sites include a range of mountain and low-elevation springs and deep and shallow wells. Water recharged during the Pleistocene may have cooler recharge temperatures relative to more recent conditions. Samples with Pleistocene (older than 12,000 years) apparent carbon-14 ages are differentiated from samples having apparent ages less than 12,000 years (table 6.7).

The calculated recharge temperatures are between 1 and 57°C (34–135°F). Most samples, 36 of 59, have average recharge temperatures less than 10°C (50°F) (table 6.7, figures 6.21 and 6.22). Recharge temperatures between 10 and 15°C (50–59°F) were calculated for 11 samples, and 9 samples have recharge temperatures of 15 to 25°C (59–77°F). The remaining three samples have recharge temperatures greater than 25°C (77°F).

Low recharge temperatures (less than 10°C [(50°F]) are located in and near the Snake Range and to the east and north across the floor of Snake Valley and at a single site in the adjoining west part of Tule Valley. These temperatures are likely typical of recharge within the mountain block. Eight of the low-recharge-temperature samples have Pleistocene ages, and these samples may have recharged along the valley floor or in or near the mountain block during a cooler climate.

Recharge temperatures between 10 and 15°C (50–59°F) occur east of Gandy, at the north end of Fish Springs and at Needle Point Spring in Snake Valley. Samples in this temperature range may be examples of Holocene valley floor or low-elevation mountain front recharge conditions. Five of these samples contain water recharged during the Pleistocene and may be the result of recharge in areas of elevated water-table temperatures due to a deep water table and/or high geothermal heat flow.

Recharge temperatures between 15 and 25°C (59–77°F) exist in Tule Valley, at Fish Springs, and at site 4 in southern Snake Valley. These higher recharge temperatures may result from modern recharge in areas of deep water tables where the temperature at this depth is affected by the geothermal gradient. Alternately, these higher temperatures may result from reequilibration and degassing during regional flow through geologic barriers (Thomas and others, 2003), or reequilibration near the sample sites at major springs including Fish Springs and Coyote Spring. Pleistocene-age water is indicated for four of the samples in this temperature range.

The remaining three samples have recharge temperatures greater than 25°C (77°F) and Pleistocene apparent ages. This contradiction may indicate at least partial degassing or reequilibration of the dissolved gases in these samples. Samples collected from Well 22 and PW18 indicate recharge across a deep water table affected by the geothermal gradient. Sample contamination by drilling fluids is also possible, particularly for site PW19C.

6.3.2 Stable Isotopes

6.3.2.1 Introduction

The stable isotopes of hydrogen and oxygen (^{2}H and ^{18}O) occur in small concentrations relative to the more common isotopes of hydrogen and oxygen (^{1}H and ^{16}O) in the water molecule. The relative concentration of heavy (^{2}H and ^{18}O) and light (^{1}H and ^{16}O) isotopes in meteoric waters is driven by change in the ratio of heavy to light isotopes (fractionation) that occurs as water is evaporated or condensed. Heavy isotopes are concentrated (depleted) during condensation and diluted (enriched) during evaporation relative to light isotopes. Cooler temperatures during fractionation yield increases in depletion or decreases in enrichment. These fractionation processes control the isotopic composition of precipitation and yield depleted (lower) isotopic ratios for cooler precipitation and enriched

Table 6.7. *Dissolved gas data and modeled recharge temperatures for select samples.*

Station ID[1]	Location	Sample date	Sample source[2]	Sample type	Elevation (ft)[3]	TDGP (mm Hg)[4]	^{4}He (ccSTP/g)	^{20}Ne (ccSTP/g)	^{40}Ar (ccSTP/g)	^{84}Kr (ccSTP/g)	^{129}Xe (ccSTP/g)	A_e[5]	F[6]	$\Sigma\chi^2$[7]	Hrmin (ft)[8]	Trmax (°C)	Hrmax (ft)[9]	Trmin (°C)	Hravg (ft)	Travg (°C)[10]	Pleistocene[11]
2	PW01A	7/29/2009	UGS	diffussion sampler	5312	774	5.31E-8	1.91E-7	3.86E-4	5.04E-8	3.23E-9	0.100	0.77	0.05	5312	9.4	10500	4.4	7906	6.9	--
4	PW01B	7/29/2009	UGS	diffussion sampler	5312	724	5.38E-8	1.91E-7	3.72E-4	5.07E-8	3.39E-9	0.002	0.00	0.20	6100	4.6	10500	0.8	8300	2.7	--
7	PW02B	7/30/2009	UGS	diffussion sampler	5459	671	1.11E-7	2.89E-7	3.64E-4	4.91E-8	3.24E-9	0.008	0.00	0.10	5459	8.4	10500	3.2	7980	5.8	--
9	PW03A	5/19/2009	UGS	diffussion sampler	5325	765	9.57E-8	2.19E-7	4.08E-4	5.41E-8	3.39E-9	0.028	0.61	0.73	5325	6.6	10500	2.1	7913	4.3	--
11	PW03B	5/18/2009	UGS	diffussion sampler	5325	696	7.53E-8	1.77E-7	3.78E-4	5.29E-8	3.44E-9	0.100	0.87	0.79	5500	5.9	10500	1.0	8000	3.4	--
17	PW05B	7/29/2009	UGS	diffussion sampler	5080	786	6.06E-8	1.84E-7	4.21E-4	5.49E-8	3.97E-9	0.063	0.87	0.91	5080	2.7	8202	0.2	6641	1.5	x
19	PW05C	5/19/2009	UGS	diffussion sampler	5080	681	2.19E-7	1.86E-7	4.05E-4	5.31E-8	3.73E-9	0.043	0.84	0.75	5080	4.3	9842	0.2	7461	2.3	x
26	PW06C	5/19/2009	UGS	diffussion sampler	5001	750	6.59E-7	3.67E-7	3.99E-4	5.10E-8	3.19E-9	0.013	0.00	0.02	5001	10.1	10400	5.0	7700	7.5	--
32	PW07A	7/28/2009	UGS	diffussion sampler	5020	678	4.32E-7	1.91E-7	4.03E-4	5.56E-8	3.86E-9	0.003	0.46	0.03	5020	2.4	7546	0.2	6283	1.3	x
35	PW07B	5/19/2009	UGS	diffussion sampler	5020	675	6.28E-7	1.91E-7	3.94E-4	5.36E-8	3.50E-9	0.031	0.78	0.42	7000	3.8	10500	0.8	8750	2.3	x
38	PW08B	5/18/2009	UGS	diffussion sampler	5750	616	8.61E-8	1.96E-7	3.19E-4	4.30E-8	2.90E-9	0.003	0.00	2.48	5750	11.0	10800	6.3	8275	8.7	x
46	PW11C	5/18/2009	UGS	diffussion sampler	5665	610	2.79E-7	1.92E-7	3.41E-4	4.65E-8	3.00E-9	0.003	0.00	0.70	5665	8.5	10500	3.5	8082	6.0	x
51	AG13A	6/18/2010	UGS	diffussion sampler	5264	663	4.50E-8	1.59E-7	3.16E-4	4.39E-8	2.80E-9	0.001	0.00	0.97	5264	10.2	10100	5.5	7682	7.9	--
52	AG13B	6/18/2010	UGS	diffussion sampler	5262	677	5.06E-8	1.74E-7	3.25E-4	4.29E-8	2.62E-9	0.100	0.81	0.70	5262	15.2	10500	8.8	7881	12.0	--
53	AG13C	6/18/2010	UGS	diffussion sampler	5262	726	5.60E-8	1.95E-7	3.67E-4	4.81E-8	3.13E-9	0.015	0.65	0.09	5262	8.3	10500	3.7	7881	6.0	--
54	AG14A	5/20/2010	UGS	diffussion sampler	5010	782	6.26E-8	1.95E-7	3.79E-4	4.18E-8	3.29E-9	0.021	0.68	12.06	5010	10.2	10300	5.2	7655	7.7	--
55	AG14B	5/20/2010	UGS	diffussion sampler	5010	827	7.08E-8	2.10E-7	4.08E-4	5.57E-8	3.35E-9	0.100	0.70	1.90	5010	9.3	10500	3.6	7755	6.4	--
56	AG14C	5/20/2010	UGS	diffussion sampler	5010	845	7.71E-8	2.19E-7	4.18E-4	5.37E-8	3.58E-9	0.023	0.61	0.00	6400	4.4	10500	0.8	8450	2.6	--
57	AG15	6/17/2010	UGS	diffussion sampler	5528	606	5.77E-8	1.61E-7	3.29E-4	4.64E-8	2.86E-9	0.100	0.92	1.94	5528	10.0	9000	7.9	7264	8.9	--
59	AG16A	7/30/2009	UGS	diffussion sampler	5414	701	8.44E-8	1.82E-7	3.86E-4	4.99E-8	3.54E-9	0.024	0.81	0.57	6300	4.5	10500	0.9	8400	2.7	--
61	AG16B	7/30/2009	UGS	diffussion sampler	5415	649	5.49E-8	1.99E-7	4.07E-4	5.51E-8	3.64E-9	0.026	0.73	0.27	5415	4.1	10170	0.1	7792	2.1	--
63	AG16C	7/30/2009	UGS	diffussion sampler	5415	654	4.68E-7	1.79E-7	3.89E-4	5.47E-8	3.70E-9	0.007	0.76	0.37	5415	2.8	8530	0.2	6972	1.5	x
66	PW17A	5/20/2009	UGS	diffussion sampler	4507	730	2.44E-7	2.04E-7	3.29E-4	4.10E-8	2.79E-9	0.003	0.00	0.82	4507	13.5	6300	8.5	5404	11.0	x
75	PW19C	5/20/2009	UGS	diffussion sampler	4635	710	1.83E-7	1.74E-7	1.68E-4	1.67E-8	9.69E-10	0.004	0.00	0.02	4635	63.6	10500	50.9	7567	57.2	x
77	SG21C	7/14/2009	UGS	diffussion sampler	4310	671	3.07E-7	1.70E-7	3.15E-4	4.01E-8	2.63E-9	0.005	0.68	0.03	4310	14.0	7600	10.9	5955	12.5	x
78	SG22B	7/14/2009	UGS	diffussion sampler	4310	673	2.25E-7	1.44E-7	2.66E-4	3.39E-8	2.28E-9	0.000	0.00	0.82	4310	19.2	10500	11.5	7405	15.3	x
79	SG23B	6/17/2010	UGS	diffussion sampler	5450	731	7.87E-8	1.92E-7	4.27E-4	6.11E-8	3.90E-9	0.100	0.82	1.67	5450	2.6	9514	0.1	7482	1.4	--
81	SG24C	7/29/2009	UGS	diffussion sampler	4820	680	1.13E-6	1.89E-7	3.87E-4	5.37E-8	3.49E-9	0.015	0.76	0.80	4820	5.1	10500	0.3	7660	2.7	x
82	SG25A	6/18/2010	UGS	diffussion sampler	4789	605	3.11E-7	1.67E-7	3.15E-4	4.02E-8	2.51E-9	0.100	0.85	0.06	4789	16.5	10500	11.1	7645	13.8	--
83	SG25B	6/18/2010	UGS	diffussion sampler	4789	589	6.32E-7	1.65E-7	3.18E-4	4.67E-8	3.07E-9	0.001	0.00	3.96	4789	9.7	10500	2.7	7645	6.2	--
84	SG25C	6/18/2010	UGS	diffussion sampler	4789	557	5.17E-7	1.53E-7	2.94E-4	3.92E-8	2.51E-9	0.000	0.00	0.20	4789	14.2	7000	12.1	5895	13.2	x
85	SG25D	6/18/2010	UGS	diffussion sampler	4789	593	2.38E-7	1.61E-7	3.13E-4	3.36E-8	2.50E-9	0.031	0.85	12.64	4795	17.5	10500	12.3	7648	14.9	--
86	SG26B	7/14/2009	UGS	diffussion sampler	4794	508	4.46E-7	1.32E-7	2.55E-4	3.29E-8	2.32E-9	0.000	0.35	12.07	4794	20.5	10500	11.5	7647	16.0	--
87	SG26C	7/14/2009	UGS	diffussion sampler	4794	672	5.82E-7	1.79E-7	3.38E-4	4.51E-8	2.91E-9	0.003	0.45	0.25	4794	10	10500	4.8	7647	7.4	--
88	SG27A	6/18/2010	UGS	diffussion sampler	4823	602	5.59E-8	1.85E-7	3.40E-4	4.11E-8	2.73E-9	0.025	0.73	0.63	4823	13.8	7300	11.5	6062	12.7	--
95	Big Springs	6/14/2006	UGS	diffussion sampler	5577	644	7.62E-8	1.63E-7	3.44E-4	4.44E-8	3.29E-9	0.001	0.00	1.62	5577	7.0	10500	2.2	8039	4.6	--
98	Twin Springs	6/14/2006	UGS	diffussion sampler	4820	717	1.28E-6	1.56E-7	3.13E-4	3.99E-8	2.53E-9	0.100	0.93	0.52	4820	14.4	6300	13.5	5560	13.9	--
100	Persey Spring	6/15/2006	UGS	diffussion sampler	4315	654	1.06E-7	1.53E-7	2.65E-4	3.35E-8	2.04E-9	0.005	0.79	0.20	4315	21.5	10500	15.2	7408	18.4	--
101	Mirror Springs	6/15/2006	UGS	diffussion sampler	4342	589	2.20E-7	1.51E-7	2.65E-4	3.36E-8	2.15E-9	0.001	0.00	0.13	4342	20.4	10500	13.3	7408	18.4	--
103	(C-16-18)26cba[twin mx]	7/28/2009	USGS	diffussion sampler	4880	615	6.23E-7	1.54E-7	3.28E-4	4.51E-8	2.96E-9	0.000	0.00	0.31	4880	9.0	10500	2.7	7690	5.8	--
104	Coyote Spring	6/3/2008	USGS	diffussion sampler	4420	566	3.39E-7	1.34E-7	2.21E-4	2.83E-8	1.90E-9	0.095	1.03	4.55	4420	26.0	10500	18.2	7460	22.1	x
108	(C-18-15)36cdd-1	9/8/2008	USGS	diffussion sampler	4530	590	1.11E-7	1.74E-7	3.01E-4	3.96E-8	2.36E-9	0.008	0.65	1.36	4530	16.4	5200	15.8	4865	16.1	--

Table 6.7. *continued*

Station ID[1]	Location	Sample date	Sample source[2]	Sample type	Elevation (ft)[3]	TDGP (mm Hg)[4]	^{4}He (ccSTP/g)	^{20}Ne (ccSTP/g)	^{40}Ar (ccSTP/g)	^{84}Kr (ccSTP/g)	^{129}Xe (ccSTP/g)	A_e[5]	F[6]	$\Sigma\chi^2$[7]	Hrmin (ft)[8]	Trmax (°C)	Hrmax (ft)[9]	Trmin (°C)	Hravg (ft)	Travg (°C)[10]	Pleistocene[11]
109	PW06D	9/9/2008	UGS	diffusion sampler	5001	722	5.12E-7	2.33E-7	3.58E-4	5.07E-8	3.08E-9	0.005	0.00	4.56	5001	8.9	10500	2.8	7750	5.8	--
110	PW09B	9/9/2008	UGS	diffusion sampler	5140	812	2.62E-7	2.45E-7	4.12E-4	5.52E-8	3.52E-9	0.008	0.21	0.81	5140	4.9	10500	0.3	7820	2.6	--
112	PW11B	5/18/2009	UGS	diffusion sampler	5665	606	3.14E-7	1.68E-7	3.38E-4	4.74E-8	3.26E-9	0.001	0.00	1.36	5665	6.8	10500	1.5	8082	4.1	--
127	PW04B	11/16/2010	UGS/USGS	diffusion sampler	6181	1,113	1.40E-7	4.44E-7	3.75E-4	3.65E-8	2.55E-9	0.019	0.00	19.97	6181	26.0	10500	19.9	8341	23.0	x
128	PW10B	11/17/2010	UGS/USGS	diffusion sampler	5266	644	1.26E-7	2.01E-7	3.29E-4	4.35E-8	2.91E-9	0.003	0.00	1.27	5266	11.2	10200	5.4	7733	8.3	--
129	PW18	11/17/2010	UGS/USGS	diffusion sampler	5185	928	7.44E-8	1.01E-7	1.81E-4	1.68E-8	1.23E-9	0.000	5.89	26.30	5185	41.7	10500	33.6	7842	37.7	x
140	PW17C	5/20/2009	UGS	diffusion sampler	4507	521	2.01E-7	3.47E-7	3.12E-4	3.85E-8	2.49E-9	0.012	0.00	25.74	4507	24.3	10500	16.2	7503	20.3	--
130	Well 22	6/15/2011	UGS	copper tube	4811	--	7.58E-8	1.21E-7	1.87E-4	2.08E-8	1.34E-9	0.000	0.00	1.70	1466	36.7	3200	29.4	2333	33.3	x
131	Ibex Well	6/15/2011	UGS	copper tube	4779	--	6.87E-8	1.44E-7	2.50E-4	2.91E-8	2.10E-9	0.001	0.00	3.61	1457	22.5	3200	15.0	2329	18.6	x
132	Wah Wah Well	6/15/2011	UGS	copper tube	4645	--	9.83E-8	1.55E-7	2.84E-4	3.99E-8	2.56E-9	0.001	0.00	1.61	1416	14.8	3200	7.7	2308	11.2	x
133	Guyman Well	6/15/2011	UGS	copper tube	5085	--	7.95E-8	1.56E-7	2.81E-4	3.62E-8	2.50E-9	0.001	0.00	0.68	1550	15.7	3200	9.1	2375	12.3	x
141	Dearden Ranch Spring	10/7/2011	UGS	diffusion sampler	5420	609	1.67E-7	1.54E-7	2.96E-4	3.99E-8	2.61E-9	0.001	0.00	0.24	1652	12.8	3200	6.7	2426	9.7	--
205	Mustang Spring	7/14/2005	USGS	diffusion sampler	10194	518	3.59E-8	1.43E-7	3.24E-4	4.38E-8	3.21E-9	0.001	0.53	0.38	10194	2.3	10500	2.1	10347	2.2	--
208	Gandy Springs	12/15/2005	USGS	diffusion sampler	5238	677	7.19E-7	1.34E-7	2.59E-4	3.60E-8	2.40E-9	0.100	1.09	1.68	5500	14.3	6300	13.6	5900	14.0	--
220	Caine Spring	12/12/2005	USGS	diffusion sampler	5024	719	1.15E-7	1.80E-7	3.31E-4	4.29E-8	2.56E-9	0.004	0.41	0.00	5024	11.1	9900	6.1	7462	8.6	--
221	Clay Spring	5/18/2010	USGS	diffusion sampler	5440	564	9.20E-8	1.47E-7	3.00E-4	4.35E-8	2.76E-9	0.000	0.35	2.86	5500	10.7	10500	4.7	8000	7.7	--
226	MX Well 100 (N11 E70 36BDDD)	12/13/2005	USGS	diffusion sampler	5545	600	4.42E-8	1.72E-7	3.41E-4	4.60E-8	3.07E-9	0.001	0.00	0.07	5545	7.8	10500	3.2	8023	5.5	--

[1] Station ID and location match those on figure 6.1.

[2] Sample source is either Utah Geological Survey (UGS) or the U.S. Geological Survey (USGS).

[3] Elevation of ground surface at sample site.

[4] Total dissolved gas pressure measured at position of diffusion sampler.

[5] Excess air concentration parameter following method of Aeschbach-Hertig and others (2000). This and subsequent table fields are the work of P. Gardner at the USGS, Salt Lake City, UT.

[6] Excess air fractionation parameter following method of Aeschbach-Hertig and others (2000).

[7] Chi-squared misfit between measured and modeled recharge parameters.

[8] Minimum recharge elevation, equal to the land surface elevation at the sample site. Used as input to calculate the maximum possible recharge temperature Trmax.

[9] Maximum recharge elevation, equal to the highest elevation at which recharge may occur upgradient of a given sample. Used as input to calculate the minimum possible recharge temperature.

[10] Average temperature of recharge taken as the midpoint between the caculated minimum and maximum values.

[11] Apparent age based on carbon-14. Samples with x have an apparent age greater than 12,000 years and may have been recharged during substantially different temperature regimes. See carbon isotope section for details.

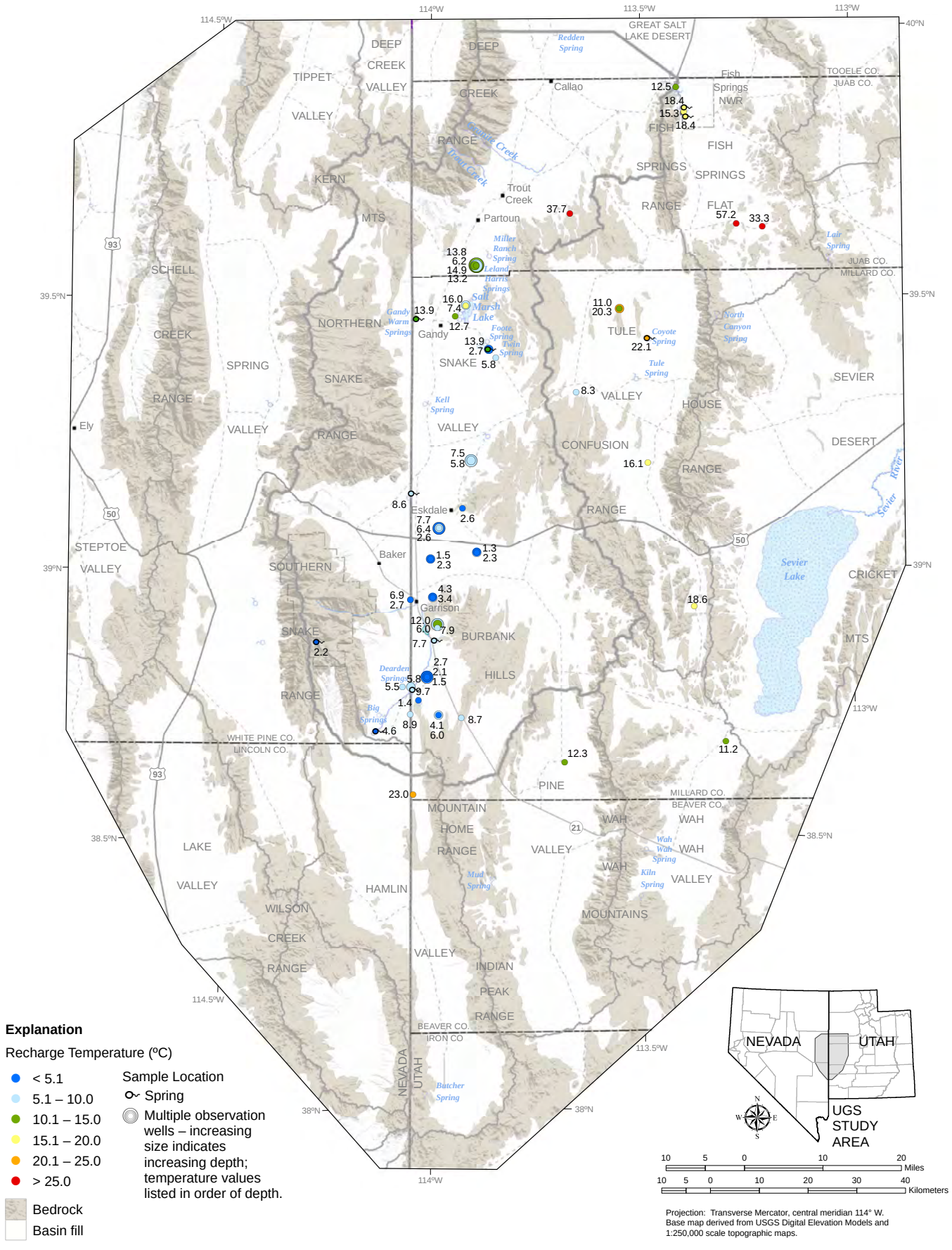

Figure 6.21. *Recharge temperatures estimated from dissolved noble-gas concentrations for select wells in the UGS study area (table 6.7).*

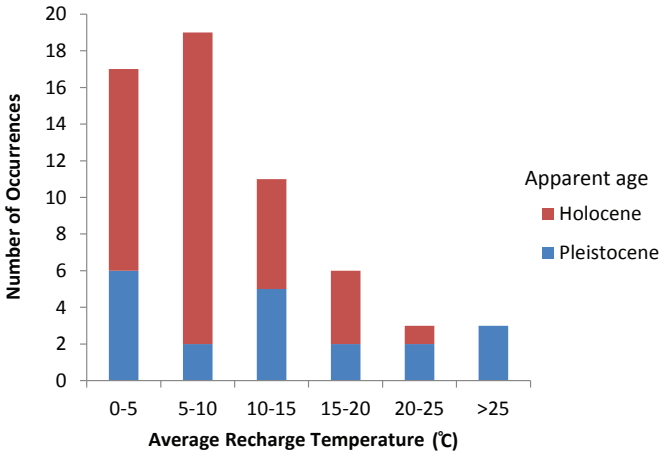

Figure 6.22. *Histogram of average groundwater recharge temperatures (table 6.7).*

(higher) isotopic ratios for warmer precipitation. Measured isotopic ratios of oxygen (^{16}O and ^{18}O) and hydrogen (^{1}H and ^{2}H) in precipitation therefore vary systemically with topography, temperature, and distance from the ocean and tend to plot along known trends (Craig, 1961; Dansgard, 1964; Clark and Fritz, 1997).

Following precipitation, isotopic ratios in surficial and near-surface groundwater may be altered by evaporation (Clark and Fritz, 1997). This process generally yields an increase in the $^{18}O/^{16}O$ ratio relative to the $^{2}H/^{1}H$ ratio. Beneath the water table, few processes other than mixing and mineral-water interaction at temperatures greater than 50°C (112°F) alter the stable isotopic ratios of $^{18}O/^{16}O$ and $^{2}H/^{1}H$. Stable isotopic ratios measured in groundwater therefore record vital information concerning the character and sources of groundwater recharge (Clark and Fritz, 1997) and offer an important direct measurement of the sources, sinks, and flow paths of groundwater.

6.3.2.2 Stable Isotope Results

Water samples collected for this study were analyzed for the stable-isotopic ratios of hydrogen ($\delta^{2}H$) and oxygen ($\delta^{18}O$). Most stable isotope samples were collected using a standard downhole pump. A smaller number were collected using drill rig airlifting following well completion. Repeat sampling of sites via airlift and downhole pump methods have shown that potential error in $\delta^{2}H$ is within or near measurement error (reported from the laboratory), whereas the $\delta^{18}O$ value sampling error may be slightly greater than measurement error but still relatively low. For subsequent discussions the $\delta^{2}H$ value is therefore considered the most accurate stable isotope and $\delta^{18}O$ is considered to be inherently less accurate. All samples from compiled sources are assumed to have been collected using a standard downhole or peristaltic sampling pump.

The stable-isotope ratios were measured at the Brigham Young University Hydrogeochemistry Laboratory using a Finnigan Delta^{plus} isotope ratio mass spectrometer, and were normalized to the VSMOW/SLAP scale following the procedures of Coplen (1996) and Nelson (2000). Laboratory procedures and methods for compiled samples are discussed in detail in the respective reports from which the data are taken (see Hershey and Mizell, 1995; Thomas and others, 2006; Hershey and others, 2007; Thomas and Mihevc, 2007; Gillespie, 2008; Acheampong and others, 2009).

Isotopic ratios of hydrogen ($^{2}H/^{1}H$) and oxygen ($^{18}O/^{16}O$) are reported as delta (δ) values in units of parts per thousand (per mil, or ‰) relative to a reference standard (Standard Mean Ocean Water) (Craig, 1961) via the following equation:

$$\delta x = \left(\frac{Rsample}{Rstandard} - 1 \right) \cdot 1000 \qquad (6.1)$$

where:

δx = delta^{18}O or ^{2}H (‰)

Rsample = $^{18}O/^{16}O$ or $^{2}H/^{1}H$ in the sampled water

Rstandard = $^{18}O/^{16}O$ or $^{2}H/^{1}H$ in the reference standard

Values greater than zero for δx indicate a sample is enriched relative to the standard and δx values less than zero indicate a sample is depleted relative to the standard. Natural waters in western North America commonly are depleted and therefore have negative values for both $\delta^{2}H$ and $\delta^{18}O$ (Bowen and Revenaugh, 2003). The values for both $\delta^{2}H$ and $\delta^{18}O$ for precipitation in the study area vary spatially, with both isotopes becoming enriched (increasing values) progressively from north to south (Friedman and others, 2002)

A subset of 160 stable isotope samples was chosen from the compiled dataset and the samples collected for this study (table 6.8) to examine trends and patterns in the stable isotopic composition of groundwater in the study area. Stable isotope values for the study area range from -97.3 to -125.9 for $\delta^{2}H$ with an average of -112.4 and from -12.3 to -17.2 for $\delta^{18}O$ with an average of -14.8. These values are within the range of previous data for both precipitation and groundwater from the study area (Friedman and others, 2002; Gillespie and others, 2012). Deuterium and oxygen-18 composition of groundwater follows a predictable trend defined by the global meteoric water line (Craig, 1961). Figure 6.23 is a plot of $\delta^{18}O$ versus $\delta^{2}H$ values and shows both the global meteoric water line and a local meteoric water line typical of stable isotopic

Table 6.8. *Isotopic data and apparent age results for selected samples in the broader UGS study area.*

Station ID[1]	Location	^{2}H (‰)	^{2}H_error (‰)	^{18}O (‰)	^{18}O_error (‰)	^{13}C (‰)	pmc (%)	pmc_error (%)	Tritium (TU)	Tritium_error (TU)	Tritium source	Tritium Age[2] (yr)	Qualitative age[3]	Uncor[4] (yr)	Ave Modern[5] (yr)	P-H[6] (yr)	C-F[7] (yr)	F-G[8] (yr)	Average Age[9] (yr)
2	PW01A	-112.10	0.50	-14.94	0.20	-8.72	66.53	0.20	5.06	0.47	UofU	38	Modern	--	--	--	--	--	--
4	PW01B	-113.90	0.50	-15.53	0.20	-7.27	28.85	0.11	0.08	0.10	UofU	--	Old	10,300	6,800	1,100	5,500	2,500	4,000
5	PW02A	-113.84	1.00	-14.69	0.20	--	--	--	--	--	--	--	--	--	--	--	--	--	--
7	PW02B	-114.00	0.50	-15.07	0.20	-11.46	33.59	0.12	0.03	0.10	UofU	--	Old	9,000	5,600	3,600	8,000	3,400	5,200
9	PW03A	-103.06	1.00	-13.80	0.20	-9.10	66.00	0.31	2.34	0.15	UofU	35	Modern	--	--	--	--	--	--
11	PW03B	-103.75	1.00	-13.91	0.20	-9.70	66.26	0.35	2.63	0.12	UofU	29	Modern	--	--	--	--	--	--
12	PW03P	-104.20	1.00	-13.26	0.20	-9.40	65.06	0.25	2.20	0.20	BYU	--	Modern	--	--	--	--	--	--
16	PW05A	-114.60	0.50	-15.43	0.20	-7.64	51.46	0.16	0.08	0.10	UofU	--	Premodern	--	--	--	--	--	--
17	PW05B	-125.90	0.50	-16.77	0.20	-8.04	3.96	0.03	0.21	0.10	UofU	--	Old	26,700	23,300	18,400	22,700	19,400	20,900
19	PW05C	-124.31	1.00	-16.62	0.20	-5.30	1.57	0.11	0.06	0.10	UofU	--	Old	34,300	30,900	22,600	26,900	24,800	26,300
21	PW06A	-108.70	0.50	-13.87	0.16	-6.66	22.87	0.15	0.40	0.20	BYU	--	Old	12,200	8,800	2,300	6,700	4,500	5,600
23	PW06B	-109.69	1.00	-14.93	0.20	-6.30	27.10	0.19	0.17	0.10	UofU	--	Old	10,800	7,400	500	4,800	2,000	3,700
26	PW06C	-109.32	1.00	-14.75	0.20	-7.70	30.77	0.19	0.17	0.10	UofU	--	Old	9,700	6,300	1,100	5,400	2,300	3,800
32	PW07A	-125.30	0.50	-16.57	0.20	-3.20	2.19	0.03	0.02	0.10	UofU	--	Old	31,600	28,200	15,700	20,000	20,500	21,100
35	PW07B	-121.54	1.00	-16.61	0.20	-2.20	6.76	0.12	0.05	0.03	UofU	--	Old	22,300	18,800	3,200	7,600	21,000	12,700
36	PW08A	-111.00	1.00	-15.39	0.20	--	--	--	--	--	--	--	--	--	--	--	--	--	--
38	PW08B	-112.04	1.00	-15.32	0.20	-6.80	8.54	0.13	0.11	0.10	UofU	--	Old	20,300	16,900	10,600	15,000	12,200	13,700
40	PW09A	-107.30	0.50	-14.44	0.16	-7.88	32.48	0.18	0.20	0.10	BYU	--	Old	9,300	5,900	800	5,200	2,200	3,500
44	PW11B	-115.90	1.00	-15.69	0.20	-6.00	3.55	0.11	0.21	0.10	UofU	--	Old	27,600	24,200	16,900	21,200	18,600	20,200
46	PW11C	-115.80	1.00	-15.90	0.20	-7.20	4.66	0.11	0.08	0.10	UofU	--	Old	25,300	21,900	16,100	20,500	17,400	19,000
48	PW11E	-115.93	1.00	-15.94	0.20	-7.90	4.36	0.12	0.24	0.10	UofU	--	Old	25,900	22,500	17,400	21,800	18,200	20,000
49	NPA1B (11P)	-115.60	1.00	-15.59	0.20	--	--	--	--	--	--	--	--	--	--	--	--	--	--
50	PW12	-107.63	1.00	-14.42	0.20	--	--	--	--	--	--	--	--	--	--	--	--	--	--
51	AG13A	-111.46	1.00	-14.98	0.20	-9.90	79.35	0.34	3.45	0.16	UofU	18	Modern	--	--	--	--	--	--
52	AG13B	-113.07	1.00	-15.19	0.20	-10.40	64.79	0.23	0.87	0.10	UofU	41	Modern	--	--	--	--	--	--
53	AG13C	-113.48	1.00	-15.41	0.20	-9.07	62.92	0.22	0.42	0.10	UofU	54	Premodern	--	--	--	--	--	--
54	AG14A	-107.10	1.00	-15.22	0.20	-7.50	20.31	0.11	0.20	0.10	BYU	--	Old	13,200	9,700	4,300	8,600	5,600	7,100
55	AG14B	-110.80	1.00	-15.00	0.20	-9.53	18.91	0.10	0.40	0.20	BYU	--	Old	13,800	10,300	6,900	11,200	7,300	8,900
56	AG14C	-112.90	1.00	-15.12	0.20	-8.40	13.04	0.08	0.10	0.20	BYU	--	Old	16,800	13,400	8,900	13,200	9,800	11,300
57	AG15A	-111.49	1.00	-14.09	0.20	-7.49	58.50	0.02	0.10	0.20	UofU	--	Premodern	--	--	--	--	--	--
59	AG16A	-108.50	0.50	-14.42	0.20	-9.85	76.21	0.22	1.34	0.23	UofU	17	Modern	--	--	--	--	--	--
61	AG16B	-111.10	0.50	-14.87	0.20	-9.58	14.38	0.07	0.02	0.10	UofU	--	Old	16,000	12,600	9,200	13,500	9,300	11,100
63	AG16C	-123.90	0.50	-16.38	0.20	-8.95	3.67	0.03	0.09	0.10	UofU	--	Old	27,300	23,900	19,900	24,200	20,600	22,100
66	PW17A	-109.64	1.00	-14.65	0.20	-4.40	3.18	0.11	0.38	0.10	UofU	--	Old	28,500	25,100	15,200	19,600	17,400	19,300
71	PW19A	-116.50	0.50	-14.99	0.20	--	--	--	--	--	--	--	--	--	--	--	--	--	--
73	PW19B	-116.10	0.50	-14.65	0.20	-1.23	2.94	0.04	0.20	0.10	BYU	--	Old	29,200	25,700	5,300	9,700	16,500	14,300
75	PW19C	-116.06	1.00	-15.41	0.20	-1.80	0.72	0.10	0.50	0.10	UofU	--	Mix	40,800	37,400	20,100	24,400	28,000	27,500
77	SG21C	-110.30	0.50	-14.40	0.20	-3.84	7.10	0.04	0.14	0.10	UofU	--	Old	21,900	18,400	7,400	11,800	11,600	12,300
78	SG22B	-110.50	1.00	-14.05	0.20	-3.38	3.84	0.04	0.70	0.20	BYU	--	Mix	26,900	23,500	11,500	15,800	15,400	16,600
79	SG23B	-109.41	0.10	-14.71	0.20	-7.33	18.61	0.10	0.05	0.10	UofU	--	Old	13,900	10,500	4,800	9,200	5,800	7,600
80	SG24B	-107.90	1.00	-14.11	0.20	-6.45	18.93	0.10	0.60	0.20	BYU	--	Mix	13,800	10,300	3,600	8,000	5,000	6,700
81	SG24C	-105.37	1.00	-14.16	0.20	-6.25	2.98	0.04	0.30	0.20	BYU	--	Old	29,000	25,600	18,600	23,000	20,200	21,800

Table 6.8. *continued*

Station ID[1]	Location	^{2}H (‰)	^{2}H_error (‰)	^{18}O (‰)	^{18}O_error (‰)	^{13}C (‰)	pmc (%)	pmc_error (%)	Tritium (TU)	Tritium_error (TU)	Tritium source	Tritium Age[2] (yr)	Qualitative age[3]	Uncor[4] (yr)	Ave Modern[5] (yr)	P-H[6] (yr)	C-F[7] (yr)	F-G[8] (yr)	Average Age[9] (yr)
82	SG25A	-121.13	1.00	-14.73	0.20	-6.01	20.18	0.09	0.03	0.10	UofU	--	Old	13,200	9,800	2,500	6,900	4,400	5,900
83	SG25B	-121.90	1.00	-15.13	0.20	-6.34	13.15	0.08	0.01	0.10	UofU	--	Old	16,800	13,300	6,500	10,800	8,400	9,800
84	SG25C	-122.77	1.00	-16.14	0.20	-7.20	8.82	0.06	0.06	0.10	UofU	--	Old	20,100	16,600	10,800	15,200	12,200	13,700
85	SG25D	-122.50	1.00	-16.23	0.20	-6.82	30.81	0.11	0.03	0.10	UofU	--	Old	9,700	6,300	100	4,400	2,300	3,300
86	SG26B	-122.40	1.00	-16.20	0.20	-6.46	22.03	0.12	0.04	0.14	BYU	--	Old	12,500	9,100	2,400	6,700	4,300	5,600
87	SG26C	-122.70	0.50	-16.15	0.20	-6.39	13.65	0.09	0.20	0.10	BYU	--	Old	16,500	13,000	6,200	10,600	8,200	9,500
88	SG27A	-120.40	1.00	-15.40	0.20	-8.89	70.58	0.27	0.05	0.10	UofU	--	Premodern	--	--	--	--	--	--
89	(C-13-14)25dac[19mx]	-116.80	0.50	-15.81	0.16	-2.08	2.01	0.03	0.09	0.10	UofU	--	Old	32,300	28,900	12,800	17,100	20,700	19,900
90	(C-16-18)26cba[twin mx]	-107.20	0.50	-14.23	0.16	-4.94	12.18	0.09	0.20	0.10	BYU	--	Old	17,400	14,000	5,100	9,400	7,800	9,100
91	(C20-18)32abd[PW7 mx]	-106.90	0.50	-13.49	0.16	-7.43	26.40	0.10	0.06	0.10	UofU	--	Old	11,000	7,600	2,000	6,400	3,400	4,800
92	Indian Trail well	-121.28	1.00	-15.77	0.16	-3.20	19.48	0.20	0.20	0.20	BYU	--	Old	13,500	10,100		1,900	600	4,200
94	Tule Mx #1 well	-119.88	1.00	-15.49	0.16	-4.77	20.84	0.20	0.20	0.50	BYU	--	Old	13,000	9,500	300	4,700	2,900	4,400
95	Big Spring	-110.84	1.00	-14.86	0.16	-4.95	15.88	0.17	2.14	0.10	UofU	30	Mix	15,200	11,800	2,900	7,200	5,800	6,900
96	Davies well	-108.16	1.00	-13.96	0.16	-5.77	16.98	0.22	2.00	0.40	BYU	--	Mix	14,700	11,200	3,600	7,900	5,800	7,100
97	Shell-Baker well	-112.57	1.00	-14.72	0.16	-9.27	44.47	0.30	0.20	0.30	BYU	--	Old	6,700	3,300	--	3,900	200	2,400
98	Twin Springs	-108.48	1.00	-13.85	0.16	-11.14	74.42	0.46	0.12	0.10	UofU	--	Premodern	--	--	--	--	--	--
99	West Buckskin well	-107.01	1.00	-13.49	0.16	-13.55	73.40	0.45	0.30	0.30	BYU	--	Premodern	--	--	--	--	--	--
100	Persey Spring	-116.28	1.00	-13.82	0.16	-8.10	36.35	0.26	0.20	0.20	UofU	--	Old	8,400	4,900	100	4,500	600	2,500
101	Mirror Spring	-110.73	1.00	-13.96	0.16	-9.39	49.27	0.44	0.20	0.20	UofU	--	Old	5,900	2,400	--	3,200	--	2,800
102	North Spring	-115.73	1.00	-13.84	0.16	-4.67	15.19	0.16	0.60	0.20	BYU	--	Mix	15,600	12,100	2,800	7,100	8,900	7,700
104	Coyote Springs	-107.86	1.00	-14.35	0.16	-2.77	4.12	0.17	0.19	0.19	UofU	--	Old	26,400	22,900	9,200	13,600	13,900	14,900
106	(C-15-15)30bdd-1	-107.83	1.00	-14.15	0.16	-3.74	4.17	0.13	0.09	0.19	UofU	--	Old	26,300	22,800	11,600	16,000	14,200	16,200
108	(C-18-15)36cdd-1	-111.52	1.00	-14.29	0.16	-6.00	10.00	0.09	0.12	0.19	UofU	--	Old	19,000	15,600	8,300	12,600	10,100	11,700
109	PW06D	-109.14	1.00	-14.40	0.16	-6.60	29.51	0.16	0.02	0.19	UofU	--	Old	10,100	6,700	100	4,500	1,900	3,300
110	PW09B	-106.45	1.00	-13.93	0.16	-7.43	32.57	0.17	0.24	0.19	UofU	--	Old	9,300	5,800	300	4,600	1,500	3,100
111	(C-20-17)9cad-1 BLM LVW	-113.78	1.00	-14.62	0.16	-5.67	7.60	0.08	0.16	0.19	UofU	--	Old	21,300	17,900	--	14,400	12,200	14,800
113	SG23A	-109.68	1.00	-14.53	0.16	-8.64	18.10	0.12	0.10	0.19	UofU	--	Old	14,100	10,700	6,400	10,800	7,000	8,700
114	C20	-119.80	0.50	-15.85	0.20	--	--	--	--	--	--	--	--	--	--	--	--	--	--
115	C32 (C-11-17)11aaa-1	-119.40	5.00	-15.77	0.20	--	--	--	--	--	--	--	--	--	--	--	--	--	--
116	RSW02	-121.90	0.50	-15.80	0.20	-7.69	43.22	0.16	0.20	0.05	UofU	--	Old	6,900	3,500		2,600		3,000
117	CO2	-123.60	0.50	-16.20	0.20	-10.72	37.32	0.14	0.12	0.04	UofU	--	Old	8,100	4,700	2,200	6,600	1,800	3,800
118	C9	-122.20	0.50	-16.08	0.20	-12.39	89.45	0.27	7.90	0.20	UofU	--	Modern	--	--	--	--	--	--
119	C29	-120.90	0.50	-16.03	0.20	-11.41	79.85	0.24	2.50	0.11	UofU	--	Modern	--	--	--	--	--	--
120	C199	-117.70	0.50	-15.48	0.20	-10.90	88.81	0.28	12.38	0.55	UofU	--	Modern	--	--	--	--	--	--
121	(C-11-16)36cdb	-111.40	0.50	-13.88	0.20	-4.23	6.27	0.05	0.01	0.09	UofU	--	Old	22,900	19,500	9,300	13,600	19,700	15,500
122	Kell Spring	-116.50	0.50	-15.24	0.20	--	--	--	0.17	0.06	UofU	--	--	--	--	--	--	--	--
123	SG24a	-107.50	0.50	-13.46	0.20	-8.18	20.42	0.09	0.04	0.03	UofU	--	Old	13,100	9,700	5,000	9,300	5,900	7,500
124	SG21a	-108.50	0.50	-13.70	0.20	-2.34	4.83	0.04	0.01	0.06	UofU	--	Old	25,100	21,600	6,500	10,900	16,300	13,800
125	SG21b	-109.20	0.50	-13.41	0.20	-4.40	6.00	0.05	0.10	0.03	UofU	--	Old	23,300	19,800	10,000	14,300	17,200	15,300
126	SG22a	-109.30	0.50	-13.92	0.20	-2.62	3.90	0.04	0.14	0.05	UofU	--	Old	26,800	23,400	9,200	13,600	16,700	15,700
127	PW04b	-98.47	0.50	-12.30	0.20	-9.98	50.74	0.17	0.10	0.10	UofU	--	Premodern	--	--	--	--	--	--
128	PW10b	-116.31	0.50	-15.23	0.20	-9.84	7.99	0.13	0.20	0.10	UofU	--	Old	20,900	17,500	14,200	18,600	14,400	16,200

Table 6.8. *continued*

Station ID[1]	Location	^{2}H (‰)	^{2}H_error (‰)	^{18}O (‰)	^{18}O_error (‰)	^{13}C (‰)	pmc (%)	pmc_error (%)	Tritium (TU)	Tritium_error (TU)	Tritium source	Tritium Age[2] (yr)	Qualitative age[3]	Uncor[4] (yr)	Ave Modern[5] (yr)	P-H[6] (yr)	C-F[7] (yr)	F-G[8] (yr)	Average Age[9] (yr)
129	PW18	-107.43	0.50	-13.70	0.20	-6.57	17.93	0.09	0.20	0.10	UofU	--	Old	14,200	10,800	4,200	8,600	9,400	8,200
130	Well 22	-115.00	0.50	-14.62	0.20	-3.89	5.12	0.04	0.12	0.05	UofU	--	Old	24,600	21,100	10,200	14,600	16,000	15,500
131	Ibex Well	-110.50	0.50	-14.37	0.20	-6.52	7.16	0.05	0.21	0.08	UofU	--	Old	21,800	18,400	11,700	16,100	13,700	15,000
132	Wah Wah Well	-106.00	0.50	-14.09	0.20	-9.19	7.43	0.05	0.08	0.05	UofU	--	Old	21,500	18,100	14,300	18,600	16,100	16,800
133	Guyman Well	-104.70	0.50	-13.77	0.20	-9.56	10.64	0.06	0.01	0.05	UofU	--	Old	18,500	15,100	11,600	16,000	12,200	13,700
134	Mountain Home Spring	-110.80	0.50	-14.56	0.20	-9.85	48.81	0.15	1.60	0.10	BYU	--	Mix	5,900	2,500	--	3,600	--	3,100
136	Antelope Spring	-112.70	0.50	-12.70	0.20	-12.22	54.21	0.17	0.14	0.05	UofU	--	Premodern	--	--	--	--	--	--
139	Gyp Seep	-112.70	0.50	-12.70	0.20	-7.82	63.91	0.19	0.70	0.10	BYU	--	Modern	--	--	--	--	--	--
140	PW17c	-108.90	0.50	-14.06	0.20	-6.42	3.59	0.03	0.01	0.05	UofU	--	Old	27,500	24,100	17,300	21,700	19,600	20,700
141	Dearden Ranch Spring	-110.40	0.50	-14.69	0.20	-9.01	16.48	0.08	0.01	0.05	UofU	--	Old	14,900	11,500	7,500	11,900	8,400	9,800
201	Kious Spring	-110.00	--	-14.50	--	-10.40	83.10	--	3.40	--	--	--	Modern	--	--	--	--	--	--
202	Barrel Spring	-99.00	--	-13.36	--	--	--	--	--	--	--	--	--	--	--	--	--	--	--
203	Cedar Cabin Spring	-105.85	--	-14.07	--	--	--	--	--	--	--	--	--	--	--	--	--	--	--
204	DecathonSpring	-107.63	--	-14.41	--	-11.05	--	--	6.70	--	--	--	--	--	--	--	--	--	--
205	Mustang Spring	-110.90	--	-15.30	--	-10.50	95.40	--	5.30	--	--	--	Modern	--	--	--	--	--	--
206	South Spring (D7)	-107.40	--	-14.57	--	--	--	--	--	--	--	--	--	--	--	--	--	--	--
207	SpringCreekSpring	-112.50	--	-15.21	--	--	--	--	--	--	--	--	--	--	--	--	--	--	--
208	GandySprings	-119.70	--	-15.72	--	-7.00	39.60	--	3.90	--	--	--	Mix	7,700	4,200	--	2,500	--	3,400
209	UnnamedSpring#4	-106.70	--	-14.48	--	--	--	--	--	--	--	--	--	--	--	--	--	--	--
210	Unnamed Spring #5 (D10)	-105.40	--	-13.82	--	--	--	--	--	--	--	--	--	--	--	--	--	--	--
211	CobbSpring	-103.70	--	-13.74	--	--	--	--	--	--	--	--	--	--	--	--	--	--	--
212	UnnamedSpring#12	-116.60	--	-15.89	--	-13.70	89.90	--	--	--	--	--	--	--	--	--	--	--	--
213	Unnamed Spring, 195 N16 E69 19 1	-115.70	--	-15.38	--	--	--	--	--	--	--	--	--	--	--	--	--	--	--
214	UnnamedSpring#13	-113.70	--	-14.64	--	--	--	--	--	--	--	--	--	--	--	--	--	--	--
215	RyanSpring	-103.80	--	-13.62	--	--	--	--	--	--	--	--	--	--	--	--	--	--	--
216	MerrilsCampSpring	-102.30	--	-14.05	--	--	--	--	--	--	--	--	--	--	--	--	--	--	--
217	RipgutSpring	-105.10	--	-14.24	--	--	--	--	--	--	--	--	--	--	--	--	--	--	--
218	Unnamed Spring #1 (WM-8)	-109.60	--	-15.05	--	--	--	--	--	--	--	--	--	--	--	--	--	--	--
219	Butcher Spring	-103.20	--	-14.22	--	--	--	--	--	--	--	--	--	--	--	--	--	--	--
220	Caine Spring	-113.90	--	-15.17	--	-8.66	78.80	--	1.00	--	--	--	Modern	--	--	--	--	--	--
221	Clay Spring	-112.10	--	-14.79	--	-5.81	16.00	--	0.30	--	--	--	Old	15,100	11,700	4,100	8,500	6,400	7,700
222	Cold Spring	-119.20	--	-15.42	--	-8.59	--	--	1.20	--	--	--	--	--	--	--	--	--	--
223	Knoll Spring	-108.20	--	-14.05	--	-6.13	32.90	--	0.40	--	--	--	Old	9,200	5,800	--	2,700	400	2,900
224	Needle Pt Spring Box	-108.58	--	-14.32	--	-10.00	39.40	--	<0.2	--	--	--	Old	7,700	4,300	1,000	5,200	1,500	3,000
225	North Little Springs	-110.70	--	-14.97	--	-8.17	48.10	--	3.60	--	--	--	Mix	6,100	2,600	--	1,900	--	2,300
226	MX Well 100 (N11 E70 36BDDD)	-109.70	--	-14.38	--	-7.79	23.60	--	0.40	--	--	--	Old	11,900	8,500	3,200	7,400	4,700	5,900
227	MX-Observation (N08 E69 35CDDD)	-114.20	--	-14.82	--	-8.51	23.00	--	0.60	--	--	--	Mix	12,200	8,700	4,100	8,300	5,200	6,600
228	Unnamed Spring #7 (SN-29)	-117.20	--	-15.96	--	--	--	--	--	--	--	--	--	--	--	--	--	--	--
229	Unnamed Spring #9 (SN-31)	-114.00	--	-15.58	--	--	--	--	--	--	--	--	--	--	--	--	--	--	--
230	Unnamed Spring #10 (SN-33)	-115.40	--	-15.28	--	--	--	--	--	--	--	--	--	--	--	--	--	--	--
231	Marble Spring (SN-34)	-115.30	--	-15.61	--	--	--	--	--	--	--	--	--	--	--	--	--	--	--
232	Unnamed Spring #17 (SN-35)	-116.50	--	-15.78	--	--	--	--	--	--	--	--	--	--	--	--	--	--	--

Table 6.8. *continued*

Station ID[1]	Location	^{2}H (‰)	^{2}H_error (‰)	^{18}O (‰)	^{18}O_error (‰)	^{13}C (‰)	pmc (%)	pmc_error (%)	Tritium (TU)	Tritium_error (TU)	Tritium source	Tritium Age[2] (yr)	Qualitative age[3]	Uncor[4] (yr)	Ave Modern[5] (yr)	P-H[6] (yr)	C-F[7] (yr)	F-G[8] (yr)	Average Age[9] (yr)
233	Unnamed Spring #18 (SN-36)	-115.10	--	-15.57	--	--	--	--	--	--	--	--	--	--	--	--	--	--	--
234	Unnamed Spring #19 (SN-37)	-115.20	--	-15.56	--	--	--	--	--	--	--	--	--	--	--	--	--	--	--
235	Unnamed Spring #20 (SN-38)	-115.00	--	-15.83	--	--	--	--	--	--	--	--	--	--	--	--	--	--	--
236	Unnamed Spring #21 (SN-39)	-114.60	--	-15.62	--	--	--	--	--	--	--	--	--	--	--	--	--	--	--
237	Unnamed Spring #22 (SN-40)	-113.10	--	-15.57	--	--	--	--	--	--	--	--	--	--	--	--	--	--	--
238	Unnamed Spring #23 (SN-41)	-113.10	--	-15.49	--	--	--	--	--	--	--	--	--	--	--	--	--	--	--
239	Unnamed Spring #24 (SN-42)	-114.40	--	-15.20	--	--	--	--	--	--	--	--	--	--	--	--	--	--	--
240	Coyote Spring	-119.20	--	-15.49	--	--	--	--	--	--	--	--	--	--	--	--	--	--	--
241	Pipe Spring	-121.70	--	-15.35	--	-7.20	--	--	1.10	--	--	--	--	--	--	--	--	--	--
242	Rowland Spring	-112.90	--	-14.88	--	-12.56	--	--	6.90	--	--	--	--	--	--	--	--	--	--
243	Marmot Spring	-115.90	--	-15.33	--	-15.03	--	--	4.80	--	--	--	--	--	--	--	--	--	--
244	SnakeCampsite#2	-114.50	--	-15.02	--	-11.20	--	--	7.40	--	--	--	--	--	--	--	--	--	--
245	SnakeCreekRiver	-113.60	--	-15.04	--	-8.24	--	--	8.80	--	--	--	--	--	--	--	--	--	--
246	Wilson Health Spring 2	-106.90	--	-12.71	--	--	--	--	--	--	--	--	--	--	--	--	--	--	--
247	House Spring	-110.50	--	-14.26	--	--	--	--	--	--	--	--	--	--	--	--	--	--	--
248	Deadman Spring	-109.20	--	-13.91	--	--	--	--	--	--	--	--	--	--	--	--	--	--	--
249	Cold Spring	-112.00	--	-14.07	--	--	--	--	--	--	--	--	--	--	--	--	--	--	--
250	Laird Spring	-108.10	--	-13.54	--	-10.20	77.10	--	<0.08	--	--	--	Premodern	--	--	--	--	--	--
251	North Canyon Spring	-109.40	--	-14.57	--	--	--	--	--	--	--	--	--	--	--	--	--	--	--
252	Walter Spring	-110.30	--	-14.48	--	--	--	--	1.00	--	--	--	--	--	--	--	--	--	--
253	Antelope Spring(C-17-12)30ba (Unlisted #1)	-117.00	--	-15.87	--	-9.20	86.80	--	12.40	--	--	--	Modern	--	--	--	--	--	--
254	Lime Spring	-123.80	--	-17.20	--	--	--	--	--	--	--	--	--	--	--	--	--	--	--
255	Trough Spring	-113.60	--	-15.33	--	-11.70	92.80	--	16.60	--	--	--	Modern	--	--	--	--	--	--
256	Skunk Spring	-121.40	--	-16.34	--	-7.60	34.70	--	<0.08	--	--	--	Old	8,800	5,300	--	4,300	1,200	3,600
257	Tule Spring	-109.40	--	-14.88	--	-4.00	4.63	--	<0.08	--	--	--	Old	25,400	22,000	11,300	15,700	16,500	16,400
258	Painter Spring	-108.30	--	-14.55	--	-12.20	109.90	--	7.80	--	--	--	Modern	--	--	--	--	--	--
259	Kiln Spring	-100.80	--	-13.31	--	--	--	--	<0.08	--	--	--	--	--	--	--	--	--	--
260	Buckhorn Spring	-105.20	--	-14.22	--	-7.90	75.00	--	<0.08	--	--	--	Premodern	--	--	--	--	--	--
261	Mud Spring	-106.40	--	-14.44	--	--	--	--	--	--	--	--	--	--	--	--	--	--	--
262	Willow Spring(Wah Wah Valley)	-97.33	--	-12.73	--	-13.30	106.94	--	4.80	--	--	--	Modern	--	--	--	--	--	--
263	Willow Spring(Pine Valley)	-99.00	--	-12.70	--	-9.50	104.60	--	--	--	--	--	--	--	--	--	--	--	--
264	Water Hollow Spring	-104.20	--	-14.79	--	-13.00	106.20	--	1.90	--	--	--	Modern	--	--	--	--	--	--
265	Miller Spring	-117.18	--	-15.59	--	-2.70	5.80	--	<0.08	--	--	--	Old	23,500	20,100	6,200	10,500	12,800	12,400
266	South Tule Spring	-109.10	--	-15.09	--	--	--	--	--	--	--	--	--	--	--	--	--	--	--

[1] Station ID corresponds with those in tables D.1 and D.2.

[2] Modeled age of recharge based on dissolved gas data. Only calculated for sites with tritium >0.5 and complete dissolved gas data.

[3] Qualitative age based on tritium and pmc; modern = tritium > 0.5 and pmc > 50, premodern = tritium < 0.5 and pmc > 50, mixed = tritium 0.5 and pmc < 50, old = tritium < 0.5 and pmc < 50.

[4] Apparent age pmc corrections; Uncor = age calculated using initial pmc = 100 and standard decay equation, see text for details.

[5] Ave Modern = age calculated using initial pmc of 66 and standard decay equation, see text for details.

[6] P-H = age calculated using correction of Pearson and Hanshaw (1970), see text for details.

[7] C-F = age calculated using correction of Clark and Fritz (1997), see text for details.

[8] F-G = age calculated using the correction of Fontes and Garnier (1979), see text for details.

[9] Average apparent age of the old fraction for samples having < 50 pmc. Average apparent age calculated as the mean of the previous age corrections including Ave Modern, P-H, C-F, and F-G.

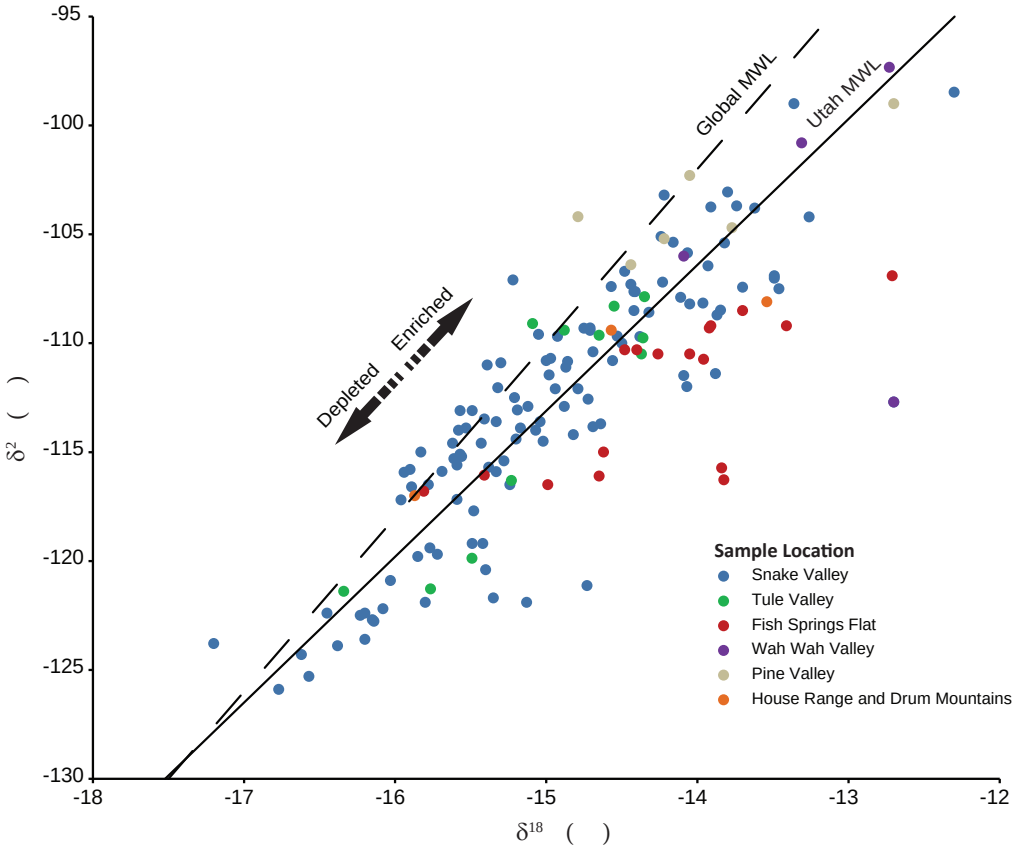

Figure 6.23. *$\delta^{18}O$ versus $\delta^{2}H$ for select wells and springs (table 6.8). The global MWL (meteoric water line) is taken from Craig (1961) and the Utah MWL from Kendall and Coplen (2001).*

samples collected in Utah (Kendall and Coplen, 2001). Samples collected for this study plot along and near the local meteoric water line, and generally below the global meteoric water line. Samples are also grouped based on geographic location. There is general overlap among samples taken from different basins and geographic locations. The range of stable isotope values of samples from Tule Valley is similar to the range of samples from Snake Valley. Most samples from Fish Springs Flat also plot within the extent of the Snake Valley samples. Samples from Wah Wah Valley and Pine Valley are enriched relative to most of the other samples, but still plot largely within the range of samples collected in Snake Valley. Three samples from the House Range and Drum Mountains also plot within the range of samples collected from Snake Valley. The overlap of stable isotopic concentrations across the study area limits the value of these tracers to constrain regional groundwater flow paths. Stable isotopes cannot be used to rule out interbasin flow in the manner presented by Gillespie and others (2012) because comparable stable isotope concentrations are found in adjoining basins and at upgradient and downgradient locations across the study area.

Stable isotopic values range from depleted end members characterized by samples collected at sites PW05B, PW05C, and PW07B, to enriched end member samples from PW04B and Willow Spring. The depleted end members all have percent modern carbon (pMC) values less than 10 (see subsequent carbon isotope sections) and are located in fine-grained basin fill of east-central Snake Valley. These samples may represent groundwater recharged by cool Pleistocene-age water derived from the southern Snake Range and are likely along relatively slow flow paths. The enriched end members are located in the southern part of the study area, and their relative enrichment may result from the regional trend of increasingly enriched stable isotopic composition of precipitation with decreasing latitude, typical of the Intermountain West (Friedman and others, 2002). Several samples collected at and near Fish Springs plot farthest away from the global meteoric water line, including Wilson Health Springs, North Spring, and Persey Spring. The isotopic shift in these samples may result from water-rock interaction at temperatures greater than 50°C (122°F) along deep, regional flow paths that feed these springs, or may also include a component of evaporative enrichment that occurs at the spring pools and areas of shallow groundwater near

where these samples were collected. Other samples that plot at a significant distance below the global meteoric water line including SG25A, SG25B, and SG21B, were collected from relatively shallow piezometers near areas of spring flow, and it is likely these samples have undergone evaporative enrichment typical of areas of discharge near springs. Many of the remaining samples plot near and just below the Utah meteoric water line (Kendall and Coplen, 2001) and may define a regional meteoric trend for the study area.

Plots of $\delta^{18}O$ and $\delta^{2}H$ show the spatial distribution of stable isotopic measurements across the study area (figures 6.24 and 6.25). Values of $\delta^{2}H$ are most enriched (highest) in the southwest and most depleted (lowest) in the northwest part of the study area along the west flank of Snake Valley between Gandy and Callao. Values elsewhere in Snake Valley vary from relatively depleted values north of Garrison, to more enriched values northeast of Garrison in eastern Snake Valley. Values of $\delta^{2}H$ in Tule Valley and Fish Springs Flat vary within the range of $\delta^{2}H$ values in the eastern and northern parts of Snake Valley. Notable localized variation in $\delta^{2}H$ exists near Fish Springs, and near and south of Garrison (figure 6.24). The range of $\delta^{2}H$ near Fish Springs may result from flow path convergence that likely occurs at the Fish Springs discharge area. Variation south of Garrison may occur from a combination of different recharge sources in this area that may include direct infiltration of precipitation, infiltration of relatively cool surface water sourced from the Snake Range, and recharge of unconsumed irrigation water. The distribution of $\delta^{18}O$ shows similar trends of depleted and enriched samples with $\delta^{2}H$. There is a greater degree of variation amongst sites in Fish Springs Flat and a notably low value at PW18 (figure 6.25). Variation in $\delta^{18}O$ near these areas may result from high-temperature water-rock interaction along deep flow paths that feed these areas. The spatial variability of the stable isotopes implies multiple sources of recharge both in time and space for the regional groundwater system. Despite this variation, there is broad overlap of stable isotopic concentrations across much of the study area.

6.3.3 Tritium

6.3.3.1 Introduction

Tritium (^{3}H) is a radioactive isotope of hydrogen generated naturally in small quantities in the upper atmosphere. It was also artificially produced in large quantities (three orders of magnitude above natural concentrations) during above-ground thermonuclear testing that peaked in the early 1960s. Tritium has a half-life of 12.32 years and is incorporated in small amounts in precipitation and surface waters. As precipitation or surface water infiltrates and becomes groundwater, tritium decays and its presence in groundwater provides an important direct measurement of recent groundwater recharge.

Tritium concentrations are reported in tritium units (TU), where one TU is equivalent to one tritium-containing water molecule per 10^{18} water molecules that lack tritium. Concentrations in meteoric water, measured during the past 60 years, range from natural background levels of 4 to 10 TU to values greater than 1000 TU generated during frequent above-ground thermonuclear testing in the late 1950s and early 1960s (Clark and Fritz, 1997). Due to the short half-life and relatively low initial natural input concentrations, tritium concentrations in groundwater reach levels of less than 0.5 TU in 50 to 60 years. Samples with values less than 0.5 TU therefore consist of water that was recharged prior to the 1950s. Concentrations of tritium greater than 0.5 TU are evidence of at least some component of recharge in the past 60 years, and concentrations greater than 1.0 indicate a sample contains a significant fraction of recharge since 1950 (Clark and Fritz, 1997).

Tritium concentration was measured via two distinct methods at either the University of Utah or at Brigham Young University. Analysis at Brigham Young University was done via sequential electrolytic enrichment of the sample followed by low-level liquid scintillation counting using a Perkin Elmer Quantulus 1220 ultra-machine. All samples were evaluated against blanks and an NIST traceable standard (SRM 4361C) (David Tingey, Brigham Young University, written communication, 2008). Analysis at the University of Utah was done via a tritium-^{3}He ingrowth method detailed by Solomon and Cook (2000). This method measures the concentration of the daughter product of the radioactive decay of tritium, the ^{3}He isotope, during a discrete interval.

Several replicate samples were submitted to each lab and the results overlap within measurement error. Analytical precision varies between the two tritium concentration measurement methods. It is commonly assumed that the lower limit for repeatable tritium measurements using the method used by Brigham Young University is just less than 0.5 TU. The ingrowth method used by the University of Utah is assumed to have a slightly lower threshold of repeatability of 0.3 TU (Vic Heilweil, USGS, personal communication, 2010). Reported concentrations below these values therefore carry inherent error and may record either very low tritium values or no tritium. For subsequent discussions, samples with less than 0.5 TU may be considered to contain negligible tritium concentrations. Both methods yield tritium concentrations sufficient for relative dating and qualitative age estimates.

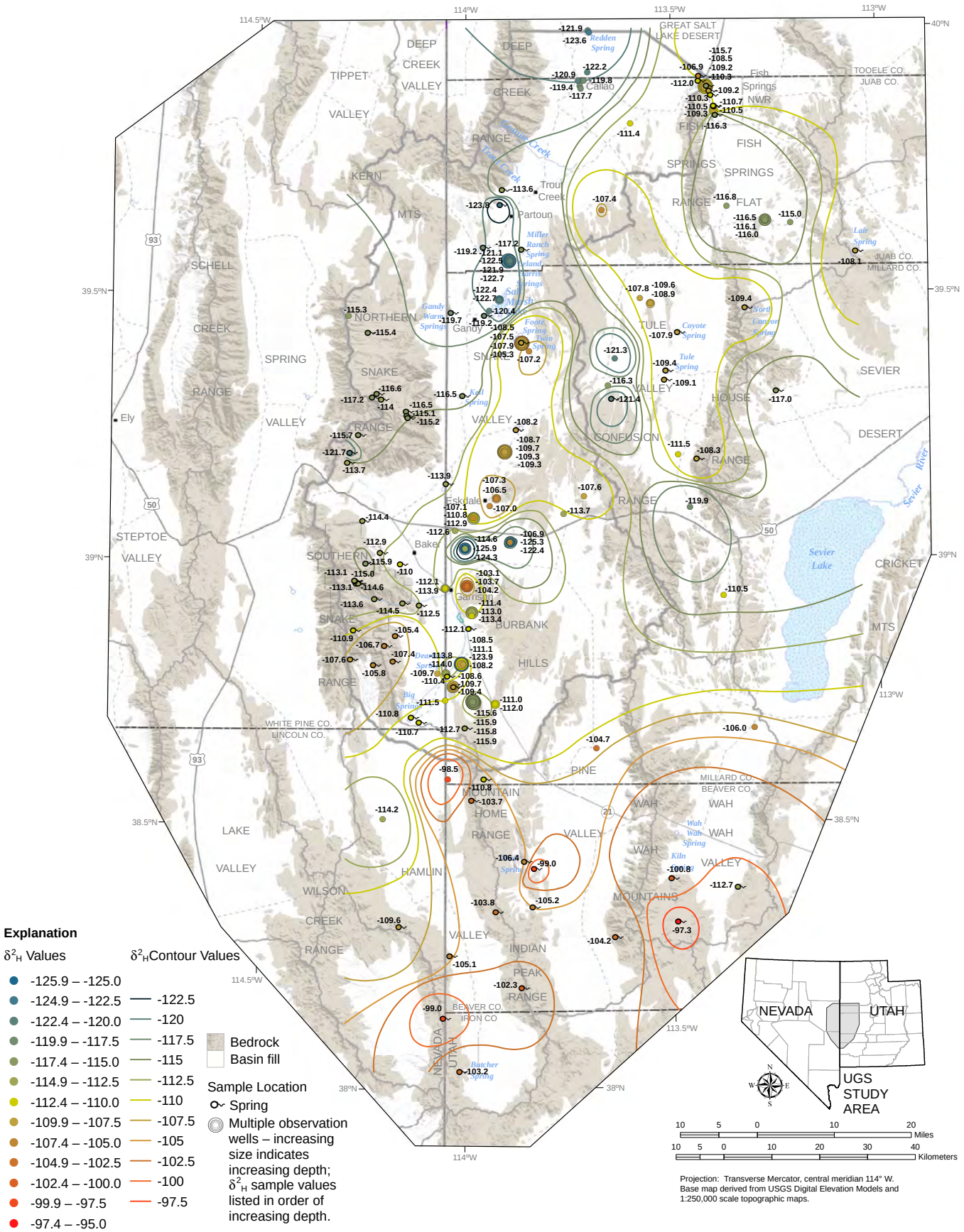

Figure 6.24. *Values of δ^2H for select wells and springs in the UGS study area (table 6.8).*

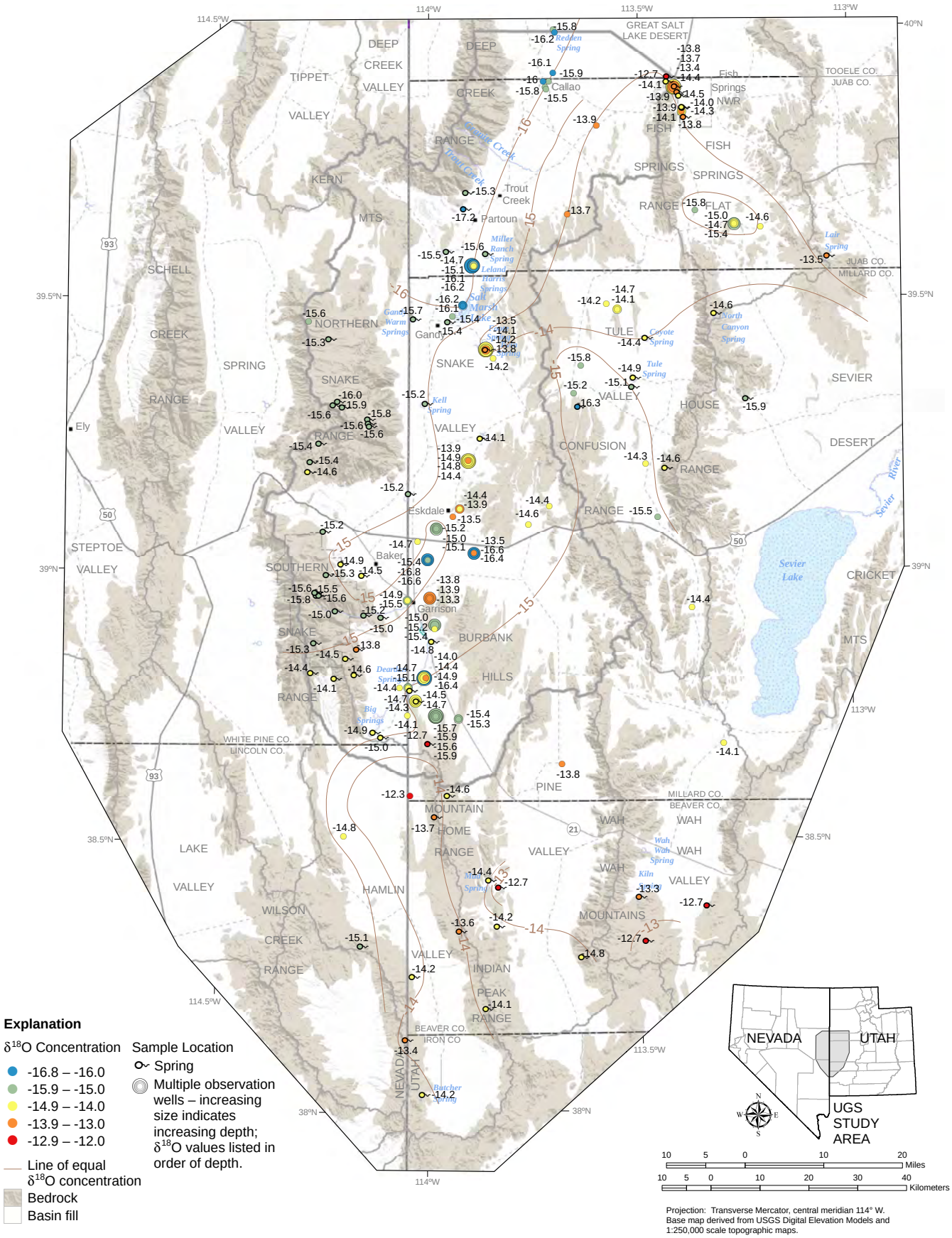

Figure 6.25. *Values of $\delta^{18}O$ for select wells and springs in the UGS study area (table 6.8).*

6.3.3.2 Tritium Results

A subset of 114 samples with tritium data were chosen for further analysis. Tritium values ranged from non-detect to 16.6 TU, and most samples (77) contained less than 0.5 TU (table 6.8). The remaining 37 samples have tritium concentrations greater than 0.5 TU, and 9 samples have tritium concentrations between 0.5 and 1 TU. Six samples have tritium concentration between 1 and 2 TU, and 22 samples have tritium concentrations greater than 2 TU. Based on tritium data alone, two-thirds of these samples show no evidence of recharge since 1950. The remaining one-third have tritium concentrations greater than 0.5 TU and contain varying amounts of water recharged since 1950. More detailed discussion and synthesis of these data with carbon isotopic results is presented in subsequent sections to give a more complete account of both the qualitative and apparent age of given samples.

The spatial distribution of tritium concentrations defines areas that received recent recharge (tritium concentration greater than 1.0 TU) and areas with little (0.5 to 1.0 TU) or no recent recharge (less than 0.5 TU). Samples having tritium concentrations greater than 1.0 TU are located near and south of Garrison on the western flank of Snake Valley, near the Deep Creek Range, at a single piezometer near the Leland Harris spring system north of Gandy, and at isolated springs and wells near the House Range and Wah Wah Mountains (figure 6.26). Samples of groundwater from the spring head at Big Springs and Gandy Springs contain tritium greater than 1.0 TU, and therefore contain a significant fraction of water recharged since 1950. All samples in both Tule Valley and Fish Springs Flat contain less than 1.0 TU. Significant modern recharge (since 1950) is therefore limited to western Snake Valley and near mountain ranges in the remainder of the study area. Several sites in Tule Valley and Fish Springs Flat have tritium concentrations equal to or slightly greater than 0.5 TU, possibly indicating a small fraction of localized modern recharge. Alternately, these samples may result from atmospheric contamination of samples taken from spring pools at Fish Springs, or incomplete well development or purging in the case of samples from PW19C and early samples collected from PW17C. Tritium concentrations are generally less than 0.5 TU, indicating no significant modern recharge, away from mountain ranges and across most of the study area.

6.3.3.3 Apparent Tritium Ages

The apparent age of a sample may be calculated by the tritium ingrowth method, which uses the concentration of ^{3}He and certain assumptions concerning the dissolved gas characteristics of recharge water to model the age of a groundwater sample (Solomon and Cook, 2000). The apparent age estimates presented here were modeled by P. Gardner (U.S. Geological Survey) using spreadsheets available from the University of Utah Dissolved Gas Laboratory. Gardner and Heilweil (2014) presented complete dissolved gas data and methodology for these samples. Apparent age is calculated for eight of the sites that have tritium concentrations greater than 0.5 TU and total dissolved gas measurements. These samples are shown on figure 6.26 along with tritium concentration data. These sites have apparent ages of recharge that range from 17 to 54 years (table 6.8). Most of these sites (PW01B, PW03A, PW03B, AG13A, AG13B, and AG13C) are located in agricultural areas near Garrison. Groundwater in this area may receive recharge from both unconsumed irrigation water and surficial recharge from Snake Creek and Pruess Lake. Site 16A is located to the south near Davies Ranch in an area where unlined canals and irrigation may provide the source of recharge. The remaining sample was collected from the springhead at Big Springs, with an apparent tritium age of 30 years and a pMC less than 50, representing a mix of old and modern water. Recent recharge at Big Springs likely occurs from runoff and infiltration of precipitation from the nearby southern Snake Range.

6.3.4 Carbon Isotopes

6.3.4.1 Introduction

The isotopes of carbon dissolved in groundwater, ^{13}C and ^{14}C, provide quantitative information about residence time, recharge rates, flow paths, and the hydrochemical evolution of the aqueous and mineral phases of a groundwater system (Plummer and others, 1994; Clark and Fritz, 1997). The radiogenic isotope ^{14}C has a half-life of 5730 years, and by making assumptions about the recharge conditions and hydrochemical sources and sinks for this isotope in the groundwater system, both qualitative age and apparent age of the old component of a groundwater sample can be estimated (Plummer and others, 1994). Measurements of ^{14}C in groundwater use percent modern carbon (pMC) which is the percent of ^{14}C relative to an atmospheric standard taken in the 1950s. Measurements of ^{13}C are commonly presented as an isotopic ratio ($^{13}C/^{12}C$) and reported as delta (δ) values in units of parts per thousand (per mil, or ‰) relative to the standard Pee Dee Belemnite (PDB) reference sample standard using methods described by Coplen (1996).

Radiogenic carbon (^{14}C) is generated naturally in the upper atmosphere and subsequently incorporated into very small quantities of CO_2 gas molecules. Atmospheric concentrations of ^{14}C are approximately one ^{14}C bearing CO_2 molecule for every 10^{12} ^{14}C-free CO_2 molecules (Clark and Fritz, 1997). The stable isotope of carbon (^{13}C) also

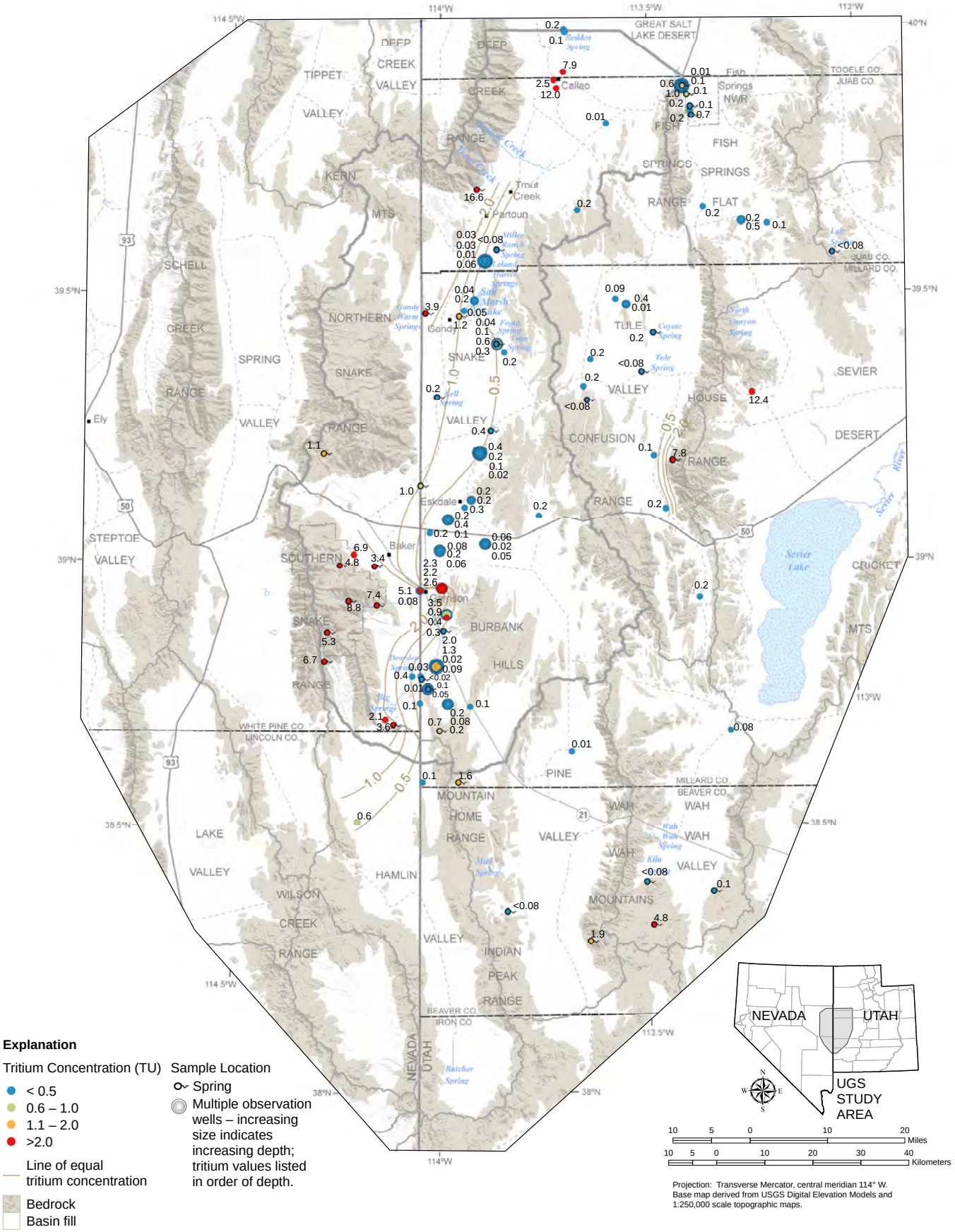

Figure 6.26. *Tritium concentration values (TU) for select wells and springs in the UGS study area (table 6.8).*

exists in measurable and distinct concentrations in atmospheric, hydrologic, and mineralogic parts of the carbon system. As CO_2 gas is circulated in the atmosphere and biosphere, radiogenic ^{14}C and stable ^{13}C are distributed in relatively consistent concentrations throughout the atmosphere. Recharge that infiltrates through the unsaturated zone dissolves a component of soil gases, including CO_2, with atmospheric concentrations of ^{14}C and plant-modified ^{13}C concentrations. This isotopic signature is incorporated into groundwater, primarily as dissolved inorganic carbon (DIC). DIC in groundwater at typical pH and temperatures is dominated by the bicarbonate anion. This anion readily interacts with carbonate minerals (primarily calcite and dolomite) and the potential exists for isotopic fractionation (generally producing a lower pMC concentration) as ^{14}C-free mineral carbon is exchanged for part of the DIC in groundwater. The ^{13}C isotope is also fractionated during this process, generally yielding more enriched or larger $\delta^{13}C$ values.

PMC concentrations in recently recharged groundwater are typically less than atmospheric concentrations (~100 pMC) (Plummer and others, 1994; Clark and Fritz, 1997; Zhu and Murphy, 2000), and may be as low as ~50 pMC in recently recharged groundwater due to fractionation in the unsaturated zone. Values of pMC decrease following recharge, and the rate of decrease is dependent on radioactive decay and gas and mineral interactions. Carbon isotopic fractionation and evolution in the aqueous system is recorded by the $\delta^{13}C$ value (Clark and Fritz, 1997). Generally more enriched $\delta^{13}C$ (higher values) corresponds with increased residence time and carbon mass transfer (Clark and Fritz, 1997). Relatively depleted $\delta^{13}C$ (lower values) likely represents decreased residence time, where the carbon isotopic system is less evolved and there is less hydrochemical evidence of interaction between the aquifer matrix and groundwater (Plummer and others, 1994).

All samples collected by the UGS for carbon isotope analysis were processed to concentrate at the Brigham Young University Hydrogeochemistry Laboratory and then shipped to the University of Georgia Center for Applied Isotope Studies and analyzed by accelerator mass spectrometry. Samples were analyzed for ^{13}C and ^{14}C using a National Electrostatics Corporation Model 1.5SDH-1 AMS.

6.3.4.2 Carbon Isotope Results

Carbon isotope results for 108 samples were chosen from the compiled dataset and the samples collected for this study for more detailed analysis (table 6.8). This subset includes the most recent sample collected by this study from a given site using either a downhole or peristaltic sampling pump. Values of pMC range between 0.72 and 109. The mean pMC concentration is 35, and 31 samples have a pMC value greater than 50 indicative of premodern (less than about 1000 years and before 1950) or modern (since the 1950s) groundwater recharge. Of the remaining 77 samples, 46 have pMC between 10 and 50, and 31 samples have pMC less than 10. Samples with pMC less than 50 contain a significant fraction of groundwater recharged hundreds to thousands of years ago and may be examined in greater detail to estimate the apparent age of the old fraction of groundwater in a given sample. The values of $\delta^{13}C$ range between -1.23 and -13.70‰ and have a mean of -7.62‰.

The relationship between stable and radiogenic carbon isotopes in the DIC of groundwater in the study area is summarized by a plot of $\delta^{13}C$ versus pMC (figure 6.27). Recently recharged groundwater samples plot to the lower right and older groundwater samples that may have undergone significant water-mineral isotopic fractionation plot in the upper left. The correlation of decreasing pMC with enriched $\delta^{13}C$ is consistent with mineral-DIC interactions being the dominant process by which isotopic fractionation of carbon is occurring (Clark and Fritz, 1997). Significant spread exists among samples, suggesting a large variation in the relative amount and type of mineral-DIC interactions and likely variations in the initial carbon isotopic content of groundwater recharged at different times and in different locations. Samples are symbolized by geographical group to show trends in carbon isotopic composition based on location. Samples from Snake Valley define a broad zone that follows the general trend of increasing $\delta^{13}C$ with decreasing pMC, and include both recently recharged and older groundwaters that may have undergone varying amounts of carbon isotope exchange and fractionation. Samples from Tule Valley plot in a range that overlaps those from Snake Valley. Samples from Fish Springs Flat show relatively little carbon isotope variability and primarily consist of low-pMC and high-$\delta^{13}C$ groundwater. Values of $\delta^{13}C$ are variable for given pMC values across the samples, supporting varying degrees of isotopic fractionation and radioactive decay that produce measured pMC values.

The spatial patterns of carbon isotope concentrations show broad trends of recharge and discharge that are similar in most cases, with areas of low pMC corresponding with areas of high $\delta^{13}C$ (figures 6.28 and 6.29). The highest pMC values, greater than 75 pMC, are located near or in upland mountain ranges that include the northern and southern Snake Range, Deep Creek Range, House Range, and Wah Wah Mountains. Values of pMC decrease away from these areas, and the lowest values are found in and near Coyote Springs in Tule Valley, at Fish Springs, and to the south in Fish Springs Flat at site PW19C. Within

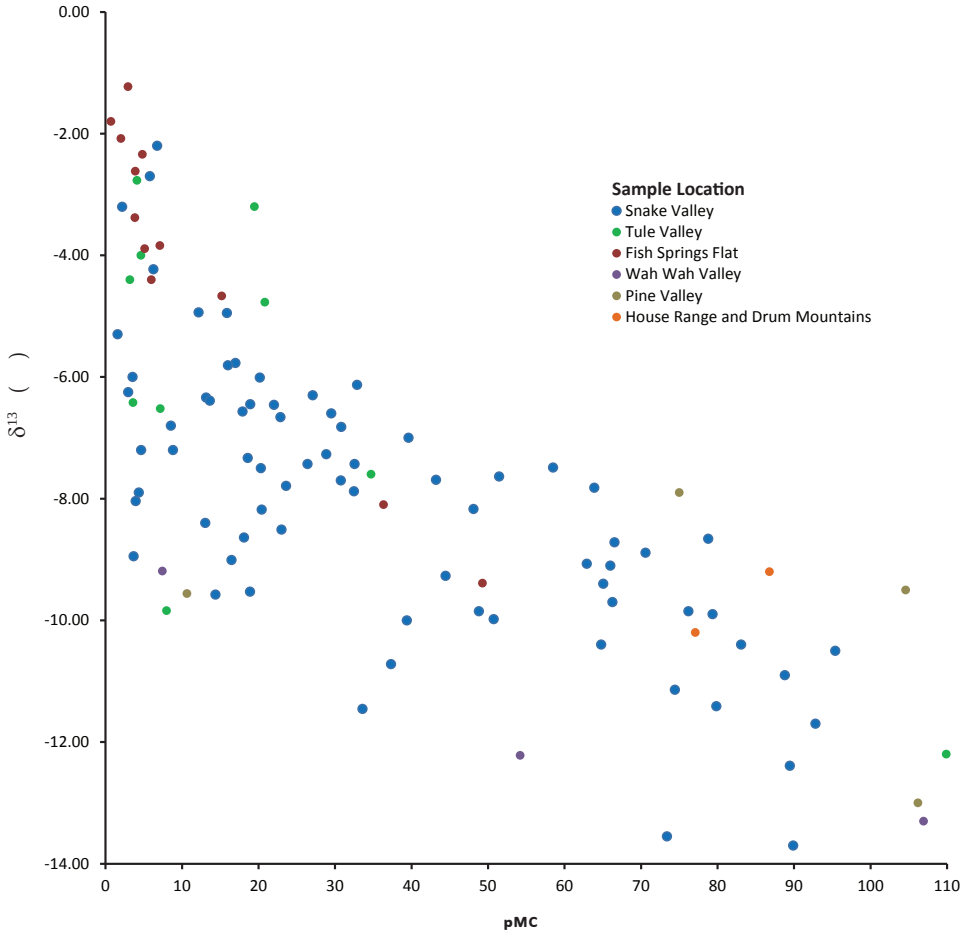

Figure 6.27. *$\delta^{13}C$ versus percent modern carbon (pMC) for select wells and springs (table 6.8).*

Snake Valley, pMC values generally decrease west to east, and the lowest pMC values are at piezometers completed in relatively low-permeability basin fill (sites PW05B and C, and PW07A and B) and near Twin Springs (SG24B). The distribution of $\delta^{13}C$ is correlated with pMC; lower $\delta^{13}C$ values correlate with areas of recharge and high pMC, and higher $\delta^{13}C$ values are found in areas with low pMC.

6.3.4.3 Apparent Carbon Isotopic Ages

An apparent age may be calculated when initial and final concentrations of radiogenic isotopes are known or estimated. Apparent age of recharge may therefore be directly calculated for samples using ^{14}C concentration (pMC), a standard decay equation, and the known half-life. The apparent age of the old component is calculated for samples with pMC less than 50 via several different methods detailed below. Groundwater commonly represents a mixture of water recharged at different times; all apparent age data should be assumed to represent the mean age of a given sample, weighted according to the relative percentage of different recharge components.

Apparent-age calculations use pMC measured in groundwater, the standard exponential decay function, and ^{14}C half-life of 5730 years. The simplest form of this calculation assumes the initial pMC in DIC is equal to the atmospheric concentration of 100%. This uncorrected age (table 6.8) represents the oldest possible age for a given sample. In many groundwater systems and particularly in the study area, there is the potential for significant carbon isotope exchange and fractionation between DIC and mineral or gas phases that yield initial pMC values much less than 100% both in the saturated and unsaturated zone. To account for carbon isotope exchange and fractionation and provide a reasonable range of apparent ages for a given sample, three formula-based corrections and one correction based on average pMC of modern recharge were also calculated. The formula-based corrections use the measured $\delta^{13}C$ value (Pearson and Hanshaw, 1970; Clark and Fritz, 1997) and hydrochemistry (Fontes and Garnier, 1979) of a given sample to estimate initial pMC and

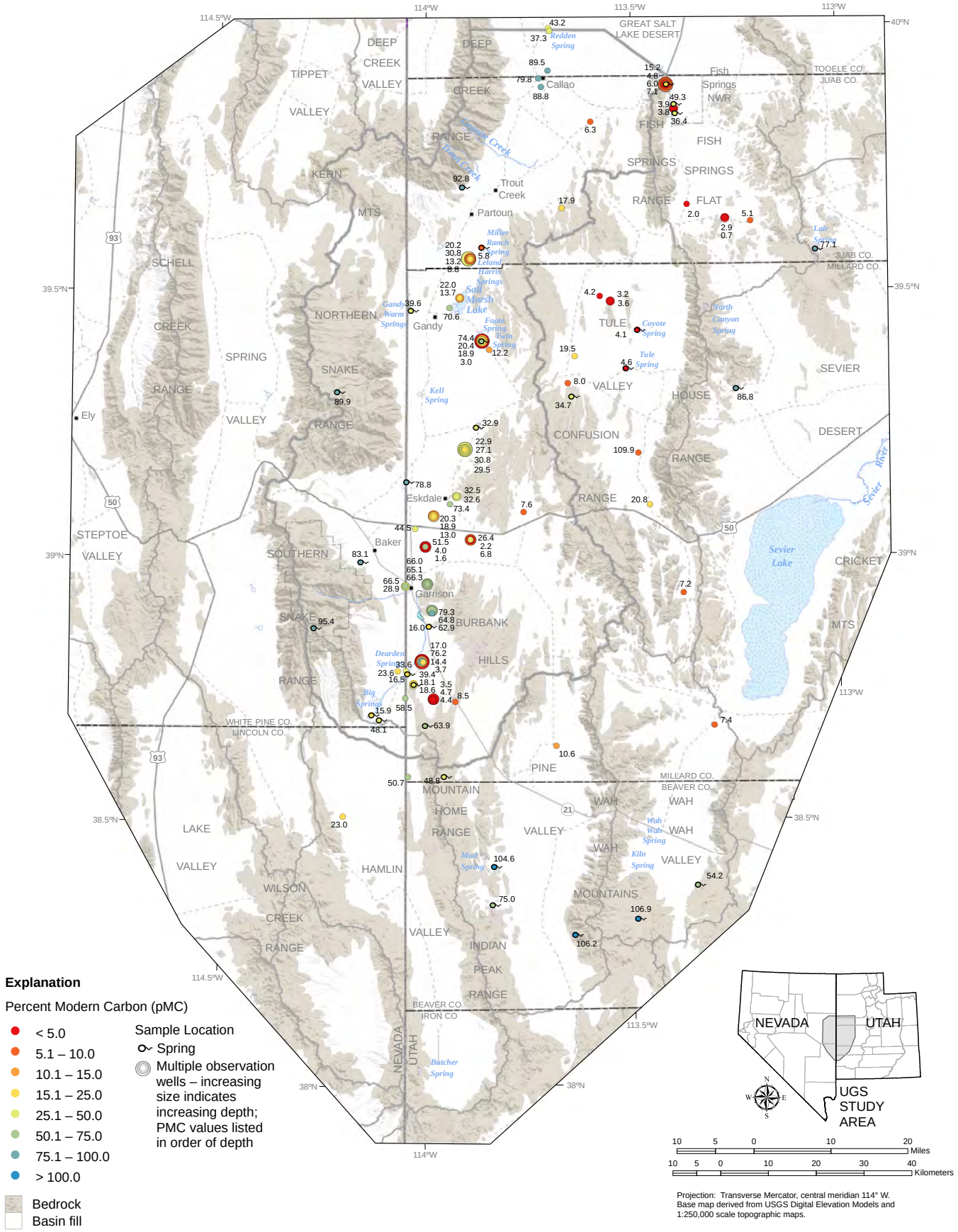

Figure 6.28. *Percent modern carbon (pMC) for select wells and springs in the UGS study area (table 6.8).*

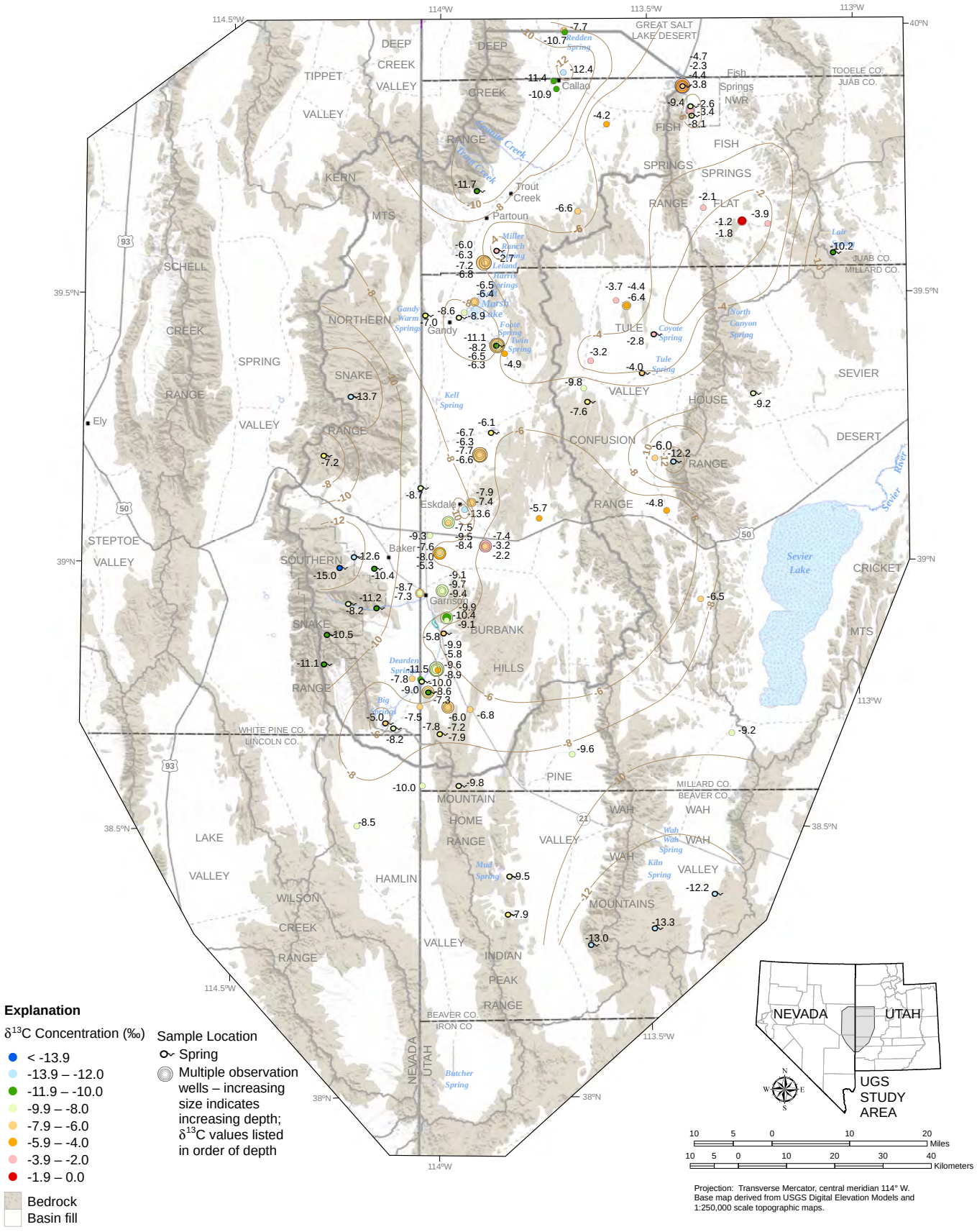

Figure 6.29. *Values of $\delta^{13}C$ for select wells and springs in the UGS study area (table 6.8).*

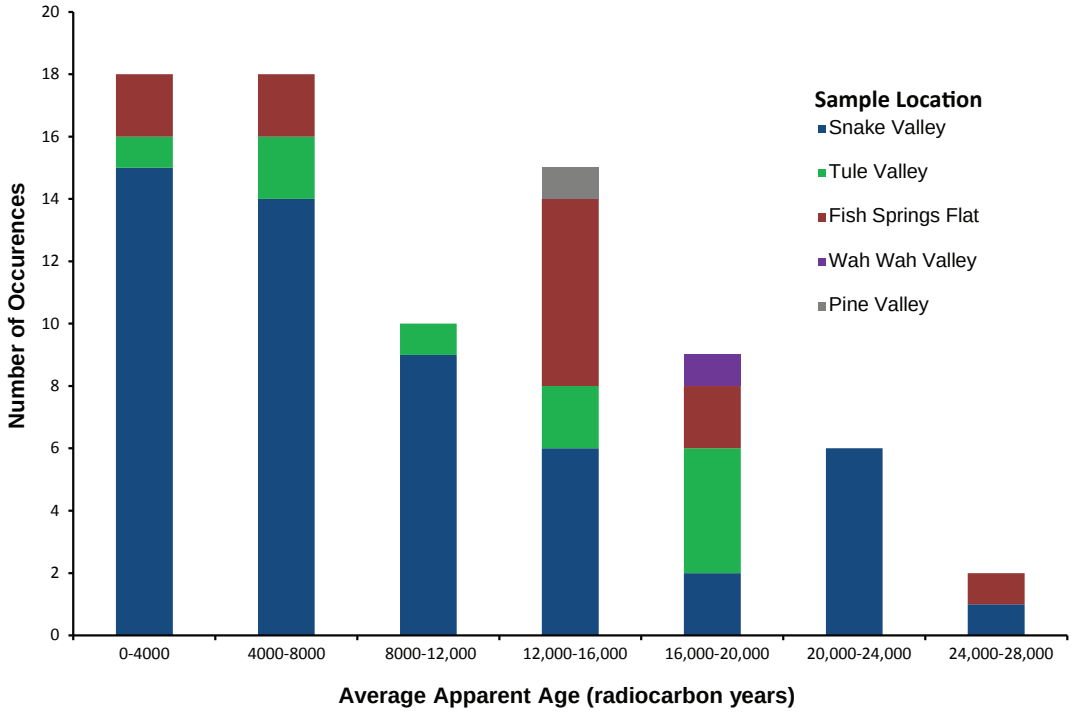

Figure 6.30. *Histogram of average apparent age for select samples (table 6.8).*

apparent age. Carbon isotope assumptions used for these models include (1) ^{14}C soil gas = 100 pMC, (2) carbonate-mineral ^{14}C = 0 pMC, (3) $\delta^{13}C$ soil gas = −22.5‰, and (4) carbonate-mineral $\delta^{13}C$ = 0‰. Isotopic assumptions are based on recent measurements of soil gas in Utah (Hart and others, 2010) and worldwide measurements of the isotopic composition of carbonate minerals (Clark and Fritz, 1997). These formulas do not always yield reasonable ages (greater than zero or less than the uncorrected value) and individual samples may not have a calculated apparent age via each method. Apparent age is also estimated assuming initial pMC concentration for a given sample is equal to the average value (pMC = 66) of samples identified as modern (recharged since 1950) in previous sections. Each sample in table 6.8 may therefore have up to five unique estimates of apparent age of the old fraction, all of which are hydrochemically plausible. These apparent ages provide a reasonable range of the old component of groundwater in the sample, but not a unique age. The average of the four corrected ages is presented as the best estimate of apparent age for a given sample because it includes all reasonable age corrections (table 6.8).

Apparent age is calculated for a subset of 77 samples classified as old or mixed age. The mean of the average age is 10,500 years and the median is 9000 years. The maximum average age is 27,500 years and the minimum age is 2300 years. A histogram of average apparent age by geographic area shows that most samples in Snake Valley contain water recharged in the past 12,000 years (figure 6.30). Samples corresponding to hydrochemical group 2 have average ages of less than 8000 years. Samples from Tule Valley include apparent ages that range to 24,000 years and generally are evenly distributed across this range. Most samples from Fish Springs Flat have average ages between 12,000 and 16,000 years, but this group also includes several samples younger and older than this range.

The spatial distribution of average apparent age is complex, but generally groundwater age increases to the north and east across the study area (figure 6.31). Fish Springs Flat and Tule Valley have numerous samples with ages greater than 12,000 years, whereas much of Snake Valley is characterized by average apparent ages less than 8000 years. The heterogeneous but generally increasing apparent ages with decreasing elevation mirrors much of the previous isotopic results that indicate active recharge occurs primarily along the eastern flank of the Snake Range and Deep Creek Range; elsewhere, away from uplands, most groundwater recharged thousands of years ago. The apparent age of samples collected at and near Fish Springs show important variability with ages ranging from 6700 years near North Spring to 16,600 years for site SG21B, indicating that groundwater of various ages and, necessarily, various flow paths is discharging at Fish Springs. Samples from Persey and Mirror Springs both have apparent ages less than 3000 years that may result from atmospheric contamination of carbon isotopes at these spring pools.

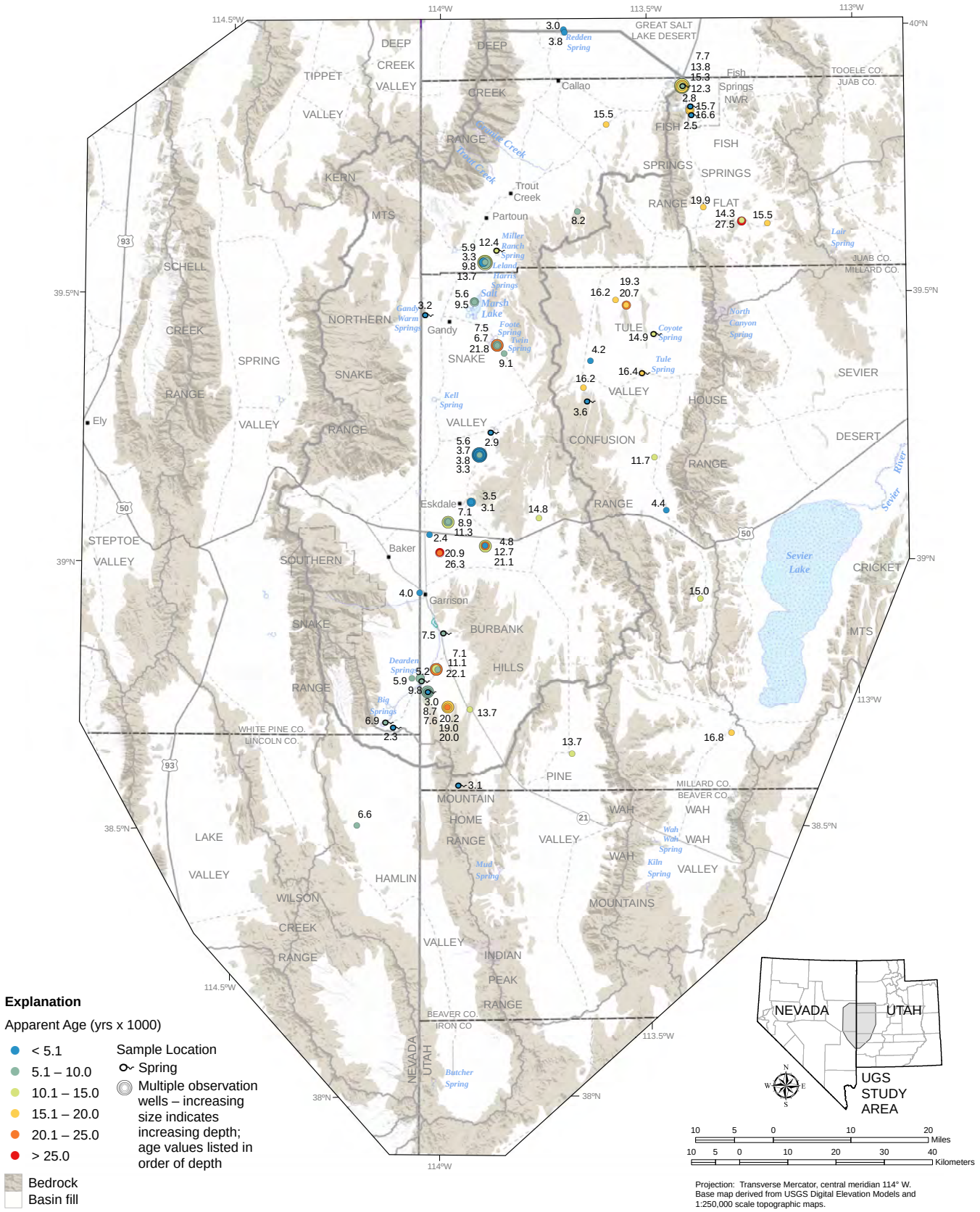

Figure 6.31. *Apparent groundwater age from select wells and springs in the UGS study area.*

6.3.5 Age of Groundwater

Tritium and pMC concentrations provide two independent measures of the relative age of a groundwater sample. By combining data from these radiogenic tracers for a given sample, a robust qualitative estimate of the residence time can be made. These qualitative age constraints were applied to a subset of 106 samples that include both carbon isotope and tritium data (table 6.8).

Samples having tritium concentrations greater than 0.5 TU and pMC greater than 50 consist of a large fraction of water recharged since 1950, and are termed modern in table 6.8. A second category of young, premodern groundwater is assigned to samples that contain pMC greater than 50 but have tritium concentrations less than 0.5 TU. Apparent age of these samples may be assumed to be greater than 50 to 60 years but less than 1000 years, and many of these samples were likely recharged hundreds of years ago. All of the remaining samples contain a significant fraction of old water recharged more than 1000 years ago. These samples have pMC values less than 50 and either tritium less than 0.5 TU, in the case of old samples, or tritium greater than 0.5 TU for samples that are termed mixed. Mixed samples contain at least a small amount of tritiated groundwater recharged since 1950 (tritium greater than 0.5 TU) in addition to a significant fraction of old groundwater (pMC less than 50).

There are 29 samples that have pMC values greater than or equal to 50, thus lacking a significant fraction of old water. Nineteen of these samples are classified as modern, consisting primarily of groundwater recharged since 1950, and 10 samples are classified as premodern, consisting of groundwater recharged prior to 1950 but within the last 1000 years. All 77 remaining samples have pMC values less than 50 and contain a significant fraction of groundwater recharged more than 1000 years ago. Of the samples having pMC less than 50, 10 also have tritium concentrations greater 0.5, and these samples represent mixed groundwater with both old and young fractions. Sixty-seven samples are classified as old with pMC less than 50 and tritium less than 0.5 TU (figure 6.32).

The spatial distribution of relative ages mirrors many of the previous isotopic distributions and shows that significant recent recharge (modern or premodern) occurs along the west flank of Snake Valley, near Garrison, and near isolated uplands elsewhere (House Range, Wah Wah Mountains, Mountain Home Range) (figure 6.33). Most samples collected from sites along the floor of Snake Valley, Tule Valley, and Fish Springs Flat are either old or mixed-age samples and show little evidence of recent recharge. Samples from the springhead at Gandy Warm Springs and

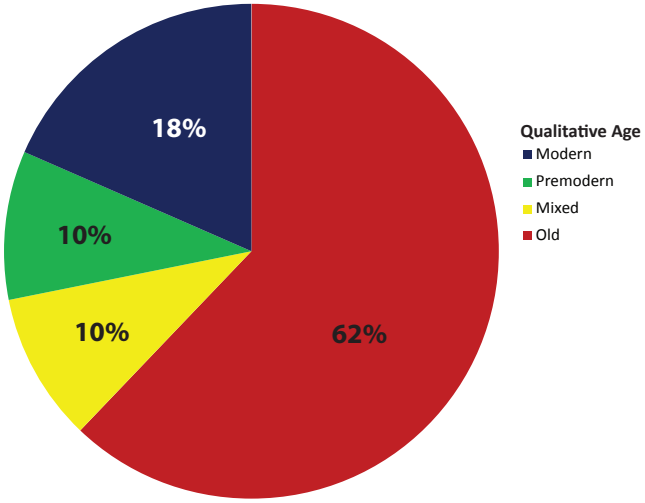

Figure 6.32. *Qualitative ages of select wells and springs.*

Big Springs indicate mixed-age groundwater with significant components of both young and old groundwater. Elsewhere, most samples indicate groundwater recharge that occurred more than 1000 years ago, and most sites from Fish Springs and Tule Valley indicate old (either far or slowly traveled) groundwater. Minor amounts of modern recharge mixing with much older water occur in all valleys, but most groundwater sampled in the study area away from upland sources of recharge is old.

6.4 DISCUSSION

The distribution of major solute concentrations in the Snake Valley area of western Utah follows systematic spatial and compositional trends. Groundwater chemistry is generally correlated with location along hypothesized flow paths from recharge to discharge areas. Groundwater types range from calcium-bicarbonate typical of upland recharge areas to chloride or sulfate type groundwater in areas of discharge. Groundwater quality is generally good and most samples have TDS concentrations less than 1000 mg/L. High TDS, greater than 1000 mg/L, occurs primarily in Tule Valley and Fish Springs Flat. Nitrate concentrations are generally low and within drinking water standards. Isolated samples of high nitrate are localized and do not appear related to land use. Concentrations of arsenic are locally high, and nearly a quarter of the samples have concentrations greater than 10 µg/L and just less than half of samples have concentrations greater than 5 µg/L.

Factor analysis of solute chemistry suggests relatively simple water-rock interactions dominated by dissolution of calcite, dolomite, gypsum, and halite; these water-rock interactions account for most of the variability

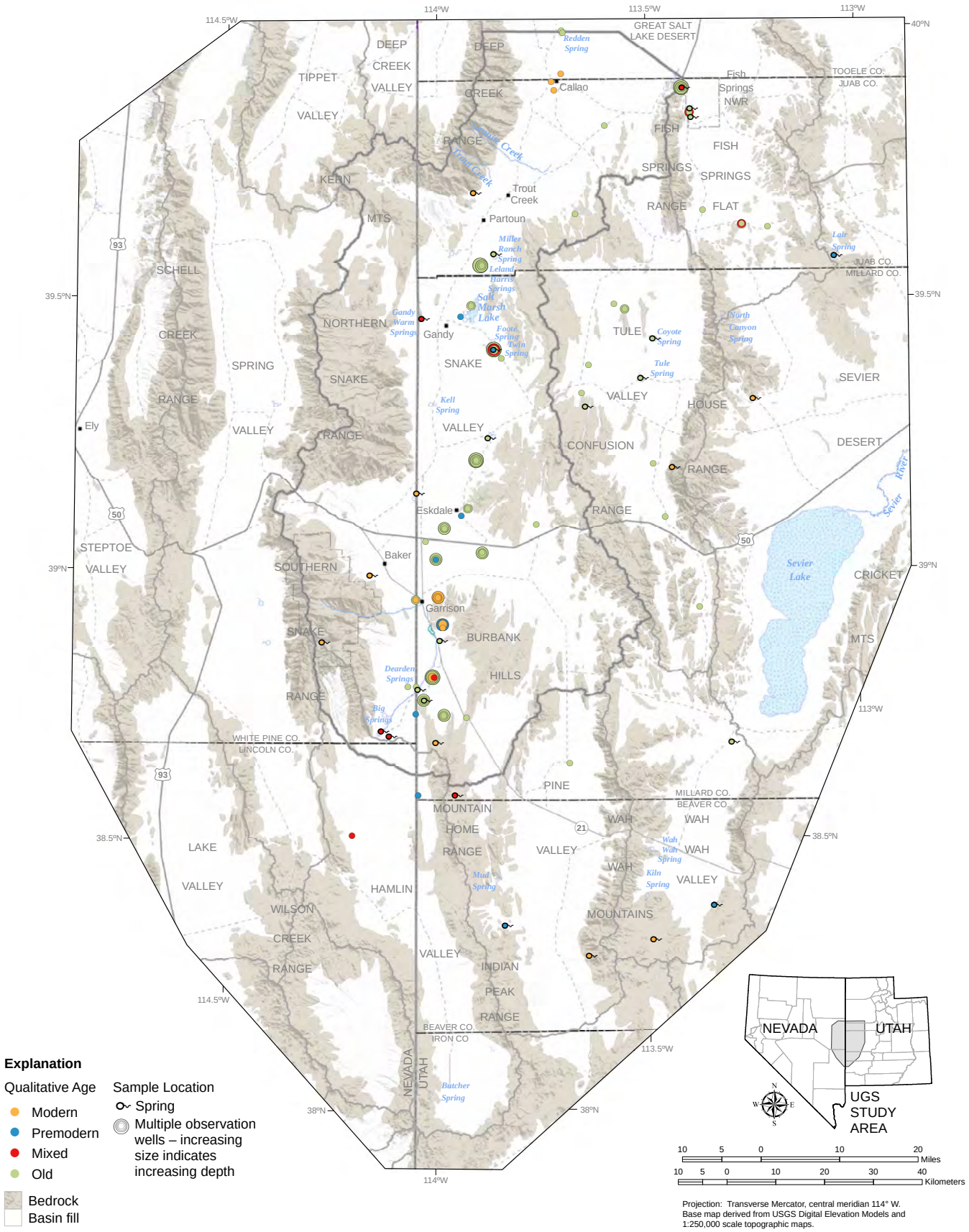

Figure 6.33. *Qualitative ages of select wells and springs in the UGS study area.*

among solute concentrations. Hierarchical cluster analysis yields six sample groupings and groundwater types that objectively categorize solute chemistry into six water types (hydrochemical groups) based primarily on increasing concentrations of chloride, sulfate, and sodium. These clusters are generally robust with each group consisting of similar ranges of concentrations of sodium, chloride, and sulfate. There is overlap amongst the constituents of calcium, magnesium, and bicarbonate. The spatial distribution of the hydrochemical facies follows a predictable pattern, where groups having low relative concentrations of chloride and sulfate are located near areas of recharge along the eastern flanks of the Snake Range and Deep Creek Range and at mountain ranges elsewhere in the study area. As groundwater elevation decreases, and near areas of discharge including Fish Springs and the lower reaches of Tule Valley, chloride and sulfate composition increase and calcium is replaced by sodium as the principal cation. Chemical composition and hydrochemical grouping is dependent on residence time and hydrogeology. Simple inverse hydrochemical models constrained by measured solute chemistry and mineral saturation states can account for changes in groundwater between the six groups along a series of hypothesized flow paths.

The model results necessarily represent an oversimplified view of the potential hydrochemical evolution of the groundwater system. These models cannot account for all possible initial and final water compositions or potentially available mineral and gas phases. The models also do not examine the potential for waters not included in the dataset (e.g., deep-basin brines) to interact with water in the active groundwater system. Instead, these models provide simple and consequently robust hydrochemical links between most of the groundwater groups and groundwater samples in this dataset. The plausibility of the hydrochemical models implies that flow paths are possible among the hydrochemical groups, and therefore across much of the study area. Because of inherent ambiguity and error in simplified hydrochemical modeling relative to actual hydrochemical processes, unknowns, and gaps in characterization of groundwater chemistry, these results alone do not require groundwater flow across topographic basin boundaries, such as between Snake Valley and Tule Valley. However, they lend support to localized flow across topographic basin boundaries.

Based on the data presented above, groundwater chemistry across the study area may represent a continuum of hydrochemical evolution as water moves from recharge to discharge areas. This has important implications for groundwater flow between hydrographic basins (chapter 8), and ultimately the recharge area for major springs and discharge zones to the north and east of Snake Valley.

Dissolved-gas recharge temperatures indicate that most groundwater in Snake Valley was recharged under cool temperatures (<10°C), indicative of direct infiltration of upland precipitation in the Snake Range and Deep Creek Range and at upland areas to the east. The temperature of recharge is greater than 10°C across eastern parts of Snake Valley and parts of Tule Valley and Fish Springs Flat, and may indicate limited recharge along valley floors and/or recharge in deep water-table settings potentially affected by the geothermal gradient. Samples with recharge temperatures greater than 20°C occur in Tule Valley and Fish Springs Flat and may result from deep water-table recharge or gas loss (gas stripping), either in the aquifer (Thomas and others, 2003) or upon sample collection.

The isotopic ratios δ^2H and $\delta^{18}O$ from groundwater in the Snake Valley area plot along the local meteoric water line of Kendall and Coplen (1996) and generally below the global meteoric water line of Craig (1961). General overlap exists amongst samples taken from different basins and geographic locations. Samples collected in Tule Valley plot within the extent of samples collected in Snake Valley. Most samples from Fish Springs Flat also plot within the extent of the Snake Valley samples. Samples from Wah Wah Valley and Pine Valley are enriched relative to most of the other samples, but still plot largely within the range of samples collected in Snake Valley. Three samples from the House Range and Drum Mountains also plot within the range of samples collected from Snake Valley.

Data for both tritium and pMC provide additional support for a conceptual model where most groundwater recharge occurs along and near the mountain front of the Snake Range and Deep Creek Range and at isolated upland locations to the east in the House Range and elsewhere. Away from these locations groundwater recharge is generally minimal. Percent modern carbon generally decreases and apparent age generally increases away from sources of recharge near the Snake Range and Deep Creek Range. This is broadly consistent with longer flow paths and residence times for groundwater in Tule Valley and Fish Springs Flat. Groundwater discharging at Fish Springs is old, but contains a range of apparent ages consistent with multiple flow paths from different locations (some of which could come from northern parts of Snake Valley) converging at these springs.

Environmental-tracer data indicate that more than half of the groundwater sampled in the Snake Valley area is old, and modern recharge comprises less than a fifth of all the samples. Samples classified as premodern or mixed comprise the remaining 25% of the dataset. Modern water is limited to parts of southern Snake Valley and other isolated areas, likely supplied by uplands having relatively high

precipitation and recharge rates. Apart from these areas, most groundwater is old, implying that low recharge rates and/or long flow paths are typical of much of the Snake Valley groundwater system. The environmental-tracer results suggest that away from localized major sources of recharge in mountain ranges, groundwater is recharged very slowly, if at all.

Environmental-tracer data and measured groundwater levels in wells and springs, collected by the UGS, provide the basic data that constrain the Snake Valley groundwater flow system. All other refinements of our understanding of groundwater in Snake Valley, including numeric models and hydrogeologic framework studies, must also explain the distribution of basic hydrochemistry, dissolved gas composition, and environmental tracers such as stable isotopes, carbon-14, and tritium. These data, therefore, provide the fundamental information that allows water managers to make informed decisions concerning water allocation and use.

6.5 CHAPTER 6 REFERENCES

Acheampong, S.Y., Farnham, I.M., and Watrus, J.M., 2009, Geochemical characterization of ground water and surface water of Snake Valley and the surrounding areas in Utah, *in* Tripp, B.T., Krahulec, K., and Jordan, J.L., editors, Geology and geologic resources and issues of western Utah: Utah Geological Association Publication 38, p. 325–344.

Aeschbach-Hertig, W., Peeters, F., Beyerle, U., and Kipfer, R., 1999, Interpretation of dissolved atmospheric noble gases in natural waters: Water Resources Research, v. 35, p. 2779–2792.

Aeschbach-Hertig, W., Peeters, F., Beyerle, U., and Kipfer, R., 2000, Paleotemperature reconstruction from noble gases in ground water taking into account equilibration with entrapped air: Nature, v. 405, p. 1040–1043.

Anderson, M.P., 2005, Heat as a groundwater tracer: Groundwater, v. 43, p. 951–968.

Back, W.B., Hanshaw, B., Plummer, L.N., Rahn, P.H., Rightmire, C.T., and Rubin, M., 1983, Process and rate of dedolomitization—mass transfer and ^{14}C dating in a regional carbonate aquifer: Geological Society of America Bulletin, v. 94, p. 1415–1429.

Blackett, R.E., 2011, Temperature profiles of water monitoring wells in Snake Valley, Tule Valley, and Fish Springs Flat, Millard and Juab Counties, Utah: Utah Geological Survey Open-File Report 578, 13 p.

Bolke, E.L., and Sumsion, C.T., 1978, Hydrologic reconnaissance of the Fish Springs Flat area, Tooele, Juab, and Millard Counties, Utah: Utah Department of Natural Resources Technical Publication No. 64, 30 p.

Bowen, G.J., and Revenaugh, J., 2003, Interpolating the isotopic composition of modern meteoric precipitation: Water Resources Research, v. 39, p. 9–13.

Carlton, S.M., 1985, Fish Springs multibasin flow system, Nevada and Utah: Reno, University of Nevada, M.S. thesis, 103 p.

Clark, I., and Fritz, P., 1997, Environmental isotopes in hydrogeology: New York, Lewis Publishers, 328 p.

Coplen, T.B., 1996, New guidelines for reporting stable hydrogen, carbon, and oxygen isotope-ratio data: Geochimica et Cosmochimica Acta, v. 60, p. 3359–3360.

Craig, H., 1961, Isotopic variation in meteoric waters: Science, v. 133, p. 1702–1703.

Dalton, M.G., and Upchurch, S.B., 1978, Interpretation of hydrochemical facies by factor analysis: Ground Water, v. 16, no. 4, p. 228–233.

Dansgaard, W., 1964, Stable isotopes in precipitation: Tellus, v. 16, p. 436–467.

Dawd, D.R., and Feth, J.H., 1967, Applications of factor analysis in study of chemistry of groundwater quality, Mojave River Valley, Californa: Water Resources Research, v. 3, no. 2, p. 505–510.

Domenico, P.A., and Schwartz, F.W., 1997, Physical and chemical hydrogeology: New York, John Wiley and Sons, 506 p.

Everitt, B.S., and Torsten, H., 2006, A handbook of statistical analyses using R: Boca Raton, Florida, Chapman and Hall/CRC, 304 p.

Fontes, J.C., and Garnier, J.M., 1979, Determination of the initial ^{14}C activity of the total dissolved carbon—a review of the existing models and a new approach: Water Resources Research, v. 15, p. 399–413 (doi: 10.1029/WR015i002p00399).

Freeze, R.A., and Cherry, J.A., 1979, Groundwater: Englewood Cliffs, New Jersey, Prentice Hall, 604 p.

Friedman, I., Smith, G.I., Johnson, C.A., and Moscati, R.J., 2002, Stable isotope compositions of waters in the Great Basin, United States, 2, modern precipitation: Journal of Geophysical Research, v. 107, p. 1–21 (doi: 10.1029/2001JD000566).

Gardner, P.M., Heilweil, V.M., 2014, A multiple-tracer approach to understanding regional groundwater

flow in the Snake Valley area of the eastern Great Basin, USA.: Applied Geochemistry, v. 45, p. 33–49.

Gardner, P.M., Masbruch, M.D., Plume, R.W., and Buto, S.G., 2011, Regional potentiometric surface map of the Great Basin carbonate and alluvial aquifer system in Snake Valley and surrounding areas, Juab, Millard, and Beaver Counties, Utah, and White Pine and Lincoln Counties, Nevada: U.S. Geological Survey Scientific Investigations Map 3193.

Gates, J.S., and Kruer, S.A., 1981, Hydrologic reconnaissance of the southern Great Salt Lake Desert and summary of the hydrology of west-central Utah: Utah Department of Natural Resources Technical Publication No. 71, 55 p.

Gillespie, J.M., 2008, A conceptual model of groundwater flow in Spring Valley, Nevada, and Snake Valley, Nevada-Utah: Provo, Utah, Brigham Young University, M.S. thesis, 80 p.

Gillespie, J., Nelson, S.T., Mayo, A.L., and Tingey, D.G., 2012, Why conceptual groundwater flow models matter—a trans-boundary example from the arid Great Basin, western USA: Hydrogeology Journal (doi: 10.1007/s10040-012-0848-0).

Guler, C., and Thyne, G.D., 2006, Statistical clustering of major solutes—use as a tracer for evaluating interbasin groundwater flow into Indian Wells Valley, California: Environmental and Engineering Geoscience, v. 12, no. 1, p. 53–65.

Harrill, J.R., and Prudic, D.E., 1998, Aquifer systems in the Great Basin region of Nevada, Utah and adjacent states—summary report: U.S. Geological Survey Professional Paper 1409-A, 66 p.

Hart, R., Nelson, S.T., and Eggett, D., 2010, Uncertainty in ^{14}C model ages of saturated zone waters—the influence of soil gas in terranes dominated by C_3 plants: Journal of Hydrology (doi: 10.1016/j.jhydrol./2010.08.001).

Hershey, R.L., Heilweil, V.M., Gardner, P., Lyles, B.F., Earman, S., Thomas, J.M., and Lundmark, K.W., 2007, Groundwater chemistry interpretations supporting the Basin and Range Regional Carbonate-rock Aquifer System (BARCAS) study, eastern Nevada and western Utah: Reno, Nevada, Desert Research Institute DHS Publication No. 41230, 86 p.

Hershey, R.L., and Mizell, S.A., 1995, Water chemistry of spring discharge from the carbonate-rock province of Nevada and California: Desert Research Institute, Water Resources Center Publication No. 41140, v. 1, 45 p.

Hintze, L.F., and Davis, F.D., 2002a, Geologic map of the Wah Wah Mountains North 30′ x 60′ quadrangle and part of the Garrison 30′ x 60′ quadrangle, southwest Millard County and part of Beaver County, Utah: Utah Geological Survey Map 182, 2 plates, scale 1:100,000.

Hintze, L.F., and Davis, F.D., 2002b, Geologic map of the Tule Valley 30′ x 60′ quadrangle and parts of the Ely, Fish Springs, and Kern Mountains 30′ x 60′ quadrangles, northwest Millard County, Utah: Utah Geological Survey Map 186, 2 plates, scale 1:100,000.

Hintze, L.F., and Davis, F.D., 2003, Geology of Millard County, Utah: Utah Geological Survey Bulletin 133, 305 p.

Hood, J.W., and Rush, E.E., 1965, Water-resources appraisal of the Snake Valley area, Utah and Nevada: Utah State Engineer Technical Publication No. 14, 43 p.

Kehew, A.E., 2000, Applied chemical hydrogeology: Upper Saddle River, New Jersey, Prentice Hall, 368 p.

Kendall, C., and Coplen, T.B., 2001, Distribution of oxygen-18 and deuterium in river waters across the United States: Hydrological Processes, v. 15, p. 1363–1393.

Kirby, S.M., 2012, Statistical analysis and geochemical evolution of groundwater in the Snake Valley area of western Utah—implications for regional groundwater flow, *in* Hylland, M.D., and Harty, K.M., editors, Selected topics in engineering and environmental geology in Utah: Utah Geological Association Publication 41, p. 115–135.

Knochemus, L.A., Laczniak, R.J., Moreo, M.T., Sweetkind, S.S., Wilson, J.W., Thomas, J.M., Justet, L., Hershey, R.L., Earman, S., Lyles, B.F., and Lundmark, K.W., 2007, Groundwater conditions, *in* Welch, A.H., Bright, D.J., and Knochemus, L.A., editors, Water resources of the Basin and Range carbonate-rock aquifer system, White Pine County, Nevada, and adjacent areas in Nevada and Utah: U.S. Geological Survey Scientific Investigations Report 2007-5261, p. 37–42.

Koonce, J.E., Yu, Z., Farnham, I.M., and Stetzenbach, K.J., 2006, Geochemical interpretation of groundwater flow in the southern Great Basin: Geosphere, v. 2, no. 2, p. 88–101.

Lowe, M., and Wallace, J., 1999, The hydrogeology of Ogden Valley, Weber County, Utah, and recommended waste-water management practices to protect ground-water quality, *in* Spangler, L.E., and

Allen, C.J., editors, Geology of northern Utah and vicinity: Utah Geological Association Publication 27, p. 313–336.

Lowe, M., Wallace, J., and Bishop, C.E., 2002, Water-quality assessment and mapping for the principal valley-fill aquifer in Sanpete Valley, Sanpete County, Utah: Utah Geological Survey Special Study 102, 91 p., scale 1:100,000, CD-ROM.

Lowe, M., Wallace, J., and Bishop, C.E., 2003, Groundwater quality classification and recommended septic tank soil-absorption-system density maps, Cache Valley, Cache County, Utah: Utah Geological Survey Special Study 101, 31 p., scale 1:100,000, CD-ROM.

Manning, A.H., and Solomon, D.K., 2003, Using noble gases to investigate mountain-front recharge: Journal of Hydrology, v. 275, p. 194–207.

Meinzer, O.E., 1911, Ground water in Juab, Millard, and Iron Counties, Utah: U.S. Geological Survey Water-Supply Paper 277, 162 p.

Nelson, S.T., 2000, A simple, practical methodology for routine VSMOW/SLAP normalization of water samples analyzed by continuous flow methods: Rapid Communications in Mass Spectrometry, v. 14, p. 1044–1046.

Nolan, T.B., 1928, Potash brines in the Great Salt Lake Desert, Utah, *in* Loughlin, G.F., and Mansfield, G.R., editors, Contributions to economic geology, part 1—metals and nonmetals except fuels: U.S. Geological Survey Bulletin 795-B, p. 25–44.

Oviatt, C.G., 1991, Quaternary geology of Fish Springs Flat, Juab County, Utah: Utah Geological Survey Special Study 77, 16 p., 1 plate, scale 1:50,000.

Parkhurst, D.L., and Appelo, C.A.J., 1999, Users guide to PHREEQC (version 2)—a computer program for speciation, batch-reaction, one-dimensional transport, and inverse geochemical calculations: U.S. Geological Survey Water-Resources Investigations Report 99-4259, 312 p.

Pearson, F.J., Jr., and Hanshaw, B.B., 1970, Sources of dissolved carbonate species in groundwater and their effects on carbon-14 dating, *in* Isotope hydrology 1970: Panel Proceedings Series—International Atomic Energy Agency, p. 271–286.

Plummer, L.N., Busby, J.F., Lee, R.W., and Hanshaw, B.B., 1990, Geochemical modeling of the Madison aquifer in parts of Montana, Wyoming, and South Dakota: Water Resources Research, v. 26, p. 1981–2014.

Plummer, L.N., Prestemon, E.C., and Parkhurst, D.L., 1994, An interactive code (NETPATH) for modeling net geochemical reactions along a flow path, version 2.0: U.S. Geological Survey Water-Resources Investigations Report 94-4169, 130 p.

R Development Core Team, 2012, R—a language and environment for statistical computing: R Foundation for Statistical Computing, Vienna, Austria, online at http://www.R-project.org, accessed March 1, 2012.

Schaefer, D.H., Thiros, S.A., and Rosen, M.R., 2005, Groundwater quality in the carbonate-rock aquifer of the Great Basin, Nevada and Utah, 2003: U.S. Geological Survey Scientific Investigations Report 2005-5232, 32 p.

Snyder, C.T., 1963, Hydrology of stock-water development on the public domain of western Utah: U.S. Geological Water-Supply Paper 1475-N, p. 487–536.

Solomon, D.K., 2000, ^{4}He in groundwater, *in* Cook, P.G., and Herczeg, A.L., editors, Environmental tracers in subsurface hydrology: Boston, Kluwer Academic, p. 425–440.

Solomon, D.K., and Cook, P.G., 2000, ^{3}H and ^{3}He, *in* Cook, P.G., and Herczeg, A.L., editors, Environmental tracers in subsurface hydrology: Boston, Kluwer Academic, p. 397–424.

Stephens, J.C., 1974, Hydrologic reconnaissance of the Wah Wah Valley drainage basin, Millard and Beaver Counties, Utah: Utah Department of Natural Resources Technical Publication No. 47, 53 p.

Stephens, J.C., 1976, Hydrologic reconnaissance of the Pine Valley drainage basin, Millard, Beaver, and Iron Counties, Utah: Utah Department of Natural Resources Technical Publication No. 51, 38 p.

Stephens, J.C., 1977, Hydrologic reconnaissance of the Tule Valley drainage basin, Juab and Millard Counties, Utah: Utah Department of Natural Resources Technical Publication No. 56, 37 p.

Stute, M., and Schlosser, P., 2000, Atmospheric noble gases, *in* Cook, P.G., and Herczeg, A.L., editors, Environmental tracers in subsurface hydrology: Boston, Kluwer Academic, p. 349–377.

Suk, H., and Lee, K.K., 1999, Characterization of a ground water hydrochemical system through multivariate analysis—clustering into ground water zones: Ground Water, v. 37, no. 3, p. 358–366.

Templ, M., Filzmoser, P., and Reimann, C., 2008, Cluster analysis applied to regional geochemical data—problems and possibilities: Applied Geochemistry, v. 23, p. 2198–2213.

Thomas, J.M., Hudson, G.B., Stute, M., and Clark, J.F., 2003, Noble gas loss may indicate groundwater flow

across flow barriers in southern Nevada: Environmental Geology, v. 43, p. 568–579.

Thomas, J.M., and Mihevc, T.M., 2007, Letter report to the Southern Nevada Water Authority—stable isotope evaluation of water budgets for the White River and Meadow Valley Wash Regional Groundwater Flow Systems in east-central and southeastern Nevada: Desert Research Institute, November 2007, 189 p.

Thomas, J.M., Mihevc, T., Sada, D., Powell, R., and Rosamond, C., 2006, Letter report to the Southern Nevada Water Authority—annual data report for geochemical, isotopic, and biological monitoring for east central and southeastern Nevada: Desert Research Institute, November 2006, 139 p.

Thomas, J.M., Welch, A.H., and Dettinger, M.D., 1996, Geochemistry and isotope hydrology of representative aquifers in the Great Basin region of Nevada, Utah, and adjacent states: U.S. Geological Survey Professional Paper 1409-C, 100 p.

Tibbetts, J.R., Enright, M., and Wilberg, D.E., 2004, Water resources data, Utah, water year 2003: U.S. Geological Survey Water Data Report UT-03-1, 495 p.

U.S. Environmental Protection Agency, 2011, Current drinking water standards: Online, http://www.epa.gov/safewater/mcl.html, accessed June 27, 2011.

U.S. Geological Survey, 1977, Water-resources data for Utah, water year 1976: U.S. Geological Survey Water-Data Report UT-76-1, 634 p.

U.S. Geological Survey, 1978, Water-resources data for Utah, water year 1977: U.S. Geological Survey Water-Data Report UT-77-1, 559 p.

Usunoff, E.J., and Guzmán-Guzmán, A., 1989, Multivariate analysis in hydrochemistry—an example of the use of factor and correspondence analyses: Ground Water, v. 27, no. 1, p. 27–34.

Wilde, F.D., Radtke, D.B., Gibs, J., and Iwatsubo, R.T., editors, 1998, National field manual for the collection of water-quality data: U.S. Geological Survey, Techniques of Water-Resources Investigations book 9, chapter A4, 103 p.

Zhu, C., and Murphy, W.M., 2000, On radiocarbon dating of groundwater: Ground Water, v. 38, p. 802–804.

CHAPTER 7 | AQUIFER TESTS

by J. Lucy Jordan, Paul Inkenbrandt, Hugh Hurlow, and Walid Sabbah

A contractor operates the pump rig at site 11 while UGS personnel measure water levels in observation wells in the background, March 2009.

Bibliographic citation for this chapter:
Jordan, J.L., Inkenbrandt, P., Hurlow, H., and Sabbah, W., 2014, Aquifer tests, Chapter 7 *in* Hurlow, H., editor, Hydrogeologic studies and groundwater monitoring in Snake Valley and adjacent hydrographic areas, west-central Utah and east-central Nevada: Utah Geological Survey Bulletin 135, p. 195–232.

CHAPTER 7 CONTENTS

FIGURES

TABLES

CHAPTER 7: AQUIFER TESTS

by J. Lucy Jordan, Paul Inkenbrandt, Hugh Hurlow, and Walid Sabbah

7.1 INTRODUCTION

Hydraulic-property estimates derived from long-term aquifer tests of the basin-fill and carbonate-rock aquifers in Snake Valley were sparse prior to our work. We conducted aquifer tests at sites 11 and 3 to characterize the hydraulic properties of the upper and lower carbonate-rock aquifer, respectively, at these locations. Both tests were conducted at the maximum possible discharge rate as constrained by pump capacity, water level, and well diameter, and involved continuous monitoring of multiple observation wells using pressure transducers supplemented by manual measurements. The tests were designed to determine the hydraulic conductivity and storativity of the carbonate-rock aquifer and, for site 11, the hydraulic conductivity of the lower part of the basin-fill aquifer and the hydraulic connection between the basin-fill and upper carbonate-rock aquifers.

To determine hydraulic properties (hydraulic conductivity and storativity), aquifer-test analyses use analytical solutions, numerical solutions, and/or a combination of the two (Walton, 2007). Analytical methods in aquifer-test analysis refer to matching theoretical curves to plotted groundwater-level drawdown and recovery data, also known as curve matching. Numerical techniques generally refer to solutions obtained by numerical groundwater-flow modeling software that uses iterative processing and user-defined parameters. We used analytical and combination methods to analyze aquifer-test data from site 11, and analytical solutions to analyze aquifer-test data from site 3. Our attempt at a numerical model at site 11 was unsuccessful.

This chapter describes the geologic setting of each aquifer-test site, our methods of data collection and analysis, and the estimates of hydraulic properties that we derived from our aquifer-tests data analysis. We also compare our results to those of others. All groundwater-level data collected for the aquifer tests is included electronically in a data folder on this CD (tables DF-3 and DF-4).

7.2 SITE 11 AQUIFER TEST

7.2.1 Location and Geologic Setting

Site 11 is 15 miles (24 km) south-southeast of Garrison, Utah, at the north end of the Mountain Home Range in a geographic area denoted as The Cove on the Garrison and Wah Wah Mountains North 30′ x 60′ quadrangles (figures 7.1 and 7.2). North-trending bedrock ridges composed of Permian-Mississippian Ely Limestone (PMM) of the upper Paleozoic carbonate-rock aquifer hydrogeologic unit (UPzc on figure 4.1) form the eastern and western boundaries of The Cove.

Site 11 is on a north-sloping alluvial fan composed of gravel, sand, and clay of the Quaternary-Tertiary basin-fill aquifer (units QTcs on figure 4.1 and Qafy and Qafo on figure 7.2). The Ely Limestone is composed of fine- to medium-grained bioclastic cherty limestone having well-defined bedding about 1 to 5 feet (0.3–2 m) thick (figure 7.3a). On the north-trending bedrock ridges that bound The Cove, joints in the Ely Limestone include a set along the bedding planes, a set that strikes north-northeast to north-northwest and dips 70 to 80 degrees southeast and is spaced 1 to 5 feet (0.3–2 m) (approximate distance between fracture planes measured perpendicular to strike), and a rare set that strikes northeast to east-northeast and dips 60 to 85 degrees southeast. The Mississippian Chainman Shale of the middle Paleozoic siliciclastic-rock confining unit (MPzs on figure 4.1 and M2 on figures 7.2 and 7.4), exposed in the northern Mountain Home Range, is composed of calcareous shale and siltstone and less abundant limestone.

The north end of the Mountain Home Range is an anticline having a north-striking, nearly vertical axial plane and a north-plunging hinge line, in the hanging wall of the north-striking Mountain Home thrust fault (figures 7.2 and 7.4; Hintze, 1986). The Chainman Shale is in the core of the anticline and contains several subsidiary thrust faults and folds, and the north-trending ridge composed of Ely Limestone that bounds The Cove on the east is the overturned eastern limb of the anticline (figure 7.2). Given that the Mountain Home thrust fault extends along the eastern bounding ridge of The Cove, we postulate that other structures on the north end of the Mountain Home range may extend in the subsurface beneath the basin fill in The Cove, as shown in figures 7.2 and 7.4. However, no borehole data exist to test our interpretation. If the Chainman Shale is located as shown in figure 7.4, it would create a barrier to groundwater flow to our aquifer test at site 11. We analyze and compare the results from both an unbounded aquifer hydrogeologic setting and one with a no-flow boundary representing the faulted setting.

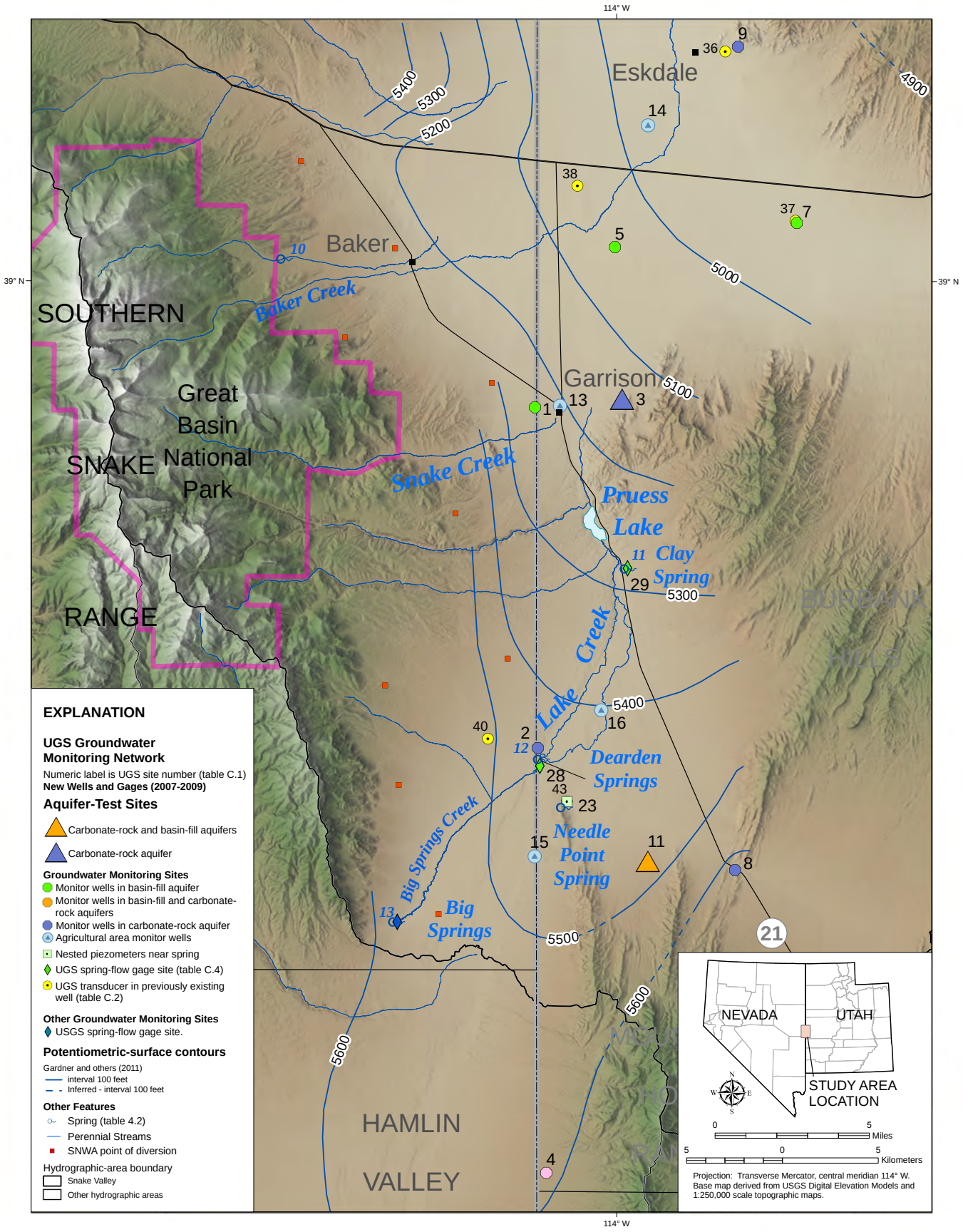

Figure 7.1. *Geographic setting of UGS aquifer-test sites.*

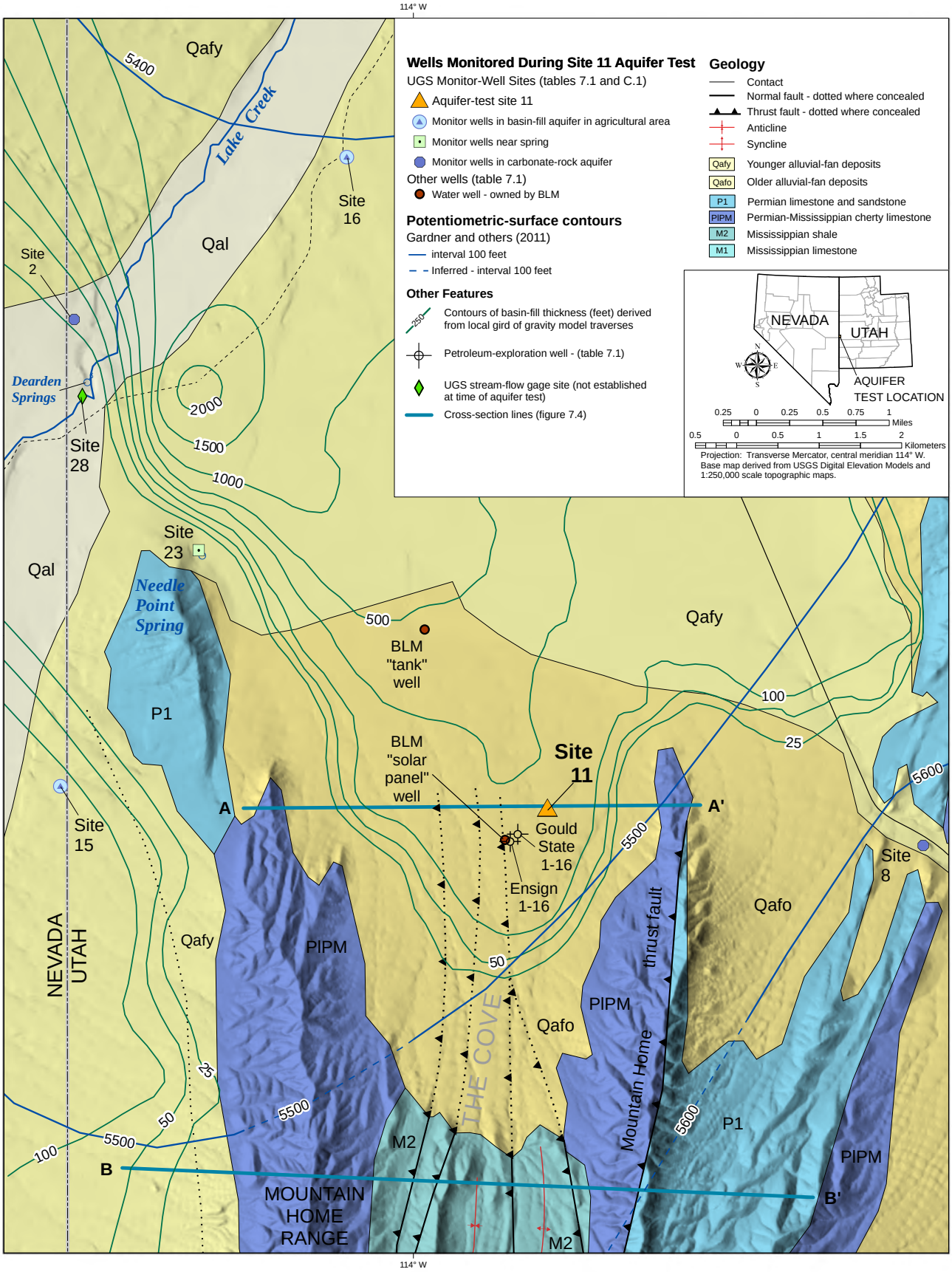

Figure 7.2. *Geologic setting of aquifer-test site 11.*

Figure 7.3. *UGS aquifer-test site 11.* ***A.*** *The Permian-Mississippian Ely Limestone on north-south striking ridge northeast of site 11. The pumping and observation wells at this site are screened in this unit. Pencil (circled) is 5.5 inches (14 cm) long.* ***B.*** *View of well NPA-1B at site 11 before reconditioning.* ***C.*** *Installing new surface casing on well NPA-1B.* ***D.*** *Discharge pit and flume during the preliminary air-lift test of NPA-1B.* ***E.*** *Installing the pump into NPA-1B prior to the aquifer test.* ***F.*** *Equipment and monitoring sites during site 11 aquifer test.*

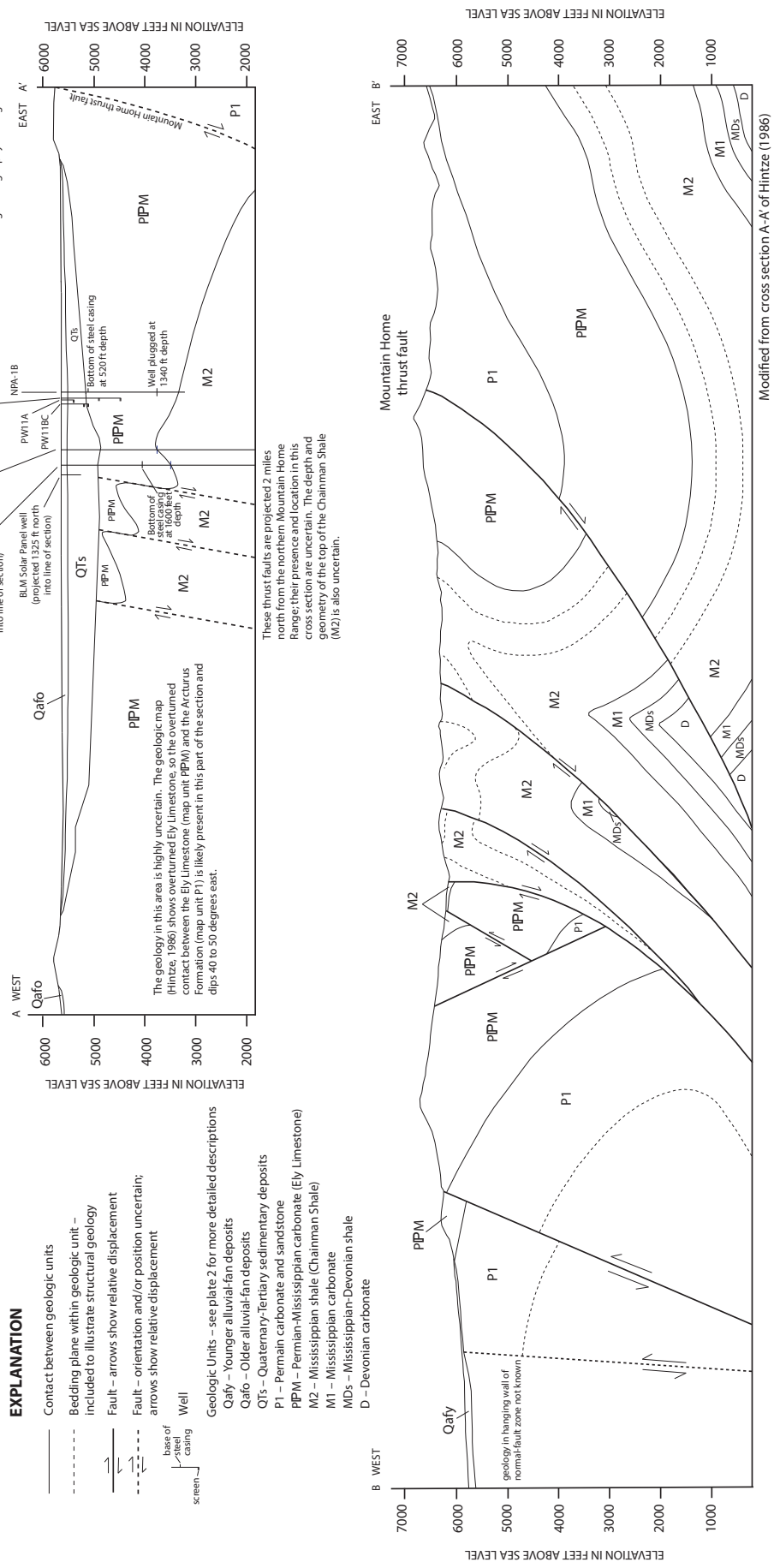

Figure 7.4. *Geologic cross sections through aquifer-test site 11. A–A': East-west section through site 11 showing pumping and observation wells. B–B': Cross section through the northern Mountain Home Range (simplified from cross section A–A' of Hintze [1986]).*

7.2.2 Site Selection and Preparation

We constructed site 11 around an "orphaned" (i.e., abandoned but not plugged) petroleum-exploration well (Needle Anticline #1-B, API #43-027-30011, hereafter NPA-1B), brought to our attention by Dustin Doucet of the Utah Division of Oil, Gas, and Mining. Before our work, NPA-1B was open at the surface (figure 7.3b), cased to 150 feet (46 m), and open from 150 to 2407 feet (46–734 m) depth. The original well penetrated basin-fill sediments from the surface to 470 feet (143 m) depth, the Ely Limestone from 470 to 2265 feet (143–690 m), and the Chainman Shale from 2265 to 2407 feet (690–734 m). The water level in NPA-1B was about 210 feet (64 m) from the top of the old surface casing before we began our work. Original well records are available online from the Utah Division of Oil, Gas, and Mining.

The abandoned site also contained an old water well located 140 feet (43 m) west of NPA-1B, which had been permitted as an oil and gas exploration well in 1974 (Commodore Resources Needle State #1, API #43-027-30009). Records for the well are incomplete but show 350 feet (107 m) of 7-inch-diameter (18 cm) steel casing (no record of perforations) in a 376-foot-deep (115 m), 10-inch-diameter (25 cm) hole that has no cement or other annular seal. We attempted to recondition this well to produce water for use during work on NPA-1B and to use as a basin-fill monitoring well during aquifer testing. A crew from the U.S. Geological Survey Western Region Research Drilling Program reconditioned the well in 2008 by removing a non-functional water pump, flushing the 7-inch-diameter (18 cm) well to 280 feet (85 m) below surface (obstructions and caving problems were encountered between 250 and 280 feet [76–85 m]), and installing 4-inch-diameter (10 cm) PVC casing to 255 feet (78 m) to protect a new temporary submersible pump. The new PVC casing has a screen from 235 to 255 feet (72–78 m) and the annulus between the PVC and steel casings is sand packed from 99 to 255 feet (30–78 m) below surface. The reconditioned well is completed borehole PW11A (tables C.1 and 7.1).

To prepare well NPA-1B for pumping, the drillers constructed a drilling pad, installed new surface casing (figure 7.3c), installed 10-inch-diameter (25 cm) steel casing to 520 feet (158 m), ran a drill bit to approximately 1350 feet (410 m) to flush the hole, installed a cement plug at 1340 feet (408 m), and developed the well by air-lifting. Next, the drill crew installed completed borehole PW11BC, located 216 feet (66 m) west of NPA-1B. We then conducted an air-lift pump test, described below. Finally, we constructed completed borehole PW11DE north of NPA-1B. We conducted the full-scale aquifer test approximately 11 months later.

We designed the observation wells (piezometers) at site 11 based on the expected transmissivity of the Ely Limestone, the estimated pumping rate from NPA-1B, and the structural setting of the site. SNWA estimated a transmissivity range of 10,000 to 50,000 feet squared per day (930–4600 m^2/day) for fractured Ely Limestone from the results of aquifer tests on their test wells W105 and W506M in Spring Valley (James Prieur, SNWA, electronic communication, January 18, 2008). Using a simplified expression for the relation between pumping rate, drawdown, and transmissivity in a single pumped well (Theis and others, 1963; Fetter, 2001, p. 205) we estimated a transmissivity of 30,000 feet squared per day (2800 m^2/day) for the Ely Limestone, that NPA-1B could be pumped at 1200 gallons per minute (4540 L/min) for two to three weeks, and that these conditions would produce about 4 to 5 feet (1–2 m) of drawdown in observation wells about 150 to 200 feet (50–60 m) away. We expected that the hydraulic conductivity of the Ely Limestone is likely greatest in the north-south direction and least in the east-west direction, due to its location in the hinge zone of the anticline and the predominance of north-striking fractures and bedding (chapter 4, section 4.3.3).

After reconditioning PW11A and NPA-1B and using our preliminary conceptual model of the site, we installed completed borehole PW11BC 216 feet (66 m) west-southwest of NPA-1B. The screens in piezometers PW11B and PW11C are as close to the basin fill-bedrock contact as possible (figure 7.5, tables 7.1 and C.1), as constrained by the need to seal the contact zone in the borehole, to measure the hydraulic conductivity of each unit and the vertical hydraulic conductivity between them. The lithologic log of borehole PW11BC (included in the Lithologic Logs data folder) shows that the lower part of the basin-fill aquifer, from 455 to 480 feet (139–146 m) depth, is composed of clay-rich gravel and sand. The relatively high clay content of the lowest 25 feet (8 m) of the basin-fill aquifer, therefore, likely has lower hydraulic conductivity than the overlying basin-fill aquifer and the underlying carbonate-rock aquifer, and may influence groundwater flow between the units.

Next, we conducted a preliminary air-lift test during which the drillers injected air into the well to discharge water at 880 gallons per minute (3300 L/min) for 6 hours (figure 7.3d). We monitored the discharge rate using a 3-inch Parshall flume at the downstream end of a pit excavated for the test. Because of the air injection, the groundwater level in NPA-1B could not be measured during the test, but within 10 minutes after air lifting ceased, the groundwater level recovered to within 0.5 feet (0.2 m) of pre-test static water level. We monitored groundwater levels in piezometers PW11B and PW11C at 1- to 30-minute intervals

Table 7.1. *Well data for UGS aquifer tests. See table C.1 for additional well data.*

Well Name	Land Elevation (ft)[1]	Screened Geologic Unit[2]	Casing Diameter (in)	Screened Interval (ft)	Screen Elevation (ft)	Distance from Pumping Well (ft)	Static Depth to Water (ft)[3]	Drawdown at End of Pumping (ft)	Summary Log[2]
Site 11 Aquifer Test									
NPA-1B[4]	5666.39	PIPMe	12.25	520–1340	5146–4326	0	215.18	66.39	QTs to 470 ft; PIPMe to 2270 ft; Mc to TD at 2407 ft
UGS PW11A[5]	5664.88	QTs	4.0	235–255	5430–5410	147	214.1	0.15	QTs to TD at 255 ft
UGS PW11B	5665.04	QTs	2.0	435–455	5230–5210	216	214.01	1.71	QTs to 480 ft; PIPMe to TD at 540 ft
UGS PW11C	5665.04	PIPMe	2.0	519–539	5146–5126	216	213.77	2.83	Same borehole as PW11B
UGS PW11D	5659.50	PIPMe	1.0	720–740	4940–4920	144	208.36	3.92	QTs to 480 ft; PIPMe to TD at 1263 ft
UGS PW11E	5659.50	PIPMe	2.0	1139–1159	4521–4501	144	208.11	7.50	Same borehole as PW11E
BLM solar panel[6]	5702.57	QTs	8.0	355–>370?	5348–<5333	2107	253.44	0	Unknown
Gould State 1-16[7]	5695	NA	NA	plugged	NA	1588	NA	NA	QTs to 770 ft; PIPMe to 1860 ft?; Mc to 4200 ft; Mj to TD at 9239 ft
Ensign 1-16[8]	5710	NA	NA	plugged	NA	2009	NA	NA	QTs to 750 ft; PIPMe to ~2140 ft; Mc to 4142 ft; Mj to fault at 5420 ft; Dg to TD at 12,362 ft
BLM tank[9]	5469.04	QTs?		30–130	5439–5339	8445	70.67	0	Unknown
Site 3 Aquifer Test									
UGS PW03P[10]	5316.61	Dg, Ds	12.0	296–845[8]	5021–4472	0	181.35	30.20	Dg to fault at 740 ft; Ds to TD at 845 ft
UGS PW03Z	5310.63	Dg	2.0	200–220	5111–5091	137	172.97	5.77	Dg to TD at 220 ft
UGS PW03A	5324.97	Dg	2.0	280–320	5045–5005	164	199.66	7.65	Dg to fault at 705 ft; Ds to TD at 968 ft
UGS PW03B	5324.97	Ds	2.5	820–860	4505–4465	164	195.97	7.01	Same borehole as PW03A

[1] Elevation of top of concrete pad at base of steel surface casing. Vertical Datum: NAVD88.

[2] QTs, Quaternary-Tertiary sediment; PIPMe, Permian-Mississippian Ely Limestone; Mc, Mississippian Chainman Formation; Mj, Mississippian Joana Limestone; Dg, Devonian Guilmette Formation; Ds, Devonian Simonson Dolomite.

[3] Depth to water at beginning of pumping, referenced to top of concrete pad at base of steel surface casing.

[4, 5, 6, 7, and 8] Additional detailed information about petroleum-exploration wells is available from the Utah Division of Oil, Gas, and Mining at <http://oilgas.ogm.utah.gov>.

[4] Pumping well for site 11 aquifer test. Original well name is Commodore Resources Needle Anticline 1-B, API number 4302730011. Well is cased to 520 ft and open to bedrock from 520 to 1340 ft.

[5] Original well name is Commodore Resources Needle State #1, API number 4302730009. Well was rehabilitated for aquifer test. Screen interval is inside un-perforated steel casing.

[6] Possible water supply well for nearby petroleum-exploration wells (API numbers 4302730005 and 4302730021). July 2006 downhole camera revealed 8-inch casing, possibly perforated from 355 to total inspected depth of 370 ft. Debris and sediment in the well at 368 ft precluded further inspection.

[7] API number 4302730005. Plugged and abandoned oil exploration well drilled to 9239 feet. Land elevation interpolated from 1:24,000 topographic map.

[8] API number 4302730021. Plugged and abandoned oil exploration well drilled to 12,362 feet. Water well located nearby is probably the BLM solar panel well. Land elevation interpolated from 1:24,000 topographic map.

[9] Old well refurbished in February 2009 to provide water for wildlife. Pump set at 102 ft. Pumped 15 gpm for 1 hr with 8 to 9 ft of drawdown. January 2009 downhole camera revealed the well was silted in at 131 ft.

[10] Pumping well for site 3 aquifer test. Well is cased to 296 feet and open to bedrock from 296 to 845 feet.

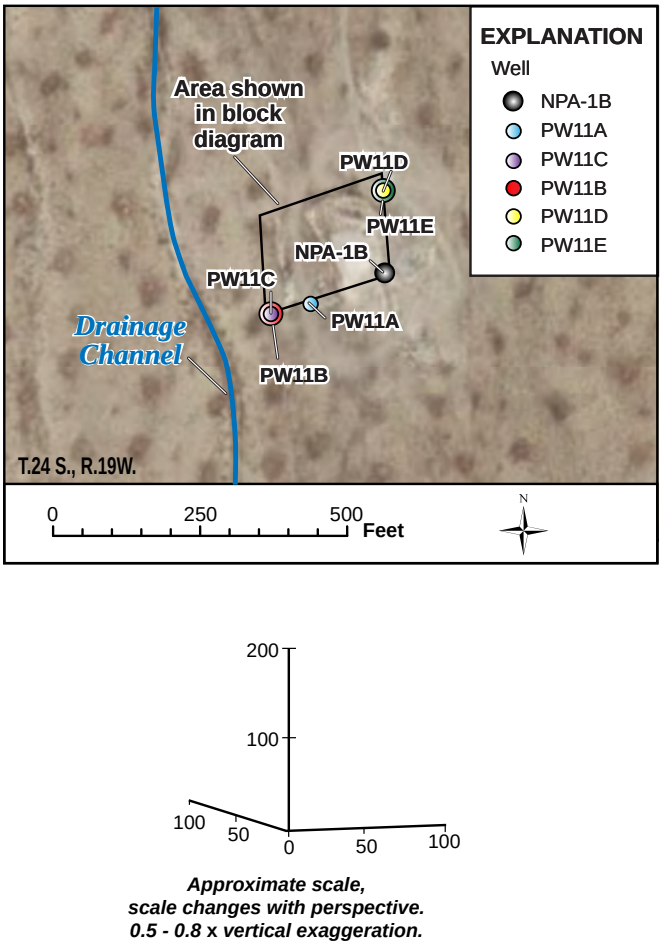

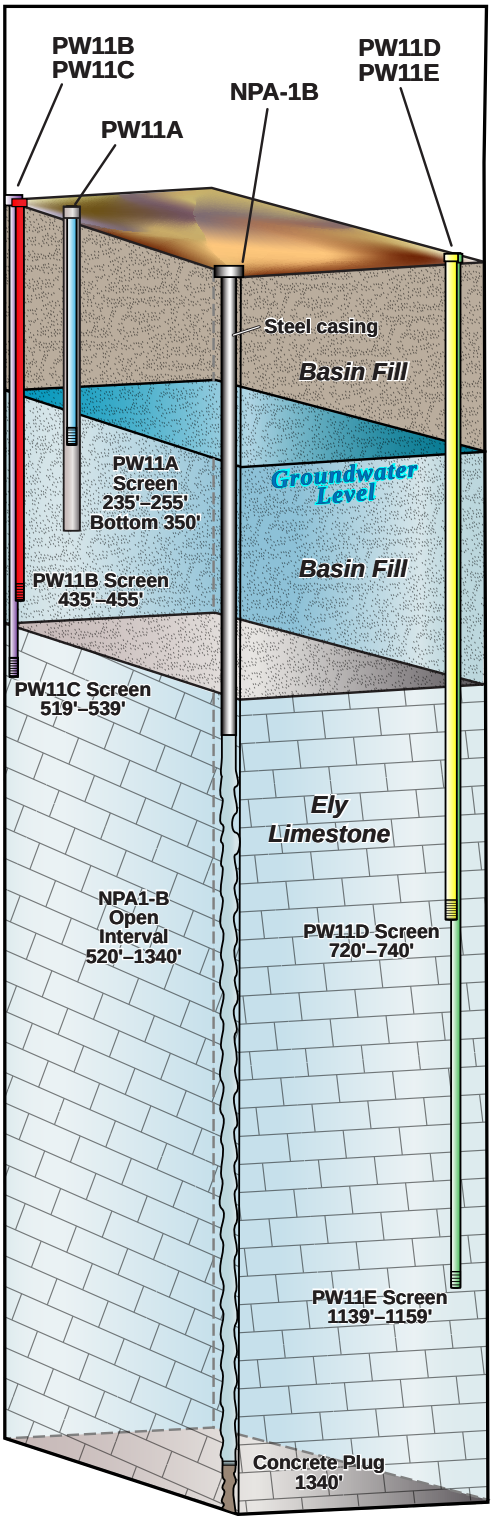

Figure 7.5. *Site 11 3D perspective showing pumping well (NPA-1B), observation wells, geologic contacts, and the water table.*

during the air-lifting and recovery periods using electronic pressure transducers. Drawdown in PW11B and PW11C at the end of the 6-hour test was 0.77 and 1.54 feet (0.23–0.47 m), respectively. We matched drawdown versus time plots of observation-well data to analytical solutions for a variety of aquifer types (Theis, 1935; Hantush and Jacob 1955; Neuman and Witherspoon, 1969; Moench, 1984) using AQTESOLV v. 3.5 computer software program (Duffield, 2003). From these solutions, we estimated a transmissivity of 24,000 to 45,000 feet squared per day (2200–4200 m^2/day) for the Ely Limestone and that NPA-1B could sustain our original production estimate of 1200 gallons per minute (4540 L/min) for three weeks.

Based on the air-lift test data, we placed completed borehole PW11DE 143 feet (44 m) north of NPA-1B, slightly closer to the pumping well than completed borehole PW11BC and with progressively deeper screen intervals to investigate the performance of the deeper part of the carbonate-rock aquifer (figure 7.5; tables 7.1 and C.1). Piezometers PW11D and PW11E are screened at elevations where fractured zones are present in both the piezometers and in NPA-1B (figure 7.5), as interpreted from the geophysical logs, in an attempt to maximize the hydraulic connection between the pumped well and the observation wells. This design does not necessarily ensure maximum possible drawdown in the

observation wells because flow to wells in fractured rock occurs through fracture networks that are hydraulically connected to the pumped well (Long and Witherspoon, 1985; Parney and Smith, 1995), and there is no guarantee that the factures adjacent to the well screens are hydraulically connected to the rest of the aquifer. Delineating the subsurface geometry of hydraulically connected fracture networks would require geophysical logging and surveying combined with extensive aquifer testing in which discrete zones in the pumping and observation wells were isolated using pneumatic packers (Hsieh, 1987).

7.2.3 Test Design and Implementation

We conducted the drawdown portion of the test in March to coincide with the time of year when water levels in observation wells are at their most stable, and before the start of the irrigation season. The basin-fill and carbonate-rock aquifers west and northwest of site 11 are profoundly affected by seasonal irrigation pumping from Granite Peak Ranch and Davies Ranch area irrigation wells (chapter 5, section 5.2.4.1; Dong and others, 2011; Halford and Plume, 2011). Groundwater monitoring data from sites 23, 15, 16, and 2 (figure 7.2) indicate that water levels in March and April typically either are slowly rising or stable and are at their highest (most recovered condition) since the previous irrigation season than at any other time of the year. In spring 2009, April 9 was the earliest any of the above-mentioned wells responded to local agricultural pumping (wells AG16A and AG16B near Davies Ranch), and the well west of Needle Point that monitors basin-fill aquifer conditions near Granite Peak Ranch's pumping wells (well AG15) showed no seasonal drawdown until after April 21. Water-level monitoring before and during the drawdown portion of site 11 aquifer test and for most of the recovery portion of the test was conducted prior to any influence from 2009 agricultural pumping.

For the site 11 aquifer test, the pump contractor set a multi-stage submersible pump (figure 7.3e) in NPA-1B at a depth of 480 feet (146 m) below the top of the surface casing using 6-inch-diameter (15 cm) pump column within the 10-inch-diameter (25 cm) well casing. The pump was equipped with a variable frequency drive (VFD), which allowed us to constrain the discharge to a constant 1200 gallons per minute (4540 L/min) as measured by an in-line electromagnetic flow meter. Two pressure transducers were set above the top of the pump to monitor the water level during pumping.

We conducted a preliminary test for 27 minutes on March 5, 2009, to ensure that the pump was operating properly and that the well could sustain the projected pumping rate of 1200 gallons per minute (4540 L/min) without lowering the water level to expose the pump. The full test began at 9:00 a.m. on March 6, and continued for 17 days and 3 hours until 13:00 on March 23 (24,660 minutes).

A pipe conveyed the pump discharge 370 feet (110 m) west-southwest of the pumping well and 130 feet (40 m) west of completed borehole PW11BC (to the right of the area shown in figure 7.3f) to a small dry drainage channel where it flowed north away from the site. Because the water table is over 200 feet (60 m) deep, infiltration from the drainage channel to the water table over the pumping and recovery period is unlikely. During the 411-hour test, the pump discharged approximately 91 acre-feet (0.11 hm^3) of water. Infiltration rate declines as soil moisture increases (Maidment, 1993), and water not infiltrated is lost to evapotranspiration, surface runoff, and shallow subsurface flow. Based on the Green-Ampt estimate of infiltration rate and estimates of soil parameters (Maidment, 1993), water would likely infiltrate at a rate of about 0.26 feet per hour (0.08 m/hr), and at a slower rate if the soil had significant water content. We calculate that water produced from NPA-1B would take approximately 760 hours to infiltrate through the unsaturated zone at a rate of 0.26 feet per hour (0.08 m/hr) before reaching the saturated zone 200 feet (60 m) below the surface. Based on these calculations, we assume water levels in the carbonate-rock aquifer were not affected by recharge of produced water during the test period.

7.2.4 Water-Level Observations and Trend Corrections

We monitored groundwater levels in all wells at site 11, two old water-supply wells 0.4 miles (0.6 km) southwest and 1.6 miles (2.6 km) northwest of site 11 (the BLM "solar panel" and "tank" wells, respectively) and piezometers at UGS sites 8, 15, 16, and 23 (figure 7.2). We collected drawdown data from March 6 to March 23, 2009, at site 11 using pressure transducers, supplemented by electronic water-level tape readings. The interval of measurement set on the transducers increased logarithmically during the first 24 hours of the test from 10 readings per second at the beginning of the test to a maximum of one reading every 15 minutes. We monitored groundwater levels in the more distal wells using pressure transducers recording twice per day and electronic water-level tapes for backup. We collected recovery data through May 21, 2009, using the same data-collection schedule as in the pumping part of the test. We corrected the time stamp of transducer readings for the 1-hour time advancement for Daylight Savings Time, which occurred during the test. Water-level data are provided electronically in table DF-3 in the Aquifer Test Data folder on this CD.

Before we began our analyses, we considered stresses on the aquifer system and water levels other than aquifer-test pumping. Changes in barometric pressure, earth tides, seasonal recharge and discharge, irrigation well pumpage, and aspects of well construction can influence groundwater levels, masking drawdown produced by pumping for an aquifer test. The groundwater levels measured in all of the site 11 wells display apparent influences by earth tides and barometric pressure. Long-term seasonal influences may exist as well.

Barometrically induced groundwater-level fluctuations occur because barometric pressure changes instantly affect groundwater levels in wells, whereas the aquifers transfer a portion of the change in atmospheric load to the water column over time. The difference in stress between the aquifer and well creates a pressure gradient, causing groundwater levels in the well to change. An increase in barometric pressure will cause a decrease in groundwater level and vice versa (Rasmussen and Crawford, 1997). Because both the basin-fill and Ely Limestone aquifers are unconfined and/or leaky in this area, their response to changes in barometric pressure should show a time lag (Rasmussen and Crawford, 1997). To account for the possibility of time lag, we determined barometric efficiency for each well using two techniques: MRCX in Excel (Mackley and others, 2010), and a visual method as outlined by Gonthier (2007). We did not apply Clark's method (Gonthier, 2007) to these data because they exhibit lag due to the unconfined nature of the aquifer.

Groundwater levels in wells at site 11 also show earth-tide influence. As the moon and sun pass over a well, the change in gravitational force dilates the pore spaces in the surrounding aquifer, which decreases the head pressure and causes a decrease in groundwater level in the well. Fractured media have a greater response to gravitational forces than porous media due to the geometry of the fractures and lower compressibility (Rojstaczer and Agnew, 1989).

The variables influencing groundwater levels can be treated as components of the groundwater-level signal. We are interested only in the drawdown component of the measured groundwater levels for aquifer-test analysis. We used a technique developed by Halford (2006) to evaluate the magnitude of influence of background signals on drawdown. Halford (2006) created "synthetic" groundwater levels that match the measured groundwater levels by varying the phase and amplitude of various components, such as barometric pressure or earth tide, that affect the measured groundwater levels. These components are subtracted from the resulting synthetic groundwater-level record to produce an estimated drawdown curve. The accuracy of the estimated drawdown curve depends on how well the synthetic water levels fit the measured water levels. We also analyzed the raw, unprocessed data to compare the influence of the smoothing process proposed by Halford (2006). Wells PW11B, C, D, E, and NPA-1B all had sufficient drawdown that fluctuations caused by barometric pressure and earth tides did not interfere with acceptable drawdown analysis, so we chose to use the unprocessed data in our analysis. Well PW11A had significant levels of noise from earth tides and atmospheric influences and required the Halford (2006) analysis to resolve the drawdown curve. Groundwater-level records from the BLM solar panel well and BLM tank well were examined with the Halford (2006) analysis. We attempted to include the influence of drawdown induced by pumping NPA-1B as a component of groundwater-level change in the data from the solar panel and tank wells, but we could not create sufficient matches between the observed water levels and the model drawdown.

7.2.5 Aquifer Response

Drawdown in each observation well at the end of the pumping portion of the aquifer test is listed in table 7.1 and the drawdown and recovery response in site 11 wells is shown on figure 7.6. Drawdown in the pumping well at the end of the pumping period was more than 66 feet (20 m), whereas site 11 piezometers experienced between 0.2 and 7.5 feet (0.06–2.3 m) of drawdown (table 7.1). All other wells monitored during this test showed no effect from NPA-1B pumping. Individual well responses are described below.

We observed a small 0.15-foot (0.05 m) response in PW11A (table 7.1, figure 7.6), but suspect poor communication between the well and the aquifer. A large amount of drilling mud was used during well rehabilitation to try to clear obstructions in the original steel well casing. After installation of the new PVC casing inside the steel casing, we had difficulty developing the drilling mud out of the well. The necessary placement of the new PVC well screen and sand pack within the un-perforated steel casing also likely limits aquifer connection. Additionally, we were unable to remove significant water-level fluctuations in the PW11A data even considering atmospheric influences and earth tides. Our doubts about aquifer connection and the residual water-level fluctuations prevented us from obtaining meaningful matches of PW11A data to analytical type curves.

Piezometers screened in the carbonate-rock aquifer at site 11 (PW11C, PW11D, and PW11E) displayed more drawdown (2.38 to 7.50 feet [0.73–2.29 m]) than the alluvial piezometer PW11B (1.71 feet [0.52 m]) (table 7.1, figure 7.6). The greatest drawdown occurred in the deepest

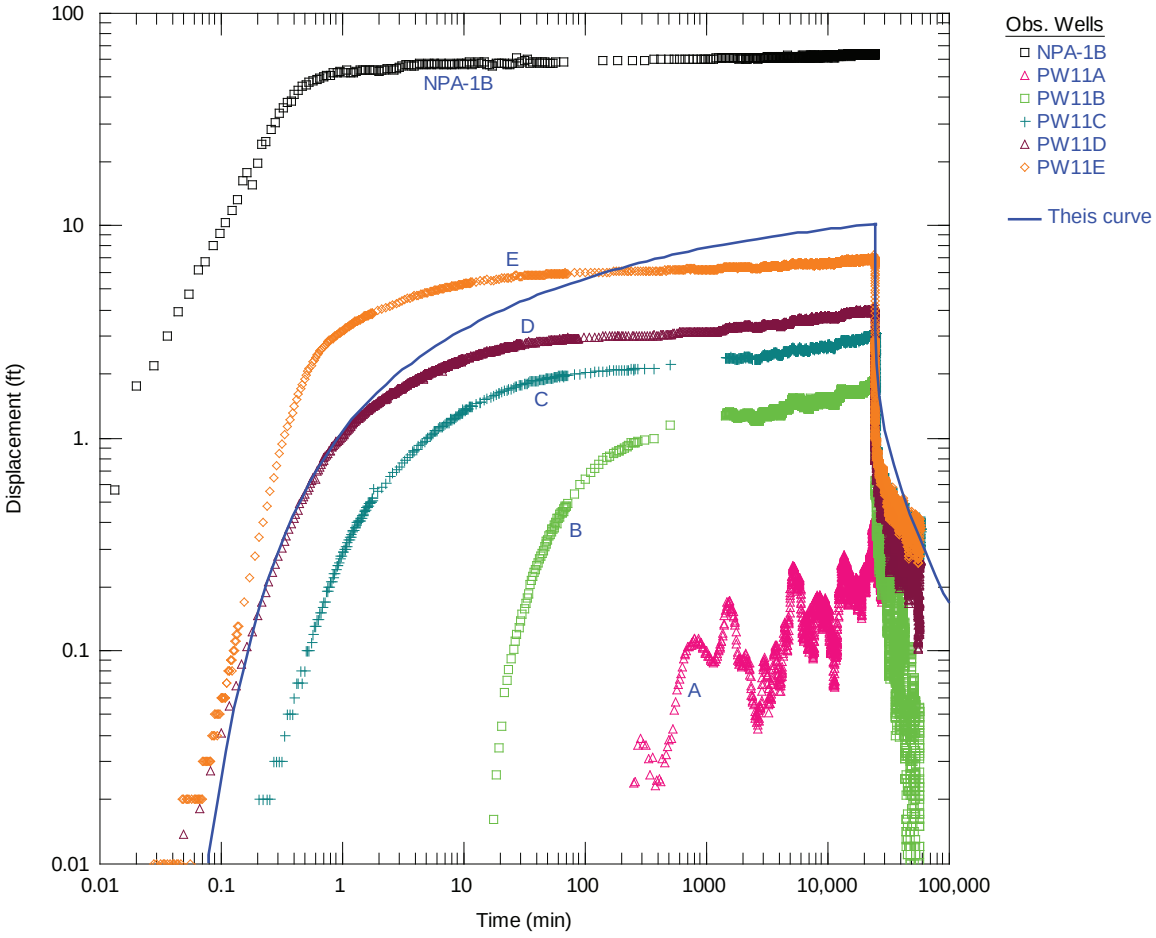

Figure 7.6. *Site 11 pumping- and observation-well response during the aquifer test. Piezometer PW11C took slightly longer to respond than PW11D or E, likely because it is more distant from the pumping well. The 16-minute time lag before PW11B water level began to decline is likely because this well is open to the overlying basin-fill aquifer, which was not pumped. PW11A may not be in communication with the basin-fill aquifer.*

completion, PW11E. Groundwater levels in piezometers PW11D and PW11E, which are located 144 feet (44 m) from the pumping well (horizontal distance), began to decrease after less than 0.05 minutes, and piezometer PW11C, 216 feet (66 m) away from the pumping well, responded after 0.2 minutes (figure 7.6). The groundwater level in piezometer PW11B, which is completed in the overlying basin-fill aquifer, began to decline 16 minutes after pumping began.

The early-time data drawdown curve in the pumping well is a straight line with a slope of approximately 1 (figure 7.6), indicating that borehole storage dominated drawdown during the first 30 seconds of pumping (Renard and others, 2009; Kruseman and de Ridder, 2000, pg. 219). The observation-well time-drawdown curves are more linear in late time as compared to the Theis curve, which is characteristic of leaky aquifer systems or aquifers having recharge boundaries (Renard, 2005; Kruseman and de Ridder, 2000). We would expect the rate of drawdown in late time to increase if the drawdown cone intersected a no-flow boundary (Renard, 2005), that is, the drawdown curve would steepen. We suspect that leakage from the overlying basin-fill aquifer could compensate for the lack of recharge to the well from the west if the no-flow boundary is present. The leakage may mask the characteristic increase in slope typically seen in a bounded aquifer.

7.2.5.1 Aquifer Response as a Function of Depth

We visualize drawdown through the vertical section by contouring the drawdown at the end of pumping on a two-dimensional cross section through site 11 wells (figure 7.7). We made no adjustment to the contours on figure 7.7 for the interface between the bedrock and basin-fill aquifers. We observed greater drawdown per distance from the pumping well's open interval in piezometers PW11D and PW11E. Piezometer PW11C, near the top of the pumping well open

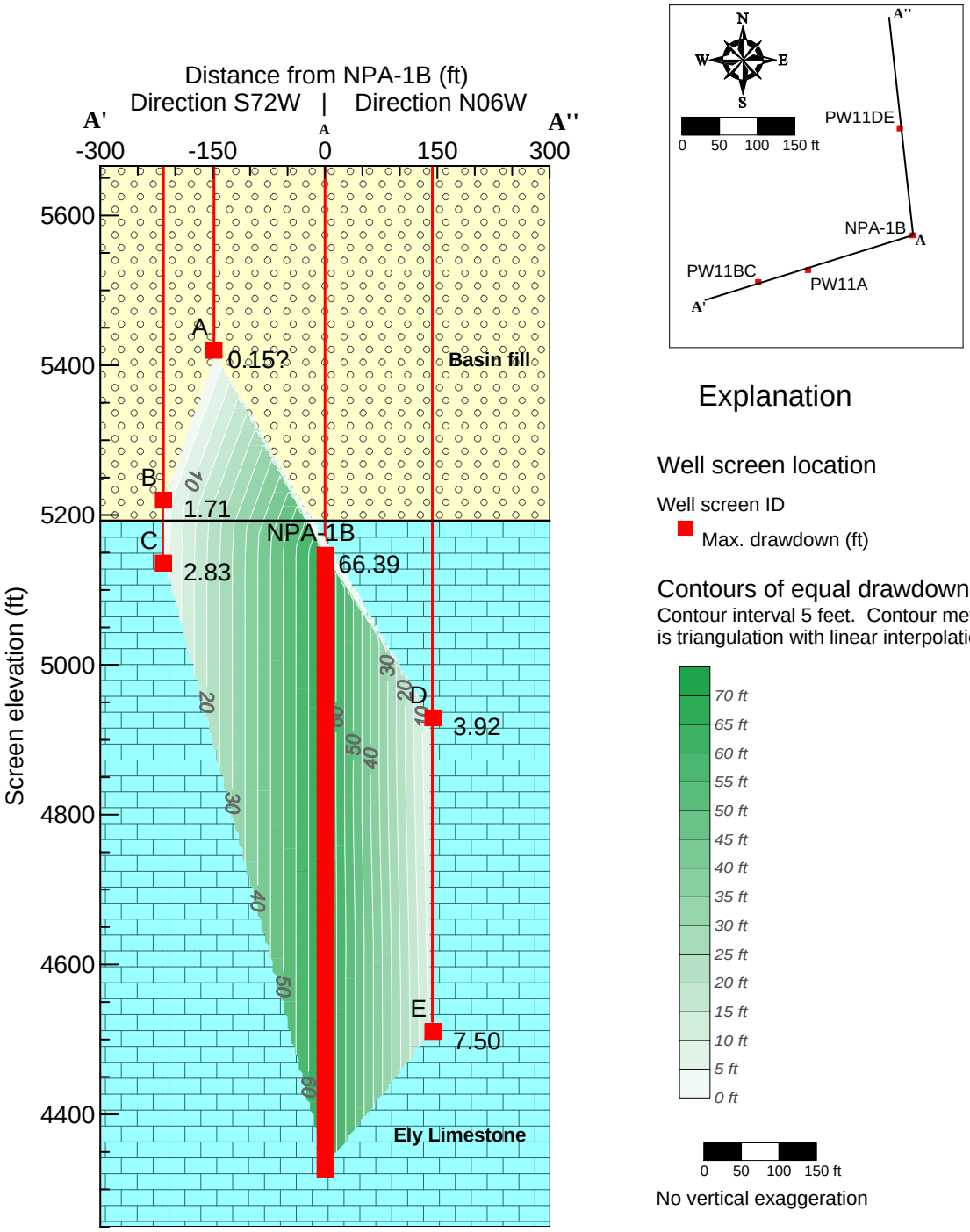

Figure 7.7. *Cross section through site 11, showing drawdown in the westerly direction (PW11A, B, and C) and northerly direction (PW11D and E). The closer spacing of drawdown contours north of the pumping well as compared to west of the well may indicate hydraulic anisotropy (i.e., lower transmissivity in the N–S direction). Alternative explanations for more drawdown in the deeper piezometers are that the aquifer has decreased transmissivity with depth or that leakage from the overlying basin-fill aquifer to the aquifer surrounding the shallow-bedrock completion (PW11C) masked some of the drawdown that would otherwise have occurred there.*

interval and nearest the interface with the overlying basin-fill aquifer, had a drawdown per distance only half that of piezometer PW11D. Possible reasons for the differences in drawdown vertically in the aquifer are discussed in section 7.2.9.2 and include partial penetration, leakage from the overlying aquifer, and/or horizontal or vertical anisotropy.

7.2.5.2 Areal Extent of Pumping Influence

We performed a simple analysis to evaluate the lack of water-level response to pumping NPA-1B in the distal observation wells (wells at sites 8, 15, 16, and 23) and the closer BLM wells (solar panel and tank). Using reasonable estimated ranges of aquifer transmissivity (30,000 ft^2/day [2800 m^2/day]) and storativity (0.001) of the carbonate-rock aquifer as input to AQTESOLV v4.50 (Duffield, 2007), we extrapolated a theoretical cone of depression to estimate the possible extent of influence pumping NPA-1B has on the aquifer. In this type of simple application, AQTESOLV does not show the effects of anisotropy or heterogeneity, and therefore represents contours of equal drawdown as circles in map view (figure 7.8). Based on the reasonable transmissivity and storativity input, at the end of pumping on March 23, 2009, the measureable (>0.1 foot [0.03 m]) cone of depression in the carbonate-rock aquifer should have extended several miles from NPA-1B, beyond even the most distal monitoring wells (figure 7.8A). However, we were unable to detect drawdown in wells other than at site 11 in either the carbonate-rock or basin-fill aquifers; possible reasons are discussed below.

Our extrapolated cone of depression suggests that the maximum drawdown in the carbonate-rock aquifer at the BLM solar panel well, which is approximately 2100 feet (640 m) from the pumping well, should have been approximately 3.5 feet (1.1 m) (figure 7.8A). Variations in groundwater-level data at the BLM solar panel well do not exceed 0.4 foot (0.12 m), and analysis of these data using the Halford (2006) methodology indicates that pumping-induced drawdown did not occur in this well. An exhaustive search of well records held by the Utah Divisions of Water Rights and Oil, Gas, and Mining turned up no well completion information for this well, and only a few clues to its purpose and drilling specifications. Consequently, we are unsure to which aquifer(s) the BLM solar panel well is open. The well likely was drilled as part of oil exploration activities in conjunction with the nearby Gould State 1-16 hole (API #43-027-30005) sometime between 1969 and 1971, either as a failed exploration hole that was completed as a water well or, more likely, specifically as a shallow water well to provide water for those activities. Reference to a water well at this location is made in the records for nearby oil exploration well Ensign 1-16 (API #43-027-30021), placing the likely completion date prior to 1971. A down-hole video of the well filmed in 2006 by the Utah Division of Water Rights shows mineral incrustation on the casing, possibly indicating casing perforations, at depths in the basin-fill (table 7.1). If the well was a failed exploration hole that once penetrated the Ely Limestone, the down-hole video suggests that the casing is now caved and the possibility of hydraulic connection with the carbonate aquifer is very small. We conclude that the most likely reason the BLM solar panel well did not drawdown as our cone of depression extrapolation predicts is that the well is open only to the basin-fill aquifer, not the pumped aquifer. However, another explanation exists for the well's lack of drawdown—a no-flow barrier.

We performed an alternative AQTESOLV analysis in which we inserted a no-flow barrier at the location that we projected thrust faults from the northern Mountain Home Range, shown in cross section A–A′ (figure 7.4). In this section, the Mississippian Chainman Shale of the middle Paleozoic siliclastic-rock confining unit creates a north-south striking flow barrier where it is thrust adjacent to the Ely Limestone of the Upper Paleozoic carbonate-rock aquifer. In this case, the BLM solar panel and tank wells are on the other side of the barrier from NPA-1B and would experience no drawdown.

In a homogeneous, isotropic, unbounded aquifer, pumping NPA-1B should have created approximately 2 feet (0.6 m) of drawdown in the carbonate-rock aquifer at the location of the BLM tank well, approximately 8400 feet (2560 m) northwest of the pumping well, as predicted by our extrapolated drawdown cone (figure 7.8A); however, we did not detect drawdown in the BLM tank well even after using the Halford (2006) technique to remove other influences. Well-completion records for the BLM tank well are not on record with the Utah Divisions of Water Rights or Oil, Gas, and Mining. A down-hole video of the well filmed in 2009 by the BLM showed the well silted in at 131 feet (40 m), but the BLM has pumped the well with some success (table 7.1). Based on this limited information, the well is likely open only to the basin-fill aquifer, which explains why we did not detect drawdown at this location.

Based on our projection of a reasonable measureable cone of depression at the end of pumping, we expected about 1 foot (0.3 m) of drawdown in piezometers PW08A and PW08B, which are located at site 8 about 3 miles (5 km) east of site 11 and are screened in the Ely Limestone of the upper Paleozoic carbonate-rock aquifer (figure 7.8A). We observed instead a linear downward trend in water levels before, during, and long after pumping, in which water levels in both piezometers declined approximately 0.2 feet (0.06 m) from the start of pumping until the end of the recovery data-collection period. Even though our

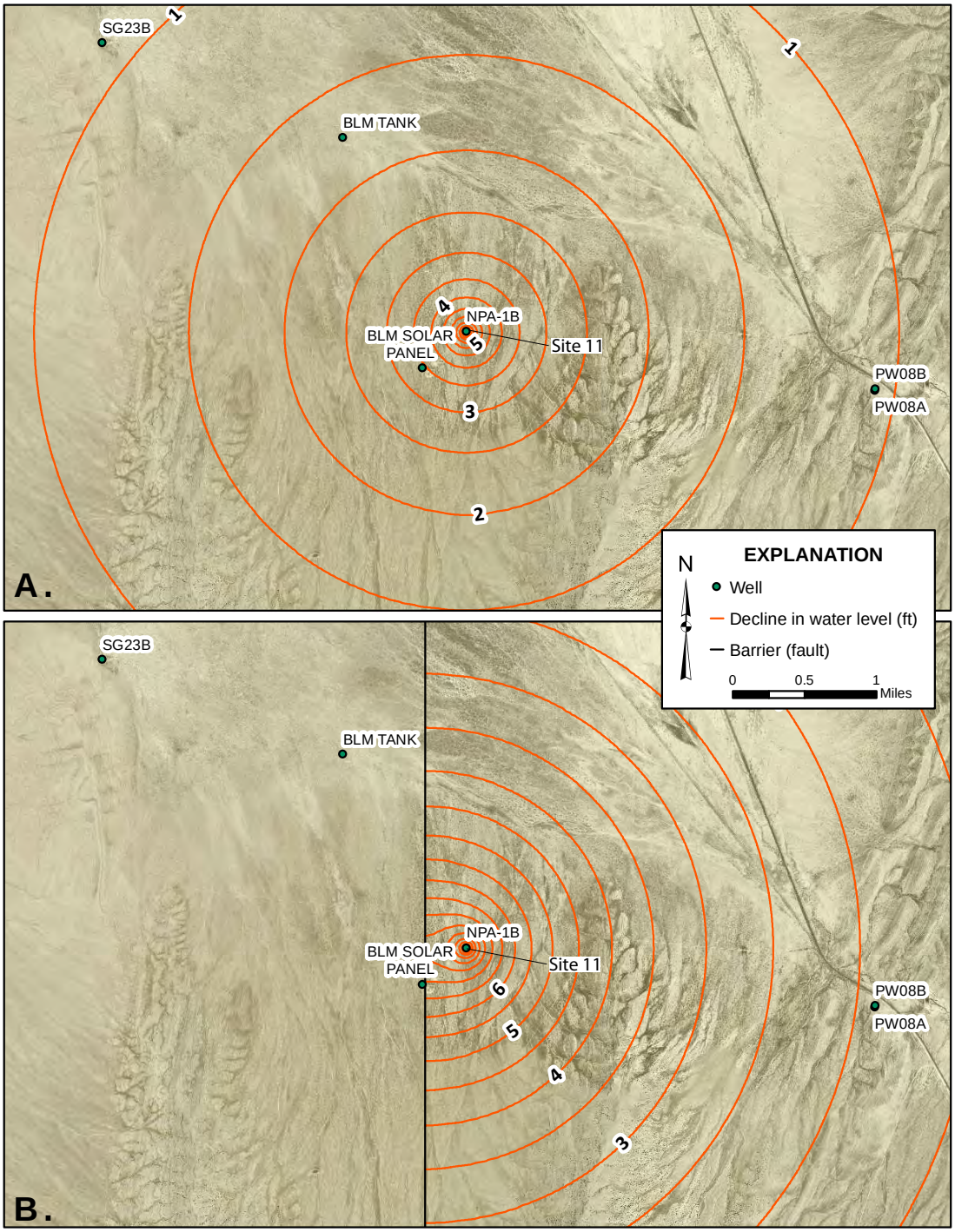

Figure 7.8. *Theoretical drawdown expected in the carbonate-rock aquifer near site 11 using the Theis estimate, storativity of 0.001, and transmissivity of 30,000 feet squared per day (2800 m²/day):* ***A*** *without a no-flow barrier boundary and* ***B*** *with a no-flow barrier placed at the approximate location of thrust faults projected from the northern Mountain Home Range.*

data were temporally limited to two transducer readings per day and supplemented by manual measurements, we are confident the downward trend observed in site 8 water levels is a regional trend not related to site 11 pumping. The most plausible reasons we did not detect the predicted drawdown at site 8 are that several thrust faults and folds, particularly the northern subsurface continuation of the Mountain Home thrust (figures 7.2 and 7.4), prohibit aquifer communication between sites 11 and 8. Also, site 8 is upgradient of the pumping well (potentiometric head at site 8 is nearly 180 feet [55 m] higher than at site 11), and is, therefore, unlikely to experience significant drawdown.

The wells we monitored that are 4 to 5 miles (6.4–8 km) away from the pumping well (Needle Point BLM, SG23B, AG15, AG16ABC) are all completed in the basin-fill aquifer. We neither expected nor observed measurable drawdown in these wells during our test.

7.2.6 Analytical Solutions

7.2.6.1 Solutions and Limitations

This section details the methods and results of our site 11 aquifer-test analysis using analytical solutions for transient conditions (non-steady state) that were pioneered by Theis (1935) and continuously refined by others following him. We used AQTESOLV v. 4.5 (Duffield, 2007) computer software program to assist our curve matching to analytical solutions.

We accounted for the properties of the wells and the hydrogeologic aspects of the basin-fill and carbonate-rock aquifers in our aquifer-test data analysis. Influences on groundwater levels in the wells include borehole storage, skin effects, and partial penetration of an aquifer. Borehole storage is the storage of water in the casing and borehole of the pumping well, and it delays drawdown of the groundwater level in the well during the early stages of the test, distorting the pumping well's drawdown curve (on a log-log plot of drawdown versus time) to be a straight line with a slope of one in early time (Kruseman and de Ridder, 2000). Some of our analytical techniques accounted for borehole storage; in those that did not, we disregarded early-time data (pumping times of less than one hour). Partial penetration effects occur when the pumping well is not open to the entire pumped aquifer. Mud cakes and other blockages in the open intervals of wells used for aquifer tests can cause skin effects and reduce well efficiency. Partial penetration, skin effects, and well inefficiency of the pumping well will increase the amount of drawdown observed in the pumping well and may yield erroneously low transmissivity estimates if not accounted for (Kruseman and de Ridder, 2000). Most of our analytical techniques corrected for partial penetration and skin effects; we note those analyses that do not and the possible effect on results. Hydrogeologic aspects of the aquifer are realized by constructing a conceptual model of the aquifer system involved in each test (Walton, 2007). We estimated aquifer thickness, pore geometry, degree of consolidation of the aquifer matrix, and presence of low permeability units based on borehole data and geologic mapping.

We obtained initial transmissivity and storativity values from our site 11 aquifer-test data analysis by fitting the unconfined Theis (1935) solution to the trend-corrected groundwater-level data. We refined the Theis (1935) values from the carbonate-rock monitoring wells by applying the Moench (1997) and Neuman and Witherspoon (1969) analytical solutions. The derivatives of the drawdown data were plotted with the drawdown data to better fit the theoretical curves (Bourdet, 2002). The derivative of the drawdown allows for further interpretation of the aquifer system, and a better analytical match (Bourdet, 2002). We attempted to match our well data to theoretical curves for fractured-rock aquifers with limited success, i.e., the curves did not match well.

We applied a Moench (1997) analysis for unconfined aquifers to the drawdown data for piezometers PW11B, C, D, and E (figure 7.9). The Moench (1997) analysis accounts for borehole storage and partial penetration. Because the Moench (1997) technique does not account for leakage from under- or overlying layers, we treated the basin fill and Ely Limestone as a single unconfined aquifer. Using methods that do not account for leakage from adjacent aquifers and aquitards can result in estimates of permeability/transmissivity that are higher than the actual value for the aquifer (Neuman and Witherspoon, 1972).

We evaluated the effect a potential no-flow boundary created by the truncation of the upper Paleozoic carbonate aquifer by shale and thrust faults would have on our hydraulic-property estimates. We inserted a north-south trending no-flow boundary 1500 feet (457 m) west of the well and re-matched the aquifer test data using AQTESOLV automatic curve matching with the Moench (1997) solution again.

Next, we applied a method that would account for the water contributed from the overlying unconsolidated basin fill when pumping from the Ely Limestone aquifer, the Neuman and Witherspoon (1969) technique (figure 7.10) using AQTESOLV v. 4.50 (Duffield, 2007). This technique allows analysis of the Ely Limestone and the overlying basin-fill deposits as separate aquifers. Although the original Neuman and Witherspoon (1969) technique was intended for overlying aquitards of very low permeability, a later publication (Neuman and Witherspoon, 1972) proved it effective for very leaky aquifer systems. We treated the basin-fill material as a very leaky aquitard for this analysis. The 25 feet (8 m) of clay-rich sediment at the base of the basin-fill aquifer was used as the thickness of the aquitard separating the two aquifers. The Neuman and Witherspoon (1969) technique does not account for the effects of borehole storage or partial penetration. To avoid the effects of borehole storage and well skin, which are most noticeable in the first few minutes of an aquifer test, we weighted the curve matches to later time data. Partial penetration will cause more drawdown in the well than the theoretical Theis (1935) estimate predicts (Kruseman and de Ridder, 2000).

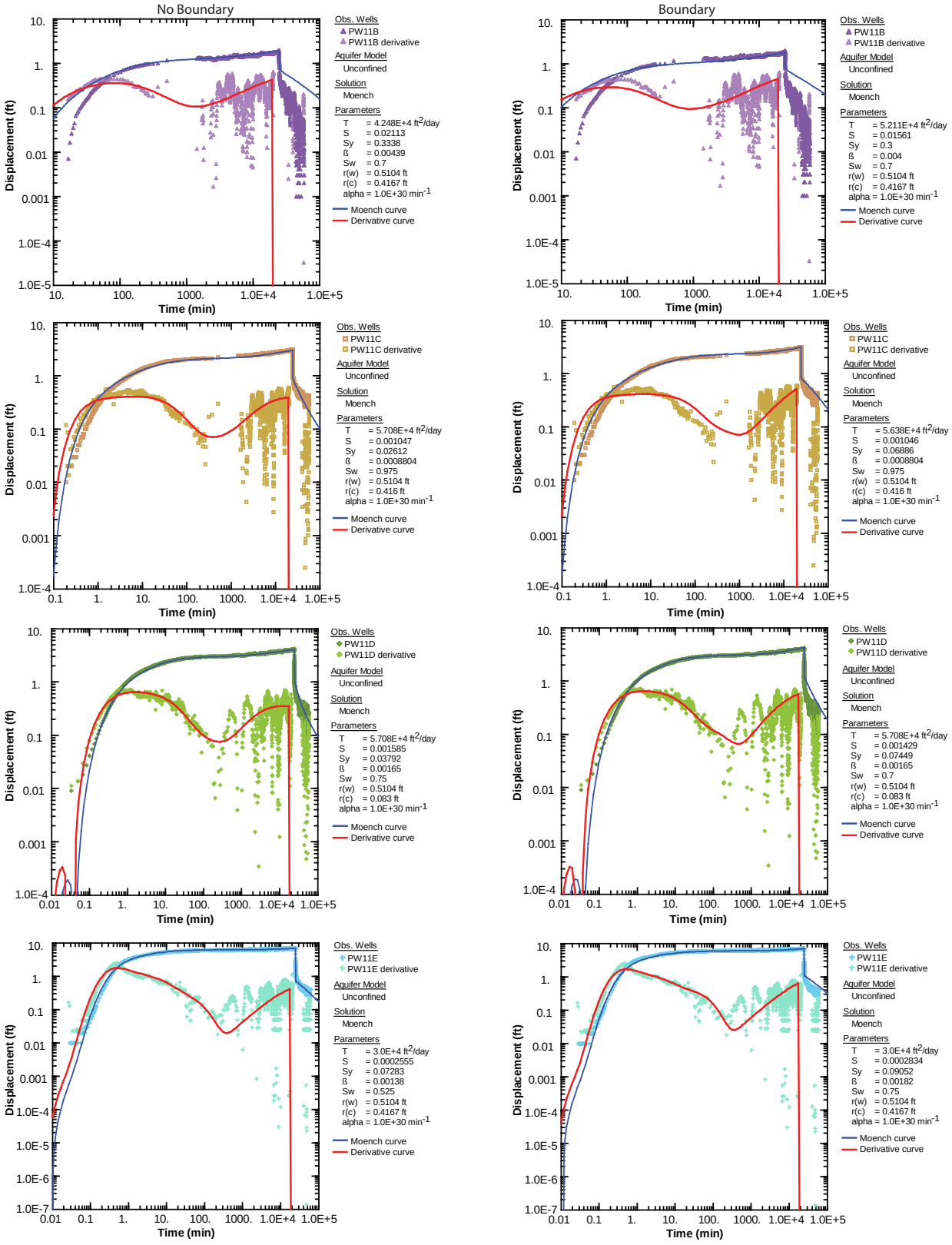

For All Plots:

T = transmissivity (ft²/day)
S = storativity (dimensionless)
Sy = specific yield (dimensionless)
β = curve family value (dimensionless)
Sw = wellbore skin factor (dimensionless)
r(w) = well radius (ft)
r(c) = nominal casing radius (ft)
alpha = Moench's empirical constant for noninstantaneous drainage at the water table

Figure 7.9. *Hydraulic-property estimates from site 11 aquifer test determined using the Moench (1997) analytical solution. The four graphs on the left side of the figure assume an aquifer of infinite areal extent, whereas a north-south trending no-flow boundary 1500 feet west of NPA-1B is included in the aquifer geometry in the analytical solutions represented by the four graphs on the right side of the figure.*

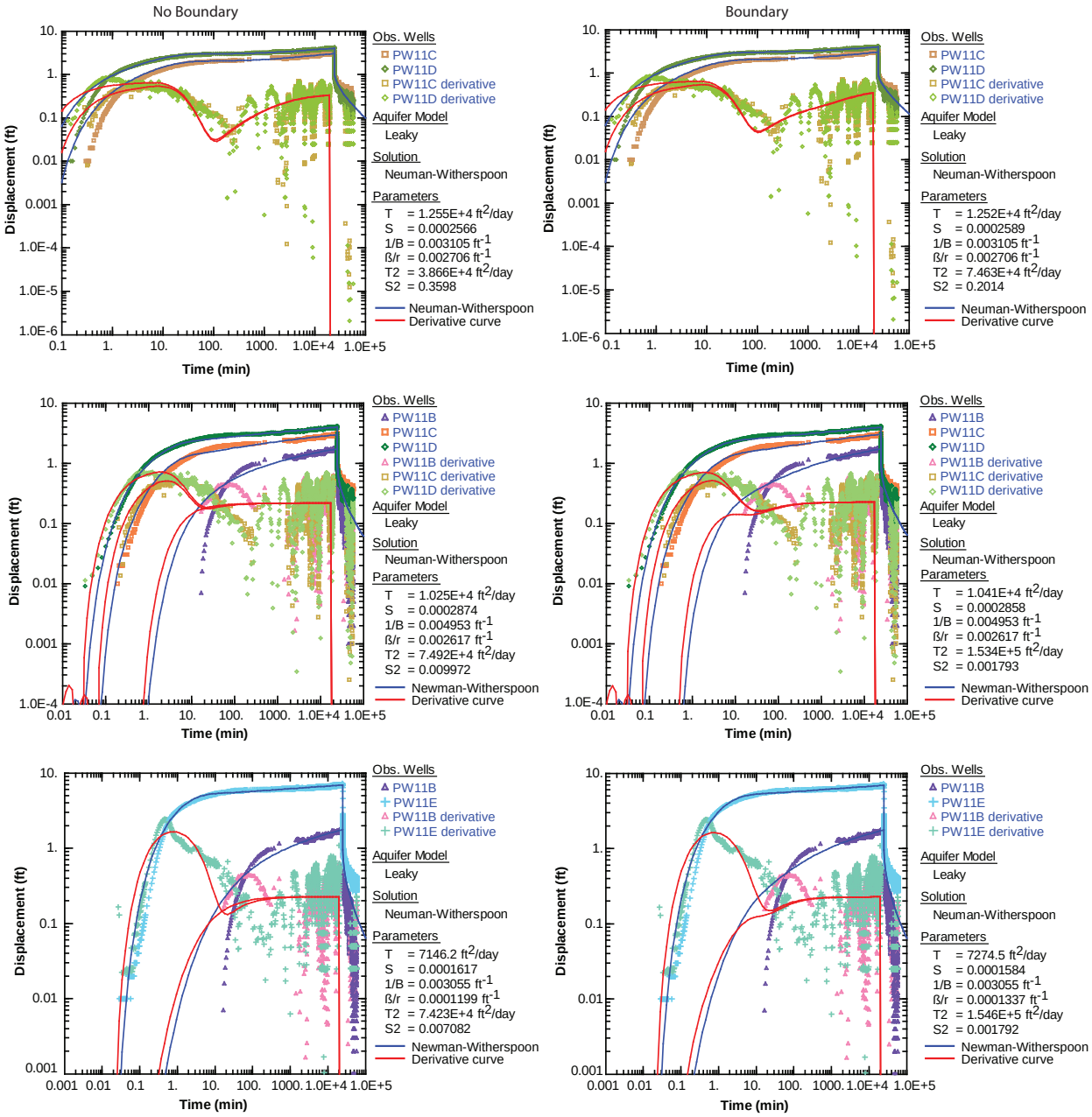

Figure 7.10. *Hydraulic-property estimates from site 11 aquifer test determined using the Neuman and Witherspoon (1969) analytical solution. This solution accommodates an unconfined basin-fill aquifer and a confined carbonate-rock aquifer. To avoid the effects of borehole storage and well skin, we matched the type curves to late-time data. The three graphs on the left side of the figure assume both aquifers are of infinite areal extent, whereas a north-south trending, no-flow boundary 1500 feet west of NPA-1B bounds both aquifers in the analytical solutions represented by the three graphs on the right side of the figure.*

The greater drawdown is caused by nonlinear flow into the partially penetrating well screen. Transmissivity estimates using the Neuman and Witherspoon (1969) technique on partially penetrating wells will be lower than if the solution could account for partial penetration.

Finally, we applied the same Neuman and Witherspoon (1969) solution but included a no-flow boundary 1500 feet (457 m) west of the well. Unfortunately, the computer software does not allow the boundary to be placed in a single aquifer. The no flow boundary in this analytical solution extends vertically through both the carbonate-rock and basin-fill aquifers, contrary to our interpretation of the possible hydrogeologic setting involving the truncation of the carbonate-rock aquifer by shale (figure 7.4). The effect of a no-flow boundary spanning both aquifers is that the transmissivity calculated by AQTESOLV for both aquifers will be higher than in the unbounded case, whereas we would expect only the carbonate-rock aquifer transmissivity to be higher had we been able to bound only the lower aquifer.

7.2.6.2 Hydraulic-Property Estimates from Analytical Curve Matching

We do not discuss the results of the Theis (1935) analyses because we obtained more accurate results from the Moench (1997) and Neuman and Witherspoon (1969) analyses.

Our analysis of site 11 observation well data using the Moench (1997) solution, in which we treated the basin-fill and carbonate-rock aquifers as one 2060-foot- (628 m) thick aquifer, resulted in transmissivity estimates that range from 30,000 to 57,100 feet squared per day (2800–5300 m^2/day) (table 7.2). The hydraulic conductivity ranges from 15 to 28 feet per day (4–8 m/day). Storativity ranged over two orders of magnitude, from 3 x 10^{-4} to 2 x 10^{-2}, and specific yield ranged from 0.03 to 0.09 in the carbonate-rock aquifer wells and was 0.33 in the well completed in the basin-fill aquifer. Analysis of the pumping well drawdown response yielded a lower transmissivity estimate of 18,000 feet squared per day (1700 m^2/day), likely due to more drawdown in the pumping well than expected because of well loss unaccounted for in the analytical solution. Estimates of the vertical to horizontal hydraulic conductivity ratio are obtained from the Moench (1997) solution, which includes the ratio as a variable parameter in the iterative matching procedure. The solution estimated the vertical to horizontal hydraulic conductivity ratio of the site 11 combined aquifers to be between 0.1 and 0.4.

For comparison, the hydraulic properties obtained using the Moench (1997) solution on the combined basin-fill and carbonate-rock aquifer, but with a no-flow boundary 1500 feet (457 m) west of the well, are listed on table 7.2. For most of the observation wells, the boundary did not appreciably change the transmissivity or storativity estimates. Only the transmissivity estimate for the basin-fill well, PW11B, was significantly higher than in the unbounded case. Specific yield in the carbonate-rock wells, however, did increase in the bounded case, suggesting that this solution is not unique in the case of transmissivity.

Our most robust and realistic analysis of site 11 aquifer-test data used the Neuman and Witherspoon (1969) solution and treated the site as a leaky aquifer overlying an 1800-foot-thick (550 m) confined aquifer, separated by a 25-foot-thick (8 m) aquitard. Transmissivity estimates of the Ely Limestone range from 7300 to 12,600 feet squared per day (660–1200 m^2/day) (table 7.2). Based on a saturated thickness of 1800 feet (550 m), the hydraulic conductivity of the Ely Limestone is between 4 and 7 feet per day (1–2 m/d). Our estimate of basin-fill transmissivity using the Neuman and Witherspoon (1969) solution is approximately 75,000 feet squared per day (7000 m^2/day) (table 7.2). Based on a saturated thickness of 260 feet (79 m), hydraulic conductivity of the basin fill ranges is approximately 290 feet per day (88 m/day). Storativity of the Ely Limestone estimated using Neuman and Witherspoon (1969) is approximately 3 x 10^{-4}. Storativity of the basin fill is approximately 1 x 10^{-2}.

The transmissivity estimates of the carbonate-rock aquifer using the two-aquifer solution but also including a no-flow boundary 1500 feet (457 m) west of the site 11, are not appreciably different from the estimates of the unbounded setting (table 7.2). The transmissivity of the bounded basin-fill aquifer is approximately twice that of the unbounded case. If our software program had been able to model the aquifer boundary only in the carbonate-rock aquifer, the results would have shown higher transmissivity in the bounded carbonate-rock aquifer and little difference in the unbounded basin-fill aquifer transmissivity.

Transmissivity estimates obtained by treating site 11 as one aquifer and matching the groundwater-level data using the Moench (1997) solution, which does not account for leakage, are likely overestimates. Transmissivity estimates using the Neuman and Witherspoon (1969) technique on our partially penetrating carbonate-rock aquifer well data are likely underestimates because the solution does not account for partial penetration. A median value between the values from each solution is likely the most representative of actual aquifer transmissivity.

Independent of the analysis applied, transmissivity generally decreases as depth of the open intervals of the wells increases.

7.2.7 Combination Solution (MLU)

As an alternative to the strictly analytical solutions described above, we performed aquifer analyses with MLU (Multi-Layer Unsteady state) for Windows aquifer-test analysis software (Hemker, 1999; Hemker and Post, 2009), a robust and flexible application which uses a combination of analytical and numerical techniques to derive solutions (Hemker, 1999; Carlson and Randall, 2012). MLU models hydraulic properties based on a best-fit analytical solution to measured data using an automatic curve-fitting algorithm that optimizes hydraulic properties and fitted drawdown. MLU, unlike analytical technics such as AQTESOLV, is based on a single analytical solution technique for well flow. This technique allows for examination of multiple aquifer layers. We used the light version of this software, which allows two aquifers and two observation wells.

MLU uses the Stehfest (1970) numerical method to apply the Laplace equation to groundwater potential. MLU also includes programming that applies the superposition principle in space (wells at different locations) and

Table 7.2. *Hydraulic properties at site 11 determined using analytical solutions (AQTESOLV).*

Solution: Moench (1997) for an unconfined aquifer, accomodates borehole storage and partial penetration

INPUT					RESULTS Combined basin-fill and carbonate-rock aquifers					
Observation Wells	Boundary	Basin-fill thickness (ft)	Ely Limestone thickness (ft)	Total saturated thickness (ft)	K_z/K_r [1]	Transmissivity (ft^2/day)	Storativity	Specific yield	S_w [2]	K
PW11B	No	NA: Units are combined		2060	0.4	42,500	2E-02	0.33	0.7	21
	Yes	NA: Units are combined		2060	0.1	52,100	1E-02	0.30	0.7	25
PW11C	No	NA: Units are combined		2060	0.1	57,100	1E-03	0.03	1.0	28
	Yes	NA: Units are combined		2060	0.1	56,400	1E-03	0.07	1.0	27
PW11D	No	NA: Units are combined		2060	0.3	57,100	2E-03	0.04	0.8	28
	Yes	NA: Units are combined		2060	0.3	57,100	1E-03	0.07	0.7	28
PW11E	No	NA: Units are combined		2060	0.3	30,000	3E-04	0.07	0.5	15
	Yes	NA: Units are combined		2060	0.4	30,000	3E-04	0.09	0.8	15
NPA-1B	No	NA: Units are combined		2060	0.3	18,000	NA	NA	4.8	9

Solution: Neuman-Witherspoon (1969) for a leaky, two aquifer system

INPUT						RESULTS					
						Ely Limestone			Basin fill		
Observation Wells[4]	Boundary	Basin-fill thickness (ft)	Ely Limestone thickness (ft)	Total saturated thickness (ft)	K_z/K_r [1]	Transmissivity (ft^2/day)	Storativity	K	Transmissivity (ft^2/day)	Storativity	K
PW11C,D	No	260	1800	2060	0.1	12,600	3E-04	7	NA	NA	NA
	Yes	260	1800	2060	0.1	12,500	3E-04	7	NA	NA	NA
PW11B,C,D	No	260	1800	2060	0.1	10,300	3E-04	6	74,900	1E-02	290
	Yes	260	1800	2060	0.1	10,400	3E-04	6	153,000	2E-03	590
PW11B,E	No	260	1800	2060	0.1	7300	2E-04	4	74,200	7E-03	290
	Yes	260	1800	2060	0.1	7400	2E-04	4	155,000	2E-03	600

NA: Not applicable.

[1] K_z is vertical hydraulic conductivity; K_r is horizontal (radial) hydraulic conductivity.

[2] S_w is wellbore skin factor (dimensionless).

[3] Pumping well data do not produce reliable estimates of storativity.

[4] If multiple wells are listed, multiple curves were matched simultaneously to the data.

[5] Estimate not applicable because there is no observation well in the basin fill.

time (variable discharges of each well). MLU applies the Levenberg-Marquardt algorithm for parameter optimization (automated curve fitting) to match the modeled behavior to measurements (Pujol, 2007).

MLU requires the user to assign boundaries and parameters to model aquifer response to pumping. For the site 11 MLU model, we designated the Chainman Shale of the middle Paleozoic siliciclastic-rock confining unit as an aquitard. We modeled the system as a two-aquifer system (basin-fill and carbonate-rock). Although MLU allows the user to input factors describing the nature of well screens, we did not include this feature because we did not know the efficiency of the wells used for this test. MLU requires the user to specify hydraulic-property variables for the model. We allowed the transmissivity and storativity of each of the two aquifers to vary. To simplify the model, we set the vertical hydraulic conductivity of the model aquitard layer arbitrarily low (1×10^{-6} ft/day [3×10^{-7} m/day]).

We conducted three MLU model runs using two observation wells in each run (PW11B and PW11C, PW11B and PW11D, and PW11B and PW11E) so that in each case, we could determine the hydraulic properties for both the basin fill and Ely Limestone. We did not include in this report our analyses from well PW11A or pumping well NPA-1B, due to suspect data and incomplete data in those wells, respectively. However, examination of MLU models using the available pumping well data resulted in comparable hydraulic-property estimates.

Results of modeling using MLU are summarized in table 7.3 and figure 7.11. The results indicate a transmissivity range from 54,200 to 89,000 feet squared per day (5040–8270 m^2/day) for the basin-fill aquifer and 11,700 to 37,100 feet squared per day (1090–3450 m^2/day) for the Ely Limestone (upper Paleozoic carbonate-rock aquifer hydrogeologic unit). Transmissivity in the deepest tested portion of the carbonate-rock aquifer is about one third that of the shallowest level. Storativity of the basin fill ranges from 0.0003 to 0.004, and the Ely Limestone aquifer storativity ranges from 0.0004 to 0.001.

7.2.8 Attempt to Model Site 11 Aquifer Test Numerically

We constructed a digital numerical groundwater-flow model of site 11 using MODFLOW-2000 (Harbaugh and others, 2000) modeling software. A groundwater-flow model would be useful for site 11 site because (1) hydraulic properties for both aquifers can be estimated simultaneously, a task less easily done using curve-matching software, (2) the volume of vertical leakage from the basin-fill to the carbonate-rock aquifer can be simulated, and (3) it would provide another means of aquifer-test analysis to compare to analytical and combination methods.

Our first numerical model of site 11 extended from the surface down to the Chainman Shale aquitard and laterally out from site 11 about 3 miles in each direction, or to the ridges of the Mountain Home Range surrounding the site. This large model proved to be ineffective at predicting water levels because we lacked water-level data at the more distal areas of the model domain to calibrate the model. We scaled the model down to an area of 7.8 acres (3.2 ha) around NPA-1B and the site 11 observation wells (584 feet [178 m] square), which allowed us to discretize the digital model into a fine grid and model short time steps while keeping computational time within reason; however, this area proved to be so small as to violate the assumption that the aquifers have infinite areal extent. Therefore, we do not present the results of our numerical modeling in this report.

7.2.9 Discussion

7.2.9.1 Summary of Hydraulic Properties and Comparison to Other Studies

We compiled the results of our analyses of the multiple-well aquifer test at site 11 (tables 7.2 and 7.3) and comparable results from other studies into table 7.4. Our results show the transmissivity of the basin-fill aquifer to be between 54,200 and 89,000 feet squared per day [5000–8300 m^2/day], which is about two to five times greater than that of the carbonate-rock aquifer (7300 to 37,100 feet squared per day [660–3500 m^2/day]) (table 7.4). Storativity is approximately an order of magnitude larger in the basin fill (3×10^{-4} to 1×10^{-2}) as carbonate rock (2×10^{-4} to 1×10^{-3}) (table 7.4). Our one estimate of specific yield from the basin-fill observation well (PW11B) was 0.33, slightly higher than values typically reported for unconsolidated sand and gravel aquifers (0.23 to 0.28 [Johnson, 1967]).

Our hydraulic-property estimates are significantly different from estimates determined from the BARCAS study (Sweetkind and others, 2007). The arithmetic mean of 13 hydraulic conductivity measurements of the finer basin-fill material reported in the BARCAS study is 34 feet per day (10 m/day) and the coarser basin-fill material is 40 feet per day (12 m/day) (43 measurements), which are lower than our estimates of hydraulic conductivity from the site 11 aquifer test by up to as much as an order of magnitude (table 7.4). The BARCAS study reports that Mississippian age carbonates in the area have an average hydraulic conductivity of 145 feet per day (44 m/day) (12 measurements) (Sweetkind and others, 2007), which is higher than our estimates of hydraulic conductivity by about one order of magnitude (table 7.4). Our test represents only one

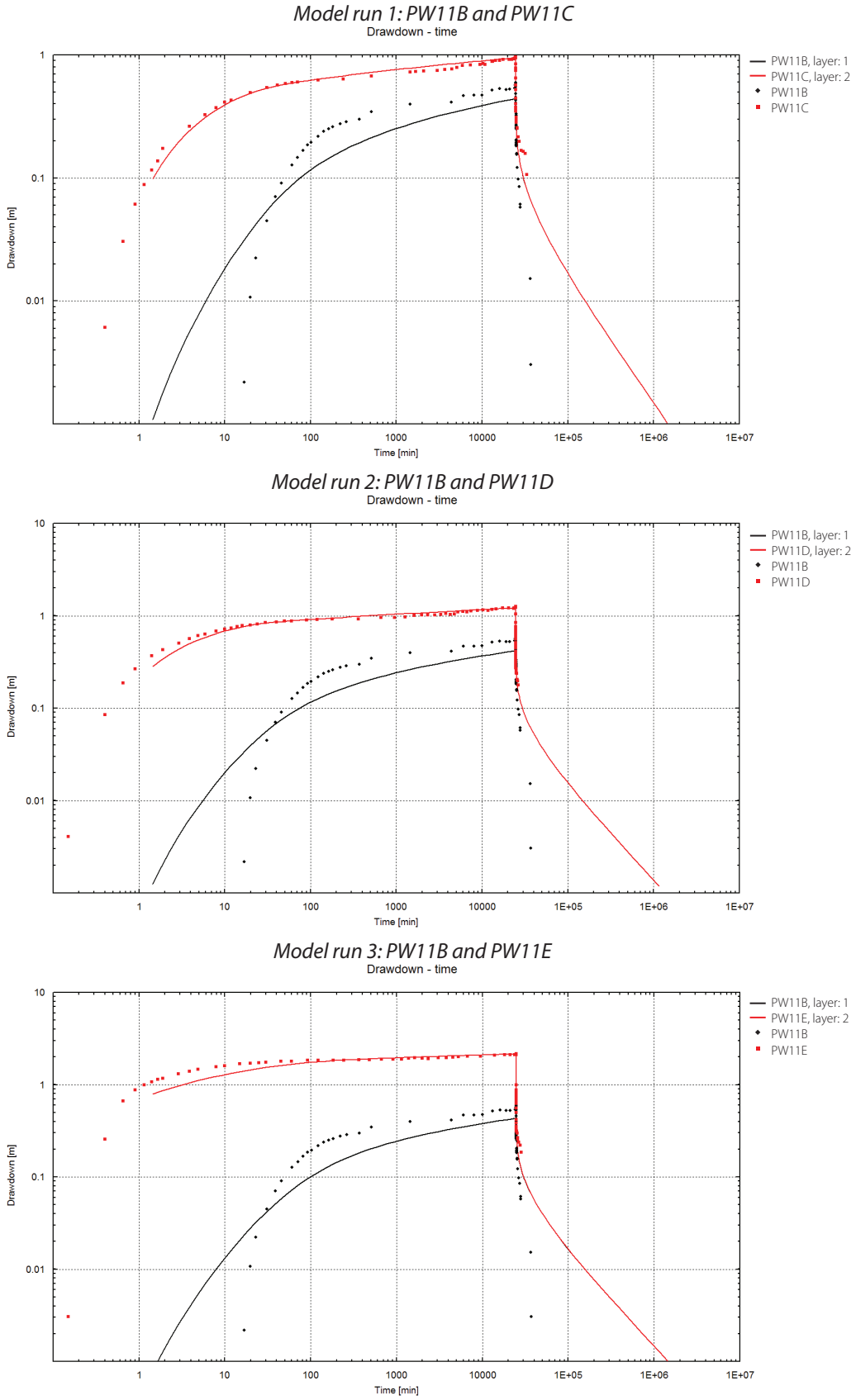

Figure 7.11. *Drawdown at site 11 (solid lines) modeled to observed water levels (points) using a combined analytical and numerical technique (MLU). Table 7.3 shows aquifer-parameter results.*

Table 7.3. *Hydraulic-property estimates of transmissivity (T), storativity (S), and horizontal hydraulic conductivity (K) obtained by modeling a two-aquifer system at site 11 using a combined analytical and numerical technique (MLU for Windows).*

Model run	Well	Aquifer	Base elevation (ft)	Thickness (ft)	T (ft²/day)	T error[1] (ft²/day)	S	S error[1]	K (ft/day)
1	B	Basin fill	5207	259	54,200	7400	3.E-04	2.E-04	210
2	B	Basin fill	5207	259	81,600	6300	4.E-03	1.E-03	310
3	B	Basin fill	5207	259	89,000	7500	1.E-03	6.E-04	340
1	C	Ely Limestone	3405	1801	37,100	3900	1.E-03	2.E-04	21
2	D	Ely Limestone	3405	1801	20,400	1900	9.E-04	1.E-04	11
3	E	Ely Limestone	3405	1801	11,700	1200	4.E-04	6.E-05	6

[1]Error is based on measures of goodness of fit of the theoretical curve to the actual data.

Table 7.4. *Summary and comparison of hydraulic-property estimates for the basin-fill and upper Paleozoic carbonate-rock aquifers from tests at site 11 or in Snake or Spring Valleys.*

Source	Transmissivity (ft²/d)	Hydraulic conductivity (ft/d)	Storativity or Specific Yield (Sy) where noted
Basin fill			
This study, analytical solutions	75,000	290	$7x10^{-3}$–$1x10^{-2}$
This study, combination	54,200–89,000	210–340	$3x10^{-4}$–$4x10^{-3}$
BARCAS (Sweetkind and others, 2007)	NC	34–40	NC
Needle Point well field multi-year test (Dong and others, 2011)	1200–1300	0.6	0.12–0.13 (Sy)
Big Springs NW well (Halford, 2010a)	10,000	25	>0.05
Baker/Eskdale well field multi-year test (Halford and Plume, 2011)	5600–9000	NC	0.12–0.13 (Sy)
upper Paleozoic carbonate-rock aquifer			
This study, analytical solutions	7300–12,600	4–8	$2x10^{-4}$–$3x10^{-4}$
This study, combination	11,700–37,100	6–21	$4x10^{-4}$–$1x10^{-3}$
BARCAS (Sweetkind and others, 2007)	NC	145	NC
Needle Point well field multi-year test (Dong and others, 2011)[1]	7000–16,000	7–15	0.001–0.006 (Sy)
Big Springs SW well (Halford, 2010b)	4,000	NC	>0.05
2 SNWA wells in Spring Valley (Prieur and others, 2010; Halford and Plume, 2011)	10,000–55,000	NC	0.02–0.04 (Sy)
Combined basin fill and bedrock			
This study, analytical solutions	30,000–57,100	15–28	$3x10^{-4}$–$2x10^{-2}$

NC: not compared
[1] The carbonate-rock aquifer west of Needle Point in which Granite Peak Properties' wells are completed is likely the Permian Arcturus formation, which is part of the upper Paleozoic carbonate-rock aquifer.

location, which may be one reason for the difference.

Researchers from SNWA and U.S. Geological Survey estimated hydraulic properties by analyzing water-level changes induced by seasonal agricultural irrigation pumping from a well field (Granite Peak Ranch) along the Nevada–Utah border, west of Needle Point (Dong and others, 2011). The Needle Point analysis used a MODFLOW 3D groundwater-flow model (Harbaugh and MacDonald, 1996) to match simulated water-level response to measured water levels in four observation wells affected by well-field pumping over a period of 3 years. Reported transmissivity and specific yield of the basin-fill aquifer are 1200 to 1300 feet per day (110–120 m^2/d) and 0.12 to 0.13, respectively. For comparison, our basin-fill transmissivity estimates (54,200 and 89,000 feet squared per day [5000–8300 m^2/day]) are much higher. Dong and others' (2011) transmissivity and specific yield of the carbonate-rock aquifer in the Needle Point area (most likely composed of the Permian Arcturus formation, which is also in the upper Paleozoic carbonate aquifer unit) are 7000 to 16,000 feet squared per day (650–1500 m^2/d) and 0.001 to 0.006. Compared to our Ely Limestone transmissivity estimates (7300 to 37,100 feet squared per day [660–3500 m^2/day]), the Arcturus Formation has similar transmissivity to the Ely Limestone.

The U.S Geological Survey (Halford, 2010a, 2010b) conducted two single-well aquifer tests in Snake Valley, about 8 miles (13 km) west of site 11. The reported transmissivity for the basin-fill aquifer from those tests is 10,000 feet squared per day (930 m^2/day) (Halford, 2010a), whereas the transmissivity of the fractured carbonate-rock aquifer (unit not specified, but likely is the Ely Limestone) is 4000 feet squared per day (470 m^2/day) (Halford, 2006). Halford's (2010a, 2010b) transmissivity estimates are lower than our estimates for the basin-fill aquifer (54,200 to 89,000 feet squared per day [5000–8300 m^2/day], table 7.4), and the Ely Limestone (7300 to 37,100 feet squared per day [660–3500 m^2/day]). The discrepancy may result from (1) greater saturated thickness of the basin-fill aquifer at site 11, (2) differences in sedimentary texture, or (3) inaccuracy of the methods applied (for both tests). The relative differences in transmissivity between the Ely Limestone and the basin fill are similar. Halford (2010a) estimated a storage coefficient of >0.05 for the basin-fill aquifer, at the high end of our estimates (table 7.4).

SNWA estimated a transmissivity range of 10,000 to 55,000 feet squared per day (900–4600 m^2/day) for the Ely Limestone in Spring Valley (Prieur and others, 2010; Halford and Plume, 2011). The results of our multiple-well aquifer-test analyses are similar to these values.

Our result using the Moench (1997) analysis (T = 30,000 to 57,100 feet squared per day [2800–5300 m^2/day], table 7.4) represents a bulk transmissivity of the entire saturated thickness in the aquifer-test area, including both the basin-fill and carbonate-rock aquifers, which skews the estimate to values that are intermediate between basin fill and bedrock.

7.2.9.2 Anisotropy

One objective of the site 11 aquifer test was to evaluate horizontal anisotropy of hydraulic conductivity in the Ely Limestone, by siting observation wells in directions parallel (north) and perpendicular (west) to the local fold axis projected from the northern Mountain Home Range, relative to the pumping well (figure 7.2). However, we compromised our ability to easily analyze horizontal anisotropy by placing the carbonate-rock observation wells at different depths, in order to collect information about vertical anisotropy (figure 7.5). Therefore, we can make only general observations on the nature of horizontal anisotropy and heterogeneity within the carbonate-rock aquifer at site 11.

Contours of drawdown projected onto the vertical cross section through site 11 (figure 7.7) show that equipotential lines are more widely spaced in the direction of piezometer PW11C (west) than PW11D and E (north). In a well that fully penetrates a confined aquifer, this condition would indicate that transmissivity is greater in the direction of PW11C (perpendicular to the fold axis) as compared to PW11D and E (parallel to the fold axis) (Ferré and Thomasson, 2010), contrary to our original assumption. However, partial penetration by the pumping and observation wells and leakage of water from the overlying basin-fill aquifer would tend to decrease drawdown in PW11C relative to PW11D and E, which, if not accounted for in the analysis, would artificially increase the transmissivity calculation from PW11C data. Fortunately, most of the analysis techniques we used factor leakage into the analysis and generate hydraulic properties that are representative of the aquifer.

Transmissivity decreases with depth at site 11. The results from combination solutions (table 7.3) clearly show that the transmissivity at the bottom of the tested interval (1200 feet [370 m]) is about one-fifth of the transmissivity near the top of the carbonate-rock aquifer. Although not as straightforward, the analytical curve matching results also show decreasing transmissivity with depth. Observation wells PW11C and PW11D (table 7.2, figures 7.9 and 7.10) show higher transmissivity than the deeper observation well PW11E.

Most of our analytical results show more similar transmissivity values in the upper and middle parts of the carbonate-rock aquifer compared to the lower carbonate-

rock aquifer (results from observation PW11C and PW11D as compared to PW11E, table 7.2). PW11C and PW11D are at right angles to the pumping well, suggesting that horizontal anisotropy is not large in the upper and middle part of bedrock aquifer.

7.2.9.3 Hydraulic Connection Between Aquifers

Proof that the basin-fill aquifer is supplying water to the bedrock aquifer is provided by the nearly 2 feet of drawdown in the basin-fill observation well (PW11B), despite the fact that NPA-1B has no screen or open interval in this aquifer. The significant time delay between the response of observation well PW11B and the start of pumping NPA-1B (16 minutes) as compared to the nearly immediate response of the carbonate-rock monitoring wells, indicates that the basin-fill and carbonate-rock aquifers are hydraulically connected but do not act as one aquifer.

7.3 SITE 3 AQUIFER TEST

7.3.1 Location and Geologic Setting

Site 3 is 2 miles (3 km) east-northeast of Garrison, Utah, on the northwest margin of the Burbank Hills (figure 7.12). Irrigation wells supply water for about 1000 acres (400 ha) of cropland (chiefly alfalfa) within about 2.5 miles (4 km) of the Garrison town center. These irrigation wells are screened in the basin-fill aquifer, whereas the pumping and observation wells at site 3 are screened in rocks of the lower Paleozoic carbonate-rock aquifer (LPzc on figure 4.1). Site 3 is approximately 2 miles (3 km) east-northeast of site 13 and 3 miles (5 km) east-northeast of site 1.

Site 3 is on the northwestern margin of the Burbank Hills, in faulted and tilted rocks of the lower member of the Devonian Guilmette Formation of the lower Paleozoic carbonate-rock aquifer (figure 7.12; plates 1 and 2; Hintze, 1997). Outcrops are composed of healed autoclastic breccia, in which the carbonate clasts are medium to dark gray, fine-grained limestone and dolomite, and the matrix is composed of similar material (figure 7.13a). White calcite veins up to several millimeters thick cut clasts and matrix. Poorly defined bedding strikes northeast and dips about 20 to 30 degrees southeast (figure 7.13b). Fractures include a more abundant set that strikes north-northeast, dips 75 to 85 degrees northwest, and is spaced 3 to 10 feet (1–3 m), and a less abundant set that strikes west-northwest, dips 70 to 85 degrees north-northeast, and is spaced 5 to 15 feet (2–5 m). Several northwest- to northeast-striking normal faults occur in the northwestern Burbank Hills, and a north-striking, steeply west-dipping thrust fault juxtaposes the lower (hanging wall) and middle (footwall) members of the Guilmette Formation 0.5 mile (0.8 km) east of site 3 (figures 7.12 and 7.14) (Hintze, 1997). Boreholes PW03AB and PW03P intercept a gently northwest-dipping fault that places the lower member of the Guilmette Formation on the Devonian Simonson Dolomite; its precise orientation is unknown because only two control points exist (figures 7.14 and 7.15). We interpret this fault as the northward continuation of an "attenuation" fault (i.e., a gently dipping fault that accomplishes structural thinning) shown near the northwestern end of Hintze's (1997) cross section B–B′. In our interpretation, the site 3 wells are in the hanging wall of a northeast-striking, northwest-side-down normal fault whose trace lies along the base of the northwestern Burbank Hills (figures 7.14 and 7.15).

The northwestern Burbank Hills comprises the southeast-dipping limb of a northeast-striking syncline that is in the footwall of a northeast-striking, southeast-dipping thrust fault (plate 1). The thrust fault and syncline hinge are about 4 miles (6.4 km) southeast of site 3. Two to 3 miles (3–5 km) east of site 3 are two structural domes that are 1 to 2 miles long (3–6 km) and 1 mile (2 km) wide, and have cores composed of Devonian Pilot Shale and rims composed of the Mississippian Joanna Limestone, both of the middle Paleozoic siliciclastic-rock confining unit (MPzs).

7.3.2 Site Selection and Preparation

We decided to perform an aquifer test at site 3 because the lower Paleozoic carbonate-rock aquifer, by virtue of its thickness, structural position, and areal distribution, likely accommodates flow and storage of large volumes of groundwater in the study area, and estimates of its hydraulic conductivity and storativity will provide constraints on these parameters for existing and future numerical groundwater flow models.

A crew from the U.S. Geological Survey Western Region Research Drilling Program installed completed borehole PW03AB (tables C.1 and 7.1) in September 2007. During summer 2008, the U.S. Geological Survey crew installed the pumping well PW03P and another contractor installed observation well PW03Z, 164 feet and 302 feet (50 and 92 m), respectively, northwest of PW03AB (table 7.1, figure 7.15). PW03P is cased to 296 feet (90 m) and is open from the base of the casing to its total depth of 845 feet (258 m) (table 7.1). The borehole is in the Devonian Guilmette Formation to approximately 740 feet (225 m), where we place the contact with the underlying Devonian Simonson Dolomite at the attenuation fault described above, which we interpret to be the same fault encountered at 705 feet (215 m) in borehole PW03AB. The lower part of borehole PW03P, from 810 to 845 feet (247–258 m) depth, inter-

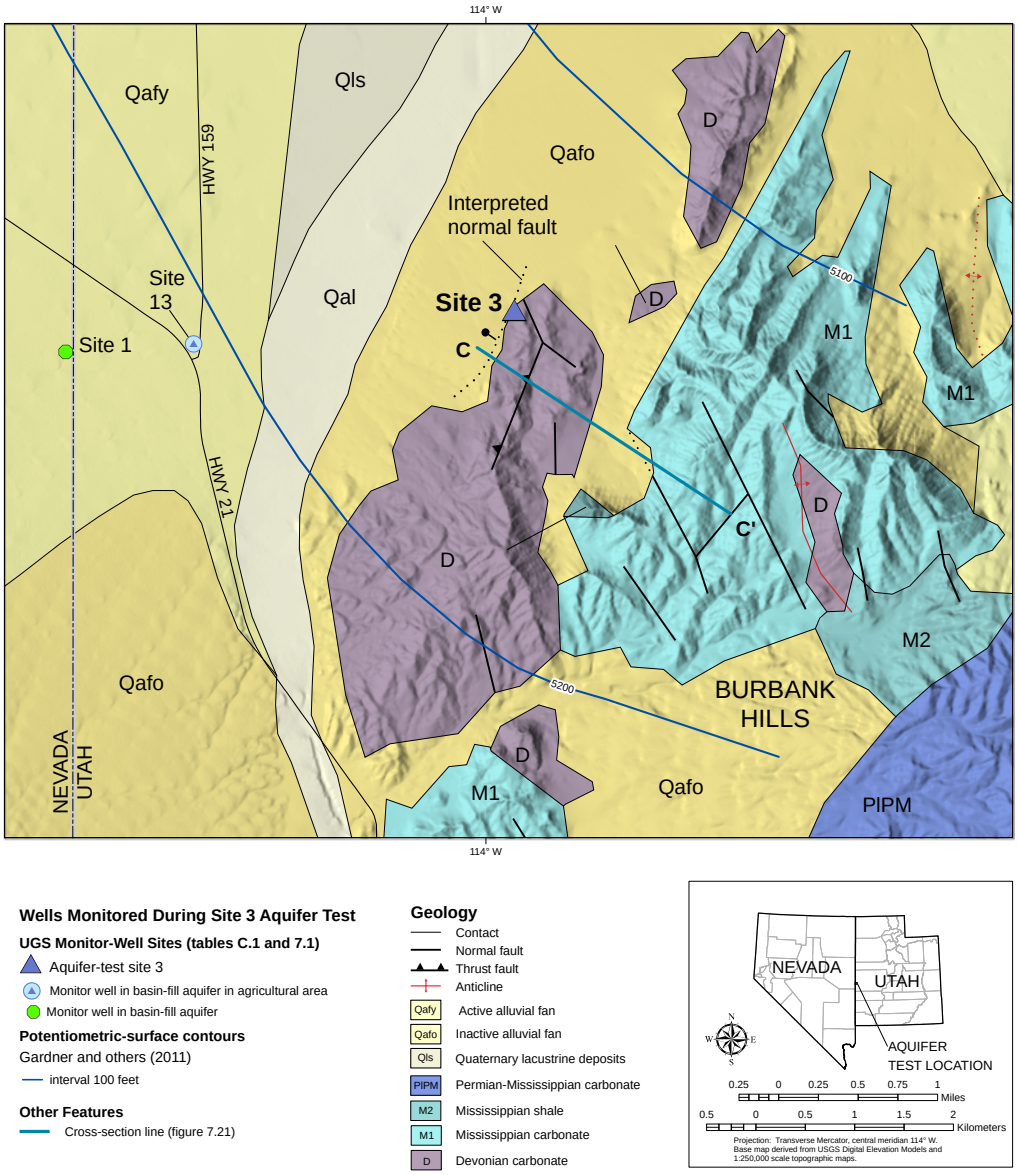

Figure 7.12. *Geologic setting of UGS aquifer-test site 3.*

sects a water-bearing fracture zone. Borehole PW03AB intersects a water-bearing fracture zone from 830 to 835 feet (253–255 m) depth (figure 7.15). The elevation of the bottom of the steel casing in PW03P is 4 feet (1.2 m) below that of the screen midpoint in observation well PW03A, which is completed in the Guilmette Formation; the bottom of PW03P is 7 feet (2.1 m) higher than the bottom of the screen in observation well PW03B, which is completed in the Simonson Dolomite (figure 7.15). This configuration ensures that the pumping well is open to the carbonate-rock aquifer at approximately the same elevations as the screens in the observation wells. The midpoint of the screened interval in observation well PW03Z is 80 feet (24 m) higher than the base of the casing in PW03P (table 7.1, figure 7.15) and about 40 feet (12 m) below the water table, which allows PW03Z to monitor water-level response to pumping near the top of the saturated zone.

SNWA estimated a transmissivity range of 9000 to 38,000 feet squared per day (800–3500 m^2/day) for the Guilmette Formation and Simonson Dolomite combined from the results of an aquifer test they conducted on their test wells W101 and W502M in Spring Valley (James Prieur, SNWA, electronic communication, January 18, 2008). Based on these results and on constraints imposed by well geometry and groundwater levels at site 3, we anticipated conducting our aquifer test at 800 to 1000 gallons per minute (3030–3790 L/min).

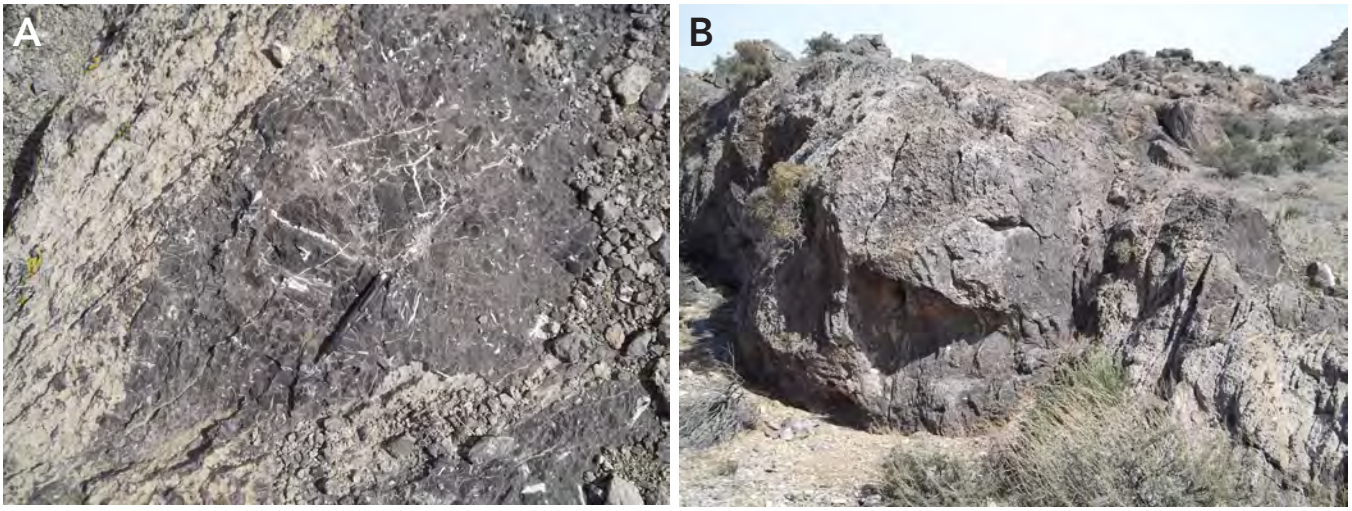

Figure 7.13. *Devonian Guilmette Formation of the lower Paleozoic carbonate-rock hydrogeologic unit at UGS aquifer-test site 3. The pumping and observation wells at this site are in this unit and the underlying Devonian Simonson Dolomite.* ***A.*** *Close-up of carbonate autobreccia.* ***B.*** *Outcrop view facing southeast showing gently southeast-dipping bedding and vertical joints.*

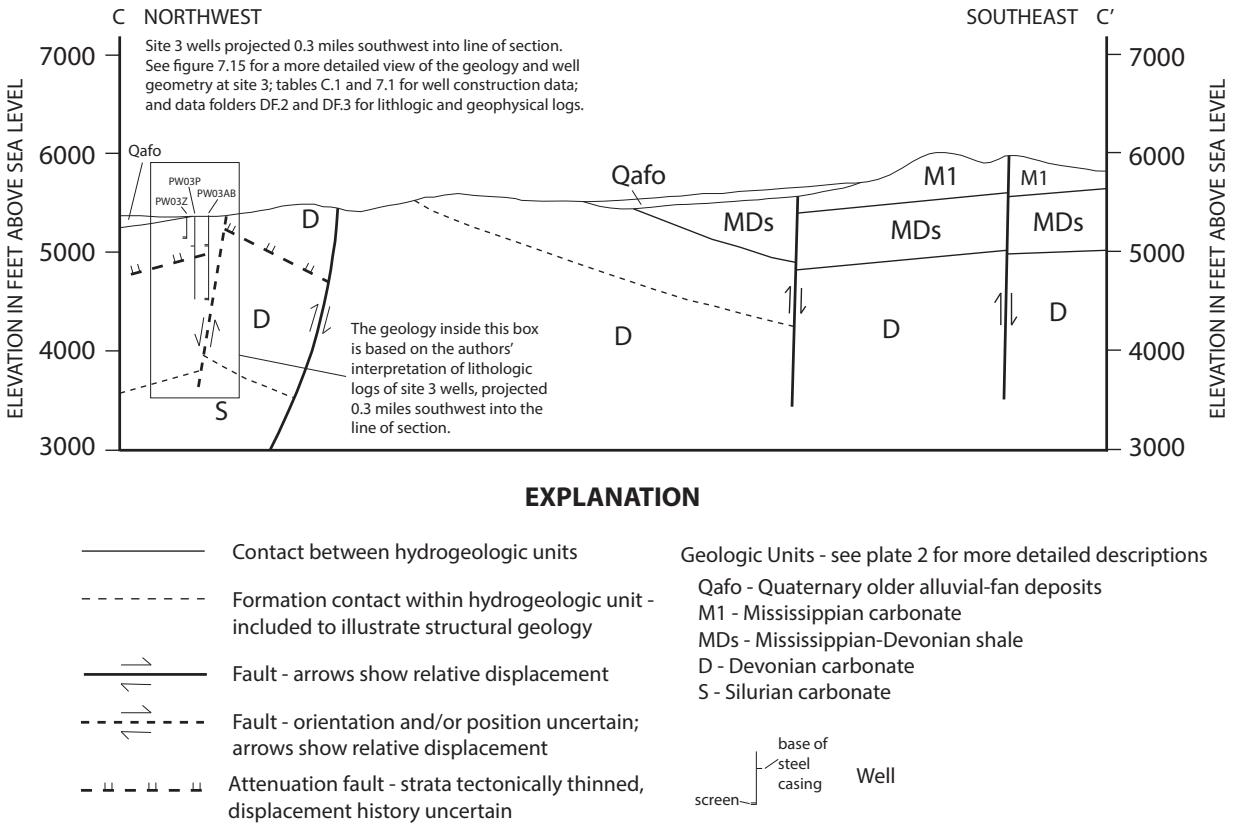

Figure 7.14. *Geologic cross section through aquifer-test site 3. Simplified and modified from section B-B' of Hintze (1997).*

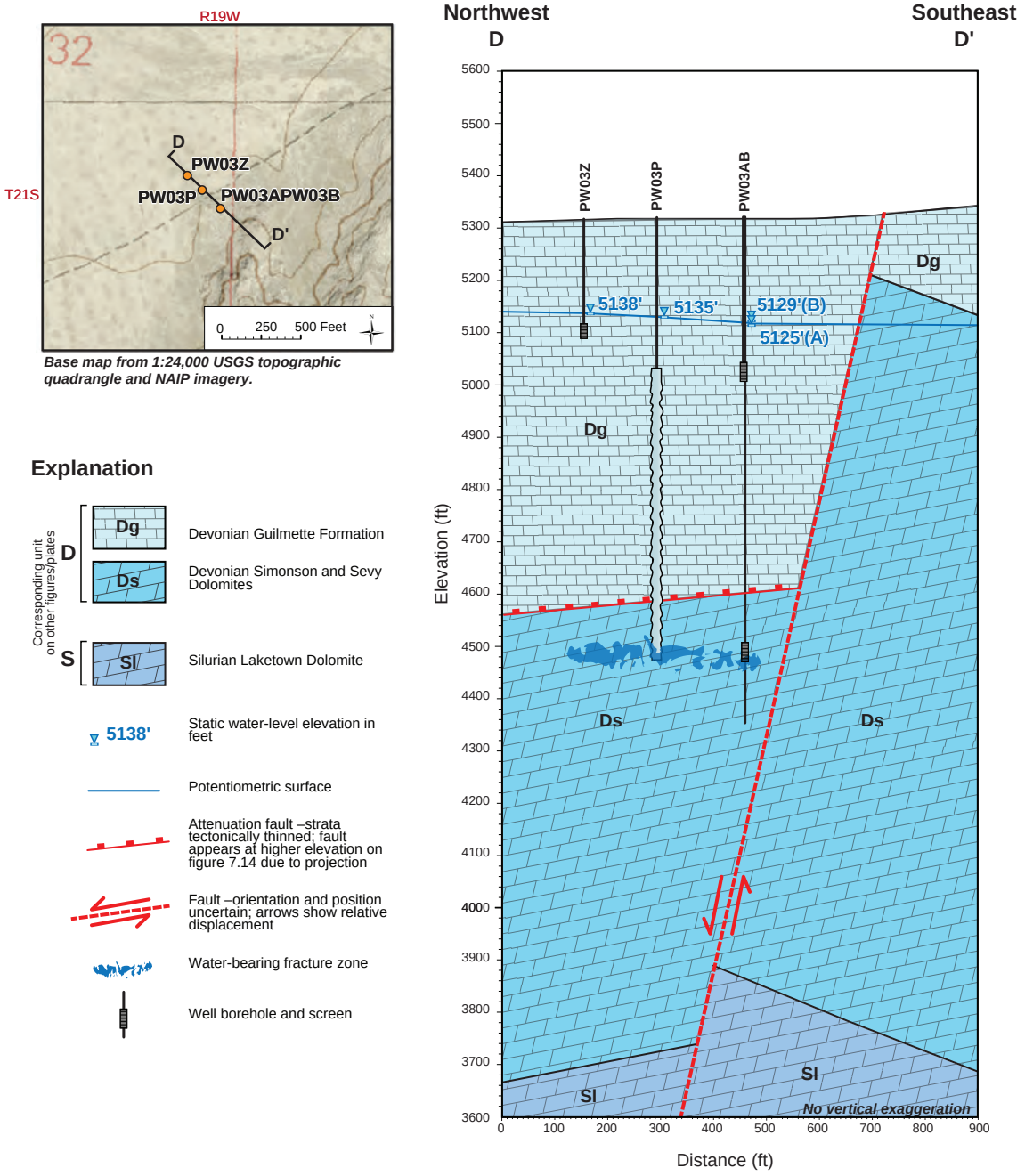

Figure 7.15. *Site 3 cross section showing the relation of well screens, the water table, geologic contacts, and interpreted geologic structure.*

7.3.3 Test Design and Implementation

We conducted the drawdown portion of the test in March 2009 to coincide with the time of year when water levels in wells near Garrison are at their most stable, and before the start of the irrigation season. In chapter 5, section 5.2.4.1, we describe the influence Garrison area agricultural pumping has on the basin-fill and carbonate-rock aquifers (wells at sites 3, 13, and 1). Groundwater monitoring data from sites 13 and 1 indicate that water levels in February and early March 2009 before the start of our test were either slowly rising or stable and were at their most recovered condition since the previous irrigation season. Wells at site 3 were on a long-term steady decline, as discussed below; we accounted for this decline in our aquifer test analysis. Water-level monitoring before and during the drawdown portion of site 3 aquifer test and for most of the recovery portion of the test was conducted prior to any influence from 2009 agricultural pumping.

The pump contractor performed a preliminary test on March 9, 2009, after setting a line-shaft pump with the top of the pump bowls at 273 feet (83 m) deep and the water intake at 277 feet (84 m). Pumping at our desired rate of 800 gallons per minute (3030 L/min) resulted in a very fast rate of drawdown, so the contractor reduced the pumping rate to 230 gallons per minute (870 L/min) for 20 minutes, then to 180 gallons per minute (680 L/min) for 4 minutes. The depth to water reached 252 feet (77 m) below land surface. The contractor determined that pumping the well at 180 gallons per minute (680 L/min) would produce a stable water level safely above the pump intake during a 12-day aquifer test. The contractor obtained a different submersible pump, which he set with the top at 282 feet (86 m) and the intake at 290 feet (88 m) below land surface.

The drawdown part of the site 3 aquifer test began at 9:30 a.m. on March 13, 2009. The pump contractor quickly stabilized discharge at 180 gallons per minute (680 L/min) by adjusting an orifice valve to keep the height of the water-column in a pitot tube connected to the discharge line at a constant level. Flow was measured by a McCrometer in-line propeller-type flow meter. The 180 gallons per minute (681 L/min) pumping rate remained constant for the duration of the test. The drawdown test ended at 10:30 a.m. on March 25, 2009, after pumping for 12 days, 1 hour (17,340 minutes).

To avoid infiltration of discharge from pumping well PW03P through the alluvial fan to the water table, thereby affecting the drawdown response in our observation wells, we piped the discharge from PW03 approximately 500 feet (150 m) northwest of the well and 360 feet (110 m) from well PW03Z (figure 7.16b). From the end of the pipe, the discharge flowed northwest in a small drainage channel where it infiltrated into the alluvium. Before the test, the static depth to water in well PW03Z was approximately 175 feet (53 m). We calculated that at an infiltration rate of 0.3 feet per hour (0.09 m/hr), recharge would reach the static water table after approximately 570 hours, almost twice the amount of time that we pumped. We saw no noticeable effects of surface recharge on the drawdown data or their derivatives.

7.3.4 Water-Level Observations and Trend Corrections

We measured water levels in all wells at sites 3, 13, and 1 using pressure transducers supplemented by electronic-tape measurements. The data-collection interval in the transducers at site 3 was one reading per second at the beginning of the test, increased by a log-time scale to 5 minutes during the first 3 hours, and was set to 15 minutes thereafter. We encountered several problems with operation of the transducers, so we have no transducer water-level data for the first approximately 1.5 hours of the test in the pumping well and after a few days in two of the observation wells; however, we have manual measurements for those time periods. Water levels in observation wells at distal well sites 1 and 13 were measured twice daily during the test using pressure transducers and checked by electronic-tape measurements. We collected recovery data through May 21, 2009, using the same data-collection schedule as in the pumping part of the test. Water-level data are provided electronically in table DF.4 in the Aquifer Test Data folder on this CD.

First we removed a continuous downward linear trend in water levels at site 3 wells from the background, pumping, and recovery water-level data. To remove the trend, we determined the rate of downward trend over time (slope) from 4 months of pre-test water-level measurements. We also examined the slope of the water-level data collected during the year following the test to determine the likelihood of seasonal changes in slope during the springtime when we were conducting the aquifer test. Based on examination of the following year's slope and trends of the post- and pre-test data, we determined that significant slope changes in the downward trend of the groundwater-level data were unlikely. We subtracted the downward trend from the data to get de-trended water levels.

We also examined the data for influence on the groundwater level from barometric pressure changes or earth tides, but because drawdown greatly exceeded the possible magnitudes of these effects for all of the observation wells, we did not remove those trends.

7.3.5 Aquifer Response

Aquifer response in the pumping and observation wells is shown on figure 7.17. Water levels in all wells began drawing down within 30 seconds of the start of pumping. The drawdown curves of observation wells PW03P and PW03B are flattened in late time compared to a typical homogeneous, confined aquifer (figure 7.17). The flattened shape of the drawdown curves and the shape of the derivative curves (figure 7.18) suggest either a fractured or unconfined aquifer system (Bourdet, 2002; Renard and others, 2009). PW03Z, the shallowest completion at site 3, experienced less drawdown (5.77 feet [1.76 m], table 7.1) than the deeper completions, the response most typical of a confined homogeneous aquifer, even though this well is the closest to water table and therefore most likely to show an unconfined water-table response. PW03A and PW03B are at the top and bottom of the pumping well open interval, respectively. PW03A experienced more drawdown than PW03B (7.65 feet [2.33 m] versus 7.01 feet [2.14 m], table

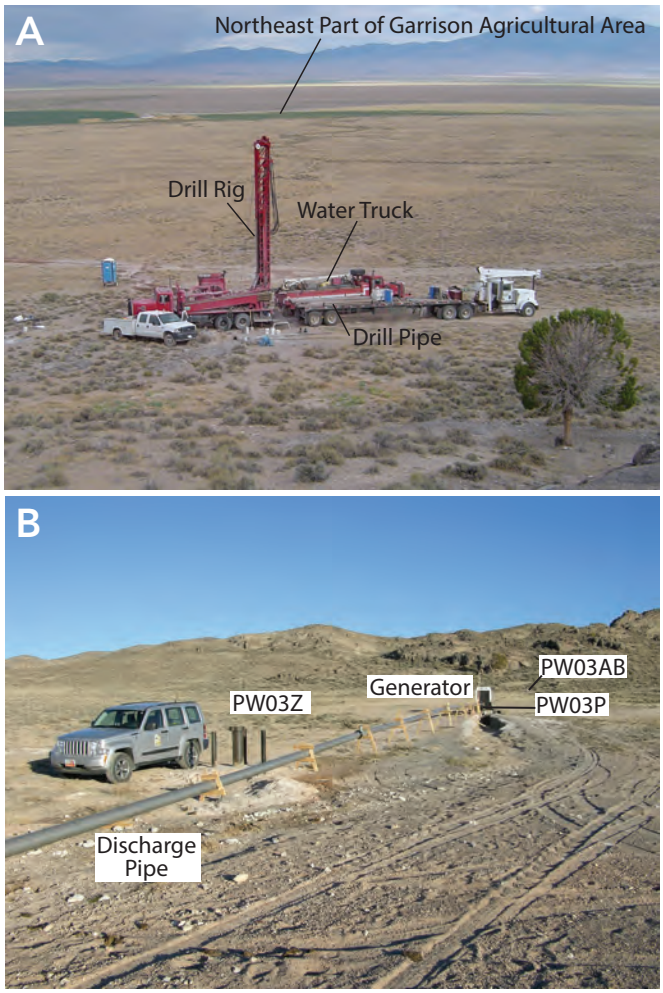

Figure 7.16. *Drilling and aquifer-test operations at site 3.* ***A.*** *View northwest of site 3 during installation of PW03AB, September 2007.* ***B.*** *View southeast of discharge pipe and surface casing of completed borehole PW03Z in foreground, and generator running pump in background during site 3 aquifer test.*

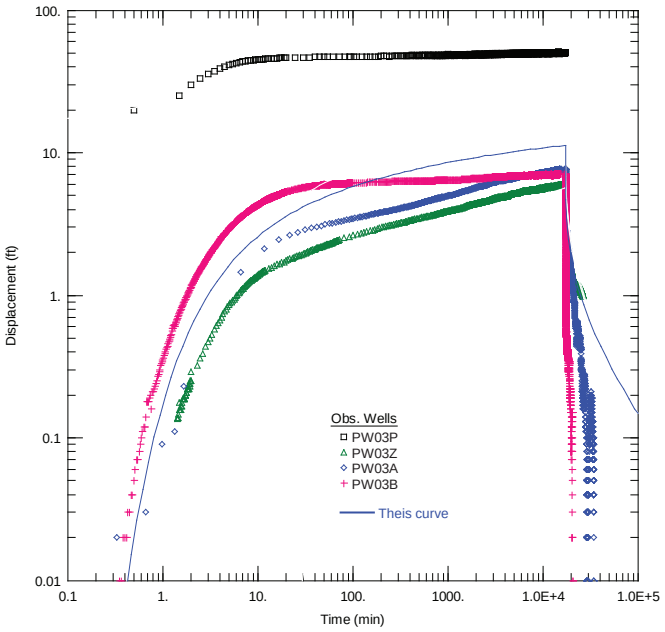

Figure 7.17. *Site 3 pumping- and observation-well response during the aquifer test. The responses of piezometers PW03A and PW03Z are typical of a homogeneous confined aquifer, as shown by their similarity to the Theis curve.*

7.1). The pumping well is open to two different geologic formations, the Guilmette Formation and the Simonson Dolomite, and we suspect the differences in drawdown response between PW03A and PW03B may be due to their positions in different geologic formations, which may have different hydraulic conductivities, and/or because the attenuation fault between the completions (figure 7.15) may limit hydraulic connection between the formations above and below the fault.

7.3.6 Data Analysis

7.3.6.1 Analyses Techniques

We used AQTESOLV v. 4.5 (Duffield, 2007) computer software program to assist our curve matching to analytical solutions.

We accounted for the properties of the wells and the hydrogeologic aspects of the basin-fill and carbonate-rock aquifers in our analysis. As discussed in section 7.2.6.1 for site 11 aquifer-test data, influences on water levels in the wells include borehole storage, skin effects, and partial penetration of an aquifer. Some of our analytical techniques accounted for borehole storage; in those that did not, we disregarded early-time data (pumping times of less than one hour). Most of our analytical techniques corrected for partial penetration and skin effects; we note those analyses that do not and the possible effect on results. We estimated aquifer thickness, pore geometry, degree of consolidation of the aquifer matrix, and presence of low permeability units based on borehole data and geologic mapping.

We obtained initial transmissivity and storativity values from our site 3 aquifer-test data analysis by fitting the unconfined Theis (1935) solution to the trend-corrected water-level data. We refined the Theis (1935) values by applying the Moench (1997) analyses for unconfined aquifers. This analysis accounts for partial penetration and borehole storage. We used a vertical to horizontal hydraulic conductivity ratio of 0.3 to 0.7 based on a reasonable range and trial and error during curve matching. We plotted the derivatives of the drawdown data with the drawdown data to aid our analysis (Bourdet, 2002). We also matched the data to a double-porosity fractured rock solution (Moench, 1984) and a leaky aquifer solution (Neuman and Witherspoon, 1969).

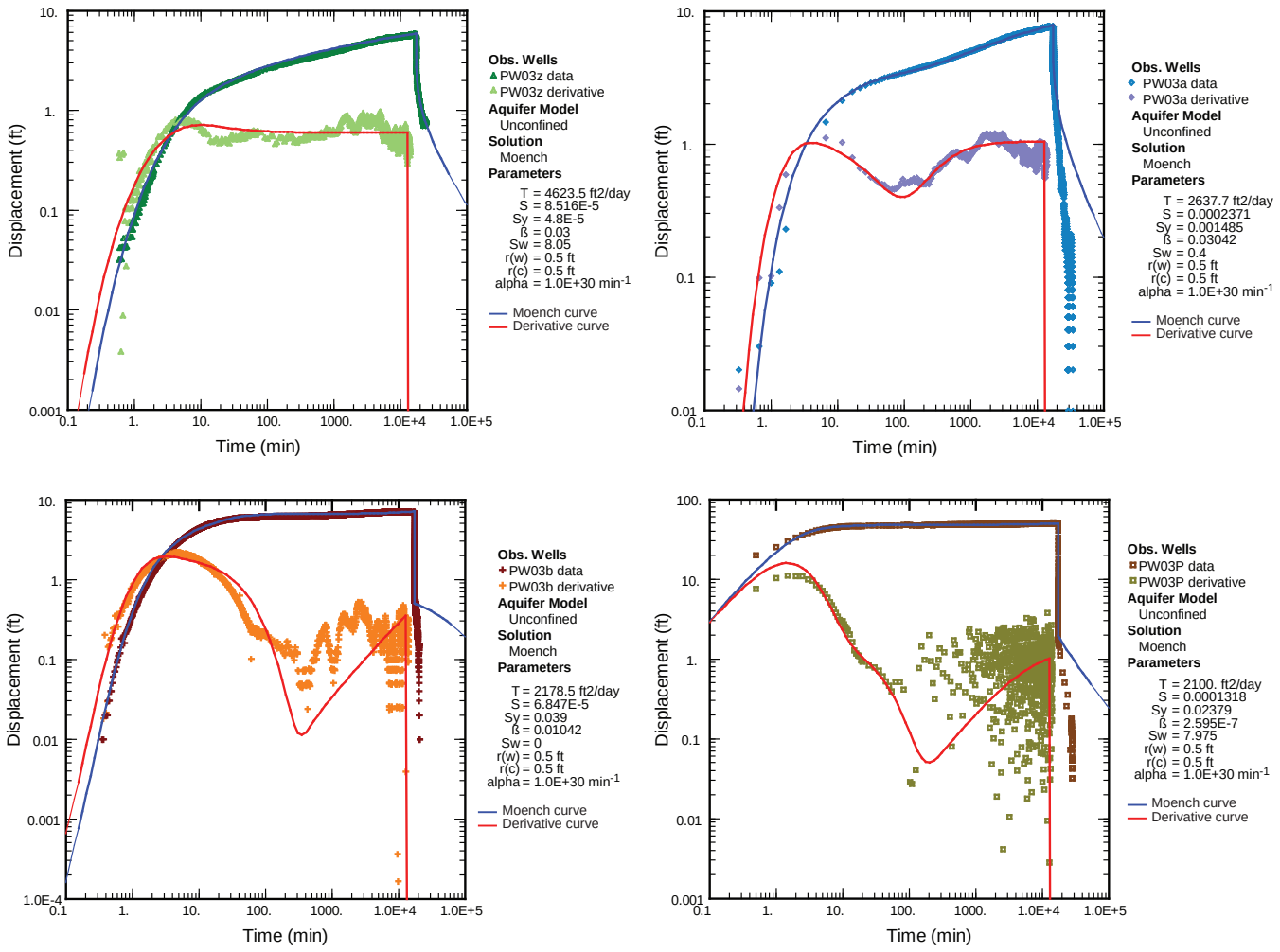

For All Plots:
T = transmissivity (ft²/day)
S = storativity (dimensionless)
Sy = specific yield (dimensionless)
β = curve family value (dimensionless)
Sw = wellbore skin factor (dimensionless)
r(w) = well radius (ft)
r(c) = nominal casing radius (ft)
alpha = Moench's empirical constant for noninstantaneous drainage at the water table

Figure 7.18. *Hydraulic-property estimates from site 3 aquifer test determined using the Moench (1997) analytical solution for an unconfined aquifer.*

7.3.6.2 Results

The theoretical curves derived using the Moench (1997) unconfined aquifer solution match the data and their derivatives well (figure 7.18). Our estimate of the transmissivity of the lower Paleozoic carbonate-rock aquifer (Guilmette Formation and Simonson Dolomite) at site 3 is 2100 to 4600 feet squared per day (200–430 m^2/day) (table 7.5). Storativity estimates range from 6 x 10^{-5} to 2 x 10^{-4}. Transmissivity values decrease with depth by about half from the depth of the shallowest observation well at approximately 40 feet (12 m) below the water table to the depth of our deepest well at approximately 640 feet (200 m) below the water table. Estimated transmissivity values are similar to those given in table 7.5 and figure 7.18 when we match the data using the fractured-rock aquifer solution of Moench (1984) and the leaky aquifer solution of Neuman and Witherspoon (1969), but the uncertainties of the curve fits are greater than those shown on figure 7.18. Our results suggest the transmissivity of the lower Paleozoic carbonate-rock aquifer at site 3 is four to eight times less than the same rock unit tested by SNWA in Spring Valley.

7.4 SUMMARY

We conducted two long-term, multiple-well aquifer tests in southern and central Snake Valley. From these data, we estimated hydraulic properties for the basin-fill aquifer and the upper and lower Paleozoic carbonate-rock aquifers, and gained a better understanding of hydraulic connection

Table 7.5. *Hydraulic properties determined for the lower Paleozoic carbonate-rock aquifer determined using the Moench (1997) solution for an unconfined aquifer to site 3 aquifer-test data.*

INPUT			RESULTS				
Observation Well	K_z/K_r [1]	Total saturated thickness (ft)	Transmissivity (ft^2/day)	Storativity	Specific yield	S_w [2]	K_r [1] (ft/day)
PW03Z	0.7	660	4600	9E-05	5E-05	8.1	7
PW03A	0.5	660	2600	2E-04	1E-03	0.4	4
PW03B	0.3	660	2100	6E-05	3E-02	3.7	3
PW03P	0.5	660	2100	NA[3]	NA[3]	8.0	3

NA: Not applicable.

[1] K_z is vertical hydraulic conductivity; K_r is horizontal (radial) hydraulic conductivity.

[2] S_w is wellbore skin factor (dimensionless).

[3] Pumping well data do not produce reliable estimates of storativity.

between the basin-fill aquifer and carbonate-rock aquifer. Our work at site 11 resulted in estimates of hydraulic conductivity, transmissivity, specific storage, specific yield, storativity, and vertical and horizontal anisotropy characteristics. Understanding the hydraulic properties of these three large aquifers is important to our understanding of groundwater flow in Snake Valley.

Site 11 was the location of our longest and most involved test. We refurbished a 1970s era oil exploration well in southern Snake Valley to have 820 feet (250 m) of open interval in the Permian-Mississippian Ely Limestone, a fine- to medium-grained cherty limestone having well-defined bedding planes. The Ely Limestone is part of the upper Paleozoic carbonate-rock aquifer. Overlying the Ely Limestone at site 11 is 260 feet (79 m) of saturated, unconsolidated or semi-consolidated, medium- to coarse-grained basin fill. We installed four new observation wells in two boreholes located about 150 feet (50 m) north and northwest, respectively, from the pumping well. In March 2009, we pumped for 17 days at a rate of 1200 gallons per minute (4540 L/min), measuring water levels in the pumping well, the four new observation wells, and 11 new, existing, or refurbished wells in the surrounding area. The test provided us an excellent opportunity to determine hydraulic properties and communication between the basin-fill and carbonate-rock aquifers.

Water levels responded rapidly to pumping in the three observation wells at site 11 that are completed in the same unit as the pumping well (upper Paleozoic carbonate-rock aquifer), taking less than 12 seconds to begin declining. The observation well that is completed in the overlying basin-fill aquifer responded to pumping after 16 minutes. Total drawdown at the end of the 17-day pumping period ranged from 1.7 feet to 7.6 feet (0.52–2.3 m) in the four observation wells. The water level in the pumping well declined more than 66 feet (20 m) by the end of pumping, and none of the 11 wells outside of site 11 that we monitored experienced a measurable water-level decline that we could attribute to pumping.

We applied two methods to analyze the site 11 aquifer-test data: (1) matching the data to type curves derived from various analytical aquifer solutions using AQTESOLV computer software, and (2) applying a combination analytical and numerical solution that uses an integrated analytical solution that is independent of aquifer type to model the aquifer-test data.

Based on geologic mapping and hydrogeologic information from our well drilling, the aquifer model that best fits the hydrogeologic setting at site 11 is an unconfined, mostly homogeneous unconsolidated aquifer overlying a somewhat fractured carbonate aquifer having high secondary porosity. We applied an analytical aquifer solution (Neuman and Witherspoon, 1969) that takes into account both these aquifer types. We also had good curve matching results when we treated the entire aquifer as one unconsolidated aquifer with the Moench (1997) solution. We also analyzed site 11 data using MLU for Windows, a program that uses a curve matching technique that is not specific to a hydrogeologic model and can include multiple aquifers.

We repeated our aquifer-test analysis after modifying our hydrogeologic setting to include a no-flow aquifer boundary 1500 feet (457 m) west of the pumping well to simulate the possible presence of a series of thrust faults that place the Chainman Shale adjacent to the carbonate-rock aquifer.

Transmissivity of the basin-fill aquifer derived from the site 11 aquifer test is between 54,200 and 89,000 feet squared per day [5000–8300 m^2/day]. The transmissivity of the upper Paleozoic carbonate-rock aquifer is comparatively lower, between 7300 and 37,100 feet squared per day

(660–3500 m^2/day). Storativity is approximately an order of magnitude larger in the basin fill (3×10^{-4} to 1×10^{-2}) than in carbonate rock (2×10^{-4} to 1×10^{-3}) (table 7.4). Specific yield of the basin fill is 0.33.

Limiting the aquifer 1500 feet (457 m) away from the pumping well had a smaller effect on our calculated transmissivity estimates than we would predict, a probable artifact of our analytical software. We would expect the transmissivity values of the carbonate-rock aquifer to be about fifty percent higher in an aquifer that is limited to 1500 feet in one direction. Our results are reasonable when compared within the range of previously published estimates for the same hydrogeologic units in the eastern Great Basin.

We confirmed our assumption that transmissivity decreases with depth and estimate that at nearly 1200 feet (370 m) below the water table, the deepest interval tested at site 11, transmissivity is about one-third of the value near the top of the aquifer. We were unable to determine if significant horizontal anisotropy exists at site 11.

We chose a site 2 miles (3 km) east-northeast of Garrison, Utah, for our other multiple-well aquifer test because of the site's proximity to an important area of agricultural groundwater use and its hydrogeologic setting. Site 3 wells, which consist of one pumping and three observation wells constructed under the direction of UGS for this study, have their open intervals in the lower Paleozoic carbonate-rock aquifer hydrogeologic unit and the water table was approximately 170 to 200 feet (50–60 m) below land surface at the time of the test. The two shallower observation wells are completed in the Devonian Guilmette Formation (primarily limestone) above a fault and the deeper observation well is completed in the Devonian Simonson Dolomite below the fault. The pumping well is cased from the surface to 300 feet (91 m) below land surface and has an open hole intersecting the fault. The borehole is open to approximately 100 feet (30 m) of the Guilmette Formation above the fault and 450 feet (140 m) of the Simonson Dolomite below the fault.

We extracted 180 gallons per minute (681 L/min) from the site 3 pumping well for 12 days in March 2009, during which time its water level declined by approximately 30 feet (9 m). We measured drawdown in the observation wells, which are located 137 and 164 feet (42 and 50 m) away from the pumping well, of between 5.8 and 7.7 feet (1.8–2.4 m). We removed a long-term downward trend in water-level elevation before analyzing the pumping and recovery data by matching analytical solutions to our data. We achieved the best curve-matching results when we treated the lower Paleozoic carbonate-rock aquifer hydrogeologic unit as a homogeneous unconfined aquifer with the Moench (1997) solution.

We estimate that the transmissivity of the Guilmette Formation and Simonson Dolomite of the lower Paleozoic carbonate-rock aquifer hydrogeologic unit ranges from 2100 to 4600 feet squared per day (200–430 m^2/day) (table 7.5). Storativity estimates range from 6×10^{-5} to 2×10^{-4}. Transmissivity values decrease with depth by about half through the 600 feet (190 m) of aquifer tested.

Analysis of groundwater-level data collected during two multiple-well aquifer tests conducted by the UGS in southern and central Snake Valley provides a range of hydraulic-property estimates for the basin-fill and upper and lower Paleozoic carbonate-rock aquifers. These data add to our understanding that the basin-fill aquifer is generally more transmissive than the bedrock aquifers, and can be an important source of leakage or recharge to the underlying aquifers when the potentiometric head in the bedrock is lowered by pumping. Transmissivity decreases with depth, even within units we interpret from drilling data to be one aquifer.

7.5 CHAPTER 7 REFERENCES

Bourdet, D., 2002, Well test analysis—the use of advanced interpretation models: New York, Elsevier, 426 p.

Carlson, F., and Randall, J., 2012, MLU—a Windows application for the analysis of aquifer tests and the design of well fields in layered systems: Ground Water, v. 50, no. 4, p. 504–510 (doi: 10.1111/j.1745-6584.2012.00945.x).

Dong, W., Naranjo, R.C., and Halford, K.J., 2011, Analysis of water level fluctuations from pumpage for irrigation during multiple drought years in Snake Valley, HA195, near Needle Point and south of Garrison, Utah: U.S. Geological Survey Memorandum to Devin Galloway, U.S. Geological Survey Western Region: Online, http://nevada.usgs.gov/water/AquiferTests/2011_Halford_Snake_Needlept/00_NeedlePt-SnakeV_%20AquiferTestReport.pdf, 16 p., accessed June 4, 2013.

Duffield, G.M., 2003, AQTESOLV for Windows aquifer test analysis software, professional edition: Reston, Virginia, HydroSOLVE, Inc., version 3.5.

Duffield, G.M., 2007, AQTESOLV for Windows aquifer test analysis software, professional edition: Reston, Virginia, HydroSOLVE, Inc., version 4.5.

Fetter, C.W., 2001, Applied hydrogeology: New York,

Macmillan, 598 p.

Ferré, T.P.A., and Thomasson, M.J., 2010, The influence of formation material properties on the response of water levels in wells to earth tides and atmospheric loading: Ground Water, v. 48, no. 4, p. 478–479.

Gardner, P.M., Masbruch, M.D., Plume, R.W., and Buto, S.G., 2011, Regional potentiometric surface map of the Great Basin carbonate and alluvial aquifer system in Snake Valley and surrounding areas, Juab, Millard, and Beaver Counties, Utah, and White Pine and Lincoln Counties, Nevada: U.S. Geological Survey Scientific Investigations Map 3193.

Gonthier, G.J., 2007, A graphical method for estimation of barometric efficiency from continuous data—concepts and application to a site in the Piedmont, Air Force Plant 6, Marietta, Georgia: U.S. Geological Survey Scientific Investigation Report 2007–5111, 29 p.

Halford, K.J., 2006, Documentation of a spreadsheet for time-series analysis and drawdown estimation: U.S. Geological Survey Scientific Investigations Report 2006-5024, 38 p.

Halford, K.J., 2010a, AQUIFER TEST—analysis of BS-NW, single-well aquifer test of basin-fill aquifer, southwestern Snake Valley, HA195, near Great Basin National Park, NV: U.S. Geological Survey Memorandum to Devin Galloway, U.S. Geological Survey Western Region: Online, http://nevada.usgs.gov/water/AquiferTests/2010_BigSprings-NW/Report/00_BigSprings-NW-SnakeV_%20AquiferTestReport.v2.pdf, 9 p., accessed numerous times during 2012.

Halford, K.J., 2010b, AQUIFER TEST—analysis of BS-SW single-well aquifer test of carbonate-rock aquifer, southwestern Snake Valley, HA195, near Great Basin National Park, NV: U.S. Geological Survey Memorandum to Devin Galloway, U.S. Geological Survey Western Region: Online, http://nevada.usgs.gov/water/AquiferTests/2010_BigSprings-SW/Report/00_BigSprings-SW-SnakeV_%20AquiferTestReport.v2.pdf, 5 p., accessed numerous times during 2012.

Halford, K.J., and Plume, R.W., 2011, Potential effects of groundwater pumping on water levels, phreatophytes, and spring discharges in Spring and Snake Valleys, White Pine County, Nevada, and adjacent areas in Nevada and Utah: U.S. Geological Survey Scientific Investigations Report 2011-5032, 52 p.

Hantush, M.S., and Jacob, C.E., 1955, Non-steady radial flow in an infinite leaky aquifer: American Geophysical Union Transactions, v. 36, p. 95–100.

Harbaugh, A.W., Banta, E.R., Hill, M.C., and McDonald, M.G., 2000, MODFLOW-2000, the U.S. Geological Survey modular ground-water model—user guide to modularization concepts and the ground-water flow process: U.S. Geological Survey Open-File Report 00-92, 121 p.

Harbaugh, A.W., and McDonald, M.G., 1996, User's documentation for MODFLOW-96, an update to the U.S. Geological Survey modular finite-difference groundwater flow model: U.S. Geological Survey Open-File Report 96-485, 56 p.

Hemker, C.J., 1999, Transient well flow in layered aquifer systems—the uniform well-face drawdown solution: Journal of Hydrology, v. 225, p. 19–44.

Hemker, C.J., and Post, V.E.A., 2009, MLU for Windows, lite version 2.25.14: Amsterdam, Netherlands.

Hintze, L.F., 1986, Geologic map of the Mormon Gap and Tweedy Wash quadrangles, Millard County, Utah, and Lincoln and White Pine Counties, Nevada: U.S. Geological Survey Map MF-1872.

Hintze, L.F., 1997, Interim geologic map of the Burbank Pass quadrangle, Millard County, Utah: Utah Geological Survey Open-File Report 356, scale 1:24,000.

Hsieh, P.A., 1987, Characterizing the hydraulic properties of fractured rock masses—methodology and case studies, *in* Farmer, I.W., Daemen, J.J.K., Desai, C.S., Glass, C.E., and Neuman, S.P., editors, Proceedings of the 28th U.S. Symposium on Rock Mechanics: Tuscon, Arizona, p.465–472.

Johnson, A.J., 1967, Specific yield—compilation of specific yields for various materials: U.S. Geological Survey Water Supply Paper 1662-D, 74 p.

Kruseman, G.P., and de Ridder, N.A., 2000, Analysis and evaluation of pumping test data (2nd ed.): Wageningen, The Netherlands, International Institute for Land Reclamation and Improvement Publication 47, 377 p.

Long, J.C.S., and Witherspoon, P.A., 1985, The relationship of the degree of interconnection to permeability in fracture networks: Journal of Geophysical Research, v. 90, p. 3087–3098.

Mackley, R.D., Spane, F.A., Pulsipher, T.C., and Allwardt, C.H., 2010, Guide to using multiple regression in Excel (MRCX v.1.1) for removal of river stage effects from well water levels: Pacific Northwest National Laboratory PNNL-19775, 55 p.

Maidment, D.R., 1993, Handbook of hydrology: New York, McGraw-Hill, 1147 p.

Moench, A.F., 1984, Double-porosity models for a fissured groundwater reservoir with fracture skin: Water

Resources Research, v. 20, no. 7, p. 831–846.

Moench, A.F., 1997, Flow to a well of finite diameter in a homogeneous, anisotropic water-table aquifer: Water Resources Research, v. 33, no. 6, pp. 1397–1407.

Neuman, S.P., and Witherspoon, P.A., 1969, Theory of flow in a confined two aquifer system: Water Resources Research, v. 5, no. 4, p. 803–816.

Neuman, S.P., and Witherspoon, P.A., 1972, Field determination of the hydraulic properties of leaky multiple aquifer systems: Water Resources Research, v. 3, no. 5, p. 1284–1298.

Parney, R., and Smith, L., 1995, Fluid velocity and path length in fractured media: Geophysical Research Letters, v. 22, p. 1437–1440.

Prieur, J.P., Farnham, I.M., and Ashinhurst, C.S., 2010, Hydrologic data anaylsis report for test well 184W101 in Spring Valley hydrographic area 184: Las Vegas, Nevada, Southern Nevada Water Authority Document No. DAR-ED-003, 79 p.

Pujol, J., 2007, The solution of nonlinear inverse problems and the Levenberg-Marquardt method: Geophysics, v. 72, no. 4, p. W1–W16.

Rasmussen, T.C., and Crawford, L.A., 1997, Identifying and removing barometric pressure effects in confined and unconfined aquifers: Ground Water, v. 35, no. 3, p. 502–511.

Renard, P., 2005, Hydraulics of wells and well testing, *in* Anderson, M.G., editor, Encyclopedia of hydrological sciences, v. 4: Hoboken, New Jersey, Wiley, 591 p.

Renard, P., Glenz, D., and Mejias, M., 2009, Understanding diagnostic plots for well-test interpretation: Hydrogeology Journal, v. 17, no. 3, p. 589–600 (doi: 10.1007/s10040-008-0392-0).

Rojstaczer, S., and Agnew, D.C., 1989, The influence of formation material properties on the response of water levels in wells to earth tides and atmospheric loading: Journal of Geophysical Research, v. 94, no. B9, p. 403–412.

Stehfest, H., 1970, Algorithm 368—numerical inversion of Laplace transform: Communication of the Association for Computing Machinery (ACM), v. 13, no. 1, p. 47–49.

Sweetkind, D.S., Knochenmus, L.A., Ponce, D.A., Wallace, A.R., Scheirer, D.S., Watt, J.T., and Plume, R.W., 2007, Hydrogeologic framework, *in* Welch, A.H., Bright, D.J., and Knochenmus, L.A., editors, Water resources of the Basin and Range carbonate-rock aquifer system, White Pine County, Nevada, and adjacent areas in Nevada and Utah: U.S. Geological Survey Scientific Investigations Report 2007-5261, 96 p.

Theis, C.V., 1935, The relation between the lowering of the piezometric surface and the rate and duration of discharge of a well using groundwater storage: American Geophysical Union Transactions, v. 16, p. 519–524.

Theis, C.V., Brown, R.H., and Meyer, R.R., 1963, Estimating the transmissibility of aquifers from the specific capacity of wells: U.S. Geological Survey Water-Supply Paper 1536-I, 10 p.

Walton, W.C., 2007, Aquifer test modeling: Boca Raton, Florida, CRC Press, 222 p.

CHAPTER 8

EVALUATION OF GROUNDWATER FLOW PATHS IN SNAKE VALLEY AND ADJACENT HYDROGRAPHIC AREAS

by Hugh Hurlow and Stefan Kirby

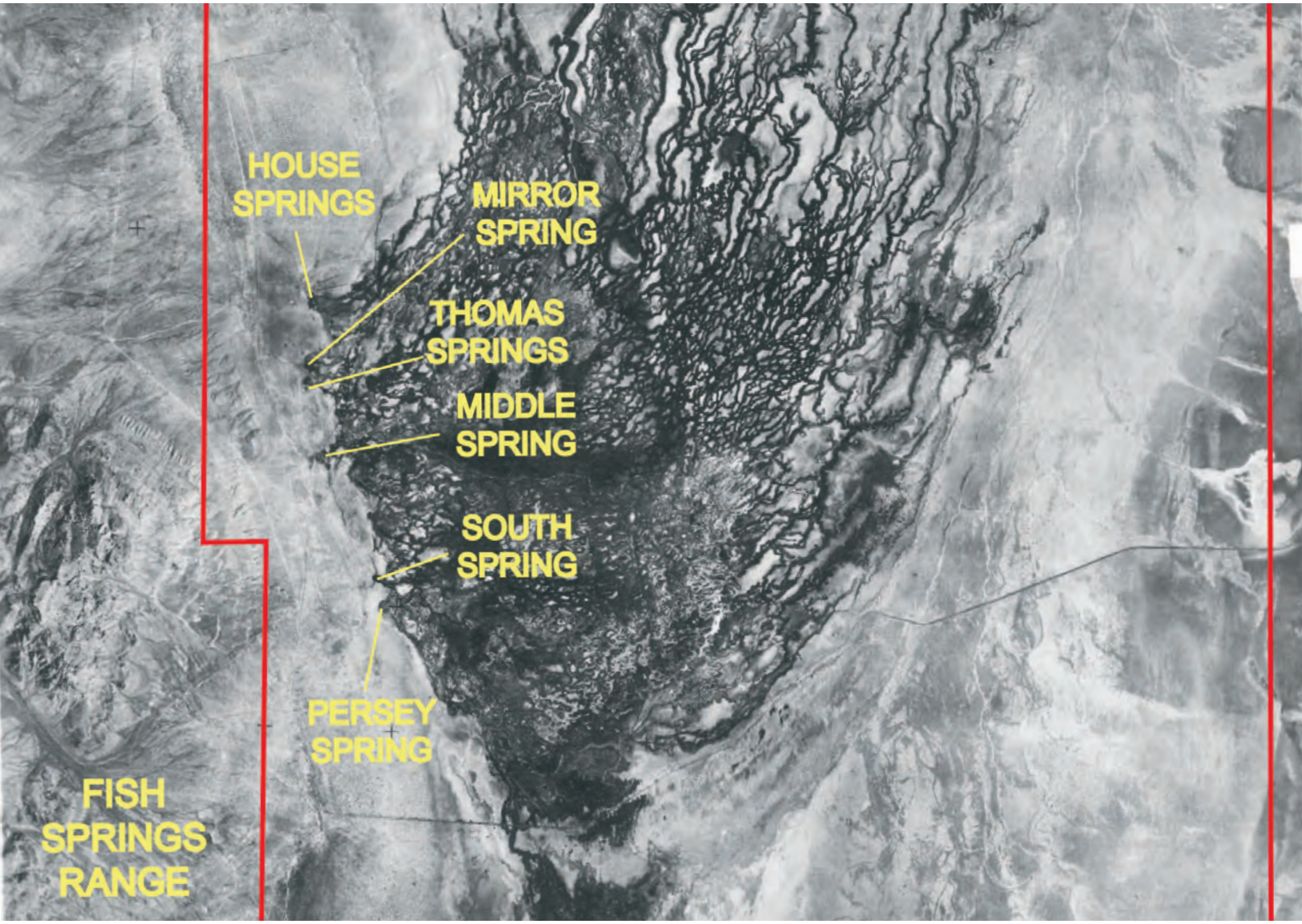

Aerial view of Fish Springs National Wildlife Refuge about 1958 at time of refuge establishment (U.S. Fish and Wildlife Service, 2004). Red line is Refuge boundary. The Fish Springs complex is the main discharge point of the Fish Springs sub-regional flow system of the Great Salt Lake Desert regional flow system.

Bibliographic citation for this chapter:
Hurlow, H., and Kirby, S., 2014, Evaluation of groundwater flow paths in Snake Valley and adjacent hydrographic areas, Chapter 8 *in* Hurlow, H., editor, Hydrogeologic studies and groundwater monitoring in Snake Valley and adjacent hydrographic areas, west-central Utah and east-central Nevada: Utah Geological Survey Bulletin 135, p. 233–256.

CHAPTER 8 CONTENTS

FIGURES

TABLES

CHAPTER 8: EVALUATION OF GROUNDWATER PATHS IN SNAKE VALLEY AND ADJACENT HYDROGRAPHIC AREAS

by Hugh Hurlow and Stefan Kirby

8.1 INTRODUCTION

In this chapter we evaluate the implications of new UGS hydrogeologic and hydrochemical data and selected data from other studies, as presented and interpreted in the preceding chapters, for previously published conceptual models of groundwater flow in the UGS study area. Most previously published conceptual models of groundwater flow in the Great Basin carbonate-rock province conclude that groundwater flow from recharge areas to discharge areas occurs at scales ranging from local flow in shallow basin-fill and carbonate-rock aquifers over a few miles, to interbasin flow in the deeper parts of the carbonate-rock aquifers over tens to hundreds of miles (Eakin, 1966; Gates and Kruer, 1981; Carlton, 1985; Harrill and others, 1988; Prudic and others, 1995; Laczniak and others, 2007; Belcher and others, 2009; SNWA, 2009; Sweetkind and others, 2011). In these conceptual models, deep groundwater flows through carbonate-rock aquifers from Snake Valley to Tule Valley and Fish Springs Flat. Groundwater recharged in the Snake Range and Deep Creek Mountains is at least a partial source for discharge from major springs and evapotranspiration in Tule Valley (including Coyote Spring) and Fish Springs Flat (including Fish Springs) (Carlton, 1985; Harrill and others, 1988; Prudic and others, 1995).

Necessary conditions to interpret that groundwater flows from Snake Valley to Tule Valley and Fish Springs Flat, or across any other interbasin boundary, include that the basins are connected by permeable aquifer systems, the potentiometric surface varies continuously from highest elevation in the recharge areas to lowest elevation in the discharge areas, and hydrochemical constituents (major-ion and isotopic compositions and apparent age) vary systematically from recharge to discharge areas. These basic assumptions form a set of criteria by which to evaluate the likelihood that interbasin flow occurs within particular flow systems and flow paths. The UGS groundwater-monitoring network provides abundant new data on groundwater levels and chemistry to which these criteria can be applied, to test previously published concepts of interbasin flow and better delineate groundwater flow within Snake Valley.

A flow system comprises recharge area(s), aquifer(s), and discharge area(s) connected by groundwater flow (Toth, 1963; Harrill and others, 1988). Toth (1963) delineated local-, intermediate-, and regional-scale flow systems based on increasing distance from recharge to discharge area, depth of circulation, and travel time. Table 8.1 shows our subjective application of Toth's (1963) classification scheme to the UGS study area, in which local- and intermediate-scale flow systems are within a hydrographic area, whereas regional-scale flow systems traverse one or more hydrographic-area boundaries and, therefore, include flow through bedrock aquifers below a surface-water divide (i.e., interbasin flow). For example, the Fish Springs flow system (Carlton, 1985; Harrill and others, 1988) includes recharge areas in several mountain ranges and discharge areas in three hydrographic areas (Tule Valley, Fish Springs Flat, and southern Great Salt Lake Desert [GSLD]). The physical dimensions used to delineate the three scales of flow systems in our study area generally follow illustrations in Toth (1963, figure 3), Harrill and others (1988, figure 4), and Sweetkind and others (2011, figure C-1). Depth of circulation in these systems is poorly constrained. We describe the physical and chemical characteristics of these flow systems in greater detail in sections 8.2 and 8.4.

Flow paths comprise specific, physically connected recharge areas, aquifer systems (including hydrographic-area boundaries for interbasin flow), and discharge areas connected by groundwater flow, within a larger flow system. For example, the Fish Springs flow system includes several possible flow paths, including one from the southern Snake Range recharge area, through basin-fill and carbonate-rock aquifers below southern and south-central Snake Valley, interbasin flow through carbonate-rock aquifers in the central and southern Confusion Range, and discharge in Tule Valley. In section 8.3 and table 8.1 we designate this flow path as the "south-central Snake Valley to Tule Valley and Fish Springs" flow path 3a.

Sections in this chapter briefly review previously published conceptual models of regional (interbasin) and local groundwater-flow systems in the UGS study area (section 8.2), evaluate previously proposed interbasin flow paths

Table 8.1. *Summary of general hydrogeologic and hydrochemical characteristics of local-, intermediate-, and regional- (interbasin) scale groundwater-flow systems in Snake Valley and adjacent hydrographic basins, west-central Utah and east-central Nevada.*

Flow System Scale	Recharge Area	Discharge Area	Total Length (miles)	Circulation Depth (feet)	Potentiometric Elevation of Recharge Area(s) (feet)	Potentiometric Elevation of of Discharge Area(s) (feet)	Hydro-chemical Group[1] in Discharge Area	Ground-water Temp. (°C)	Tritium Units	Percent Modern Carbon	Apparent Age (years)	Quali-tative Age	Dissolved-Gas Model Recharge Temp. (°C)
Local (intrabasin)	Mountain block (in-place) and mountain front (runoff)	Adjoining valley floor	<10	<500(?)	10,000–6000(?)	5500–4800	Group 3	<15	>0.5	50–75	<1000	modern	0–10
Intermediate (intrabasin)	Mountain block (in-place) and mountain front (runoff)	Valley axis springs and ET zones	10 to 25	<1000(?)	10,000–6000(?)	5000–4300	Group 3 or 4	15–20	<0.5	<50	3000–10,000	mixed to old	0–15
Regional (interbasin)	Carbonate-rock mountain block and mountain front	Fault controlled	<100	500–4000(?)	10,000–6000(?)	4500–4200	Group 5 or 6	20+	<0.5	<50	3000–>10,000	old or mixed	10–>20

[1]See table 6.3 for hydrochemical group-mean compositions.

based on hydrogeologic and hydrochemical (solute chemistry, inverse chemical modeling, isotopic compositions, and dissolved-gas) criteria to (section 8.3), and delineate generalized local and intermediate flow systems in Snake Valley based on variations in hydraulic head and hydrochemistry (section 8.4). Appendix E presents a detailed hydrogeologic analysis of interbasin flow from Snake Valley to Tule Valley.

8.2 PREVIOUS WORK

Harrill and others (1988, sheet 2) delineated major groundwater-flow systems in the Great Basin carbonate-rock province. A groundwater-flow system includes recharge and discharge areas connected by a permeable aquifer system, following the concepts of Toth (1962, 1963) and Freeze and Witherspoon (1966, 1967), and flow systems may vary from local (a few miles) to regional (up to hundreds of miles) scales. The UGS study area is in the southern part of Harrill and others' (1988) GSLD regional flow system, which includes 16 hydrographic areas in eastern Nevada and western Utah (figure 1.3). In their model, groundwater in the GSLD flow system moves from higher potentiometric-surface elevation in mountain-block recharge areas, through the carbonate-rock aquifer, to lower hydraulic-head elevation in valley-floor discharge areas (distributed ET and large springs). The UGS study area encompasses the Fish Springs sub-regional flow system within the GSLD (figure 1.3) as delineated by Carlton (1985), which consists of eight hydrographic areas thought to be hydraulically connected and contribute to the flow from the Fish Springs complex and discharge from central Tule Valley.

Gates and Kruer (1981), Harrill and others (1988), Prudic and others (1995), and Laczniak and others (2007) suggested that groundwater in the Fish Springs flow system moves from primary recharge areas in the Snake Range, Deep Creek Mountains, Schell Creek Range, and Egan Range, through the carbonate-rock aquifer, to primary discharge areas in Tule Valley, Fish Springs, and southern GSLD. These studies did not provide detailed analyses of specific flow paths, but suggested that interbasin flow occurs across numerous hydrographic-area boundaries in the Fish Springs flow system (figure 8.1). In this chapter we evaluate whether hydrogeologic and hydrochemical criteria support the proposed flow system as a whole, and selected paths within the flow system.

Contrasting views of interbasin flow in the UGS study area exist. Rowley and others (2009, p. 258–259 and 262–263) and Rowley and Dixon (2011, p. 2-6 to 2-12) emphasized the role of major range-bounding normal-fault zones as

barriers to cross-fault flow and conduits for fault-parallel flow, and suggested that west-to-east interbasin flow perpendicular to the main north-south structural grain is minimal. Dixon and others (2007) and Rowley and Dixon (2011, p. 4-74 to 4-75) characterized the potential for interbasin flow from Snake Valley eastward through the Confusion Range to Tule Valley as "unlikely," except in the southern Confusion Range, based on their evaluation of the hydrogeologic setting. They stated that range-bounding normal-fault zones act as barriers to cross-fault groundwater flow, noted the presence of the middle Paleozoic siliciclastic confining unit in the Confusion Range between Snake Valley and Tule Valley and concealed plutonic rocks below the Fish Springs Range between northeastern Snake Valley and Fish Springs, and interpreted them as flow barriers. Rowley and Dixon (2011, p. 4-67 to 4-69) discounted interbasin flow from northern Spring Valley to northern Snake Valley based on hydrogeologic setting. Burns and Drici (2011, p. 7-5 to 7-8) and Rowley and Dixon (2011, p. 4-70 to 4-74) acknowledged that some interbasin flow occurs from southern Spring Valley to southern Snake Valley, but asserted that the range-bounding normal-fault zones on either side of the mountain pass between the two hydrographic areas are flow barriers and limit this flow. Gillespie and others (2012) discounted significant (greater than a few hundred acre-feet per year) interbasin flow from southern Spring Valley to northern Hamlin Valley and, by analogy, most hydrogeologically similar hydrographic-area boundaries in the region, based on their evaluation of the hydrogeologic setting and isotopic compositions of groundwater on either side of the boundary.

Analysis of hydrochemistry can support or refute interbasin flow by evaluating whether variations in solute composition, isotopic composition, and model recharge temperature between the postulated recharge and discharge areas are consistent with expected changes due to known chemical processes over space and time. Thomas and others (1996) used the isotopic composition of groundwater to delineate interbasin flow in the White River flow system, and a flow system within the Las Vegas basin. Hershey and others (2007) used hydrochemistry, isotopic data, and water-rock reaction modeling to show that interbasin flow from southern Spring Valley to northern Hamlin Valley and from northern Spring Valley to central Snake Valley is feasible. Acheampong and others (2009) interpreted variations in hydrochemistry and isotopic composition between Snake Valley and Tule Valley to suggest that the basins are not hydraulically connected. Thomas and Milhevc (2011) used hydrochemistry, including geochemical modeling of major-ion composition and stable- and radiogenic-isotope composition, to evaluate interbasin flow paths in the basin-fill and carbonate-rock aquifer systems of the White River flow system in eastern Nevada. The latter two studies identified possible interbasin-flow paths that are consistent with hydrogeologic data and concepts, and ruled out flow paths that are inconsistent with the hydrochemical data.

Harrill and others (1988, sheet 2) schematically depicted local- to intermediate-scale groundwater-flow patterns in the basin-fill and upper carbonate-rock aquifers in the eastern Great Basin. For Snake Valley, they illustrated groundwater flow generally to the north-northeast in northern Snake Valley, generally to the northeast in central Snake Valley including along the eastern valley margin, and generally to the north in southern Snake Valley. Flow directions implied by Gardner and others' (2011) potentiometric-surface contours generally agree with those of Harrill and others (1988, sheet 2) but are constrained by significantly more data and show greater detail. Neither authors delineated flow systems within Snake Valley that illustrated source areas for and flow paths to important springs and discharge areas. For Tule Valley, Harrill and others (1988, sheet 2) illustrated groundwater flow in the basin-fill and shallow carbonate-rock aquifers to the north in southern Tule Valley, and radially inward to the valley-floor discharge area in central and northern Tule Valley. For Fish Springs Flat, Harrill and others (1988, sheet 2) illustrated shallow groundwater flow generally to the northwest.

8.3 HYDROGEOLOGIC AND HYDROCHEMICAL EVALUATION OF INTERBASIN FLOW

8.3.1 Introduction

This section presents evaluations of hydrogeologic and hydrochemical data to test the likelihood of previously proposed groundwater-flow systems and flow paths in the UGS study area, principally Snake Valley and the hydrographic areas to the east. We apply a set of criteria to the hydrogeologic and hydrochemical data presented in chapters 4 and 6 to test the general validity of the Fish Springs flow system and hypothetical flow paths therein, resulting in subjective rankings of "valid," "conditionally valid," or "not valid". Criteria for inferring interbasin flow (i.e., a valid or conditionally valid ranking) include (1) the interbasin-boundary zone (see section 8.3.2 for discussion) is composed of aquifers and/or fault zones that have sufficient transmissivity to accommodate a significant rate of groundwater flow, (2) groundwater levels on either side of the interbasin-flow zone define a flow potential, and (3) variations in major-ion and isotopic compositions are consistent with the postulated flow direction. We are concerned with interbasin-flow rates that are significant

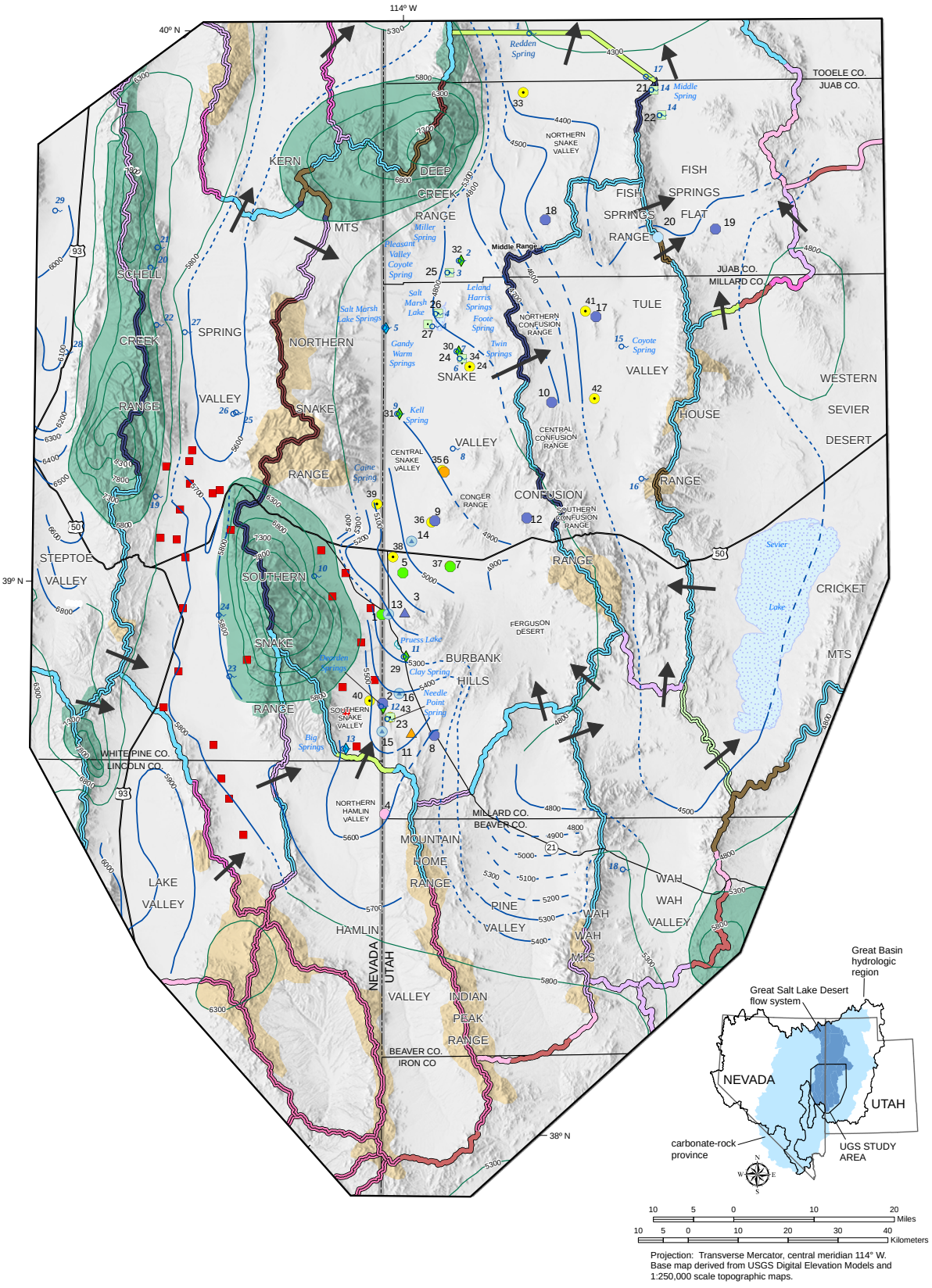

Figure 8.1. *Hydrogeologic classification of interbasin-boundary zones, based on the predominant hydrogeologic unit and orientation of bedding, faults, and folds relative to the principal hydraulic-gradient direction. For simplicity the interbasin-boundary zones are shown as lines along the hydrographic-area boundaries, but the classification is based on hydrogeologic units and structures throughout the entire width of the mountain blocks and thickness of the saturated zone. Boundaries between different classification types are shown as abrupt but may actually be gradational.*

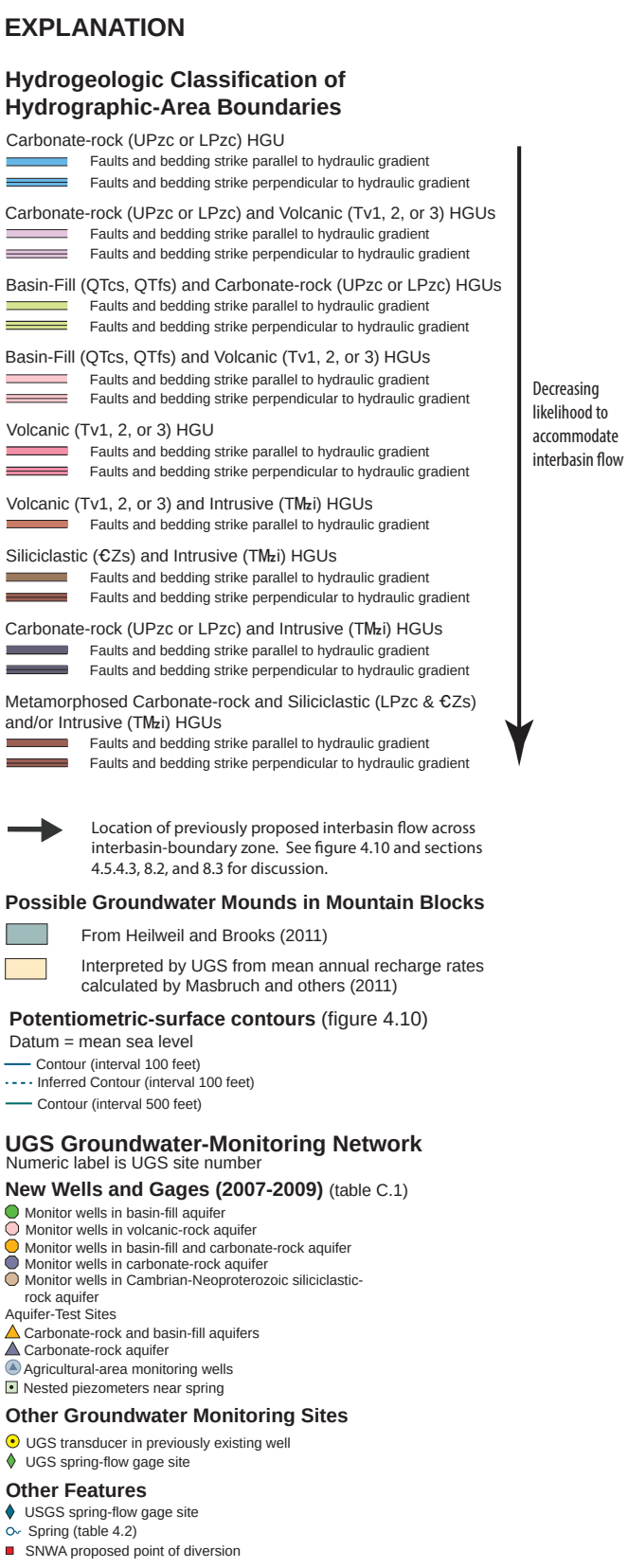

Explanation of map symbols on figure 8.1.

relative to the water budgets of the adjacent basins, i.e., about 3000 acre-feet per year (3.6 hm^3/year) or more. For such flow to occur, the upgradient hydrographic area should have substantially greater mean annual recharge (including interbasin flow from other hydrographic areas, if applicable) than discharge, so that groundwater must flow out of the basin for the water budget to balance and storage to remain constant (section 4.5.4.4).

8.3.2 Hydrogeologic Evaluation of Interbasin-Boundary Zones

Most interbasin groundwater-flow paths in west-central Utah and east-central Nevada are through either topographically low areas at the ends of mountain ranges, or transverse ridges (subsurface or exposed) that form the basin margins (Plume, 1996; Dixon and others, 2007; Laczniak and others, 2007; Sweetkind and others, 2007; Rowley and others, 2009; Rowley and Dixon, 2011). In this report, we refer to the areas in which groundwater moves below hydrographic-area boundaries as interbasin-boundary zones. Groundwater moving through interbasin-boundary zones likely flows from basin-fill and/or carbonate-rock aquifers of the upgradient valley margins, into bedrock aquifers in the interbasin-boundary zone, and into the basin-fill aquifer and/or carbonate-rock aquifer of the downgradient hydrographic area.

Figure 8.1 shows our hydrogeologic characterization of interbasin-boundary zones in the UGS study area. We applied hydrogeologic criteria, particularly the presence of thick, continuous sections of aquifer hydrogeologic units and/or faults that strike parallel to the principal hydraulic-gradient direction (i.e., approximate flow direction), to qualitatively rank interbasin-boundary zones by their likelihood to accommodate interbasin flow. Figure 8.1 classifies interbasin-boundary zones by the predominant hydrogeologic unit(s) within about 4000 feet (1200 m) of the land surface (section 4.2.3), and by the predominant orientation of bedding, faults, and folds relative to the principal hydraulic-gradient direction across the interbasin-boundary zone. Interbasin-boundary zones composed mainly of aquifer hydrogeologic units accommodate interbasin flow more readily than those dominated by confining hydrogeologic units. Interbasin-boundary zones in which most bedding and/or faults strike within about 45 degrees of the principal hydraulic-gradient direction likely accommodate interbasin flow more readily than those where this angle is greater than about 45 degrees, because hydraulic conductivity is greater parallel to bedding planes and fault planes than across them (section 4.3). Our hydrogeologic classification of interbasin-boundary zones is similar to that of Sweetkind and others (2007, figure 15), and gener-

ally more permissive of interbasin flow than that of Dixon and others (2007, figure 4-33).

Our evaluation of hydrogeologic setting and hydraulic-gradient in the Fish Springs flow system (table 8.2; figure 8.2) identifies valid interbasin flow paths, i.e., areas of transmissive aquifers and structures in interbasin-boundary zones between hydrographic areas having significantly different potentiometric surfaces, through which interbasin flow is likely. We also identify interbasin-boundary zones that include hydrogeologic barriers (confining hydrogeologic units and/or structures), through which interbasin flow is unlikely (invalid). Flow across these interbasin-boundary zones was suggested by previous authors as summarized in section 8.2 and illustrated on figures 8.1 and 4.10, and listed in table 4.6. The interbasin-boundary zones are parts of longer flow paths from recharge to discharge areas. In the following paragraphs, we delineate these hypothetical flow paths based on previous studies (section 8.2) and our evaluation of the potentiometric-surface contours of Gardner and others (2011). We describe the hypothetical flow paths and evaluate them based on hydrogeologic criteria in the following paragraphs, then test their validity based on hydrochemical criteria in section 8.3.3.

Flow-path names and numbers correspond with the numerical labels on the variously colored arrows used to schematically illustrate the flow paths in figure 8.2, and with the flow-path names and numbers in tables 8.2 and 8.3.

1. Northern Snake Valley to Fish Springs flow path. The hypothetical flow path from recharge in the Deep Creek Mountains, through northern Snake Valley, the central Fish Springs Range, and Fish Springs Flat, to discharge at Fish Springs (flow path 1a) is conditionally valid (i.e., flow is within aquifers but must cross several faults) based on hydrogeologic and hydraulic-gradient criteria. Physically continuous or adjacent aquifer systems are present along the flow paths, but flow must cross range-bounding normal-fault zones on either side of the Fish Springs Range, likely limiting the flow rate.
2. North-central Snake Valley to Fish Springs flow path. The hypothetical flow path from recharge in the northern Snake Range, through northern and/or north-central Snake Valley through the Middle Range (flow path 2a), to discharge from Fish Springs is not valid, based on the presence in the Middle Range of the steeply dipping, north-south striking middle Paleozoic siliciclastic confining unit. The flow path from north-central Snake Valley through the northern Confusion Range (flow path 2b) is also not valid, based on the presence of the middle Paleozoic siliciclastic hydrogeologic unit in both limbs of a north- to northwest-striking syncline that comprises the entire range (appendix E).
3. South-central Snake Valley to Tule Valley and Fish Springs flow paths. Several hypothetical flow paths from recharge in the southern Snake Range, through south-central Snake Valley and the central and southern Confusion Range, to discharge in central Tule Valley, or Fish Springs, are valid based on hydrogeologic criteria. After crossing through the Confusion Range, groundwater may flow through western Tule Valley, either to the east to discharge at Coyote Spring and by ET in central Tule Valley (flow path 3atv), or to the north-northeast through northwestern Tule Valley, the southern Fish Springs Range, and Fish Springs Flat to discharge from Fish Springs (flow path 3afs). Groundwater may flow from southern and south-central Snake Valley, through the southern Confusion Range, to discharge from central Tule Valley (flow path 3b). Appendix E provides a more detailed hydrogeologic analysis of the Confusion Range interbasin-boundary zone.
4. Pine Valley and Wah Wah Valley to Tule Valley flow paths. Two hypothetical flow paths from recharge in the mountains bounding Pine Valley and Wah Wah Valley, north through southern Tule Valley to discharge at Coyote Spring and adjacent springs and ET areas in central Tule Valley, are valid based on hydrogeologic criteria. Groundwater may flow from the northern Pine Valley basin-fill aquifer, through south-central Snake Valley (Ferguson Desert area) and the southern Confusion Range, to Tule Valley (flow path 4a) (Gates and Kruer, 1981), or from northern Pine Valley, through northern Wah Wah Valley and southern Tule Valley (flow path 4b). The lower Paleozoic carbonate-rock and coarse-grained basin-fill aquifers and north-south striking faults are present along the flow path.
5. Western Sevier Desert to Fish Springs flow path. The hypothetical flow paths from recharge in mountain ranges in the western Sevier Desert, particularly the House Range, through the lower Paleozoic carbonate-rock and volcanic-rock aquifer and along north- to northwest-striking faults, to discharge at Fish Springs, are valid. Precipitation and recharge to this area are low compared to the Snake Range and Deep Creek Mountains (figure 4.5; Flint and others, 2011; Masbruch and others, 2011), and potentiometric and groundwater-chemical data are sparse. Harrill and others (1988, sheet 2) and Prudic and others (1995, p. D84) suggested that the western Sevier Desert is a partial source of Fish Springs discharge.

Table 8.2. *General descriptions of hypothetical interbasin flow paths in the Fish Springs flow system. Red text indicates invalid flow path based on hydrogeologic and/or hydrochemical evaluation discussed in text.*

Flow Path[1] Number	Flow Path[1] Name	Recharge Area(s)	Interbasin-Boundary Zone[2]	Discharge Area	Inverse Hydrochemical Model[3]
1a[#]	Northern Snake Valley to Fish Springs	Deep Creek Mts	Central Fish Springs Range	Fish Springs	Deep Creek E.2 and E.3
2a[$#]	North-central Snake Valley to Fish Springs	Northern Snake Range and Deep Creek Mts(?)	Middle Range and southern Fish Springs Range	Fish Springs	Gandy Springs
2b[$]		Northern Snake Range	Northern Confusion Range and southern Fish Springs Range	Fish Springs	Northern Snake Range E.2 and E.3
3atv	South-central Snake Valley to Tule Valley and Fish Springs	Southern and northern(?) Snake Range	Central Confusion Range	Tule Valley (Coyote Spring)	Snake Creek E.2 and E.3[4]
3afs		Southern and northern(?) Snake Range	Central Confusion Range and southern Fish Springs Range	Fish Springs	Snake Creek E.2 and E.3[4]
3b		Southern Snake Range	Central and southern Confusion Range	Tule Valley (Coyote Spring)	Southern Snake Range E.2 and E.3[5]
4a	Pine Valley and Wah Wah Valley to Tule Valley	Mtn Home, Indian Peak, and Wah Wah Ranges	Southern Confusion Range	Coyote Spring	Pine Valley D.3, to E.1 and/or E.2
4b		Mtn Home, Indian Peak, and Wah Wah Ranges	Southern Confusion Range	Coyote Spring	Pine Valley D.2, to E.2 and/or E.3
5a	Western Sevier Desert to Fish Springs	House Range	Southwestern boundary of Fish Springs Flat	Fish Springs	North Canyon Spring
5b		Drum Mts./Thomas Range	Southwestern boundary of Fish Springs Flat	Fish Springs	Laird Spring
6a	Southern Spring Valley to southern Snake Valley[6]	Southern Snake Range and Schell Creek Range	Southern Snake Range-northern Limestone Hills divide	Southern Snake Valley	Hershey and others (2007)[8]
6b		Southern Snake Range and Schell Creek Range	Southern Snake Valley-northern Hamlin Valley divide[7]	Southern Snake Valley	Hershey and others (2007)[8]
7a[$]	Northern Spring Valley to central Snake Valley[9]	Northern Snake Range and Schell Creek Range	Northern Snake Range - Kern Mountains	North-Central Snake Valley	Hershey and others (2007)[8]
8a	Northern Snake Valley to southern GSLD[10]	Northern Snake Range and Deep Creek Mts	Northern Snake Valley - southern GSLD divide[10]	GSLD	n/a
9a	Southern Steptoe Valley to southern Spring Valley[11]	Schell Creek Range and Egan Range[12]	Southern Schell Creek Range	Southern Snake Valley[14]	Laczniak and others (2007)[15]
9b		Schell Creek Range and Egan Range[12]	S. Schell Creek Range, N. Lake Valley, N. Fortification Range[13]	Southern Snake Valley[14]	Laczniak and others (2007)[15]

#: Flow path not supported by chemical criteria (figure 8.2; table 8-3).

$: Flow path not supported by hydrogeologic evaluation (table 8.3; figures 8.1 and 8.2).

[1] Flow path names and numbers correspond with those in table 8.3 and on figure 8.2.

[2] See figure 8.1 and table 8.3 for hydrogeologic evaluation.

[3] See table 8.3, section 6.2.4, and figure 6.19, or reference cited. Only valid and conditionally valid hydrochemical models are shown. n/a: Hershey and others (2007) found insufficient geochemical data to construct an inverse chemical flow-path model.

[4] Recharge in northern part of southern Snake Range, underlain by hydrogeologic units CZs and Mzi, starting composition represented by Snake Creek (sample 245, table 6.1). Some flow may come from groundwater recharged in the southern part of the northern Snake Range, based on potentiometric-surface contours.

[5] Recharge in southern part of southern Snake Range underlain by hydrogeologic unit LPzc, starting composition represented by Big Springs.

[6] See Hershey and others (2007, p. 50–64), Laczniak and others (2007, p. 71-80), Rowly and Dixon (2011, p. 4-70 to 4-74), and Burns and Drici (2011, p. 7-5 to 7-6) for more detailed discussions.

[7] Divide is topographically indistinct, and is defined by geophysical data (Sweetkind and others, 2007, p. 33–36).

[8] Hershey and others (2007; table 4, p. 47-54) and Laczniak and others (2007, p. 75–77. table 8).

[9] Rowley and Dixon (2011, p. 4-67 to 4-69) and Burns and Drici (2011, p. 7-3 to 7-5) dispute the validity of this flow path based on hydrogeologic setting.

[10] Great Salt Lake Desert. See Gates and Kruer (1981) for more detailed discussion. Divide is topographically indistinct, and is defined by geophysical data (Sweetkind and others, 2007, p. 33–36).

[11] This flow path is not discussed in chapter 8. See section 4.5.4.3 for discussion of water budgets. Dixon and others (2007, figure 4-10) and Rowley and Dixon (2011, p. 4-54, 4-60, and 4-63) rated interbasin flow across this boundary as "unliklely" based on hydrogeologic setting. If interbasin flow from southern Steptoe Valley to southern Spring Valley occurs at a significant rate, then this flow path is part of the Fish Springs flow system. If insignificant flow occurs, this flow path should not be considred part of the Fish Springs flow system. In this report we subjectively regard a "signficant" interbasin-flow rate as about >3% of the average annual discharge rate of either of the adjacent hydrographic areas, i.e., about 3,000 acre-feet per year for most hydrogaphic areas in the study area.

[12] The Egan Range forms the western boundary of Steptoe Valley, and is immediately west of the UGS study area.

[13] Laczniak and others (2007) proposed that groundwater moves from southern Steptoe Valley, through northern Lake Valley, to southern Spring Valley.

[14] Laczniak and others (2007) proposed that flow paths 9a and 9b join flow paths 6a and 6b through southern Spring Valley to southern Snake Valley.

[15] Laczniak and others (2007, p. 75–77. table 8) and Hershey and others (2007, p. 64–65).

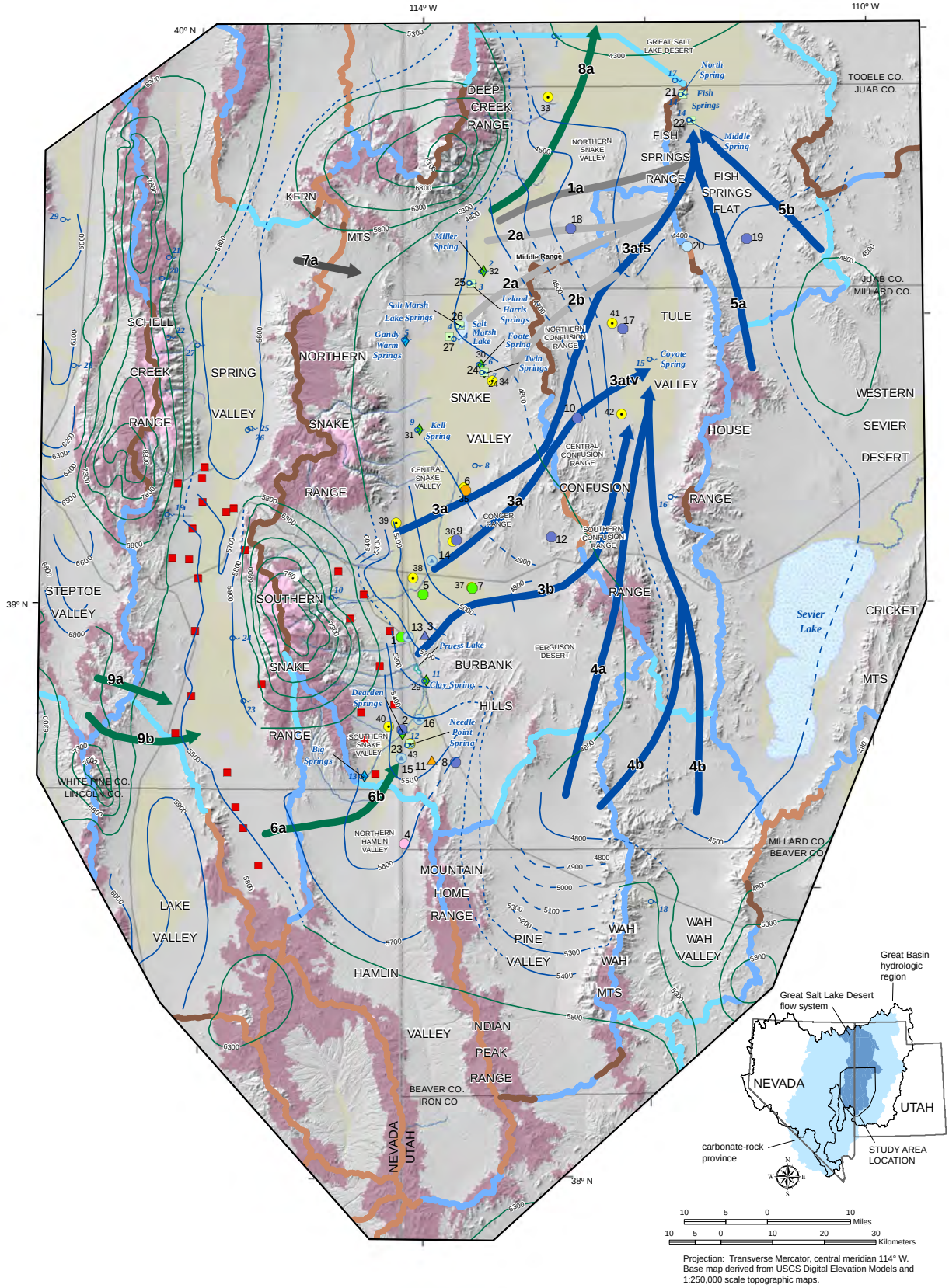

Figure 8.2. *Flow paths in the Fish Springs flow system (table 8.2), schematically illustrated by arrows drawn through the approximate centers of the regions where flow occurs. Groundwater flow occurs over wider areas than the arrows suggest, and the lateral boundaries of the flow paths are indistinct. Where arrows merge, convergence and mixing of groundwater from different flow systems is implied. Numeric labels on flow-path arrows correspond to the Flow Path Number column in tables 8.2 and 8.3. Flow paths are classified according to whether they meet hydrogeologic and hydrochemical criteria to be considered valid and conditionally valid, i.e., they accommodate significant amounts of interbasin groundwater flow (see section 8.3 and tables 8.2 and 8.3 for details).*

Figure 8.2 continued. *Green arrows represent valid flow paths, and gray arrows represent invalid flow paths. Also shown are (1) interbasin-boundary zones, classified according to their likelihood to accommodate interbasin flow, simplified from figure 8.1, (2) potentiometric-surface contours, simplified from figure 4.10, (3) mountain-block areas having relatively high potential recharge and runoff rates, modified from Masbruch and others (2011, figures D-5 and D-6, respectively), and (4) generalized valley-floor discharge areas from Gardner and others (2011).*

Table 8.3. *Evaluation of hydrogeologic and hydrochemical criteria for selected possible interbasin-flow paths, based on simple linear geochemical evolution from recharge area to discharge area. Red text indicates invalid flow path based on hydrogeologic and/or hydrochemical evaluation discussed in text.*

Flow Path[1] Number	Flow Path[1] Name	Hydrogeologic Units[2]	Structures[3]	Average Hydraulic Gradient[4]	Radiogenic Isotopes[5]	Temp.[6]	Stable Isotopes[7]	Inverse Hydrochemical Model[8]	Hydrochemical Evolution[9]	Dissolved Gas Model Recharge Temp.[10]	Overall Ranking[11]
1a	Northern Snake Valley to Fish Springs	QTcs-UPzc-LPzc-QTcs	mixed	0.003	No[a]	No[e]	No[i]	Deep Creek	Yes[k]	n/a[m]	Not Valid
2a	North-central Snake Valley to Fish Springs	LPzc-QTcs-UPzc-LPzc-QTcs	unfavorable	0.004	Yes[b]	No[f]	No	Gandy Springs	Yes[k]	No[n]	Not Valid
2b		LPzc-QTcs-UPcz-LPzc-QTcs	unfavorable	0.003	No[a]	Yes[g]	No	Northern Snake Range	Yes[k]	No[n]	Not Valid
3atv	South-central Snake Valley to Tule Valley and Fish Springs	LPzc-QTcs-UPzc-LPzc	favorable	0.011	Yes[c]	Yes[g]	No	Snake Creek	Yes[k]	No[n]	Conditionally valid – valid if water moves directly from group 4 to group 6 water
3afs		LPzc-QTcs-UPzc-LPzc-QTcs	favorable	0.007	Yes[c]	Yes[g]	No	Snake Creek	Yes[k]	No[n]	Conditionally valid – valid if water moves directly from group 4 to group 6 water
3b		UPzc-QTcs-UPzc-LPzc	favorable	0.004	Yes[d]	Yes[h]	No	Southern Snake Range	Yes[k]	No[n]	Conditionally valid – valid if flow path begins with first two legs of Snake Creek Path
4a	Pine Valley and Wah Wah Valley to Tule Valley	UPzc-QTcs-UPzc-LPzc	favorable	0.002	Yes[c]	Yes[g]	No	Pine Valley	Yes[l]	No[n]	Conditionally valid – valid if water moves directly from group 4 to group 6 water
4b											
5a	Western Sevier Desert to Fish Springs	LPzc-QTcs	favorable	0.017	Yes	Yes	Yes	North Canyon Spring	Yes	n/a[m]	Valid
5b		Tv-QTcs	favorable	0.011	Yes	Yes	No[j]	Laird Spring	Yes	n/a[m]	Valid

[1] Flow path name and number shown in table 8.2 and on figure 8.2.

[2] See figure 4.1 for explanation of hydrogeologic-unit symbols.

[3] Evaluation of whether the predominant orientation of most bedding, faults, and fold axes relative to the general potentiometric-surface gradient are favorable or unfavorable for interbasin flow. Interbasin flow is more likely where these structures strike parallel to or within 45 degrees of the principal potentiometric-surface gradient. However, flow through structures oriented at higher angles to the gradient is not precluded, gradients within interbasin-flow zones are poorly known, and flow paths are likely tortuous in detail.

[4] Hydraulic gradient (dimensionless) between chemical model starting and ending points as measured at sampled wells or springs. Inspection of the potentiometric-surface contours shown on figure 8.1 suggests that the hydraulic gradient varies along the flow paths.

[5] Evaluation based on whether both ^{14}C percent modern carbon and tritium concentrations decrease linearly along flow path. Violation of criterion suggests that either mixing of groundwater having different residence times occurs, or the flow path is invalid. Caveats: a. lowest pmc is in middle of path; b. pmc unknown for several samples; c. valid if group 5 sample is excluded; d. valid if path begins with first two legs of Snake Creek path.

[6] Evaluation based on whether temperature does not decrease along flow path. Violation of this criterion suggests that either mixing of groundwater from different depths occurs, or the flow path is not valid. Caveats: e. highest temperature is in the middle; f. temperature increases and decreases along path; g. valid if path through group 5 excluded; h. valid if path begins with first two legs of Snake Creek Path.

[7] Evaluation based on whether both deuterium and ^{18}O compositions are consistent within analytical error for all data points along the proposed flow path. Violation of criterion suggests that either mixing of groundwater having different starting compositions, due to recharge at different latitudes and/or ages, occurs, or flow path is invalid. Caveats: i. last legs to Fish Springs are consistent; j. just slightly outside of uncertainty.

[8] Inverse chemical model shown on figure 6.20. See section 6.2.4 for discussion.

[9] Inverse model results. See section 6.2.4 and figure 6.20. "Yes and "no" indicate whether data set supports or does not support the flow path. Caveats: k. direct evolution from group 4 to group 6, or mixing of groups 4 and 5, required for final leg for model to be valid; l. mixing or direct evolution from group 3 to 5 required for middle legs.

[10] Evaluation based on whether model recharge temperature is consistent along flow path. "Yes" and "No" indicate whether data set supports or does not support the flow path. Uncertainty of model recharge temperatures are not well known but are relatively large, so violation does not necessarily invalidate the flow path. Caveats: m. no data for starting points; n. model recharge temperatures are not equal within error.

[11] General evaluation of flow path based on all hydrogeologic and hydrochemical criteria. See table 6.3 for hydrochemical group-mean compositions and section 8.3.4 for discussion.

6. Southern Spring Valley to southern Snake Valley flow path. This groundwater flow path is conditionally valid (flow is within aquifers but must cross several faults), based on our interpretations of data and discussions in Laczniak and others (2007), Rowley and Dixon (2011, p. 4-67 to 4-69), Burns and Drici (2011, p. 7-3 to 7-5), and Prudic and Sweetkind (in review). Flow is from recharge in the southern Snake Range and the southern Schell Creek Range, through the coarse-grained basin-fill, lower Paleozoic carbonate-rock and volcanic-rock aquifers in the southern Snake Range and northern Limestone Hills, and the basin-fill and upper and lower Paleozoic carbonate-rock aquifers in northern Hamlin Valley, to discharge at Big Springs and Dearden Springs in southern Snake Valley. Flow must cross north-striking range-bounding normal-fault zones along both sides of the Limestone Hills, but east- to southeast-striking faults along the northern margin of the Limestone Hills (Rowley and Dixon, 2011, figure 4-73) may accommodate flow. Appendix E discusses estimates of interbasin-flow rates across this interbasin-boundary zone in greater detail. North-striking intrabasin faults below northern Hamlin Valley and southern Snake Valley (Rowley and Dixon, 2011, figure 4-73) may accommodate flow to the north toward the discharge areas, parallel to the principal hydraulic-gradient direction. The majority of discharge from Big Springs and to Lake Creek is likely part of a local groundwater-flow system having its recharge area in the southern Snake Range (section 8.4; Prudic and Sweetkind, in review). Dearden Springs discharges old groundwater (table 6.8), suggesting that the faults that control its location tap deeper groundwater flow (recharge area unknown, but possibly interbasin flow from southern Spring Valley) and not the local flow system (section 8.4).

Table 8.2 includes three additional flow paths (northern Spring Valley to west-central Snake Valley, flow path 6a; northern Snake Valley to southern GSLD, flow path 7a; and southern Steptoe Valley to southern Spring Valley, flow paths 8a and 8b) that are part of the Fish Springs flow system (with the possible exceptions of flow paths 8a and 8b; see table 8.2) discussed by previous authors. UGS data do not directly address the likelihood of these flow paths, so we do not discuss them here.

The hydrogeologic evaluations in the previous list do not address estimates of flow volumes or rates, which must be done in conjunction with water-budget analysis (section 4.5.4.4). Estimating the relative contributions of various flow paths to discharge in Tule Valley and Fish Springs is an important problem that requires additional data and study. Previous authors (Laczniak and others, 2007, p. 72–75; SNWA, 2009, table 8.1; Burns and Drici, 2011, p. 7-5 to 7-8) used Darcy's Law to estimate flow rates across various interbasin-boundary zones in the study area. In appendix E, we combine hydrogeologic analysis of previously published cross sections through part of the Confusion Range (Greene and Herring, 2012) and Darcy's Law to estimate possible interbasin flow rates from central Snake Valley to western Tule Valley.

Published estimates of the interbasin-flow rate from Snake Valley to Tule Valley range from about 14,000 to 33,000 acre-feet per year, and the most recent estimates from conceptual and numerical groundwater-flow models range from 15,000 acre-feet per year (18.5 hm^3/yr) (SNWA, 2009, table I-2) to 17,000 acre-feet per year (21.0 hm^3/yr) (Durbin and Loy, 2010, table 3.1-1) (table 4.6). The regional hydraulic-gradient direction between east-central Snake Valley and west-central Tule Valley varies from east-northeast to northeast (figure 8.2) (Gardner and others, 2011). Faults, folds, and hydrostratigraphy define four northeast-striking groundwater compartments in the Confusion Range (figure E.1), composed of the upper or lower Paleozoic carbonate-rock aquifer hydrogeologic units. Bedding, faults, and folds within the groundwater compartments predominantly strike northeast, parallel to the regional hydraulic gradient (figure E.1). Although the groundwater flow paths are likely tortuous in detail, the structural grain and along-strike continuity of the groundwater compartments in the Confusion Range collectively favor northeastward groundwater flow. Estimates using Darcy's Law show that these groundwater compartments can accommodate the entire estimated interbasin flow volume from central Snake Valley to central Tule Valley (appendix E).

We conclude from our hydrogeologic analysis that interbasin flow from Snake Valley to Tule Valley occurs at a rate within the range of estimates from recent groundwater-flow models because (1) the possible total flow rate through the interbasin flow area, based on Darcy's Law, exceeds rates from published groundwater flow models and water-budget analyses, (2) the southeastern end of the Conger Range is not separated from the Snake Valley basin-fill aquifer by a major range-bounding normal-fault zone, so a major barrier that may inhibit movement of groundwater from the Snake Valley basin-fill aquifer into the interbasin flow zone is absent there, (3) the range-bounding normal-fault zones on either side of the Confusion Range likely contain permeable segment-boundary zones that provide local pathways for cross-fault groundwater flow, and (4) geochemical modeling and isotopic data permit this interpretation (chapter 6; section 8.4).

A source of uncertainty in the application of Darcy's Law as in appendix E is that potentiometric gradients in interbasin-boundary zones are poorly known, and are likely highly variable due to complex geology. UGS groundwater-monitoring sites in interbasin-boundary zones include site 10 in west-central Tule Valley adjacent to east-central Snake Valley, site 12 in east-central Snake Valley adjacent to southwestern Tule Valley, site 18 in northeastern Snake Valley adjacent to northern Tule Valley, and site 20 in northeastern Tule Valley adjacent to Fish Springs Flat (figure 8.1). Groundwater levels at these sites provide important, previously unavailable constraints on hydraulic gradients in interbasin-boundary zones. Several examples follow.

We used groundwater levels at site 6 in east-central Snake Valley and site 10 in west-central Tule Valley to define the hydraulic gradient used in the Darcy's Law calculations (appendix E). The groundwater level at site 12 in the southern Confusion Range is similar to those in Tule Valley and substantially lower than in eastern Snake Valley, suggesting that local recharge is sparse and that either a flow barrier exists between southeastern Snake Valley and site 12, or groundwater at site 12 is not connected to the regional aquifer system. Consequently, we estimated the regional potentiometric gradient through the southern Confusion Range using the contours of Gardner and others (2011), which do not use the groundwater level at site 12. Although the Sand Pass transverse zone provides a potential path for flow from northeastern Tule Valley to southwestern Fish Springs Flat, we do not think that such flow occurs, at least at relatively shallow depths, because the potentiometric surface at UGS groundwater-monitoring site 20 is about 4 feet (1.2 m) higher than in central Tule Valley. Deeper groundwater flow through this zone is possible, but we do not have data to support or refute this idea.

Another possible complication of determining hydraulic gradients in interbasin-boundary zones is the presence of large areas of relatively high groundwater levels and steep hydraulic gradients ("groundwater mounds") in areas of high recharge rate. Sweetkind and others (2011, p. 5 and p. 7) discuss these groundwater mounds and suggest that they divert groundwater flow, and the groundwater-level map of Heilweil and Brooks (2011, plate 2) shows their distribution in the eastern Great Basin. Figure 8.1 shows likely areas of groundwater mounding in mountain blocks, based on water-level contours from Heilweil and Brooks (2011, plate 2). We interpret the presence of additional possible groundwater mounds in areas of relatively high potential recharge (Masbruch and others, 2011, figures D-5 and D-6). We consider interbasin flow beneath these groundwater mounds unlikely.

8.3.3 Evaluations of Flow Paths Based on Major-Ion, Isotopic, and Dissolved-Gas Compositions

In this section, we use hydrochemical data presented in chapter 6 to evaluate whether spatial variations in major-ion hydrochemistry, aquifer temperature, and hydrochemical tracers (radiogenic-isotope and noble-gas compositions) are consistent with expected changes along the hypothetical flow paths discussed in the previous section.

Changes in most hydrochemical constituents support the conceptual model of the Fish Springs flow system. From the major recharge areas to the major discharge areas, major-ion compositions and statistically defined hydrochemical groups trend toward more chemically evolved types (figures 6.7 and 6.13), groundwater temperature remains constant or does not decrease (figure 6.3), tritium concentration decreases (figure 6.26), and percent modern carbon decreases (figure 6.28). Variations in ∂^2H (figure 6.24) and ∂^{18}O (figure 6.25) and model recharge temperature do not support a simple model of direct, closed-system groundwater flow. Stable-isotope compositions vary beyond analytical error between upgradient and downgradient hydrographic areas in the flow system. Model recharge temperatures derived from dissolved-gas compositions differ between Snake Valley and most samples from Tule Valley and Fish Springs Flat. Gardner and Heilweil (2014) presented similar conclusions from a detailed study of noble-gas tracers. Overall, variations in most chemical constituents support the conceptual model of flow in the Fish Springs flow system, and suggest some mixing or other processes may occur (see discussion in section 8.3.4).

Hypothetical flow paths in the Fish Sprigs flow system can be evaluated further by considering variations in hydrochemistry measured in individual wells and springs from recharge areas to discharge areas. Table 8.3 summarizes the hydrogeology and hydraulic gradients of proposed flow paths, and evaluates whether variations in major-ion chemistry, radiogenic-isotope composition, groundwater temperature, stable-isotope composition, inverse-hydrochemical modeling, and model recharge temperatures support the flow paths delineated in table 8.2 and on figure 8.2. Criteria for evaluating whether constituents support the flow paths are as follows:

1. Major-ion chemistry (section 6.2.3; figures 6.7 and 6.13) – whether compositions become more chemically evolved with increasing distance from the recharge area, and the changes are consistent with aquifer mineralogy,
2. Radiogenic isotopes (sections 6.3.3 and 6.3.4; figures 6.26 and 6.28) – whether both the tritium and

percent-modern-carbon concentrations decrease progressively (i.e., increasing residence time) along the flow path,

3. Temperature (section 6.2.1.3; figure 6.3) – whether groundwater temperature does not decrease along the flow path,
4. Stable isotopes (section 6.3.2; figures 6.24 and 6.25) – whether values of ^{2}H and ^{18}O are consistent within error along the flow path,
5. Inverse hydrochemical modeling (section 6.2.4; figure 6.20) – whether valid models exist for statistically defined geochemical groups and compositions measured from individual wells and springs along the flow path,
6. Dissolved-gas model recharge temperatures (section 6.3.1; figure 6.21) – whether model recharge temperatures are consistent within error along the flow path.

These criteria are listed in order of decreasing confidence, based on our subjective evaluation of the relative degree of uncertainty, potential for modification along the flow paths by processes such as mixing or evaporation in discharge areas, non-uniqueness of model results, and uncertainty of assumptions required to perform calculations.

In table 8.3 we evaluate whether changes in chemical constituents along the flow paths are consistent with a simple model of progressive, unidirectional change between successive discrete data points (well or spring samples). Violation of this criterion for any step along the flow path results in either a "conditionally valid," or "not valid" ranking for the flow path. A conditionally valid ranking indicates that not all constituents change in a manner consistent with the simple flow model, but that the variation can be explained by an additional, reasonably likely process such as mixing of groundwater from different flow paths (see discussion in section 8.3.4). Evaluation of variations in major-ion composition, temperature, and radiogenic-isotope concentration results in valid or conditionally valid rankings for the north-central Snake Valley to Fish Springs (2b; not supported by hydrogeology), south-central Snake Valley to Tule Valley and Fish Springs (3afs and 3atv), Pine Valley and Wah Wah Valley to Tule Valley (4a and 4b), and Western Sevier Desert to Fish Springs (5a and 5b) flow paths (table 8.3; figure 8.2). The hydrochemical evaluation results in a not valid ranking for the northern Snake Valley to Fish Springs (1a) or north-central Snake Valley to Fish Springs (2a; not supported by hydrogeology) flow paths (table 8.3; figure 8.2).

Stable-isotope compositions vary beyond analytical error in all but the western Sevier Desert to Fish Springs (5a and 5b) flow paths. This variation can be explained by mixing of groundwater recharged at different latitudes, elevations, or ages, so violation of this criterion does not necessarily invalidate the flow paths. Model recharge temperatures fail to support any of the proposed interbasin flow paths that include dissolved-gas samples from recharge, intermediate sample points, and discharge areas. In section 8.4.3 we discuss possible reasons for the disagreement between most hydrogeologic and geochemical criteria and the dissolved-gas model temperatures.

The final column in table 8.3 presents our subjective evaluations of whether the hydrochemistry of samples along the flow paths collectively support the proposed flow paths. We conclude that the western Sevier Desert to Fish Springs (5a and 5b) flow path is valid and the south-central Snake Valley to Tule Valley and Fish Springs (3afs and 3atv) and Pine Valley and Wah Wah Valley to Tule Valley (4a and 4b) flow paths are conditionally valid, and we consider interbasin groundwater flow along these paths likely. Our analyses do not support significant groundwater flow along the northern Snake Valley to Fish Springs (1a), and north-central Snake Valley to Fish Springs (2a and 2b) flow paths.

8.3.4 Discussion

Application of hydrogeologic and hydrochemical criteria to interbasin flow in the Fish Springs flow system identifies several flow paths that satisfy hydrogeologic and hydrochemical criteria for valid flow paths. This evaluation does not address the important question of flow rates, and the relative contributions of different flow paths to the major discharge areas in Tule Valley and Fish Springs.

Potentiometric-surface contours (Gardner and others, 2011) support the conceptual model of the Fish Springs flow system at the regional scale (figure 8.1). These contours are based on significantly more groundwater-level data than were available to Carlton (1985) and Harrill and others (1988), particularly from the carbonate-rock aquifer, which they hypothesized to accommodate the interbasin flow. Variations in major-ion composition, temperature, and radiogenic-isotope concentration support the conceptual model. Variations in stable-isotope composition and model recharge temperatures derived from dissolved-gas composition do not support a simple model of closed-system groundwater flow between recharge and discharge areas, but do not necessarily disprove the model, as discussed below.

In the Fish Springs flow system, structurally complex aquifer systems exist between the proposed recharge and discharge areas, and define several distinct flow paths (table 8.2; figures 8.1 and 8.2). Along these flow paths, adjacent

hydrographic areas are hydraulically connected through interbasin-boundary zones (figures 8.1 and 8.2). Although the concept of interbasin flow is controversial and data are sparse, our interpretation of the hydrogeology of selected interbasin-boundary zones indicates that sufficient groundwater flow may occur through them to support the general model of the Fish Springs flow system and the existence of the specific flow paths discussed in section 8.3.3 and delineated in table 8.2 and on figure 8.2. Evaluation of hydrochemical variations among specific wells and springs from recharge areas to discharge areas (table 8.3) suggests that groundwater in the Fish Springs flow system does not conform to a simple closed-system flow model, and some of the flow paths proposed based on hydrogeologic criteria are not valid. Evaluation of variations in hydrochemistry supports the western Sevier Desert to Fish Springs (5a and 5b) flow path, and conditionally supports the south-central Snake Valley to Tule Valley and Fish Springs (3a and 3b) and Pine Valley and Wah Wah Valley to Tule Valley (4a and 4b) flow paths. Hydrogeologic and hydrochemical data do not support the northern Snake Valley to Fish Springs (1a), and north-central Snake Valley to Fish Springs (2a and 2b) flow paths (table 8.3).

The south-central Snake Valley to Tule Valley and Fish Springs flow paths (3a and 3b), which represent flow from the southern Snake Range recharge area though the central and southern Confusion Range, either to the Tule Valley discharge area (including Coyote Spring), or through northern Tule Valley, the southern Fish Springs Range, and Fish Springs Flat to discharge at Fish Springs, are conditionally valid. We consider groundwater flow along this path possible provided that a) some flow occurs from eastern Snake Valley to Fish Springs without mixing with or evolving to the sulfate-bearing groundwater present in the Tule Valley discharge area, b) the variation in stable-isotope compositions between eastern Snake Valley, Tule Valley, and Fish Springs can be explained by recognized processes that would affect hydrochemistry along the flow path, and c) variation in model recharge temperatures can be explained by processes that change the dissolved-gas concentrations from their values obtained during recharge, or by the uncertainties in the assumptions necessary for model calculation.

The lack of valid inverse models for major-ion evolution from group 5 (Na-Ca-Cl-SO_4 type) to group 6 (Na-Cl type) groundwater (tables 6.3 and 6.5; section 6.2.4) makes identifying a valid flow path from Snake Valley through Tule Valley to Fish Springs Flat difficult. Coyote Spring, the largest spring in the Tule Valley discharge area, has group 6 groundwater, similar to the groundwater that issues from Fish Springs. One possible scenario for the geographic proximity of groups 5 and 6 is that group 5 groundwater represents relatively shallower flow that obtains its sulfate from water-rock chemical reactions with gypsum-bearing upper Paleozoic rocks and/or Quaternary-Tertiary lakebed deposits, whereas the fault zones that localize Coyote Spring and Fish Springs directly access group 6 groundwater, which is part of a deeper flow system in the carbonate-rock aquifer that does not interact with these geologic units. This inference is supported by the work of Carlton (1985, p. 34–37) who used silica composition, temperature, and an assumed geothermal gradient to estimate that the circulation depth of groundwater issuing from the major springs in the Fish Springs flow system ranges from about 2000 to 4000 feet (610–1219 m). We do not have similar estimates for group 5 groundwater, but these samples are from wells less than 1000 feet (305 m) deep. Groups 5 and 6 groundwater may be parts of different flow systems. Flow from Snake Valley to Coyote Spring and Fish Springs may occur within the deeper flow system that produces group 6 groundwater.

Considering that Tule Valley and Fish Springs each have several possible source areas of interbasin flow and local recharge (figures 8.1 and 8.2), these discharge areas likely represent convergence and mixture of groundwater from different flow paths recharged in different aquifers, latitudes, and times (i.e., climatic conditions) (chapter 6). Mixing of groundwater from different source areas could result in stable-isotopic compositions in the discharge area that are not consistent with values presently measured in one or more of the recharge areas or at sample points intermediate in the flow path. Differences in stable-isotopic composition along the Fish Springs flow system and flow paths therein, therefore, do not necessarily invalidate the concept of interbasin flow or the individual flow paths. This scenario would explain the mixing of groundwater required to generate some valid inverse models of major-ion evolution (tables 6.5 and 8.1), and radiogenic-isotope compositions would also represent mixtures of groundwater recharged at different times and potentially under different geochemical conditions.

Model recharge temperatures based on dissolved-gas compositions require estimates of the changes in temperature with land-surface elevation and depth to the groundwater table at the time of recharge (section 6.3.1) and carry large uncertainties, which may partly explain the discordant model-recharge temperatures between Snake Valley and Tule Valley and Fish Springs Flat. Alternatively, contamination or disequilibrium processes may have resulted in anomalously high model recharge temperatures in some samples west of Snake Valley (section 6.3.1). However, the model recharge temperatures are systematically different

and suggest that groundwater in Tule Valley and Fish Springs Flat was recharged under different thermal conditions (lower elevation and/or higher geothermal gradient) than in Snake Valley. Another possibility, discussed in section 8.5, is that the shallow groundwater in Tule Valley and northeastern Snake Valley (group 5, Na-Ca-Cl-SO_4 type) is not derived from Snake Valley, but the groundwater discharging from Fish Springs and Coyote Spring (group 6, Na-Cl type) is derived from Snake Valley and is tapped by faults controlling these springs. The noble gas compositions of this groundwater may have been altered during deep circulation and/or mixing with other flow paths in these discharge areas. On the whole, the dissolved-gas data do not corroborate the other hydrogeologic and hydrochemical data considered in this report and are not easily explained. Gardner and Heilweil (2014) used noble-gas tracers to delineate flow systems and address the apparent discordance between these data and other groundwater-chemical constituents.

If interbasin flow from Snake Valley to Tule Valley and/or Fish Springs Flat occurs, evolution of hydrochemistry along this flow path cannot be described by a simple, closed-system model. In figure 8.3 we attempt to schematically illustrate the physical and chemical evolution of groundwater in this and similar flow paths, accounting for flow across structurally complex interbasin-boundary zones, mixing of groundwater from local and distant sources, and discharge to fault-controlled springs or upward flow from the deep carbonate-rock aquifer to the basin-fill or shallow carbonate-rock aquifers. In the Tule Valley and Fish Springs discharge areas, convergence and mixing of groundwater from different flow paths having different starting compositions and path lengths could result in variations in groundwater chemistry that do not fit the simple evolutionary model used to evaluate the interbasin flow paths in table 8.3. Additional study is required to evaluate the contributing sources for the Tule Valley and Fish Springs discharge areas.

Alternatively, the disagreement between the model recharge temperatures and analysis of other chemical problems may imply that the proposed flow paths from Snake Valley to Tule Valley and Fish Springs are invalid, and that variations in groundwater-chemical constituents that are consistent with the hypothesized flow paths are either non-unique or coincidental. This option is presently unsatisfactory to us because it contradicts the evaluations based on hydrogeology and most other chemical data, and does not provide a source for the excess discharge in Tule Valley and Fish Springs Flat (section 4.5.5.4), but suggests that future work should focus on delineating flow systems that contribute to these discharge areas.

8.4 GROUNDWATER FLOW IN SNAKE VALLEY

8.4.1 Introduction

The majority of new hydrochemical samples from this project are from Snake Valley. In this section we use potentiometric-surface and hydrochemical data to delineate local- and intermediate-scale flow systems (table 8.1) in Snake Valley, at a level of detail not possible before this study. Local flow systems include relatively young (predominantly modern to premodern qualitative ages) groundwater directly downgradient from the areas of highest average annual precipitation and recharge in the Snake Range and Deep Creek Mountains, and intermediate flow systems represent longer, and likely deeper, flow paths from the mountains and mountain fronts to springs and evapotranspiration (ET) areas in the valley centers.

8.4.2 Local Flow Systems

We delineate five local groundwater-flow systems in Snake Valley (figure 8.4) based on potentiometric-surface contours, and variations in major-ion, radiogenic- and stable-isotope compositions, and model recharge temperatures:

1. the Callao local flow system includes recharge in the Deep Creek Mountains mountain block and mountain front, and discharge by springs, ET, and agricultural pumping in the Callao area,
2. the Gandy local flow system includes recharge in the northern part of the northern Snake Range, and the component of young groundwater that discharges from Gandy Warm Springs,
3. the central Snake Valley local flow system includes recharge in the central part of the northern Snake Range mountain block and mountain front, and discharge by springs (including Kell Spring and Caine Spring) and ET in central Snake Valley,
4. the Garrison/Baker local flow system includes recharge in the northern part of the southern Snake Range mountain block and mountain front, and discharge to Lake Creek, ET, and agricultural pumping from an approximate southern boundary a few miles south of Pruess Lake on the south to the Baker, Nevada, area to the north, and
5. the Big Springs local flow system includes recharge in the southern part of the southern Snake Range mountain block and mountain front, and discharge to springs (including Big Springs), surface water (Big Springs Creek in Nevada and Lake Creek

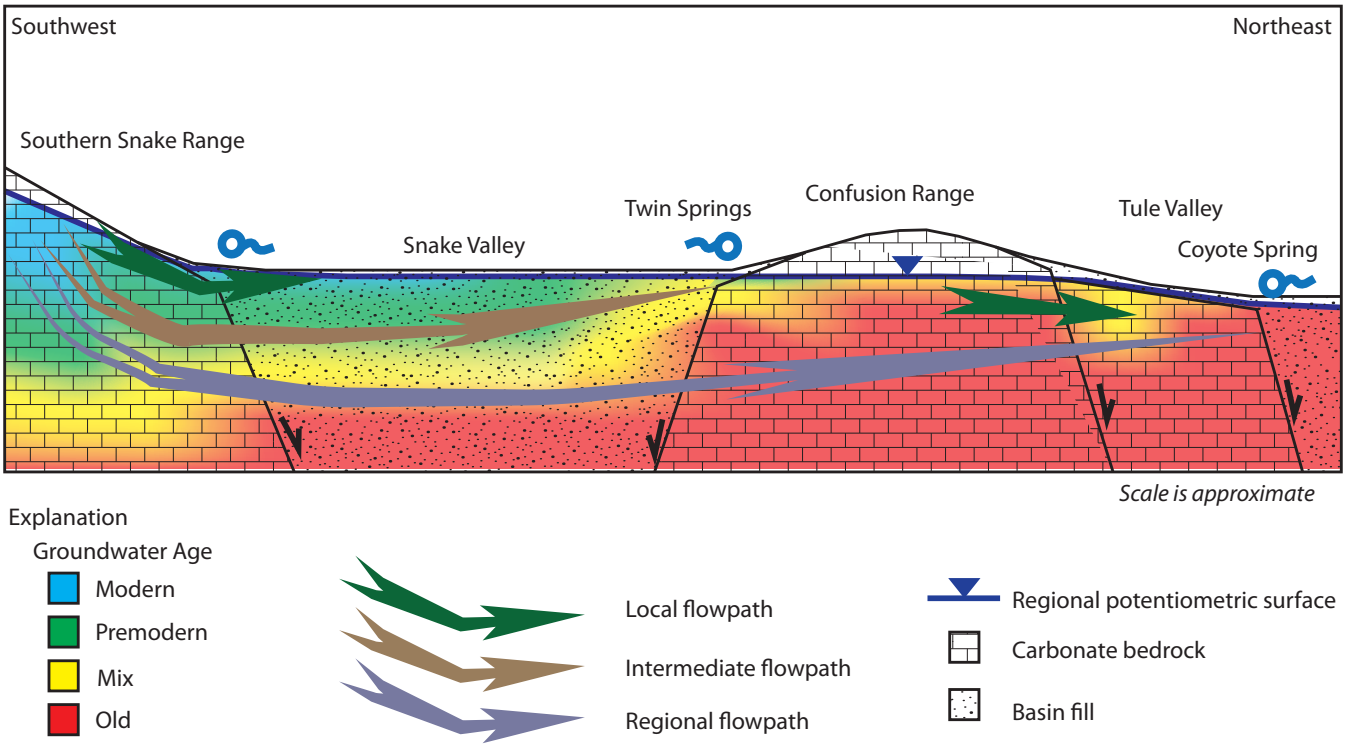

Figure 8.3. *Idealized section of groundwater flow along local and intermediate flow paths in Snake Valley, and regional (interbasin) flow from Snake Valley to Tule Valley. Arrows represent generalized flow paths, and colors symbolize groundwater of different residence times. Other chemical constituents, such as major-ion or isotope composition, may vary in a similar manner. Mixing may occur in transition zones between flow systems of different scales, in discharge areas such as Twin Springs and Coyote Spring, and from local recharge as illustrated by green arrow below the Confusion Range.*

in Utah), ET areas along the creeks and adjacent valley floors, and agricultural pumping in southern Snake Valley.

Groundwater in local flow systems in Snake Valley moves from recharge areas in the mountain blocks and on the adjacent mountain fronts, through the basin-fill and/or shallow carbonate-rock aquifers, to springs and ET areas within about 10 miles (16 km) of the mountain front. The springs may be localized by faults or by sedimentary facies transitions within the basin fill from coarser-grained alluvial-fan deposits having higher hydraulic conductivity below the mountain fronts, to finer-grained lacustrine deposits having lower hydraulic conductivity below the valley floors. Groundwater recharged in the mountain block either crosses the basin-bounding normal-fault zone in the subsurface, or enters mountain streams that flow onto the mountain fronts where it recharges into alluvial-fan deposits. Springs in Snake Valley that we interpret to discharge modern groundwater from local flow systems include springs near Callao in the Callao local flow system, Gandy Warm Springs and Pleasant Valley Coyote Spring in the Gandy local flow system, Kell Spring and Caine Spring in the central Snake Valley local flow system, and Big Springs and unnamed springs to the north and south in the Big Springs local flow system (figure 8.4), but see discussion of possible multiple-flow-system sources for some of these springs in section 8.4.

Table 8.1 summarizes the general geochemical characteristics of local flow systems in Snake Valley. Groundwater chemistry ranges from Ca-HCO_3 type (hydrochemical group 1) in recharge areas to Ca-Mg-HCO_3 type (group 2) or Ca-Mg-Na-HCO_3 type (group 3) in discharge areas (figures 8.4 and 6.13). Water-rock reaction models A and B of the northern Snake Range, Snake Creek, and southern Snake Range chemical paths describe the geochemical evolution from recharge to discharge areas (tables 6.5 and 6.6; figures 6.18 and 6.19). Groundwater temperature is generally less than 10°C (50°F) (figure 6.3).

Radiogenic-isotope concentration in Snake Valley local flow systems generally decreases from recharge areas to discharge areas. Tritium concentration ranges from greater than 2.0 tritium units in recharge areas to 0.5 tritium units in discharge areas, percent modern carbon

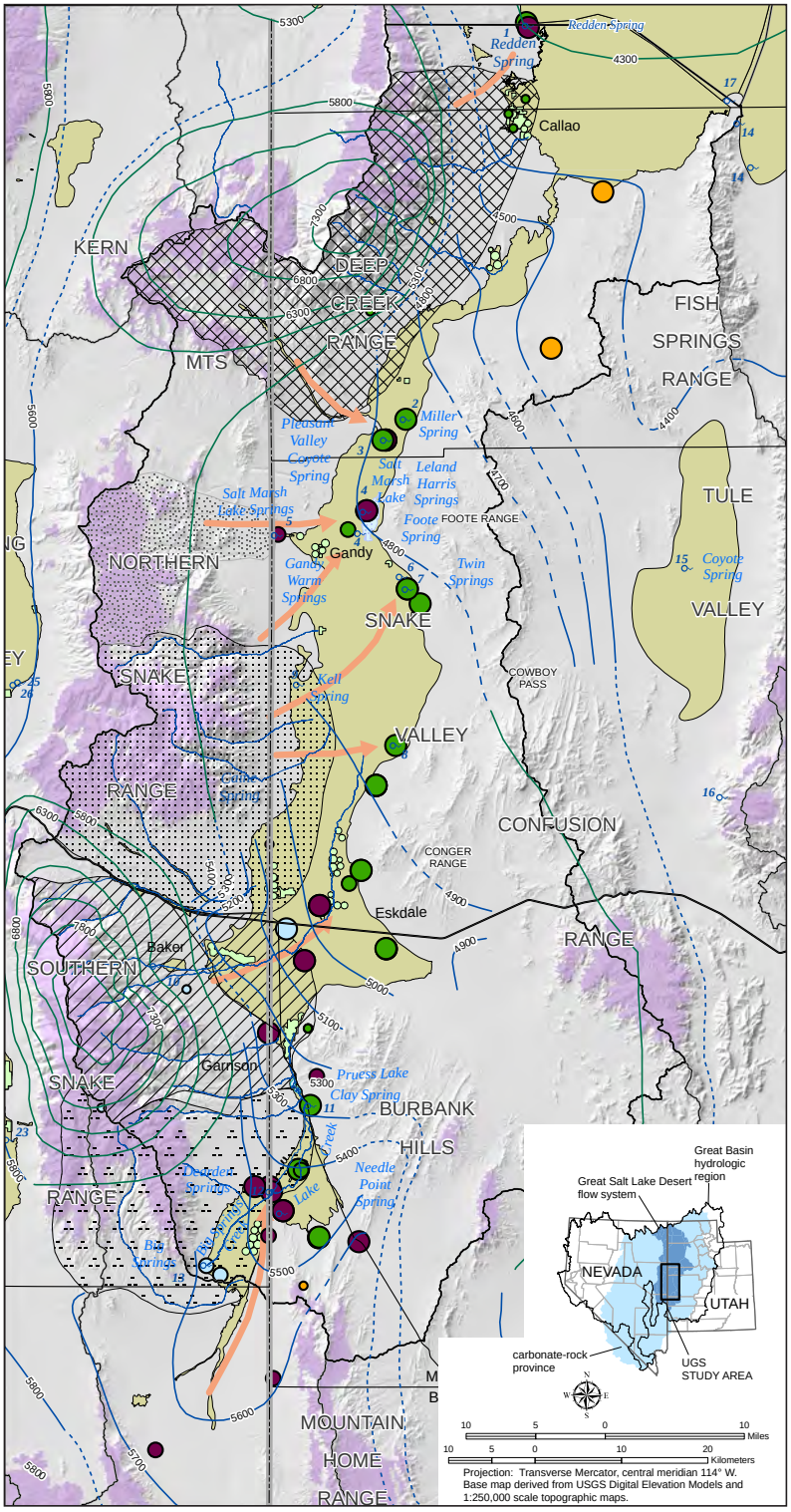

EXPLANATION

Groundwater Flow Systems

Local Flow Systems

- Callao
- Gandy
- Central Snake Valley
- Garrison/Baker
- Big Springs

Intermediate Flow System - general, schematic

Sample Geochemistry and Age

Group 2	Group 3	Group 4	Group 5
Modern	Modern	Modern	Modern
Mix	Mix	Mix	Mix
Premodern	Premodern	Premodern	
Old	Old	Old	Old

Recharge (Masbruch and others, 2011)

In-Place Recharge
6.1 - 38.0 in/yr

Recharge of runoff*
1.1 - 5.4 in/yr

*Flint and others (2011) calculated runoff of precipitation using the BCM model. Runoff is shown where it originates, in the topographically higher areas of the mountain blocks. The runoff values shown here are 10% of the total runoff generated, i.e., the estimated proportion that recharges to the basin-fill aquifer along the mountain front (Masbruch and others, 2011, p. 14).

Discharge area (Laczniak and others, 2007)

Potentiometric- surface contours (figure 4.10)

Datum = mean sea level

- Contour (interval 100 feet)
- Inferred Contour (interval 100 feet)
- Contour (interval 500 feet)

UGS Groundwater-Monitoring Network

Numeric label is UGS site number

New Wells and Gages (2007-2009) (table C.1)

- Monitor wells in basin-fill aquifer
- Monitor wells in volcanic-rock aquifer
- Monitor wells in basin-fill and carbonate-rock aquifer
- Monitor wells in carbonate-rock aquifer
- Monitor wells in Cambrian-Neoproterozoic siliciclastic-rock aquifer

Aquifer-Test Sites

- Carbonate-rock and basin-fill aquifers
- Carbonate-rock aquifer
- Agricultural-area monitoring wells
- Nested piezometers near spring

Other Groundwater Monitoring Sites

- UGS transducer in previously existing well (table C.2)
- UGS spring-flow gage site (table C.4)

Other Features

- USGS spring-flow gage site
- Spring (table 4.2)
- Perennial stream
- SNWA proposed point of diversion

Figure 8.4. *Local- and intermediate-scale groundwater-flow systems in Snake Valley, interpreted from hydrogeologic and hydrochemical data (section 8.4). Local flow systems are illustrated as broad fields, but data are insufficient to precisely define their lateral extent and depth. Intermediate-scale flow systems are illustrated as arrows pointing to springs that discharge groundwater interpreted to be more chemically evolved and older (i.e., longer-traveled) than that which discharges from local flow systems. The source areas of these springs are likely broader than illustrated by the arrows. Graduated symbols show variations in major-ion composition and qualitative age.*

values are greater than 50, apparent ages are less than 1000 years, and the groundwater is qualitatively classified as modern or premodern (figures 6.25, 6.27, and 6.30, and 6.32, respectively). Most model recharge temperatures estimated from dissolved-gas compositions range from 0 to 10°C (32–50°F) (figure 6.20), consistent with recharge in the higher-elevation parts of the mountain blocks or along the mountain fronts in areas dominated by recharge of surface runoff, such as the highest-altitude parts of the Snake Range. Most ∂^2H and ∂^{18}O values in the discharge areas of local flow systems are similar or enriched (i.e., less negative) compared to values measured in the nearby upgradient recharge areas (figures 6.23 and 6.24). The difference in stable-isotope composition may reflect mixtures of groundwater recharged at a variety of elevations and times, including (1) groundwater that may have recharged to mountain-block aquifers, discharged to mountain streams, and recharged to the groundwater table lower in the mountain block or along the mountain front (e.g., Wilson and Guan, 2004), and (2) irrigation return flow near agricultural areas.

8.4.3 Intermediate Flow Systems

Groundwater discharging to springs and ET areas (as sampled by wells) on the Snake Valley floor and eastern margin is more chemically evolved and older than groundwater in local flow systems (table 8.1; figure 8.4). Flow systems that end in these discharge areas are here referred to as "intermediate" because they are longer than local flow systems but do not cross hydrographic-area boundaries (figures 8.3 and 8.4; Sweetkind and others, 2011, figure C-1). Discharge areas of intermediate flow systems in Snake Valley include, from north to south, the Redden Springs area in northern Snake Valley, the Miller Spring-Leland Harris Springs area and Salt Marsh Lake Springs in north-central Snake Valley, the Bishop Springs area (including Twin Springs and Foote Spring) in east-central Snake Valley, and discharge by pumping in the Eskdale agricultural area and nearby ET areas in south-central Snake Valley.

Groundwater discharging from intermediate-scale flow systems in Snake Valley likely recharges in the same areas as groundwater in local flow systems, but either moves to greater depths in the recharge area and flows along longer, deeper flow paths compared to local flow systems (figure 8.3), based on the conceptual models of flow systems outlined by Toth (1963), Freeze and Witherspoon (1967), Harrill and others (1988), Laczniak and others (2007), and Sweetkind and others (2011, figure C-1), or represents relatively shallower groundwater that does not discharge from local-system areas but continues to flow to the east or northeast. Flow paths are complex and may cross intrabasin normal-fault zones where hydrogeologic conditions permit. The distance between recharge and discharge areas is about 10 to 25 miles (16–40 km).

Groundwater chemistry in discharge areas of intermediate-scale flow systems ranges from Ca-Mg-Na-HCO_3 type (group 3) to Na-Ca-Mg-HCO_3-SO_4 type (group 4) (figure 8.4). Water-rock reaction models A through C of the Gandy Springs, northern Snake Range, and Snake Creek chemical paths, and A and B of the southern Snake Range chemical path (tables 6.5 and 6.6; figures 6.18 and 6.19) describe the hydrochemical evolution from recharge to discharge in intermediate flow systems in Snake Valley. Groundwater temperatures range from about 10 to 15°C (50–59°F) (figure 6.3).

Tritium concentration in intermediate-scale flow systems discharge areas is less than 0.5 tritium units, percent modern carbon ranges from about 25 to 50, apparent ages range from about 3000 to 10,000 years, and the water is qualitatively classified as premodern, old, or mixed (figures 6.25, 6.27, and 6.30, and 6.32, respectively). Most ∂^2H and ∂^{18}O values are less depleted than values in local flow systems (figures 6.23 and 6.24), perhaps reflecting recharge under different climatic conditions, or evaporation in the discharge areas (section 6.3.2). Model recharge temperatures estimated from dissolved-gas composition that range from 0 to 10°C (32–59°F) are consistent with recharge in the mountain block or along the mountain front where recharge rates are high. Model recharge temperatures of 10 to 15°C (50–59°F) suggest recharge either along the mountain front where recharge rates are low, or in the mountain block where the water table is deeper or the geothermal gradient is higher (section 6.3.1) (Gardner and Heilweil, 2014).

8.4.4 Discussion

Although they are situated in the discharge areas of local flow systems, radiogenic-isotope data suggest that Big Springs and Gandy Warm Springs discharge groundwater from both local and intermediate and/or interbasin flow systems. Tritium is present in measurable quantities suggesting recharge younger than 50 years, whereas percent modern carbon is less than 50 and model apparent ages are older than about 2000 years (table 6.7; figures 6.25, 6.27, and 6.30, respectively; Hershey and others, 2007). The intermediate-depth piezometer at Twin Springs (piezometer SG24B, UGS groundwater-monitoring site 24) also yields mixed-source radiogenic isotope data. In contrast, Dearden Springs is located in the Lake Creek local flow system but discharges old groundwater to Lake Creek (table 6.7), so its source is likely an intermediate-scale flow system and/or interbasin flow from southern Snake Valley.

Faults that localize the springs (Kistinger and others, 2009) may tap deeper groundwater than the local flow system, and the strong upward flow prevents local recharge from mixing with the deeper-sourced water.

8.5 SUMMARY AND CONCLUSIONS

The UGS groundwater-monitoring network, along with other recent groundwater-monitoring and sampling projects by the U.S. Geological Survey and SNWA, has substantially increased the hydraulic-head and hydrochemical data available in Snake Valley and adjacent hydrographic areas to the east that comprise the Fish Springs flow system. Among the many possible applications of these new data, is evaluation of previously proposed conceptual models of regional groundwater flow and interbasin-flow paths. Better delineating flow systems will identify general source areas for environmentally and economically important discharge areas, to aid future evaluations of the potential effects of groundwater development (chapter 9).

The conceptual model of regional flow systems in the carbonate-rock province of the eastern Great Basin has been developed and adopted by numerous hydrogeologic studies that include part or all of the UGS study area (Harrill and others, 1988; Prudic and others, 1995; Laczniak and others, 2007; Sweetkind and others, 2011). In this model, groundwater moves below surface-flow divides that define hydrographic-area boundaries and, therefore, in many cases must cross range-bounding normal-fault zones and flow through structurally complex bedrock-aquifer systems in the mountain ranges or low passes, herein termed interbasin-boundary zones, on either side of the hydrographic-area boundaries. Interbasin flow is difficult to demonstrate in detail, and several authors are skeptical of its prevalence in the UGS study area (e.g., Acheampong and others, 2009; Rowley and others, 2009; Rowley and Dixon, 2011; Gillespie and others, 2012). In this chapter we use new hydraulic head and hydrochemical data and hydrogeologic interpretations to evaluate possible interbasin-flow paths in the Fish Springs flow system.

The conceptual model of regional groundwater-flow systems requires that hydraulic head decreases, and that sufficient permeable aquifer systems exist, continuously from recharge areas to discharge areas (e.g., Harrill and others, 1988; Prudic and others, 1995). A corollary is that the chemical composition of groundwater changes progressively in a predictable manner from recharge to discharge areas for non-conservative constituents such as major-ion composition and radiogenic-isotope concentration, or does not change for conservative constituents such as stable-isotope composition or model recharge temperature (e.g., Thomas and others, 1996; Hershey and others, 2007; Thomas and Milhevc, 2011).

Our evaluation of the potentiometric surface and hydrogeology suggests that some interbasin-flow paths from recharge areas in the Snake Range to discharge areas in Tule Valley and Fish Springs Flat, from Pine Valley to Tule Valley, and from the western Sevier Desert to Fish Springs Flat, are valid (figure 8.1). Interbasin-boundary zones composed chiefly of the upper and/or lower Paleozoic carbonate-rock aquifers, in which bedding, faults, and folds are oriented predominantly parallel to the principal potentiometric-gradient direction, are the most likely to accommodate interbasin flow. The potentiometric gradients and depth of flow in these interbasin-boundary zones are incompletely known.

Estimates of interbasin-flow rates from Snake Valley to Tule Valley through part of the Confusion Range using Darcy's Law (appendix E) suggest that sufficient permeable aquifer volume exists to accommodate recent estimates derived from groundwater-flow models of about 15,000 to 17,000 acre-feet per year (18.5–21 hm^3/yr) (SNWA, 2009; Durbin and Loy, 2010, respectively). The calculations require estimates of (1) the hydraulic conductivity of the upper and lower Paleozoic carbonate-rock aquifer hydrogeologic units (table 7.4), (2) the hydraulic gradient across the interbasin-boundary zone, and (3) the cross-sectional aquifer area available for interbasin flow between the groundwater table and 2000 feet (610 m) below land surface. Using reasonable estimates of these values, the range of estimated interbasin-flow rates can be accommodated through the Confusion Range south of Cowboy Pass (appendix E).

Hydrochemical variations generally support the conceptual model of the Fish Springs flow system. From recharge areas to discharge areas, major-ion content changes to more chemically evolved compositions, groundwater temperature increases, and radiogenic-isotope concentrations indicate longer residence times, all consistent with previously hypothesized regional flow patterns. Stable-isotope compositions do not reflect interbasin flow in a simple manner, because they vary with latitude, elevation, and time of recharge. Model recharge temperatures derived from dissolved-gas compositions are warmer in Tule Valley and Fish Springs Flat than in Snake Valley and, at face value, do not support interbasin flow.

Evaluation of changes in hydrochemistry in wells and springs sampled along flow paths that satisfy hydrogeologic criteria for interbasin flow indicates that whereas some of these flow paths are valid, most cannot be explained by a simple model of closed-system flow from recharge to discharge areas. Variations in hydrochemistry support

flow from the western Sevier Desert to Fish Springs Flat, and conditionally support flow from Snake Valley to Tule Valley and to Fish Springs Flat. Flow from eastern Snake Valley to Fish Springs Flat is valid, provided there is no interaction with or chemical evolution to sulfate-bearing groundwater present in the basin-fill and shallow carbonate-rock aquifers in Tule Valley. Fish Springs and central Tule Valley each discharge groundwater from several flow paths having different recharge conditions, aquifer systems, and residence times that converge and mix in the discharge areas. Variations in stable-isotope compositions along interbasin flow paths may be explained by mixing of groundwater recharged at different latitudes, elevations, and times, though we did not perform calculations to verify this idea. Evaluation of the implications of recharge temperatures derived from dissolved-gas compositions may be hindered by large uncertainties in the model calculations.

We define local- and intermediate-scale flow systems in Snake Valley based on potentiometric-surface contours (Gardner and others, 2011), variations in major-ion chemistry and radiogenic-isotope composition, and model recharge temperatures. Local flow systems include recharge areas in the parts of the Deep Creek Mountains and Snake Range having the highest precipitation and recharge rates, and discharge areas consisting of springs, ET from phreatophytes, and, in some cases, agricultural pumping and surface water. Qualitative groundwater age in local flow systems is predominantly modern to premodern. Intermediate flow systems likely originate in the same recharge areas as local flow systems, but flow paths are deeper, more complicated, and longer in time and distance. Discharge from springs in Snake Valley including Miller, Leland Harris, and Twin Springs and Gandy Salt Marsh, comes from intermediate flow systems.

Gandy Warm Springs and Big Springs are situated in local flow systems, but discharge a mixture of young groundwater derived from local flow systems and old groundwater derived from intermediate or interbasin flow systems. These springs are fault controlled, and the older groundwater accessed by the faults evidently mixes with younger groundwater during ascent to the spring. A similar process may occur near Twin Springs. In contrast, Dearden Springs discharges old groundwater within the geographic extent of the Lake Creek local flow system, so mixing of older/deeper and younger/shallower groundwater evidently does not necessarily occur at every major spring.

8.6 CHAPTER 8 REFERENCES

Acheampong, S.Y., Farnham, I.M., and Watrus, J.M., 2009, Geochemical characterization of ground water and surface water of Snake Valley and the surrounding areas in Utah, *in* Tripp, B.T., Krahulec, K., and Jordan, J.L., editors, Geology and geologic resources and issues of western Utah: Utah Geological Association Publication 38, p. 325–344.

Belcher, W.R., Bedinger, M.S., Back, J.T., and Sweetkind, D.S., 2009, Interbasin flow in the Great Basin with special reference to the southern Funeral Mountains and the source of Furnace Creek springs, Death Valley, California, U.S.: Journal of Hydrology, v. 369, p. 30–43.

Burns, A.G., and Drici, W., 2011, Hydrology and water resources of Spring, Cave, Dry Lake, and Delamar Valleys, Nevada and vicinity: Southern Nevada Water Authority: Online, http://water.nv.gov/hearings/past/springetal/documents.cfm?DIR=Exhibits.SNWA%20Exhibits.SNWA_Exh_258_Burns%20and%20Drici%20Report, variously paginated, accessed October 2011.

Carlton, S.M., 1985, Fish Springs multibasin flow system, Nevada and Utah: Reno, University of Nevada, M.S. thesis, 103 p.

Dixon, G.L., Rowley, P.D., Burns, A.G., Watrus, J.M, and Ekren, E.B., 2007, Geology of White Pine and Lincoln Counties and adjacent areas, Nevada and Utah—the geologic framework of regional groundwater flow systems: Las Vegas, Southern Nevada Water Authority, HAM-ED-001, variously paginated. Available *in* Southern Nevada Water Authority, 2008a, Baseline characterization report for Clark, Lincoln, and White Pine Counties Groundwater Development Project, *in* U.S. Bureau of Land Management, 2012, Clark, Lincoln, and White Pine Counties Groundwater Development Project Final Environmental Impact Statement: FES 12-33, Document BLM/NV/NV/ES/11-17+1793.

Durbin, T., and Loy, K., 2010, Development of a groundwater model, Snake Valley region, eastern Nevada and western Utah: U.S. Department of the Interior: Online, http://www.blm.gov/ut/st/en/prog/more/doi_groundwater_modeling.html, accessed July 2, 2010.

Eakin, T.E., 1966, A regional interbasin ground-water system in the White River area, southeastern Nevada: Water Resources Research, v. 2, p. 251–271.

Flint, A.L., Flint, L.E., and Masbruch, M.D., 2011,

Appendix 3: Input, calibration, uncertainty, and limitations of the Basin Characterization Model, *in* Heilweil, V.M., and Brooks, L.E., editors, 2011, Conceptual model of the Great Basin carbonate and alluvial aquifer system: U.S. Geological Survey Scientific Investigations Report 2010-5193, p. 149–163.

Freeze, A.R., and Witherspoon, P.A., 1966, Theoretical analysis of regional ground-water flow: 1. Analytical and numerical solutions to the mathematical model: Water Resources Research, v. 2, p. 641–656.

Freeze, A.R., and Witherspoon, P.A., 1967, Theoretical analysis of regional groundwater flow: 2. Effect of water-table configurations and subsurface permeability variation: Water Resources Research, v. 3, p. 623–634.

Gardner, P.M., Heilweil, V.M., 2014, A multiple-tracer approach to understanding regional groundwater flow in the Snake Valley area of the eastern Great Basin, USA.: Applied Geochemistry, v. 45, p. 33–49.

Gardner, P.M., Masbruch, M.D., Plume, R.W., and Buto, S.G., 2011, Regional potentiometric surface map of the Great Basin carbonate and alluvial aquifer system in Snake Valley and surrounding areas, Juab, Millard, and Beaver Counties, Utah, and White Pine and Lincoln Counties, Nevada: U.S. Geological Survey Scientific Investigations Map 3193.

Gates, J.S., and Kruer, S.A., 1981, Hydrologic reconnaissance of the southern Great Salt Lake Desert and summary of the hydrology of west-central Utah: Utah Department of Natural Resources Technical Publication 71, 55 p.

Gillespie, J., Nelson, S.T., Mayo, A.L., and Tingey, D.G., 2012, Why conceptual groundwater flow models matter—a trans-boundary example from the arid Great Basin, western USA: Hydrogeology Journal (doi: 10.1007/s10040-012-0848-0).

Greene, D.C., and Herring, D.M., 2013, Structural architecture of the Confusion Range, west-central Utah—a Sevier fold thrust belt and frontier petroleum province: Utah Geological Survey Open-File Report 613, 22 p., 6 plates.

Harrill, J.R., Gates, J.S., and Thomas, J.M., 1988, Major ground-water flow systems in the Great Basin region of Nevada, Utah, and adjacent states: U.S. Geological Survey Hydrologic Investigations Atlas HA-694-C, scale 1:1,000,000, 2 sheets.

Heilweil, V.M., and Brooks, L.E., editors, 2011, Conceptual model of the Great Basin carbonate and alluvial aquifer system: U.S. Geological Survey Scientific Investigations Report 2010-5193.

Hershey, R.L., Heilweil, V.M., Gardner, P., Lyles, B.F., Earman, S., Thomas, J.M., and Lundmark, K.W., 2007, Ground-water chemistry interpretations supporting the Basin and Range regional carbonate-rock aquifer system (BARCAS) study, eastern Nevada and western Utah: University of Nevada Desert Research Institute Publication 41230, 86 p.

Kistinger, G.M., Prieur, J.P., Rowley, P.D., and Dixon, G.L., 2009, Characterization of streams and springs in the Snake Valley area, Utah and Nevada, *in* Tripp, B.T., Krahulec, K., and Jordan, J.L., editors, Geology and geologic resources and issues of western Utah: Utah Geological Association Publication 38, p. 300–323.

Laczniak, R.J., Flint, A.L., Moreao, M.T., Knochenmus, L.A., Lundmark, K.W., Pohll, G., Carroll, R.W.H., Smith, J.L., Welborn, T.L., Heilweil, V.M., Pavelko, M.T., Hershey, R.L., Thomas, J.M., and Lyles, B.F., 2007, Ground-water budgets, *in* Welch, A.H., Bright, D.J., and Knochenmus, L.A., 2007, Water resources of the Basin and Range carbonate-rock aquifer system, White Pine County, Nevada, and adjacent areas in Nevada and Utah: U.S. Geological Survey Scientific Investigations Report 2007-5261, p. 43–82.

Masbruch, M.D., Heilweil, V.M., Buto, S.G., Brooks, L.E., Susong, D.D., Flint, A.L., Flint, L.E., and Gardner, P.M., 2011, Chapter D: Estimated groundwater budgets, *in* Heilweil, V.M., and Brooks, L.E., editors, 2011, Conceptual model of the Great Basin carbonate and alluvial aquifer system: U.S. Geological Survey Scientific Investigations Report 2010-5193, p. 73–125.

Plume, R.W., 1996, Hydrogeologic framework of aquifer systems in the Great Basin region of Nevada, Utah, and adjacent states: U.S. Geological Survey Professional Paper 1409-B, 64 p.

Prudic, D.E., Harrill, J.R., and Burbey, T.J., 1995, Conceptual evaluation of regional ground-water flow in the carbonate-rock province of the Great Basin, Nevada, Utah, and adjacent states: U.S. Geological Survey Professional Paper 1409-D, 102 p.

Prudic, D.E., and Sweetkind, D.S., editors, in review, Evaluating connection of aquifers to springs and streams, eastern part of Great Basin National Park and vicinity, Nevada: U.S. Geological Survey Professional Paper.

Rowley, P.D., and Dixon, G.L., 2011, Geology and geophysics of Spring, Cave, Dry Lake, and Delamar Valleys, White Pine and Lincoln Counties and adjacent areas, Nevada and Utah: The geologic framework of regional groundwater flow systems: Online: http://water.nv.gov/hearings/past/springetal/

browseabledocs/Exhibits%5CSNWA%20Exhibits/SNWA_Exh_058_Rowley%20et%20al%20Report.pdf, accessed 7/26/2011, variously paginated, accessed October 2011.

Rowley, P.D., Dixon, G.L., Burns, A.G., and Collins, C.A., 2009, Geology and hydrogeology of the Snake Valley area, western Utah and eastern Nevada, *in* Tripp, B.T., Krahulec, K., and Jordan, J.L., editors, Geology and geologic resources and issues of western Utah: Utah Geological Association Publication 38, p. 251–269.

Southern Nevada Water Authority, 2009, Conceptual model of groundwater flow for the central carbonate-rock province—Clark, Lincoln, and White Pine Counties Groundwater Development Project, in U.S. Bureau of Land Management, 2012, Clark, Lincoln, and White Pine Counties Groundwater Development Project Final Environmental Impact Statement: FES 12-33, Document BLM/NV/NV/ES/11-17+1793.

Sweetkind, D.S., Knochenmus, L.A., Ponce, D.A., Wallace, A.R., Scheirer, D.S., Watt, J.T., and Plume, R.W., 2007, Hydrogeologic framework, *in* Welch, A.H., Bright, D.J., and Knochenmus, L.A., 2007, Water resources of the Basin and Range carbonate-rock aquifer system, White Pine County, Nevada, and adjacent areas in Nevada and Utah: U.S. Geological Survey Scientific Investigations Report 2007-5261, p. 11–42.

Sweetkind, D.S., Masbruch, M.D., Heilweil, V.M., and Buto, S.G., 2011, Groundwater flow, *in* Heilweil, V.M., and Brooks, L.E., editors, 2011, Conceptual model of the Great Basin carbonate and alluvial aquifer system: U.S. Geological Survey Scientific Investigations Report 2010-5193, 22 p.

Thomas, J.M., Welch, A.H., and Dettinger, M.D., 1996, Geochemistry and isotope hydrology of representative aquifers in the Great Basin region of Nevada, Utah, and adjacent states: U.S. Geological Survey Professional Paper 1409-C, 100 p.

Thomas, J.M., and Mihevc, T.M., 2011, Evaluation of groundwater origins, flow paths, and ages in east-central and southeastern Nevada: Desert Research Institute Publication 41253, 61 p.

Toth, J., 1962, A theory of groundwater motion in small drainage basins in central Alberta, Canada: Journal of Geophysical Research, v. 67, p. 4795–4812.

Toth, J., 1963, A theoretical analysis of groundwater flow in small drainage basins: Journal of Geophysical Research, v. 68, p. 4795–4812.

U.S. Fish and Wildlife Service, 2004, Comprehensive conservation plan—Fish Springs National Wildlife Refuge: Online, http://www.fws.gov/mountain-prairie/planning/ccp/ut/fhs/fhs.html, accessed December, 2012.

Wilson, J.L., and Guan, H., 2004, Mountain-block hydrology and mountain-front recharge, *in* Phillips, F.M., Hogan, J., and Scanlon, B., editors, Groundwater recharge in a desert environment—the southwestern United States: Washington, D.C., American Geophysical Union, p. 113–137.

CHAPTER 9

POTENTIAL IMPACTS OF FUTURE GROUNDWATER DEVELOPMENT—REVIEW AND INTERPRETATION OF RECENT PUBLICATIONS

by Hugh Hurlow

View southwest of Lake Creek and associated wetlands and wet meadows, about 0.5 miles (1 km) south of Pruess Lake. Southern end of southern Snake Range in background on right side of view.

Bibliographic citation for this chapter:
Hurlow, H., 2014, Potential impacts of future groundwater development—review and interpretation of recent publications, Chapter 9 *in* Hurlow, H., editor, Hydrogeologic studies and groundwater monitoring in Snake Valley and adjacent hydrographic areas, west-central Utah and east-central Nevada: Utah Geological Survey Bulletin 135, p. 257–264.

CHAPTER 9 CONTENTS

FIGURE

CHAPTER 9: POTENTIAL IMPACTS OF FUTURE GROUNDWATER DEVELOPMENT—REVIEW AND INTERPRETATION OF RECENT PUBLICATIONS

by Hugh Hurlow

9.1 INTRODUCTION

Expected future population growth in the Great Basin and the existence of pending applications to develop groundwater (figure 1.2) suggest that demand for groundwater in west-central Utah and east-central Nevada will continue. Monitoring baseline groundwater conditions is, therefore, relevant to future water-management issues. This chapter discusses possible impacts of future groundwater development to the water budget and ecosystems in Snake Valley.

9.2 FUTURE GROUNDWATER DEVELOPMENT IN SNAKE VALLEY

The draft *Agreement for Management of the Snake Valley Groundwater System* (hereafter referred to as the interstate agreement) (Utah Division of Water Rights, 2010), although unsigned at the time of this writing, provides a model for potential amounts of future groundwater development. The draft agreement allows for new development of 35,000 acre-feet per year (43 hm^3/yr) in Nevada and 6000 acre-feet per year (7 hm^3/yr) in Utah. Currently allocated water rights are 12,000 acre-feet per year (15 hm^3/yr) in Nevada, and 55,000 acre-feet per year (68 hm^3/yr) in Utah including 20,000 acre-feet per year (25 hm^3/yr) reserved for the U.S. Fish and Wildlife Service's water rights for Fish Springs National Wildlife Refuge (Utah Division of Water Rights, 2010). Total pumping in the Snake Valley hydrographic area would be 47,000 acre-feet per year (58 hm^3/yr) in Nevada and 41,000 acre-feet per year (51 hm^3/yr) in Utah, if the maximum allowed development were to occur. Most current use is for irrigation in south-central Snake Valley near Garrison and Eskdale, Utah, and Baker, Nevada, and in southern Snake Valley in Nevada and Utah (figure 9.1; plate 4).

Based on the distribution of recent applications (figure 1.2), most of the new groundwater development would likely occur in central and southern Snake Valley. All of the newly appropriated groundwater exported to other hydrographic areas would represent increased discharge from the Snake Valley groundwater system, whereas about 95% of groundwater pumped for crop irrigation, including previously and newly appropriated amounts, represents discharge by evapotranspiration (in other words, about 5% of the amount pumped for irrigation recharges the aquifer via return flow; Welch and others, 2007, p. 68). Under these assumptions, groundwater development at the upper limit allowed by the interstate agreement would increase discharge from the Snake Valley hydrographic area by approximately 41,000 acre-feet per year (50.6 hm^3/yr).

Sweetkind and others (2007) subdivided Snake Valley and Hamlin Valley into five hydrogeologic sub-basins, and Laczniac and others (2007) estimated recharge and discharge for each sub-basin. The majority of current and likely future groundwater development occurs in Snake Valley sub-basins 3 and 4 (figure 9.1). Recharge in sub-basins 3 and 4 is about 61,000 acre-feet per year (75 hm^3/yr), and discharge by evapotranspiration is about 60,000 acre-feet per year (74 hm^3/yr) (Welch and others, 2007, appendix A). Most of the pumping is from wells that are less than 500 feet (150 m) deep, based on well-log data available from the Utah Division of Water Rights (http://www.waterrights.utah.gov/) and the Nevada Division of Water Resources (http://water.nv.gov/). Additional groundwater pumping would remove additional groundwater from storage and capture groundwater that currently flows to discharge areas and supports phreatophyte growth and spring flow.

Recharge to Snake Valley sub-basin 4 may also occur by interbasin flow from Spring Valley and by flow from Snake Valley sub-basin 5 (central and southern Hamlin Valley). Estimates of interbasin flow from Spring Valley range from about 300 to 33,000 acre-feet per year (0.4–47 hm^3/yr) (table 4.6), and Snake Valley sub-basin 5 has excess recharge of about 9000 acre-feet per year (11 hm^3/yr) (Welch and others, 2007, appendix A), much of which presumably flows north to sub-basin 4. The declining groundwater levels suggest that the flow from southern Spring Valley and Snake Valley sub-basin 5 is relatively small or that this flow is not tapped by the irrigation wells. Capture of this flow by additional groundwater development by deep

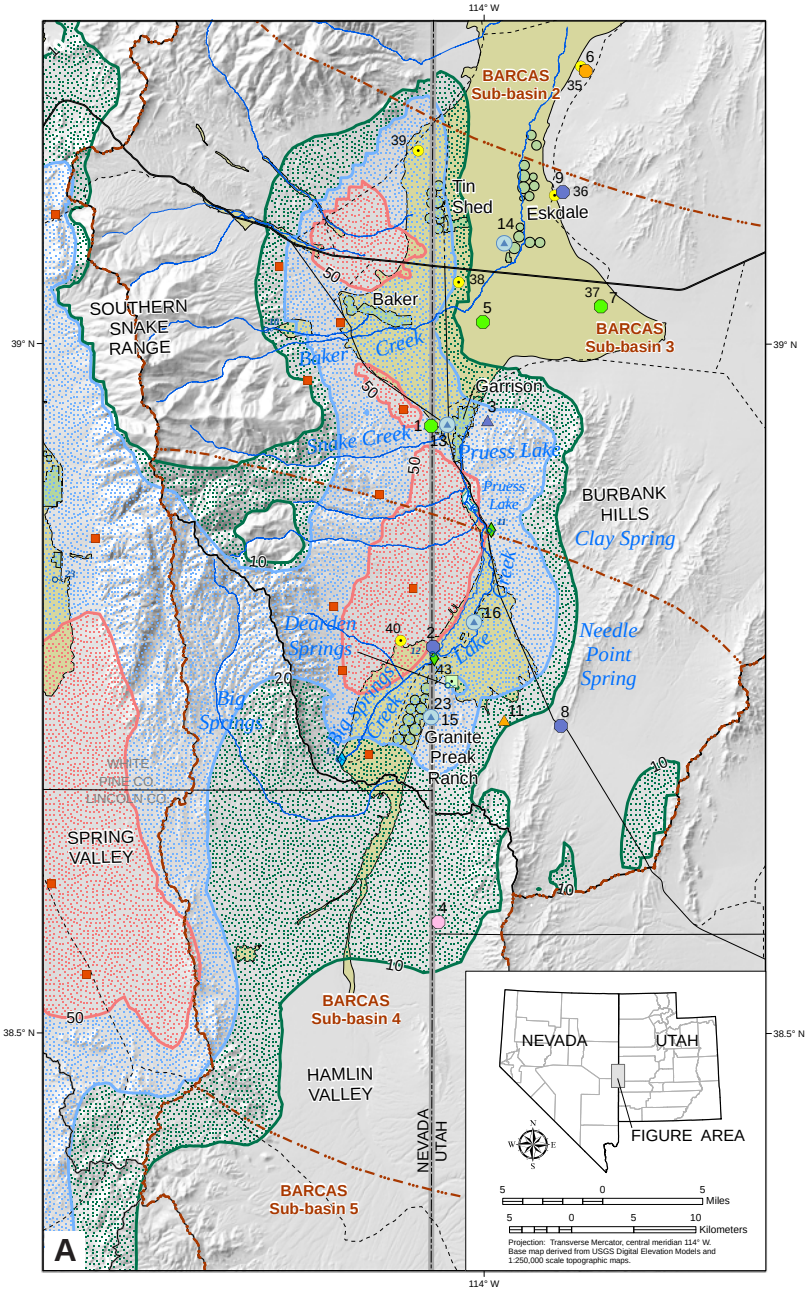

EXPLANATION

Modeled drawdown (ft) (SNWA, 2010b; U.S. BLM, 2012)

- 50 - 100
- 20 - 50
- 10 - 20
- 50 ft contour
- 20 ft contour
- 10 ft contour
- BARCAS Snake Valley sub-basin boundary (Welch and others, 2007).
- Discharge area (Laczniac and others, 2007)
- Irrigated area

UGS Groundwater-Monitoring Network

Numeric label is UGS site number

New Wells and Gages (2007–2009) (Table C.1)

- Monitor wells in basin-fill aquifer
- Monitor wells in volcanic-rock aquifer
- Monitor wells in basin-fill and carbonate-rock aquifer
- Monitor wells in carbonate-rock aquifer
- Monitor wells in Cambrian-Neoproterozoic siliciclastic-rock aquifer

Aquifer-Test Sites

- Carbonate-rock and basin-fill aquifers
- Carbonate-rock aquifer
- Agricultural-area monitoring wells
- Nested piezometers near spring

Other Groundwater Monitoring Sites

- UGS transducer in previously existing well (table C.2)
- UGS spring-flow gage site (table C.4)

Other Features

- USGS spring-flow gage site
- Spring (table 4.2)
- Perennial stream
- SNWA proposed point of diversion

Hydrographic-area boundary

- Snake Valley
- Other hydrographic areas

Figure 9.1. *Hydrologic setting of central and southern Snake Valley and northern Hamlin Valley, including Snake Valley sub-basin boundaries from Sweetkind and others (2007), and simulated drawdown of groundwater levels under the Alternative A development scenario, from SNWA's numerical groundwater-flow model (SNWA, 2010; U.S. Bureau of Land Management, 2012a). Alternative A provides for distributed pumping at rates consistent with the presently unsigned interstate agreement (Utah Division of Water Rights, 2010). Wells would be distributed within the groundwater-development areas shown on the figure, and would collectively withdraw about 36,000 acre-feet per year (44 hm3/yr) from Snake Valley aquifers to convey to the Las Vegas area via pipeline.* ***A.*** *Modeled drawdown after 75 years of pumping.*

wells may facilitate groundwater development, but may draw down groundwater levels in the agricultural areas where the deeper and shallower aquifers are connected, and would eventually reduce subsurface flow to northern Snake Valley and Tule Valley by reducing the hydraulic gradient between the two areas.

9.3 PREDICTIVE SIMULATIONS

Three recent numerical groundwater-flow models use estimates of the future development outlined in the interstate agreement to evaluate potential groundwater-level declines in Snake Valley (SNWA, 2010b; Loy and Durbin, 2010; Halford and Plume, 2011). The models cover different

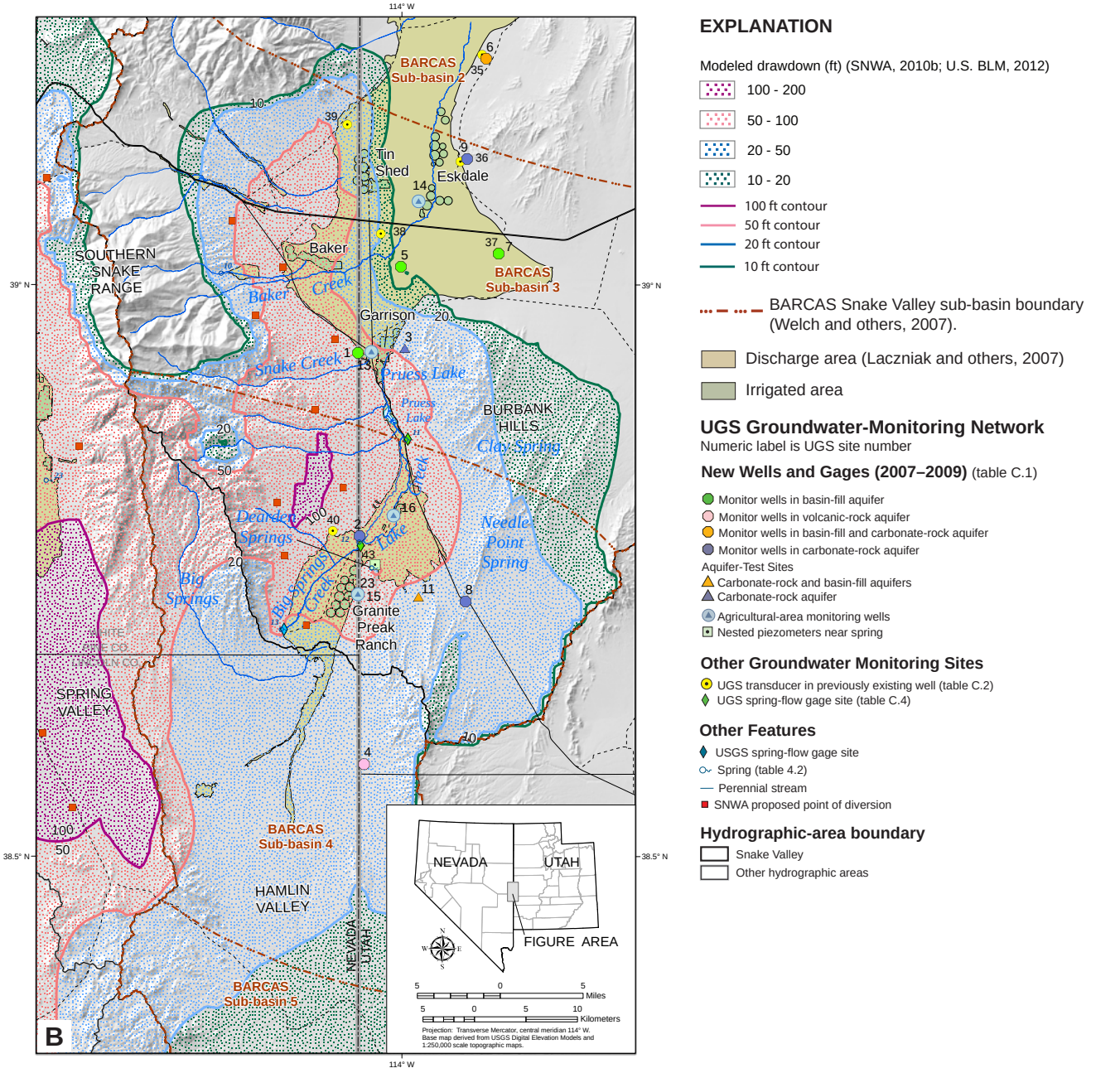

Figure 9.1. *continued.* ***B.*** *Modeled drawdown after 200 years of pumping.*

areas, and use different hydrogeologic frameworks, methods for estimating water budgets, and assumptions for calibrating steady-state conditions, and slightly different future pumping scenarios for the proposed SNWA groundwater development in Snake Valley. Despite these differences, their results are broadly similar and, in combination, provide a first approximation of changes in groundwater levels from the maximum development allowed in the interstate agreement.

Predictive simulations of groundwater pumping in Snake Valley at current rates plus additional development in central and southern Snake Valley, as outlined in the draft interstate agreement, indicate the following declines in groundwater levels (SNWA, 2010b, Alternative A, plate 2; Loy and Durbin, 2010, figures D-11 and D-13; Halford and Plume, 2011, figures 24 and 25; U.S. Bureau of Land Management 2012a, Alternative A, figures 3.3.2-13 and 3.3.2-14). After 75 years of pumping, groundwater levels within most of the proposed groundwater-development area would decline by 20 to 100 feet (6.1–30 m) (figure 9.1A). Groundwater levels would decline by 50 to 200 feet (15–61 m) from present-day depths after 200 years (figure 9.1B). Groundwater-level declines in the rest of

sub-basins 3 and 4 would decrease approximately radially away from the groundwater-development area. Within about 10 to 12 miles (16–19 km) of the wells, predicted drawdown is more than 10 feet (3 m) after 75 years of pumping (figure 9.1A) and more than 20 feet (6.1 m) after 200 years of pumping (figure 9.1B). Discharge from Big Springs and Dearden Springs would decline by about 50 to 100% after 200 years (Halford and Plume, 2011, figure 27; U.S. Bureau of Land Management, 2012a, table 3.3.2-11). Flow from Clay Spring, southeast of Pruess Lake, would presumably decline by a similar amount. The amount and distribution of these predicted declines should be regarded as general estimates, not specific predictions, as discussed thoroughly by the authors (SNWA, 2010, chapters 5 and 6; Durbin and Loy, 2010, sections 4.4 and 5.2.4; Halford and Plume, 2011, p. 24–32; U.S. Bureau of Land Management 2012a, section 3.3.2.8). At the time of this writing, the Governor of Utah has declined to sign the draft agreement in its present form, but the above evaluation allows us to examine possible impacts proposed in the agreement.

The U.S. Bureau of Land Management's Clark, Lincoln, and White Pine Counties Groundwater Development Project Final Environmental Impact Statement (FEIS) evaluates potential impacts of SNWA's proposed groundwater-development plan to hydrologic, vegetation, biologic, and water-rights resources in areas predicted to experience 10 or more feet (3 m) of drawdown up to 200 years after full implementation of the project (U.S. Bureau of Land Management 2012a). Impacts to spring flow and related spring-fed wetland ecosystems may occur in areas having less than 10 feet (3 m) of drawdown (Cooper and others, 2006; Patten and others, 2007). Springs and spring complexes in Snake Valley that support wetland ecosystems and agriculture and are outside of the simulated 10-foot (3 m) drawdown contour, but which could be adversely affected, include Gandy Warm Springs, Twin Springs and Foote Reservoir Spring, Kell Spring, Salt Marsh Lake spring complex, Leland Harris spring complex, and Miller Spring. Coyote Spring and Tule Spring in Tule Valley, and the Fish Springs complex in Fish Springs Flat could also experience slightly reduced flow, due to a decrease in regional hydraulic gradient from the lowering of groundwater levels in the groundwater-development area.

SNWA's predictive simulation for alternative A (SNWA, 2010; U.S. Bureau of Land Management, 2012a) indicates that flow from Foote Reservoir Spring and Kell Spring would decline by about 1%, whereas Gandy Warm Spring would be unaffected. Interbasin flow from Snake Valley to Tule Valley would be reduced by about 2% after 75 years and by about 6% after 200 years. This reduction in interbasin flow would presumably cause a slight decline in flow from Coyote Spring and Tule Spring, due to the hydraulic connection between Snake Valley and Tule Valley. Halford and Plume (2011) indicate that spring flow from Twin Springs and the Fish Springs complex would decline by less than 1%. These estimates depend on the hydraulic properties of the faults and hydrogeologic units along the flow paths to the springs, which are uncertain. Impacts to some of these springs could be greater if they are hydraulically connected to the proposed groundwater development area by north-south striking fault zones, or less if the transmissivity of the aquifers between the springs and the proposed groundwater development area is lower than the values specified in the models.

9.4 POTENTIAL IMPACTS OF GROUNDWATER DEVELOPMENT ON ECOSYSTEMS

Environmentally sensitive species in Snake Valley, Tule Valley, and Fish Springs Flat depend on spring-fed wetland habitats for survival (U.S. Fish and Wildlife Service, 2004; Bailey and others, 2005, 2006; Utah Division of Wildlife Resources, 2011). Least chub, Columbia spotted frog, and several species of spring snail are aquatic conservation species that use vegetation in standing water for breeding and protection from sunlight and predators (Bailey and others, 2005, 2006; Utah Division of Wildlife Resources, 2011). Many other environmentally sensitive species depend on the water and habitat in the wetlands and adjacent wet meadows and grasses (Utah Division of Wildlife Resources, 2011). Spring-fed wetlands and wet meadows occur along the margins of spring pools, along their outflow channels, and in nearby areas of shallow groundwater. The decreased flow predicted for Big Springs and Clay Spring would likely reduce the habitat available for sensitive species that live in their pools and outflow areas (Patten and others, 2007). Surface flow along Lake Creek would also decline, decreasing habitat available for sensitive species and migratory birds that use the wetlands and wet-meadow plant communities upstream from Pruess Lake. Substantial capture of discharge would also reduce available wet-meadow habitat. Such changes would reduce the quality of grazing land along the Lake Creek streambed.

SNWA's groundwater-flow model suggests that groundwater development in Snake Valley at the maximum amount allowed in the interstate agreement (Alternative A in U.S. Bureau of Land Management, 2012a, chapters 3.3 and 3.7) would likely substantially reduce flow from several springs in southern Snake Valley that provide essential habitat for sensitive species. Declining spring discharge and reduction of wetland habitat in Snake Valley and adjacent valleys may lead to listing of some aquatic species and, perhaps,

other avian and terrestrial species as threatened by the U.S. Fish and Wildlife Service. Listing of species results in mandatory compliance of current and future water-development facilities and plans with the Endangered Species Act, and transfers jurisdiction of species management from the State of Utah to the U.S. Fish and Wildlife Service (Utah Division of Wildlife Resources, 2011). Because several of the environmentally sensitive species present in Snake Valley are also present along the Wasatch Front, the mandatory compliance with the Endangered Species Act and change of jurisdiction would also apply to the heavily populated Wasatch Front area.

The reduced spring flow and drawdown of groundwater levels predicted by the groundwater-flow models (SNWA, 2010; Loy and Durbin, 2010; Halford and Plume, 2011) would substantially impact the Big Springs–Dearden Springs–Lake Creek–Pruess Lake hydrologic-ecologic system, which includes springs, surface flow, and shallow groundwater, provides habitat for environmentally sensitive species, and supports extensive grazing. Declines in groundwater levels of 10 feet (3 m) or more would induce succession of plant communities from groundwater-dependent to precipitation-dependent associations (McClendon, 2011). Aquatic, wetland, wet-meadow, and dry-meadow plant communities would be replaced by shrubland communities, either phreatophytic or non-phreatophytic, over several tens of years, depending on the rate of groundwater-level decline and precipitation rates during the transition (McClendon, 2011).

The effects of small declines in flow at Twin Springs, Salt Marsh Lake spring complex, Leland Harris spring complex, and Miller Spring on aquatic, wetland, and wet-meadow plant communities and sensitive-species habitats are difficult to predict. Changes in habitat due to decreased spring flow depend on the detailed topography of the outflow area, local stratigraphy, precipitation, magnitude of spring flow, spring-pool morphology, and the relative proportion of upwelling deep groundwater to side-inflow of shallow groundwater (Loheide and others, 2008). At several key spring-fed wetland ecosystems in Snake Valley, Three Parameters Plus (2010) performed baseline physical habitat surveys and vegetation delineations, and shallow-groundwater monitoring is ongoing (Hooker and others, 2011; data are available from the Utah Geological Survey Groundwater Monitoring Data Portal at http://geology.utah.gov/databases/groundwater/projects.php). These data form a framework for potential future modeling studies that may assess the potential effects of small decreases in spring flow on sensitive species habitat.

9.5 CHAPTER 9 REFERENCES

Bailey, C.L., Wilson, K.W., and Anderson, M.E., 2005, Conservation agreement and strategy for least chub *(Iotichthys phlegthontis)* in the state of Utah: Utah Division of Wildlife Resources Publication 05-24, 37 p.

Bailey, C.L., Wilson, K.W., and Anderson, M.E., 2006, Conservation agreement and strategy for Columbia spotted frog *(Rana lutieventris)* in the state of Utah: Utah Division of Wildlife Resources Publication 06-01, 42 p.

Cooper, D.J., Sanderson, J.S., Stannard, D.I., and Groenveld, D.P., 2006, Effects of long-term water table drawdown on evapotranspiration and vegetation in an arid region phreatophyte community: Journal of Hydrology, v. 325, p. 21–34.

Durbin, T., and Loy, K., 2010, Development of a groundwater model, Snake Valley region, eastern Nevada and western Utah: U.S. Department of the Interior: Online, http://www.blm.gov/ut/st/en/prog/more/doi_groundwater_modeling.html, accessed July 2, 2010.

Halford, K.J., and Plume, R.W., 2011, Potential effects of groundwater pumping on water levels, phreatophytes, and spring discharges in Spring and Snake Valleys, White Pine County, Nevada, and adjacent areas in Nevada and Utah: U.S. Geological Survey Scientific Investigations Report 2011-5032, 52 p.

Hooker, T.H., Jordan, J.L., and Emerson, R., 2011, Intensive monitoring of spring discharge and wetland hydrology to understand aquifer dynamics and the consequences for excessive ground-water withdrawal: Geological Society of America Abstracts With Programs, v. 43, no. 4, p. 60.

Laczniak, R.J., Flint, A.L., Moreao, M.T., Knochenmus, L.A., Lundmark, K.W., Pohll, G., Carroll, R.W.H., Smith, J.L., Welborn, T.L., Heilweil, V.M., Pavelko, M.T., Hershey, R.L., Thomas, J.M., and Lyles, B.F., 2007, Ground-water budgets, in Welch, A.H., Bright, D.J., and Knochenmus, L.A., 2007, Water resources of the Basin and Range carbonate-rock aquifer system, White Pine County, Nevada, and adjacent areas in Nevada and Utah: U.S. Geological Survey Scientific Investigations Report 2007-5261, p. 43–82.

Loheide, S.P., Deitchman, R.S., Cooper, D.J., Wolf, E.C., Hammarsmark, C.T., and Lundquist, J.D., 2008, A framework for understanding the hydroecology of impacted wet meadows in the Sierra Nevada and Cascade Ranges, California, USA: Hydrogeology Journal (doi: 10.1007/s10040-008-0380-4).

Loy, K., and Durbin, T., 2010, Simulation results report eastern Nevada—western Utah regional groundwater flow model: U.S. Department of the Interior: Online, http://www.blm.gov/ut/st/en/prog/more/doi_groundwater_modeling.html, accessed July 2, 2010.

McClendon, T., 2011, Potential effects of change in depth to water on vegetation in Spring Valley, Nevada: Southern Nevada Water Authority, variously paginated.

Patten, D.T., Rouse, L., and Stromberg, J.C., 2007, Isolated spring wetlands in the Great Basin and Mojave Deserts, USA—potential response of vegetation to groundwater withdrawal: Environmental Management (doi: 10.1007/s00267-007-9035-9).

Southern Nevada Water Authority, 2010, Simulation of groundwater development scenarios using the transient numerical model of groundwater flow for the central carbonate-rock province—Clark, Lincoln, and White Pine Counties Groundwater Development Project, *in* U.S. Bureau of Land Management, 2012, Clark, Lincoln, and White Pine Counties Groundwater Development Project Final Environmental Impact Statement: FES 12-33, Document BLM/NV/NV/ES/11-17+1793.

Southern Nevada Water Authority, 2012, Southern Nevada Water Authority Clark, Lincoln, and White Pine Counties Groundwater Development Project Conceptual Plan of Development November 2012: Online, http://www.snwa.com/assets/pdf/ws_gdp_copd.pdf, accessed March 19, 2014.

Sweetkind, D.S., Knochenmus, L.A., Ponce, D.A., Wallace, A.R., Scheirer, D.S., Watt, J.T., and Plume, R.W., 2007, Hydrogeologic framework, *in* Welch, A.H., Bright, D.J., and Knochenmus, L.A., 2007, Water resources of the Basin and Range carbonate-rock aquifer system, White Pine County, Nevada, and adjacent areas in Nevada and Utah: U.S. Geological Survey Scientific Investigations Report 2007-5261, p. 11–42.

Three Parameters Plus, 2010, Baseline physical habitat conditions of wetlands in Snake Valley, Utah—final report: Unpublished contract report prepared for the Utah Department of Natural Resources, Endangered Species Program, 2 volumes.

U.S. Bureau of Land Management, 2012a, Clark, Lincoln, and White Pine Counties Groundwater Development Project Final Environmental Impact Statement: FES 12-33, Document BLM/NV/NV/ES/11-17+1793.

U.S. Bureau of Land Management, 2012b, Clark, Lincoln, and White Pine Counties Groundwater Development Project Record of Decision: Document BLM/NV/NV/ES/11-17+1793.

U.S. Fish and Wildlife Service, 2004, Comprehensive conservation plan—Fish Springs National Wildlife Refuge: Online, http://www.fws.gov/mountain-prairie/planning/ccp/ut/fhs/fhs.html, accessed December 2012.

Utah Division of Water Rights, 2010, Snake Valley Agreement: Online, http://waterrights.utah.gov/snakeValleyAgreement/default.asp, accessed March 23, 2010.

Utah Division of Wildlife Resources, 2011, Utah Sensitive Species List: Online, http://dwrcdc.nr.utah.gov/ucdc/ViewReports/SSLAppendices20110329.pdf, accessed January 4, 2012.

Welch, A.H., Bright, D.J., and Knochenmus, L.A., 2007, Water resources of the Basin and Range carbonate-rock aquifer system, White Pine County, Nevada, and adjacent areas in Nevada and Utah: U.S. Geological Survey Scientific Investigations Report 2007-5261, 96 p.

CHAPTER 10 | SUMMARY

by Hugh Hurlow

View northwest of Lake Creek, several springs of the Dearden Springs complex to the right of the creek; and, in the background, the southern Snake Range including Wheeler Peak in Great Basin National Park. The Dearden Springs are west of the Nevada-Utah state line in southern Snake Valley, and provide significant flow to Lake Creek, the longest reach of perennial surface flow in Snake Valley. Lake Creek originates about seven miles upstream at Big Springs in Nevada.

Bibliographic citation for this chapter:
Hurlow, H., 2014, Summary, Chapter 10 *in* Hurlow, H., editor, Hydrogeologic studies and groundwater monitoring in Snake Valley and adjacent hydrographic areas, west-central Utah and east-central Nevada: Utah Geological Survey Bulletin 135, p. 265–269.

CHAPTER 10 CONTENTS

CHAPTER 10: SUMMARY

by Hugh Hurlow

This report presents results and analyses of hydrogeologic, geophysical, groundwater-monitoring, and hydrochemical studies by the Utah Geological Survey (UGS) in Snake Valley, Tule Valley, and Fish Springs Flat, Millard and Juab Counties, west-central Utah. The primary objectives of this work were (1) establish a groundwater-monitoring network to improve data on baseline groundwater-level, spring-flow, and hydrochemical conditions, (2) measure the impacts of current and proposed future groundwater pumping on these baseline conditions, (3) improve understanding of geologic controls on groundwater flow in the study area, and (4) integrate the results to test previously proposed conceptual models of groundwater flow.

Our study area is in the eastern Basin and Range Province, characterized by elongate, north-south trending mountain ranges and valleys having abrupt boundaries (mountain fronts). The valleys overlie fault-bounded sedimentary basins that formed in the hanging walls of normal-fault zones during Miocene to Quaternary time. Basin-fill deposits are alluvial and lacustrine sediments, and Eocene to Oligocene volcanic and volcaniclastic deposits at greater depths. The ranges are composed of Paleozoic carbonate rocks, Tertiary volcanic rocks, Neoproterozoic to early Paleozoic siliciclastic rocks, and Mesozoic and Cenozoic granitic intrusive rocks, in order of decreasing abundance. These rocks were variably faulted and folded during late Mesozoic to early Cenozoic crustal shortening and late Cenozoic extension.

New UGS gravity data, combined with previously existing data, were processed and modeled to reveal the subsurface structure of the basin-fill aquifer below Snake Valley and adjacent valleys to the east. The sedimentary basin below Snake Valley and northern Hamlin Valley is composed of five sub-basins separated by transverse subsurface bedrock ridges. Sedimentary deposits in these sub-basins are up to about 10,000 feet (3050 m) thick. The Tule Valley, Pine Valley, Wah Wah Valley, Fish Springs Flat, and western Sevier Desert sedimentary basins also contain sub-basins separated by subsurface bedrock ridges, and are up to about 5000 feet (1500 m) thick. The basin below southern Hamlin Valley is part of the Indian Peak Caldera complex, and is composed of up to 17,500 feet (5300 m) of volcanic deposits and related intrusions.

Geologic units in the study area are grouped into 12 hydrogeologic units, and are classified as either aquifers or confining units, although a continuum of hydraulic properties exists. Medium- to coarse-grained, Quaternary-Tertiary clastic sediment, Paleozoic carbonate rocks, and some Tertiary volcanic rocks form the principal aquifers. Subsurface continuity of the consolidated-rock aquifers is disrupted by the major normal-fault zones that form the basin-range boundaries, and by other large faults and folds. Major fault zones may permit or inhibit groundwater flow across their planes depending on the hydraulic properties of the hydrogeologic units they cut and juxtapose, fault geometry, and fault-zone composition and texture. These characteristics likely vary horizontally and vertically within major fault zones.

The UGS established a groundwater-monitoring network in Snake Valley, Tule Valley, and Fish Springs Flat in 2007 to 2009. The network consists of (1) piezometers screened at various depths in the basin-fill, carbonate-rock, and volcanic-rock aquifers, in agricultural areas, spring-fed wetlands, and remote areas, and (2) surface-flow gages at environmentally sensitive and economically important springs. All groundwater-monitoring data are available though the UGS data portal, <http://geology.utah.gov/databases/groundwater/projects.php>. The primary objectives of the monitoring are (1) establish baseline groundwater conditions, including temporal and spatial variability of groundwater levels, spring discharge, and chemistry, (2) quantify changes in groundwater conditions due to current and possible future increases in groundwater pumping, and (3) test conceptual models of groundwater flow in Snake Valley and adjacent hydrographic areas.

Records from the UGS groundwater-monitoring wells show (1) groundwater levels in areas of pumping for irrigation vary by up to 15 feet (4.6 m) seasonally, and most piezometers experienced gradual declines from 2007 to late 2012, (2) groundwater levels in remote parts of the study area were mostly constant from 2007 to late 2012, and (3) groundwater levels in nested piezometers near spring pools fluctuated due to seasonal variations in evapotranspiration rates in the spring-fed wetlands ecosystems.

Groundwater levels generally vary systematically from

recharge areas in the Snake Range and Deep Creek Mountains, to discharge areas in the Snake Valley, Tule Valley, and Fish Springs Flat valley floors. Groundwater levels in carbonate-rock aquifers are interpreted to decrease continually through mountain ranges bounding adjacent parts of east-central Snake Valley and west-central Tule Valley, northeastern Snake Valley and southwestern Fish Springs Flat, and southeastern Spring Valley and southwestern Snake Valley, suggesting interbasin flow in these areas. Groundwater temperature and total-dissolved-solids concentrations generally increase with decreasing groundwater level. Groundwater composition ranges from calcium-bicarbonate type in the recharge areas and mountain fronts, to sodium-sulfate or sodium-chloride types in the discharge areas. Stable isotope compositions (∂^2H and ∂^{18}O values) vary within and between hydrographic areas in a complex manner that suggests convergence and mixing of groundwater flow paths having different compositions. Tritium concentration and percent modern carbon generally decrease with decreasing groundwater level. Apparent groundwater ages are generally <50–5000 years in the mountain fronts, 5000–28,000 years in the valley floors, and 12,000–17,000 years in regional and sub-regional springs. These generally systematic variations reflect slow flow from recharge to discharge areas, including interbasin flow from Snake Valley to Tule Valley and Fish Springs Flat.

Hierarchical cluster analysis of solute chemistry yields six sample groupings that objectively define six groundwater types distinguished primarily on increasing concentrations of chloride, sulfate, and sodium. Simple inverse geochemical models constrained by measured major-ion chemistry and mineral saturation states can account for changes in groundwater chemistry between the six groups along a series of defined flow paths.

Environmental-tracer data suggest that more than half of the groundwater sampled in the Snake Valley area recharged over one thousand years ago, implying that low recharge rates and/or long or slow flow paths predominate. Active groundwater recharge occurs locally in parts of Snake Valley adjacent to the mountain fronts, and is supplied by mountain-block areas having relatively high rates of precipitation and runoff.

We conducted aquifer tests at UGS groundwater-monitoring sites 11 and 3. Analysis of aquifer-test data from site 11 using standard curve-matching analytical solutions and MLU modeling resulted in estimates of transmissivity of 54,200 to 89,000 feet squared per day (5040–8270 m^2/day) and storativity of 3 x 10^{-4} to 4 x 10^{-3} for the basin-fill aquifer, and estimates of transmissivity of 11,700 to 37,000 feet squared per day (1100–3440 m^2/day) and storativity of 4 x 10^{-4} to 1 x 10^{-3} for the upper Paleozoic carbonate-rock aquifer. From analysis of aquifer-test data from site 3 using standard curve-matching techniques, we estimated transmissivity of 2100 to 4600 feet squared per day (200–430 m^2/day), and storativity of 6 x 10^{-5} to 1 x 10^{-4} for the lower Paleozoic carbonate-rock aquifer.

The UGS study area is in the Fish Springs sub-regional groundwater flow system of the Great Salt Lake Desert regional groundwater flow system, as defined by previous workers (Harrill and others, 1988; Prudic and others, 1995) who postulated that deep groundwater in the upper and lower carbonate-rock aquifers moves below surface-flow divides (hydrographic-area boundaries) toward major discharge areas in Tule Valley, Fish Sprigs Flat, and the southern Great Salt Lake Desert. Variations in the regional potentiometric surface, hydrogeology, and hydrochemistry support this hypothesis, and are consistent with locations and rates of interbasin flow derived from recent groundwater flow models. In addition, we define local- and intermediate-scale flow systems in Snake Valley from our data and analyses. Local flow systems discharge from springs and by evapotranspiration along the mountain fronts and nearby valley floors about 10 miles (16 km) or less from the recharge areas. Groundwater in the local flow systems is the youngest and least chemically evolved of the samples we analyzed. Intermediate flow systems discharge from springs on the valley floors or fault-controlled springs on the mountain fronts, about 10 to 25 miles (16–40 m) from the recharge areas and within the same hydrographic area. Groundwater in intermediate flow systems is more chemically evolved and substantially older than in local flow systems. Interbasin (regional) flow systems discharge from large spring complexes and by evapotranspiration up to 100 miles (160 km) from, and in different hydrographic areas than, their recharge areas. Groundwater discharging from regional flow systems is the most chemically evolved and oldest measured in this study.

Pressure to pump groundwater from the basin-fill and carbonate-rock aquifers for local use and export to other places of use will likely continue. Predictive simulations using the numerical groundwater-flow model developed by the Southern Nevada Water Authority (SNWA) for the Environmental Impact Statement (SNWA, 2010; U.S. Bureau of Land Management, 2012) and the model developed by the U.S. Geological Survey to evaluate potential impacts on Great Basin National Park and surrounding areas (Halford and Plume, 2011), provide the best available estimates of the consequences of future groundwater development. Groundwater levels would eventually decline by 10 to more than 100 feet (3–30 m) in much of southern and central Snake Valley (Halford and Plume, 2011; U.S. Bureau of Land Management, 2012) in the

modeled pumping scenarios. The Big Springs–Dearden Springs–Lake Creek–Pruess Lake hydrologic system would experience dramatically or entirely reduced spring and surface flow, due to capture of groundwater discharge by the new pumping and decline of groundwater levels due to removal of groundwater from storage (Halford and Plume, 2011; U.S. Bureau of Land Management, 2012). Wetlands and wet meadow plant communities would be succeeded by non-phreatophytic shrubland vegetation (Patten and others, 2007; McClendon, 2011), resulting in reduced or lost habitat for some environmentally sensitive species and reduced grazing land. Details of these changes cannot be accurately predicted without more complete geologic and hydrologic data and specific information about development plans. Spring flow and sensitive species habitat beyond the modeled 10-feet (3.1 m) drawdown contour could also be reduced. Small changes in spring flow could have important negative impacts on habitat depending on local hydrogeology and topography.

CHAPTER 10 REFERENCES

Halford, K.J., and Plume, R.W., 2011, Potential effects of groundwater pumping on water levels, phreatophytes, and spring discharges in Spring and Snake Valleys, White Pine County, Nevada, and adjacent areas in Nevada and Utah: U.S. Geological Survey Scientific Investigations Report 2011-5032, 52 p.

Harrill, J.R., Gates, J.S., and Thomas, J.M., 1988, Major ground-water flow systems in the Great Basin region of Nevada, Utah, and adjacent states: U.S. Geological Survey Hydrologic Investigations Atlas HA-694-C, scale 1:1,000,000, 2 sheets.

McClendon, T., 2011, Potential effects of change in depth to water on vegetation in Spring Valley, Nevada: Southern Nevada Water Authority, variously paginated. Online: http://water.nv.gov/hearings/past/springetal/browseabledocs/Exhibits%5CSNWA%20Exhibits/SNWA_Exh_037_McLendon%20Report.pdf, accessed July 26, 2011.

Patten, D.T., Rouse, L., and Stromberg, J.C., 2007, Isolated spring wetlands in the Great Basin and Mojave Deserts, USA—potential response of vegetation to groundwater withdrawal: Environmental Management (doi: 10.1007/s00267-007-9035-9).

Prudic, D.E., Harrill, J.R., and Burbey, T.J., 1995, Conceptual evaluation of regional ground-water flow in the carbonate-rock province of the Great Basin, Nevada, Utah, and adjacent states: U.S. Geological Survey Professional Paper 1409-D, 102 p.

Southern Nevada Water Authority, 2010, Simulation of groundwater development scenarios using the transient numerical model of groundwater flow for the central carbonate-rock province—Clark, Lincoln, and White Pine Counties Groundwater Development Project, *in* U.S. Bureau of Land Management, 2012, Clark, Lincoln, and White Pine Counties Groundwater Development Project Final Environmental Impact Statement: FES 12-33, Document BLM/NV/NV/ES/11-17+1793.

U.S. Bureau of Land Management, 2012, Clark, Lincoln, and White Pine Counties Groundwater Development Project Final Environmental Impact Statement: FES 12-33, Document BLM/NV/NV/ES/11-17+1793.

APPENDIX A | GRAVITY DATA-COLLECTION & REDUCTION METHODS

by Hugh Hurlow

Instrument: Lacoste-Romberg G-264, borrowed from the University of Utah Department of Geology and Geophysics.

Base Station: USAF Gravity Station BAKER (ACIC Ref. 2360-1), value 979,543.36 milligals.

Elevation Control: Measured at each station using Trimble 5800 Series Base and Rover antennae in RTK and Infill mode. Elevation uncertainty ranged from 0.02 to 0.06 m.

Data Reduction Sequence (Geosoft Inc., 2010):

- Instrument drift
- Earth-tide correction
- Free Air Anomaly: absolute gravity (corrected for instrument drift and earth tide) – latitude correction +(0.308596 * station elevation [m]).
- Bouguer Anomaly: $g_{ba} = g_{fa} - 0.0419088*(\rho h_s) + g_{curv}$,

  where

  g_{ba} = Bouguer anomaly in milligals

  g_{fa} = free air anomaly in milligals

  ρ = Bouguer density of rock (2.67 g/cm^3)

  h_s = station elevation in meters

  g_{curv} = earth-curvature correction
- Terrain correction: calculated using the algorithm of Geosoft Inc. (2010), with 30-meter digital elevation models for the local (up to 1000 m from station) and regional (1 to 167 km from station) corrections.
- Complete Bouguer anomaly = g_{ba} + terrain correction

The estimated uncertainty of individual complete Bouguer anomaly values is 0.04 ± 0.02 mgal, based on the precision of elevation control and repeated station occupations. This estimate does not include uncertainties associated with deviation of the Bouguer reduction density from the true density of the rocks, and inaccuracy of the terrain correction in areas having significant topographic relief.

- Isostatic Residual Anomaly: depth of sea level compensation = 30 km, Bouguer density = 2.67 g/cm^3, Moho density contrast = 0.33 g/cm^3, radius of compensation = 166.7 km. The Geosoft platform uses the algorithms of Simpson and others (1983, 1986).

Geophysical Modeling Units

Modeling Unit	Density (g/cm^3)	Susceptibility (dimensionless)
Upper Sedimentary Basin Fill	2.02	0
Middle Sedimentary Basin Fill	2.12	0–0.0015
Lower Sedimentary Basin Fill	2.32	0.0015
Middle Volcanic Basin Fill	2.27	0
Lower Volcanic Basin Fill	2.32	0.001
Granitic Intrusion	2.50	0.0015
Bedrock/Geophysical Basement 1	2.67	0
Bedrock/Geophysical Basement 2	2.67	0.0015
Neoproterozoic Metasediments 1	2.8	0.00055
Neoproterozoic Metasediments 2	2.8	0

Density values of sedimentary and volcanic basin fill are from Saltus and Jachens (1995). Other density values and all magnetic susceptibility values are from Geosoft (2010).

APPENDIX A REFERENCES

Geosoft Inc., 2010, Montaj gravity and terrain correction v. 7.1: Toronto, Ontario, Canada, Geosoft Incorporated, 50 p.

Saltus, R.W., and Jachens, R.C., 1995, Gravity and basin depth maps of the Basin and Range Province, western United States: U.S. Geological Survey Map GP-1012, scale 1:2,500,000.

Simpson, R.W., Jachens, R.C., and Blakely, R.J., 1983, AIRYROOT—A Fortran program for calculating the gravitational attraction of an Airy isostatic root out to 166.7 km: U.S. Geological Survey Open-File Report 83-883, 66 p.

Simpson, R.W., Jachens, R.C., Blakely, R.J., and Saltus, R.W., 1986, A new isostatic residual gravity map of the conterminous United States with a discussion on the significance of isostatic residual anomalies: Journal of Geophysical Resources, v. 91, p. 8348–8372.

APPENDIX B | HYDROGEOLOGIC UNIT DESCRIPTIONS & PHOTOGRAPHS

by Hugh Hurlow

APPENDIX B CONTENTS

FIGURES

B.1 QTcs and QTfs – Quaternary-Tertiary coarse-grained sedimentary aquifer and fine-grained sedimentary confining unit (younger basin fill)

Younger basin-fill deposits that form aquifers include interbedded gravel, sand, silt, and mud deposited in alluvial-fan environments along the range-valley margins (figure B.1), thinner and less extensive alluvial deposits below the valley centers, and lacustrine shoreline deposits that are locally interbedded with the distal parts of the alluvial-fan deposits. Confining units are mud and silt deposited in lake-bottom (figure B.2), playa, and spring-outflow environments, found mainly in the valley center. Contacts between aquifers and confining units are gradational due to continuous lateral variation in average grain size and texture, and interlayering of deposits in varying proportions. For example, the alluvial-fan deposits generally fine toward the valley centers where they are interbedded with fine-grained lacustrine mud. Lithologic logs of boreholes at UGS groundwater-monitoring sites in the valley centers (chapter 5) show that gravel and sand deposits are interbedded with lacustrine mud in the upper parts of the sedimentary basin centers.

Figure B.1. *Layered sorted alluvial-fan conglomerate of the younger basin-fill aquifer hydrogeologic unit (QTcs). (Camera case is 4 inches (10 cm) long.)*

Figure B.2. *Fine-grained lacustrine marl of the younger basin-fill aquifer hydrogeologic unit (QTfs). Case (circled) is 2.5 inches (6 cm) long.*

The two younger basin-fill hydrogeologic units are coeval and range from Holocene to mid-Miocene in age. The base of the younger basin-fill deposits corresponds to a change from volcanic, lacustrine, and alluvial depositional environments in the older basin fill to predominantly alluvial and lacustrine depositional environments in the younger basin fill. This transition occurred when topography and drainage patters changed due to initiation of basin-and-range faulting. In the Sacramento Pass area, the transition is marked by a gradational contact between interbedded lacustrine limestone, alluvial sandstone, and tuffaceous deposits below, and alluvial-fan deposits above, that occurred at about 17 Ma (Miller and Grier, 1995). The lower deposits correspond to hydrogeologic unit Ts (section 4.2.3.2) and the alluvial-fan deposits correspond to the lowest part of hydrogeologic unit QTcs. In Big Wash on the eastern flank of the Southern Snake Range, tilted volcaniclastic deposits exposed on the lower part of the south-facing canyon wall are in hydrogeologic unit Ts, whereas the gently dipping alluvial deposits above the angular unconformity are in hydrogeologic unit QTcs (figure B.3). However, thickness distribution of the younger basin-fill deposits is uncertain due to sparse subsurface data, and lack of age control in the relatively few wells that have detailed lithologic logs.

Thickness estimates of the younger basin-fill deposits are available from several locations in the study area. The alluvial-fan deposits in the Sacramento Pass area are up to about 4900 feet (1500 m) thick (Miller and Grier, 1995). Based on lithology and drilling records from boreholes at UGS groundwater monitoring sites, the younger basin fill is over 1517 feet (460 m) thick at site PW01, in which 975 feet (297 m) of predominantly sand and gravel (hydrogeologic unit QTcs) overlie gravel and sand in a sticky clay matrix (QTfs); over 1000 feet (300 m) thick in PW05 (mostly QTcs); and over 1400 feet (430 m) thick in PW07,

Figure B.3. *View northwest of poorly sorted conglomerate of the younger basin-fill aquifer hydrogeologic unit (QTcs) overlying tilted volcaniclastic conglomerate and coarse-grained sandstone of the older basin-fill aquifer hydrogeologic unit in Big Wash, on the eastern mountain front of the southern Snake Range.*

in which 860 feet (260 m) of interbedded QTcs and QTfs overlie semi-consolidated limestone-clast gravel (QTcs). Lithologic logs of several petroleum-exploration wells in Hamlin Valley also provide approximate constraints on the thickness of the younger basin fill hydrogeologic units. The younger basin fill is less than 1250 feet (380 m) thick in Outlaw Federal 1 (well I, table 3.1), in which 1254 feet (380 m) of "valley fill" (QTcs, QTfs, and Ts undifferentiated) overlies carbonate rock. In Fletcher No. 1 (well J, table 3.1), 2240 feet (680 m) of "basin fill" (QTcs and QTfs undifferentiated) overlies 3630 feet (1100 m) of anhydrite (shallow lacustrine and playa evaporite deposits; QTfs and/or Ts), which overlies 1820 feet (555 m) of clay, lacustrine limestone, and conglomerate (Ts) that rests on volcanic rocks (hydrogeologic unit Tvt2, section 4.2.3.3). In Hamlin Wash 18-1 (well L, table 3.1), 2600 feet (792 m) of "basin fill" (QTcs, QTfs, and Ts undifferentiated) overlie Tertiary volcanic rocks. In Hamlin Wash 19-1, (well K, table 3.1) 1602 feet (488 m) of "valley fill" (QTcs and QTfs undifferentiated) overlies 1870 feet (570 m) of anhydrite (QTfs or Ts).

The isopach map derived from gravity data (figure 3.14) provides an estimate of the thickness and structure of the younger and older basin-fill deposits combined, but the depth-density function used for the basin fill does not distinguish between the hydrogeologic units. In central and northern Snake Valley, central Spring Valley, and Tule Valley, where older volcanic deposits are likely absent or relatively thin (Sweetkind and others, 2007, figure 14), gravity-data modeling suggests that basin-fill deposits are up to 10,000 feet (3050 m) thick (figure 3.14), a reasonable maximum value for hydrogeologic units QTcs and QTfs (younger basin fill) and Ts (older basin fill) combined.

Plate 1 and figure 4.2 show the surface distribution of the younger basin-fill deposits. Below the surface, the lateral extent, thickness, and texture of hydrogeologic units QTcs and QTfs may differ substantially from the map patterns due to variations in climate, sediment supply, and tectonic subsidence of the valley floor through time (Leeder and Gawthorpe, 1987). The distribution of aquifers and confining units in the subsurface cannot, therefore, be predicted with confidence without detailed subsurface data. Such data are absent in the study area except in central Snake Valley, where detailed lithologic logs of boreholes at UGS groundwater monitoring sites exist.

Hydraulic-property estimates for younger basin-fill deposits in the Basin and Range Province vary substantially, depending on the textures and relative proportions of sedimentary facies that compose the tested interval. Reported values for hydraulic conductivity range from about 0.003 to 430 ft/day (9 x 10^{-4}–131 m/day) with a geometric mean of 3 to 7 ft/day (0.9–2.1 m/day), and reported values for specific yield range from 4 x 10^{-4} to 0.2 with a mean of 0.03 (Belcher and others, 2001; SNWA, 2009). The UGS conducted an aquifer test at groundwater monitoring site PW11, and derived a hydraulic-conductivity value of 210 to 340 ft/day (64–104 m/day) and a specific-storage value of 3 x 10^{-4} to 1 x 10^{-2} for the semi-consolidated basin-fill deposits (chapter 7). The hydraulic conductivity and effective porosity of the basin-fill aquifer unit likely decrease with depth (e.g., SNWA, 2009, appendix C) due to compaction and cementation. Exposures of the lower part of hydrogeologic unit QTcs on range flanks and in valleys are semi-consolidated to weakly consolidated, suggesting that the lower part of this unit has substantially lower hydraulic conductivity than the upper part. Drilling data and lithologic logs from boreholes at UGS groundwater-monitoring sites suggests that this transition typically occurs at 800 to 1000 feet (250–300 m) depth.

B.2 Ts – Tertiary sedimentary-rock aquifer (older basin fill)

Hydrogeologic unit Ts includes Oligocene and Eocene map units Ts1 and Ts2 (plates 1 and 2), and is composed of sedimentary rocks that predate, are interbedded with, and post-date the volcanic rocks of hydrogeologic unit Tvt2 (section 4.2.3.3). These rocks are exposed in the eastern part of the study area in the northern Schell Creek, Antelope, and Wilson Creek Ranges, and near Sacramento Pass (section 4.2.3.1), and presumably form part of the basin fill in much of the study area. The unit consists of interbedded conglomerate, tuff, and lacustrine limestone, alluvial and lacustrine sandstone and siltstone, and local deposits of sedimentary breccia. The best exposures of this unit are east of Sacramento Pass and in the southern Egan Range southwest of the study area. The hydraulic properties of unit Ts are intermediate between the younger basin-fill and carbonate-rock aquifers and the siliciclastic-rock confining units (table 4.1; figure 4.3).

B.3 Tvt1, Tvt2, Tvf – Tertiary volcanic-rock aquifers

Tertiary volcanic rocks in the study area range from Eocene to Miocene in age, are mostly andesite and dacite composition but range from basalt to rhyolite, and formed as tuff, breccia, and flow deposits that erupted from calderas or cones (plates 1 and 2). The volcanic rocks contain interbedded sedimentary deposits in places (Dixon and others, 2007; Sweetkind and others, 2007). Hydrogeologic units Tvt1 and Tvt2 correspond directly to lithostratigraphic units Tv1 and Tv2, respectively, and hydrogeologic unit Tvf includes lithostratigraphic unit Tv3 (figure 4.1). The lithology, thickness, and distribution of these units vary substantially within the study area.

Hydrogeologic unit Tvt1 includes tuff and breccia deposits exposed mainly in the Antelope Range, northern Snake Range, and southern Kern Mountains in the northwestern part of the study area (Rowley, 1998; Dixon and others, 2007). The eruptive center for these 38 to 35 Ma deposits underlies basin-fill deposits in northern Spring Valley (Watt and Ponce, 2007; figures 3.4 and 4.2). The rocks are over 500 feet (150 m) thick within and adjacent to the caldera, and occur in an east-west trending belt in outcrop and subsurface, that thins east to its boundary near the northern Confusion Range (Sweetkind and others, 2007, figure 14). This unit is an aquifer in northern Snake Valley beneath the sedimentary basin-fill units.

Figure B.4. *Welded tuff of the Oligocene Wah Wah Springs Tuff of the volcanic-rock hydrogeologic unit (Tvt2) in the central Confusion Range.*

Hydrogeologic unit Tvt2 consists primarily of Oligocene (32 to 27 Ma) tuff, volcanic breccia, and shallow intrusive rocks of the Indian Peak caldera complex (figure B.4) (Best and others, 1989a). The caldera complex is exposed in the Indian Peak and Wilson Creek Ranges in the southern part of the study area (figures 2.1 and 4.2), and related welded tuff deposits crop out as far north as the central Confusion Range and are present in the lower part of the basin fill below Hamlin and Snake Valleys (figure 2.2; Sweetkind and others, 2007). The volcanic and intrusive rocks are 8000 to 14,000 feet (2400–4300 m) thick within the caldera (figure 3.14) (Dixon and others, 2007; Sweetkind and others, 2007), and thin to the north where they are less than 500 feet thick (150 m) or absent north of Garrison, Utah (Sweetkind and others, 2007), although subsurface data to quantify this trend are sparse. The logs of three petroleum wells in Hamlin Valley (wells J, K, and L, table 3.1) denote volcanic rocks interbedded with tuffaceous sandstone in the basin fill below 2600 feet (800 m) depth. UGS borehole PW04AB on the western flank of the Mountain Home Range encountered welded tuff from 88 to 981 feet (27–299 m) depth. UGS borehole PW01, one mile west of Garrison, Utah, encountered volcaniclastic sandstone but no welded tuff from 345 to 735 feet (105–224 m) depth. In central Snake Valley east of Baker, Nevada, UGS boreholes PW05ABC and PW07B, drilled to 1000 and 1400 feet depth (305

and 427 m) , respectively, encountered no volcanic or volcaniclastic deposits.

Hydrogeologic unit Tvf includes (1) rhyolite and basalt flows in the southern Indian Peak Range and southeastern White Rock Mountains (units Tv3 and Tv on plate 1) (Best, 1987), (2) rhyolite and basalt flows in the southern Wah Wah Mountains and south of the San Francisco Mountains in the southeastern part of the study area, where they overlie flows and tuff of hydrogeologic unit Tvt2 (Best and others, 1987c, 1989b), (3) basalt cinder cones and flows and a rhyolite extrusive dome in the northern Confusion Range, and (4) rhyolite flows, tuff, and extrusive domes in the Thomas Range in the northeastern part of the study area (Lindsey, 1979).

The Tertiary volcanic units on plates 1 and 2 show significant lithologic variation with distance from their eruptive centers. For example, map unit Tv2 includes volcanic breccia, tuff, and shallow intrusive rocks (Best and others, 1987a, 1989a). Within and adjacent to the Indian Peak caldera boundary, this unit consists of welded tuff, volcanic breccia, and flow rock that vary from structureless and homogeneous to complexly interlayered in composition and texture. Dikes, plugs, and small plutons intrude the eruptive rocks. The degree of induration, mineral composition and grain size, and volume of lapilli and lithic fragments can vary over hundreds of feet. The less indurated, coarser-grained facies may have sufficient primary porosity to be classified as aquifers, and the densely welded tuff and flow rocks may form aquifers where they are fractured and below the water table. The limited lateral extent and greater degree of alteration characteristic of intracaldera rocks probably limit their ability to function as regional aquifers (Laczniak and others, 1996; Belcher and others, 2001). A few miles from the caldera boundary and beyond, the welded tuffs are tabular, layered, and highly indurated, as revealed in exposures along the western flank of the Mountain Home Range (Best and others, 1987b; Hintze and Best, 1987). These units have greater lateral extent and more uniform thickness than the intracaldera units. At UGS groundwater monitoring site PW04, the Oligocene Cottonwood Wash Tuff produced up to about 60 gallons per minute (230 L/min) during drilling, below a thin zone of calcite-filled fractures encountered at about 660 feet (200 m) depth. Water levels in the two piezometers in the borehole are nearly identical (table C.1), suggesting that the aquifer is hydraulically connected between 680 feet and 935 feet (207–285 m).

The only estimate of the hydraulic properties of volcanic rocks within the study area is from SNWA test well W508M, which yielded a transmissivity of 70 ft^2/day (6.5 m^2/day) (SNWA, 2009). In the Death Valley region, similar volcanic rocks have been extensively tested and yielded hydraulic conductivity values ranging from 0.04 to 179 ft/day (0.01–55 m/day), with geometric means of 1 ft/day (0.3 m/day) for flow rocks and 8 ft/day (2.4 m/day) for tuffs (table 4.1; figure 4.3) (Belcher and others, 2001; Sweetkind and others, 2007). Hydrogeologic units Tvt1 and Tvt2 are likely low-conductivity aquifers or confining units within and adjacent to their calderas, due to heterogeneous facies distribution and the presence of low-hydraulic conductivity facies. Welded ash-flow tuffs of both units more than about a mile from the caldera margins are potentially fractured-rock aquifers, especially along fault zones and areas of high joint density. The Indian Peak and Wilson Creek Ranges are underlain by hydrogeologic unit Tvt2, and have more perennial streams and mountain springs than ranges composed predominantly of carbonate rocks, suggesting that the volcanic-rock hydrogeologic units are generally less permeable than the carbonate-rock hydrogeologic units. Hydrogeologic unit Tvf is likely an aquifer that occurs in the upper part of the saturated zone below the southern parts of Hamlin, Pine, and Wah Wah Valleys.

B.4 TMzi – Tertiary and Mesozoic intrusive-rock confining unit

Intrusive rocks in the study area range from Jurassic to Miocene in age, and from tonalite to granite in composition; most are quartz monzonite or granodiorite. Isolated stocks and plutons occur in the Deep Creek Range, Kern Mountains (figure B.5), southern Snake Range, House Range, and San Francisco Mountains, whereas intrusive rocks in the northern Snake Range and Indian Peak Range form stocks and dikes distributed over several square miles. Although fractured intrusive rocks may yield water to wells, on a regional scale they retard regional groundwater flow and are classified as a confining unit (Plume, 1996; Sweetkind and others, 2007). The range of hydraulic-conductivity estimates from aquifer tests is considerably lower than those of hydrogeologic units QTcs, UPzc, and LPzc (table 4.1; figure 4.3). The intrusive rocks may not significantly impede groundwater flow

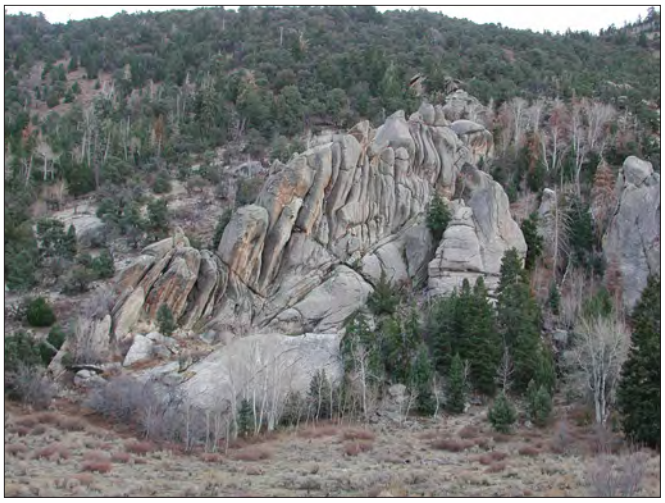

Figure B.5. *Cretaceous granite of the Tertiary-Mesozoic intrusive-rock hydrogeologic unit (TMzi) in the northwestern Kern Mountains.*

Figure B.6. *Jointed fine-grained calcareous sandstone of the Permian Arcturus Formation of the upper Paleozoic carbonate-rock aquifer hydrogeologic unit (UPzc) in the central Confusion Range. Hammer is 11 inches (28 cm) long.*

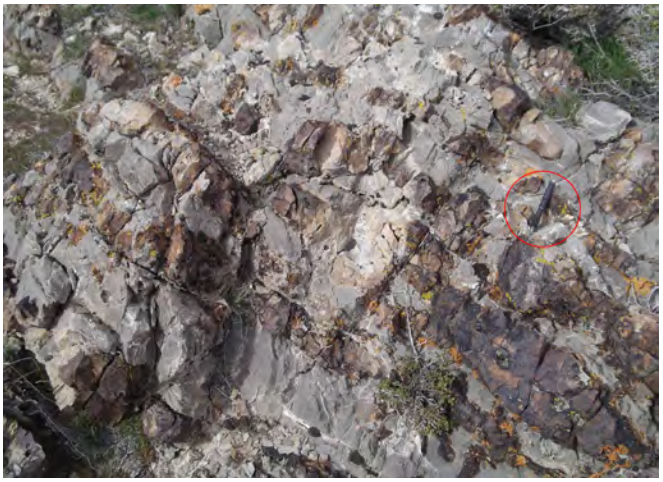

Figure B.7. *Cherty limestone of the Mississippian-Permian Ely Limestone of the upper Paleozoic carbonate aquifer hydrogeologic unit (UPzc) in the northern Mountain Home Range. Pencil (circled) is 5.5 inches (14 cm) long.*

parallel to major fault planes due to high joint density in the damage zones associated with the faults (section 4.3.2).

B.5 TMzs – Mesozoic sedimentary-rock confining unit

Triassic, Jurassic, and Cretaceous sedimentary rocks were largely eroded from the study area during the Cretaceous-Eocene Sevier Orogeny (Long, 2012), so only small exposures exist in the southern part of the study area, and these rocks are likely not present below the basin-fill and Tertiary volcanic units. Three small exposures of the Jurassic Navajo Sandstone occur in the southern Wah Wah Mountains, where they underlie rocks of the lower Paleozoic carbonate-rock aquifer hydrogeologic unit below a thrust fault. The Navajo Sandstone is a regional aquifer in parts of the Basin and Range and Colorado Plateau provinces, but in our study area this unit is likely highly segmented in the subsurface due to thrust faulting, eruption of volcanic material from the Indian Peak caldera complex, and normal faulting. Therefore, hydrogeologic unit Mzs is not relevant to regional groundwater flow in the study area.

B.6 UPzc – Upper Paleozoic carbonate-rock aquifer

The upper Paleozoic carbonate-rock aquifer hydrogeologic unit includes the Late Mississippian to Early Permian Ely Limestone, the Permian Arcturus Formation, and the Permian Park City Group (plate 2). This hydrogeologic unit is about 6800 to 7100 feet (2073–2164 m) thick, and is exposed in the northern Mountain Home Range, Burbank Hills, and northern Confusion Range in the central part of the study area, and in the southern Schell Creek Range in the western part of the study area (figure 4.2, plate 1).

The Ely Limestone is fine- to medium-grained cherty limestone having well-defined bedding, nodular to bedded chert, and little or no silt (figure B.6), the Arcturus Formation is fine-grained calcareous sandstone and limestone (figure B.7), and the Park City Group is limestone, dolomite, and silty limestone. Primary porosity is likely negligible in all of these formations, so hydraulic conductivity and storage are derived primarily from fractures (Winograd and Thordarson 1975; Belcher and others, 2001). Field observations indicate that joints are common in the Ely Limestone and

Figure B.8. *Fine-grained calcareous siltstone of the Mississippian Chainman Formation of the middle Paleozoic sedimentary-rock confining unit hydrogeologic unit (Pzs) in the central Confusion Range. Pencil is 5.5 inches (14 cm) long.*

Arcturus Formation, typically manifested by two sets perpendicular and one parallel to bedding. Fracture density is greatest adjacent to faults and within and adjacent to fold axes.

Boreholes at UGS groundwater-monitoring sites 2, 6, 15, and 23 encountered the Arcturus Formation below basin-fill sediment. In each of these boreholes, high fracture density and weathering of the Arcturus Formation at the unconformity resulted in severe lost-circulation problems during drilling, suggesting high transmissivity along this surface. During drilling of borehole PW06D using a button-hammer bit and pressurized air, water fountained from piezometer PW06B in already-completed borehole PW06ABC, suggesting a strong hydraulic connection over several hundred yards. The water level in piezometer PW06C, although it was closer to the drilling point, did not rise as much as that in PW06B, suggesting that the hydraulic connection is along a specific set of highly transmissive, interconnected fractures.

Hydraulic-conductivity estimates derived from aquifer tests of the upper Paleozoic carbonate-rock aquifer range from 0.00003 to 2690 ft/day (9×10^{-6}–880 m/day), including tests on unfractured and fractured rock (Winograd and Thordarson, 1975; Dettinger and others, 1995; Belcher and others, 2001; Sweetkind and others, 2007). The range for fractured carbonate rock is 0.01 to 2690 ft/day (3×10^{-3}–820 m/day), the geometric mean is approximately 1 to 9 ft/day (0.3–2.7 ft/day), and median values are 3 to 4.5 ft/day (0.9–1.4 m/day) (table 4.1; figure 4.3) (Dettinger and others, 1995; Belcher and others, 2001; Sweetkind and others, 2007). The UGS conducted an aquifer test on the Ely Limestone at groundwater monitoring site 11. Hydraulic-conductivity estimates ranged from 4 to 8 ft/day (1.2–2.4 m/day), consistent with the range of values from aquifer tests in others parts of the Great Basin.

B.7 MPzs – Middle Paleozoic siliciclastic-rock confining unit

This hydrogeologic unit ranges from Late Devonian to Mississippian in age, consists of the Mississippian Chainman Formation (figure B.8), Mississippian Joana Limestone, and Mississippian-Devonian Pilot Shale, and is about 2100 to 3000 feet (640–900 m) thick where structurally unmodified. Significant structural thickening and thinning may occur in fold hinges and limbs, respectively. The Pilot Shale and Chainman Formation are chiefly composed of carbonaceous siltstone and silty shale. In the Confusion Range, the Chainman Formation includes several quartzite beds and two limestone beds, up to 30 feet (9 m) thick, that are bounded above and below by thick shale sequences. The Joana Limestone is 300 to 500 feet (90–150 m) thick, and is composed of medium-grained cherty limestone. Joints and solution features occur in the Joana Limestone in the Burbank Hills and Buckskin Hills. This unit could be a local aquifer where it is structurally continuous between a recharge area and the saturated zone in the subsurface, but is not likely a regional-scale aquifer because it is bounded above and below by several hundred feet of shale having low hydraulic conductivity. Aquifer tests indicate that the hydraulic conductivity of the middle Paleozoic siliciclastic rocks is about two orders of magnitude less than that of the carbonate-rock aquifers (table 4.1; figure 4.3).

B.8 LPzc – Lower Paleozoic carbonate-rock aquifer

Middle Cambrian to Devonian marine carbonate rocks comprise a regional aquifer composed mainly of fine- to medium-grained limestone and dolomite, 16,750 to 18,600 feet (5100–5650 m) thick in total (Plume, 1996). Previous studies group this sequence into a single hydrogeologic unit, but hydraulic properties likely vary due to lithologic variations within the stratigraphic sequence. The upper 12,000 feet (3650 m) of the lower Paleozoic carbonate-rock aquifer includes dolomite and limestone of the Devonian Guilmette Formation (figure B.9) and underlying

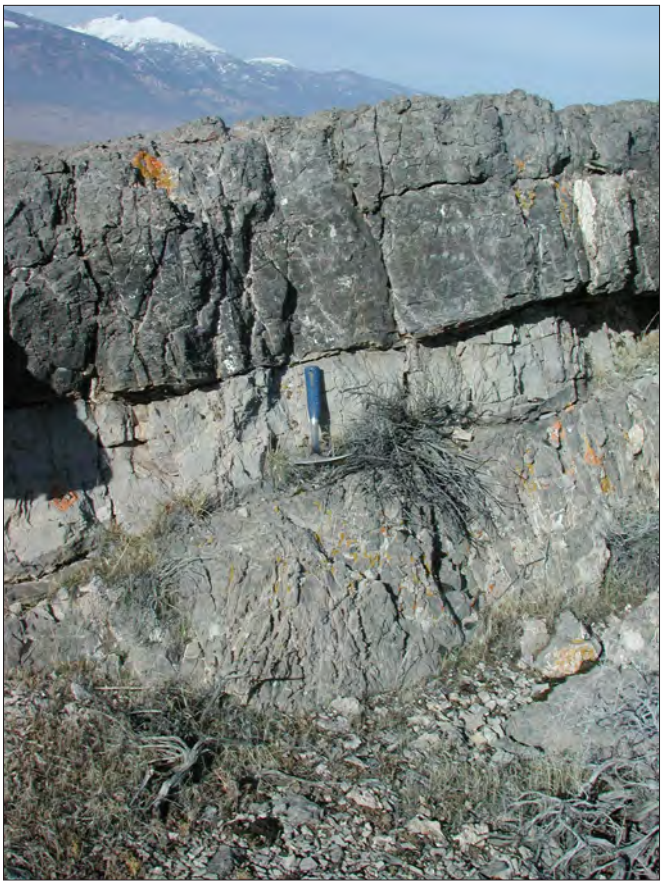

Figure B.9. *Limestone and dolomite of the Devonian Guilmette Formation of the lower Paleozoic carbonate-rock aquifer hydrogeologic unit (LPzc) in the Buckskin Hills. Hammer is 11 inches (28 cm) long.*

Figure B.10. *Jointed limestone of the Ordovician House Limestone of the lower Paleozoic carbonate-rock aquifer hydrogeologic unit (LPzc) in the southern Snake Range. Hammer is 11 inches (28 cm) long.*

Devonian through Early Cambrian formations (figure B.10). Ordovician quartzite and sandstone units including the Eureka Quartzite occur near the middle of this sequence. The upper part of the Cambrian Orr Formation contains interbedded shale and limestone that is about 860 feet (260 m) thick and likely forms a confining unit. Below the upper Orr Formation are 2400 to 3400 feet (730–1040 m) of Cambrian limestone and dolomite. The lowest 1700 to 2400 feet (520–730 m) of the lower Paleozoic carbonate-rock aquifer includes six Cambrian formations composed of limestone, silty limestone, and shale. The hydraulic conductivity of these units may be lower than in the rest of the hydrogeologic unit due to the presence of low-permeability shale beds that likely limit the extent and connectivity of fractures. The inferences that the upper Orr Formation and the lower shale and shaly limestone units may form confining units or relatively less transmissive intervals within the regional lower Paleozoic carbonate-rock aquifer are based on lithology; aquifer-test results that address this issue are not available. Borehole PW19AC at UGS groundwater-monitoring site 19 in southern Fish Springs Flat encountered the upper shale-rich part and lower limestone member of the Orr Formation. Groundwater production during drilling increased markedly below the upper Orr Formation, and the static water level is about 50 feet (15 m) above its upper contact, suggesting that it forms a confining layer at that site.

Aquifer tests of fractured lower Paleozoic carbonate rocks in central and southwestern Nevada yielded hydraulic-conductivity values of about 0.03 to 8900 ft/day (0.01–2700 m), with a geometric mean of about 13 ft/day (4.0 m/day) and an arithmetic mean of 554 ft/day (169 m/day) (Winograd and Thordarson, 1975; Dettinger and others, 1995; Belcher and others, 2001). Sweetkind and others (2007, p. 33) reported a range of hydraulic-conductivity values for the lower carbonate-rock aquifer of 0.009 to 2704 ft/day (2.7×10^{-3}–824 m/day), with a geometric mean of 4 ft/day (1.2 m/day) and a median value of 4 ft/day (1.2 m/day). Prieur and others (2010) calculated a hydraulic-conductivity value of 7.6 to 8.0 ft/day (2.3–2.4 m/day) from an aquifer test of the Devonian Guilmette Formation at their test-well site 184W101 in southeastern Spring Valley. The UGS conducted an aquifer test of the Guilmette Formation and underlying Simonson Dolomite at site 3, and derived hydraulic-conductivity estimates of 3, 4, and 7 ft/day (0.9, 1.2, and 2.1 m/day) from data from monitoring wells open at different depths (chapter 7).

Winograd and Thordarson (1975) and subsequent studies attributed the locally high hydraulic conductivity of the lower carbonate aquifer to solution widening of joints and faults, and presented outcrop-scale evidence of solution features including caves and solution-widened joints in the Nevada Test Site area. In the UGS study area, outcrop-scale solution features, including caves, occur in the Guilmette Formation and Joana Limestone. The Cambrian Pole Canyon Limestone hosts several extensive cave systems that influence spring and stream flow in Great Basin National Park (Elliot and others, 2006), and Gandy Warm Springs in northwestern Snake Valley emerge from this unit (Gans and others, 1999). Snake Creek Cave, east of Great Basin National Park on the eastern flank of the Southern Snake Range, is in the Devonian Guilmette Formation (Whitebread, 1969). These caves typically form along fracture intersections, but they are not ubiquitous, so their subsurface occurrence and influence on regional groundwater flow cannot be predicted.

B.9 €Zs – Lower Cambrian and Neoproterozoic siliciclastic-rock confining unit

The oldest hydrogeologic unit in the study area consists of Neoproterozoic quartzite, siltstone, and phyllite of the McCoy Creek Group in the western part of the study area and similar units in the southeastern part of the study area (figure B.11; map units p€s and p€m, plates 1 and 2), overlain by feldspathic quartzite of the Lower Cambrian Prospect Mountain Quartzite and siltstone and phyllite of the Lower Cambrian Pioche Formation (map unit €1, plates 1 and 2). This hydrostratigraphic unit is over 13,000 feet (4000 m) thick. Major exposures of unit €Zs are in the Schell Creek Range, Snake Range, and southern Deep Creek Range in the western part of the study area, where they are metamorphosed to greenschist grade, and in the southern Wah Wah Mountains, San Francisco Mountains, and Cricket Range in the southeastern part of the study area.

Hydrogeologic studies and aquifer-test results indicate that unit €Zs is a regional confining unit. Hydraulic-conductivity estimates range from 9 x 10^{-8} to 15 ft/day (2.7 x 10^{-8}–4.6 m/day) with a geometric mean of 2 x 10^{-6} ft/day (8 x 10^{-8} m/day) (table 4.1; figure 4.3) (Dettinger and others, 1995; Belcher and others, 2001; Sweetkind and others, 2007). Due to thorough cementation of pore space, porosity and permeability are almost entirely derived from fractures. Thick sequences

Figure B.11. *Neoproterozoic quartzite of the Cambrian-Neoproterozoic siliciclastic-rock confining unit hydrogeologic unit (€Zs) in the southern Deep Creek Range. Hammer is 11 inches (28 cm) long.*

of Prospect Mountain Quartzite may transmit some groundwater, especially where faulted (Belcher and others, 2001, p. 19), but hydraulic conductivity is substantially lower than that of the carbonate-rock and basin-fill aquifers. Abundant phyllite beds within the Neoproterozoic rocks likely prevent significant groundwater flow through this unit. Drilling data from UGS groundwater monitoring site 20 suggest that the upper 300 feet (90 m) of the Prospect Mountain Quartzite has moderate transmissivity.

Hydrogeologic unit €Zs likely inhibits regional groundwater flow where it is present in the saturated zone, primarily below and adjacent to mountain ranges dominated by exposures of this unit. Subsurface interbasin groundwater flow is unlikely to pass below these ranges. Substantial groundwater flow may occur in this unit where it is cut by range-bounding normal-fault zones, for example along the Schell Creek Range, central and northern House Range, southern Wah Wah Mountains, and Cricket Mountains mountain fronts, by segment boundaries and displacement-transfer zones in these normal-fault zones, or by transverse faults such as in the Sand Pass transverse zone between the Fish Springs and House Ranges.

Unit €Zs is less permeable to infiltration of precipitation and snowmelt in mountain blocks, so these areas have a higher number of perennial streams and greater proportion of recharge of runoff along their alluvial fans compared to mountains underlain by the carbonate-rock aquifers (Sweetkind and others, 2007; Heilweil and Brooks, 2011).

B.10 APPENDIX B REFERENCES

Belcher, W.R., Elliot, P.E., and Geldon, A.L., 2001, Hydraulic-property estimates for use with a transient ground-water flow model of the Death Valley regional ground-water flow system, Nevada and California: U.S. Geological Survey Water-Resources Investigations Report 01-4120, 28 p.

Best, M.G., 1987, Geologic map and sections of the area between Hamlin Valley and Escalante Desert, Iron County, Utah: U.S. Geological Survey Miscellaneous Investigations Series Map I-1774, 1:50,000.

Best, M.G., Christiansen, E.H., and Blank, R.H., Jr., 1989a, Oligocene caldera complex and calc-alkaline tuffs and lavas of the Indian Peak volcanic field, Nevada and Utah: Geological Society of America Bulletin, v. 101, p. 1076–1090.

Best, M.G., Grant, S.K., Hintze, L.F., Cleary, J.G., Hutsinpiller, A., and Saunders, D.M., 1987a, Geologic map of the Indian Peak (southern Needle) Range, Beaver and Iron counties, Utah: U.S. Geological Survey Miscellaneous Investigations Series Map I-1795, 1: 50,000.

Best, M.G., Hintze, L.F., and Holmes, R.D., 1987b, Geologic map of the southern Mountain Home and northern Indian Peak Ranges (central Needle Range), Beaver County, Utah: U.S. Geological Survey Miscellaneous Investigations Series Map I-1796, 1: 50,000.

Best, M.G., Lemmon, D.M., and Morris, H.T., 1989b, Geologic map of the Milford quadrangle and east half of the Frisco quadrangle, Beaver County, Utah: U.S. Geological Survey Miscellaneous Investigations Series Map I-1904, 1: 50,000.

Best, M.G., Morris, H.T., Kopf, R.W., and Keith, J.D., 1987c, Geologic map of the southern Pine Valley area, Beaver and Iron Counties, Utah: U.S. Geological Survey Miscellaneous Investigations Series Map I-1794, 1:50,000.

Dettinger, M.D., Harrill, J.R., Schmidt, D.L., and Hess, J.W., 1995, Distribution of carbonate-rock aquifers and the potential for their development, southern Nevada and parts of Arizona, California, and Utah: U.S. Geological Survey Water-Resources Investigations Report 91-4146, 100 p.

Dixon, G.L., Rowley, P.D., Burns, A.G., Watrus, J.M, and Ekren, E.B., 2007, Geology of White Pine and Lincoln Counties and adjacent areas, Nevada and Utah—the geologic framework of regional groundwater flow systems: Las Vegas, Southern Nevada Water Authority, HAM-ED-001, variously paginated. Available *in* Southern Nevada Water Authority, 2008, Baseline characterization report for Clark, Lincoln, and White Pine Counties Groundwater Development Project, *in* U.S. Bureau of Land Management, 2012, Clark, Lincoln, and White Pine Counties Groundwater Development Project Final Environmental Impact Statement: FES 12-33, Document BLM/NV/NV/ES/11-17+1793.

Elliot, P.E., Beck, D.A., and Prudic, D.E., 2006, Characterization of surface-water resources in the Great Basin National Park area and their susceptibility to groundwater withdrawals in adjacent valleys, White Pine County, Nevada: U.S. Geological Survey Scientific Investigations Report 2006-5099, 156 p.

Gans, P.B., Miller, E.L., and Lee, J., 1999, Geologic map of the Spring Mountain quadrangle, Nevada: Nevada Bureau of Mines and Geology Field Studies Map 18, scale 1:24,000.

Heilweil, V.M., and Brooks, L.E., editors, 2011, Conceptual model of the Great Basin carbonate and alluvial aquifer system: U.S. Geological Survey Scientific Investigations Report 2010-5193.

Hintze, L.F., and Best, M.G., 1987, Geologic map of the Mountain Home Pass and Miller Wash quadrangles, Miller and Beaver Counties, Utah, and Lincoln County, Nevada: U.S. Geological Survey Miscellaneous Field Studies Map MF-1950, scale 1:24,000.

Laczniak, R.J., Cole, J.C., Sawyer, D.A., and Trudeau, D.A., 1996, Summary of hydrogeologic controls on ground-water flow at the Nevada test site, Nye County, Nevada: U.S. Geological Survey Water-Resources Investigations Report 96-4109, 59 p.

Leeder, M.R., and Gawthorpe, R.L., 1987, Sedimentary models for extensional tilt-block/half-graben basins, *in* Coward, M.P., Dewey, J.F., and Hancock, P.L., editors, Continental extensional tectonics: Geological Society of London Special Publication 28, p. 139–152.

Lindsey, D.A., 1979, Geologic map and cross-sections of Tertiary rocks in the Thomas Range and northern Drum Mountains, Juab County, Utah: U.S. Geological Survey Miscellaneous Investigations Series Map I-1176, 1: 50,000.

Miller, E.L., and Grier, S.P., 1995, Geologic map of Lehman Caves 7.5′ quadrangle, White Pine County, Nevada: U.S. Geological Survey Map GQ-1758, scale 1:24,000.

Miller, E.L., Dumitru, T.A., Brown, R.W., and Gans, P.B., 1999, Rapid Miocene slip on the Snake Range–Deep

Creek Range fault system, east-central Nevada: Geological Society of America Bulletin, v. 111, p. 886–905.

Plume, R.W., 1996, Hydrogeologic framework of aquifer systems in the Great Basin region of Nevada, Utah, and adjacent states: U.S. Geological Survey Professional Paper 1409-B, 64 p.

Prieur, J.P., Farnham, I.M., and Ashinhurst, C.S., 2010, Hydrologic data analysis report for test well 184W101 in Spring Valley hydrographic area 184: Las Vegas, Nevada, Southern Nevada Water Authority Document No. DAR-ED-003, 79 p.

Rowley, P.D., 1998, Cenozoic transverse zones and igneous belts in the Great Basin, western United States—their tectonic and economic implications, *in* Faulds, J.E., and Stewart, J.H., editors, Accommodation zones and transfer zones—the regional segmentation of the Basin and Range Province: Boulder, Colorado, Geological Society of America Special Paper 323, p.195–228.

Southern Nevada Water Authority, 2009, Conceptual model of groundwater flow for the central carbonate-rock province—Clark, Lincoln, and White Pine Counties Groundwater Development Project, *in* U.S. Bureau of Land Management, 2012, Clark, Lincoln, and White Pine Counties Groundwater Development Project Final Environmental Impact Statement: FES 12-33, Document BLM/NV/NV/ES/11-17+1793.

Watt, J.T., and Ponce, D.A., 2007, Geophysical framework investigations influencing ground-water resources in east-central Nevada and west-central Utah: U.S. Geological Survey Open-File Report 2007-1163, 43 p.

Whitebread, D.H., 1969, Geologic map of the Wheeler Peak and Garrison quadrangles, Nevada and Utah: U.S. Geological Survey Miscellaneous Geologic Investigations Series Map I-578, scale 1:48,000

Winograd, I.J., and Thordarson, W., 1975, Hydrogeologic and hydrochemical framework, south-central Great Basin, Nevada-California, with special reference to the Nevada Test Site: U.S. Geological Survey Water-Supply Paper 712-C, 126 p.

APPENDIX C | WELL RECORDS

The well record files (listed below) can be found on the DVD.

Table C.1 UGS Well Data

Table C.2 Other Wells

Table C.3 USGS Wells

Table C.4 UGS Surface Gages

APPENDIX D | HYDROCHEMICAL DATA

The hydrochemical data files (listed below) can be found on the DVD.

Figure D.1 Mass Transfer Graphs

Table D.1 Hydrochemistry and Isotopic Data for Collected Samples

Table D.2 Compiled Hydrochemistry and Isotopic Data

APPENDIX E

HYDROGEOLOGIC ANALYSIS OF INTERBASIN FLOW FROM SNAKE VALLEY TO TULE VALLEY AND FROM SOUTHERN SPRING VALLEY TO NORTHERN HAMLIN VALLEY

by Hugh Hurlow

APPENDIX E CONTENTS

FIGURES

TABLES

E.1 HYDROGEOLOGIC ANALYSIS OF GROUNDWATER FLOW FROM SNAKE VALLEY TO TULE VALLEY

E.1.1 Introduction

In chapter 8 we evaluate the proposed Fish Springs flow system and specific flow paths therein based on new and previously published hydrogeologic and hydrochemical data, and conclude that the flow system as a whole, and certain flow paths within, are supported by most data. One valid flow path is from recharge in the southern Snake Range, through southern and south-central Snake Valley, the central Confusion Range, and either (1) through western Tule Valley to discharge at Coyote Spring and nearby pats of central Tule Valley, or (2) through northern Tule Valley, the southern Fish Springs Range, and Fish Springs Flat to discharge at Fish Springs (flow paths 3a and 3b, respectively, in tables 8.2 and 8.3). In this appendix I estimate possible groundwater-flow rates from Snake Valley to Tule Valley through the Confusion Range, by applying Darcy's Law using hydraulic-potential gradients and hydraulic-conductivity values determined from this study and recently published cross sections (Greene and Herring, 2013). I show that these estimates are comparable to interbasin-flow-rate estimates from recent groundwater-flow models derived principally from groundwater budgets.

This flow path was schematically illustrated by Harrill and others (1988, sheet 1) and discussed by Prudic and others (1995, p. 33, also see discussion on p. D84). SNWA (2009a, table I-2) and Durbin and Loy (2010, table 3.1-1) estimated interbasin-flow rates from Snake Valley to Tule Valley of 15,000 acre-feet per year (18.5 hm^3/yr) and 17,200 acre-feet per year (21.2 hm^3/yr), respectively, based on groundwater-budget analyses as part of their conceptual groundwater-flow models, and SNWA (2009b, table 6-4) estimated an interbasin-flow rate of 15,127 acre-feet per year (18.7 hm^3/yr) based on their transient numerical model.

Sweetkind and others (2007, figure 15) and Sweetkind and others (2011, plate 1) rated the possibility of groundwater flow from Snake Valley to Tule Valley through the Confusion Range interbasin-boundary zone as "permitted" and "high," respectively, based on hydrogeologic criteria. In contrast, Dixon and others (2007, figure 4-10) rated the potential for interbasin flow along only a limited part of the southern Confusion Range as "permissible," and rated most of the boundary as having "unlikely" potential. Rowley and others (2009, p. 262–263) and Rowley and Dixon (2011, p. 4-74 to 4-75) argued against significant flow from Snake Valley to Tule Valley based on the likely presence of range-bounding normal faults along the Confusion Range-Snake Valley boundary, and of the middle Paleozoic siliciclastic-rock confining hydrogeologic unit in the Confusion Range, that form barriers to west-to-east groundwater flow.

This appendix describes the structural geology and hydrogeology of the Confusion Range interbasin-boundary zone (figure E.1), including an estimate of possible groundwater-flow rates through the Confusion Range using Darcy's Law (table E.1), to assess whether the hydrogeology of the interbasin-boundary zone is compatible with interbasin-flow-rate estimates from Snake Valley to Tule Valley from the recent conceptual and numerical models summarized above (SNWA, 2009a, 2009b; Durbin and Loy, 2010). This boundary warrants detailed investigation because flow through it is a necessary component of the hypothesized hydraulic connection from Snake Valley to Tule Valley and Fish Springs, and divergent opinions about the degree of this connection have been published.

Groundwater that flows from Snake Valley to Tule Valley moves from the Snake Valley basin-fill and/or carbonate-rock aquifers, across range-bounding normal faults into bedrock aquifers in the Confusion Range interbasin-boundary zone (i.e., mountain block) (section E.1.2), through the Confusion Range interbasin-boundary zone (sections E.1.3 and E.1.4), and across range-bounding normal-fault zones to the basin-fill and/or carbonate-rock aquifers in west-central Tule Valley (section E.1.5). I subdivide the interbasin-boundary zone into the northern, central (Cowboy Pass-Conger Range area), and southern Confusion Range (figure E.1) based on hydrogeologic characteristics described in the following sections. Section E.2 examines use of Darcy's Law to estimate interbasin-flow rates using the example of flow from southern Spring Valley to northern Hamlin Valley, where two highly divergent estimates have been published using the same technique (Laczniak and others, 2007; Burns and Drici, 2011), to illustrate some of the difficulties with this approach.

E.1.2 Hydrogeology of the Snake Valley–Confusion Range Boundary

A concealed normal-fault zone likely forms the structural boundary between east-central Snake Valley and the northern and central parts of the Confusion Range (figure E.1). This fault zone is approximately located based on gravity and well data and range morphology, and consists of several north- to northwest-striking strands from the Bishop Springs area, where they localize Twin Springs and Foote Spring (Kistinger and others, 2009), to south of Cowboy Pass (figure E.1). The principal hydraulic-potential-gradient direction in this area is to the east, from Snake

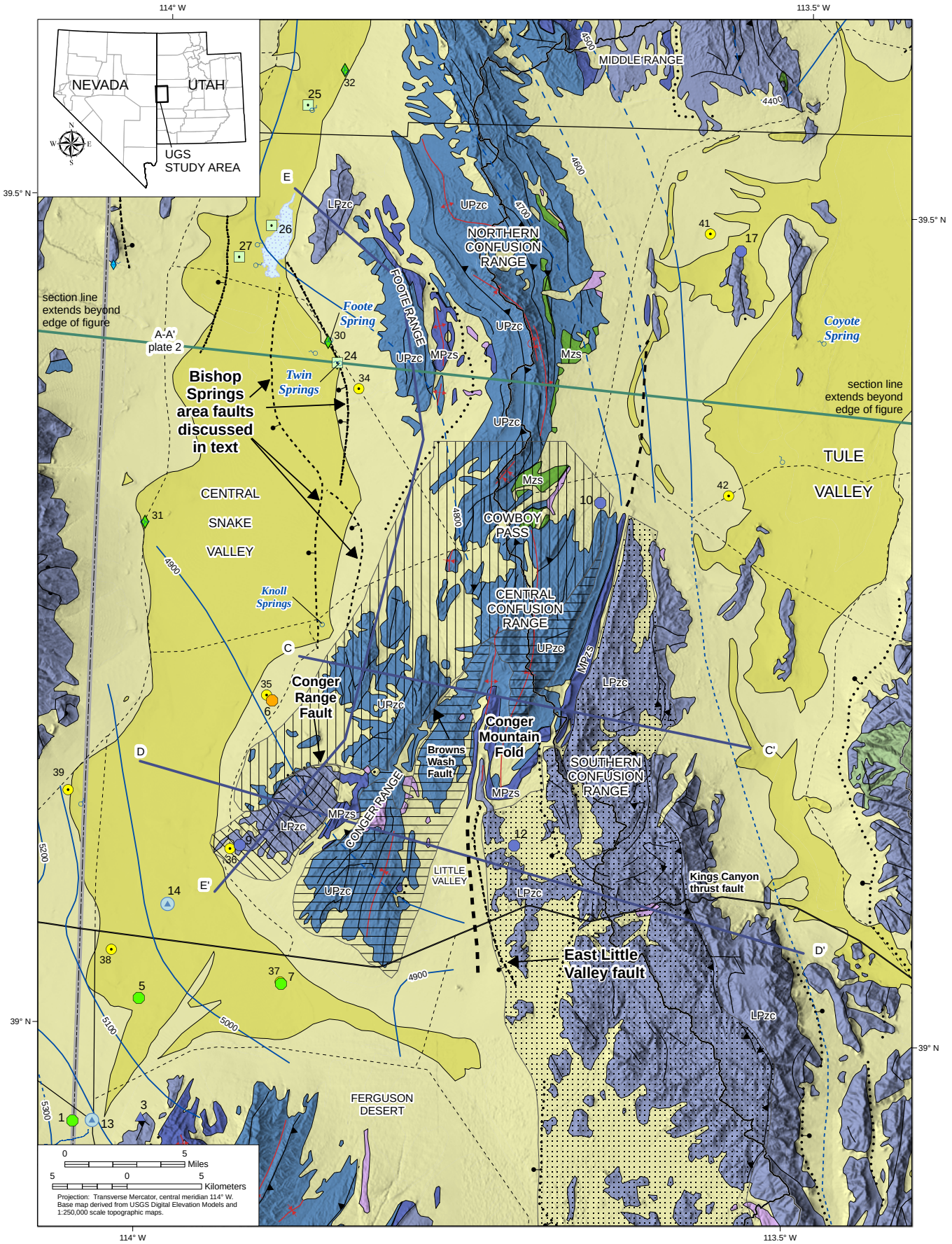

Figure E.1. *Hydrogeologic setting of the Confusion Range interbasin-boundary zone.*

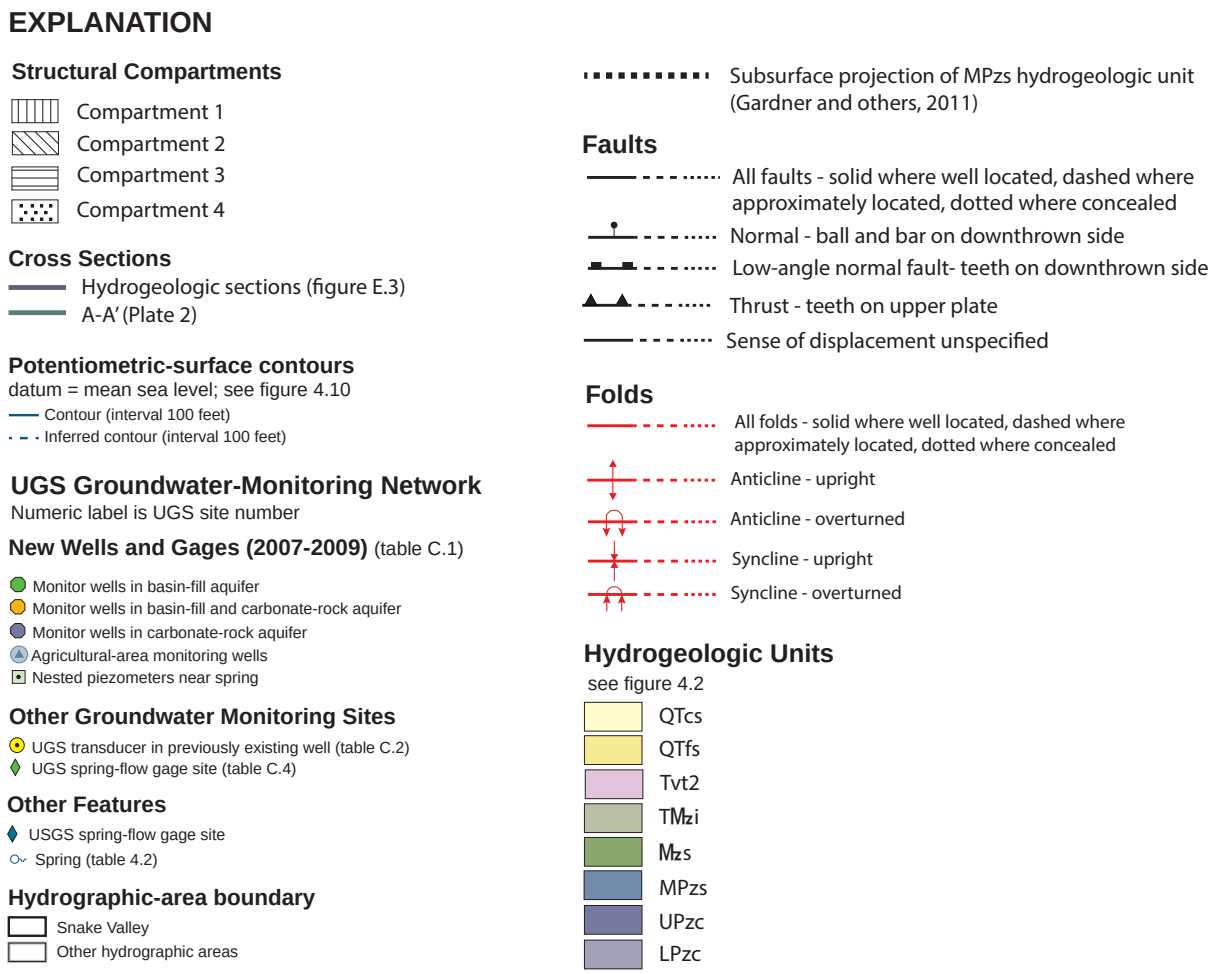

Explanation of map symbols on figure E.1.

Valley toward the Confusion Range, and the presence of Twin Springs and Foote Spring on a fault strand along the eastern margin of Snake Valley suggests that the faults and/or hydrogeology of the adjacent mountain block prevent flow into the northern Confusion Range.

South of Bishop Springs and southwest of the Cowboy Pass area, bends and intersections in strands of the range-bounding normal-fault zone are likely sites of segment-boundary zones and/or cross-faults. These features may permit cross-fault groundwater flow to the east, and no springs are present, suggesting the lack of a major flow barrier. The fault strands intersect the northeast-southwest-trending Conger Range where they terminate, continue into the range, or bend to strike southwest. One of these faults or a fault-intersection line likely localizes Knoll Springs (figure E.1; table 4.2).

Groundwater that encounters the southwest margin of the Conger Range does not need to cross a major range-bounding normal-fault zone to enter the upper and lower Paleozoic carbonate-rock aquifer hydrogeologic units. Groundwater-level records at UGS groundwater-monitoring site 9 in the lower Paleozoic carbonate-rock aquifer hydrogeologic unit reflect a pressure response to groundwater pumping from the basin-fill aquifer in the Eskdale agricultural area (chapter 5; plate 3), suggesting that the basin-fill and bedrock aquifers are hydraulically connected in this area. Groundwater levels indicate that the principal hydraulic-potential gradient direction in the Eskdale area is generally northeast (figure E.1). I conclude that the hydrogeologic setting of the Cowboy Pass-Conger Range area permits groundwater flow from Snake Valley to the Confusion Range, particularly along the southeastern margin of the Conger Range.

The groundwater level in UGS piezometer PW12A, screened in the Devonian Guilmette Formation of the lower Paleozoic carbonate-rock aquifer hydrogeologic unit, is 465 feet (142 m) lower than that in the U.S. BLM's Little Valley well 3.5 miles (5.6 km) to the southwest, screened in basin-fill deposits. The relatively high vertical hydraulic-potential gradient suggests that either the basin-fill and carbonate-rock aquifers are not hydraulically connected, or

Table E.1. *Summary of possible flow rates through the Confusion Range interbasin-boundary zone, estimated from calculations using Darcy's Law and the assumptions listed in the table footnotes.*

Cross Section	Hydraulic-Potential Gradient[1]	Compartments & HGUs[2]								Sum[5] Flow (ac-ft/yr)	Range[6]
		1 – UPzc		2 – LPzc		3 – UPzc		4 – LPzc			
		Area[3] (ft²)	Flow[4] (ac-ft/yr)	Area[3] (ft²)	Flow[4] (ac-ft/yr)	Area[3] (ft²)	Flow[4] (ac-ft/yr)	Area[3] (ft²)	Flow[4] (ac-ft/yr)		
Cowboy Pass - UPzc Hydrogeologic unit											
E–E′	0.002	51	10,000	n/a	n/a	n/a	n/a	n/a	n/a	10,000	3000–18,000
Conger Range - UPzc and LPzc Hydrogeologic units											
C–C′	0.002	86.8	18,000	0.0	0	5.0	1000	n/a	n/a	19,000	6000–32,000
D–D′	0.002	46.7	10,000	12.7	3000	11.4	2000	n/a	n/a	15,000	5000–16,000
Average	0.002	66.8	14,000	6.4	1500	8.2	1500	n/a	n/a	17,000	5000–32,000
Southern Confusion Range - LPzc Hydrogeologic unit											
C–C′	0.003	n/a	n/a	n/a	n/a	n/a	n/a	28.5	10,000	10,000	3000–16,000
D–D′	0.003	n/a	n/a	n/a	n/a	n/a	n/a	35.2	12,000	12,000	4000–20,000
Average	0.003	n/a	n/a	n/a	n/a	n/a	n/a	31.9	11,000	11,000	6000–14,000
									Average flow in three cross sections combined:	38,000	14,000–64,000

Darcy's Law

Q = -K*I*W*b*0.0084

Q = flow (acre-feet/year),

K = hydraulic conductivity (ft/day)

I = hydraulic gradient (ft/ft)

W = horizontal width of flow section (feet)

b = aquifer thickness (feet)

Hydraulic Conductivity in feet per day (table 7.4)

HGU	Mean	Low	High
UPzc	12.5	4	21
LPzc	4.7	3	7

[1] Hydraulic-potential gradients are estimated from groundwater levels at UGS groundwater-monitoring sites 6 and 10 for the Cowboy Pass and Conger Range areas, and from the difference between the 4900-foot hydraulic-potential surface contour and the elevation of Coyote Spring in Tule Valley for the southern Confusion Range.

[2] See section E.1.3 for discussion of subdivision of Conger Range into structural compartments. Cross section E-E′ was not subdivided into structural compartments.

[3] Cross-section areas estimated from rectangles drawn on cross sections by Greene and Herring (2013) (figure E.3), after simplifying their geologic units to the hydrogeologic units used in this study and assuming a maximum depth of significant groundwater flow of 2000 feet (620 m). Values are estimated area in square feet x 10-6.

[4] Flow-rate estimates are rounded to the nearest 1000 acre-feet per year.

[5] Values in Sum column are based on mean hydraulic-conductivity estimates from UGS aquifer tests (table 7.4).

[6] Values in Range column are based on minimum and maximum hydraulic-conductivity estimates from UGS aqifer tests (table 7.4).

a barrier to west-to-east groundwater flow exists between the two wells. Two geologic features are candidates for barriers. The middle Paleozoic siliciclastic-rock confining unit is below the Little Valley basin-fill deposits, where it strikes approximately north-south and dips steeply west, and may form a barrier to northeastward groundwater flow (Gardner and others, 2011). The second possible barrier is a fault that bounds the eastern margin of Little Valley (figure E.1). This fault is exposed in a wash in the northeast corner of Little Valley, where it cuts a sandy facies of the Guilmette Formation and develops a thick zone of deformation bands (figure E.2) which are impermeable to groundwater flow across their planes (Antonellini and Aydin, 1994). Assuming the sandy facies and associated fault-zone fabrics are present along the fault plane in the saturated zone, the eastern Little Valley fault may form a barrier to west-to-east groundwater flow across its plane. I conclude that little interbasin flow occurs through the area of Little Valley and UGS groundwater-monitoring site 12. Groundwater flow from Snake Valley to Tule Valley likely enters the southern Confusion Range in the Ferguson Desert area south of Little Valley, as proposed by Gates and Kruer (1981).

E.1.3 Hydrogeology of the Confusion Range

The following discussion of the hydrogeology of the Confusion Range mountain block is based on cross sections published by Hintze and Davis (2002) through the northern and central Confusion Range, and balanced cross sections by Greene and Herring (2013) through the central and southern Confusion Range. Figure E.3 shows the upper 5000 to 6000 feet (1520–1830 m) of Greene and Herrings' (2013) cross sections, with their geologic units combined into the hydrogeologic units used in this study.

In the northern Confusion Range, most faults, folds, and bedding predominantly strike north to northwest, approximately normal to the regional principal hydraulic-potential gradient direction (figure E.1). The faults and the middle Paleozoic siliciclastic-rock confining hydrogeologic unit in the syncline that occupies the central part of the mountain block (cross section A–A′, plate 2; Hintze and Davis, 2002) likely form barriers to east-flowing groundwater. We conclude that little interbasin flow occurs through the northern Confusion Range.

In the central Confusion Range (Cowboy Pass-Conger Range area, figure E.1), most bedding, faults, and folds strike north-northeast to northeast, parallel to the principal hydraulic-potential gradient direction. The Conger Mountain fold strikes northwest, and has rocks of the middle Paleozoic siliciclastic-rock confining hydrogeologic unit in its core (cross sections C–C′ and D–D′, figure E.3). Rocks

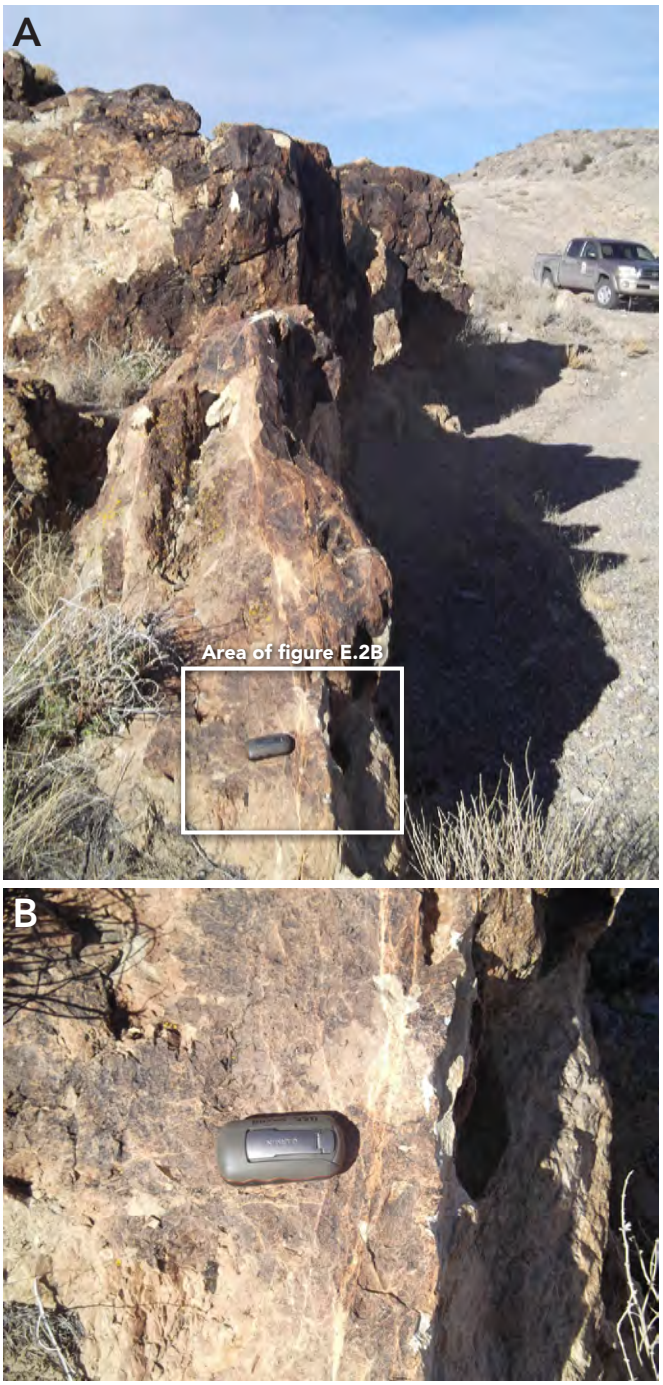

Figure E.2. *View to the north of fault-zone fabrics in the east Little Valley fault zone, showing steeply dipping deformation bands (distinct planar features bleached white) in penetratively brecciated silicified sandstone (brown). These fault-zone fabrics would form a barrier to groundwater flow across the fault plane (i.e., west-to-east) if they are present below the water table. Handheld GPS unit is 4 inches (10 cm) long.*

of the upper and lower Paleozoic carbonate-rock aquifer hydrogeologic units in the northwest and southeast limbs, respectively, of the Conger Mountain fold likely allow groundwater flow to the northeast (cross sections C–C′ and D–D′, figure E.3).

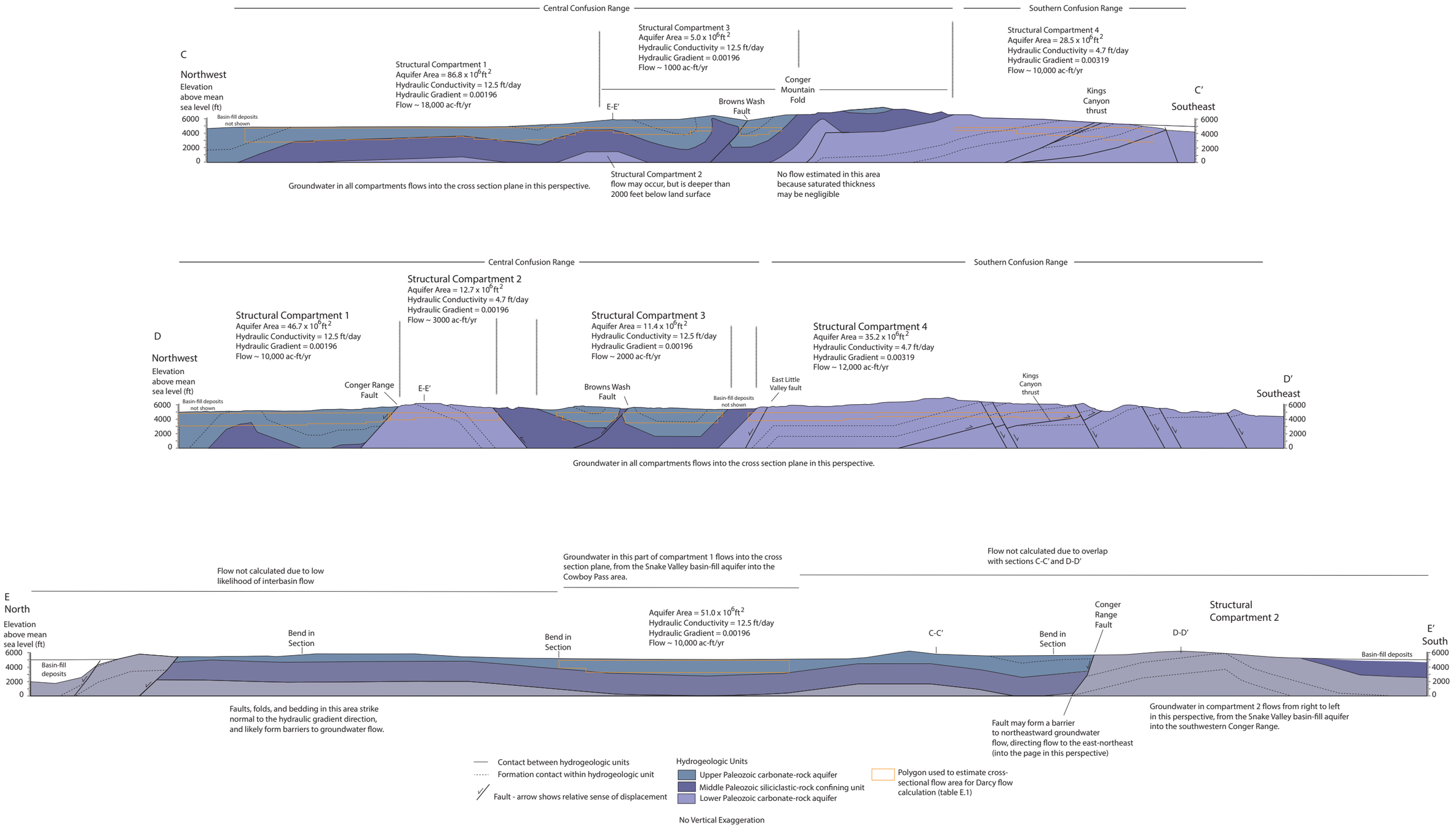

Figure E.3. *Hydrogeologic cross sections through the Confusion Range, modified from Greene and Herring (2013). See figure 4.1 and section 4.2.3 for descriptions of hydrogeologic units, and figure E.1 for locations and geologic setting. Hydrogeologic units are simplified from the map units of Greene and Herring (2013), and dotted formation contact lines are selected contacts unmodified from those sections, included here to illustrate the general internal structure of the interpreted groundwater compartments. See Greene and Herring (2013) for original sections and geologic base map. Greene and Herring (2013) used the mapping of Hintze and Davis (2002) as their base map. The geologic maps on plate 1 and figure 8.3 of this report are derived from, and are similar to but not exact matches with, Hintze and Davis' (2002) geologic map.*

Figure E.3 illustrates the interpretation that hydrostratigraphy, faults, and folds partition the central and southern Confusion Range into four northeast-trending (i.e., parallel to the hydraulic-potential gradient) groundwater compartments: (1) upper Paleozoic carbonate-rock aquifer northwest of the Conger Range fault, (2) lower Paleozoic carbonate-rock aquifer between the Conger Range fault and Conger Mountain fold, (3) upper Paleozoic carbonate-rock aquifer southeast of the Conger Mountain fold, and (4) lower Paleozoic carbonate-rock aquifer between the Conger Mountain fold and Kings Canyon thrust. These compartments are separated by northeast-striking faults and/or sections of the middle Paleozoic siliciclastic-rock confining hydrogeologic unit in the core and limbs of the Conger Mountain fold.

In the southern Confusion Range, rocks of the lower Paleozoic carbonate-rock aquifer hydrogeologic unit are less deformed than those in the northern and central Confusion Range. Widely spaced normal faults strike northwest and northeast, and several north-striking thrust faults, including the Kings Canyon thrust, are exposed in the eastern part of the area (figure E.1) (Hintze and Davis, 2002). Within the large mass of relatively little-deformed bedrock, groundwater likely travels through joints parallel and perpendicular to the gently dipping bedding planes, and along fault planes. The thrust faults in the eastern part of this area may form barriers to cross-fault flow and direct groundwater flow to the north.

E.1.4 Application of Darcy's Law to Flow in the Confusion Range

Interbasin-flow rates can be estimated using Darcy's Law in its unexpanded form (e.g., Feltis, 1967; Laczniak and others, 2007, p. 72–75; Burns and Drici, 2011, chapter 7 and appendix E):

$$Q = -K*I*W* b*0.0084$$

where

Q = groundwater flow rate (acre-feet per year),
K = hydraulic conductivity (feet per day),
I = horizontal hydraulic gradient (water level difference in feet per unit length in feet),
W = horizontal width of flow section (feet),
b = aquifer thickness (feet), the depth of significant flow in the aquifer,
0.0084 = conversion factor from cubic feet per day to acre-feet per year.

Application of Darcy's Law to interbasin flow involves simplifying assumptions, including porous-media flow, spatially homogeneous distribution of hydraulic conductivity within each hydrogeologic unit, and that the hydraulic conductivity, potentiometric gradient, and aquifer thickness are reasonably well known. Uncertainties in all of these values suggest that flow-rate estimates should be regarded as approximate. The method is applied here to evaluate whether sufficient aquifer area and potentiometric gradient exist to accommodate previously published estimates of interbasin groundwater-flow rates, not to provide a new rate estimate.

The balanced cross sections of Greene and Herring (2013) (figure E.3) provide a template for estimating the cross-sectional area of aquifers through which interbasin flow through the Confusion Range interbasin-boundary zone occurs (table E.1). Calculations were performed assuming (1) an average hydraulic-potential gradient of 0.00196 through the Cowboy Pass-Conger Range area, from the difference between groundwater elevations at UGS groundwater-monitoring sites 6 and 10, both screened in the upper Paleozoic carbonate-rock aquifer hydrogeologic unit, (2) an average hydraulic-potential gradient of 0.00319 through the southern Confusion Range, based on the difference between the 4900-foot (1500 m) potentiometric-surface contour (Gardner and others, 2011) and the elevation of Coyote Spring (4424 feet [1348 m]), the highest-flowing spring in the central Tule Valley discharge area (the groundwater elevation in UGS piezometer PW12A was not used because it is inconsistent with other groundwater levels in eastern Snake Valley and Tule Valley and, as explained above, may be isolated from Snake Valley groundwater by hydrogeologic barriers), (3) hydraulic conductivity of 12.5 feet per day (3.8 m/d) for the upper Paleozoic carbonate-rock aquifer hydrogeologic unit, the average of hydraulic-conductivity estimates from the UGS aquifer test at groundwater-monitoring site 11 (table 7.4), (4) hydraulic conductivity of 4.7 feet per day (1.4 m/d) for the lower Paleozoic carbonate-rock aquifer, the average of hydraulic-conductivity estimates from the UGS aquifer test at groundwater-monitoring site 3 (table 7.5), and (5) cross-sectional areas of saturated aquifers (figure E.3) assuming an average depth to water of 150 feet (46 m) west of Cowboy Pass, 250 feet (76 m) in the Conger Range, and 1000 feet (305 m) in the southern Confusion Range, and volumetrically significant flow to 2000 feet (610 m) below land surface.

Estimates using Darcy's Law suggest the following possible approximate groundwater-flow rates (table E.1): (1) through the Cowboy Pass area of the central Confusion Range (cross section E–E′, figure E.3), 10,000 acre-feet per year (12.3 hm^3/yr), (2) through the Conger Range area of the central Confusion Range (averages of values estimated from cross sections C–C′ and D–D′, figure E.3), 14,00 acre-

feet per year (17.3 hm^3/yr) through compartment 1, 1500 acre-feet per year (1.8 hm^3/yr) through compartment 2, and 1500 acre-feet per year (1.8 hm^3/yr) through compartment 3 (total of 15,000 acre-feet per year [18.5 hm^3/yr]), and (3) through compartment 4 in the southern Confusion Range, 11,000 acre-feet per year (13.6 hm^3/yr).

In total, the carbonate-rock aquifers in the central and southern Confusion Range interbasin-boundary zone can accommodate about 38,000 acre-feet per year (46.9 hm^3/yr) of northeastward groundwater flow from Snake Valley to Tule Valley (table E.1). Based on the ranges of hydraulic conductivities of the upper and lower Paleozoic carbonate-rock aquifer hydrogeologic units, the range of possible flow estimates is about 14,000 to 64,000 acre-feet per year (17.3–78.9 hm^3/yr) (table E.1). Adding reasonable ranges in the regional hydraulic-potential gradient and depth of groundwater flow (as much as 4000 feet [1220 m] below land surface; section 4.2.2) would increase this range and possibly change the mean estimate. Actual flow rates may be limited by the range-bounding normal-fault zones along the Snake Valley–Confusion Range boundary, which are likely less transmissive than the fractured rock within the Confusion Range.

The Darcy's Law calculations indicate that the central and southern parts of the Confusion Range together contain sufficient cross-sectional area of permeable aquifer to accommodate all of the groundwater flow from Snake Valley to Tule Valley estimated by published conceptual and numerical groundwater-flow models. The actual flow rate and volume are presently best constrained by the most recently published values of 15,000 acre-feet per year (18.5 hm^3/yr) (SNWA, 2009a, table I-2) and 17,200 acre-feet per year (21.2 hm^3/yr) (Durbin and Loy, 2010, table 3.1-1) (table 4.6).

E.1.5 Hydrogeology of the Confusion Range–Tule Valley Boundary

North-striking normal faults occur along the boundary between the Confusion Range and western Tule Valley (figure E.1), and the middle Paleozoic siliciclastic confining unit strikes north below thin basin-fill deposits west of the faults (Gardner and others, 2011). The closely spaced potentiometric-surface contours in this area (figure E.1) (Gardner and others, 2011) likely reflect low west-to-east transmissivity. The range-bounding faults likely contain segment-boundary zones and/or cross faults where the range front is concave-east at the latitude of Cowboy Pass. These fault bends are possible paths for interbasin flow from the Confusion Range mountain block to the central Tule Valley discharge area.

E.1.6 Summary

Hydrogeologic and geochemical data presented in this report and previously published water-budget analyses and groundwater-flow models support the hypothesis that some of the excess discharge from the Tule Valley hydrographic area is derived from interbasin flow from Snake Valley (chapter 8). Published estimates of the interbasin flow rate range from about 14,000 to 33,000 acre-feet per year (17.3–40.7 hm^3/yr), and the most recent estimates from conceptual and numerical groundwater-flow models are 15,000 acre-feet per year (18.5 hm^3/yr) (SNWA, 2009a, table I-2) and 17,200 acre-feet per year (21.2 hm^3/yr) (Durbin and Loy, 2010, table 3.1-1) (table 4.6).

The regional principal hydraulic-potential gradient direction between east-central Snake Valley and west-central Tule Valley varies from east-northeast to northeast (figure E.1). Little interbasin flow likely crosses the northern Confusion Range, where a thick section of the middle Paleozoic siliciclastic-rock confining hydrogeologic unit is in the limbs of a north- to northwest-striking synclinorium, and likely forms a barrier to west-to-east groundwater flow. In the central Confusion Range, faults, folds, and hydrostratigraphy define four northeast-striking groundwater compartments composed of the upper or lower Paleozoic carbonate-rock aquifer hydrogeologic unit. Bedding, faults, and folds within these groundwater compartments predominantly strike northeast, parallel to the regional potentiometric gradient (figure E.1). Although the groundwater-flow paths are likely tortuous in detail, the structural grain and along-strike continuity collectively favor northeastward groundwater flow. In the southern Confusion Range, groundwater flow from Snake Valley to Tule Valley likely occurs through a thick, largely structurally coherent block of the lower Paleozoic carbonate-rock aquifer hydrogeologic unit between the southern end of the Little Valley and the Kings Canyon thrust. Estimates using Darcy's Law show that these areas can accommodate the entire interbasin-flow rate from Snake Valley to Tule Valley estimated from recent conceptual and numerical groundwater-flow models.

E.2 INTERBASIN FLOW FROM SOUTHERN SPRING VALLEY TO NORTHERN HAMLIN VALLEY

Evaluating flow from southern Spring Valley to northern Hamlin Valley illustrates the difficulties in quantifying interbasin flow using the Darcy's Law and water-budget analysis. Laczniak and others (2007) assumed that their estimate of 33,000 acre-feet per year (40.7 hm^3/yr) of

interbasin flow from southern Spring Valley to northern Hamlin Valley was correct, and used a hydraulic gradient of 0.00758 and an aquifer thickness of nearly 15,000 feet (4570 m) to calculate a transmissivity for the carbonate-rock aquifer of 5800 feet squared per day (539 m^2/d) and a hydraulic conductivity of 0.4 feet per day (0.12 m/d). These transmissivity and hydraulic-conductivity estimates are within the range of values calculated from aquifer tests of the carbonate-rock aquifers in the Great Basin (table 4.1), from which Laczniak and others (2007) concluded that their interbasin flow estimate is realistic even though it far exceeds previous estimates for this boundary.

In contrast, Burns and Drici (2011) calculated an interbasin flow rate of 4400 acre-feet per year (5.4 hm^3/yr) across the same boundary, assuming that significant flow occurs only at the highly faulted north and south ends of the Limestone Hills and using a hydraulic conductivity of 8 feet per day (2.4 m/d) derived from a local aquifer test in faulted Devonian carbonate rock, an aquifer thickness of 2000 feet (610 m), and a hydraulic gradient of 0.0008866. Note the great difference in aquifer thickness and hydraulic gradient assumed by the two studies.

The estimates of Laczniak and others (2007) and Burns and Drici (2011) are likely maximum and minimum values, respectively, of interbasin flow from southern Spring Valley to northern Hamlin Valley. Using hydraulic-potential data from Gardner and others (2011) and assuming that the length scale of the driving force for interbasin flow is from basin center to basin center, and that the basin-fill and carbonate-rock aquifers are hydraulically connected, the hydraulic gradient across the northern Limestone Hills is about 0.00274 and the hydraulic gradient across the central Limestone Hills is about 0.00407. Using an aquifer thickness of 2000 to 4000 feet (610–1220 m) and hydraulic-conductivity values of 8 feet per day (2.4 m/d) in the northern and southern Limestone Hills and 0.4 feet per day (0.12 m/d) in the central Limestone Hills, this boundary can accommodate about 14,000 to 28,000 acre-feet per year (17.3–34.5 hm^3/yr) of interbasin flow, depending on the depth of active groundwater flow. The hydraulic-conductivity value of 0.4 ft/day (0.12 m/d) for the central Limestone Hills is 10 times smaller than the median hydraulic conductivity of the lower Paleozoic carbonate-rock aquifer cited by Laczniak and others (2007, table 3), and is meant to represent an average value of fractured carbonate rock and fault-zone rock.

Burns and Drici's (2011) estimate of interbasin flow from southern Spring Valley to southern Snake Valley of 4400 acre-feet per year (5.4 hm^3/yr) is similar to the excess recharge of 4567 acre-feet per year (5.6 hm^3/yr) for southern Spring Valley (sub-basin 4) of Laczniak and others (2007). In Laczniak and others' (2007) evaluation, the additional 29,000 acre-feet per year (35.8 hm^3/yr) that flows into southern Snake Valley from Spring Valley originates in southern Steptoe Valley, and moves through northern Lake Valley into from southern Spring Valley. Laczniak and others' (2007) interbasin flow rate from southern Spring Valley to southern Snake Valley, therefore, ultimately depends on the amount of excess recharge in southern Steptoe Valley.

E.3 APPENDIX E REFERENCES

Antonellini, M., and Aydin, A., 1994, Effect of faulting on fluid flow in porous sandstones, petrophysical properties: American Association of Petroleum Geologists Bulletin, v. 78, p. 355–377.

Burns, A.G., and Drici, W., 2011, Hydrology and water resources of Spring, Cave, Dry Lake, and Delamar Valleys, Nevada and vicinity: Southern Nevada Water Authority, variously paginated.

Dixon, G.L., Rowley, P.D., Burns, A.G., Watrus, J.M, and Ekren, E.B., 2007, Geology of White Pine and Lincoln Counties and adjacent areas, Nevada and Utah—the geologic framework of regional groundwater flow systems: Las Vegas, Southern Nevada Water Authority, HAM-ED-001, variously paginated. Available *in* Southern Nevada Water Authority, 2008, Baseline characterization report for Clark, Lincoln, and White Pine Counties Groundwater Development Project, *in* U.S. Bureau of Land Management, 2012, Clark, Lincoln, and White Pine Counties Groundwater Development Project Final Environmental Impact Statement: FES 12-33, Document BLM/NV/NV/ES/11-17+1793.

Durbin, T., and Loy, K., 2010, Development of a groundwater model, Snake Valley region, eastern Nevada and western Utah: U.S. Department of the Interior: Online, http://www.blm.gov/ut/st/en/prog/more/doi_groundwater_modeling.html, accessed July 2, 2010.

Feltis, R.D., 1967, Ground-water conditions in Cedar Valley, Utah County, Utah: Utah State Engineer Technical Publication 16, 31 p.

Gardner, P.M., Masbruch, M.D., Plume, R.W., and Buto, S.G., 2011, Regional potentiometric surface map of the Great Basin carbonate and alluvial aquifer system in Snake Valley and surrounding areas, Juab, Millard, and Beaver Counties, Utah and White Pine and Lincoln Counties, Nevada: U.S. Geological Survey Scientific Investigations Map 3193.

Gates, J.S., and Kruer, S.A., 1981, Hydrologic reconnaissance of the southern Great Salt Lake Desert and summary of the hydrology of west-central Utah: Utah Department of Natural Resources Technical Publication 71, 55 p.

Greene, D.C., and Herring, D.M., 2013, Structural architecture of the Confusion Range, west-central Utah—a Sevier fold thrust belt and frontier petroleum province: Utah Geological Survey Open-File Report 613, 22 p., 6 plates.

Harrill, J.R., Gates, J.S., and Thomas, J.M., 1988, Major ground-water flow systems in the Great Basin region of Nevada, Utah, and adjacent states: U.S. Geological Survey Hydrologic Investigations Atlas HA-694-C, scale 1:1,000,000, 2 sheets.

Hintze, L.F., and Davis, F.D., 2002, Geologic map of the Tule Valley 30′ x 60′ quadrangle and parts of the Ely, Fish Springs, and Kern Mountains 30′ x 60′ quadrangles, northwest Millard County, Utah: Utah Geologic Survey Map 186, scale 1:100,000.

Kistinger, G.M., Prieur, J.P., Rowley, P.D., and Dixon, G.L., 2009, Characterization of streams and springs in the Snake Valley area, Utah and Nevada, *in* Tripp, B.T., Krahulec, K., and Jordan, J.L., editors, Geology and geologic resources and issues of western Utah: Utah Geological Association Publication 38, p. 300–323.

Laczniak, R.J., Flint, A.L., Moreao, M.T., Knochenmus, L.A., Lundmark, K.W., Pohll, G., Carroll, R.W.H., Smith, J.L., Welborn, T.L., Heilweil, V.M., Pavelko, M.T., Hershey, R.L., Thomas, J.M., and Lyles, B.F., 2007, Ground-water budgets, *in* Welch, A.H., Bright, D.J., and Knochenmus, L.A., 2007, Water resources of the Basin and Range carbonate-rock aquifer system, White Pine County, Nevada, and adjacent areas in Nevada and Utah: U.S. Geological Survey Scientific Investigations Report 2007-5261, p. 43–82.

Prudic, D.E., Harrill, J.R., and Burbey, T.J., 1995, Conceptual evaluation of regional ground-water flow in the carbonate-rock province of the Great Basin, Nevada, Utah, and adjacent states: U.S. Geological Survey Professional Paper 1409-D, 102 p.

Rowley, P.D., and Dixon, G.L., 2011, Geology and geophysics of Spring, Cave, Dry Lake, and Delamar Valleys, White Pine and Lincoln Counties and adjacent areas, Nevada and Utah—the geologic framework of regional groundwater flow systems: Online: http://water.nv.gov/hearings/past/springetal/browseabledocs/Exhibits%5CSNWA%20Exhibits/SNWA_Exh_058_Rowley%20et%20al%20Report.pdf, accessed July 26, 2011.

Rowley, P.D., Dixon, G.L., Burns, A.G., and Collins, C.A., 2009, Geology and hydrogeology of the Snake Valley area, western Utah and eastern Nevada, *in* Tripp, B.T., Krahulec, K., and Jordan, J.L., editors, Geology and geologic resources and issues of western Utah: Utah Geological Association Publication 38, p. 251–269.

Southern Nevada Water Authority, 2009a, Conceptual model of groundwater flow for the central carbonate-rock province—Clark, Lincoln, and White Pine Counties Groundwater Development Project, *in* U.S. Bureau of Land Management, 2012, Clark, Lincoln, and White Pine Counties Groundwater Development Project Final Environmental Impact Statement: FES 12-33, Document BLM/NV/NV/ES/11-17+1793.

Southern Nevada Water Authority, 2009b, Transient numerical model of groundwater flow for the central carbonate-rock province—Clark, Lincoln, and White Pine Counties Groundwater Development Project, *in* U.S. Bureau of Land Management, 2012, Clark, Lincoln, and White Pine Counties Groundwater Development Project Final Environmental Impact Statement: FES 12-33, Document BLM/NV/NV/ES/11-17+1793.

Sweetkind, D.S., Knochenmus, L.A., Ponce, D.A., Wallace, A.R., Scheirer, D.S., Watt, J.T., and Plume, R.W., 2007, Hydrogeologic framework, *in* Welch, A.H., Bright, D.J., and Knochenmus, L.A., 2007, Water resources of the Basin and Range carbonate-rock aquifer system, White Pine County, Nevada, and adjacent areas in Nevada and Utah: U.S. Geological Survey Scientific Investigations Report 2007-5261, p. 11–42.

Sweetkind, D.S., Masbruch, M.D., Heilweil, V.M., and Buto, S.G., 2011, Groundwater flow, *in* Heilweil, V.M., and Brooks, L.E., editors, 2011, Conceptual model of the Great Basin carbonate and alluvial aquifer system: U.S. Geological Survey Scientific Investigations Report 2010-5193, 22 p.